The Dissertation Committee for Glenn Auld Knierim

Certifies that this is the approved version of the following dissertation

CONTROLLED ELECTRODYNAMIC SUSPENSION VEHICLE DAMPING

Committee:

_____

Mircea D. Driga, Supervisor

_____

Ross Baldick

_____

W. Mack Grady

_____

Eric P. Fahrenthold

_____

Surya Santoso

CONTROLLED ELECTRODYNAMIC SUSPENSION VEHICLE DAMPING

by

Glenn Auld Knierim, M.S.E.E., B.S.M.E.

Dissertation

Presented to the Faculty of the Graduate School of

the University of Texas at Austin

in Partial Fulfillment

of the Requirements

for the Degree of

Doctor of Philosophy

The University of Texas at Austin

May 2006

To my parents and friends, Captain Thomas George and Barbara Auld Knierim, who never falter in their love, devotion, and support of their children, grandchildren, and one another.

PREFACE

Early in life I resolved to enjoy my fleeting existence to the utmost while attempting to become as good and strong a person as I am capable. This decision led me to choose a career from my greatest interests irrespective of the recognized pains and censures I would endure. I now joyfully share this path in life as one with my wonderful and loving wife, Mari Carmen, who understands that from my profession, stems a strong sense of my identity.

This work is provided through the tutelage and support of my advisor, Dr. Mircea Driga, to whom I am grateful.

CONTROLLED ELECTRODYNAMIC SUSPENSION VEHICLE DAMPING

Publication No. _____

Glenn Auld Knierim, Ph.D.

The University of Texas at Austin, 2006

Supervisor: Mircea D. Driga

Commercial application linear motion magnetically levitated, maglev, bodies are inherently unstable owing to minimal large magnitude or prolonged oscillating disturbance natural damping. Induced vibrations into large inertial, magnetically levitated bodies experience resonance under certain operating conditions. Maglev vehicles typically incorporate a non-magnetic ancillary damping suspension system as compensation. Maglev designers desire an efficient, solely magnetic based damping system without auxiliary compensation for these large inertial vehicles, but no effective system has presented itself.

This paper investigates the unstable nature of a maglev electrodynamic suspension, E.D.S., system. Electromagnetic solenoid coils operating in concert with an appropriate control law offer this solution. A hierarchy of controlled, electromagnetic damping suspension systems is theorized and analyzed and in one case designed, fabricated, and tested. These designs range from a single degree of freedom, D.O.F., maglev suspension to a dynamically coupled six D.O.F. maglev suspension. Solenoid coils form the electromagnetic damping prime mover hardware. Soft computing optimal nonlinear control forms the final electromagnetic damping control kernel for this proof of concept paper whereas soft computing adaptive nonlinear control forms the final electromagnetic damping control kernel for a proposed final system solution.

TABLE OF CONTENTS

LIST OF TABLES

Main Body Text Tables

LIST OF FIGURES

Main Body Text Figures

Appendix Figures

GLOSSARY

Base units are listed in parenthesis after each variable or constant identified in this Glossary. System international, S.I., is this document's base unit system although a particular dimension, analysis, or model occasionally deviates from this standard. The greatest deviation occurs with the length dimension. This unit is chosen as ANSI inches to correspond to the physical material availability limits such as the primary wire, primary core, and secondary material standard stock dimensions.

Acronyms & Abbreviated Words

2D	Two Dimensional
3D	Three Dimensional
AC	Alternating Current
B.O.P.	Bipolar Amplifier
C.A.D.	Computer Aided Design
C.G.	Center of Gravity = C.O.M.
C.O.M.	Center of Mass = C.G.
C.P.U.	Control Processing Unit
D.A.Q.	Data Acquisition System
D.O.F.	Degree of Freedom
E.D.S.	Electrodynamic Suspension
emf	Electromotive Force (Volts)
E.M.	Electromagnetics
E.M.S.	Electromagnetic Suspension
I.-P.D.	Integral Proportional Differential Control
L.I.M.	Linear Induction Motor
L.S.M.	Linear Synchronous Motor
L.V.D.T.	Linear Variable Differential Transformer
Maglev	Magnetic Levitation

P.D.	Proportional Differential Control
P.I.D.	Proportional Integral Differential Control
RMS	Root Mean Squared
rpm	Revolutions Per Minute
S.I.	System International Standards for Units
S.T.P.	Standard Temperature and Pressure

Arabic Letters

a	6 D.O.F. vehicle length
A	Magnetic vector potential; $n \times n$ size linear controls matrix variable; Arbitrary constant
b	6 D.O.F. vehicle width
B	Magnetic flux density (Tesla); $n \times r$ size linear controls matrix variable; Arbitrary constant
c	Damping constant $\left(\frac{\text{kg}}{\text{sec}}\right)$; 6 D.O.F. vehicle height
C	$p \times n$ size linear controls matrix variable; Arbitrary constant
D	Variable for operator notation; Arbitrary constant
e	State error equation array variable
E	Electric field $\left(\frac{\text{Volts}}{\text{meter}}\right)$; Arbitrary constant
f	Frequency (Hertz)
F	Thrust (Newtons)
g	Gravitational body force; Gap length (meters)
G	Arbitrary constant; Center of gravity
$G(\xi)$	Vector potential complex zeros term
h_p, h_s	Height of primary solenoid and secondary respectively
$H(\xi)$	Vector potential complex poles term

H	Magnetic field intensity $\left(\frac{\text{Ampere} \times \text{turns}}{\text{meter}}\right)$
i	Time dependent current (Amperes)
I	Current (Amperes)
j	Imaginary number operator
J	Polar moment of inertia; Equivalent current density $\left(\frac{\text{Amperes}}{\text{meter}^2}\right)$
k	Spring constant $\left(\frac{\text{kg}}{\text{sec}^2}\right)$
k_w	Winding coefficient
K, K_f	Equivalent sheet or surface current density of infinitesimally small thickness $\left(\frac{\text{Amperes}}{\text{meter}}\right)$; Free sheet or surface current density $\left(\frac{\text{Amperes}}{\text{meter}}\right)$
L	Inductance (Henries)
m	Mass (kg); Dummy series variable
n	Number of system states; Control array length variable; Dummy series variable
N	Number of windings (turns)
O	Phase III pivot axis
p	Control array length variable
P	Real power (Watts); Arbitrary point in space above current ring
q	Generalized coordinate for Lagrange's energy equations
Q	Generalized force for Lagrange's energy equations
r	Control array length variable; Radius
R	Resistance (Ω)

s	Complex frequency, assuming only using imaginary component $(j\omega)$ in paper
t	Time (seconds)
T	Kinetic energy
u	r length linear controls vector
U	Potential energy
x	Right Cartesian coordinate x used throughout document; Body reference frame propulsion direction
X	Inertial reference frame propulsion direction
y	Right Cartesian coordinate y used throughout document; Body reference frame lateral or sway direction
Y	Inertial reference frame lateral or sway direction
z	Right Cartesian coordinate z used throughout document; State variable; Controls output variable; Body reference frame vertical or heave direction
Z	Impedance (Ω); Inertial reference frame vertical or heave direction

Greek Letters & Special Symbols

[]	Matrix indicator when single variable inside brackets
{}	Array indicator when single variable inside braces
$\hat{a}$	Unit vector indicator, use for any lower case, single variable below carrot
$\dot{a}$	Single dot product or single derivative of variable below dot
$\ddot{a}$	Double dot product or double derivative of variable below dots
a'	Single derivative of variable in front of slash
a''	Double derivative of variable in front of slashes

$\hat{A}$	Phasor A indicator, use for any upper case, single variable below carrot; State error equation variables
$\bar{A}$	Vector A indicator, use for any single variable below arrow
$\tilde{A}$	Fourier transform of A indicator, use for any single variable below tilde
A^*	Complex conjugate of A indicator, use for any single variable; Co-energy of A indicator, use for any single variable
α	Characteristic equation constant
β	Traveling wave constant or wave number $\left(\frac{1}{\text{meters}}\right)$; General traveling magnetic flux density wave component
γ	Fourier transform differential operator; Quadratic form of the ξ poles.
δ	Phase angle; Skin depth (meters)
ϕ	Mechanical pitch angle
Φ	Magnetic flux (Webers)
λ	Magnetic flux linkage $(\text{Weber} \times \text{turns})$
μ	Linear state space control closed loop pole; Permeability $\left(\frac{\text{Henries}}{\text{meters}}\right)$
μ_o	Permeability of free space $\left(\frac{\text{Henries}}{\text{meters}}\right)$
ε	Semicircle radius for Cauchy Principle Value point on analytic contour
ν	Velocity $\left(\frac{\text{meters}}{\text{second}}\right)$
θ	Mechanical roll angle
ρ	Resistivity $(\text{Ohm} \times \text{meters})$

σ	Conductivity $\left(\frac{\text{mhos}}{\text{meter}}\right)=\left(\frac{\text{Amperes}}{\text{Volt}\times\text{meter}}\right)$
τ	Pole pitch (meters)
ω	Primary power supply electrical angular frequency $\left(\frac{\text{Radians}}{\text{second}}\right)$
ξ_1, ξ_2	Vector potential poles from the Residue Theorem; x or y propulsion axis dynamic boundary conditions
ψ	Mechanical yaw angle
ℓ	Integration path of a circulation (meters)

Subscripts

1	Primary region; Phase III mechanical linear mass
2	Secondary region; Phase III mechanical linear and rotational mass
2%	Type of linear state control settling time
3	Air gap region below secondary
4	Air gap region above secondary
A	Aft of 6 D.O.F. vehicle
B	Bow of 6 D.O.F. vehicle
c	Control system
Cntl	Control system
com	Center of mass
g	Air gap in the respective coordinate axis direction in line with the coordinate axis
G	Center of mass
g_init	Initial gap position
G_init	Initial position about point G
HA	Halbach array
I	Integrator constant

l	Principal or primary levitation system
mechy	Phase III y directed mechanical spring constant
mechz	Phase III z directed mechanical spring constant
L	6 D.O.F. vehicle lateral direction
N	Normal component
O	Phase III pivot axis
original	Original equation form determined
prime_ξ	Derivative of the pole form of γ^2 with the appropriate pole value substitution
Prin	Principal system
P	Power; Percent overshoot; Port side of 6 D.O.F. vehicle
rms	Root mean squared
s	Steady state component; Synchronous component; Secondary sheet surface resistivity for the sheet current
S	Starboard side of 6 D.O.F. vehicle
T	Total air gap between primary & secondary; Tangential component
V	6 D.O.F. vehicle vertical direction
x	Right Cartesian coordinate x used throughout document
xx	Polar moment of inertia coordinate
y	Right Cartesian coordinate y used throughout document
z	Right Cartesian coordinate z used throughout document

Figure Diagram and Schematic Color Code

Blue	Mechanical ground
Cyan	Mechanical subsystem
Green	Controls; Control levitation and guidance system; Acceptable simulation performance

Magenta	Overall coil primary; Principal levitation and guidance system; Coil primary iron; Electrical subsystem
Red	Highlighted area of interest; Unacceptable simulation performance
Yellow	Overall plant of block diagrams; Secondary conductor; Coil primary winding; Complex plane contour map; Desired simulation performance levels

CHAPTER 1 INTRODUCTION

1.1 BACKGROUND

1.1.a Overall Maglev Concept

Magnetically levitated bodies benefit from a non-contact distance or air gap between the primary and secondary which removes all mechanical bearing friction and mechanical vibration. A maglev body also benefits from no appreciable magnetic damping when the levitation axis is predominately parallel to the magnetic flux density lines, the magnetic orientation required for a more efficient maglev propulsive axis. A designer makes use of these benefits in devices such as high and low speed maglev trains, magnetic bearings, and non-contact bodies such as wind tunnel prototypes.

Magnetically levitated bodies also pay a penalty from this negligible orthogonal damping benefit. All pure maglev suspensions are unstable under certain operating conditions. For over half a century this fact plagued commercial application maglev vehicle design. Electromagnetic damping, mechanical auxiliary suspension damping, aerodynamic auxiliary suspension damping, the studied but not implemented propulsive active to reactive power converter current angle suspension damping, or a suspension system combination is deemed necessary to achieve adequate vehicle performance. Common rotary magnetic systems, such as rotary magnetic bearings, exhibit gyroscopic motion which benefits their stability over linear systems, such as maglev systems. The majority of proposed commercial maglev train suspensions researched to date, where ride quality is crucial, incorporate mechanical auxiliary suspension damping to absorb the induced kinetic energy. Maglev train designers desire a fully electromagnetic suspension, but no commercially viable solution currently presents itself.

Earnshaw's theorem stated simply in Moon [16], "A body with steady charges, magnetization, or currents placed in a steady electric or magnetic field

cannot rest in stable equilibrium under the action of electric and magnetic forces alone." Exceptions to Earnshaw's theorem such as levitation of a permanent magnet in a superconducting potential bowl or suspension of a permanent magnet in a ferrofluid are not applicable to maglev systems and are not considered in this work. This theorem requires active instead of passive control for all magnetic suspensions. A magnetic suspension can actively force magnetic damping at the expense of the intrinsic magnetic spring constant. Since active control is required for maglev systems, all maglev control systems considered are assumed active.

1.1.b Maglev System Basics

1.1.b.i E.D.S. VS. E.M.S. MAGLEV SYSTEMS

Figure 1.1-1: General Atomics Urban Maglev Low Speed E.D.S. Maglev Train

Maglev suspension systems are classified into two main categories as per the means of magnetic levitation. E.D.S. maglev systems operate on the principle of electrodynamic repulsion. Electromagnetic suspension, E.M.S., maglev systems operate on the principle of electromagnetic attraction.

Simple E.D.S. systems can be made relatively stable inside of a magnetic potential well construct and therefore can be operated under open loop control. Complex E.D.S. maglev systems are unstable and therefore require closed loop active control for operation. E.D.S. maglev trains can be levitated with air gaps around six to ten centimeters with acceptable power loss. Some superconductor based E.D.S. systems even acquire a thirty centimeter air gap, Moon [17].

Figure 1.1-1, provided courtesy of General Atomics low speed maglev technology program, is an example of a conventional magnet, low speed E.D.S. maglev train. This system's levitation prime mover operates on the principle of permanent magnets arranged in a Halbach array.

E.M.S. systems are inherently unstable under all configurations and therefore require closed loop active control for operation. E.M.S. maglev train air gaps are much smaller than E.D.S. maglev train air gaps. A typical E.M.S. air gap is around one to two centimeters. Figure 1.1-2, provided courtesy of General Atomics who is affiliated with Transrapid USA, provides an example of a conventional magnet high speed E.M.S. maglev train.

Figure 1.1-2: Transrapid High Speed E.M.S. Maglev Train

This suspension air gap distance, vertical levitation and lateral guidance, is crucial to the implementation of commercial maglev trains. High speed maglev trains maintain relatively cheap preventative maintenance costs, operating costs, capital investment costs, and a more environmentally sound technology compared to conventional high speed trains, but politics opposing maglev trains in numerous countries around the globe have thus prohibited their commercial use. Therefore any means to lower maglev train costs is desired. The initial guideway capital investment is by far the greatest cost of any maglev system. The large E.D.S. air gap allows for lower guideway mechanical tolerances than the E.M.S. air gap and hence lower capital cost of the maglev system from this point of view. Therefore the larger air gap, E.D.S. system is often desired commercially and is the focus of this research paper. A recent caveat to the maglev global implementation statement above is the German based Transrapid International high speed maglev train demonstration opened in the year 2004 for short distance, twenty mile, operation in Shanghai, China.

1.1.b.ii Maglev System Damping

Energy Components

In physics energy components are broadly classified as inertial, capacitive, or dissipative. Understanding what these components represent electromechanically is crucial to understanding the maglev damping relationship. Inertial and capacitive components store energy whereas dissipative components dissipate energy. In a mechanical system these components are defined as mass, spring, or dashpot elements respectively. In an electrical system these components are defined as inductor, capacitor, or resistor elements respectively. An example of basic mechanical and electrical energy components arranged with the capacitive and dissipative components in parallel between the inertial component and ground plane, which is the same orientation as a maglev suspension, is demonstrated in Figure 1.1-3.

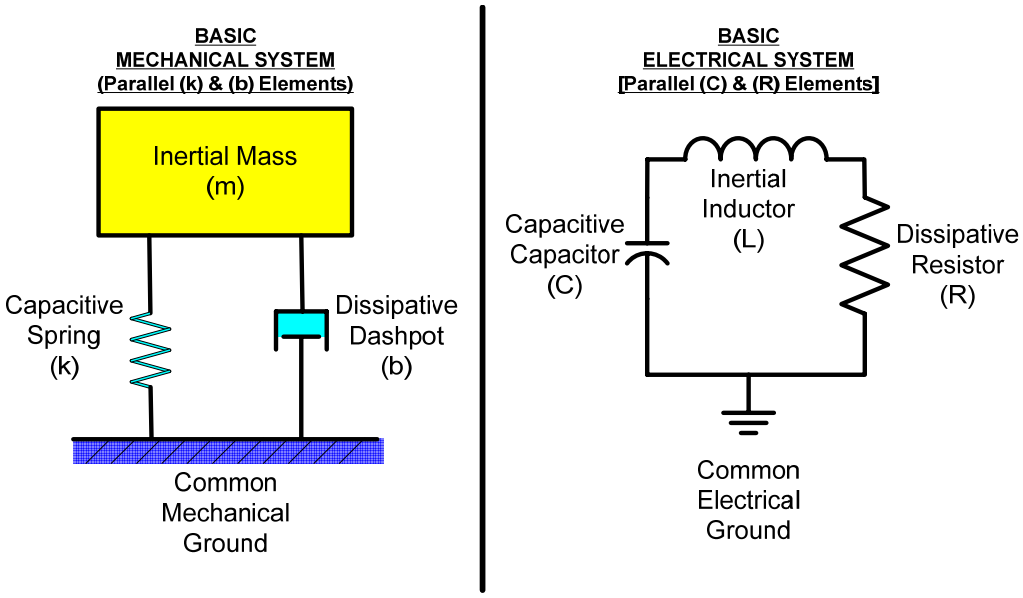

Figure 1.1-3: Basic Energy Element Example

A maglev suspension is dominated by its' inertial and capacitive components. Hence the electrical equivalent of a maglev suspension is composed of inductor and capacitor elements with negligible resistive elements. Such a system is often unstable across parts of its' operational range when negligible damping is present. The unstable nature of the system developed in this paper is presented later in the discussion revolving around equation (3.97). High magnitude disturbance and prolonged oscillation inputs can introduce ride quality oscillation peak and damping time constant issues in addition to potential worse case scenario maglev vehicle health issues. The oscillations in this system depend on system magnetic wavelengths, critical propulsive velocity values where the electrical angle between the levitation system and its' image allows vertical energy input, total sprung inertia where the mass is often limited to a fixed range of values for a particular design, spring and damping values, and harmonic and transient perturbation forces. These values particularly affect large mass systems with insignificant damping once the disturbance energy is transformed into the mechanical inertial energy since the natural period of oscillation is governed by equation (1.1) where m is the sprung mass

and k is the spring constant. In a real system there is always some level of damping present and therefore equation (1.1) does not strictly apply. Equation (1.1) is still useful when considering maglev systems where parasitic damping is only a second order effect. Particularly in cases where the natural period of oscillation is much greater than allowable ridership quality level time constants. Another form of equation (1.1) is provided later in equation (3.3).

$$\begin{pmatrix}\text{Natural Period}\\ \text{of Oscillation}\end{pmatrix} = \tau = 2\pi\sqrt{\frac{m}{k}} \tag{1.1}$$

In providing E.D.S. system stability there are limitations on a maglev designer's options. Maglev designers do not want to limit the inertial maglev system component, the system mass, to a fixed range of values. Maglev designers also do not want to raise the capacitive maglev system component, the system spring constant stiffness, to levels that create unacceptable ride quality while raising resonant frequency values whereas too low of a capacitive maglev system component produces a large oscillatory amplitude. Therefore providing a magnetic system damping constant is the variable chosen to provide system stability.

Static vs. Dynamic Maglev Systems

The introduction of a maglev propulsive component, the maglev's magnetic component other than pure levitation or guidance, differentiates the static and dynamic maglev systems. A static maglev system has no propulsive component whereas a dynamic maglev system is actively moved via a propulsive force.

As mentioned previously in this chapter, in reality dynamic maglev trains have a measurable amount of natural aerodynamic damping and velocity dependent eddy current power dissipation that can take the form of damping. Maglev trains are still unstable over their range of operation and require another damping source to reduce introduced oscillations. This is demonstrated in Sinha [20] where the underdamped vertical frequency of a superconducting E.D.S. maglev is 1.6 Hz. Since the common human motion sickness frequency range is 0.5 Hz to 1.5 Hz, persistent

vertical oscillations around this frequency are obviously unacceptable for commercial transit maglev applications. Static and dynamic maglev systems both experience this coupled no damping problem but in different manners.

A static maglev is inherently unstable with typically nominal electromagnetic damping from induced eddy currents. These eddy currents may stem from prime mover sources such as the primary levitation or guidance magnetic forces exciting secondary eddy currents or from relative mechanical motion between the primary and secondary resulting in velocity dependent parasitic drag effects from the stray magnetic flux penetrating support structure conducting materials. A dynamic maglev system can build upon the existing static eddy current damping forces, such as the addition of the relative primary to secondary propulsive velocity vector mechanical motion, as well as potentially introduce more eddy current damping originating from the primary motor employed for thrust itself. As reported in Moon [17], the oscillation of a magnetic field source near a stationary conductor producing the induced eddy currents in the body normally results in damping forces. Therefore underdamped oscillations in a maglev system are only introduced by external forces above a minimum oscillation energy threshold.

The multiple D.O.F. of a maglev system are always coupled. All multiple D.O.F. maglev systems in this paper are also dynamic maglev systems. Besides coupling between the static levitation and guidance maglev D.O.F., a dynamic maglev system also experiences a coupling between the static maglev D.O.F. and any magnetically propulsive D.O.F. This extra complexity in the dynamic maglev system model allows possible negative damping in a convective magnetomechanical system. Stated another way, the possibility of negative damping occurs when the field source and conductor experience a relative velocity transverse to a vibration between the field source and conductor, as mentioned in Moon [16]. This occurs when the translating propulsive motion adds energy into the vertical or lateral vibrating D.O.F. through negative magnetic damping.

1.1.b.iii Damping Control Coil Solution

Defining Principal & Control Coils

In this research paper principal coils are defined as the coils within the principal solenoid or solenoids that are used as the prime mover for vertical levitation as well as lateral guidance. In general the principal solenoids may be a lumped parameter approximation of the forces and dynamics that an actual maglev system represents.

The control coils are defined as the coils within the control solenoid or solenoids that are introduced via this paper into the maglev system under analysis for magnetic air gap damping control in both the levitation and lateral guidance directions.

The system could potentially suffice with the principal coils as combined levitation and guidance as well as damping control coils by superimposing the required electrical coil inputs to perform each respective task. This research paper assumes that a separate control solenoid system is both required due to the probable faster time constant and desired due to the smaller energy requirements than the principal solenoid system. Since the principal coils assume no controllability upon themselves which thereby increases the control coil energy and control logic requirements, the principal coils are therefore assumed to only have an “On” or “Off” power state throughout this analysis. These issues are discussed further in Chapter 2.4.

Magnetic Attraction vs. Repulsion Damping Control Coils

Magnetic air gap linear vibrations oscillate in a two stroke gap widening and gap closing fashion. Magnetically attractive or repulsive control coil systems dampen oscillations by lessening or increasing their respective control force. In this sense these control coils act as trim coils which fine tune the levitation and guidance gap

distances of a respective body. Proper phase angle control between system oscillations and the control coil output force provides the damping solution.

A low level of principal and control coil damping is always present in the secondary material due to the primary energy used to establish the secondary currents. In all actuality the addition of these new magnetic solenoid controlling devices for vertical levitation and lateral guidance purposes cannot provide a high amount of direct velocity dependent damping in the axis in which they are meant to control and hence are oriented, although they can provide a high damping component in the propulsive velocity direction where the velocity is completely orthogonal to solenoid axis. Physically the addition of control solenoids only increases the magnetic spring stiffness of each respective air gap. Air gap oscillation damping is only achieved through the air gap position and velocity dependent control of the introduced control solenoid's magnetic flux density output and hence a controlled magnetic spring stiffness value. This control of the solenoid provides the actual damping mechanism.

Magnetically attractive control coil systems can be direct current amplitude based instead of the more complicated alternating current amplitude and frequency based, although magnetically attractive systems typically include ferrous materials as coil cores and secondary reaction plates. Ferrous materials introduce undesired increased system inductance and lower response times over air cores. This difference in transient response times and higher system reactance leads the analysis of this paper to the magnetically repulsive control coil system. The primary of a conventional magnetically repulsive scheme also commonly includes ferrous materials, but the overall amount of ferrous materials in this system is typically much lower than the attractive system.

Magnetically repulsive control coil systems with a passive secondary, the system chosen for this research paper, must induce an emf, electromotive force, into the secondary conductor. This reaction typically requires more energy than the magnetic material pole alignment of a magnetically attractive system. Also the

introduction of ferrous materials effectively focuses the magnetic flux density into a designed path which typically leads to a lower energy requirement than an air core system to attain a similar magnetic pressure. This higher energy requirement introduces a larger repulsive coil system than a magnetically attractive system. Although magnetically repulsive control coil systems often experience higher coil energy requirements than their magnetically attractive system counterparts, their much desired faster electrical transient times retains them as the focus of this paper.

1.1.c Past Work

Stability is a recognized design challenge for any commercial maglev train. The problem's crux lays in the inherent no damping nature of the system. Iwamoto *et al.* [1] discovered the critical damping propulsive speed of $\approx 50 \frac{\text{m}}{\text{sec}}$, above which negative damping predominates a maglev train's electromagnetic suspension. Fortunately this negative damping is typically dominated by the maglev train's aerodynamic damping. As noted in Thompson and Thornton [21], the conclusion of many early maglev ride control studies is that some form of damping is needed for acceptable ride quality, even in the presence of aerodynamic damping. It is also noted that many of the reported instabilities are related to magnetic coupling between the maglev's suspension and propulsion. It is concluded that E.D.S. maglev needs some sort of auxiliary suspension or active damping control.

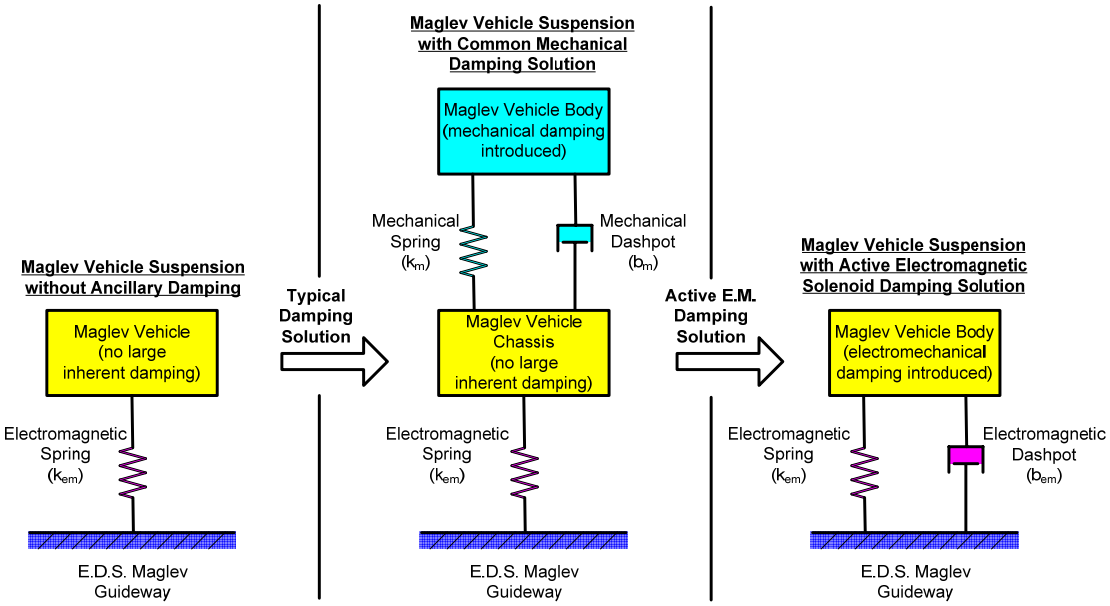

Note: Springs and Dashpots in each model represent the superposition of energy elements for all 6 D.O.F.

Figure 1.1-4: Maglev Suspension Energy Element Example

Most maglev train research programs compensated for the greatly underdamped electromagnetic primary suspension by providing auxiliary mechanical suspensions that incorporate damping mechanisms as demonstrated in Figure 1.1-4. This solution attempts to ignore the difficulties and even worse case scenario potential danger to an underdamped electromagnetic suspension while introducing mechanical system preventative maintenance issues. Researchers have studied this unstable E.D.S. maglev problem for half a century, but still find no commercially viable solution presents itself, although there are a few laboratory successes. Thompson and Thornton [21] discovered that with an electromagnetic suspension using high temperature superconductors reacting with a conductive rotating wheel, it is possible to actively control the magnet position to achieve good ride quality within reasonable source power and energy levels.

1.2 OBJECTIVE

1.2.a Problem Statement

Large mass maglev vehicles, where the oscillation damping effects of system eddy currents and aerodynamics are minimal, are unstable systems under certain common maglev operating conditions. Maglev system designers desire an electromagnetic based damping system to control this instability while maintaining a low overall system profile. Such oscillations introduce ride quality issues and potential worse case scenario system heath issues. These systems involve large magnetic levitation, guidance, and propulsion energies which are reluctant to change. Therefore no commercial application large mass, solely magnetically damped, E.D.S. maglev vehicle is available today. Instead non-magnetic auxiliary damping is commonly implemented to compensate. Components of an E.D.S. magnetically based damping are developed at various research centers, but a final system which pulls all components together still eludes technology.

1.2.b Original Achievement

Produce a unique proof of concept simulation prototype which economically maximizes magnetically based damping with no auxiliary system damping requirement for a large mass E.D.S. linear propulsive maglev vehicle for any common range of operation.

1.2.c Goal

The goal of this research paper is to theoretically understand, analyze, and control instabilities in a proof of concept maglev system. This achievement is accomplished by inserting external magnetic damping control systems into a general E.D.S. maglev system. This goal must eventually be achieved economically regarding monetary, energy, and sizing costs in a full scale system, but although these issues are mentioned throughout this paper they are not the focus of this paper. In Phase I this research paper focuses on the general principle of electrodynamic repulsion. Where applicable the General Atomics E.D.S. maglev vehicle is used for a specific base comparison study. In Phases II and III this research shifts focus to this particular E.D.S. maglev system, the General Atomics Halbach array principal levitation maglev vehicle. The shift to this specific vehicle is used to detail testing recommendations on existing equipment at General Atomics from the theory and analysis formulated in this research paper. These testing recommendations can be applied in a general sense to any E.D.S. maglev, but the focusing on this particular real world hardware helps present these recommendations in a clear fashion. Phase IV then shifts back to a general E.D.S. maglev system configuration for analysis and simulation but still exploits the General Atomics maglev vehicle example to clearly demonstrate a means of applying these general equations to a specific vehicle.

Applying this work on each E.D.S. maglev configuration available today requires modification of this work, but the governing damping theory hypothesized in this research paper applies to any E.D.S. maglev system. Therefore the governing theory and control scheme devised creates a basis for electromagnetic damping work

on any E.D.S. type system. The extreme overlap between the E.D.S. and E.M.S. magnetic systems allows this work to also serve as an E.M.S. damping system basis.

The analytical development of this paper assumes multiple approximations. A judicious choice of these assumptions provides the final analysis goal which focuses on a general air gap magnetic damping proof of concept system. Therefore analytical complexity is maintained for the air gap magnetic spring constant and supporting control system, but is minimized wherever else possible. A list of main analysis assumptions for the final equations used or not used is provided in Table 1.2-1.

Table 1.2-1: Main Analysis Assumptions

ANALYSIS ASSUMPTIONS FOR FINAL EQUATIONS USED				
Main Assumption Category	**Item #**	**Effects Phase**	**Main Assumptions *NOT* Used List**	**Described in Chapter(s)**
Mechanical	1	III & IV	Small angle approximation	3.5.a.i & 3.6.a.i
Main Assumption Category	**Item #**	**Effects Phase**	**Main Assumptions Used List**	**Described in Chapter(s)**
Mechanical	1	III & IV	Vehicle C.O.M. = Vehicle geometric center	3.5.a.i & 3.6.a.i
	2	IV	3D vehicle boundary limits	3.6.a.i
	3	All	Rigid body motion applies	3.5.a.i & 3.6.a.i
	4	III & IV	System starts from a static equilibrium point	3.3.a.iv
	5	All	Perturbation amplitudes high compared to normal operation	5.1
	6	IV	Maglev vehicle in steady state propulsion	5.3.c.i
	7	IV	Principal & control solenoids share the same geometric location	3.6.a.i
	8	IV	Rotational wheel test facility approximates a linear system	4.3.c.i

Controls	9	II & III	Rotary wheel motor is properly and smoothly controlled through a separate control scheme	2.3.c
	10	IV	L.S.M. is properly and smoothly controlled through a separate control scheme	2.3.e
Electrical	11	All	Isolated electrical source	5.1
	12	All	Principal solenoids only have total “on” or “off” power states	1.1.b.iii
	13	All	Perfect sinusoidal electrical input voltage for all solenoid coils	3.2.b.i, 3.3.a.i, & 3.3.a.ii
	14	All	Uncoupled mutual inductance from air gap distance	3.2.b.iii
	15	All	Median resonant frequency approximation	5.2.d.iv
Thermal	16	All	Thermal analysis solenoid lumped parameters	3.2.b.vi
	17	All	S.T.P. ambient thermal conditions	3.2.b.vi
	18	All	No conductive or forced convective cooling	3.2.b.vi
Magnetic	19	IV	Magnetic analysis solenoid lumped parameters	1.1.b.iii& 3.6.a.i
	20	All	Solenoid stator may comprise either the armature primary or secondary	2.1.a
	21	All	Secondary is a purely passive conductor	2.1.a & 3.3.a.ii
	22	All	All materials are linear, homogeneous, & isotropic	3.3.a.ii
	23	All	All primary $\vec{B}$ enters secondary	3.3.a.ii
	24	All	Iron core saturation step function with no hysteresis effects	3.2.b.iii& 5.3.c.ii
	25	I	Solenoid magnetic isolation	6.2.c.vii
	26	All	Uncoupled saturating $\vec{B}$ from primary current	3.2.b.iii
	27	II, III, & IV	Solenoid secondary conducting sheet assumed to be a ring secondary	3.3.a.iii
	28	All	Primary & secondary have approximately equivalent radii	3.3.a.ii
	29	All	Primary inside radii does not effect $\vec{B}$	3.3.a.ii

	30	II, III, & IV	Magnetic drag approximation	3.3.a.iii
	31	All	2D Cartesian coordinate approximation for the cylindrical system	3.3.a.ii
	32	All	Only the covered stator portion of the primary current contributes to the magnetic vector potentials	3.3.a.ii
	33	All	Fixed magnetic wave length from primary geometry	3.3.a.ii
	34	All	Fourier methods for $\vec{B}$ entering secondary for a particular propulsive velocity & x coordinate length	3.3.a.ii
	35	All	Permeability values	3.3.a.ii
	36	All	Parallel facing & coaxial primary & secondary with $\vec{B}$ constant at all secondary radial points	3.3.a.iii
	37	All	Magnetic bounding regions continue without change to infinity	3.3.a.ii
	38	All	Primary is a purely non-conducting source where the magnetic vector potential only flows in the x axis direction	3.3.a.ii
	39	All	Magnetic gradient has only y axis component in region 2	3.3.a.ii
	40	All	Simple pole proximity to origin	3.3.a.ii
	41	All	Residue theorem has two contours of interest to solve	3.3.a.ii
	42	All	Residue theorem contour radius, ε, is equivalent for both real axis poles	3.3.a.ii

This research paper is not meant to optimize or completely design a maglev principal solenoid, control solenoid, or control kernel. A maglev system is extremely complex and therefore a complete design requires much more work than this paper allows. Therefore maglev design primary power, energy, and system efficiency values are not considered. This research paper is also not concerned with exact passenger ride quality levels. A damping system solution that achieves electromagnetic damping while amenable to general ride quality requirements is considered adequate.

1.3 RESEARCH PAPER OUTLINE

This introductory chapter describes the background and basics behind maglev systems while outlining the focus of this research paper. Chapter 2 outlines the general proposal behind this work and procedures for solving each phase. This chapter initially discusses the overall methodology for solving the problem at hand. Then the system modeling, control theory, fabrication, and testing methods used in this research paper are discussed. Chapter 3 details the analysis and control algorithm derivation for each phase model described. Chapter 4 details the Phase I test setup and models and Phases II, III, and IV proposed test setups and models. Chapter 5 provides system modeling results, governing physical laws, control and optimization theory results, and Phase I system testing results. Chapter 6 presents the conclusion for each phase and the overall conclusion for this research paper. The Appendices provide the program flow charts, analytical programs, numerical programs, test and control programs, computational outputs, and detailed design and assembly drawings. Appendix A provides the Mathcad® exact solution programs. Appendix B provides the Opera™ electromagnetic computational solutions. Appendix C provides the Matlab® and Simulink® numerical system simulation programs. Appendix D provides the detailed Labview™ test and control program. Appendix E provides test article hardware supplemental fabrication information, pictures, and drawings of assemblies and subassemblies.

CHAPTER 2 PROPOSAL

2.1 METHODOLOGY

2.1.a Overall Methodology

In order to properly solve this previously discussed unstable E.D.S. system issue, this work must first model the complete electromechanical system including the introduced electromagnetic damping control solution hardware. The focus then reverts to controlling the system with the introduced electromagnetic damping hardware. This research paper evolved around a hierarchal increasing level of complexity and verification methodology. This method provides a proper understanding of governing parameters and laws while verifying final solution accuracy. This hierarchal approach is witnessed in the overall research paper phase structure described throughout Chapter 2, modeling and control techniques of Chapter 3, Phase I implemented and Phases II, III, and IV recommended test techniques of Chapter 4, and within this research paper's chapter titles. This hierarchal approach embodies a tedious analysis and control method of basic observation and redundancy. Since each consecutive part or phase of this research paper is only an expansion of the previous part, the completion time for this overall research methodology is not prohibitive.

This research paper centers on understanding and control of the E.D.S. electromagnetic damping system itself. The electromagnetic system only depends on the relative position between the electromagnetic primary and secondary regardless of other influences, assuming everything else being equal. Therefore the stator can comprise either the electromagnetic primary or secondary as long as the modeling and control systems correspond with their respective test apparatus. The secondary is a purely passive conductor.

2.2 INNER PHASE METHODOLOGY

Although the physical laws of the final maglev system model are nonlinear, many of the system's components are based on linear physical laws. Linearity approximations and superposition techniques lend themselves to direct hierarchal construct of increased complexity. Therefore linear analytical techniques are initially applied to approximate the outcome of a particular system model or phase. Then nonlinear analytical techniques are introduced to construct a more exact model for each particular system.

In implementing this methodology, this work initially compares the linear and nonlinear analytic models through analytic parameter observation and numerical simulation. The next step is dynamic and electromechanical computational model creation for comparison with the analytic models wherever appropriate. Now the work devises the companion control scheme for the respective linear and nonlinear analytic models. Linear state space control methods use linear analytic equations. Nonlinear control methods, such as soft computing optimal and soft computing adaptive control methods, use nonlinear analytic equation methods. Before proceeding to the each successive phase the project compares the linear and nonlinear control schemes and then discusses a devised test apparatus for each phase. These steps are briefed in Table 2.2-1. This method of increasingly complex models is applied in an effort to understand the physical laws and control the simpler linear model before proceeding to a more complex but accurate nonlinear system model. Note that only the Phase I test apparatus is completely fabricated and tested. Phase II, III, and IV test recommendations are introduced as a guideline for any future work.

Table 2.2-1: Phases I to IV Overall Procedure

Overall Procedure Steps on a Per Phase Basis		
Step #	**Category**	**Step Description**
1	Component Models	Analytical Component Modeling
2		Computational Component Modeling (Driven by Analytical Model)
3	Control	Linear Control (Phase I and II only)
4		Nonlinear Control
5		Compare Linear and Nonlinear Control
6	System Models	Nonlinear System Modeling
7		Compare Models Between Project Phases
8	Test	Design & Fabrication of Components & Test Apparatus
9		Test System
10		Obtain Empirical Data
11	Empirical Results Analysis	Compare Empirical Data with Models and Control Schemes
12		Use Empirical Data to Lead Corrections of Models & Control Schemes
13		Compare Data Between Project Phases

2.3 INTRA PHASE METHODOLOGY

2.3.a Overall Intra Phase Methodology

Final 6 D.O.F. System

To facilitate this work without adding unnecessary complexities, one of the simplest six D.O.F., E.D.S. maglev systems conceivable is chosen for discussion. The final maglev system model analyzed in Chapter 3.6 is purposely not this exact model but a slight variant, where the lateral guidance coils are switched to the inside with an outer conducting track area, to demonstrate how easily one may apply this analysis to slight permutations of the basic E.D.S. model. In the E.D.S. system discussed here the vehicle encloses the top of a central guideway allowing a six D.O.F. vehicle with certain D.O.F. dependencies. In this model each magnetic source for magnetic force or control is only located on a primary axis plane which by definition ideally only

provides orthogonal magnetic interactions. Therefore the various simplified D.O.F. never have a translation to translation D.O.F. or rotation to rotation D.O.F. coupling. Figure 2.3-1 provides a representation of this six D.O.F. maglev vehicle with the central guideway removed. The often continuous maglev suspension system itself is separated into multiple contiguous yet discernable maglev modules. Such a modular suspension separation allows another logical module modeling step prior to modeling the entire maglev system.

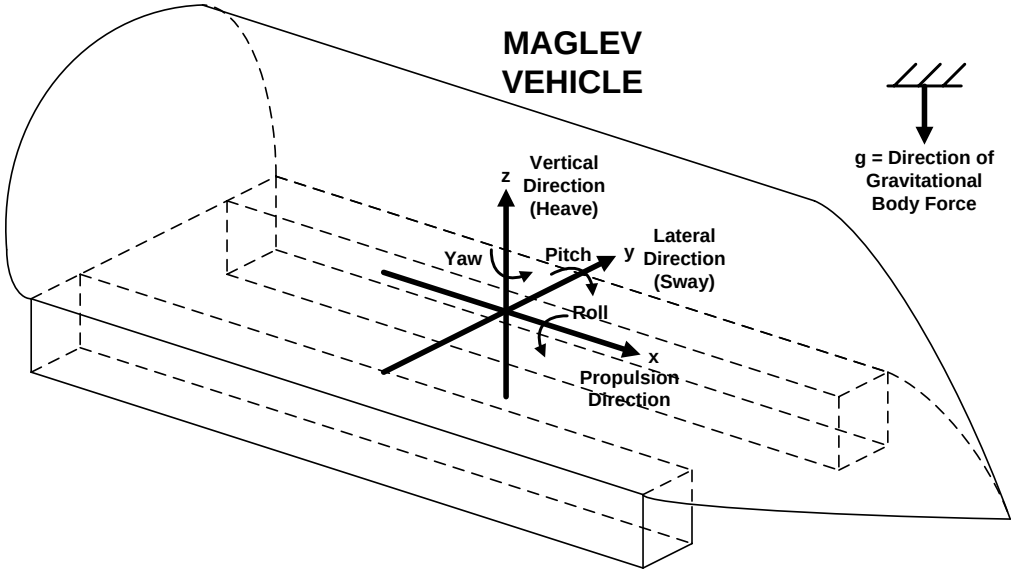

Figure 2.3-1: The Maglev Vehicle's 6 D.O.F.

Intra Phase Methodology Specifics

This intra phase methodology embodying this multiple phase approach as outlined in Figure 2.3-2 is based on understanding the complexity of the final system model. Therefore the final damping solution for the six D.O.F., E.D.S. maglev system is broken into separate models. This research paper takes advantage of this hierarchal approach by organizing these models into distinct chapter sections of increasing complexity. Each model type or set of chapters sections is then termed a particular research phase. Note that in Figure 2.3-2 the particulars of each phase is provided by

the bullet points within the boxes whereas the bullet points next to the phase boxes indicates the level of effort performed on each phase in this research paper.

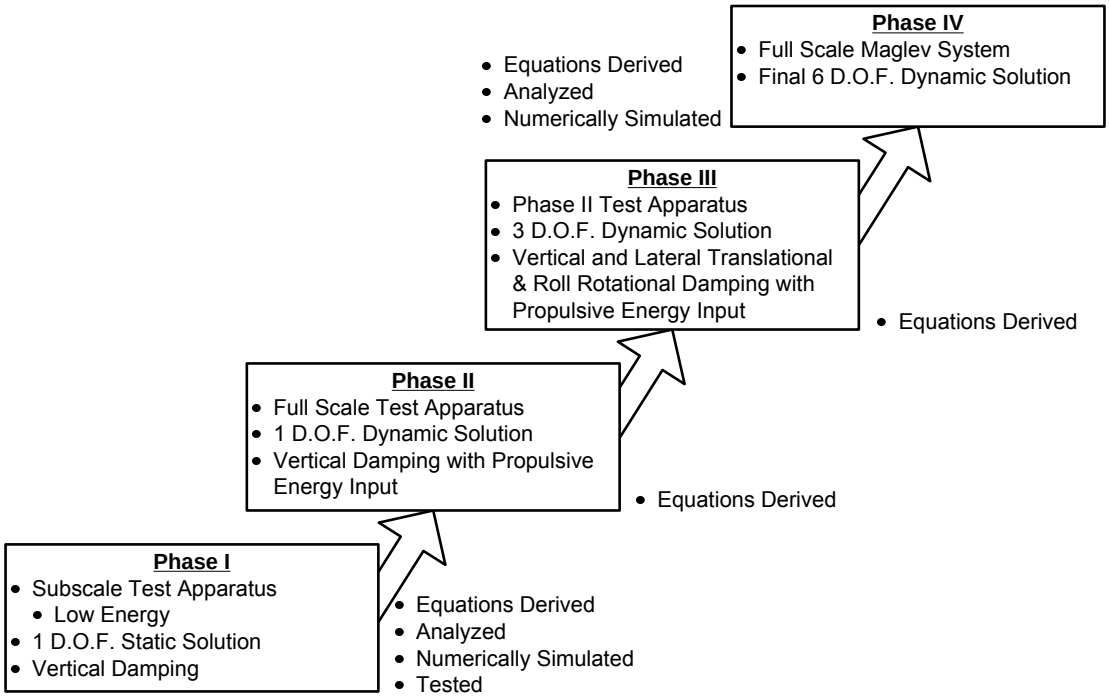

Figure 2.3-2: Intra Phase Methodology

Phase I is used to determine basic control hardware and algorithm capabilities to be implemented in Phase IV. Phase II and III are only used to help develop a final Phase IV prototype by outlining a logical succession of prototype systems. Since this research paper is meant for theoretical proof of concept purposes only, the governing equations behind Phases II and III are determined to help facilitate a final system solution, but their simulation analysis or test is not required for this proof of concept determination and hence is not performed.

As stated at the end of Chapter 2.2, only the Phase I test apparatus is developed and used for actual testing. This setup provides a minimum of empirical data necessary to assist in this proof of concept feasibility study. Phase II through IV test apparatus are only proposed systems.

2.3.b Phase I Goals

Phase I provides a static, single D.O.F., E.D.S. maglev system. This is the most rudimentary system allowable. This system provides basic E.D.S. system modeling and control proof of concept before introducing mode coupling or dynamic motion. Phase I is subscale compared to a full maglev suspension system size. A subscale prototype allows monitoring of the initial governing equations and honing of the nonlinear control system while maintaining proper system parameters prior to incorporating a more expensive, more unwieldy, and larger energy system into the analysis.

2.3.c Phase II Goals

Phase II builds on Phase I by simply introducing a full scale, dynamic single D.O.F., E.D.S. maglev system where the propulsive vehicle energy is dynamically coupled to and can feed the vertical oscillation component energy. This common maglev suspension system phenomenon provides the next level of complexity, full scale dynamic motion interaction, while still isolating multiple D.O.F. and hence mode coupling.

Phase II and III analysis is modeled around the General Atomics rotating wheel test facility as pictured in Figure 4.3-1, Figure 4.3-2 and Figure 4.4-1. This facility provides an almost optimum test bed for these logical steps in testing and analysis. The rotary wheel motor is assumed to be properly and smoothly controlled through a separate control scheme.

2.3.d Phase III Goals

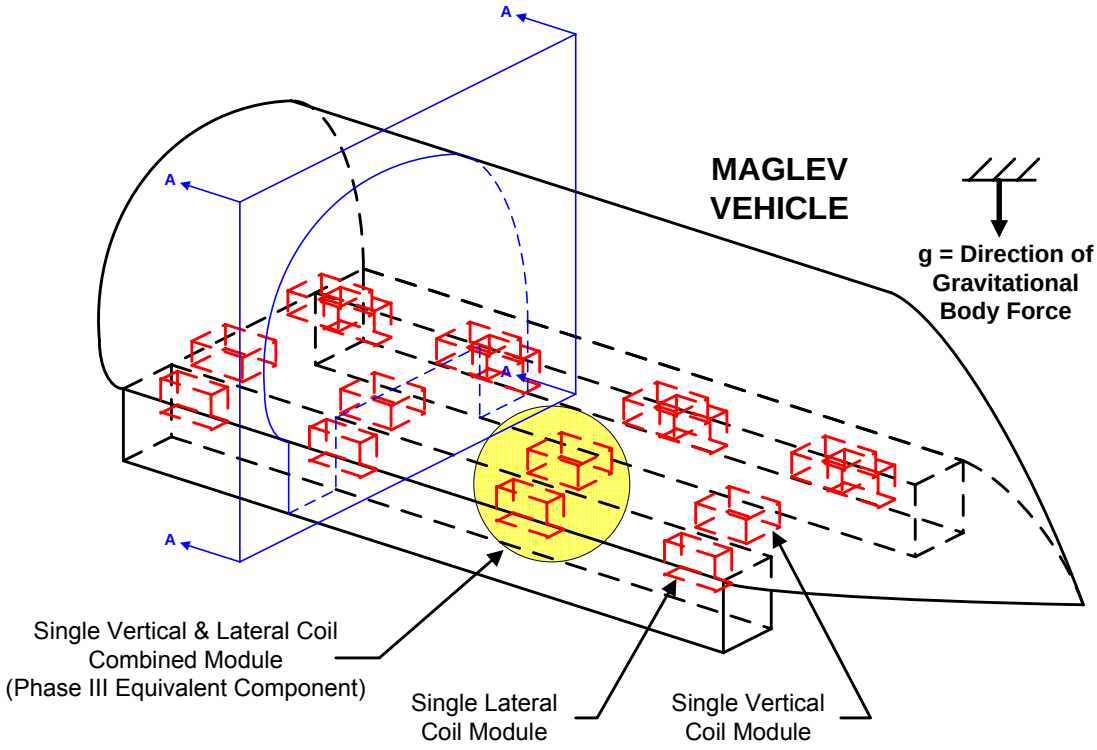

Figure 2.3-3: E.D.S. Maglev Vehicle with Vertical & Lateral Coil Modules

Phase III introduces multiple D.O.F. into the full scale, dynamic E.D.S. maglev system equation. Uncoupled, multiple D.O.F. individually provide no extra data beyond the previous Phase I and Phase II work. Therefore Phase III introduces coupling between multiple D.O.F. Phase III goes one step further by looking into Phase IV work. Phase IV provides a six D.O.F. vehicle with certain D.O.F. dependencies. The actual E.D.S. maglev system modeled in Phase IV is chosen for

ease of modeling and control by providing these multiple discernable maglev suspension modules. Each Phase III module is a combined lateral and vertical control coil set for Phase IV's final E.D.S. maglev system as shown in Figure 2.3-3.

Phase III therefore intends to model one of these Phase IV modules as a three D.O.F. individual entity. In reality Phase III simulates a single linear D.O.F. of the six D.O.F. vehicle lateral guidance coil spring constants, a single linear D.O.F. of the six D.O.F. vehicle levitation coil spring constants, and the full Phase III linear and rotational three D.O.F. control coil spring constants.

A more accurate partial Phase IV, six D.O.F. model would occur if Phase III simulated the full three D.O.F. in both the vehicle and control systems. Unfortunately the current General Atomics rotating wheel mechanical layout used as a basis for this analysis limits any vehicle representation to two linear translational components. This limitation downsizes the control coils, particularly the lateral control coil, and affects the model simulation and control system, but controlling the Phase III coupled three D.O.F. still assists in understanding and designing the final Phase IV control system.

2.3.e Phase IV Goals

Phase IV is the final six D.O.F., E.D.S. maglev vehicle model as shown in Figure 2.3-1 and Figure 2.3-3. The General Atomics low speed maglev test vehicle chassis, pictured in Figure 4.5-1 and Figure 4.5-2, is chosen as the basis for the Phase IV test bed discussion. This test bed allows testing on an actual, full scale maglev vehicle. As mentioned in the previous paragraph, this model is chosen for ease of modeling hierarchy throughout the Phase I to Phase IV process. As shown in Figure 2.3-4, the suspension coils are assumed to be on the maglev vehicle. The guideway is assumed to consist of passive rails that interact with the maglev vehicle's suspension coils. The guideway also provides propulsion through a linear synchronous motor, L.S.M. The L.S.M. or its' interaction with the vehicle is not depicted in Figure 2.3-4. In actuality this research paper only controls five D.O.F. since the L.S.M. propulsion control is not taken directly into account and assumed properly and smoothly

controlled through a separate L.S.M. control scheme. Therefore any perturbations in the L.S.M. are not directly controlled here. Although the vertical gap distance of an E.D.S. maglev vehicle is propulsive velocity dependent and hence propulsive thrust dependent. This system still controls any adverse effect the propulsive motor may have on the vertical and lateral controls. Therefore although the control scheme produced here only truly controls five D.O.F., this control scheme does control any energy introduced into the controlled five D.O.F. through the vehicle's six D.O.F.

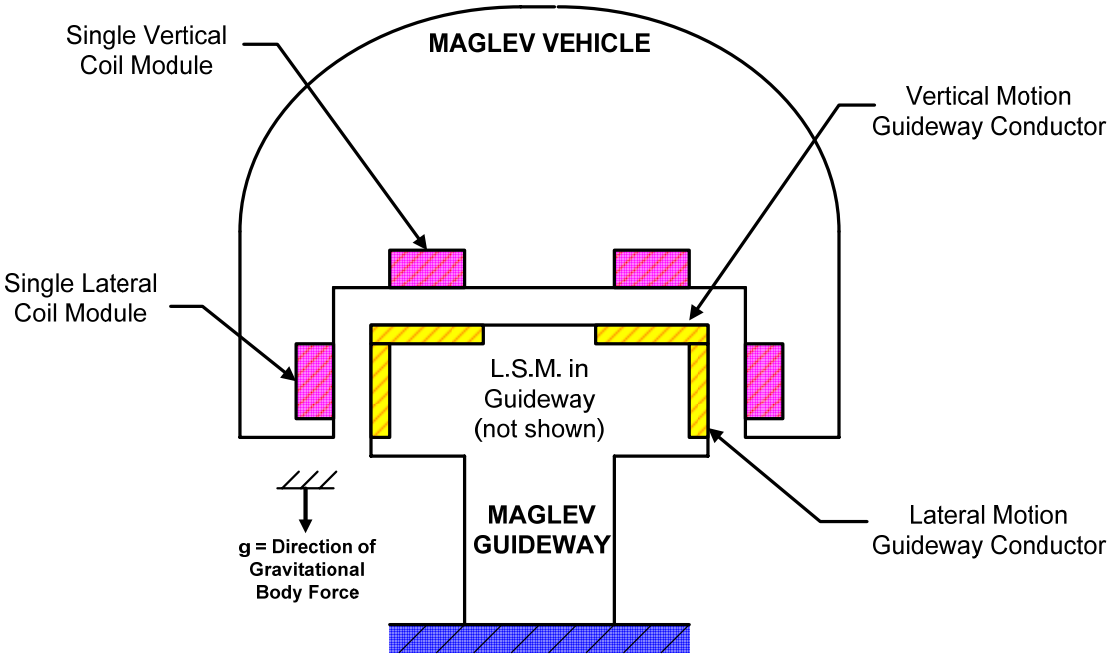

Figure 2.3-4: Maglev Train X-Section View (Section A-A of Figure 2.3-3)

2.4 CONTROL SYSTEM HARDWARE

Since the introduced electromagnetic control hardware must respond to mechanical mode and transient vibrations at an appreciably higher electrical frequency, they cannot contain large amounts of stored energy. Stored energy hinders their required response time. Therefore the maglev system's principal levitation, guidance, and propulsions system is separate from the control system as Chapter 1.1.b.iii suggests. A system of control solenoid coils is chosen for control hardware.

This choice is based on the simplistic nature of solenoids. A solenoid is an unsophisticated system that attains a reasonably high energy density output. Here the energy density refers to the energy per unit volume of the entire solenoid body, but in all future discussions in this paper the energy density is defined as the energy in an air gap height between a primary and secondary under consideration.

Referring to the most power and energy demanding air gap from an introduced control coil standpoint, a larger vertical coordinate axis principal levitation gap requires a higher levitation energy density within the gap. A corresponding vertical control coil system would likewise require more energy density to effectively operate across this higher levitation gap distance, although the control coil does not require nearly as much energy density as the principal levitation system. Therefore from a vibration control standpoint a smaller levitation gap is desired. This vertical principle levitation system must maintain enough energy storage and delivered power to preserve an ideally steady state levitation air gap distance which for a large mass body requires a very large energy density across the entire air gap. Comparatively the introduced control coils only require enough operational energy storage and delivered power for the often transient case of removing the lower oscillation amplitude energy density in the air gap, although note that a more higher energy and power rated control coil may be required to remove an oscillation within a set period or at a high frequency rate and hence the control system transient power requirements may be excessive due to a high oscillation amplitude or frequency. Figure 2.4-1 shows a direct comparison of these energy density requirements. The principle levitation air gap height is much greater than the controller's oscillation amplitude height. This directly translates to a principal levitation energy density much greater than the required control system energy density. The lower control system energy density permits a control system with a lower hardware energy rating and a higher operational frequency or transient time than the principal levitation system. This salient fact is the main reason a control system separate from the principal levitation or any other principal electromagnetic vehicle guidance system is able to control the

electromagnetic principle levitation or guidance system. The required control system force in Chapter 3.2.b is based on this principle.

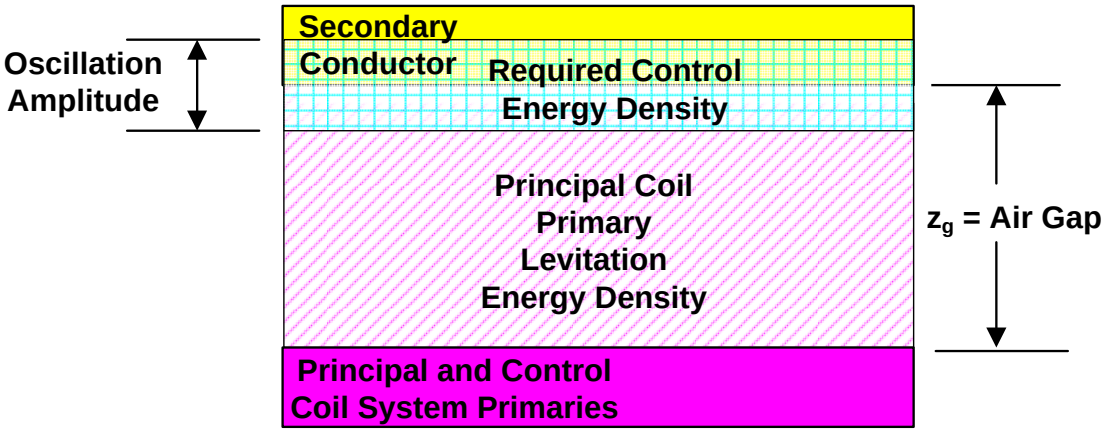

Figure 2.4-1: Air Gap Energy Densities

Equation (2.1) provides the general form of the energy gap concept. The potential energy is U, the lift force is F, the system inductance is L, the primary current is i, and the lift displacement spatial component is z.

$$\frac{dU}{dz} = F = \frac{\Delta\left(\frac{1}{2}Li^2\right)}{\Delta z} \tag{2.1}$$

There is also a possible magnetic coupling concern which may adversely affect the operation of the control coils. Chapter 4.1 details experiments where the control coils are both magnetically coupled and partially magnetically isolated from the principal coils. These experiments determine if the final system requires control coil magnetic isolation.

2.5 SYSTEM MODELING

2.5.a Overall System Modeling

Analytical closed form exact solution methods, numerical integration methods, and computational solution gradient methods are three of the most basic

virtual modeling environments available today. It is typically desired to create models across these various environments. This allows a reasonably inexpensive comparison of one model type relative to another before necessitating tests of actual system prototypes. Analytical solutions often provide a rough but quick estimate of a final solution through various approximations as well as provide inputs for a numerical or computational study. Numerical solutions are often implemented in the form of state space equations and accompanying simulations when no analytical closed form exact solution presents itself. Computational solutions, the most accurate of these methods but also the most computationally time consuming, are often used to verify and hone the less accurate analytical and numerical solution as well as provide stand alone solutions. Computational solutions are seldom used to completely model a complex system simulation due to their excessive computational time requirement, but instead focus on pieces of the total simulation fixed for a particular system configuration. The growth of computing power should eventually allow computational solutions or equivalent to dominate the analysis environment, but to date system dynamics and control are routinely cumbersome when run through a computational solution. When analytical, numerical, and computational tools are working properly, development of a reasonable laboratory prototype system initiates. This prototype allows comparisons between the virtual computer models and real world empirical data. Such comparisons allow for final simulation adjustments and error determination between the models and real world prior to designing and building the final system.

The complete electromechanical system in this research paper is analytically and numerically modeled whereas only part of the electromechanical system is computationally modeled. The analytical effort comprises linear and nonlinear closed form analytic equation solutions. Numerical integration techniques then simulate desired indeterminate variables within the closed form analytic solutions. Whenever applicable, computational models verify and hone the closed form analytic and numerical solution accuracies. The solenoid design of Chapter 3.2.b describes an example of this process.

The overall model that describes the complete system with all components is coined the system model. The system subcomponents such as the maglev magnetics model, the maglev mechanical model, the controls model, and the controls power model are all coined the subsystem component design models as indicated in Figure 2.5-1. A strong bond exists between the control subsystem model and all other subsystem models. The maglev subsystem, maglev mechanical subsystem, and electrical subsystem models form the plant of the control subsystem. Ideally this simulated plant and the real prototype plant components are completely interchangeable. Therefore control subsystem development occurs in situ with all other subsystem model development.

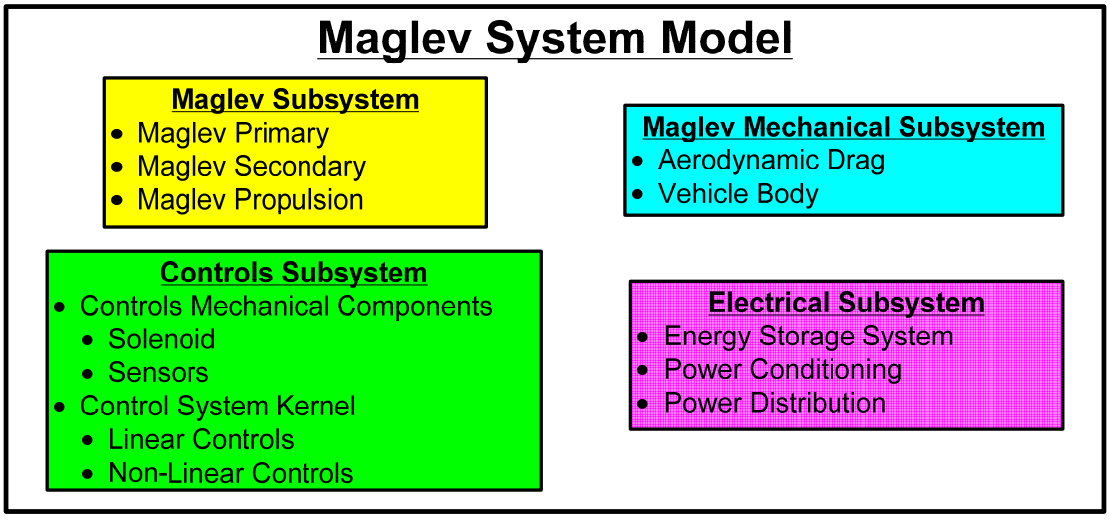

Figure 2.5-1: Maglev System Model Structure

2.5.b Modeling Implementation

The analytically based model is developed within Mathsoft's Mathcad® software environment. This environment is used to size the principal and control solenoid coils and provide a closed form solution to approximate the solenoid geometric, electrical, magnetic, thermal, and mechanical output values.

Numerical solutions are simulated within the Mathworks' Matlab® and Simulink® software platforms. These platforms are used to simulate the system model plant and controller for each phase analyzed. The Matlab® and Simulink® code numerical integration routines developed assist in simulation effectiveness by make full use of the computer's C.P.U., central processing unit, efficiency over computer hard drive or random access memory for solving the extensive simulation computations. In Phases II, III, & IV these software platforms are also configured to communicate with and control real world test devices through real time environment dedicated computer C.P.U.'s and National Instruments Labview™ software.

The computational solutions provide a means of ascertaining the validity and accuracy of the closed form analytic and numerical solutions by comparing the output trend plots from analytical and numerical technique solutions to the more accurate computational technique solution. This research only uses third party purchased and available computational modeling packages for the computational electromagnetic and thermal models, instead of developing the solutions as in every other software package mentioned. The Ansys® and Vector Fields Inc. Opera™ software packages are both used to verify the electromagnetic system magnetic energy, which indirectly provides system inductance, and force outputs. The Ansys® model is only used to support the main outputs provided by Opera™ model.

2.6 CONTROL THEORY

2.6.a Overall Controls

2.6.a.i Overall Control Theory

The control solution is divided into time domain state space linear and soft computing methods nonlinear control schemes. Both modern control methods employ closed loop vector control as indicated in Figure 2.6-1. In vector control the vector indicates instantaneous values of the system. The control algorithm then manipulates this space vector either directly or through observable parameters which feed a comparator. Observation is the estimation of directly immeasurable state variables.

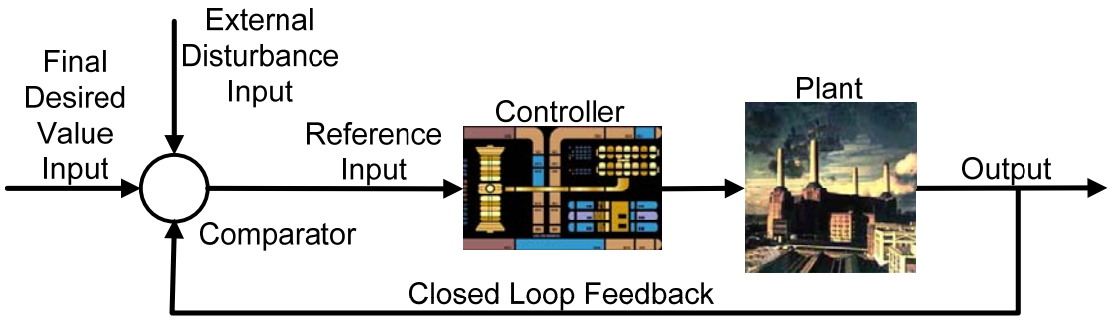

Figure 2.6-1: Basic Closed Loop Control Schematic

Phase I and II are nonlinear single D.O.F. systems. Geometrically these nonlinearities stem from the vertical position, vertical velocity, and horizontal propulsive velocity dependence of the magnetic spring constants as well as the repulsive only force condition of these spring constants. All phases also experience material nonlinearities through the primary iron cores of both the principal and control solenoids until complete magnetic saturation occurs. An easily developed linear control method initially attempts to control these Phase I and II systems. Use of linear controls provides an understanding for the level of nonlinearities experienced within these basic systems. A nonlinear soft computing control method is then employed and tested against the linear control method. Phase I and II nonlinear

control system testing provides a foundation for controlling the more complex Phase III and IV nonlinear, coupled D.O.F. systems. Phase III and IV systems not only witness the same nonlinearities experienced in Phase I and II systems, but also experience a strong coupling between these nonlinearities as well as the coupling between the added D.O.F. Only nonlinear soft computing control methods are employed in these later phases.

Phase IV control requirements drive the type of nonlinear control system developed. Nonlinear optimal controls methods such as the Lyapunov nonlinear control were considered in place of soft computing controls methods, but are not employed due to their dependence on a hard computing fixed performance index. Although Lyapunov nonlinear control methods can adequately stabilize and control Phase I and II systems, they are not considered sufficient for the wide range of coupled nonlinear parameter values expected by the Phase III and IV systems. Future work could consider utilizing Lyapunov's second method for stability analysis which is discussed in [13] and [25], but this method is not employed in this research paper. Phases III and IV are nonlinear, stochastic systems where parameters vary in an unpredictable fashion, witness large variations, or witness rapid variations. This leads to a goal driven soft computing control scheme capable of dealing with large nonlinear uncertainties by continuously measuring control parameters and adapting their compensation to this measurement. This requirement defines a nonlinear soft computing control system. Therefore soft computing optimal fuzzy control methods, which provide nonlinear optimal control for a wide range of potential system disturbances, are initially incorporated as the control system used in this research paper. Soft computing adaptive control methods, which adapt the control parameters for a changing environment instead of relying on a fixed optimization index, is mentioned as a potential upgrade for final Phase IV implementation. This upgrade would modify the fuzzy logic controller into a hybrid neuro-fuzzy controller. The neuro-fuzzy control algorithm then adapts the control space vector gains through a neural network learning process via the closed loop feedback system. A myriad of

references, [2], [4], [6], [9], [15], [18], and [25], were researched to understand and achieve the proper implementation of fuzzy logic, neural networks, and neuro-fuzzy control soft computing methods for this research paper.

2.6.a.ii Overall Control Implementation

Control Software Implemented

Both control schemes are operated on a Microsoft Windows® operating system, personal computer platform inside of the Matlab® and Labview™ software platforms. The National Instruments Simulation Interface Toolkit software provides an interface between Matlab® Real Time Workshop running inside of Simulink® and National Instruments Labview™ software platforms. This two software platform execution is intended to minimize overall system cost while maintaining system flexibility.

The Simulink® software forms the controller's mathematical kernel. Simulink® runs inside the Labview™ software environment as a subroutine via Labview™ call functions. Note that Labview™ also runs various control and coding routines inside of the Labview™ compiler. This research paper opts to use a single computer code for both analysis and control with minimal modifications between analysis and control algorithms. Simulink® performs these desired analysis and control functions. Labview™ allows a simplistic yet powerful graphical controller interface platform which forms the controller's data acquisition, control input, and control output.

Non-Deterministic Processing & Time Constants

When considering data accuracy and system controllability, the control scheme must consider all system time constants. Personal computer processes operating inside of the Microsoft Windows® operating system are non-deterministic. In the control scheme's case this means a control process is not necessarily operating

in real time but may be interrupted by an unpredictable operating system background operation before resuming software performance. Therefore a dedicated control and D.A.Q. real time computer processor is required for Phase II through IV, but a non-dedicated processor will suffice for the simplistic and low energy Phase I system test.

Scrutiny of the control system used indicates that the most probable controller time bottlenecks are the computer control process time and the control solenoid time constant. The computer control process time indicates the time required for the computer control system to run through a single control process cycle. The control solenoid time constant indicates the minimum time required to change the current value in a fully energized control solenoid. Experience dictates that a worse case computer control process time is around a 500 Hz minimum. This translates into a 2 milli second time constant. Initial rough inductance over resistance calculations for the expected Phase I control single coil hardware sized with 2289 turns, 1.6 inch inside diameter, 1.6 inch height, and a 30 gage wire produces a maximum 7.6 milli second time constant value. Therefore the expected absolute minimum computer control process time operates just under the maximum control solenoid time constant. The conclusion is that the relatively frugal, non-deterministic control scheme used here is considered just adequate for this research, but aliasing effects may present themselves in the final test data. This system is not adequate for commercial applications. In such cases the controllers would require a more robust real time dedicated processor computer configuration.

The D.A.Q. hardware itself operates at sweep rate across all channels at 500,000 samples per second or 500 kHz which is not an issue in comparison to the computer processor time.

The National Instruments Labview™ software incorporates tools for determining computing real time computer process times. In this research paper Labview™ is coded to embed these times in the empirical data. The empirical data also provides information that provides the control solenoid's instantaneous time

constant as well as the maximum solenoid time constant. Chapter 4.1 uses these tools for the Phase I test apparatus. Chapter 5.2.e test results provide a more accurate assessment of the final test system time constants and test limitations realized.

2.6.b Linear State Space Control

Maglev linear control schemes are commonly unstable. Velocity dependent damping is introduced into the linear state space control system via linear pole placement techniques. This feedback control system depends on mechanical equations of motion and hence is a servo system. This desired pole placement control method may be used for damping when a system is completely state controllable. The basic proportional differential, P.D., controller for servo systems does not improve the system control type. Therefore P.D. control is only useful for regulator systems that do not track inputs. Kuo [12] discusses how most control systems, including the control system used in this research paper, must track inputs. Integral control allows input tracking. This leads to proportional integral differential, P.I.D., control. This scheme compares real parameters with theoretical variables computed from the assumed analytical model of the system. The differences between the real and theoretical values are then minimized through a comparator by adjusting the parameter estimates to provide an estimated output control value. P.I.D. control can also be adapted for approximating nonlinear systems, but here it is a uniquely linear control methodology and hence only uses the linear closed form analytic equations. The main drawbacks to this method are the need for proper initial selection of gain coefficients and the non-optimal dynamic response to instantaneous system changes. This dynamic response drawback stems from the P.D. control portion saturating the control signal during sudden input transients. I.-P.D., integral proportional derivative, control solves this problem as discussed in Ogata [19] by separating the integral and P.D. control portions of P.I.D. control. The result is an I.-P.D. controller that can handle sudden transients but responds slower than a corresponding P.I.D. controller.

Since sudden transients are expected in this system the I.-P.D. controller is chosen as the preferred linear system controller.

2.6.c Soft Computing Nonlinear Control

Nonlinear Control Problem

Active suspensions require precise control systems to be effective. Typical linear, piecewise linear, and nonlinear state space control systems require accurate knowledge of vehicle behavior to be precise. Predicting such knowledge is often unfeasible in a complex dynamic system such as a nonlinear six D.O.F., E.D.S. maglev vehicle in operation due to unpredictable vehicle behavior and unpredictable external perturbations. Therefore a maglev vehicle controller is required to operate without explicit system functional relations, identify vehicle behavior in real time, and continuously modify the control parameters and/or the control algorithm to obtain and maintain optimal operating conditions.

Soft computing methods are chosen to solve this problem. Fuzzy logic, neural networks, and genetic algorithms may be considered the principal constituents of soft computing. Each method provides a different tact in solving a problem and these various methods can be combined to assist in solving particular solutions. These soft computing methods, which provide the foundation for the emerging field of conceptual intelligence, are tolerant of imprecision which differs from conventional hard computing methods. Uncertainties and approximations are naturally embedded into any real world problem. Hence an ideal solution to a real world problem would seamlessly incorporate these uncertainties and approximations. Soft computing methods exploit the imprecise nature of reality to achieve a more robust and tractable system through a smooth transitioning gain scheduler in comparison to hard computing methods which incorporate no true variance for the imprecise nature of reality.

Soft Computing Optimal Control

This research paper is concerned with the feasibility study of performing magnetic air gap damping on proof of concept simulations. Therefore a reasonable set of extreme but known system disturbances are applied to the dynamic simulations and their respective controllers to solve this feasibility problem. Such knowledge of external perturbations allows the use of soft computing optimal control as the main nonlinear controller implemented in this paper. Prototype factory acceptance test beds are recommended to start with this type of nonlinear control before adding future adaptive control complexities which build on the optimal control foundation.

Fuzzy controllers are a form of soft computing optimal controllers which provide an acceptable output parameter solution within a reasonable time frame by defining acceptable input parameter ranges, assigning degrees and mapping the input to output values through fuzzy inference techniques which effectively provide a smooth control gain transition for the range of inputs, and then monitoring the performance of the output parameters through a gradient vector during the real time control process. The heart of fuzzy logic is fuzzy inference which involves membership functions, fuzzy logic operators, and if-then rules. Much of the power of fuzzy control comes from allowing the fuzzy if-then rules to be performed via a set of intuitive linguistic approximation values in what is called the calculus of fuzzy rules and multivalued logic instead of set discrete numerical values and bivalent “yes-no” logic. In all complex control applications the bivalent rule set must be larger than the fuzzy rule set to attain equivalent system performance to the fuzzy rule set for a known extreme disturbance. Another bivalent rule set shortcoming is the inability to adapt for unexpected perturbations. Even though a fuzzy control system is an optimal system which therefore is set to optimize the control output for known disturbances. The fuzzy controller readily handles many severe and unexpected perturbations with just a relatively small rule set. Such performance is witnessed in results output of Chapter 5.2 for Phase I and Chapter 5.3 for Phase IV.

As with most control methods the three main objectives of fuzzy control as listed in Trzynadlowski [22] are minimizing the control errors, limiting system variables to allowable ranges, and avoiding unnecessary action if the control errors remain within predefined tolerance bands. This paper primarily incorporates fuzzy control to limit the control action to an acceptable bandwidth of values instead of discrete control action values thereby lessening the overall control system operational requirements.

Soft Computing Adaptive Control

A final operational maglev system, the final goal of this research paper, is concerned with performing magnetic air gap damping during real life operations. The set of all large system disturbances experienced by a maglev vehicle are never fully known, but a reasonable set can be determined. Identifying nondeterministic vehicle behavior in real time and using this information to continually optimize the control system avoids these shortcomings of imprecise system state knowledge. This requirement defines soft computing adaptive controls, nicknamed universal approximators as defined in [18], as the main nonlinear controller implemented in the field or at least used to determine the proper set of optimal control rules and associated gains. All proposed full scale test apparatus are recommended to initially implement optimal control for system feasibility studies, but full scale test apparatus and the final operational maglev system are recommended to eventually build upon the optimal controller developed and implement an adaptive nonlinear control that has undergone extensive training cycles. This adaptive controller then is either retained as the final maglev vehicle system control kernel or the optimal control particulars learned from the adaptive controller training cycles are placed into a final optimal control scheme which is then used for the final maglev vehicle system control kernel.

Neural networks and fuzzy logic are two powerful soft computing control methods that have the ability to approximate functions such as system dynamics with

external disturbances in real time. This leads to the neuro-fuzzy adaptive control hybrid which developed to combine the power of neural networks and fuzzy logic into one control algorithm. In this control algorithm the neural network learns information about the control and system response data sets in the form of training before and during implementation into the control kernel. The control algorithm then uses this information to compute optimal fuzzy logic membership function parameters for the tested data sets. These dynamic membership function parameters then provide an adaptation of control gains and sometimes even rules to achieve the needed dynamically varying optimal control to compensate for the dynamically varying environment. The combination of neural networks and fuzzy logic allows nonlinear, adaptive control while maintaining a reasonable time for each control operation when implemented on a final operational system.

Neural networks, the added adaptive component of the controller, incorporate training and real time monitoring functions for maintaining optimum control parameters through various learning methods. Fausett [1] describes neural nets as mathematical models of information processing that use two modules, an emulator and a controller, when integrated into control systems. Through a training process the emulator learns to simulate a system for a variety of conditions. The controller learns to control the trained emulator and over time optimize this control for a particular set of conditions. The power of neural networks lies in the algorithm's ability to adjust control parameters in real time without the need for a complete system mathematical model.

The neuro-fuzzy adaptive control recommended in this research paper is a direct parameter adaptive approach. This type of machine intelligence control intimately combines neural network principles with fuzzy logic principles. The Takagi-Sugeno-Kang or Sugeno method of fuzzy inference, the fuzzy component method recommended in this paper for neuro-fuzzy adaptive control, is well suited for adaptive techniques and constructing fuzzy models where the membership functions are tuned using a back propagation algorithm in combination with a least

squares method to control the system dynamics and hence learn from the system data. This recommended Sugeno type inference method maps the inputs to outputs by fuzzifying the inputs, applying the membership functions, and then defuzzifying the outputs through a singleton technique. An important component of any fuzzy process is the final defuzzification method. This singleton technique uses a computationally efficient linear or constant output which is amenable to nonlinear input to output systems to achieve the final solution. This scheme uses real parameters to directly estimate the output control value and readily handles linear or nonlinear controls.

Although adaptive control techniques are performed during the system analysis, they are not required for achieving the desired performance for the system types analyzed. This is because the main focus of the simulations performed was achieving acceptable system performance for a low powered control system relative to the power of the principal system. Since the control system in the simulations is so low in power the optimal control of full power to the control coils during the majority of the magnetic damping stroke for every perturbation type was simple to achieve. In this case only the damping of small secondary oscillations benefits from adaptive control algorithms. The other simulation focus of provide a control solenoid on the same order of power as the principal solenoid, as well as any control scheme that doesn't require full control solenoid power for the majority of the magnetic damping control stroke, could benefit from adaptive control, but this level of detail requires final design damping requirements which is not necessary for this proof of concept paper. Therefore neuro-fuzzy adaptive control techniques are only discussed but are not presented in this paper.

2.7 FABRICATION AND TESTING

Prototype testing permits real life verification of all computer models, control schemes, and governing system laws. Prototype empirical data directs final computer models, controller optimization and final system design efforts.

Fabrication and testing of Phase I occurs entirely at the author's home laboratory as described in Chapter 4.1. This includes a manual winding machine design and fabrication for building solenoid coils, solenoid coil design and fabrication, test apparatus design and fabrication, test software design and implementation, and complete testing program. Phase II, III, and IV proposed testing descriptions are based on modified test apparatus in the author's workplace as described in Chapter 4.3 for Phase II, Chapter 4.4 for Phase III, and Chapter 4.5 for Phase IV. Each test apparatus maintains simplicity to lower test cost and complexity.

The National Instruments Labview™ software and associated hardware discussed in Chapter 2.6.a.ii operates as a D.A.Q., data acquisition system, to acquire all test data while operating the controller through various sensors. This research paper requires implementation of a variety of sensors. Phase I directly senses the vertical heave acceleration via an accelerometer. Phase II senses vertical heave position via a Linear Variable Differential Transformer, L.V.D.T., which is a linear potentiometer or linear encoder. Acceleration and velocity are easily deduced from this device when an appropriately fine encoder grid and quadrature sensing method is employed. The vertical acceleration is also sensed with an accelerometer. Phase III use the same sensors as Phase II with a second accelerometer placed for lateral acceleration. The angular roll acceleration is calculated through the two existing linear accelerometers and known geometry. Phase IV senses all six D.O.F. through a suite of sensors already designated for normal service on this vehicle. All phases require voltage and current measurement for all principal and control coils used.

CHAPTER 3 ANALYSIS & CONTROL ALGORITHM DERIVATION

3.1 OVERALL SYSTEM SOLUTION

3.1.a Solution Outline

All modeling and control algorithms derived in Chapter 3 are modeled in the appendices, the salient results are presented in Chapter 5, and final conclusions are presented in Chapter 6.

3.1.b Linear Variable Definitions

In the subsequent force equation derivation and equations of motion for Phases I through IV it is important to understand the subtle differences behind the linear variables used. The variable z has the most variety and hence is chosen for the majority of this discussion. Throughout this paper multiple figures indicate the coordinate axis with x, y, and z components. These x, y, and z parameters indicate the right handed Cartesian coordinate zero reference axis position and positive direction of each axis. Here the coordinate axis parameters are interchangeable with their respective unit vector values $\hat{a}_x$, $\hat{a}_y$, and $\hat{a}_z$. These x, y, and z parameters also provide the scale of Cartesian coordinate axis distance values from zero onwards. For the equations of motion but not the force equation derivation, y, and z parameters provide the purely linear gap motion from a set initial condition to the next time stepped value as per the following z based equation. Here the $\sum f_z(angle)$ component provides the sum of linear z displacements for all angular rotations.

$$z_g = \left\{ z_{g\_init} + \left[z + \sum f_z(angle) \right] \right\} = \left[\left(\text{Initial } z_{gap} \right) + \left(z_{gap} \text{ Time Step Motion} \right) \right] =$$
$$= \left(z_{g\_init} + z_\Delta \right)$$

In Phases I and II there is no angular motion and hence $z_\Delta = z$. In Phases III and IV angular motions are present and hence sometimes $z_\Delta = z + \sum f_z(angle)$. The

linear displacement of the angular motions is noted as “sometimes” since the linear gap distance values may not be the same for all parts of the same equation. Examples are seen in the potential energy derivation terms of Phase III, equations (3.141) to (3.142), and Phase IV, equations (3.163) and (3.164). One must therefore determine each component of a particular equation and decide how this linear gap distance term is defined. These notions are extremely important when using the derived force equations as part of the equations of motion.

The gap distance variances presented above is not witnessed in any linear or angular rate parameters thanks to the simple fact of constants equaling zero in any rate derivation.

3.2 OVERALL PLANT ANALYSIS

3.2.a Control Solenoid Plant Representation

The plant dynamics equations of all four phases include plant and control coil components. The control solenoid is controlled via an observed velocity feedback to produce the desired damping effect. Even with velocity control, the solenoid force is electromagnetic in nature and hence a distance dependent mechanism which must be reflected as such in the plant derivation.

3.2.b Control Solenoid Design

3.2.b.i Overall Solenoid Design

Initial solenoid design steps provide a physical design and simulation spring constants. Every solenoid design conforms to a trade study. At the top level of this trade study the solenoid design must balance between solenoid geometry versus system time constants, thermal limitations, source current limitations, and maximum magnetic force obtainable for a particular geometry and source current.

The principal levitation solenoid of Phase I and the control solenoids of all four Phases follow a similar design path. Solenoid design forcing functions are

determined analytically and verified and honed computationally as described in Chapter 2.5.a. An initial first order analytical model provides an initial solenoid design and indicates design parameter trends. The solenoid design equations throughout every design phase, including Phase I which is a static only case, are chosen to capture both the transformer and motional eddy current effects witnessed in Phase II, III, and IV dynamic systems. This initial approximation identifies design areas requiring more modeling accuracy, allows optimization from parameterization studies, provides a basis for state space numerical simulations, and provides input for computational design runs. Figure 3.2-1 shows the expected secondary trends for an E.D.S. system experiencing relative motion between the primary and secondary systems. The motion itself may be mechanical or electrical in nature as long as the secondary conductor moves relative to the primary magnetic flux density source. A computational model then tests and hones the solenoid design parameters. The analytical solenoid design is modified to properly approximate the computational design outputs. This analytical model modification takes the form of either updating the base analytical equations or incorporated into the analytical model interpolated computational model parameter trends. The numerical state equation system simulation is based on the final analytical system model.

The magnetic flux density tangential, B_T, and normal, B_N, primary and secondary resultant components from the magnetic interaction between the primary and secondary provide the secondary forces. The resultant B_N provides the initial induced current for all secondary forces, the secondary shear force which translate to a side propulsive or axial centering force depending on the system geometry, and if a ferrous material or properly aligned permanent magnet resides on the secondary it provides a secondary attractive force. The resultant B_T provides the secondary repulsive or lift force depending on the system geometry. As the resultant $\vec{B}$ on the secondary surface approaches a dominant B_T component, which indicates a maximum secondary current is produced, this resultant $\vec{B}$ approaches complete

expulsion from the secondary and the secondary magnetic pressure and hence the secondary repulsive levitation is maximized. Referring to Figure 3.2-1, this case is approached as the relative motion between the primary and secondary is maximized. This is the obviously the preferred case in this solenoid repulsive system.

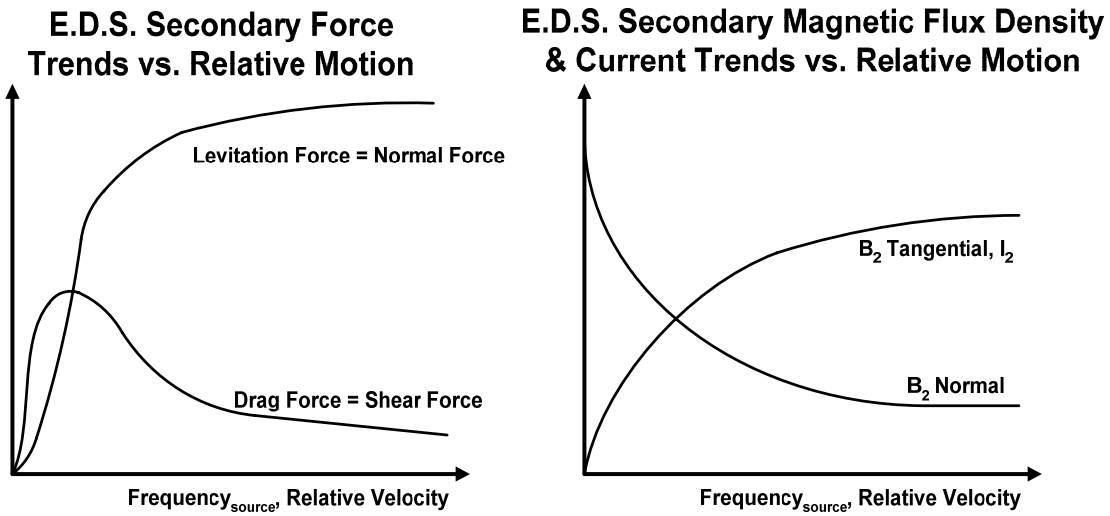

Figure 3.2-1: Expected E.D.S. Secondary Trends

The control force requirements produce the initial inputs for the solenoid design equations of Chapter 3.3.a.i. All solenoid analyses assume a specified input voltage and solve for the output force. This output force is then compared with the required control force, or perturbation force the control system is required to control as described in Chapter 2.4. The solenoid design parameters are listed in Table 3.2-1.

Table 3.2-1: Solenoid Design Parameters

Parameter Type	Parameter Name	Parameter Description
Ranged Parameters	r_2	Secondary Radius
	z_g	Total Linear Gap Distance
Primary Point Parameters	N_{turns}	Number of Solenoid Turns
	r_{2_in}	Solenoid Inner Radius

	v_{rms}	Solenoid Input Voltage (Phase I: = 120 V_{rms})
Secondary Point Parameters	ϕ_{wire}	Solenoid Wire Diameter w/o Insulation
	h_1	Solenoid Height
	h_2	Secondary Thickness (Phase I: = δ)
	freq	Solenoid Input Frequency (Phase I: = 60 Hz)

3.2.b.ii Plant Perturbation Input Force and Energy

Assuming constant plant geometric, material, and perturbation values, magnetic pressure determines input force and energy when the plant forcing function axis is magnetic. An approximate magnetic flux density at the perturbed secondary surface is found from Maxwell's magnetic stress tensor, equation (3.1).

$$\left|\vec{T}\right| = \frac{B^2}{2\mu} \tag{3.1}$$

The perturbation energy is determined from the perturbation distance and force on the secondary surface as indicated in equation (2.1).

3.2.b.iii Solenoid Magnetic Material & Mutual Inductance

The magnetic equations in this analysis also do not provide for the primary iron B-H curve in either the principal or control solenoid. Instead the magnetic flux density, B, is set with a step function to purely saturate at a constant value. Although only the real component of the B is used in physical outputs such as force and current density as briefly discussed in the magnets output area of Chapter 5.3.c.ii, this saturating value is applied to both the real and imaginary B components for numerical purposes. This magnetic saturation is only placed upon the B and not upon the inductance of each coil and thereby uncoupling the saturating magnetic flux density from the primary current. This is incorrect since in reality as the primary iron saturates the inductance will lower at that state and allow more current into the coils for a unit voltage increase compared to a unit voltage increase of an unsaturated core. Assuming no resonant capacitor, this will raise the coil temperatures as well as B in

an increasingly linear fashion with the increased current which in turn saturates the iron even more yet only providing an increasingly linear output force. This process continues with increased current until the primary iron is completely saturated and linear. This incorrect uncoupling of the saturating magnetic flux density from the primary current is acceptable for this analysis for the following two specific reasons. The first is due to the introduced series resonance capacitor used with each solenoid as discussed in Chapter 4.2.c.i. As the coil primary iron saturates the introduced resonance capacitor will no longer be in resonance with the solenoid. Therefore as the solenoid coil inductances vary the capacitor will restrict the source current and in turn the B through its' own reactive losses. The second is that for best performance it is desired to operate in a resonant capacitor to coil inductor condition with maximum B and as low a primary current per coil as possible due to thermal limitations. Therefore even though taking the saturation of the B and not coupling this value with the coil inductance provides an incorrect result, it also provides the combined effective material, geometric, and electrical operational bandwidths to avoid. Therefore the proper system operation should naturally avoid these operational bandwidth areas by designing a system that experiences only a low saturation during peak performance.

The magnetic equations in this analysis do not provide for a gap distance dependent coupling of the mutual inductance for either the principal or control solenoids. Instead the mutual inductance is set to a typical operational constant value. In reality a decreased air gap provides a lower inductance which allows a higher current into the primary through the lowered reactance. This higher current generates a higher induced repulsive Lorentz force on the secondary which provides a stiffer spring constant. In the principal coil this variable inductance effect sends the secondary farther and faster away from the primary which establishes a higher oscillation amplitude. In the control coil this variable inductance provides for a higher damping force at the smaller air gap values.

Since the purpose of this research paper is to establish whether or not damping is feasible in the magnetic air gap, these approximations will not adversely affect that

effort and are deemed acceptable. These approximations must be removed in order to properly simulate and test a final maglev system model.

3.2.b.iv Plant Natural Oscillation Values

Assume this underdamped plant is a perfect harmonic oscillator. The plant spring constant, k, is known from equation (3.2). This provides the natural frequency, ω_n, of the plant from equation (3.3). Another form of equation (3.3) is provided previously in equation (1.1).

$$k = \left(\frac{\text{Force to Levitate}}{\text{Distance Levitated}} \right) \tag{3.2}$$

$$\omega_n = \sqrt{\frac{k}{mass}} \tag{3.3}$$

3.2.b.v Control System Force and Period Values

Assume that each peak to peak oscillation removes an equal amount of energy for every stroke and throughout the half stroke for repulsion. This information provides the total control force per perturbation oscillation. Chapter 3.3.a.i equations use this total control force per perturbation oscillation to design the solenoid control coils per each phase. The final solenoid designs consider solenoid power, voltage, current, solenoid heating, and mechanical plant natural time constants versus solenoid electrical time constants.

3.2.b.vi Solenoid Heat Transfer Analysis

The solenoid heat transfer analysis is a non-rigorous analysis. Lumped parameter values are used to approximate the solenoid heating under adiabatic and then natural or free convective cooling conditions. Such values approximate whether a design is acceptable in its' current state or the system requires either re-design or active cooling.

Adiabatic Conditions

The adiabatic conditions approximate the power input of a solenoid under absolute worse case scenario starting from S.T.P., standard temperature and pressure. Heat generation is given by the following equation.

$$\text{Power Input: } q = \left| i_{Source}^2 R \right|$$

The solenoid wire temperature rise is given by the following equation where C_p = (Specific Heat) and $\rho = \left(\text{Material Density}\right)$.

$$\Delta Temp_{Wire} = \frac{q_{Wire\_Volume} t_{Temp\_Time}}{\rho C_p}$$

The resistivity change of the solenoid wire is given by the following equation

$$\rho_{res} = \frac{\left(1 + \left(\text{Coef. of Temp. of Material}\right)\Delta Temp_{Wire}\right)}{\left(\text{Material Conductivity}\right)}$$

Natural Convection & Radiative Conditions

This natural convection condition is performed by assuming no forced convection and negligible conduction. The radiative losses are assumed negligible for all thermal calculations excluding the final temperature rise over time equation provided below. The temperature rise values are compared with material yield temperatures. Convective heat generation is given by the following equation.

$$q_{conv.} = \begin{pmatrix}\text{Convection}\\ \text{Coef.}\end{pmatrix}\begin{pmatrix}\text{Solenoid External}\\ \text{Surface Area}\end{pmatrix}\Delta Temp_{Wire}$$

The thermal time constant at which point the temperature achieves steady state for a particular steady state temperature when convective cooling dominates the heat loss is given by the following equation.

$$\begin{pmatrix}\text{Thermal Time}\\ \text{Constant}\end{pmatrix} = \tau_t = \frac{\left(\text{Thermal Capacitance}\right)}{\begin{pmatrix}\text{Convection}\\ \text{Coef.}\end{pmatrix}\begin{pmatrix}\text{Solenoid External}\\ \text{Surface Area}\end{pmatrix}}$$

Temperature rise over time is provided via the following equation where T_{init} = (Initial Temperature), T_{∞} = (T_{init} + Final Temperature), and T_{rise} = (Rising Temperature Range).

$$\begin{pmatrix} \text{Steady State} \\ \text{Temp. Rise Time} \end{pmatrix} = t_{Rise} = \tau_t \left(\frac{T_{init} - T_{\infty}}{T_{rise} - T_{\infty}} \right)$$

If radiative cooling is no longer negligible then a first order, lumped mass temperature rise over time analysis is readily provided by the following equation where T_{sur} = (Surrounding Temperature), I = (Current), R = (Electrical Resistance), h = (Free Convective Coefficient), A_S = (Surface Area), ε = (Emissivity), σ = (Stefan-Boltzmann Constant), ρ = (Material Density), C_p = (Specific Heat), and V = (Volume).

$$\frac{dT}{dt} = \frac{\overbrace{I^2 R}^{\text{Electrical Internal Heat Generation}} - \overbrace{hA_S\left(T_{rise} - T_{\infty}\right)}^{\text{Free or Natural Convective Cooling}} - \overbrace{\varepsilon\sigma A_S\left(T_{rise}^4 - T_{sur}^4\right)}^{\text{Radiative Cooling}}}{\rho C_p V}$$

3.3 PHASE I

3.3.a Analytical Equation Derivation

3.3.a.i 1st Order Solenoid $\vec{B}$ and Secondary $\vec{J}$ Analysis

Overall Solution Method

Any electromagnetic system can be solved from a magnetic viewpoint which solves for the developed magnetic flux or electrical viewpoint which solves for the inductance coupling. This analysis assumes the magnetic viewpoint. There are two useful magnetically based methods to solve for the magnetic flux density, $\vec{B}$, at a point in space. The first method is solving for $\vec{B}$ at a point in space from each individual solenoid coil turn. The second method is solving for the current in a single turn ring that approximates the solenoids' ampere-turns. Then use this solution to

solve for the $\vec{B}$ at a point in space. This research paper uses the second method by solving for a single turn rung at the longitudinal solenoid end which produces an equal $\vec{B}$ at the solenoid's center axis as the solenoid itself.

Direct equation analysis determines the force produced. The direct equation analysis starts by determining magnetic flux density on the axis of the solenoids ends. The current in an equivalent ring is then determined from this axial magnetic flux density value. The ring is then used to determine the magnetic flux density equations for a point in space away from the ring in spherical coordinates. These magnetic flux density equations allow for an approximation of the surface magnetic flux density for a chosen conducting secondary surface area. Symmetry involving the secondary surface chosen for this analysis allows for a direct solution in two-dimensional right Cartesian coordinates. Therefore the magnetic flux density equations are transformed from spherical to Cartesian coordinates. The normal and tangential components of the surface magnetic flux density are determined. The surface magnetic flux density is then placed into the diffusion equation, Bullard's form of the diffusion equation is used and is shown below, which is used to find the diffused magnetic flux density and hence current density and force density in the secondary conductor. The normal component of the magnetic flux density creates the induced current for all forces, the side propulsive or centering force, and the normal attractive force if a ferrous material resides on the secondary. The tangential component of the magnetic flux density creates the repulsive and hence levitation force and rotational propulsive force.

There are numerous assumptions taken in this analysis. Many of these assumptions are listed in the analytical equation development. Therefore the predicted forces given are exaggerated values. These output forces are still useful since they allow approximate values for the output forces.

Solenoid Ring Approximation

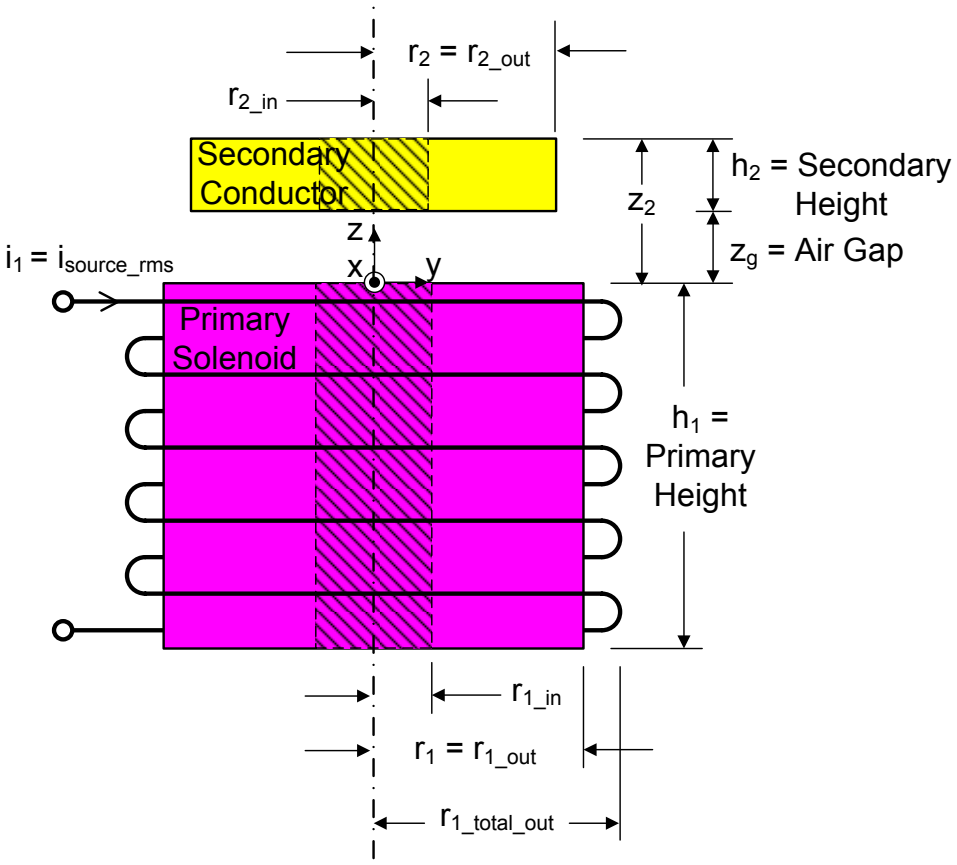

Figure 3.3-1: Phase I Solenoid Schematic

Figure 3.3-1 provides the solenoid geometry of interest. The chosen coordinate system relates a co-axial secondary disk and solenoid with parallel primary and secondary opposing faces irrespective of the world coordinates. Therefore gravity does not play into the solenoid equations. The flux density at the longitudinal end of a solenoid on the axis of the solenoid is given by the following equation.

$$B_{\text{Solenoid Axis}} = \frac{\mu N i}{2\sqrt{R_1^2 + h_1^2}}$$

Here the current, i, is the source current given by the following assumption which follows from the perfect sinusoidal source voltage assumption.

$$i = i(t) = |i|\cos(\omega t)$$

Approximate the solenoid as a single turn ring at end z=h. The magnetic flux density, B, at the ring center is given by the following equation.

$$B_{\text{Ring}} = \frac{\mu i}{4\pi R_1}\int_0^{2\pi} d\phi_{\text{Ring}} = \frac{\mu i}{2R_1}$$

Setting $B_{\text{Ring}} = B_{\text{Solenoid Axis}}$ provides the ring current.

$$i_{\text{Ring}} = \frac{R_1 N i_{Source}}{\sqrt{R_1^2 + h_1^2}}$$

$\vec{B}$ at a Point P in Space

Use i_{Ring} to find $\vec{B} = \nabla \times \vec{A}$ at a point in free space as depicted in Figure 3.3-2. Note that $\phi = \frac{\pi}{2}$ at point P is chosen for convenience.

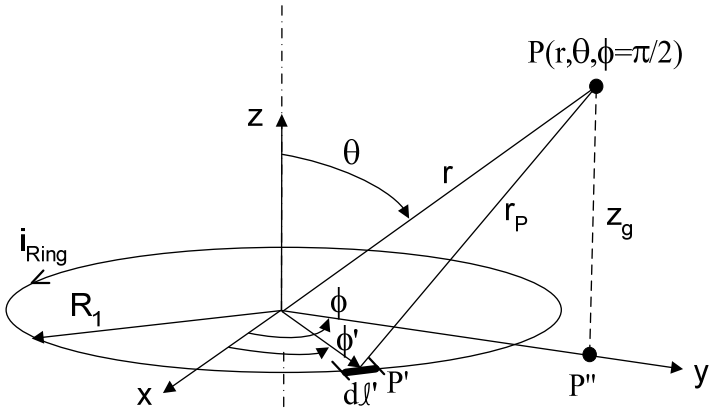

Figure 3.3-2: Phase I Solenoid i_{Ring} Schematic Isometric View

The vector magnetic potential, $\bar{A}_P$, is defined for a point P on the secondary surface from the primary ring source $Id\ell'$ as defined by the contour integral $\oint_{c'}$.

$$\text{Vector Magnet Potential} = \bar{A}_P = \frac{\mu_0 I}{4\pi}\oint_{c'}\frac{d\ell'}{r_1}$$

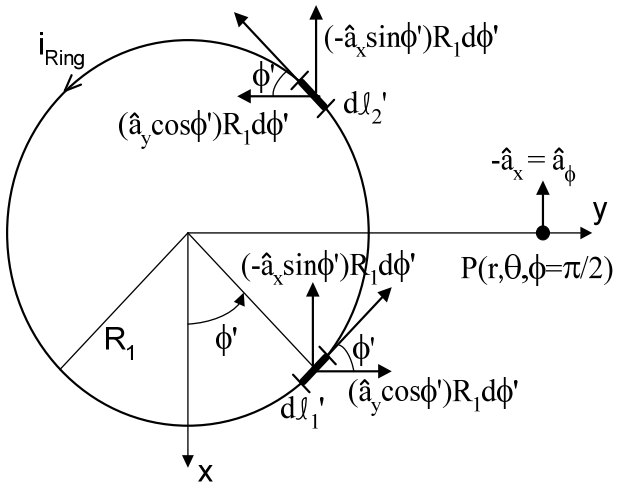

Figure 3.3-3: Phase I Solenoid i_{Ring} Schematic Plan View

In Cartesian coordinate terms the point P is located above the y axis as indicated in Figure 3.3-3. The positive x axis side of the contour $Id\ell_1'$ contributes an

equal an opposite $\vec{A}_P$ than the negative x axis side of the contour $Id\ell'_2$. Symmetry relations cancel the $\vec{A}_P(\hat{a}_x)$ and $\vec{A}_P(-\hat{a}_x)$ components leaving only a $\vec{A}_P\hat{a}_y$ component. In other words $\vec{A}_P$ is independent of the field point P angle ϕ. This symmetry relationship is witnessed in the following set of equations.

$$\ell'_1 \text{ contour: } -90° \le \phi' \le 90°$$

$$\ell'_2 \text{ contour: } 90° \le \phi' \le -90°$$

$$d\ell'_1 = \left(-a_x \sin\phi' + a_y \cos\phi'\right) R_1 d\phi'$$

$$d\ell'_2 = \left(-a_x \sin\phi' - a_y \cos\phi'\right) R_1 d\phi'$$

$$d\ell' = \left(d\ell'_1 + d\ell'_2\right) = \left(-a_x \sin\phi'\right) R_1 d\phi' \tag{3.4}$$

Equation (3.4) shows symmetry canceling the $\hat{a}_y$ components. Note that $\left(d\ell'_1 + d\ell'_2\right) \neq 2\left(-a_x \sin\phi'\right) R_1 d\phi'$ since the $d\ell'$ contour itself only provides a direction and no magnitude. Figure 3.3-3 demonstrates that at point P $\left(-\hat{a}_x\right) = \hat{a}_\phi$.

$$\vec{A}_P = \left[\frac{\mu_0 i_{Ring}}{4\pi}\int_0^{2\pi} \frac{R_1 \sin\phi'}{r_P} d\phi'\right]\left(-\hat{a}_x\right)$$

$$\vec{A}_P = \left[\frac{\mu_0 i_{Ring} R_1}{2\pi}\int_{-\frac{\pi}{2}}^{\frac{\pi}{2}} \frac{\sin\phi'}{r_P} d\phi'\right]\left(\hat{a}_\phi\right)$$

Set r_P equal to the following equation to attain equation (3.5).

$$r_P = r\sqrt{1 + \frac{R_1^2}{r^2} - \frac{2R_1}{r}\sin\theta\sin\phi'}$$

$$\vec{A}_P = \left[\overbrace{\frac{\mu_0 i_{Ring} R_1}{2\pi r}}^{C_1}\int_{-\frac{\pi}{2}}^{\frac{\pi}{2}} \overbrace{\frac{1}{\sqrt{1 + \frac{R_1^2}{r^2} - \frac{2R_1}{r}\sin\theta\sin\phi'}}}^{C_2} \sin\phi' d\phi'\right]\left(\hat{a}_\phi\right) \tag{3.5}$$

Introduce the general form of the Binomial Series, equation (3.6), to solve for the constant C_2.

$$(a+x)^n = a^n + na^{n-1}x + \frac{n(n-1)}{2!}a^{n-2}x^2 + \frac{n(n-1)(n-2)}{3!}a^{n-3}x^3 + \ldots \qquad (3.6)$$

Take the Binomial Series to the 3rd term for approximate accuracy and set $n = -\frac{1}{2}$, a=1, and $x = \frac{R_1^2}{r^2} - \frac{2R_1}{r}\sin\theta\sin\phi'$. This gives the following equation for C_2.

$$C_2 = (a+x)^n \simeq 1 + \left[-\frac{1}{2}\left(\frac{R_1^2}{r^2} - \frac{2R_1}{r}\sin\theta\sin\phi' \right) \right] +$$

$$+ \left[\frac{3}{8}\left(\frac{R_1^4}{r^4} - \frac{4R_1^3}{r^3}\sin\theta\sin\phi' + \frac{4R_1^2}{r^2}\sin^2\theta\sin^2\phi' \right) \right] =$$

$$= \overbrace{\left[1 - \frac{R_1^2}{2r^2} + \frac{3R_1^4}{8r^4} \right]}^{D_1} + \overbrace{\left[\frac{R_1}{r}\sin\theta - \frac{3R_1^3}{2r^3}\sin\theta \right]}^{D_2}\sin\phi' + \overbrace{\left[\frac{3R_1^2}{2r^2}\sin^2\theta \right]}^{D_3}\sin^2\phi'$$

Plug the set constants into equation (3.5).

$$\vec{A}_P = C_1\hat{a}_\phi \left[-D_1\cos\phi + \frac{D_2}{2}(\phi - \sin\phi\cos\phi) + D_3\left(-\cos\phi + \frac{1}{3}\cos^3\phi \right) \right]\Bigg|_{-\frac{\pi}{2}}^{\frac{\pi}{2}} =$$

$$= C_1\hat{a}_\phi \left[\left(\frac{\pi}{4}D_2 \right) + \left(\frac{\pi}{4}D_2 \right) \right] = \frac{\pi}{2}C_1D_2\hat{a}_\phi = \frac{\pi}{2}\left(\frac{\mu_0 i_{Ring}R_1}{2\pi r} \right)\left(\frac{R_1}{r}\sin\theta - \frac{3R_1^3}{2r^3}\sin\theta \right)\hat{a}_\phi =$$

$$= \left(\frac{\mu_0 i_{Ring}R_1^2\sin\theta}{4r} \right)\left(1 - \frac{3R_1^3}{2r^2} \right)\hat{a}_\phi$$

Find $\vec{B}_P$ from $\vec{B} = \nabla \times \vec{A}$ and with spherical coordinates (r, θ, ϕ) applied to the unit vector $\hat{a}_\phi$.

$$\vec{B}_P = \left(\frac{1}{r\sin\theta}\right)\left(\frac{\partial\left(A_\phi \sin\theta\right)}{\partial\theta}\right)\hat{a}_r - \frac{1}{r}\left(\frac{\partial\left(rA_\phi\right)}{\partial r}\right)\hat{a}_\theta =$$

$$= \left\{\left(\frac{1}{r\sin\theta}\right)\frac{\partial}{\partial\theta}\left[\left(1-\frac{3R_1^2}{2r^2}\right)\left(\frac{\mu_0 i_{Ring} R_1^2}{4r^2}\right)\sin^2\theta\right]\right\}\hat{a}_r -$$

$$-\left\{\left(\frac{1}{r}\right)\frac{\partial}{\partial r}\left[\left(\frac{\mu_0 i_{Ring} R_1^2 \sin\theta}{4r^2}\right)-\left(\frac{3\mu_0 i_{Ring} R_1^4 \sin\theta}{8r^3}\right)\right]\right\}\hat{a}_\theta$$

Solve the partial derivatives by assuming all else is constant at the point in question. In this case r and θ are the differential variables and hence are constant and unique for the point P in space. The actual r and θ values used in every $\vec{B}$ equation including equation (3.7) are described later when discussing the time average force solutions.

$$\vec{B}_P = \left[\left(\frac{1}{r\sin\theta}\right)\left(1-\frac{3R_1^2}{2r^2}\right)\left(\frac{\mu_0 i_{Ring} R_1^2}{4r^2}\right)2\sin\theta\cos\theta\right]\hat{a}_r -$$

$$-\left\{\frac{1}{r}\left[\left(\frac{9\mu_0 i_{Ring} R_1^4 \sin\theta}{8r^2}\right)-\left(\frac{\mu_0 i_{Ring} R_1^2 \sin\theta}{4r^2}\right)\right]\right\}\hat{a}_\theta = \left(E_1\right)\hat{a}_r + \left(E_2\right)\hat{a}_\theta \qquad (3.7)$$

Secondary Normal and Tangential $\vec{B}$ Components at Point P

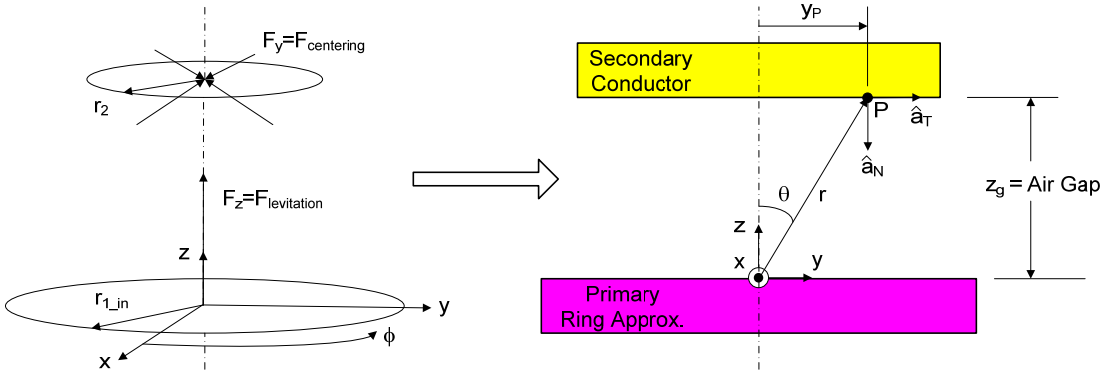

Figure 3.3-4: Phase I Solenoid System Transformation

Find the B_T and B_N components impinging on the secondary surface at point P. Typically a solution of this form could require a tedious transformation from spherical to cylindrical coordinates. In this case $\vec{B}$ is constant with respect to ϕ about the primary solenoid axis. Symmetry then allows the direct transform of coordinates as indicated by the unit vectors $\hat{a}_N$ and $\hat{a}_T$ as shown in Figure 3.3-4. The transformation is completed in the two dimensional plane from two dimensional spherical to two dimensional right Cartesian coordinates. The system's two dimensional right Cartesian coordinate system constraint equations and transformation components are listed in Table 3.3-1.

Table 3.3-1: Phase I Solenoid System Transformation

Here	Typical Transform	Constraints
$\hat{a}_T = \hat{a}_y$	$r = \sqrt{x^2 + y^2 + z^2}$	x=0, $y = 0$ to y_P, $z = z_g$
$\hat{a}_N = -\hat{a}_z$	$\theta = \cos^{-1}\left(\frac{z}{\sqrt{x^2 + y^2 + z^2}}\right)$	Equations $\phi = 90°$ and $B_x = 0$
	$\phi = \tan^{-1}\left(\frac{y}{x}\right)$	Assume: Planar Cartesian 2-D Coordinates.

Which gives $r = \sqrt{y_P^2 + z_g{}^2}$, $\theta = \cos^{-1}\left(\frac{z_g}{\sqrt{y_P^2 + z_g{}^2}}\right) = \sec\left(\frac{z_g}{\sqrt{y_P^2 + z_g{}^2}}\right)$, and $\phi = 90^\circ$ as typical transform output. The constraint $z = z_g$ gives the secondary disk vertical location desired. Use these constraints to find B_T and B_N at point P on the secondary in the right Cartesian coordinate system. This gives equations (3.8) and (3.9). Equations (3.8) and (3.9) use the following unit vector dot product relations when transforming from spherical coordinates to Cartesian coordinate tangential and normal components.

$$\hat{a}_r \bullet \hat{a}_y = \sin\theta \sin\phi$$

$$\hat{a}_\theta \bullet \hat{a}_y = \cos\theta \sin\phi$$

$$\hat{a}_r \bullet \hat{a}_z = \cos\theta$$

$$\hat{a}_\theta \bullet \hat{a}_z = -\sin\theta$$

$$B_{TP} = B_y = \vec{B}_P \bullet \hat{a}_y = \left(E_1 \hat{a}_r - E_2 \hat{a}_\theta\right) \bullet \hat{a}_y = E_1 \sin\theta \cancel{\sin\phi}^{1} - E_2 \cos\theta \cancel{\sin\phi}^{1} = \\ = E_1 \sin\theta - E_2 \cos\theta \tag{3.8}$$

$$B_{NP} = -B_z = -\left(\vec{B}_P \bullet \hat{a}_z\right) = -\left(E_1 \hat{a}_r - E_2 \hat{a}_\theta\right) \bullet \hat{a}_z = \\ = -\left[E_1 \cos\theta - E_2\left(-\sin\theta\right)\right] = -\left[E_1 \cos\theta + E_2 \sin\theta\right] \tag{3.9}$$

$$\vec{B}_P = B_{TP} + B_{NP} \tag{3.10}$$

$\vec{B}_P$ is defined as the approximate point magnetic flux density on a currently undefined right Cartesian plane located above the solenoid's surface. $\vec{B}$ separates into normal and tangential Cartesian components. Via the diffusion equation, $\vec{B}_{SA}$ provides the diffused $\vec{B}$, current density, $\vec{J}$, and force density into a geometrically defined secondary. This secondary must remain within reasonable geometric limits with respect to the primary.

Recall how $\vec{B}$ is constant with respect to ϕ about the primary solenoid axis. Symmetry then allowed the direct transform of coordinates as indicated by the unit vectors $\hat{a}_N$ and $\hat{a}_T$ as shown in Figure 3.3-4. Regarding the secondary surface area this means that each ϕ primary solenoid axis B_{NP} and B_{TP} point component of the surface area superimposes without cancellation. The $\vec{B}$ formula solved here originates with the Biot-Savart law. The Biot-Savart law solves $\vec{B}$ at a certain distance from a source but breaks down in validity at the source since the law erroneously takes $\vec{B}$ to infinity at the source. This $\vec{B}$ going to infinity artifact is seen in equation (3.7) when the distance r is set to zero. Since in reality an infinite $\vec{B}$ is not possible, start all analysis with a non-zero gap between the primary solenoid and secondary.

Diffusion Equation for $\vec{B}$ into Secondary

Since $\vec{B}$ for each point on the surface is known from equation (3.10), determine the diffusion components of the magnetic flux density in the secondary conductor. Since magnetic fields superimpose, the diffusion components are solved in parts. Note that it is at times advantageous to use equations such as Gauss's Law in the divergence or point form, $\nabla \bullet \vec{B} = 0$, to solve for applicable field components. Here start with a form of the diffusion equation known as Bullard's equation, equation (3.11).

$$\frac{1}{\mu\sigma}\nabla^2\vec{B} + \frac{\partial \vec{B}}{\partial t} = \nabla \times \left(\vec{v} \times \vec{B}\right) \tag{3.11}$$

Again, $\vec{B}$ for each point on the secondary surface is known, so now solve the assumed exponential form of the diffusion equation where the secondary flux density and current density have the same traveling wave dependence as the primary current source. Recall again that in this case $\hat{a}_T = \hat{a}_y$ and $\hat{a}_N = -\hat{a}_z$.

$$\vec{B} = \vec{B}(y,t) = \mathrm{Re}\left[\left(B_T + B_N\right)e^{j(\omega t - \beta y)}\right] = \mathrm{Re}\left[\left(B_T(y) + B_N(y)\right)e^{j(\omega t - \beta y)}\right]$$

$$\vec{B}(y,t) \rightarrow B_y(y,t) \text{ and } \left[-B_z(y,t)\right] \rightarrow \vec{J} = \vec{J}(y,t)$$

Where in the above equations $\beta = (\text{Wave Number}) = \left(\frac{1-j}{\delta}\right)$, $\delta = (\text{Skin Depth}) = \sqrt{\frac{2}{\omega\mu\sigma}}$, and $\omega = (\text{Electrical Angular Frequency})$. In Phase I the secondary thickness, thk, is assumed to equal the skin depth, δ.

Secondary $\vec{J}$

The components of $\vec{B}$ and $\vec{J}$ above only depend on y and t. $\vec{J}$ comes from symmetry and the point form of Ampere's Circuit Law given in equation (3.12).

$$\vec{J} = \vec{J}_{free} + \frac{\partial \cancel{D}^{0}}{\partial t} = \nabla \times \vec{H} = \frac{1}{\mu}\nabla \times \vec{B} = \frac{1}{\mu} \bullet \begin{vmatrix} \hat{a}_x & \hat{a}_y & \hat{a}_z \\ \frac{\partial}{\partial x} & \frac{\partial}{\partial y} & \frac{\partial}{\partial z} \\ 0 & \vec{B}_y & -\vec{B}_z \end{vmatrix} \tag{3.12}$$

Some $\vec{J}$ terms in equation (3.12) equal zero since $\vec{B} = \vec{B}(y,t)$ and does not depend on x or z. This given the following equation for $\vec{J}$.

$$\vec{J} = \frac{1}{\mu}\left[\hat{a}_x\left(-\frac{\partial B_z}{\partial y} - \frac{\partial \cancel{B_y}^{0}}{\partial z}\right) - \hat{a}_y\left(-\frac{\partial \cancel{B_z}^{0}}{\partial x}\right) + \hat{a}_z\left(-\frac{\partial \cancel{B_y}^{0}}{\partial x}\right)\right] = -\frac{1}{\mu}\frac{\partial B_z}{\partial y}\hat{a}_x = -\frac{1}{\mu}\frac{dB_z}{dy}\hat{a}_x$$

Notice that the current direction follows Lenz's Law in that the induced current is in the opposite direction of the source current so that the induced current produces a $\vec{B}$ that cancels the source $\vec{B}$. Now plug in the following equation to obtain the final form of $\vec{J}$ in equation (3.13).

$$-\frac{dB_z}{dy} = \frac{d}{dy}\left[B_N e^{j(\omega t - \beta y)}\right]$$

$$\vec{J} = \hat{J}_x = J_x(y,t) = \frac{1}{\mu} \bullet \frac{d}{dy}\left(B_N e^{j(\omega t - \beta y)}\right) \tag{3.13}$$

Summary of 1st Order Analytical Solenoid Design Approximation

The first order analytical solenoid design approximation method is only intended to provide a rough solenoid design that approximates output trends. This approximation identifies design areas requiring more modeling accuracy and provides input for computational design runs. The final solution requires enough complexity to serve as a working state space simulation as well as a parameter optimization design tool. This first order approximation method now assumes the role of a learning tool for more complex models. The learning curve starts by reviewing the approximations chosen for the first order analytical solenoid design model. The solenoid design method of Chapter 3.3.a.i assumes three main approximations. This starts with a single current ring approximation that produces an equivalent solenoid end axis $\vec{B}$ modeling the entire solenoid $\vec{B}$. In the second approximation the Biot-Savart law uses this solved ring center $\vec{B}$ to solve for the $\vec{B}$ impinging on the secondary surface. Biot-Savart law is only completely valid for a point source which cannot be assumed in this case. In the third approximation the body force equations solve the secondary force density in variable time and variable space coordinates orthogonal to the secondary surface but constant with respect to the two secondary surface tangential spatial coordinates.

In reality $\vec{B}$ is normal when entering the air gap from the solenoid iron core, but $\vec{B}$ is also centered about the solenoid winding and hence the maximum $\vec{B}$ is never located at the solenoid axis when the solenoid aspect ratio of solenoid height to diameter is low. $\vec{B}$ also maintains both a variable normal and tangential component throughout the secondary material and a proper diffusion equation analysis must reflect this fact instead of only a variable normal component.

3.3.a.ii Higher Order Solenoid $\vec{B}$ and Secondary $\vec{J}$ Analysis

Overall

Intuition and review of the computational Opera™ runs of Appendix B.1.a indicate that two higher order analytical solutions and one computational solution readily present themselves. The first analytical solution is based on the current first order analytical solenoid design solution. Instead of only using one current ring to approximate the solenoid $\vec{B}$, superimpose multiple rings with a distributed current density throughout each. Higher numbers of multiple rings will asymptotically approach a solenoid sheet current. This solution is possible, but it still requires time consuming calculation in human and computer time of many rings in order to approach a proper solenoid simulation. This approach also does not solve for the secondary $\vec{B}$ variable in two space coordinates. Therefore this approach is both cumbersome and still not a good approximation. The second analytical solution requires rework starting with Maxwell's equations. This approach, which is similar to a double sided, high speed linear induction motor method used in the author's Master thesis [11] and more remotely to Yamamura [24], requires a wave equation approach which assumes an effective wavelength for the fundamental wave as presented in Figure 3.3-5. In this case the general wave equation, $\vec{B} = B_1 e^{j\omega t} + B_2 e^{-j\omega t}$, immediately collapses to $\vec{B} = B_0 e^{-j(\omega t - \beta y)}$ from boundary conditions where the wave number is $\beta = \frac{2\pi}{\lambda_{eff}} = \frac{\pi}{\tau_{eff}}$. This method solves for $\vec{B}$ in time and multi- dimensional space as determined by the wave equation distribution. This approach of determining $\vec{B}$ is a bit more cumbersome to solve but much more exact than using the Biot-Savart law. Also the effective wavelength, λ_{eff}, must be approximated since solenoid geometry does not provide a fixed value, but the value may be approximated through computational techniques. The third solution uses the power of gradient based computational answers. By taking a known geometric configuration, material

properties, and current density a computational solution may be formed. Determining forces from multiple computational runs over a variable gap distance provides point data. Interpolation of points from an accurate model typically provides a trend line with an accurate solution.

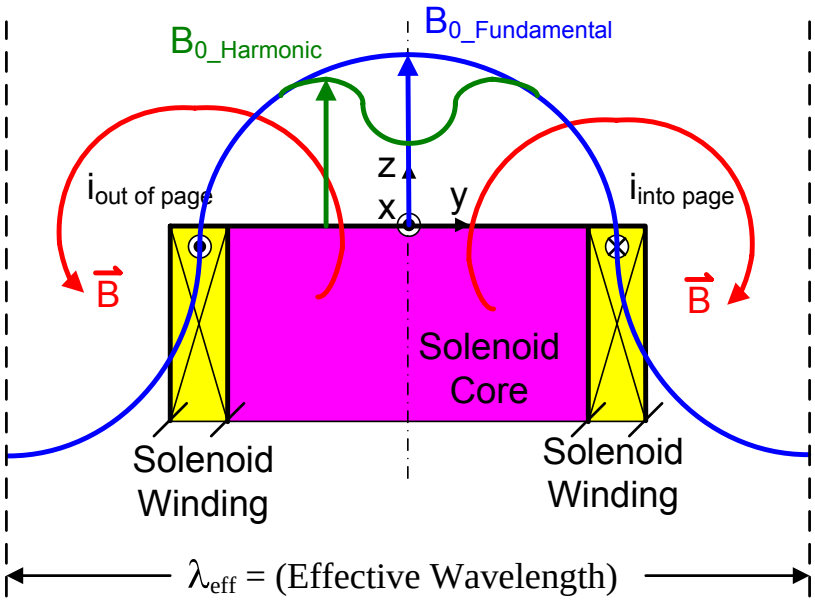

Figure 3.3-5: Wave Equation Solenoid Design Cross Section

The first solution, multiple solenoids solution, is not considered adequate. This leaves the second analytical, wave equation solution, and third computational solutions. The wave equation analytical solution is the chosen route with the computational solution verifying and honing the analytical solution outputs.

The magnetic flux density is composed of a general traveling wave component, an outside secondary radius end dynamic motion traveling wave component, and an inside secondary radius dynamic motion traveling wave end component. The dynamic motion end components are produced by any fast lateral motion between the solenoid primary and secondary. This lateral motion is witnessed in the Phase II, III, and IV dynamic applications of this system. Although Phase I is a static lateral motion system, this lateral motion dynamic effect is solved now to

negate future rework. Due to the periodic nature of the excitation, Fourier methods instead equivalent methods such as superimposing impulses or steps are used to superimpose each linear variable of interest. The superposition of these components provides an approximation for the magnetic flux density entering the secondary for a particular propulsive velocity and x axis coordinate location along the vehicle's secondary length. Source frequency and lateral velocity dependent performance calculations are derived from this magnetic flux density.

Derivation of Diffusion Equation Form Used

General Diffusion Equation Form:

Begin with the quasi-static magnetic field system assuming that all materials are linear, homogeneous, and isotropic. Thus start with the following equations as described in Hayte [5].

$$\nabla \times \vec{H} = \vec{J}_f \tag{3.14}$$

$$\nabla \bullet \vec{B} = 0$$

$$\vec{B} = \mu \vec{H} \tag{3.15}$$

$$\nabla \times \vec{E} = -\frac{\partial \vec{B}}{\partial t}$$

$$\vec{J}_f = \sigma\left(\vec{E} + \vec{v} \times \vec{B}\right) \tag{3.16}$$

The desired diffusion equation form involves operations on the vector potential, A. Introduce the vector potential with equations (3.17) and (3.18).

$$\vec{B} = \nabla \times \vec{A} \tag{3.17}$$

$$\vec{E} = -\frac{\partial \vec{A}}{\partial t} \tag{3.18}$$

Where the chosen vector potential holds for the condition $\nabla \bullet \vec{A} = 0$.

From equations (3.14), (3.15), and (3.17) obtain the following.

$$\vec{J} = \vec{J}_f = \nabla \times \left(\mu \vec{B}\right) \rightarrow \vec{J} = \left(\frac{1}{\mu}\right)\left[\nabla \times \left(\nabla \times \vec{A}\right)\right]$$

This equation is solved with the use of the following vector identity to obtain equation (3.19).

$$\nabla \times \left(\nabla \times \vec{A} \right) = \cancel{\nabla \left(\nabla \bullet \Phi \right)} - \nabla^2 \vec{A} = -\nabla^2 \vec{A}$$

$$\nabla^2 \vec{A} = -\mu \vec{J} \tag{3.19}$$

Plugging equations (3.18) and (3.19) into equation (3.16) attains equation (3.20).

$$\nabla^2 \vec{A} = \mu\sigma \left\{ \left(\frac{\partial \vec{A}}{\partial t} \right) - \left[\vec{v} \times \left(\nabla \times \vec{A} \right) \right] \right\} \tag{3.20}$$

This is a vector potential operator form of Bullard's Equation. Bullard's Equation is the Diffusion Equation with time varying motion as described in Woodson and Melcher [23]. This analysis uses the simpler vector potential equation forms instead of the magnetic flux density equation forms.

2-D Problem Specific Equation Form:

The 2-D problem starts with lessons learned from Chapter 3.3.a.i and corresponding Opera™ runs. Figure 3.3-6 indicates the general solenoid design. 2-D right Cartesian coordinates are used to simplify the initial analysis for this cylindrical system. Cylindrical coordinates and the assumptions to this geometry are later used when solving the force density equations as shown in Chapter 3.3.a.iii. Cartesian coordinates are allowable when the secondary face is parallel to the opposing primary face and when the secondary is concentric with the primary or when the y axis is located on the coordinates of any eccentricity. Figure 3.3-7 depicts the geometric approximations used for this 2-D analysis which is equivalent to the geometry of a single sided linear induction motor. Note that the secondary inner radius parameter indicates if the solenoid is a ring or disc. The 2-D model for the solenoid is broken into four analysis regions as shown in Figure 3.3-6 and Figure 3.3-7. Region 1 is the solenoid's iron core. Region 2 is the solenoid's secondary conductive sheet. Region 3 and region 4 are the solenoid's air gaps.

The solution determines the governing magnetic vector potential and hence the magnetic flux density equations for each region in two dimensions within the assumptions listed throughout the solution. Solving the governing equation constants provides a closed form analytic solution. The boundary conditions between each region determine these equation constants. Symmetry or material values at infinity removes equation constants from governing equations and helps solve the governing equation sets. Regions 1 and 4 are assumed to approach infinity under set conditions which allows the closed form solution to these governing equations.

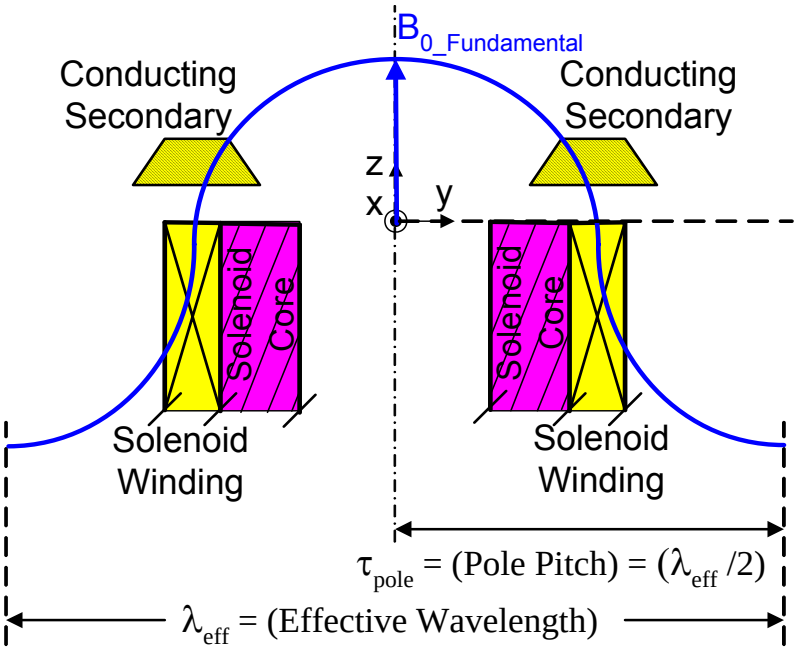

Figure 3.3-6: Ring Core & Secondary Solenoid Cross Section

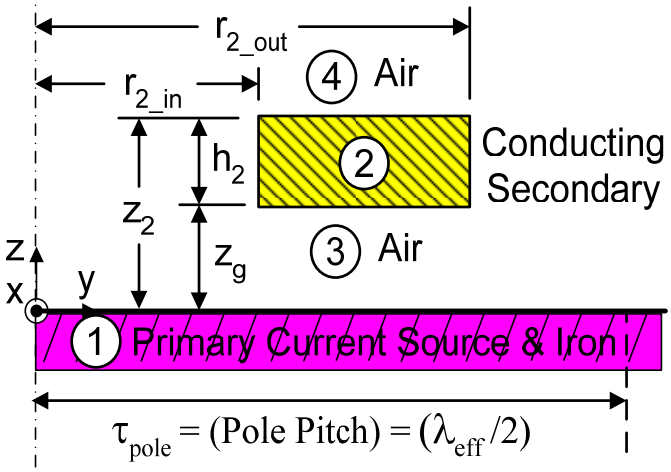

Figure 3.3-7: Ring Core & Secondary Solenoid Cross Section Analysis Regions

The primary inside radius, r_{1_in}, shown in Figure 3.3-1 is assumed to be 0 or small enough such that the effect of any hole has a negligible effect on $\vec{B}$. In actuality a hollow primary solenoid may impose an unnecessary financial burden with no analytical gain, but the r_{1_in} term is maintained in the certain equations in case a hole is deemed desirable or necessary at a later date. Therefore the primary current is taken to flow uniquely as a sheet current in the x direction across the entire y axis boundary as shown in Figure 3.3-7. Hence equation (3.14) indicates that $\vec{B}$ and $\vec{H}$ only have y and z directed components. The primary current direction and equation (3.18) also indicates that $\vec{A}$ only flows in the x direction. Therefore for this analysis assume that $\vec{A} = A_x = A$. Due to this homogenous primary sheet current assumption, this analysis cannot accurately predict a secondary outside radius that varies greatly from the primary outside radius. Therefore in practice the primary and secondary maximum radii must maintain approximately the same value.

Equation (3.17) then gives the following equation.

$$\vec{B} = \nabla \times A = \begin{vmatrix} \hat{a}_x & \hat{a}_y & \hat{a}_z \\ \frac{\partial}{\partial x} & \frac{\partial}{\partial y} & \frac{\partial}{\partial z} \\ A & 0 & 0 \end{vmatrix} = \overbrace{0}^{B_x}\hat{a}_x + \overbrace{\frac{\partial A}{\partial z}}^{B_y}\hat{a}_y - \overbrace{\frac{\partial A}{\partial y}}^{B_z}\hat{a}_z \tag{3.21}$$

In region 2 equation (3.20) takes the following form where the radial velocity is $v_y = v_{radial} = v$ and is not the air gap velocity in the z direction. This velocity component is not used in the static case of Phase I, but instead is solved now for future use in the dynamic cases of Phases II through IV.

$$\frac{\partial^2 A_2}{\partial y^2} - \frac{\partial^2 A_2}{\partial z^2} = \mu_2 \sigma_2 \left\{ \frac{\partial A_2}{\partial t} - \left[v_y \times \left(\frac{\partial A_2}{\partial z}\hat{a}_y - \frac{\partial A_2}{\partial y}\hat{a}_z \right) \right] \right\}$$

$$\frac{\partial^2 A_2}{\partial y^2} - \frac{\partial^2 A_2}{\partial z^2} = \mu_2 \sigma_2 \left(\frac{\partial A_2}{\partial t} + v \frac{\partial A_2}{\partial y} \right) \tag{3.22}$$

In regions 1, 3, and 4, where the conductivity is zero, equation (3.20) takes the following Laplacian equation forms. Note that region 1 is assumed to comprise an infinitely thin sheet current with a low conducting back iron with respect to the conducting secondary of region 2. Therefore assume region 1 is a purely non-conducting current source.

$$\frac{\partial^2 A_1}{\partial y^2} + \frac{\partial^2 A_1}{\partial z^2} = 0 \tag{3.23}$$

$$\frac{\partial^2 A_3}{\partial y^2} + \frac{\partial^2 A_3}{\partial z^2} = 0 \tag{3.24}$$

$$\frac{\partial^2 A_4}{\partial y^2} + \frac{\partial^2 A_4}{\partial z^2} = 0 \tag{3.25}$$

Boundary Conditions across y-Coordinate Region Interfaces

The boundary conditions for the z axis coordinate region interfaces are chosen and hence developed for both sides of the secondary.

Tangential Boundary Condition (Between Regions 1 & 3):

The tangential boundary condition between region 1, iron core, and region 3, air gap, follows the relation $H_{T\_1} - H_{T\_3} = K \rightarrow H_{y\_1} - H_{y\_3} = K$ where $\vec{K} = \vec{K}_1$ is the surface current density at the boundary. An assumed pure sinusoidal primary sheet current gives.

$$\vec{K}_1 = \left|K_1\right| e^{j(\omega t - \beta x)} \tag{3.26}$$

In units of amperes per meter where $\beta = \frac{2\pi}{\lambda_{eff}} = \frac{\pi}{\tau_{eff}}$ is the wave number described above for equation (3.26). The exponential component $e^{-j\beta x}$ provides the general traveling wave component of the $\vec{B}$ when combined with the time factor $e^{j\omega t}$.

This gives the following boundary condition between regions 1 and 3.

$$\frac{B_{y\_1}}{\mu_1} - \frac{B_{y\_3}}{\mu_3} = \vec{K}_1 \quad ; \text{For: } z = 0$$

In terms of the vector potentials in equation (3.21), this boundary condition takes the following form.

$$\frac{1}{\mu_1}\frac{\partial A_1}{\partial z} - \frac{1}{\mu_3}\frac{\partial A_3}{\partial z} = \vec{K}_1 \quad ; \text{For: } z = 0 \tag{3.27}$$

Tangential Boundary Condition (Between Regions 2 & 3 and Regions 2 & 4):

The tangential boundary condition between region 2, secondary conductor, and region 3 or 4, air gap and free space, follows a similar relation where $K_2 = 0$ since there is no secondary current source. This then gives the following equation for the boundary condition between regions 2 and 3 and regions 2 and 4 respectively.

$$\frac{1}{\mu_2}\frac{\partial A_2}{\partial z} - \frac{1}{\mu_3}\frac{\partial A_3}{\partial z} = 0 \quad ; \text{For: } z = z_g \; ; \text{With: } r_{2\_in} < y < r_{2\_out} \tag{3.28}$$

$$\frac{1}{\mu_2}\frac{\partial A_2}{\partial z} - \frac{1}{\mu_4}\frac{\partial A_4}{\partial z} = 0 \quad ; \text{For: } z = z_2 \; ; \text{With: } r_{2\_in} < y < r_{2\_out} \tag{3.29}$$

Region 2 does not exist when $r_{2\_in} > y > r_{2\_out}$.

Normal Boundary Condition (Between Regions 1 & 3):

The normal boundary condition between region 1, iron core, and region 3, air gap, follows the relation $B_{N\_1} = B_{N\_3} \rightarrow B_{z\_1} = B_{z\_3}$.

This gives the following boundary condition between regions 1 and 3.

$$B_{z\_1} = B_{z\_3} \quad ; \text{For: } z = 0$$

In terms of the vector potentials in equation (3.21), this boundary condition takes the following form.

$$\frac{\partial A_1}{\partial y} = \frac{\partial A_3}{\partial y} \quad ; \text{For: } z = 0 \tag{3.30}$$

Normal Boundary Condition (Between Regions 2 &3 and Regions 2 & 4):

The normal boundary condition between region 2, secondary conductor, and region 3 or 4, air gap and free space, follows a similar relation. This then gives the following boundary condition between regions 2 and 3 and regions 2 and 4 respectively.

$$\frac{\partial A_2}{\partial y} = \frac{\partial A_3}{\partial y} \quad ; \text{For: } z = z_g \; ; \text{With: } r_{2\_in} < y < r_{2\_out} \tag{3.31}$$

$$\frac{\partial A_2}{\partial y} = \frac{\partial A_4}{\partial y} \quad ; \text{For: } z = z_2 \; ; \text{With: } r_{2\_in} < y < r_{2\_out} \tag{3.32}$$

Region 2 does not exist when $r_{2\_in} > y > r_{2\_out}$.

General Fourier Transformed Vector Potentials

Due to the periodic nature of the excitation as in the 1-D case, Fourier methods instead of equivalent methods such as superimposing impulses or steps are used to superimpose each linear variable of interest. Therefore assume the following form from the periodic function.

$$A(x, y, z) = A(y, z)e^{j\omega t} \tag{3.33}$$

Where from Euler's Identity $e^{j\omega t} = \cos(\omega t) + j\sin(\omega t)$.

General Equation for Region 2 (Conductivity ≠ 0):

This gives the following equation with the frequency domain substitution $\frac{\partial}{\partial t} \rightarrow s = j\omega$.

$$\overbrace{\frac{\partial^2 A_2}{\partial y^2} + \frac{\partial^2 A_2}{\partial z^2}}^{\nabla^2 A_2} = \mu_2\sigma_2\left(\frac{\partial A_2}{\partial t} + \nu\frac{\partial A_2}{\partial y}\right) = \overbrace{\mu_2\sigma_2\frac{\partial}{\partial t}}^{j\omega\mu_2\sigma_2} A_2 + \overbrace{\mu_2\sigma_2\nu\frac{\partial}{\partial y}}^{\nu\mu_2\sigma_2\frac{\partial}{\partial y}} A_2$$

Note that the gradient is assumed to have no y component for this case which gives the following equation.

$$\left(\nabla^2 - j\omega\mu_2\sigma_2 - \nu\mu_2\sigma_2\frac{\partial}{\partial y}\right)A_2 = 0 \tag{3.34}$$

This problem is a boundary value problem. Fourier Transforms are tailored to such problems whereas Laplace Transforms are tailored to initial value problems. The

general form of the Fourier Transform is $F\{f(x)\} = \tilde{f}(\xi) = \int_{-\infty}^{\infty} f(x) e^{-j\xi x} dx$ where f(x) is the equation's math kernel.

Now the dummy integration variable of equation (3.34) is changed from y to ξ. Therefore the transform of A(y,z) with respect to y is now denoted by $\tilde{A}(\xi, z)$ with respect to ξ. This gives $\tilde{A}(\xi, z) = \int_{-\infty}^{\infty} A(y, z) e^{-j\xi y} dy$.

Now Fourier Transform the first and last components of equation (3.34) with the frequency domain substitution $\frac{\partial}{\partial y} \rightarrow s = j\xi \rightarrow s^2 = -\xi^2$.

$$\nabla^2 A_2 = \left(0 + \frac{\partial^2 A_2}{\partial y^2} + \frac{\partial^2 A_2}{\partial z^2}\right) \xrightarrow{\text{Fourier Transform}} \left[\left(j^2\xi^2\right) A_2(y,z) e^{-j\xi y}\right] + \left[\frac{\partial^2}{\partial y^2} A_2(y,z) e^{-j\xi y}\right] =$$

$$= -\xi^2 \tilde{A}_2 + \frac{\partial^2}{\partial z^2} \tilde{A}_2$$

$$\frac{\partial}{\partial y}\left[A_2(y,z) e^{-j\xi y}\right] = (-j\xi)\left[A_2(y,z) e^{-j\xi y}\right] = -j\xi \tilde{A}_2$$

Which gives $\left[\left(-\xi^2 + \frac{d^2}{dz^2}\right) - j\omega\mu_2\sigma_2 - (j\xi) v\mu_2\sigma_2\right] \tilde{A}_2(\xi, z) = 0$.

Rearrange to obtain equation (3.35) where γ is a form of the dispersion equation as described in Woodson and Melcher [23], Melcher [14], and Hayte [5]. Here γ is used as the Fourier Transform differential operator. The physical meanings of ξ and γ are discussed more when solving for the vector potential poles in equation (3.76).

$$\frac{d^2 \tilde{A}_2}{dz^2} = \overbrace{\left(\xi^2 + jv\mu_2\sigma_2\xi + j\omega\mu_2\sigma_2\right)}^{\gamma^2} \tilde{A}_2 = \gamma^2 \tilde{A}_2 \qquad (3.35)$$

<u>General Equations for Regions 1, 3, and 4 (Conductivity = 0):</u>

For region 1 substitute equation (3.33) into equation (3.23).

$$\overbrace{\frac{\partial^2 A_1}{\partial y^2}+\frac{\partial^2 A_1}{\partial z^2}}^{\nabla^2 A_1}=0$$

This gives $\nabla^2 A_1 = 0$.

Fourier Transform the previous equation to obtain the following.

$$\left(-\xi^2+\frac{d^2}{dz^2}\right)\tilde{A}_1 = 0$$

$$\frac{d^2\tilde{A}_1}{dz^2} = \xi^2\tilde{A}_1 \tag{3.36}$$

By the same methodology substitute equation (3.33) into equations (3.24) and (3.25) respectively to obtain the following equations.

$$\frac{d^2\tilde{A}_3}{dz^2} = \xi^2\tilde{A}_3 \tag{3.37}$$

$$\frac{d^2\tilde{A}_4}{dz^2} = \xi^2\tilde{A}_4 \tag{3.38}$$

General Fourier Equation Forms:

Equations (3.35), (3.37), and (3.38) are all second order differential equations following the general form $y(x) = C_1 e^{\lambda_1 x} + C_2 e^{\lambda_2 x} + \ldots + C_n e^{\lambda_n x}$ where C is an arbitrary constant. Therefore equations (3.35), (3.36), (3.37), and (3.38) assume the forms of the following equations respectively.

$$\tilde{A}_2 = C_{2A}e^{\gamma z} + C_{2B}e^{-\gamma z} \tag{3.39}$$

$$\tilde{A}_1 = C_{1A}e^{\xi z} + C_{1B}e^{-\xi z} \tag{3.40}$$

$$\tilde{A}_3 = C_{3A}e^{\xi z} + C_{3B}e^{-\xi z} \tag{3.41}$$

$$\tilde{A}_4 = C_{4A}e^{\xi z} + C_{4B}e^{-\xi z} \tag{3.42}$$

Defining Magnetic Potential $z \to \pm\infty$ Boundary Conditions:

Note that in an assumed infinitely long back iron for region 1 $\tilde{A}_1 \to 0$ as $z \to -\infty$. Therefore equation (3.40) turns into the following.

$$\tilde{A}_1 = C_{1A}e^{\xi z} + \cancelto{0}{C_{1B}}e^{-\xi z} = C_{1A}e^{\xi z} = C_1 e^{\xi z} \tag{3.43}$$

By a similar argument with assuming an infinitely long air region 4 above region 2 $\tilde{A}_4 \to 0$ as $z \to +\infty$. Therefore equation (3.42) turns into the following.

$$\tilde{A}_4 = \cancelto{0}{C_{4A}}e^{\xi z} + C_{4B}e^{-\xi z} = C_{4B}e^{-\xi z} = C_4 e^{-\xi z} \tag{3.44}$$

Fourier Transformed Boundary Conditions across Region Interfaces

Fourier Transform of the Sheet Current Density:

Fourier transforming equation (3.26) provides the following.

$$\tilde{K}_1 = \int_{-\infty}^{\infty} K_1 e^{-j\xi y}dy = \int_{-\infty}^{\infty}\left(\left|K_1\right|e^{-j(\omega t-\beta y)}\right)e^{-j\xi y}dy = \left|K_1\right|e^{j\omega t}\int_{-\infty}^{\infty} e^{-j(\xi+\beta)y}dy =$$

$$= \left\{\left|K_1\right|e^{j\omega t}\left[\frac{-1}{j(\xi+\beta)}\right]e^{-j(\xi+\beta)y}\right\}\Bigg|_{y=-\infty}^{\infty}$$

Assume that only the covered stator portion of the primary current contributes to the vector potentials. Therefore the primary current integration limits are from secondary inner to outer radii. This provides the sheet current density equation (3.45).

$$\tilde{K}_1 = \left[\frac{j\left|K_1\right|e^{j\omega t}}{\beta+\xi}e^{-j(\beta+\xi)y}\right]\Bigg|_{y=r_{2\_in}}^{r_{2\_out}} = \left(\frac{j\left|K_1\right|e^{j\omega t}}{\xi+\beta}\right)\left[e^{-j(\xi+\beta)r_{2\_out}} - e^{-j(\xi+\beta)r_{2\_in}}\right] \tag{3.45}$$

Note that if $r_{2\_in} = 0$ then equation (3.45) assumes the following form.

$$\tilde{K}_1 = \left[\frac{j\left|K_1\right|e^{j\omega t}}{\beta+\xi}e^{-j(\beta+\xi)y}\right]\Bigg|_{y=r_{2\_in}}^{r_{2\_out}} = \left(\frac{j\left|K_1\right|e^{j\omega t}}{\xi+\beta}\right)\left[e^{-j(\xi+\beta)r_{2\_out}} - 1\right]$$

Fourier Transform of the Tangential Boundary Conditions:

Fourier transforming equation (3.27) provides the following.

$$\int_{-\infty}^{\infty}\left(\frac{1}{\mu_1}\frac{\partial A_1}{\partial z} - \frac{1}{\mu_3}\frac{\partial A_3}{\partial z}\right)e^{-j\xi y}dy = \tilde{K}_1 \;\text{; For: } z = 0$$

$$\frac{1}{\mu_1}\frac{\partial \tilde{A}_1}{\partial z} - \frac{1}{\mu_3}\frac{\partial \tilde{A}_3}{\partial z} = \tilde{K}_1 \;\text{; For: } z = 0 \tag{3.46}$$

By similar arguments we obtain the following equations from equations (3.28) and (3.29) respectively.

$$\frac{1}{\mu_2}\frac{\partial \tilde{A}_2}{\partial z} - \frac{1}{\mu_3}\frac{\partial \tilde{A}_3}{\partial z} = 0 \quad ; \text{For: } z = z_g \; ; \text{With: } r_{2\_in} < y < r_{2\_out} \tag{3.47}$$

$$\frac{1}{\mu_2}\frac{\partial \tilde{A}_2}{\partial z} - \frac{1}{\mu_4}\frac{\partial \tilde{A}_4}{\partial z} = 0 \quad ; \text{For: } z = z_2 \; ; \text{With: } r_{2\_in} < y < r_{2\_out} \tag{3.48}$$

Fourier Transform of the Normal Boundary Conditions:

Fourier transforming equation (3.30) provides the following.

$$\int_{-\infty}^{\infty}\left(\frac{\partial A_1}{\partial y} - \frac{\partial A_3}{\partial y}\right)e^{-j\xi y}dy = \int_{-\infty}^{\infty}(0)e^{-j\xi y}dy$$

$$\int_{-\infty}^{\infty}\left(\frac{\partial A_1}{\partial y}\right)e^{-j\xi y}dy - \int_{-\infty}^{\infty}\left(\frac{\partial A_3}{\partial y}\right)e^{-j\xi y}dy = 0$$

Recall that $\frac{\partial}{\partial y} \rightarrow s = j\xi$ which gives $j\xi\left(\tilde{A}_1 - \tilde{A}_3\right) = 0$.

$$\tilde{A}_1 = \tilde{A}_3 \quad ; \text{For: } z = 0 \tag{3.49}$$

By similar arguments we obtain the following equations from equations (3.31) and (3.32) respectively.

$$\tilde{A}_2 = \tilde{A}_3 \quad ; \text{For: } z = z_g \; ; \text{With: } r_{2\_in} < y < r_{2\_out} \tag{3.50}$$

$$\tilde{A}_2 = \tilde{A}_4 \quad ; \text{For: } z = z_2 \; ; \text{With: } r_{2\_in} < y < r_{2\_out} \tag{3.51}$$

Fourier Transformed Vector Potential Constants

The six unknown constants, C_1, C_{2A}, C_{2B}, C_{3A}, C_{3B}, and C_4, are now solved in order to determine the magnetic vector potentials. Start by solving the following partial differential equations.

$$\frac{\partial \tilde{A}_1}{\partial z} = C_1\xi e^{\xi z} = \xi\left(C_1 e^{\xi z}\right) = \xi\tilde{A}_1 \tag{3.52}$$

$$\frac{\partial \tilde{A}_2}{\partial z} = C_{2A}\gamma e^{\gamma z} - C_{2B}\gamma e^{-\gamma z}$$

$$\frac{\partial \tilde{A}_3}{\partial z} = C_{3A}\xi e^{\xi z} - C_{3B}\xi e^{-\xi z}$$

$$\frac{\partial \tilde{A}_4}{\partial z} = -C_4\xi e^{-\xi z} = -\xi\left(C_4 e^{-\xi z}\right) = -\xi\tilde{A}_4 \tag{3.53}$$

The various boundary conditions of the preceding equations are implied but are no longer listed explicitly in the following equations for brevity. In the exponential z term cases of $z = z_g$ and $z = z_2$, the z terms are replaced with z_g and z_2 respectively. In the exponential z term case of z=0, the z term retains the exponential z form in all governing equations solved analytically in case future work produces a non-zero exponential z value.

Tangential Boundary Condition (Between Regions 2 & 3):

Obtain the following equation by substituting equations (3.39) and (3.41) into equation (3.47).

$$\frac{1}{\mu_2}\left[C_{2A}\gamma e^{\gamma z_g} - C_{2B}\gamma e^{-\gamma z_g}\right] - \frac{1}{\mu_3}\left[C_{3A}\xi e^{\xi z_g} - C_{3B}\xi e^{-\xi z_g}\right] = 0$$

Rearrange to solve for the constants C_{3A} and C_{3B}.

$$C_{3A} = \left[\left(\frac{\gamma\mu_3}{\mu_2}\right)\left(C_{2A}e^{\gamma z_g} - C_{2B}e^{-\gamma z_g}\right) + \left(\xi C_{3B}e^{-\xi z_g}\right)\right]\left(\frac{1}{\xi e^{\xi z_g}}\right) \tag{3.54}$$

$$C_{3B} = -\left[\left(\frac{\gamma\mu_3}{\mu_2}\right)\left(C_{2A}e^{\gamma z_g} - C_{2B}e^{-\gamma z_g}\right) - \left(\xi C_{3A}e^{\xi z_g}\right)\right]\left(\frac{1}{\xi e^{-\xi z_g}}\right) \tag{3.55}$$

Normal Boundary Condition (Between Regions 2 & 3):

Obtain the following equation by substituting equations (3.39) and (3.41) into equation (3.50).

$$C_{2A}e^{\gamma z_g} + C_{2B}e^{-\gamma z_g} = C_{3A}e^{\xi z_g} + C_{3B}e^{-\xi z_g}$$

Rearrange to solve for the constants C_{3A} and C_{3B}.

$$C_{3A} = e^{-\xi z_g}\left(C_{2A}e^{\gamma z_g} + C_{2B}e^{-\gamma z_g} - C_{3B}e^{-\xi z_g}\right) \tag{3.56}$$

$$C_{3B} = e^{\xi z_g}\left(C_{2A}e^{\gamma z_g} + C_{2B}e^{-\gamma z_g} - C_{3A}e^{\xi z_g}\right) \tag{3.57}$$

To solve for C_{3A} substitute equation (3.55) into equation (3.56).

$$C_{3A} = e^{-\xi z_g}\left\{C_{2A}e^{\gamma z_g} + C_{2B}e^{-\gamma z_g} + \left[\left(\frac{\gamma\mu_3}{\xi\mu_2}\right)\left(C_{2A}e^{\gamma z_g} - C_{2B}e^{-\gamma z_g}\right) - \left(C_{3A}e^{\xi z_g}\right)\right]\right\}$$

Re-arrange to obtain the constant C_{3A}.

$$C_{3A} = \left(\frac{e^{-\xi z_g}}{2}\right)\left[C_{2A}e^{\gamma z_g} + C_{2B}e^{-\gamma z_g} + \left(\frac{\gamma\mu_3}{\xi\mu_2}\right)\left(C_{2A}e^{\gamma z_g} - C_{2B}e^{-\gamma z_g}\right)\right] \tag{3.58}$$

To solve for C_{3B} substitute equation (3.54) into equation (3.57).

$$C_{3B} = e^{\xi z_g}\left\{C_{2A}e^{\gamma z_g} + C_{2B}e^{-\gamma z_g} - \left[\left(\frac{\gamma\mu_3}{\xi\mu_2}\right)\left(C_{2A}e^{\gamma z_g} - C_{2B}e^{-\gamma z_g}\right) + C_{3B}e^{-\xi z_g}\right]\right\}$$

Re-arrange to obtain the constant C_{3B}.

$$C_{3B} = \left(\frac{e^{\xi z_g}}{2}\right)\left[C_{2A}e^{\gamma z_g} + C_{2B}e^{-\gamma z_g} - \left(\frac{\gamma\mu_3}{\xi\mu_2}\right)\left(C_{2A}e^{\gamma z_g} - C_{2B}e^{-\gamma z_g}\right)\right] \tag{3.59}$$

Normal Boundary Condition (Between Regions 1 & 3 and Regions 2 & 4):

Obtain the following equation by substituting equation (3.49) into equation (3.52).

$$\frac{\partial\tilde{A}_1}{\partial z} = \xi\tilde{A}_3 = \xi\left(C_{3A}\cancel{e^{\xi 0}}^{1} + C_{3B}\cancel{e^{-\xi 0}}^{1}\right) = \xi\left(C_{3A} + C_{3B}\right) \tag{3.60}$$

By the same methodology obtain the following equation by substituting equation (3.51) into equation (3.53).

$$\frac{\partial\tilde{A}_4}{\partial z} = -\xi\tilde{A}_2 = -\xi\left(C_{2A}e^{\gamma z_2} + C_{2B}e^{-\gamma z_2}\right) \tag{3.61}$$

Tangential Boundary Condition (Between Regions 1 & 3 and Regions 2 & 4):

Obtain the following equation by substituting equation (3.60) into equation (3.46).

$$\frac{\xi}{\mu_1}\left(C_{3A} + C_{3B}\right) - \frac{\xi}{\mu_3}\left(C_{3A} - C_{3B}\right) = \tilde{K}_1 \tag{3.62}$$

By the same methodology obtain the following equation by substituting equation (3.61) into equation (3.48).

$$\frac{\gamma}{\mu_2}\left(C_{2A}e^{\gamma z_2}-C_{2B}e^{-\gamma z_2}\right)+\frac{\xi}{\mu_4}\left(C_{2A}e^{\gamma z_2}+C_{2B}e^{-\gamma z_2}\right)=0 \tag{3.63}$$

Solving for Magnetic Vector Potential Constants:

Solve for the remaining unknown four constants, C_{2A}, C_{2B}, C_{3A}, and C_{3B}, via the four equations (3.58), (3.59), (3.62), and (3.63).

Rearrange equation (3.62) to obtain the following.

$$C_{3A}=\left[\frac{1}{\xi\left(\frac{1}{\mu_1}-\frac{1}{\mu_3}\right)}\right]\left[\tilde{K}_1-\xi C_{3B}\left(\frac{1}{\mu_1}+\frac{1}{\mu_3}\right)\right] \tag{3.64}$$

Rearrange equation (3.63) to obtain the following.

$$C_{2A}=\left[\frac{C_{2B}e^{-\gamma z_2}\left(\frac{\gamma}{\mu_2}-\frac{\xi}{\mu_4}\right)}{e^{\gamma z_2}\left(\frac{\gamma}{\mu_2}+\frac{\xi}{\mu_4}\right)}\right]=\overbrace{\left[\frac{\mu_4\gamma-\mu_2\xi}{\mu_4\gamma+\mu_2\xi}\right]}^{C_5}\frac{C_{2B}}{e^{2\gamma z_2}}=\left(\frac{C_5}{e^{2\gamma z_2}}\right)C_{2B} \tag{3.65}$$

Substitute equations (3.59) and (3.64) into equation (3.58) to obtain the following.

$$\left[\frac{1}{\xi\left(\frac{1}{\mu_1}-\frac{1}{\mu_3}\right)}\right]\left\{\tilde{K}_1-\xi\left(\frac{1}{\mu_1}+\frac{1}{\mu_3}\right)\left(\frac{e^{\xi z_g}}{2}\right)\left[\begin{array}{l}C_{2A}e^{\gamma z_g}+C_{2B}e^{-\gamma z_g}-\\-\left(\frac{\gamma\mu_3}{\xi\mu_2}\right)\left(C_{2A}e^{\gamma z_g}-C_{2B}e^{-\gamma z_g}\right)\end{array}\right]\right\}=$$

$$=\left(\frac{e^{-\xi z_g}}{2}\right)\left[C_{2A}e^{\gamma z_g}+C_{2B}e^{-\gamma z_g}+\left(\frac{\gamma\mu_3}{\xi\mu_2}\right)\left(C_{2A}e^{\gamma z_g}-C_{2B}e^{-\gamma z_g}\right)\right]$$

Rearrange the previous equation.

$$2\tilde{K}_1 e^{\xi z_g} = \xi\left(\frac{1}{\mu_1}+\frac{1}{\mu_3}\right)\left(\frac{e^{\xi z_g}}{2}\right)\left[C_{2A}e^{\gamma z_g}+C_{2B}e^{-\gamma z_g}-\left(\frac{\gamma\mu_3}{\xi\mu_2}\right)\left(C_{2A}e^{\gamma z_g}-C_{2B}e^{-\gamma z_g}\right)\right]+$$
$$+\xi\left(\frac{1}{\mu_1}-\frac{1}{\mu_3}\right)\left[C_{2A}e^{\gamma z_g}+C_{2B}e^{-\gamma z_g}+\left(\frac{\gamma\mu_3}{\xi\mu_2}\right)\left(C_{2A}e^{\gamma z_g}-C_{2B}e^{-\gamma z_g}\right)\right]$$

Substitute the previous equation into equation (3.65) to find C_{2B}.

$$C_{2B}=\left\{\frac{2\tilde{K}_1 e^{\xi z_g}}{\begin{array}{l}\xi\dfrac{e^{\xi z_g}}{2}\left(\dfrac{1}{\mu_1}+\dfrac{1}{\mu_3}\right)\left[C_5 e^{\gamma z_g-2\gamma z_2}+e^{-\gamma z_g}-\left(\dfrac{\gamma\mu_3}{\xi\mu_2}\right)\left(C_5 e^{\gamma z_g-2\gamma z_2}-e^{-\gamma z_g}\right)\right]+\\ +\xi\left(\dfrac{1}{\mu_1}-\dfrac{1}{\mu_3}\right)\left[C_5 e^{\gamma z_g-2\gamma z_2}+e^{-\gamma z_g}+\left(\dfrac{\gamma\mu_3}{\xi\mu_2}\right)\left(C_5 e^{\gamma z_g-2\gamma z_2}-e^{-\gamma z_g}\right)\right]\end{array}}\right\}$$

If μ_1 is assumed to be completely iron and μ_3 is air then $\mu_1 \gg \mu_3$. Therefore μ_1 may be assumed infinite compared to μ_3. This sets $\frac{1}{\mu_1}\simeq 0$. The remaining $\frac{1}{\mu_3}$ term of the equation is placed in the numerator. Rearrange to obtain the following solution for C_{2B}.

$$C_{2B}=\left\{\frac{2\mu_3\tilde{K}_1 e^{\xi z_g}}{\xi\left\{\begin{array}{l}\dfrac{e^{(\gamma+\xi)z_g-2\gamma z_2}}{2}\left[C_5\left(1-\dfrac{\gamma\mu_3}{\xi\mu_2}\right)+\left(1+\dfrac{\gamma\mu_3}{\xi\mu_2}\right)\right]-\\ -e^{\gamma z_g-2\gamma z_2}\left[C_5\left(1+\dfrac{\gamma\mu_3}{\xi\mu_2}\right)+\left(1-\dfrac{\gamma\mu_3}{\xi\mu_2}\right)\right]\end{array}\right\}}\right\}$$

Looking at the denominator, assume the materials in the equation are a pure conductor for μ_2 and air for μ_3 and μ_4. Therefore $\mu_2 = \mu_3 = \mu_4 = \mu_0$ which gives $\frac{\mu_3}{\mu_2} = 1$. Rewrite the denominator of the C_{2B} equation in simplified form for convenience and then reduce in each of the following equations.

$$\frac{\xi e^{(\gamma+\xi)z_g - 2\gamma z_2}}{2}\left[\left(\frac{\frac{\gamma}{\mu_2} - \frac{\xi}{\mu_4}}{\frac{\gamma}{\mu_2} + \frac{\xi}{\mu_4}}\right)\left(1 - \frac{\gamma\mu_3}{\xi\mu_2}\right) + \left(1 + \frac{\gamma\mu_3}{\xi\mu_2}\right)\right] -$$

$$-\xi e^{\gamma z_g - 2\gamma z_2}\left[\left(\frac{\frac{\gamma}{\mu_2} - \frac{\xi}{\mu_4}}{\frac{\gamma}{\mu_2} + \frac{\xi}{\mu_4}}\right)\left(1 + \frac{\gamma\mu_3}{\xi\mu_2}\right) + \left(1 - \frac{\gamma\mu_3}{\xi\mu_2}\right)\right]$$

$$\frac{\xi e^{(\gamma+\xi)z_g - 2\gamma z_2}}{2}\left[\left(\frac{\gamma - \xi}{\xi + \gamma}\right)\frac{(\xi - \gamma)}{\xi} + \frac{(\xi + \gamma)}{\xi}\right] -$$

$$-\xi e^{\gamma z_g - 2\gamma z_2}\left[\left(\frac{\gamma - \xi}{\xi + \gamma}\right)\frac{(\xi + \gamma)}{\xi} + \frac{(\xi - \gamma)}{\xi}\right]$$

$$\frac{\xi e^{(\gamma+\xi)z_g - 2\gamma z_2}}{2}\left[\frac{\left(-\cancel{\gamma^2} + 2\gamma\xi - \cancel{\xi^2}\right) + \left(\cancel{\gamma^2} + 2\gamma\xi + \cancel{\xi^2}\right)}{\xi(\xi + \gamma)}\right] -$$

$$-\xi e^{\gamma z_g - 2\gamma z_2}\left[\frac{\left(\cancel{\gamma^2} - \cancel{\xi^2}\right) + \left(-\cancel{\gamma^2} + \cancel{\xi^2}\right)}{\xi(\xi + \gamma)}\right]$$

This then gives the following equation for C_{2B}.

$$C_{2B}=\left\{\frac{2\mu_3\tilde{K}_1e^{\xi z_g}}{\dfrac{\xi\gamma e^{(\gamma+\xi)z_g-2\gamma z_2}}{(\xi+\gamma)}}\right\}=\left\{\frac{2\mu_3\tilde{K}_1(\xi+\gamma)e^{\gamma(2z_2-z_g)}}{\xi\underbrace{\gamma}_{H(\xi)}}\right\}= \tag{3.66}$$

$$=\left\{\frac{2\mu_3\tilde{K}_1(\xi+\gamma)e^{\gamma(2z_2-z_g)}}{\xi H(\xi)}\right\}$$

Substitute equation (3.66) into equation (3.65) to find C_{2A}.

$$C_{2A}=\frac{2\mu_3\tilde{K}_1(\xi+\gamma)e^{-\gamma z_g}C_5}{\xi H(\xi)} \tag{3.67}$$

Now solve for C_{3A} and C_{3B}.

Substitute equations (3.66) and (3.67) into equation (3.58) to find C_{3A}.

$$C_{3A}=\left(\frac{e^{-\xi z_g}}{2}\right)\frac{2\mu_3\tilde{K}_1(\xi+\gamma)}{\xi H(\xi)}\left[C_5+e^{2\gamma(z_2-z_g)}+\left(\frac{\gamma\mu_3}{\xi\mu_2}\right)\left(C_5-e^{2\gamma(z_2-z_g)}\right)\right]$$

Rearrange to obtain the following equation.

$$C_{3A}=\frac{\mu_3\tilde{K}_1(\xi+\gamma)e^{-\xi z_g}}{\xi H(\xi)}\left[C_5\left(1+\frac{\gamma\mu_3}{\xi\mu_2}\right)+\left(1-\frac{\gamma\mu_3}{\xi\mu_2}\right)e^{2\gamma(z_2-z_g)}\right] \tag{3.68}$$

Substitute equations (3.66) and (3.67) into equation (3.59) to find C_{3B}.

$$C_{3B}=\left(\frac{e^{\xi z_g}}{2}\right)\frac{2\mu_3\tilde{K}_1(\xi+\gamma)}{\xi H(\xi)}\left[C_5+e^{2\gamma(z_2-z_g)}-\left(\frac{\gamma\mu_3}{\xi\mu_2}\right)\left(C_5-e^{2\gamma(z_2-z_g)}\right)\right]$$

Rearrange to obtain the following equation.

$$C_{3B}=\frac{\mu_3\tilde{K}_1(\xi+\gamma)e^{\xi z_g}}{\xi H(\xi)}\left[C_5\left(1-\frac{\gamma\mu_3}{\xi\mu_2}\right)+\left(1+\frac{\gamma\mu_3}{\xi\mu_2}\right)e^{2\gamma(z_2-z_g)}\right] \tag{3.69}$$

General Vector Potential Solutions

Final Solution of Fourier Transformed Vector Potentials:

At this point it is important to note the various methods available for attaining the desired solution. Previously the magnetic vector potentials for all regions of

interest were determined. Now this information can be used to solve the problem in the following three ways. Each of these three methods detailed here assume a non-magnetic and non-conducting air gap, a non-magnetic yet conducting secondary, and either all of the energy is transferred across the air gap from the primary to the secondary or the air gap losses are known. The first method places a Maxwell stress tensor on an infinitely thin surface of the secondary between the air gap and secondary regions. The resulting magnetic pressure provides the repulsive and lateral forces. This method has the drawback of assuming that the secondary is sufficiently deep such that skin depth effects do not effect the secondary performance calculations. The second method uses a body force equation, a co-energy equation, or magnetic volume tensor in the air gap region, region 3. The third method again uses a body force equation as employed by this paper, a co-energy equation, or magnetic volume tensor in the secondary conductive region for determining the diffusion of the magnetic flux density and the subsequent and interacting current density. Both methods two and three allow approximate determinations of eddy current losses, secondary current and flux diffusion mapping, and skin depth effects if the secondary is thinner than the skin depth effective region.

This analysis primarily focuses on determining the magnetic vector potential in the air gap, $\tilde{A}_3$, and secondary, $\tilde{A}_2$, which lends itself to solenoid performance calculations. Due to the assumptions made for the primary as well this main analysis focus, there is no need to determine the vector potential of the primary iron, $\tilde{A}_1$, or air region behind the secondary, $\tilde{A}_4$.

Solve for $\tilde{A}_2$ by substituting equations (3.66), (3.67), and (3.45) into equation (3.39). The $e^{j\omega t}$ term in $\tilde{K}_1$ of equation (3.45) is assumed present but dropped for simplification purposes. This gives the maximum amplitude value with respect to time only. Note that $h_2 = \left(z_2 - z_g \right)$.

$$\tilde{A}_2 = \left[\frac{j2\mu_3|K_1|}{\xi(\xi+\beta)H(\xi)}\right]\overbrace{(\xi+\gamma)\left[\begin{matrix}C_5 e^{(z-z_g)\gamma} + \\ +e^{\gamma(2z_2-z_g-z)}\end{matrix}\right]}^{G_2(\xi,z)}\left[e^{-j(\xi+\beta)r_{2\_out}} - e^{-j(\xi+\beta)r_{2\_in}}\right]$$

$$\tilde{A}_2 = \left[\frac{j2\mu_3|K_1|}{\xi(\xi+\beta)H(\xi)}\right]\overbrace{(\xi+\gamma)\left[\begin{matrix}C_5 e^{(z-z_g)\gamma} + \\ +e^{\gamma[h_2+(z_2-z)]}\end{matrix}\right]}^{G_2(\xi,z)}\left[e^{-j(\xi+\beta)r_{2\_out}} - e^{-j(\xi+\beta)r_{2\_in}}\right] \quad (3.70)$$

Solve for $\tilde{A}_3$ in a similar fashion as $\tilde{A}_2$. Substitute equations (3.68), (3.69), and (3.45) into equation (3.41). Again note that $h_2 = (z_2 - z_g)$.

$$\tilde{A}_3 = \left[\frac{j\mu_3|K_1|}{\xi(\xi+\beta)H(\xi)}\right](\xi+\gamma)\overbrace{\left\{\begin{matrix}\left[\begin{matrix}C_5\left(1+\frac{\gamma\mu_3}{\xi\mu_2}\right)+ \\ +\left(1-\frac{\gamma\mu_3}{\xi\mu_2}\right)e^{2h_2\gamma}\end{matrix}\right]e^{(z-z_g)\xi} + \\ +\left[\begin{matrix}C_5\left(1-\frac{\gamma\mu_3}{\xi\mu_2}\right)+ \\ +\left(1+\frac{\gamma\mu_3}{\xi\mu_2}\right)e^{2h_2\gamma}\end{matrix}\right]e^{(z_g-z)\xi}\end{matrix}\right\}}^{G_3(\xi,z)}\left[\begin{matrix}e^{-j(\xi+\beta)r_{2\_out}} - \\ -e^{-j(\xi+\beta)r_{2\_in}}\end{matrix}\right] \quad (3.71)$$

An intuitive check of the equations is performed through an understanding of the diffusion physics behind the z direction dependency of $\tilde{A}$. Note the forms of the z dependent exponentials in equations (3.70) and (3.71). Equation (3.71) for $\tilde{A}_3$, the air gap region, has two z dependent exponential forms. The exponential forms $e^{(z-z_g)\xi}$ and $e^{(z_g-z)\xi}$ provide variable z terms for the air gap region through the respective diminishing negative and positive air gap region traverse terms of $(z-z_g)$ and (z_g-z) as z increases. Whereas the exponents $e^{2\gamma(z_2-z_g)} = e^{2h_2\gamma}$ provide a fixed z term for the secondary conductor region through $h_2 = (z_2 - z_g)$, the secondary's thickness.

Similarly equation (3.70) for $\tilde{A}_2$, the secondary conductor region, also has two z dependent exponential forms that help decipher the physics behind the $\tilde{A}$. The exponent $e^{(z-z_g)\gamma}$ provides a variable z term for the air gap region through this diminishing negative air gap region traverse term of $\left(z-z_g\right)$ as z increases. Likewise the exponent $e^{\gamma\left(2z_2-z_g-z\right)}=e^{\gamma\left[h_2+(z_2-z)\right]}$ combines both a fixed z term for the secondary conductor region through $h_2=\left(z_2-z_g\right)$, the secondary thickness, and a variable z term for the air gap and secondary conductor regions combined through the term $\left(z_2-z\right)$.

The final value for the variable z used is solution dependent. Different z values provide different output and therefore the desired solution must dictate the final z value used. In this paper equations (3.109), (3.110), and (3.111) provide the final magnetic solution desired and hence the necessary value of z.

Place $\tilde{A}_2$ and $\tilde{A}_3$ into more solvable forms.

$$\tilde{A}_2 = j2\mu_3\left|K_1\right|\left\{\frac{G_2\left(\xi,z\right)\left[e^{-j(\xi+\beta)r_{2\_out}}-e^{-j(\xi+\beta)r_{2\_in}}\right]}{\xi\left(\xi+\beta\right)H\left(\xi\right)}\right\} \tag{3.72}$$

$$\tilde{A}_3 = j\mu_3\left|K_1\right|\left\{\frac{G_3\left(\xi,z\right)\left[e^{-j(\xi+\beta)r_{2\_out}}-e^{-j(\xi+\beta)r_{2\_in}}\right]}{\xi\left(\xi+\beta\right)H\left(\xi\right)}\right\} \tag{3.73}$$

General Vector Potential Solutions by Inverse Fourier Transforms:

The vector potentials are determined via the Inverse Fourier Transform equations shown.

$$\text{Fourier Transform: } \Im\left\{f\left(x\right)\right\}=\hat{f}\left(w\right)=\int_{-\infty}^{\infty}f\left(x\right)e^{-jwx}dx$$

$$\text{Inverse Fourier Transform: } \Im^{-1}\left\{\hat{f}\left(w\right)\right\}=f\left(x\right)=\frac{1}{2\pi}\int_{-\infty}^{\infty}\hat{f}\left(w\right)e^{-jwx}dw$$

This gives for A_2 and A_3.

$$A_2(y,z)=\frac{1}{2\pi}\int_{-\infty}^{\infty}\tilde{A}_2 e^{jy\xi}d\xi \quad ;\text{ For: } z_g \le z \le z_2$$

$$A_2(y,z)=\frac{j\mu_3|K_1|}{\pi}\int_{-\infty}^{\infty}\frac{G_2(\xi,z)\left[\begin{matrix}e^{-j(\xi+\beta)r_{2\_out}}-\\-e^{-j(\xi+\beta)r_{2\_in}}\end{matrix}\right]}{\xi(\xi+\beta)H(\xi)}e^{jy\xi}d\xi \quad ;\text{ For: } z_g \le z \le z_2$$

$$A_3(y,z)=\frac{1}{2\pi}\int_{-\infty}^{\infty}\tilde{A}_3 e^{jy\xi}d\xi$$

$$A_3(y,z)=\frac{j\mu_3|K_1|}{2\pi}\int_{-\infty}^{\infty}\frac{G_3(\xi,z)\left[e^{-j(\xi+\beta)r_{2\_out}}-e^{-j(\xi+\beta)r_{2\_in}}\right]}{\xi(\xi+\beta)H(\xi)}e^{jy\xi}d\xi \quad ; \tag{3.74}$$

For: $0 \le z \le z_g$

The vector potential integrals give a closed form bounded analytic equation with more analytic poles than zeroes. The Residue Theorem can solve such equations. Therefore the Residue Theorem is now set up and applied.

Vector Potential Poles

All poles are determined by setting equation (3.74) equal to zero and solving for the roots of the equation. It is possible to directly solve for these complex poles analytically. In this case all poles are determined by analytical inspection and logical assumptions.

The following simple poles used to find the general traveling $\vec{B}$ wave condition immediately fall out by inspecting both the A_2 and A_3 Inverse Fourier Transform equations shown above.

$$\xi = 0, -\beta$$

The remaining poles are determined by setting $H(\xi)=0$. Recall from equation (3.35) that $\gamma=\sqrt{\xi^2+jv\mu_2\sigma_2\xi+j\omega\mu_2\sigma_2}$.

$$H(\xi)=\gamma=\sqrt{\xi^2+jv\mu_2\sigma_2\xi+j\omega\mu_2\sigma_2}=0$$

A solution falls out by looking at the mathematical and material constraints in the previous equation. Even if $\xi = 0$, still $\gamma \neq 0$ in an operational system since the solenoid material constants and frequency cannot equal zero but at most only approach zero while the solenoid is operational.

ξ terms exist through the complex poles residing within the γ term. These complex poles are evaluated below which are now used to find equation (3.75).

$$\xi^2 + \left(j\nu\mu_2\sigma_2 \right)\xi + \left(j\omega\mu_2\sigma_2 \right) = \left(\xi - \xi_1 \right)\left(\xi - \xi_2 \right) = 0$$

$$H\left(\xi \right) = \gamma = \overbrace{\sqrt{\xi^2 + j\nu\mu_2\sigma_2\xi + j\omega\mu_2\sigma_2}}^{\text{Original, Quadratic Form: } \gamma_{original}} = \overbrace{\sqrt{\left(\xi - \xi_1 \right)\left(\xi - \xi_2 \right)}}^{\text{Pole Form: } \gamma_{pole}} = 0 \qquad (3.75)$$

Equation (3.75) is used to both provide a form for the γ term in the magnetic flux density equations through the original form of the equation as well as solve the poles by using the quadratic equation on both the original and pole form of the equation. This simple quadratic is now solved via the quadratic equation.

$$\xi = \xi_1, \xi_2 = \frac{-\left(j\mu_2\sigma_2\nu \right) \pm \sqrt{\left(j\mu_2\sigma_2\nu \right)^2 - 4j\mu_2\sigma_2\omega}}{2} \qquad (3.76)$$

Plugging in values for equation (3.76) indicates that ξ_1, which uses the positive sign in front of the radical value, is located in the fourth quadrant and ξ_2, which uses the negative sign in front of the radical value, is located in the second quadrant of the complex plane. This knowledge is later used to generate Figure 3.3-8 and Table 3.3-2.

The physical meaning behind ξ and γ stem from how they were originally defined to help solve the boundary value problem of equation (3.34). ξ replaced the dummy integration variable y to facilitate the Fourier Transform solution. This means that the ξ poles are x or y propulsion axis dynamic boundary conditions and γ is just a quadratic form of the ξ poles. This knowledge is used to generate Figure 3.3-8.

In reality no other pole is needed if a simple pole of zero is discovered since an analytic solution of all poles of every order could be found by Taylor's Theorem

instead of the Residue Theorem that stems from Laurent's Theorem for poles not located at the origin. Although Taylor's Theorem assumes that no other pole has a significant effect on the solution besides the pole at the origin. Therefore assume that the simple pole solution of $\xi = -\beta$ and the complex pole solutions of equation (3.76) are exceptionally closer to the origin such that they do not attenuate rapidly with respect to the simple pole at the origin. Should the poles not located at the origin end up providing a negligible solution with respect to the pole at the origin, then use of the Residue Theorem provides essentially the same answer or a slightly higher fidelity answer as the Taylor Theorem.

Residue Theorem Applied to Vector Potential Equations

As stated previously the Residue Theorem can solve the vector potential integrals since the integrals are closed form bounded analytic equations with more analytic poles than zeros.

$$\text{Residue Theorem: } \int_c \mathrm{f}(c)\,d(c) = 2\pi j \sum(\text{Residues}) \tag{3.77}$$

$$\text{Single Residue: } \mathrm{a}_{-1} = \lim_{c \to \mathrm{a}} \left\{ \frac{1}{(\text{n-1})!} \frac{d^{n-1}}{dc^{n-1}} \left[(c-a)^n \, f(z) \right] \right\} \text{ ; Where: n=order}$$

$$\text{Residue at a simple pole: } \mathrm{a}_{-1} = \lim_{c \to \mathrm{a}} \left[(c-a)\, f(z) \right]$$

The Residue Theorem is only applied to the air gap magnetic potential, A_3 with the assumption that all of the air gap magnetic potential enters the secondary. The tangential component of this magnetic potential on the secondary surface produces the repulsive lift force. The normal component of this magnetic potential on the secondary surface produces a centering force in the static solenoid case of Phase I and a drag force or drag loss in the dynamic solenoid cases of Phases II, III, and IV. The constraints of this analysis also maintain a conservation of flux as indicated by equations (3.49) and (3.50). In reality all of the primary flux produced does not enter

the secondary. Any primary flux that does not enter the secondary is a loss of some sort with respect to the primary's input.

Since only A_3 is considered, equation (3.74) is re-written in a form more suited for the Residue Theorem by manipulating the exponents.

$$A_3(y,z) = \frac{j\mu_3 |K_1|}{2\pi} \int_{-\infty}^{\infty} \frac{G_3(\xi,z) \left[e^{j(y-r_{2\_out})\xi} e^{-j\beta r_{2\_out}} - e^{j(y-r_{2\_in})\xi} e^{-j\beta r_{2\_in}} \right]}{\xi(\xi+\beta) H(\xi)} d\xi \quad ; \text{For: } 0 \le z \le z_g \tag{3.78}$$

The complex poles of equation (3.76) have both real and imaginary components where $\xi = \xi_{Real} + \xi_{Imaginary} = \xi_R + \xi_I$ holds true. By referring to the numerator inside the integral of equation (3.78), it is evident that the real and imaginary components of the complex poles determine the dynamic motion vector potential damping through the exponential sign as $\xi \to \infty$. The referenced numerator of equation (3.78) is re-written and broken into two logical components. These components are used about the physical domain $r_{2\_in} < y < r_{2\_out}$.

$$\overbrace{e^{j(y-r_{2\_out})\xi} e^{-j\beta r_{2\_out}}}^{\text{Term 1}} \overbrace{- e^{j(y-r_{2\_in})\xi} e^{-j\beta r_{2\_in}}}^{\text{Term 2}} \tag{3.79}$$

Equation (3.78) is an improper real definite integral of the form represented in the following equation.

$$\int_{-\infty}^{\infty} f(x) dx = \lim_{R_1 \to \infty} \int_{-R_1}^{0} f(x) dx + \lim_{R_2 \to \infty} \int_{0}^{R_2} f(x) dx$$

This leads to the Cauchy Principle Value since the single, combined limit exists. The integration contours themselves must enclose four singularities of significance within their domains. Two difficulties are posed in acquiring the proper integration contours. One difficulty involves the two singularities on the real axis in which the integration contour along the real axis must be modified to either include or exclude these singularities. The second difficulty involves the two complex pole singularities of significance that reside on both the positive and negative imaginary planes. Therefore two separate integration contours, one in the positive imaginary

domain and one in the negative imaginary domain, are required to obtain the complete solution of poles for the Residue Theorem. The integration contours about the poles of significance are shown in Figure 3.3-8. Now that the complex poles are solved the system is deterministic for the poles in question.

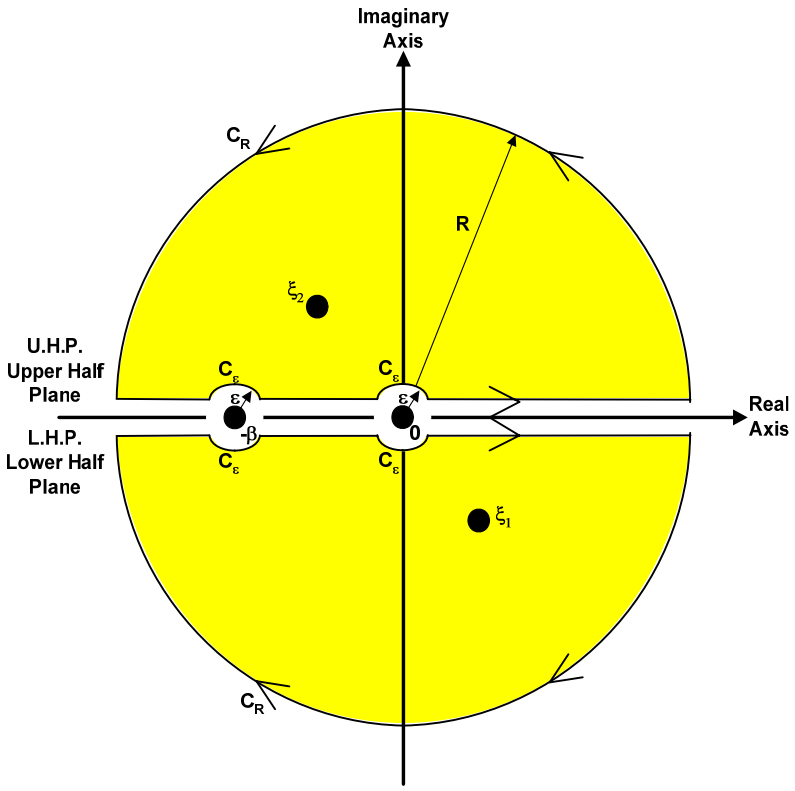

Figure 3.3-8: Vector Potential Poles and Integration Contours

The Residue Theorem has four poles of significance to solve. Figure 3.3-8 assumes two contours of interest. One contour encompasses the upper half plane, U.H.P., and the other contour encompasses the lower half plane, L.H.P. The counterclockwise contour enclosing each pole is taken as the positive direction. The complex pole $\xi = \xi_2$ is solved with a counterclockwise contour in the U.H.P. The complex pole $\xi = \xi_1$ is solved with a clockwise contour in the L.H.P. The real poles are solved with clockwise contours in the U.H.P. and counterclockwise contours in

the L.H.P. The same contour radius, ε, is assumed for both real axis poles. Both complex contours follow positive paths around the complex poles and negative paths around the negative real and zero poles. In this case the Residue Theorem, equation (3.77), follows the general format of equation (3.80) where P.V. stands for Cauchy's Principle Value.

$$\int_C f(c)\,d(c) = \int_{-\infty}^{-\varepsilon} f(c)\,dc + \int_{C_\varepsilon} f(c)\,dc + \int_{-\varepsilon}^{\varepsilon} f(c)\,dc + \int_{C_\varepsilon} f(c)\,dc + \int_{\varepsilon}^{\infty} f(c)\,dc +$$

$$\cancel{\int_{C_R} f(c)\,dc} = \int_{-\infty}^{\infty} f(c)\,dc + 2\overbrace{\int_{C_\varepsilon} f(c)\,dc}^{P.V.} = 2\pi j \sum(\text{Residues}) = \tag{3.80}$$

$$= 2\pi j \sum(\text{Enclosed Complex Plane Residues}) +$$

$$+\pi j \sum(\text{Real Axis Residues = P.V.})$$

Residue Theorem Contours from Physical Boundary Conditions

Complex plane Residue Theorem integration contours of Figure 3.3-8 are now determined for each pole as per the physical boundary condition constraints imposed by the problem. Table 3.3-2 was created to summarize these contour relations.

For $y<r_{2\_in}$:

Term 1: $[(y - r_{2\_out}) = (-d)]$: $e^{j(-d)(\xi_R + j\xi_I)} e^{-j\beta r_{2\_out}} = e^{\xi_I - j(d\xi_R + \beta r_{2\_out})}$: $(-j)$ term is in L.H.P.

Term 2: $[(y - r_{2\_in}) = (-d)]$: $-e^{j(-d)(\xi_R + j\xi_I)} e^{-j\beta r_{2\_in}} = -e^{\xi_I - j(d\xi_R + \beta r_{2\_in})}$: $(-j)$ term is in L.H.P.

For $y>r_{2\_out}$:

Term 1: $[(y - r_{2\_out}) = (d)]$: $e^{j(d)(\xi_R + j\xi_I)} e^{-j\beta r_{2\_out}} = e^{-\xi_I + j(d\xi_R - \beta r_{2\_out})}$: $(+j)$ term is in U.H.P.

Term 2: $[(y - r_{2\_in}) = (\mathrm{d})]$: $-e^{j(d)(\xi_R + j\xi_I)} e^{-j\beta r_{2\_in}} = -e^{-\xi_I + j(d\xi_R - \beta r_{2\_in})}$: $(+j)$ term is in U.H.P.

Note that the $d\xi_R$ terms are assumed to dominate the βr_2 terms.

<u>For $r_{2\_in} < y < r_{2\_out}$:</u>

Term 1: $[(y - r_{2\_out}) = (\text{-d})]$: Same solution as Term 1 for $y < r_{2\_in}$:$(-j)$ term is in L.H.P.

Term 2: $[(y - r_{2\_in}) = (\mathrm{d})]$: Same solution as Term 2 for $y > r_{2\_out}$: $(+j)$ term is in U.H.P.

Table 3.3-2: Existing Residue Theorem Integration Contours to Solve

Physical Boundary Conditions	**Equation (3.79) numerator terms**		**Poles to solve with sign of Residue Theorem from contour direction**	
	Term 1	**Term 2**	**L.H.P.**	**U.H.P.**
$y < r_{2\_in}$	L.H.P.	L.H.P.	ξ_1 w/ (-) contour	
			$0, -\beta$ w/ (+) contour	
$r_{2\_in} < y < r_{2\_out}$	L.H.P.	U.H.P.	ξ_1 w/ (-) contour	ξ_2 w/ (+) contour
			$0, -\beta$ w/ (+) contour	$0, -\beta$ w/ (-) contour
$y > r_{2\_out}$	U.H.P.	U.H.P.		ξ_2 w/ (+) contour
				$0, -\beta$ w/ (-) contour

Residues at each Pole per Physical Boundary Conditions

Table 3.3-2 helps determine the residues at each pole as per the physical boundary condition constraints imposed by the problem. Note that the boundary is defined for the y axis here, but the true boundary condition is defined for any direction which describes the relative mechanical propulsion direction and hence experiences a relative mechanical velocity component in that direction. As per Figure 3.3-7 this boundary condition may take the form or either the x or y axis or a combination of these axes.

Table 3.3-2 combined with Figure 3.3-8 illustrates the exact physical meaning of the boundary condition each pole represents. The infinitesimal integration paths about the real axis poles 0 and $-\beta$ characterize the general traveling $\vec{B}$ wave component solution along the boundary $0 \le y \le r_{2\_out}$. The U.H.P integration path about the complex pole ξ_2 characterizes the positive y axis direction dynamic motion $\vec{B}$ traveling end wave solution at the boundary $y > r_{2\_out}$. This is known as the entry end effect wave if the system has a relative mechanical velocity in the positive y axis direction. The L.H.P integration path about the complex pole ξ_1 characterizes the negative y axis direction dynamic motion $\vec{B}$ traveling end wave solution at the boundary $y < 0$. This is known as the exit end effect wave if the system has a relative mechanical velocity in the positive y axis direction. These definitions are used to categorize equation (3.100) and (3.101) components.

Differential $H(\xi)$ Term of Denominator:

In determining residues the $H(\xi)$ term of the denominator follows the product rule for differentiation. Recall that the $H(\xi)$ poles are ξ_1 and ξ_2 in equation (3.75).

$$H(\xi) = \sqrt{(\xi - \xi_1)(\xi - \xi_2)}$$

Note that the following ξ_1 and ξ_2 pole dependent residue terms of equations (3.85) through (3.94) have a $(\xi-\xi_1)$ numerator term for the $\xi=\xi_1$ pole and a $(\xi-\xi_2)$ numerator term for the $\xi=\xi_2$ pole stemming from the residue equation. This would make the entire ξ_1 and ξ_2 pole residues equal to zero which equates to no orthogonal velocity dynamic motion secondary end effects. Therefore only 0 and β general traveling wave $\vec{B}$ component pole residues remain. An example is provided in equation (3.81) for the $y<r_{2\_in}$ region.

$$\left(\text{Residue @ } \xi=\xi_1\right)= =\left(\frac{j\mu_3|K_1|}{2\pi}\right)\lim_{\xi=\xi_1}\left\{\frac{1}{(1-1)!}\frac{d^0}{d\xi^0}\left\{(\xi-\xi_1)^0\left[\frac{\left[e^{j(y-r_{2\_out})\xi}e^{-j\beta r_{2\_out}}-\right]}{\xi(\xi+\beta)}\bullet\frac{G_3(\xi,z)}{H(\xi)}\right]\right\}\right\}=0 \quad (3.81)$$

Physically the effects of the ξ_1 and ξ_2 poles are only negligible when the orthogonal velocity is relatively small for the surrounding material, geometry, and electrical frequency effects. The orthogonal velocity effect is not negligibly small in dynamic Phases II through IV and hence must be accounted. This is accomplished by multiplying each residue equation for the ξ_1 and ξ_2 poles by $\frac{\gamma_{original}}{\gamma}=1$ where $\gamma_{original}$ equals the original definition shown in equation (3.75) and γ equals the pole definition also shown in equation (3.75). Both γ forms are pole dependent as shown in later equations when the poles ξ_1, ξ_2, and $-\beta$ are inserted into the γ or $\gamma_{original}$ equations to produce the proper form of each equation. If the pole definition of γ is used in the numerator of the residue equations instead of $\gamma_{original}$ then the residues will again erroneously equal zero. The pole definition derivative of γ^2 is

now determined to provide term cancellation for the appropriate residue terms as shown in equations (3.82) through (3.84).

$$\left[H(\xi)\right]^2 = \gamma^2 = (\xi-\xi_1)(\xi-\xi_2) \tag{3.82}$$

$$\frac{d\left[H(\xi)^2\right]}{d\xi} = \left[H(\xi)^2\right]' = \left[(\xi-\xi_1)+(\xi-\xi_2)\right]$$

$$H_{prime\_\xi 1} = \left[H(\xi=\xi_1)^2\right]' = (\xi-\xi_2) = (\xi_1-\xi_2) \tag{3.83}$$

$$H_{prime\_\xi 2} = \left[H(\xi=\xi_2)^2\right]' = (\xi-\xi_1) = (\xi_2-\xi_1) \tag{3.84}$$

For $y<r_{2\_in}$:

$$(\text{Residue @ } \xi=\xi_1) =$$

$$= \left(\frac{j\mu_3|K_1|}{2\pi}\right)\lim_{\xi=\xi_1}\left\{\frac{1}{(1-1)!}\frac{d^0}{d\xi^0}\left\{(\xi-\xi_1)\left[\frac{e^{j(y-r_{2\_out})\xi}e^{-j\beta r_{2\_out}} - e^{j(y-r_{2\_in})\xi}e^{-j\beta r_{2\_in}}}{\xi(\xi+\beta)}\bullet\frac{\gamma_{original}G_3(\xi,z)}{(\xi-\xi_1)(\xi-\xi_2)}\right]\right\}\right\}$$

$$(\text{Residue @ } \xi=\xi_1) = \left(\frac{j\mu_3|K_1|}{2\pi}\right)\left\{\frac{\left[e^{j(y-r_{2\_out})\xi_1}e^{-j\beta r_{2\_out}} - e^{j(y-r_{2\_in})\xi_1}e^{-j\beta r_{2\_in}}\right]}{\xi_1(\xi_1+\beta)}\bullet\frac{\gamma_{original}G_3(\xi_1,z)}{H_{prime\_\xi 1}}\right\} \tag{3.85}$$

For $y>r_{2\_out}$:

$$(\text{Residue @ } \xi=\xi_2) =$$

$$= \left(\frac{j\mu_3|K_1|}{2\pi}\right)\lim_{\xi=\xi_2}\left\{(\xi-\xi_2)\left[\frac{e^{j(y-r_{2\_out})\xi}e^{-j\beta r_{2\_out}} - e^{j(y-r_{2\_in})\xi}e^{-j\beta r_{2\_in}}}{\xi(\xi+\beta)}\bullet\frac{\gamma_{original}G_3(\xi,z)}{(\xi-\xi_1)(\xi-\xi_2)}\right]\right\}$$

$$\left(\text{Residue @ } \xi=\xi_2\right)=\left(\frac{j\mu_3|K_1|}{2\pi}\right)\left\{\frac{\left[\begin{array}{l}e^{j\left(y-r_{2\_out}\right)\xi_2}e^{-j\beta r_{2\_out}}-\\-e^{j\left(y-r_{2\_in}\right)\xi_2}e^{-j\beta r_{2\_in}}\end{array}\right]}{\xi_2\left(\xi_2+\beta\right)}\bullet\frac{\gamma_{original}G_3\left(\xi_2,z\right)}{H_{prime\_\xi 2}}\right\} \quad (3.86)$$

For $y<r_{2\_in}$ and $y>r_{2\_out}$:

$$\left(\text{Residue @ } \xi=0\right)=$$

$$=\left(\frac{j\mu_3|K_1|}{2\pi}\right)\lim_{\xi=0}\left\{\cancel{(\xi-0)}\left[\frac{e^{j\left(y-r_{2\_out}\right)\xi}e^{-j\beta r_{2\_out}}-e^{j\left(y-r_{2\_in}\right)\xi}e^{-j\beta r_{2\_in}}}{\cancel{\xi}\left(\xi+\beta\right)}\bullet\frac{G_3\left(\xi,z\right)}{H\left(\xi\right)}\right]\right\}$$

$$=\left(\frac{j\mu_3|K_1|}{2\pi}\right)\left[\frac{\cancel{e^{0}}^{1}e^{-j\beta r_{2\_out}}-\cancel{e^{0}}^{1}e^{-j\beta r_{2\_in}}}{\left(0+\beta\right)}\bullet\frac{G_3\left(\xi,z\right)}{H\left(\xi\right)}\right]$$

$$\left(\text{Residue @ } \xi=0\right)=\left(\frac{j\mu_3|K_1|}{2\pi}\right)\left[\frac{e^{-j\beta r_{2\_out}}-e^{-j\beta r_{2\_in}}}{\beta}\bullet\frac{G_3\left(\xi=0,z\right)}{H\left(\xi=0\right)}\right] \quad (3.87)$$

$$\left(\text{Residue @ } \xi=-\beta\right)=$$

$$=\left(\frac{j\mu_3|K_1|}{2\pi}\right)\lim_{\xi=-\beta}\left\{\cancel{(\xi+\beta)}\left[\frac{e^{j\left(y-r_{2\_out}\right)\xi}e^{-j\beta r_{2\_out}}-e^{j\left(y-r_{2\_in}\right)\xi}e^{-j\beta r_{2\_in}}}{\xi\cancel{\left(\xi+\beta\right)}}\bullet\frac{G_3\left(\xi,z\right)}{H\left(\xi\right)}\right]\right\}$$

$$=\left(\frac{j\mu_3|K_1|}{2\pi}\right)\left[\frac{\cancel{e^{-j\beta y}e^{j\beta r_{2\_out}}e^{-j\beta r_{2\_out}}-e^{-j\beta y}e^{j\beta r_{2\_in}}e^{-j\beta r_{2\_in}}}^{0}}{-\beta}\bullet\frac{G_3\left(-\beta,z\right)}{H\left(-\beta\right)}\right]=0$$

$$\left(\text{Residue @ } \xi=-\beta\right)=0 \quad (3.88)$$

For $r_{2\_in}<y<r_{2\_out}$:

$$\left(\text{Residue @ } \xi=\xi_1 \text{ for Term 1}\right)=$$

$$=\left(\frac{j\mu_3|K_1|}{2\pi}\right)\lim_{\xi=\xi_1}\left\{\cancel{(\xi-\xi_1)}\left[\frac{e^{j\left(y-r_{2\_out}\right)\xi}e^{-j\beta r_{2\_out}}}{\xi\left(\xi+\beta\right)}\bullet\frac{\gamma_{original}G_3\left(\xi,z\right)}{\cancel{(\xi-\xi_1)}\left(\xi-\xi_2\right)}\right]\right\}$$

$$\left(\text{Residue @ } \xi=\xi_1 \text{ for Term 1}\right)=\left(\frac{j\mu_3|K_1|}{2\pi}\right)\left[\frac{e^{j\left(y-r_{2\_out}\right)\xi_1}e^{-j\beta r_{2\_out}}}{\xi_1\left(\xi_1+\beta\right)}\bullet\frac{\gamma_{original}G_3\left(\xi_1,z\right)}{H_{prime\_\xi 1}}\right]$$

(3.89)

$$\left(\text{Residue @ } \xi=\xi_2 \text{ for Term 2}\right)=$$

$$=\left(\frac{j\mu_3|K_1|}{2\pi}\right)\lim_{\xi=\xi_2}\left\{\cancel{(\xi-\xi_2)}\left[\frac{-e^{j(y-r_{2\_in})\xi}e^{-j\beta r_{2\_in}}}{\xi(\xi+\beta)}\bullet\frac{\gamma_{original}G_3(\xi,z)}{(\xi-\xi_1)\cancel{(\xi-\xi_2)}}\right]\right\}$$

$$\left(\text{Residue @ } \xi=\xi_2 \text{ for Term 2}\right)=\left(\frac{-j\mu_3|K_1|}{2\pi}\right)\left[\frac{e^{j(y-r_{2\_in})\xi_2}e^{-j\beta r_{2\_in}}}{\xi_2(\xi_2+\beta)}\bullet\frac{\gamma_{original}G_3(\xi_2,z)}{H_{prime\_\xi 2}}\right] \quad (3.90)$$

$$\left(\text{Residue @ } \xi=0 \text{ for Term 1}\right)=$$

$$=\left(\frac{j\mu_3|K_1|}{2\pi}\right)\lim_{\xi=0}\left\{\cancel{(\xi-0)}\left[\frac{e^{j(y-r_{2\_out})\xi}e^{-j\beta r_{2\_out}}}{\cancel{\xi}(\xi+\beta)}\bullet\frac{G_3(\xi,z)}{H(\xi)}\right]\right\}$$

$$=\left(\frac{j\mu_3|K_1|}{2\pi}\right)\left[\frac{\cancel{e^{0}}^{1}e^{-j\beta r_{2\_out}}}{(0+\beta)}\bullet\frac{G_3(\xi,z)}{H(\xi)}\right]$$

$$\left(\text{Residue @ } \xi=0 \text{ for Term 1}\right)=\left(\frac{j\mu_3|K_1|}{2\pi}\right)\left[\frac{e^{-j\beta r_{2\_out}}}{\beta}\bullet\frac{G_3(\xi=0,z)}{H(\xi=0)}\right] \quad (3.91)$$

$$\left(\text{Residue @ } \xi=0 \text{ for Term 2}\right)=$$

$$=\left(\frac{j\mu_3|K_1|}{2\pi}\right)\lim_{\xi=0}\left\{\cancel{(\xi-0)}\left[\frac{-e^{j(y-r_{2\_in})\xi}e^{-j\beta r_{2\_in}}}{\cancel{\xi}(\xi+\beta)}\bullet\frac{G_3(\xi,z)}{H(\xi)}\right]\right\}$$

$$=\left(\frac{j\mu_3|K_1|}{2\pi}\right)\left[\frac{-\cancel{e^{0}}^{1}e^{-j\beta r_{2\_in}}}{(0+\beta)}\bullet\frac{G_3(\xi,z)}{H(\xi)}\right]$$

$$\left(\text{Residue @ } \xi=0 \text{ for Term 2}\right)=\left(\frac{-j\mu_3|K_1|}{2\pi}\right)\left[\frac{e^{-j\beta r_{2\_in}}}{\beta}\bullet\frac{G_3(\xi=0,z)}{H(\xi=0)}\right] \quad (3.92)$$

$$\left(\text{Residue @ } \xi=-\beta \text{ for Term 1}\right)=$$

$$=\left(\frac{j\mu_3|K_1|}{2\pi}\right)\lim_{\xi=-\beta}\left\{\cancel{(\xi+\beta)}\left[\frac{e^{j(y-r_{2\_out})\xi}e^{-j\beta r_{2\_out}}}{\xi\cancel{(\xi+\beta)}}\bullet\frac{G_3(\xi,z)}{H(\xi)}\right]\right\}$$

$$=\left(\frac{j\mu_3|K_1|}{2\pi}\right)\left[\frac{e^{-j\beta y}e^{j\beta r_{2\_out}}e^{-j\beta r_{2\_out}}}{-\beta}\bullet\frac{G_3(-\beta,z)}{H(-\beta)}\right]$$

$$\left(\text{Residue @ } \xi=-\beta \text{ for Term 1}\right)=\left(\frac{j\mu_3|K_1|}{2\pi}\right)\left[\frac{e^{-j\beta y}}{-\beta}\bullet\frac{G_3(-\beta,z)}{H(-\beta)}\right] \qquad (3.93)$$

$$\left(\text{Residue @ } \xi=-\beta \text{ for Term 2}\right)=$$

$$=\left(\frac{j\mu_3|K_1|}{2\pi}\right)\lim_{\xi=-\beta}\left\{\cancel{(\xi+\beta)}\left[\frac{e^{j\left(y-r_{2\_out}\right)\xi}e^{-j\beta r_{2\_out}}-e^{j\left(y-r_{2\_in}\right)\xi}e^{-j\beta r_{2\_in}}}{\xi\cancel{(\xi+\beta)}}\bullet\frac{G_3(\xi,z)}{H(\xi)}\right]\right\}$$

$$=\left(\frac{j\mu_3|K_1|}{2\pi}\right)\left[\frac{-e^{-j\beta y}e^{j\beta r_{2\_in}}e^{-j\beta r_{2\_in}}}{-\beta}\bullet\frac{G_3(-\beta,z)}{H(-\beta)}\right]$$

$$\left(\text{Residue @ } \xi=-\beta \text{ for Term 2}\right)=\left(\frac{-j\mu_3|K_1|}{2\pi}\right)\left[\frac{e^{-j\beta y}}{-\beta}\bullet\frac{G_3(-\beta,z)}{H(-\beta)}\right] \qquad (3.94)$$

Vector Potential Equations: General Form

The general forms of the vector potentials in region 3, the air gap region, are determined by plugging equations (3.85) through (3.94) into equation (3.80) where the $H(\xi)$ term is determined in equation (3.75) and the appropriate derivatives of $H(\xi)$ are determined by equations (3.82) through (3.84). Recall that via the Cauchy Principle Value the simple poles on the contours of interest are multiplied by πj instead of $2\pi j$ due to the respective semicircles with radius ε. Also recall that the sign of the residues was determined in Table 3.3-2.

For $y<r_{2\_in}$:

$$A_3(y,z)=\int_c f(z)\,d(z)=-2\pi j\left(\text{Residue @ } \xi=\xi_1\right)+$$

$$+\pi j\left[\left(\text{Residue @ } \xi=0\right)+\overbrace{\left(\text{Residue @ } \xi=-\beta\right)}^{=0}\right]$$

$$A_3(y,z)=\mu_3\left|K_1\right|\left\{\left[\frac{\left[\begin{array}{l}e^{j\left(y-r_{2\_out}\right)\xi_1}e^{-j\beta r_{2\_out}}-\\-e^{j\left(y-r_{2\_in}\right)\xi_1}e^{-j\beta r_{2\_in}}\end{array}\right]}{\xi_1\left(\xi_1+\beta\right)}\bullet\frac{\gamma_{original}G_3\left(\xi_1,z\right)}{H_{prime\_\xi1}}\right]-\right.$$
$$\left.-\left[\frac{e^{-j\beta r_{2\_out}}-e^{-j\beta r_{2\_in}}}{2\beta}\bullet\frac{G_3\left(\xi=0,z\right)}{H\left(\xi=0\right)}\right]\right\} \quad (3.95)$$

For $y>r_{2\_out}$:

$$A_3(y,z)=\int_c f(z)\,d(z)=2\pi j\left(\text{Residue @ }\xi=\xi_2\right)-$$
$$-\pi j\left[\left(\text{Residue @ }\xi=0\right)+\overbrace{\left(\text{Residue @ }\xi=-\beta\right)}^{=0}\right]$$

$$A_3(y,z)=\mu_3\left|K_1\right|\left\{\begin{array}{l}-\left[\dfrac{e^{j\left(y-r_{2\_out}\right)\xi_2}e^{-j\beta r_{2\_out}}-e^{j\left(y-r_{2\_in}\right)\xi_2}e^{-j\beta r_{2\_in}}}{\xi_2\left(\xi_2+\beta\right)}\bullet\dfrac{\gamma_{original}G_3\left(\xi_2,z\right)}{H_{prime\_\xi2}}\right]+\\+\left[\dfrac{e^{-j\beta r_{2\_out}}-e^{-j\beta r_{2\_in}}}{2\beta}\bullet\dfrac{G_3\left(\xi=0,z\right)}{H\left(\xi=0\right)}\right]\end{array}\right\} \quad (3.96)$$

For $r_{2\_in}<y<r_{2\_out}$:

$$A_3(y,z)=\int_c f(z)\,d(z)=2\pi j\left[\begin{array}{l}-\left(\text{Residue @ }\xi=\xi_1\text{ for Term 1}\right)+\\\left(\text{Residue @ }\xi=\xi_2\text{ for Term 2}\right)\end{array}\right]+$$
$$+\pi j\left[\begin{array}{l}\left(\text{Residue @ }\xi=0\text{ for Term 1}\right)-\left(\text{Residue @ }\xi=0\text{ for Term 2}\right)+\\+\left(\text{Residue @ }\xi=-\beta\text{ for Term 1}\right)-\left(\text{Residue @ }\xi=-\beta\text{ for Term 2}\right)\end{array}\right]$$

$$A_3(y,z)=\mu_3|K_1|\left\{\begin{array}{l}\left[\dfrac{e^{j(y-r_{2\_out})\xi_1}e^{-j\beta r_{2\_out}}}{\xi_1(\xi_1+\beta)}\bullet\dfrac{\gamma_{original}G_3(\xi_1,z)}{H_{prime\_\xi 1}}\right]+\\ +\left[\dfrac{e^{j(y-r_{2\_in})\xi_2}e^{-j\beta r_{2\_in}}}{\xi_2(\xi_2+\beta)}\bullet\dfrac{\gamma_{original}G_3(\xi_2,z)}{H_{prime\_\xi 2}}\right]-\\ -\left[\dfrac{e^{-j\beta r_{2\_out}}}{2\beta}\bullet\dfrac{G_3(\xi=0,z)}{H(\xi=0)}\right]-\left[\dfrac{e^{-j\beta r_{2\_in}}}{2\beta}\bullet\dfrac{G_3(\xi=0,z)}{H(\xi=0)}\right]+\\ +\left[\dfrac{e^{-j\beta y}}{\beta}\bullet\dfrac{G_3(-\beta,z)}{H(-\beta)}\right]\end{array}\right\} \quad (3.97)$$

Comparing equations (3.72) and (3.73) reveal the general forms of the vector potentials in region 2, the secondary conductor region, which are determined through equation (3.97) by replacing $G_3(\xi,z)$ in the $A_3(y,z)$ equations and $2G_2(\xi,z)$ in the $A_2(y,z)$ equations along with the applicable z boundary conditions.

The unstable nature of the system developed in this paper is witnessed equation (3.97) for both the magnetic potential end effect and general waves. Lyapunov's second method for stability analysis for non-linear systems is not required if only looking at a quick piecewise linear form of the equation. As stated in Ogata [19] for a linear system which can in a general piecewise linear sense be applied to this non-linear system, if any of the closed loop poles lie in the right-half s plane, then with increasing time they give rise to the dominant mode, and the transient response increases monotonically or oscillates with increasing amplitude. This represents an unstable system. As previously mentioned in the discussion of equation (3.78) and depicted in the complex plane of Figure 3.3-8, it is evident that the real and imaginary components of the complex poles of this system determine that the dynamic motion vector potential damping is unstable.

Magnetic Flux Density Equations: General Form

The magnetic flux density equations are derived from equation (3.21). As discussed when initially applying the Residue Theorem, the tangential or y component as per Figure 3.3-7 on the secondary produces the repulsive lift force. The normal or z component of this potential on the secondary produces a centering force in the static solenoid case of Phase I and a drag force or drag loss in the dynamic solenoid cases of Phases II, III, and IV.

Normal Component (Static Centering or Dynamic Drag Force): $B_N = \vec{B}_z = -\frac{\partial A}{\partial y}\hat{a}_z$

Tangential Component (Lift Force): $B_T = \vec{B}_y = \frac{\partial A}{\partial z}\hat{a}_y$

Expand all $A_3(y,z)$ z dependent terms to find the partial derivative with respect to z for the lift force component. The only z dependent term is $G_3(\xi,z)$ which is rewritten below as equation (3.98) for convenience. Recall from equation (3.78) that $A_3(y,z)$ is only valid for the z region of $0 \le z \le z_g$ and hence the same is true for $G_3(\xi,z)$ and all of its derivatives. Taking the partial derivative of z provides the $G_3'(\xi,z)$ term shown in equation (3.99). Note that in the Lagrangian generalized coordinate potential energy derivations in Phases III and IV, as witnessed in Chapters 3.5.a.i and 3.6.a.i respectively, the second partial derivative, $G_3''(\xi,z)$, is also taken. This type of analysis not needed for the magnetic flux density or body force derivations and hence will be reserved until required.

$$G_3(\xi,z)=(\xi+\gamma)\left\{\begin{array}{l}\left[\begin{array}{l}C_5\left(1+\dfrac{\gamma\mu_3}{\xi\mu_2}\right)+\\ +\left(1-\dfrac{\gamma\mu_3}{\xi\mu_2}\right)e^{2h_2\gamma}\end{array}\right]e^{(z-z_g)\xi}+\\ +\left[\begin{array}{l}C_5\left(1-\dfrac{\gamma\mu_3}{\xi\mu_2}\right)+\\ +\left(1+\dfrac{\gamma\mu_3}{\xi\mu_2}\right)e^{2h_2\gamma}\end{array}\right]e^{(z_g-z)\xi}\end{array}\right\}\ ;\ \text{For: } 0\le z\le z_g$$

For brevity perform the following substitutions on the previous equation for $G_3(\xi,z)$ to produce equation (3.98) and all subsequent forms of $G_3(\xi,z)$.

$$C_{GA}=(\xi+\gamma)\left[\begin{array}{l}C_5\left(1+\dfrac{\gamma\mu_3}{\xi\mu_2}\right)+\\ +\left(1-\dfrac{\gamma\mu_3}{\xi\mu_2}\right)e^{2h_2\gamma}\end{array}\right]$$

$$C_{GB}=(\xi+\gamma)\left[\begin{array}{l}C_5\left(1-\dfrac{\gamma\mu_3}{\xi\mu_2}\right)+\\ +\left(1+\dfrac{\gamma\mu_3}{\xi\mu_2}\right)e^{2h_2\gamma}\end{array}\right]$$

$$G_3(\xi,z)=\left[C_{GA}e^{(z-z_g)\xi}+C_{GB}e^{(z_g-z)\xi}\right]\ ;\ \text{For: } 0\le z\le z_g \qquad (3.98)$$

$$\frac{\partial G_3(\xi,z)}{\partial z}=G_3'(\xi,z)=\xi\left[C_{GA}e^{(z-z_g)\xi}-C_{GB}e^{(z_g-z)\xi}\right]\ ;\ \text{For: } 0\le z\le z_g \qquad (3.99)$$

<u>For y<r_{2_in}:</u>

$$B_{3z}(y,z)=-j\mu_3\xi_1\left|K_1\right|\left[\frac{e^{j(y-r_{2\_out})\xi_1}e^{-j\beta r_{2\_out}}-e^{j(y-r_{2\_in})\xi_1}e^{-j\beta r_{2\_in}}}{\xi_1(\xi_1+\beta)}\bullet\frac{\gamma_{original}G_3(\xi_1,z)}{H_{prime\_\xi 1}}\right]$$

$$B_{3y}(y,z)=\mu_3|K_1|\left\{\left[\frac{e^{j(y-r_{2\_out})\xi_1}e^{-j\beta r_{2\_out}}-e^{j(y-r_{2\_in})\xi_1}e^{-j\beta r_{2\_in}}}{\xi_1(\xi_1+\beta)}\bullet\frac{\gamma_{original}G_3'(\xi_1,z)}{H_{prime\_\xi 1}}\right]-\right.$$
$$\left.-\left[\frac{e^{-j\beta r_{2\_out}}-e^{-j\beta r_{2\_in}}}{2\beta}\bullet\frac{G_3'(\xi=0,z)}{H(\xi=0)}\right]\right\}$$

For $y>r_{2\_out}$:

$$B_{3z}(y,z)=j\mu_3\xi_2|K_1|\left[\frac{e^{j(y-r_{2\_out})\xi_2}e^{-j\beta r_{2\_out}}-e^{j(y-r_{2\_in})\xi_2}e^{-j\beta r_{2\_in}}}{\xi_2(\xi_2+\beta)}\bullet\frac{\gamma_{original}G_3(\xi_2,z)}{H_{prime\_\xi 2}}\right]$$

$$B_{3y}(y,z)=\mu_3|K_1|\left\{-\left[\frac{e^{j(y-r_{2\_out})\xi_2}e^{-j\beta r_{2\_out}}-e^{j(y-r_{2\_in})\xi_2}e^{-j\beta r_{2\_in}}}{\xi_2(\xi_2+\beta)}\bullet\frac{\gamma_{original}G_3'(\xi_2,z)}{H_{prime\_\xi 2}}\right]+\right.$$
$$\left.+\left[\frac{e^{-j\beta r_{2\_out}}-e^{-j\beta r_{2\_in}}}{2\beta}\bullet\frac{G_3'(\xi=0,z)}{H(\xi=0)}\right]\right\}$$

For $r_{2\_in}<y<r_{2\_out}$:

$$B_N=B_{3z}(y,z)=-j\mu_3|K_1|\left\{\overbrace{\left[\frac{\xi_1 e^{j(y-r_{2\_out})\xi_1}e^{-j\beta r_{2\_out}}}{\xi_1(\xi_1+\beta)}\bullet\frac{\gamma_{original}G_3(\xi_1,z)}{H_{prime\_\xi 1}}\right]}^{\text{Inside Radius Dynamic Traveling Wave }\bar{B}\text{ Component}}+\right.$$
$$+\overbrace{\left[\frac{\xi_2 e^{j(y-r_{2\_in})\xi_2}e^{-j\beta r_{2\_in}}}{\xi_2(\xi_2+\beta)}\bullet\frac{\gamma_{original}G_3(\xi_2,z)}{H_{prime\_\xi 2}}\right]}^{\text{Outside Radius Dynamic Traveling Wave }\bar{B}\text{ Component}}-$$
$$\left.-\overbrace{\left[e^{-j\beta y}\bullet\frac{G_3(-\beta,z)}{H(-\beta)}\right]}^{\text{General Traveling Wave }\bar{B}\text{ Component}}\right\}\quad(3.100)$$

$$B_{3y}\left(y,z\right)=\mu_3\left|K_1\right|\left\{\begin{array}{l}\overbrace{\left[\frac{e^{j\left(y-r_{2\_out}\right)\xi_1}e^{-j\beta r_{2\_out}}}{\xi_1\left(\xi_1+\beta\right)}\bullet\frac{\gamma_{original}G_3{}'\left(\xi_1,z\right)}{H_{prime\_\xi1}}\right]}^{\text{Inside Radius Dynamic Traveling Wave }\vec{\text{B}}\text{ Component}}+\\ +\overbrace{\left[\frac{e^{j\left(y-r_{2\_in}\right)\xi_2}e^{-j\beta r_{2\_in}}}{\xi_2\left(\xi_2+\beta\right)}\bullet\frac{\gamma_{original}G_3{}'\left(\xi_2,z\right)}{H_{prime\_\xi2}}\right]}^{\text{Outside Radius Dynamic Traveling Wave }\vec{\text{B}}\text{ Component}}-\\ \overbrace{-\left[\frac{e^{-j\beta r_{2\_out}}}{2\beta}\bullet\frac{G_3{}'\left(\xi=0,z\right)}{H\left(\xi=0\right)}\right]-\left[\frac{e^{-j\beta r_{2\_in}}}{2\beta}\bullet\frac{G_3{}'\left(\xi=0,z\right)}{H\left(\xi=0\right)}\right]+}^{\text{General Traveling Wave }\vec{\text{B}}\text{ Component}}\\ +\left[\frac{e^{-j\beta y}}{\beta}\bullet\frac{G_3{}'\left(-\beta,z\right)}{H\left(-\beta\right)}\right]\end{array}\right\}$$

$$B_T=B_{3y}\left(y,z\right)=\mu_3\left|K_1\right|\left\{\begin{array}{l}\overbrace{\left[\frac{e^{j\left(y-r_{2\_out}\right)\xi_1}e^{-j\beta r_{2\_out}}}{\xi_1\left(\xi_1+\beta\right)}\bullet\frac{\gamma_{original}G_3{}'\left(\xi_1,z\right)}{H_{prime\_\xi1}}\right]}^{\text{Inside Radius Dynamic Traveling Wave }\vec{\text{B}}\text{ Component}}+\\ +\overbrace{\left[\frac{e^{j\left(y-r_{2\_in}\right)\xi_2}e^{-j\beta r_{2\_in}}}{\xi_2\left(\xi_2+\beta\right)}\bullet\frac{\gamma_{original}G_3{}'\left(\xi_2,z\right)}{H_{prime\_\xi2}}\right]}^{\text{Outside Radius Dynamic Traveling Wave }\vec{\text{B}}\text{ Component}}-\\ \overbrace{-\left[\frac{\left(e^{-j\beta r_{2\_out}}+e^{-j\beta r_{2\_in}}\right)}{2\beta}\bullet\frac{G_3{}'\left(\xi=0,z\right)}{H\left(\xi=0\right)}\right]+}^{\text{General Traveling Wave }\vec{\text{B}}\text{ Component}}\\ +\left[\frac{e^{-j\beta y}}{\beta}\bullet\frac{G_3{}'\left(-\beta,z\right)}{H\left(-\beta\right)}\right]\end{array}\right\} \quad (3.101)$$

A discussion of why equation (3.100) provides the normal $\vec{B}$ component and equation (3.101) provides the tangential $\vec{B}$ component, as indicated in each of these

equations, is provided in the next section. Note that extra ξ based terms are maintained in the equations above. This allows for easier substitutions of constants for equation components when solving the system of equations. Recall that the general dynamic motion inside end radius and dynamic motion outside end radius traveling wave $\vec{B}$ components are explained in the discussion proceeding Table 3.3-2.

Note that in Phases III and IV where angular components also add to each respective air gap distance, B_N and B_T equations assume the forms of equations (3.102) and (3.103) which account for the air gap linear distances through the angular motions in the z_g dependency. Also note that these equations are single air gap coordinate axis dependent only which in this case the equations are z coordinate axis direction dependent only. A change of each respective variable occurs for the change in air gap axis dependency. For example, the z_g dependency turns into a y_g only dependency and the y variable of equations (3.102) and (3.103) depicting the secondary radius component changes to whichever applicable axis is located orthogonal to the y coordinate axis when discussing the y coordinate axis air gap distances in Phases III and IV.

$$B_N = B_{3z}\left(y, z_g\right) = -j\mu_3 \left|K_1\right| \left\{ \overbrace{\left[\frac{\xi_1 e^{j\left(y - r_{2\_out}\right)\xi_1} e^{-j\beta r_{2\_out}}}{\xi_1\left(\xi_1 + \beta\right)} \bullet \frac{\gamma_{original} G_3\left(\xi_1, z_g\right)}{H_{prime\_\xi 1}} \right]}^{\text{Inside Radius Dynamic Traveling Wave } \bar{B} \text{ Component}} + \right.$$

$$\overbrace{\left[\frac{\xi_2 e^{j\left(y - r_{2\_in}\right)\xi_2} e^{-j\beta r_{2\_in}}}{\xi_2\left(\xi_2 + \beta\right)} \bullet \frac{\gamma_{original} G_3\left(\xi_2, z_g\right)}{H_{prime\_\xi 2}} \right]}^{\text{Outside Radius Dynamic Traveling Wave } \bar{B} \text{ Component}} - \left\} \right. \quad (3.102)$$

$$\left. - \overbrace{\left[e^{-j\beta y} \bullet \frac{G_3\left(-\beta, z_g\right)}{H\left(-\beta\right)} \right]}^{\text{General Traveling Wave } \bar{B} \text{ Component}} \right\}$$

$$B_T = B_{3y}\left(y, z_g\right) = \mu_3 \left|K_1\right| \left\{ \overbrace{\left[\frac{e^{j\left(y-r_{2\_out}\right)\xi_1} e^{-j\beta r_{2\_out}}}{\xi_1\left(\xi_1+\beta\right)} \bullet \frac{\gamma_{original} G_3'\left(\xi_1, z_g\right)}{H_{prime\_\xi 1}} \right]}^{\text{Inside Radius Dynamic Traveling Wave } \bar{B} \text{ Component}} + \right.$$

$$+ \overbrace{\left[\frac{e^{j\left(y-r_{2\_in}\right)\xi_2} e^{-j\beta r_{2\_in}}}{\xi_2\left(\xi_2+\beta\right)} \bullet \frac{\gamma_{original} G_3'\left(\xi_2, z_g\right)}{H_{prime\_\xi 2}} \right]}^{\text{Outside Radius Dynamic Traveling Wave } \bar{B} \text{ Component}} -$$

$$- \overbrace{\left[\frac{\left(e^{-j\beta r_{2\_out}} + e^{-j\beta r_{2\_in}}\right)}{2\beta} \bullet \frac{G_3'\left(\xi = 0, z_g\right)}{H\left(\xi = 0\right)} \right]}^{\text{General Traveling Wave } \bar{B} \text{ Component}} +$$

$$\left. + \left[\frac{e^{-j\beta y}}{\beta} \bullet \frac{G_3'\left(-\beta, z_g\right)}{H\left(-\beta\right)} \right] \right\} \qquad (3.103)$$

3.3.a.iii Solenoid Forcing Function and Output Parameters

Forces Impinging on Secondary

$$\vec{F} = \vec{J} \times \vec{B} \qquad (3.104)$$

$\vec{B}$ is solved for the transient and steady state wave values of the general and dynamic motion end effect traveling wave $\vec{B}$ components, normal and tangential $\vec{B}$ components on the secondary surface. Only the $\vec{B}$ that interacts with the secondary provides forces on the secondary. This occurs within the $r_{2\_in}<y<r_{2\_out}$ region at the boundary between the conductor and air gap where $z = z_g$. At this location equation (3.100) provides the normal $\vec{B}$ component and equation (3.101) provides the tangential $\vec{B}$ component. The body force equation, equation (3.104), now provides the secondary force density as described in Woodson and Melcher [23]. This time average force law integrates to solve $\vec{B}$ over the entire secondary surface opposing the primary solenoid. This is done by assuming a parallel facing and coaxial primary

and secondary with a constant $\vec{B}$ across the secondary surface at all radial points as discussed when describing Figure 3.3-7. The radial direction is provided by rotating the y axis in Figure 3.3-7.

This analysis is adequate for solving Phase I. There are three assumptions with this Phase I analysis which introduces errors in the Phase II through IV analysis. These assumptions are now described. The first assumption is the case of non-parallel primary and secondary faces. In Phase I the primary and secondary faces are held fixed in parallel. In Phases II through IV this error is considered negligible since the maximum angle from a non-parallel face condition is considered small enough to not affect the force equations. The second assumption is a non-concentric axis between the primary and secondary. In all Phases of this paper the primary is a solenoid, but the secondary is a disk or ring during Phase I where the primary and secondary are held coaxially fixed. In Phases II through IV the secondary is actually a current sheet. The geometry of Figure 3.3-7 still holds for Phases II through IV since the ring secondary of the figure represents the most conservative case of the maximum influence zone of the ring primary on the secondary only. In this case the primary is only solved for a single pole pitch as in an actual solenoid primary case. The third assumption taken is the means by which the Phase II through IV dynamic effects of the primary moving with respect to the secondary affects the system. A drag force is only produced by the primary radial current component that is orthogonal to the direction of primary to secondary relative motion. Since the primary is a circular face opposing the secondary, this orthogonal length is minimal. Therefore the magnetic drag is approximated by taking the maximum circular drag force component at the front and back ends of the primary with respect to the relative motion and assuming an effective orthogonal length for the drag force which accounts for the circular front and back end magnetic drag components. The conservative maximum drag force case of using an effective length that is two times the circular diameter is used in the dynamic case magnetic drag calculations.

Determine the forces impinging on the secondary with equation (3.104). The direct form of the real components of this equation assumes the form $\vec{F} = \mathrm{Re}(\vec{J}) \bullet \mathrm{Re}(\vec{B})$ which contains double frequency components that generate noise but do not produce a time average force. When the double frequency components are neglected the time average force density in $\left(\frac{\mathrm{N}}{\mathrm{m}^3}\right)$ S.I. units is found from the following identity, equation (3.105), where $\hat{A} = \left(\text{Phasor form of } A\right)$ and $\hat{B} = \left(\text{Phasor form of } \vec{B}\right)$.

$$\left\langle \mathrm{Re}\left(\hat{A}e^{j\omega t}\right)\mathrm{Re}\left(\hat{B}e^{j\omega t}\right)\right\rangle \equiv \frac{1}{2}\mathrm{Re}\left(\hat{A}\hat{B}^{*}\right) \tag{3.105}$$

Use equation (3.105) to solve the phasors $\hat{J}_x$, $\hat{B}_N$, and $\hat{B}_T$. The secondary current in the region of interest is expanded in equation (3.106) as per the higher order analysis solution for $\hat{B}_N$ provided by equation (3.100). Note that the $e^{j\omega t}$ phasor component is not suppressed as is common in phasor notation. This is to demonstrate the angular component cancellation witnessed in equation (3.108) for $\hat{B}_N$ and $\hat{B}_T$.

$$\text{Secondary Current: } \hat{J}_x = \frac{1}{\mu} \bullet \frac{d}{dy}\left[B_N e^{j(\omega t - \beta y)}\right]$$

<u>For $r_{2\_in} \le y \le r_{2\_out}$:</u>

Secondary Current: $\hat{J}_x(z) =$

$$= -\frac{j\mu_3 |K_1| e^{j(\omega t)}}{\mu_2} \left\{ \begin{array}{l} \overbrace{j(\xi_1 - \beta)\left[\frac{\xi_1 e^{j(y - r_{2\_out})\xi_1} e^{-j\beta r_{2\_out}} e^{-j\beta y}}{\xi_1(\xi_1 + \beta)} \bullet \frac{\gamma_{original} G_3(\xi_1, z)}{H_{prime\_\xi 1}} \right]}^{\text{Inside Radius Dynamic Traveling Wave } \bar{B} \text{ Component}} + \\ \overbrace{+ j(\xi_2 - \beta)\left[\frac{\xi_2 e^{j(y - r_{2\_in})\xi_2} e^{-j\beta r_{2\_in}} e^{-j\beta y}}{\xi_2(\xi_2 + \beta)} \bullet \frac{\gamma_{original} G_3(\xi_2, z)}{H_{prime\_\xi 2}} \right]}^{\text{Outside Radius Dynamic Traveling Wave } \bar{B} \text{ Component}} + \\ \overbrace{+ j2\beta^2 \left[\frac{e^{-j2\beta y}}{\beta} \bullet \frac{G_3(-\beta, z)}{H(-\beta)} \right]}^{\text{General Traveling Wave } \bar{B} \text{ Component}} \end{array} \right\} \quad (3.106)$$

As discussed for equations (3.102) and (3.103), in Phases III and IV equation (3.106) assumes the form of equation (3.107) which accounts for the air gap linear distances through the angular motions in the z_g dependency.

Secondary Current: $\hat{J}(z_g) =$

$$= -\frac{j\mu_3 |K_1| e^{j(\omega t)}}{\mu_2} \left\{ \begin{array}{l} \overbrace{j(\xi_1 - \beta)\left[\frac{\xi_1 e^{j(y - r_{2\_out})\xi_1} e^{-j\beta r_{2\_out}} e^{-j\beta y}}{\xi_1(\xi_1 + \beta)} \bullet \frac{\gamma_{original} G_3(\xi_1, z_g)}{H_{prime\_\xi 1}} \right]}^{\text{Inside Radius Dynamic Traveling Wave } \bar{B} \text{ Component}} + \\ \overbrace{+ j(\xi_2 - \beta)\left[\frac{\xi_2 e^{j(y - r_{2\_in})\xi_2} e^{-j\beta r_{2\_in}} e^{-j\beta y}}{\xi_2(\xi_2 + \beta)} \bullet \frac{\gamma_{original} G_3(\xi_2, z_g)}{H_{prime\_\xi 2}} \right]}^{\text{Outside Radius Dynamic Traveling Wave } \bar{B} \text{ Component}} + \\ \overbrace{+ j2\beta^2 \left[\frac{e^{-j2\beta y}}{\beta} \bullet \frac{G_3(-\beta, z_g)}{H(-\beta)} \right]}^{\text{General Traveling Wave } \bar{B} \text{ Component}} \end{array} \right\} \quad (3.107)$$

The angular components of the phasors $\hat{B}_N$ and $\hat{B}_T$ cancel as shown in equation (3.108).

Normal Component: $\hat{B}_N = B_N e^{j(\omega t - \beta y)}$

Tangential Component: $\hat{B}_T = B_T e^{j(\omega t - \beta y)}$

$$\left[e^{j(\omega t-\beta y)}\right]\left[e^{j(\omega t-\beta y)}\right]^* = e^{j(\omega t-\beta y)}e^{-j(\omega t-\beta y)} = e^0 = 1 \tag{3.108}$$

Therefore the secondary static centering or dynamic drag time average force per magnetic volume is provided by equation (3.109) and the secondary lifting or repulsive time average force per magnetic volume is provided by equation (3.110).

Normal Component (Static Centering or Dynamic Drag Force):

$$\left\langle F_y \right\rangle = \frac{1}{2}\mathrm{Re}\left(J_x B_N^*\right) \quad \left(\frac{\mathrm{N}}{\mathrm{m}^3}\right) \tag{3.109}$$

Tangential Component (Lift Force): $\left\langle F_z \right\rangle = \frac{1}{2}\mathrm{Re}\left(J_x B_T^*\right) \quad \left(\frac{\mathrm{N}}{\mathrm{m}^3}\right)$ (3.110)

The secondary lifting repulsive force is determined from the primary source interaction with the secondary magnetic energy volume. This produces equation (3.111). The secondary area facing the primary is the Maxwell stress tensor magnetic pressure area. This magnetic area component of the magnetic volume accounts for the magnetic pressure losses as the magnetic flux density decreases with an increasing magnetic air gap. The secondary thickness up to the secondary skin depth is the depth of this magnetic volume which interacts with the primary energy that crosses the magnetic air gap. Again recall that the solved $A_3(y,z)$ which is used to derive the $\hat{B}_N$, $\hat{B}_T$, and $\hat{J}_x$ is only valid for the z region of $0 \le z \le z_g$. Noting from equations (3.109) and (3.110) that the normal and tangential forces solved in this paper require a magnetic volume as presented in equation (3.111). In order to solve for the appropriate magnetic field interaction across the air gap with the secondary magnetic volume, the z variables of equations (3.98) and (3.99) are set to $z = 0$ when solving for body force equation. This allows the $A_3(y,z)$ expression to capture the entire air gap distance in the exponentials $e^{(z-z_g)\xi}$ and $e^{(z_g-z)\xi}$ of $G_3(\xi,z)$ and all of its

derivatives and hence the proper values for the magnetic flux density drop across the air gap.

$$\begin{pmatrix}\text{Magnetic}\\ \text{Volume}\end{pmatrix}=\begin{pmatrix}\text{Secondary Magnetic}\\ \text{Pressure Area}\end{pmatrix}\bullet\begin{pmatrix}\text{Secondary Thickness}\\ \text{or Skin Depth}\\ \text{(whichever is smaller)}\end{pmatrix} \qquad (3.111)$$

All secondary output forces in Phase I are physical gap distance dependent and not translational or rotational dynamic system velocity dependent. This is only true since the electrical source and inductive $\left(\frac{L}{R}\right)$ time constants are much smaller than the mechanical time constants in this system as determined in Appendix A.1.b. If the mechanical time constants are in the same range as the electrical or inductive time constants then the respective mechanical velocities could affect the output forces via magnetic diffusion.

Secondary emf, Power, and Efficiency

The secondary emf, electromotive force, power and efficiency equations are given with equations (3.112), (3.113), and (3.114) respectively where $K=\left(\text{Sheet Current Density}\right)$.

$$\left(emf\right)_2=\vec{J}\bullet\rho_2 \qquad \left(\frac{\text{V}}{\text{m}}\right) \qquad (3.112)$$

$$P_2=\frac{1}{2}\text{Re}\left[K_2^*\bullet\left(emf\right)_2\right]\left(\text{Magnetic Volume}\right) \qquad (3.113)$$

$$\left(\text{Efficiency}\right)=\eta=\left(\frac{P_2}{P_1}\right)=\left(\frac{P_2}{i_1^2R_1}\right) \qquad (3.114)$$

3.3.a.iv Plant Dynamics

Plant Equation of Motion

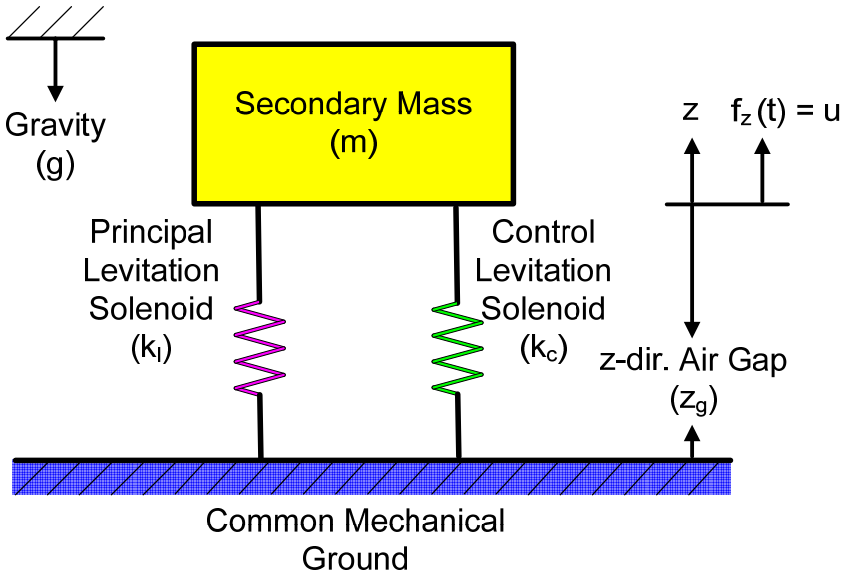

Figure 3.3-9: Phase I System Equivalent Mechanical Energy Elements

The purpose of the Phase I plant is globally described in Chapter 2.3.b. The Phase I plant mechanical system energy elements are provided in Figure 3.3-9. The z parameter definition is provided in Chapter 3.1.b. Both potential energy elements have current dependent spring constants which are voltage controlled. Equation (3.115) provides the general state space equation form for this system and equation (3.116) provides the state space equation in a differential equation form more suitable for numerical state space solution. This numerical solution equation form always isolates the highest differentials of the single respective variable under analysis.

$$m\ddot{z} + (k_c + k_l)z = u = (\text{External Force Input}) \tag{3.115}$$

$$\ddot{z} = \left(\frac{u}{m}\right) - \left(\frac{k_c + k_l}{m}\right) z \tag{3.116}$$

The spring constants k_c and k_l in equations (3.115) and (3.116) are the control and plant solenoid respective vertical spring constants determined by inputting equation (3.110) into the spring capacitance equation of F_z=kz. Therefore the equation $k = \frac{\partial F_z}{\partial z} \xrightarrow{\text{t=constant}} k = \frac{F_z}{z}$ is used for determining the spring constants k_c and k_l as shown in equation (3.117). Both spring constants are highly nonlinear. As stated in Chapter 2.6.a.i, these nonlinearities stem from the vertical position, vertical velocity, and horizontal velocity dependence of the magnetic spring constants as well as the repulsive only force condition of these spring constants.

$$k = \frac{\langle F_z \rangle \bullet (\text{Magnetic Volume})}{z_g} = \frac{\left[\frac{1}{2}\text{Re}\left(J_x B_T^*\right)\right] \bullet (\text{Magnetic Volume})}{z_g} \tag{3.117}$$

Depending on the form of equations (3.115) and (3.116), the system may start at z or $z + z_g$. Phase III assumes that the system starts about a static equilibrium point where $z = 0$. Therefore equations (3.115) and (3.116) only determine z motion from this equilibrium position and not $z + z_g$.

Frequency Domain

Since Phase I is completely linear, classical frequency domain methods can be used to determine the plant system type. First Laplace Transform equation (3.115).

$$\left(Ms^2 + K_c + K_l\right)Z(s) = U(s)$$

This Laplace Transform provides the following transfer function where $K = (K_c + K_l)$. The following is a type "0" system.

$$\frac{Z(s)}{U(s)} = \frac{1}{Ms^2 + K}$$

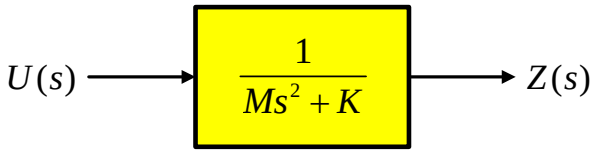

Linear State Space System Representation

Perform the following substitutions.

$$z_1 = z \qquad z_2 = \dot{z} \qquad z_3 = \ddot{z}$$

$$\dot{z}_1 = z_2 \qquad \dot{z}_2 = z_3 = \left[\left(\frac{u}{m}\right) - \left(\frac{k_c + k_p}{m}\right)z_1\right]$$

This gives the following linear state space representation of the system.

$$\text{State Space Equation Set} \begin{cases} \begin{Bmatrix} \dot{z}_1 \\ \dot{z}_2 \end{Bmatrix} = \begin{Bmatrix} z_2 \\ z_3 \end{Bmatrix} = \begin{bmatrix} 0 & 1 \\ -\left(\frac{k_c + k_l}{m}\right) & 0 \end{bmatrix} \begin{Bmatrix} z_1 \\ z_2 \end{Bmatrix} + \begin{Bmatrix} 0 \\ \left(\frac{1}{m}\right) \end{Bmatrix} u \\ z = \begin{Bmatrix} 1 & 0 \end{Bmatrix} \begin{Bmatrix} z_1 \\ z_2 \end{Bmatrix} \end{cases}$$

Which compacts when written in standard form as shown in equation (3.118) where z_n is an n length state vector, z is a p length output vector, u is an r length control vector, A is an $n \times n$ size matrix, B is an $n \times r$ size matrix, and C is an $p \times n$ size matrix.

$$\text{State Space Equation Set} \begin{cases} \{\dot{z}_n\} = [A]\{z_n\} + \{B\}u \\ z = \{C\}\{z_n\} \end{cases} \tag{3.118}$$

$$\{z_n\} = \begin{Bmatrix} z_1 \\ z_2 \\ \vdots \\ z_n \end{Bmatrix}$$

Note that single variables surrounded by brackets, [], such as [A] in equation (3.118) stands for a matrix. Also note that single variables surrounded by braces, {}, such as [B] in equation (3.118) stands for an array. The plant of equation (3.118) is represented in block diagram form in Figure 3.3-10.

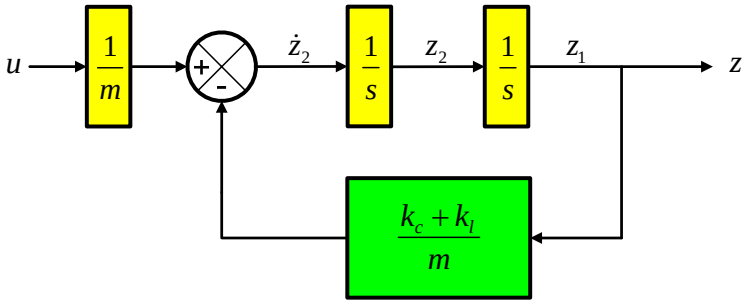

Figure 3.3-10: Phase I Plant Block Diagram

3.3.b Computational Analysis

The Ansys® and Opera™ computational analyses use equations derived in Chapter 3.3.a and presented in Appendix A.1.b to produce the output of Appendix B.1.a. Since the main outputs are provided by the Opera™ model and are only repeated by the Ansys® model for verification purposes, only the Opera™ model is presented.

3.3.c Control and Optimization Analysis

3.3.c.i Linear State Space Control Theory

State Controllability

The eigenvalues of a completely state controllable system can be arbitrarily assigned through state feedback. A state controllable system has a state controllability matrix, the first part of equation (3.119), of rank n where n is the number of input states. In Phase I n=2 as shown in the second part of equation (3.119). The state controllability matrix variables are introduced and described in equation (3.118).

$$\left[B \mid AB \mid \ldots \mid A^{n-1}B\right] \xrightarrow{n=2} \left[B \mid AB\right] \tag{3.119}$$

The following are the state controllability matrix components for Phase I.

$$AB = \begin{bmatrix} 0 & 1 \\ -\left(\frac{k_c + k_l}{m}\right) & 0 \end{bmatrix} \begin{Bmatrix} \left(\frac{1}{m}\right) \\ 0 \end{Bmatrix} = \begin{Bmatrix} \left(\frac{1}{m}\right) \\ 0 \end{Bmatrix}$$

$$\left[B \mid AB\right] = \begin{bmatrix} 0 & \left(\frac{1}{m}\right) \\ \left(\frac{1}{m}\right) & 0 \end{bmatrix}$$

$$\det\left[B \mid AB\right] = \begin{vmatrix} 0 & \left(\frac{1}{m}\right) \\ \left(\frac{1}{m}\right) & 0 \end{vmatrix} = \frac{-1}{m^2} \neq 0 \qquad (3.120)$$

Since the determinant exists or does not equal zero as shown in equation (3.120), then the matrix inverse exists.

$$\begin{bmatrix} 0 & \left(\frac{1}{m}\right) \\ \left(\frac{1}{m}\right) & 0 \end{bmatrix}^{-1} = \frac{\begin{bmatrix} 0 & -\left(\frac{1}{m}\right) \\ -\left(\frac{1}{m}\right) & 0 \end{bmatrix}}{\left(\frac{-1}{m^2}\right)} = \begin{bmatrix} 0 & m \\ m & 0 \end{bmatrix}$$

$$\left[B \mid AB\right]\left[B \mid AB\right]^{-1} = \begin{bmatrix} 0 & \left(\frac{1}{m}\right) \\ \left(\frac{1}{m}\right) & 0 \end{bmatrix}\begin{bmatrix} 0 & m \\ m & 0 \end{bmatrix} = \begin{bmatrix} 1 & 0 \\ 0 & 1 \end{bmatrix} = I \qquad (3.121)$$

Equation (3.121) is the identity matrix of rank 2. Therefore the state controllability matrix is not only nonsingular but a state controllability matrix of rank n=2. Therefore the system is completely state controllable.

Output Controllability

An output controllable system has an output controllability matrix, the first part of equation (3.122), of rank p where p is the number of output states. In Phase I n=2 and p=1 as shown in the second part of equation (3.122). The output controllability matrix variables are introduced and described in equation (3.118).

$$\left[CB \mid CAB \mid CA^2B \mid \ldots \mid CA^{p-1}B \mid D\right] \xrightarrow[n=2]{p=1} \left[CB \mid CAB\right] \qquad (3.122)$$

The following are the output controllability matrix components for Phase I.

$$CB = \begin{bmatrix} 1 & 0 \end{bmatrix} \begin{bmatrix} 0 \\ \left(\frac{1}{m}\right) \end{bmatrix} = 0$$

$$CAB = \begin{bmatrix} 1 & 0 \end{bmatrix} \begin{bmatrix} 0 & 1 \\ -\left(\frac{k_c + k_l}{m}\right) & 0 \end{bmatrix} \begin{bmatrix} 0 \\ \left(\frac{1}{m}\right) \end{bmatrix} = \begin{bmatrix} 1 & 0 \end{bmatrix} \begin{bmatrix} \left(\frac{1}{m}\right) \\ 0 \end{bmatrix} = \left(\frac{1}{m}\right)$$

$$\left[CB \mid CAB \right] = \begin{bmatrix} 0 & \left(\frac{1}{m}\right) \end{bmatrix} \tag{3.123}$$

Equation (3.123), the output controllability matrix is of rank 1 which equals p. Therefore the system is completely output controllable.

Complete Observability

An completely observable system has an observability matrix, the first part of equation (3.124), of rank n where n is the number of states. In Phase I n=2 as shown in the second part of equation (3.124). The observability matrix variables are introduced and described in equation (3.118).

$$\left[C^* \mid A^*C^* \mid \ldots \mid \left(A^*\right)^{n-1} C^* \right] \xrightarrow{n=2} \left[C^* \mid A^*C^* \right] \tag{3.124}$$

The following are the observability matrix components for Phase I.

$$C^* = \begin{bmatrix} 1 \\ 0 \end{bmatrix}$$

$$A^*C^* = \begin{bmatrix} 0 & -\left(\frac{k_c + k_l}{m}\right) \\ 1 & 0 \end{bmatrix} \begin{bmatrix} 1 \\ 0 \end{bmatrix} = \begin{bmatrix} 0 \\ 1 \end{bmatrix}$$

$$\left[C^* \mid A^*C^* \right] = \begin{bmatrix} 1 & 0 \\ 0 & 1 \end{bmatrix} = I = \left(\text{Identity Matrix}\right) \tag{3.125}$$

Equation (3.125), the output observability matrix is of rank 2 which equals n. Therefore the system is completely observable.

Completely Controllable and Observable Systems

Since the system is completely controllable and completely observable, concepts originally introduced by Kalman and presented in Ogata [19], there is no plant or controls transfer function cancellation.

Controller Block Diagram

As mentioned in Chapter 2.6.b an I.-P.D. controller is the chosen linear state space controller. Since the plant as shown in Figure 3.3-10 has no integrator, an integrator is inserted into the feed forward path between the error comparator and the plant as shown in Figure 3.3-11 and discussed in Ogata [19]. This turns the type "0" system into a type "1" system. The states are z_1 and z_2. z_1 and z_3 are sensed directly where z_2 is observed via comparing feedback and feedforward values. Note that velocity is rarely sensed in this type of system due to extreme background noise.

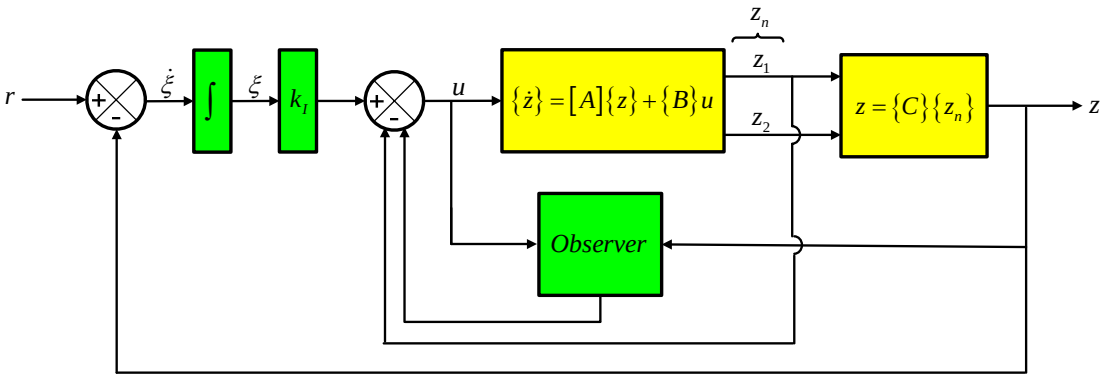

Figure 3.3-11: Phase I Controller with Observer

$z_2 = \dot{z}$ is not directly sensed, but $z_3 = \ddot{z}$ is directly sensed. Therefore instead of solving for $\dot{z}$ via tedious methods with feedback and feedforward gains, $\dot{z}$ is determined by integrating the directly sensed $\ddot{z}$. This changes the control block diagram as shown in Figure 3.3-12.

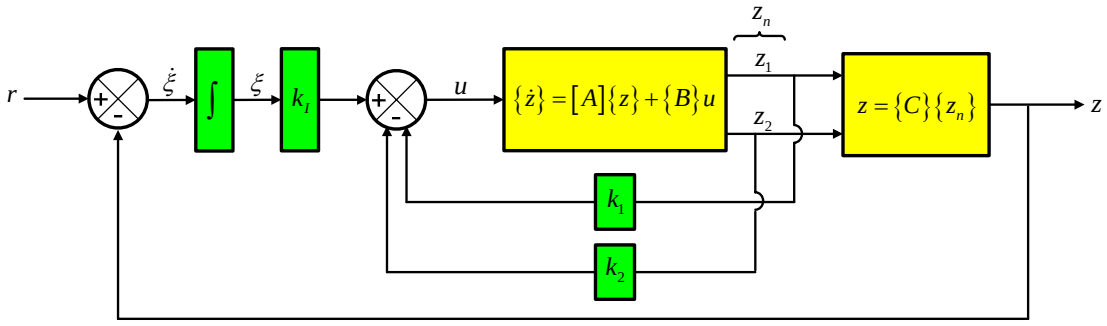

Figure 3.3-12: Phase I Controller with Direct Integration of Sensed Parameters

The following equations represent the system shown in Figure 3.3-12.

$$u = -\{K_n\}\{z_n\} + k_I \xi$$

$$\dot{\xi} = (r - z) = r - \{C\}\{z_n\}$$

The state error equation is given in equation (3.126).

$$\{\dot{e}\} = \left[\hat{A}\right]\{e\} + \left\{\hat{B}\right\} u_e \tag{3.126}$$

The following are the state error equation matrix components for Phase I.

$$\left[\hat{A}\right] = \begin{bmatrix} [A] & \{0\} \\ -\{C\} & 0 \end{bmatrix} = \begin{bmatrix} 0 & 1 & 0 \\ -\left(\frac{k_c + k_I}{m}\right) & 0 & 0 \\ -1 & 0 & 0 \end{bmatrix}$$

$$\left[\hat{B}\right] = \begin{bmatrix} \{B\} \\ 0 \end{bmatrix} = \begin{bmatrix} 0 \\ \left(\frac{1}{m}\right) \\ 0 \end{bmatrix}$$

$$u_e = -\left\{\hat{K}_n\right\}\{e\}$$

The state feedback gain matrix is provided in equation (3.127).

$$\left\{\hat{K}_n\right\} = \left[\{K_n\} \mid -k_I\right] = \begin{bmatrix} k_1 & k_2 & k_I \end{bmatrix} \tag{3.127}$$

Now we define a matrix P.

$$[P] = \begin{bmatrix} [A] & \{B\} \\ -\{C\} & 0 \end{bmatrix} = \begin{bmatrix} 0 & 1 & 0 \\ -\left(\frac{k_c + k_I}{m}\right) & 0 & \left(\frac{1}{m}\right) \\ -1 & 0 & 0 \end{bmatrix}$$

Interchange the column 1 and 2 and then columns 2 and 3 of the P matrix to produce the following triangle matrix then take the determinant of this matrix.

$$\begin{bmatrix} 1 & 0 & 0 \\ 0 & \left(\frac{1}{m}\right) & -\left(\frac{k_c+k_l}{m}\right) \\ 0 & 0 & -1 \end{bmatrix} \rightarrow \begin{vmatrix} 1 & 0 & 0 \\ 0 & \left(\frac{1}{m}\right) & -\left(\frac{k_c+k_l}{m}\right) \\ 0 & 0 & -1 \end{vmatrix} = -\left(\frac{1}{m}\right) \neq 0$$

Since the determinant does not equal zero, each matrix column is independent and hence the rank of matrix P is therefore 3. Therefore the state error equation is completely state controllable and arbitrary pole placement is allowed.

Equation (3.128) provides the characteristic equation of Phase I.

$$\left|s[I]-\left[\hat{A}\right]\right| = \begin{vmatrix} s & -1 & 0 \\ \left(\frac{k_c+k_l}{m}\right) & s & 0 \\ 1 & 0 & s \end{vmatrix} = s^3 + \left(\frac{k_c+k_l}{m}\right)s = 0 = \tag{3.128}$$

$$= s^3 + a_1 s^2 + a_2 s + a_3 = 0$$

Closed Loop Poles

The closed loop poles, s, are now determined.

$$s = \sum_{i=1}^{3} \mu_i$$

Here $\mu = x + jy$. Now choose a reasonable maximum percent overshoot, $M_P = 15\% = 0.15$, and 2% type settling time, $t_{2\%} = 2 \bullet \text{sec}$, as presented in Ogata [19]. These parameters provide the following equations which are solved in Appendix A.2.

$$x = \left(\frac{4}{t_{2\%}}\right) = 2 \tag{3.129}$$

$$M_P = e^{-\pi\left(\frac{\zeta}{\sqrt{1-\zeta^2}}\right)} \rightarrow \zeta = \frac{-\ln\left(M_P\right)}{\sqrt{\ln\left(M_P\right)^2 + \pi^2}} = 0.517$$

$$y = \left(\frac{4}{\zeta t_{2\%}}\right)\sqrt{1-\zeta^2} = 3.312 \tag{3.130}$$

Equations (3.129) and (3.130) now produce the complex, closed loop poles $\mu_1 = -2 + j3.312$ and $\mu_2 = -2 - j3.312$ from the equation $(s-\mu)$. Now locate the remaining poles on the real axis to negate stored energy effects while maximizing dissipation energy effects, in the left half closed loop complex plane to allow stability, and produce minimal system performance effects by locating far from the origin compared to solved complex poles. The final solution of $\mu_3 = 3.869$ comes from the Butterworth Pattern solution for closed loop control system poles. The solved poles now determine the characteristic equation constants of $\alpha_1 = 0.131$, $\alpha_2 = -0.507$, and $\alpha_3 = -57.916$ via equation (3.131).

$$\begin{aligned}&(s-\mu_1)(s-\mu_2)(s-\mu_3) = s^3 + 0.131s^2 - 0.507s - 57.916 = \\ &= s^3 + \alpha_1 s^2 + \alpha_2 s + \alpha_3 = 0\end{aligned} \tag{3.131}$$

Gain Constants

$[T] = [M][W]$ is the transformation matrix as provided in equation (3.132). The following sets of equations solve for the transformation matrix.

$$\left[\hat{A}\hat{B}\right] = \begin{bmatrix} 0 & 1 & 0 \\ -\left(\frac{k_c + k_l}{m}\right) & 0 & 0 \\ -1 & 0 & 0 \end{bmatrix} \begin{bmatrix} 0 \\ \left(\frac{1}{m}\right) \\ 0 \end{bmatrix} = \begin{bmatrix} \left(\frac{1}{m}\right) \\ 0 \\ 0 \end{bmatrix}$$

$$\left[\hat{A}^2\hat{B}\right] = \begin{bmatrix} -\left(\frac{k_c + k_l}{m}\right) & 0 & 0 \\ 0 & -\left(\frac{k_c + k_l}{m}\right) & 0 \\ 0 & -1 & 0 \end{bmatrix} \begin{bmatrix} 0 \\ \left(\frac{1}{m}\right) \\ 0 \end{bmatrix} = \begin{bmatrix} 0 \\ -\left(\frac{k_c + k_l}{m^2}\right) \\ -\left(\frac{1}{m}\right) \end{bmatrix}$$

$$[M]=\left[\hat{B}\mid\hat{A}\hat{B}\mid\hat{A}^2\hat{B}\right]=\begin{bmatrix}0 & \left(\frac{1}{m}\right) & 0\\ \left(\frac{1}{m}\right) & 0 & -\left(\frac{k_c+k_l}{m}\right)\\ 0 & 0 & -\left(\frac{1}{m}\right)\end{bmatrix}$$

$$[W]=\begin{bmatrix}a_2 & a_1 & 1\\ a_1 & 1 & 0\\ 1 & 0 & 0\end{bmatrix}$$

$$[T]=[M][W]=\begin{bmatrix}0 & \left(\frac{1}{m}\right) & 0\\ \left(\frac{1}{m}\right) & 0 & -\left(\frac{k_c+k_l}{m}\right)\\ 0 & 0 & -\left(\frac{1}{m}\right)\end{bmatrix}\begin{bmatrix}\left(\frac{k_c+k_l}{m}\right) & 0 & 1\\ 0 & 1 & 0\\ 1 & 0 & 0\end{bmatrix}=$$

$$=\begin{bmatrix}0 & \left(\frac{1}{m}\right) & 0\\ \left[\left(\frac{k_c+k_l}{m}\right)(m-1)\right] & -\left(\frac{k_c+k_l}{m}\right) & \left(\frac{1}{m}\right)\\ -\left(\frac{1}{m}\right) & 0 & 0\end{bmatrix} \tag{3.132}$$

Solve for the gain constants by manipulating the transformation matrix as shown in the following equations.

$$[T]^{-1}=\frac{adj[T]}{\det[T]}$$

$$|T|=-\left(\frac{1}{m^2}\right)$$

$$adj[T]=\begin{bmatrix} 0 & 0 & \left(\frac{1}{m^2}\right) \\ \left(\frac{1}{m^2}\right) & 0 & 0 \\ \left(\frac{k_c+k_l}{m^2}\right) & -\left(\frac{1}{m^2}\right) & \left[\left(\frac{k_c+k_l}{m^2}\right)(1-m)\right] \end{bmatrix}$$

$$[T]^{-1}=\begin{bmatrix} 0 & 0 & -\left(\frac{1}{m^4}\right) \\ -\left(\frac{1}{m^4}\right) & 0 & 0 \\ \left(\frac{k_c+k_l}{m^2}\right) & \left(\frac{1}{m^4}\right) & \left[\left(\frac{k_c+k_l}{m^4}\right)(m-1)\right] \end{bmatrix}$$

$$\left[\hat{K}\right]=\left[\alpha_3-a_3 \mid \alpha_2-a_2 \mid \alpha_1-a_1\right][T]^{-1}=\left[k_1 \quad k_2 \quad k_I\right]$$

$$\left[\hat{K}\right]=\left[\alpha_3 \quad \left[\alpha_2-\left(\frac{k_c+k_l}{m}\right)\right] \quad \alpha_1\right][T]^{-1}=$$

$$=\left[\left[\left(\frac{1}{m^4}\right)\left(\frac{k_c+k_l}{m}-\alpha_2\right)+\alpha_1\left(\frac{k_c+k_l}{m^4}\right)\right] \quad \left(\frac{\alpha_1}{m^4}\right) \quad \left[\alpha_1\left(\frac{k_c+k_l}{m^4}\right)(m-1)-\left(\frac{\alpha_3}{m^4}\right)\right]\right]$$

$$[K]=\left[k_1 \quad k_2\right]=\left[\left[\left(\frac{1}{m^4}\right)\left(\frac{k_c+k_l}{m}-\alpha_2\right)+\alpha_1\left(\frac{k_c+k_l}{m^4}\right)\right] \quad \left(\frac{\alpha_1}{m^4}\right)\right] \tag{3.133}$$

$$k_I=\left[\alpha_1\left(\frac{k_c+k_l}{m^4}\right)(m-1)-\left(\frac{\alpha_3}{m^4}\right)\right] \tag{3.134}$$

Equations (3.133) and (3.134) provide k_1, k_2, and k_I, the output gain constants used in Figure 3.3-12.

Inverter Plant Transformer Block

One final piece of this controller puzzle remains. This controller uses mechanical energy components to determine a controlled force value yet in reality

only the voltage or current of the physical solenoid is controlled. In this case assume that the RMS voltage is controlled. Therefore a controller transformation block is required between the controller and the system plant to convert the controller's desired force output to a controller desired RMS voltage output. This transformer block is created by inverting a few of the plant equations. The main transformation equation, shown in the following equation, transforms the controller levitation force density to an equivalent sheet current which is later transformed into an RMS voltage.

$$\left|K_{1\_Controller}\right| = \sqrt{\frac{2\left\langle F_{z\_Controller}\right\rangle}{\mathrm{Re}\left[J_x\left(\mathrm{no\ K_1}\right)B_T^*\left(\mathrm{no\ K_1}\right)\right]}}$$

3.3.c.ii Soft Computing Control Theory

As discussed in Chapter 2.6.c, the heart of fuzzy logic is fuzzy inference which involves membership functions, fuzzy logic operators, and if-then rules. This system requires two fuzzy logic inputs and one fuzzy logic output for the single control solenoid which are combined through the Mamdani type inference method as shown in Figure 3.3-13. The Simulink® model of this structure is provided in Figure 5.2-12. The Mamdani type inference method used in this paper maps the inputs to outputs by fuzzifying the inputs, applying the membership functions, and then defuzzifying the outputs through an intuitive centroid technique. An important component of any fuzzy process is the final defuzzification method. The defuzzification process solution used here is achieved via the popular method of using the distributed weighted average of a number of data points from the fuzzy inference membership function aggregation process output to find the solution centroid. The inputs are the secondary z axis velocity used for damping and the z axis position reference ratio which is required since the system is in reality a position dependent magnetic spring constant. The z axis position reference ratio is the control system comparator’s superposition quantity of the positive only desired position minus the

actual position all divided by the desired position as shown in equation (3.135). The output is the control coil RMS voltage.

$$\begin{pmatrix}\text{z axis Reference}\\ \text{Ratio}\end{pmatrix} = \frac{+\left[\left(\text{Desired Position}\right)-\left(\text{Actual Position}\right)\right]}{\left(\text{Desired Position}\right)} \qquad (3.135)$$

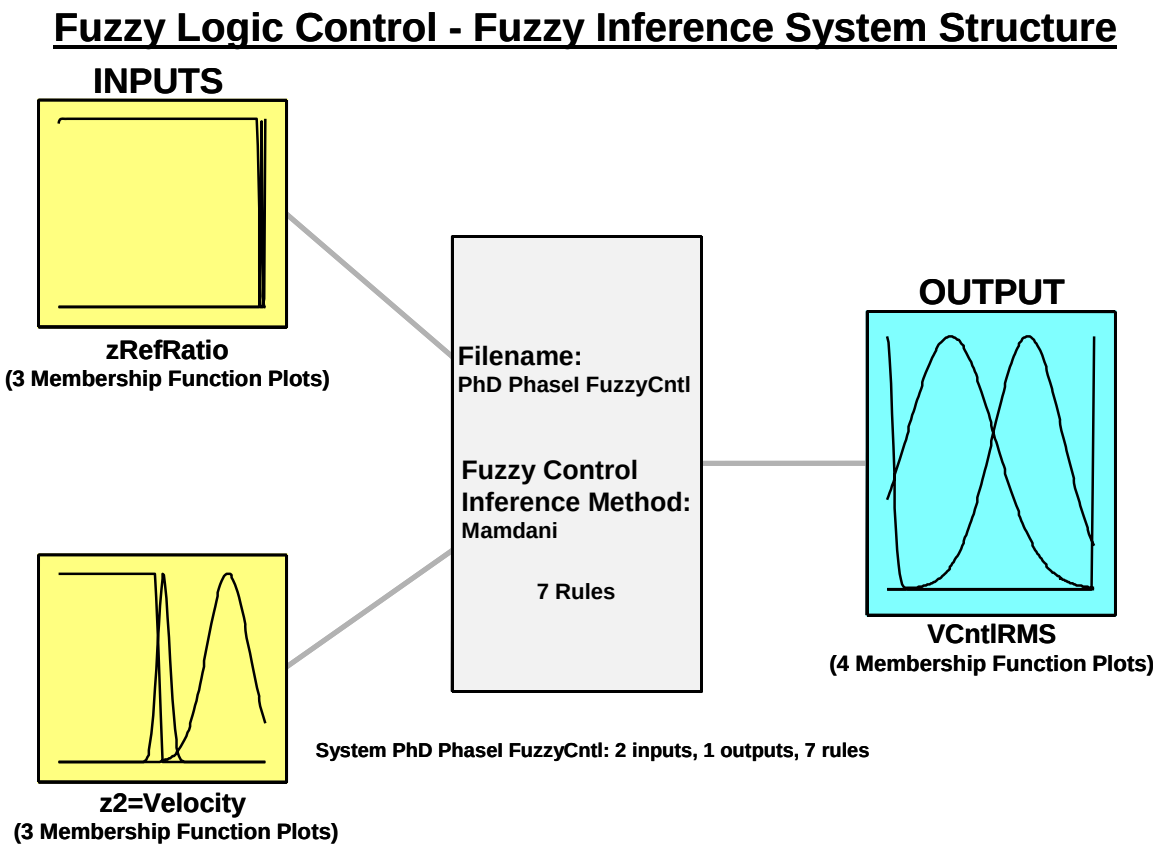

Figure 3.3-13: Phase I Fuzzy Logic Inference System Structure

The z axis reference ratio input membership function has a very low bandwidth of good solutions which is centered on achieving a uniform ratio value which is provided by a achieving an actual position above the desired reference position as shown in Figure 3.3-14.

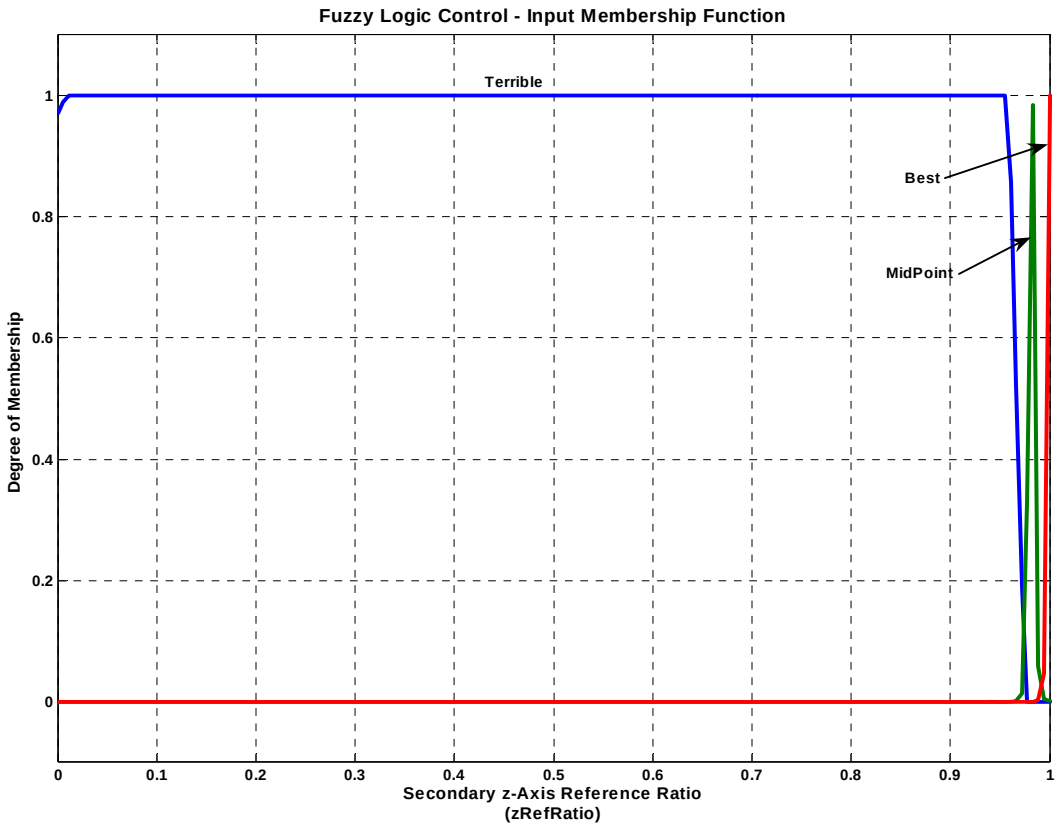

Figure 3.3-14: Phase I Fuzzy: z Axis Reference Ratio Membership Function

The z axis velocity input membership function is centered on achieving a zero secondary velocity as shown in Figure 3.3-15. Note that a negative velocity, when the secondary is moving towards the primary, results in a continually high membership function.

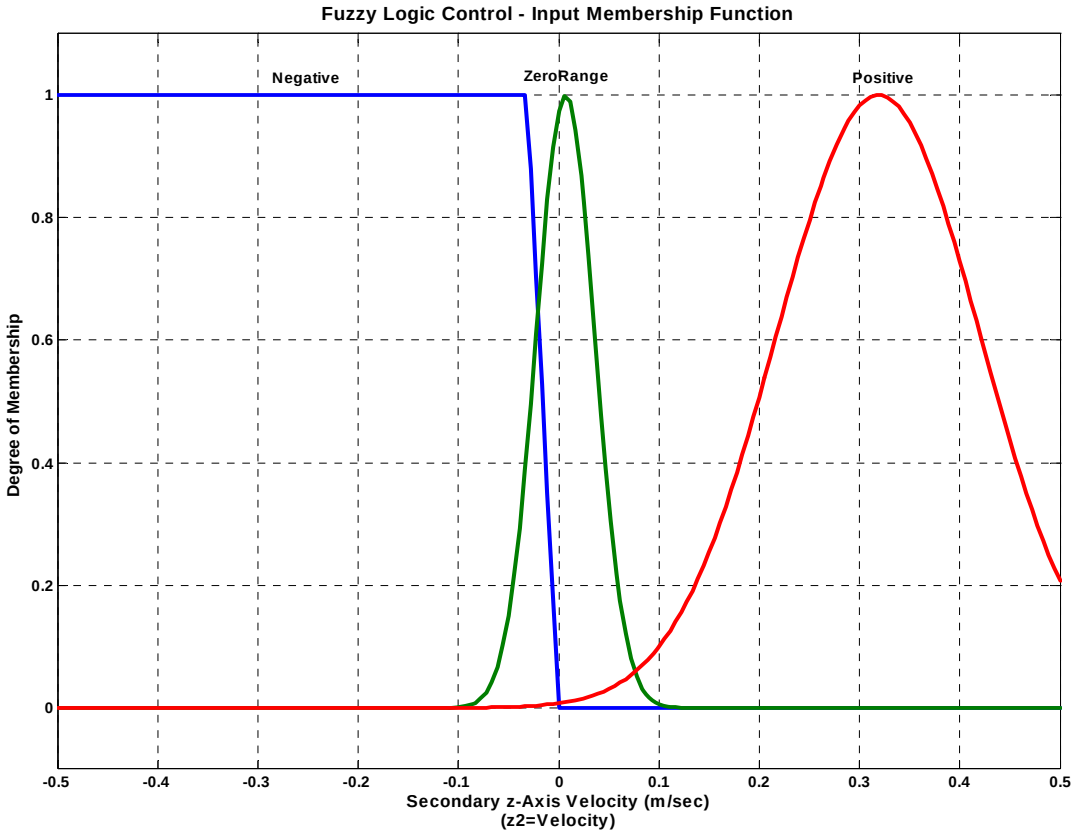

Figure 3.3-15: Phase I Fuzzy: z Axis Velocity Membership Function

The secondary control coil RMS voltage output membership function is centered on achieving a smooth variance for voltage output as shown in Figure 3.3-16.

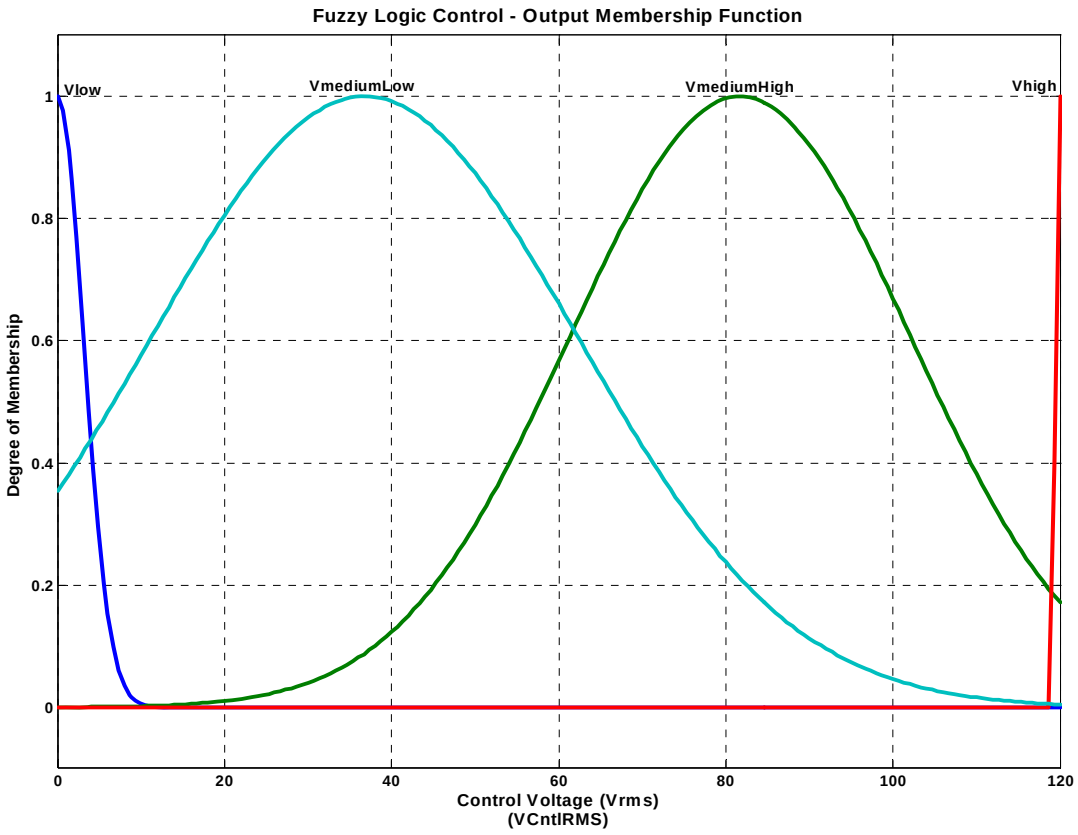

Figure 3.3-16: Phase I Fuzzy: Control RMS Voltage Membership Function

The if-then rules that correspond to the fuzzy logic membership functions are detailed in Table 3.3-3.

Table 3.3-3: Phase I Fuzzy Logic Control Rules

FUZZY LOGIC IF-THEN RULES		
Item #	**Rule Weight**	**Rule Description**
1	1	If (zRefRatio is MidPoint) and (z2=Velocity is Negative) then (VCntlRMS is Vhigh)
2	1	If (zRefRatio is MidPoint) and (z2=Velocity is Positive) then (VCntlRMS is Vlow)
3	1	If (zRefRatio is Terrible) and (z2=Velocity is Negative) then (VCntlRMS is Vhigh)
4	1	If (zRefRatio is Terrible) and (z2=Velocity is Positive) then (VCntlRMS is Vlow)
5	1	If (zRefRatio is Best) and (z2=Velocity is Negative) then (VCntlRMS is VmediumHigh)
6	1	If (zRefRatio is Best) and (z2=Velocity is ZeroRange) then (VCntlRMS is Vlow)
7	1	If (zRefRatio is MidPoint) and (z2=Velocity is ZeroRange) then (VCntlRMS is VmediumHigh)

When all of the preceding membership functions are combined into a surface plot as shown in Figure 3.3-17, this plot provides a visual representation of the fuzzy inference system structure. Note from this surface plot that the fuzzy controller will typically command a fully energized control coil for the majority of the secondary damping stroke regardless of the perturbation origination. The weighted values governing the rules of this surface plot are developed for a control coil capable of only half the energy output as the companion principal coil and hence only a portion of the magnetic spring constant. The closer the principal and solenoid magnetic spring constants are to one another, the larger the range of control provided throughout the secondary damping stroke which would allow for a less uniform surface plot.

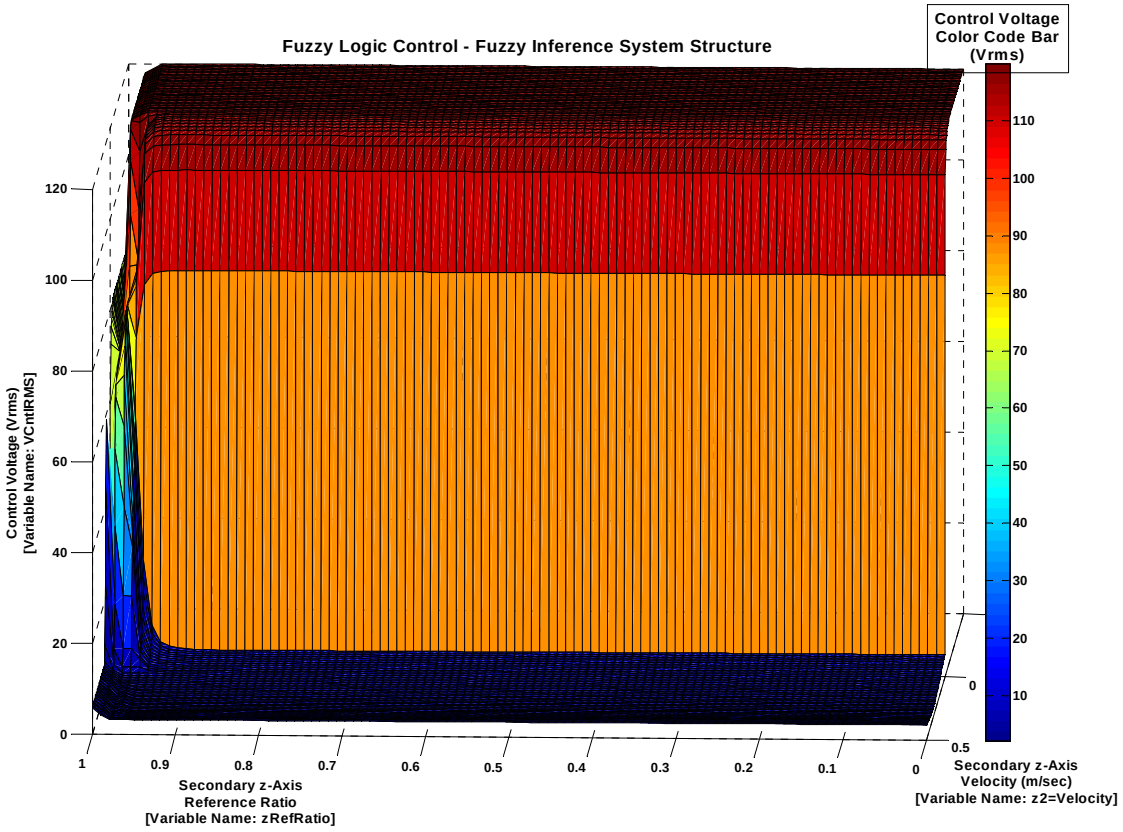

Figure 3.3-17: Phase I Fuzzy Logic Control Inference System Surface Plot

3.4 PHASE II

3.4.a Analytical Equation Derivation

3.4.a.i Plant Dynamics

Plant Equation of Motion

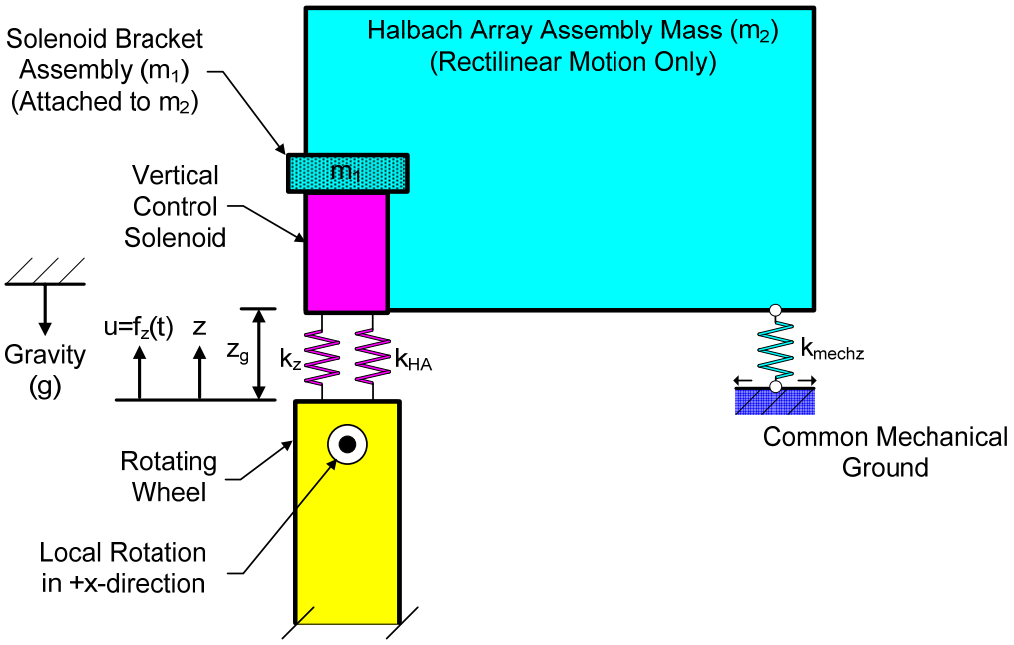

Figure 3.4-1: Phase II System Equivalent Mechanical Energy Elements

The Phase II plant mechanical system energy elements are provided in Figure 3.4-1. The z parameter definition is provided in Chapter 3.1.b. All Phase II governing equation phenomena is represented in Phase I. Phase II equations of motion are the same form as Phase I. As globally described in Chapter 2.3.c, The only two mathematical differences between Phases I and II are the introduction of an active propulsive velocity component that couples to the vertical heave motion and an increase in the energy element size with supporting power size increase. Analyzing this propulsive velocity coupling is crucial to vertical damping since certain propulsive velocity ranges feed energy into vertical heave oscillations. Both the linear

plant spring constants, k_{HA} and k_{mechz} and control solenoid coil spring constants, k_z and k_y, are shown in Figure 3.4-1. The Halbach array's magnetic spring constant, k_{HA}, and the z directed Halbach array's mechanical assembly spring constant, k_{mechz}, simulate a single linear D.O.F. of the six D.O.F. vehicle principal levitation coil spring constants. The z directed control coil's magnetic spring constant, k_z, simulates the Phase II linear, one D.O.F., control coil spring constant. The Halbach array assembly mass, m_2, is constrained to linear motion via k_{HA} and k_{mechz}. The control coil solenoid system bracket assembly mass, m_1, is constrained to linear motion via k_z. Figure 3.3-9 energy element constants k_c, k_l, m, and input force $f_z(t)$ are all changed into other constants Phase II. k_c, k_l, and m of Phase I turn into k_z, $\left(k_{HA}+k_{mechz}\right)$, and $m=\left(m_1+m_2\right)$ respectively in Phase II. The input force $f_z(t)$ must now account for propulsive dynamics in the diffusion equation analysis. Appropriate substitutions into equation (3.118) provide the proper Phase II plant equations of motion output.

Diffusion Equation for $\vec{B}$ into Secondary with Mechanical Motion

Bullard's equation, equation (3.11), is rewritten here for convenience. The mechanical velocity component of Bullard's equation discussed when solving for equation (3.22), $\vec{v}$, now assumes a nonzero value in Phase II which affects the input force $f_z(t)$.

$$\frac{1}{\mu\sigma}\nabla^2\vec{B}+\frac{\partial\vec{B}}{\partial t}=\nabla\times\left(\vec{v}\times\vec{B}\right)$$

3.4.b Computational Analysis

A Phase II computational analysis would follow a similar pattern as Phase I and described in Chapter 3.3.b. No Phase II specific computational analyses are performed.

3.4.c Control and Optimization Analysis

3.4.c.i Linear State Space Control Theory

As described in Chapter 3.4.a.i, Phase I and Phase II are extremely similar. Applying the Phase II differences outlined in Chapter 3.4.a.i, equations (3.133) and (3.134) provide k_1, k_2, and k_I, the output gain constants used in Figure 3.3-12, the Phase I linear state space control model including slightly modified output gains can be used for Phase II control.

3.4.c.ii Soft Computing Control Theory

Phase II would implement a similar soft computing method as Phase I which is described in Chapter 3.3.c.ii. No Phase III specific soft computing control methods are implemented.

3.5 PHASE III

3.5.a Analytical Equation Derivation

3.5.a.i Plant Dynamics

Plant Equation of Motion

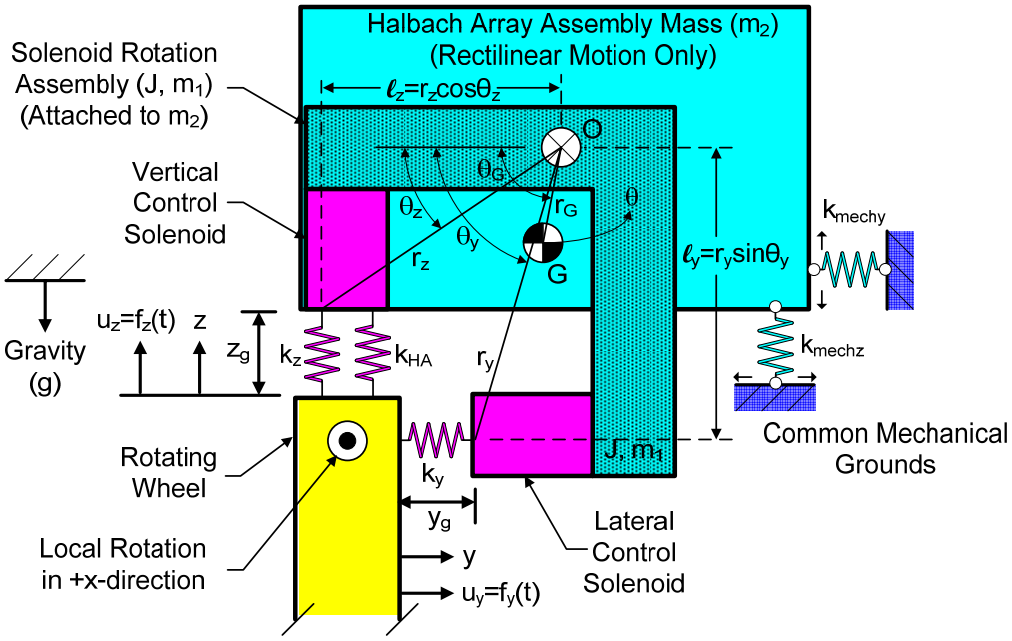

Figure 3.5-1: Phase III System Equivalent Mechanical Energy Elements

The Phase III plant mechanical system energy elements are provided in Figure 3.5-1. The y and z parameter definitions are provided in Chapter 3.1.b. All Phase III energy elements are sized equivalently to Phase II. All Phase III governing equation phenomena is represented in Phase II. As globally described in Chapter 2.3.d, the only mathematical differences between Phase II and III are nonlinearities introduced through two additional D.O.F. In Figure 3.5-1 point O represents the m_1 pivot point after the origin moved and hence point O only moves in pure translation, point G represents the m_1 center of mass or center or gravity after the origin moved, and J

represents the m_1 polar mass moment of inertia for the rigid body rotating on its own axis. By assuming a body rotation about its' own axis and taking a basic polar moment shape, J, the angular moment of inertia, may be solved with an uncoupled diagonal mass moment of inertia matrix without the complexity of a coupled mass moment of inertia matrix solution. Unless the angular coupling of the mass moment of inertia from either a complex shape or a C.O.M. location differing from the geometric center is the focus of analysis, this approximation is a common first step. After the basic performance is understood then the use of C.A.D. design and eventually test performance data will provide any necessary modifications for the simulation model and corresponding analysis. Both the linear plant spring constants, k_{HA}, k_{mechz}, and k_{mechy} and control solenoid coil spring constants, k_z and k_y, are shown in Figure 3.5-1. The y directed Halbach array's mechanical assembly spring constant, k_{mechy}, simulates a single linear D.O.F. of the six D.O.F. vehicle lateral guidance coil spring constants. The Halbach array's magnetic spring constant, k_{HA}, and the z directed Halbach array's mechanical assembly spring constant, k_{mechz}, simulate a single linear D.O.F. of the six D.O.F. vehicle levitation coil spring constants. The z directed control coil's magnetic spring constant, k_z, and the y directed control coil's magnetic spring constant, k_y, simulate the full Phase III linear and rotational three D.O.F. control coil spring constants. The distances z_g and y_g represent the z and y gap distances respectively and are interchangeable with the variables z and y superimposed with each respective initial condition when discussing their respective mechanical gap distances but not electromagnetic gap distances. The Halbach array assembly mass, m_2, is constrained to linear motion via k_{HA}, k_{mechz}, and k_{mechy}. The control coil solenoid system assembly mass, m_1, is constrained to linear and rotational motion via k_z and k_y.

System Kinematics

Assume that rigid body motion applies and that $\left(J_{xx}\right)_1 = J$ for m_1. $\theta_G = \theta_{G\_init} + \theta$, $\theta_y = \theta_{y\_init} + \theta$, and $\theta_z = \theta_{z\_init} + \theta$ define the angles. $z_g = \left\{ z_{g\_init} + \left[z + \sum f_z\left(angle\right) \right] \right\}$ and $y_g = \left\{ y_{g\_init} + \left[y + \sum f_y\left(angle\right) \right] \right\}$ define linear gap distances as originally introduced and defined in Chapter 3.1.b.

Translational kinematics for both masses m_1 and m_2 are defined in the following equations. Equation (3.136) is true for varying θ_G with respect to time since θ_{G_init} does not vary with time and hence $\theta_{G\_init} = \left(\text{A Constant}\right)$. Similar arguments apply for θ_z, θ_y, z_g, and y_g with respect to varying time, θ_z, θ_y, and θ_G with respect to varying θ, z_g with respect to varying z, and y_g with respect to varying y. Therefore, since all equations of motion solved here depend upon a rate and not an exact position, equation (3.136) shows that the values of z_g, y_g and the various forms of θ revert back to the generalized coordinates $q = \left(z, y, \theta\right)$. Note that the potential energy equation initially involves a direction dependent linear and angular position value unlike the kinetic co-energy which is purely velocity dependent. This fact is used when solving for the potential energy component of the Lagrangian.

$$\vec{v}_0 = v\hat{k} + v\hat{j} = \dot{z} + \dot{y} \rightarrow \vec{v}_0^{\,2} = \dot{z}^2 + \dot{y}^2$$

Where: $\dot{k} \bullet \dot{k} = \dot{j} \bullet \dot{j} = 1$;and: $\dot{k} \bullet \dot{j} = \dot{j} \bullet \dot{k} = 0$

$$\theta_G = \theta_{G\_init} + \theta \rightarrow \dot{\theta}_G = \frac{d\left(\theta_{G\_init} + \theta\right)}{dt} = \frac{\cancel{d\left(\theta_{G\_init}\right)}^{\,0}}{dt} + \frac{d\left(\theta\right)}{dt} = \frac{d\left(\theta\right)}{dt} \quad (3.136)$$

Rotational and translational kinematics for mass m_1 about its' respective mass center are defined in the following equations where $\dot{\theta} = \omega$.

$$\vec{r}_{origin} = \vec{r}_0 + \vec{r}_G \rightarrow \vec{v}_G = \vec{v}_0 + \cancel{\vec{v}_{relative}}^{\,0} + \left(\vec{\omega} \times \vec{r}_G\right)$$

$$\vec{v}_G = \overbrace{\left(\dot{z}+\dot{y}\right)}^{\text{Translational Component}} + \overbrace{\left[\left(\dot{\theta}\hat{i}\right)\times\left(-\hat{j}r_G\cos\theta_G - \hat{k}r_G\sin\theta_G\right)\right]}^{\text{Rotational Component about x axis}} = \tag{3.137}$$
$$= \left(\dot{z} - \hat{k}\dot{\theta}r_G\cos\theta_G\right) + \left(\dot{y} + \hat{j}\dot{\theta}r_G\sin\theta_G\right)$$

$$\vec{a}_G = \left(\ddot{z} - \ddot{\theta}r_G\cos\theta_G + \dot{\theta}^2 r_G\sin\theta_G\right)\hat{k} + \left(\ddot{y} + \ddot{\theta}r_G\sin\theta_G + \dot{\theta}^2 r_G\sin\theta_G\right)\hat{j} \tag{3.138}$$

Solve for $\vec{v}_G^{\,2}$ in equation (3.139) using equation (3.137) and the relation $\dot{k}\bullet\dot{j} = \dot{j}\bullet\dot{k} = 0$.

$$\text{For } \hat{\text{k}}\text{:} \quad \left(\hat{k}\bullet\hat{k} = 1\right) \rightarrow \left(\dot{z}^2 - 2\dot{z}\dot{\theta}r_G\cos\theta_G + \dot{\theta}^2 r_G^2\cos^2\theta_G\right)$$

$$\text{For } \hat{\text{j}}\text{:} \quad \left(\hat{j}\bullet\hat{j} = 1\right) \rightarrow \left(\dot{y}^2 - 2\dot{y}\dot{\theta}r_G\sin\theta_G + \dot{\theta}^2 r_G^2\sin^2\theta_G\right)$$

$$\vec{v}_G^{\,2} = \left(\dot{z}^2 - 2\dot{z}\dot{\theta}r_G\cos\theta_G + \dot{\theta}^2 r_G^2\cos^2\theta_G\right) +$$
$$+\left(\dot{y}^2 + 2\dot{y}\dot{\theta}r_G\sin\theta_G + \dot{\theta}^2 r_G^2\sin^2\theta_G\right) = \tag{3.139}$$
$$= \left[\dot{z}^2 + \dot{y}^2 + 2\dot{\theta}r_G\left(\dot{y}\sin\theta_G - \dot{z}\cos\theta_G\right) + \dot{\theta}^2 r_G^2\right]$$

Energy Derivations

For a simple method of maintaining desired accuracy for this three D.O.F. system, the Phase III nonlinear equations of motion are solved via Lagrange's energy method about the pure translating pivot point O which connects both masses m_1 and m_2 under analysis. The generalized coordinates are $q = (z, y, \theta)$. Solve for the kinetic co-energy, equation (3.140), and potential energy, equation (3.142). The squared energy terms in each of these equations are translational and rotational specific as well as (x, y, z) global coordinate axis specific as presented in a similar rotational motion analysis in [1].

The problem's physics and geometry defines the potential energy sign convention. A decrease in each respective magnetic air gap provides a continual increase in the respective magnetic spring constant potential energy, but the vertical gravitational potential energy decreases with a decreasing vertical air gap. The

magnetic spring constant potential energy never experiences a change in continually increasing or decreasing energies as the air gap continually increases or decreases respectively. In other words, the magnetic spring constant potential energy is unidirectional and doesn't experience a sign change with an increasing air gap that attracts the primary and secondary surfaces. This is dissimilar to most forms of mechanical spring potential energies, but quite similar to gravitational potential energy. In Figure 3.5-2, which depicts the Phase III potential energy angular component critical angles and lengths as originally shown in Figure 3.5-1, the θ sign convention indicates the direction of potential energy positive angular motion.

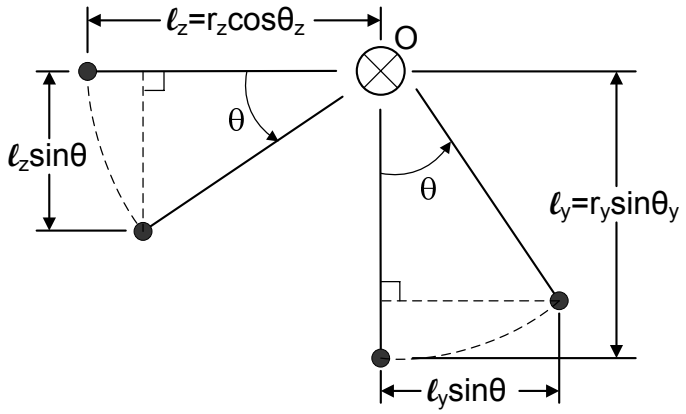

Figure 3.5-2: Potential Energy Angular Displacement Trigonometric Relations

The kinetic co-energy equation is shown in equation (3.140) and the final potential energy equation is shown in equation (3.142). As previously mentioned, the potential energy equation involves a direction dependent linear and angular position value. Therefore initially write the potential energy equation with respect to the gap lengths and change of gap lengths as in equation (3.141) and then remove the initial condition values when solving for the derivative of the potential energy as per the logic behind equation (3.136).

$$T^* = \overbrace{\frac{1}{2} m_2 \left(\dot{z}^2 + \dot{y}^2 \right)}^{\text{Body } m_2} + \overbrace{\frac{1}{2} m_1 \left[\dot{z}^2 + \dot{y}^2 + 2\dot{\theta} r_G \left(\dot{y} \sin\theta_G - \dot{z} \cos\theta_G \right) + \dot{\theta}^2 r_G^2 \right] + \frac{1}{2} J \dot{\theta}^2}^{\text{Body } m_1 \text{ at Center of Mass for } m_1} \tag{3.140}$$

$$U = \overbrace{\frac{1}{2}\left(k_z + k_{HA}\right) z_g{}^2 + \frac{1}{2} k_y y_g{}^2}^{\text{Linear \&Angular Air Gap Components}} + \overbrace{g\left(m_2 z_g + m_1 z_g\right) + \frac{1}{2}\left(k_{mechz}\right) z_g^2 + \frac{1}{2}\left(k_{mechy}\right) y_g^2}^{\text{Linear Air Gap Components Only}} \tag{3.141}$$

Rewrite the potential energy equation, equation (3.141), by substituting in the for gap length variables. Note that the mass m_2 and mechanical springs do not have an angular component to their respective z_g values. Indicate the proper sign of the respective increasing or decreasing potential energy as per the linear, z and y, and angular, θ, displacement sign conventions described above. This provides equation (3.142) for the potential energy.

$$\begin{aligned} U = {} & \frac{1}{2}\left(k_z + k_{HA}\right)\left[\overbrace{\left(z_{g\_init} - z\right) + \ell_z \sin\theta}^{=z_g}\right]^2 + \frac{1}{2} k_y \left[\overbrace{\left(y_{g\_init} - y\right) - \ell_y \sin\theta}^{=y_g}\right]^2 + \\ & + g\left\{m_2\left(z_{g\_init} + z\right) + m_1\left[\left(z_{g\_init} + z\right) - \ell_z \sin\theta\right]\right\} + \\ & + \frac{1}{2} k_{mechz}\left(z_{g\_init} - z\right)^2 + \frac{1}{2} k_{mechy}\left(y_{g\_init} - y\right)^2 \end{aligned} \tag{3.142}$$

Kinetic Energy Partial Differential Derivations

The kinetic co-energy partial differential energy equation derivations are presented in the following sets of equations. Equations (3.138), (3.139), and (3.140) are used to derive these equations.

$$\frac{\partial T^*}{\partial \dot{z}} = \left(m_1 + m_2\right)\dot{z} - m_1 r_G \dot{\theta} \cos\theta_G$$

$$\frac{\partial T^*}{\partial \dot{y}} = \left(m_1 + m_2\right)\dot{y} + m_1 r_G \dot{\theta}\sin\theta_G$$

$$\frac{\partial T^*}{\partial \dot{\theta}} = m_1 r_G\left(\dot{y}\sin\theta_G - \dot{z}\cos\theta_G\right) + m_1 r_G^2\dot{\theta} + J\dot{\theta}$$

$$\frac{d}{dt}\left(\frac{\partial T^*}{\partial \dot{z}}\right) = \left(m_1 + m_2\right)\ddot{z} - m_1 r_G\left(\ddot{\theta}\cos\theta_G - \dot{\theta}^2\sin\theta_G\right)$$

$$\frac{d}{dt}\left(\frac{\partial T^*}{\partial \dot{y}}\right) = \left(m_1 + m_2\right)\ddot{y} + m_1 r_G\left(\ddot{\theta}\sin\theta_G + \dot{\theta}^2 cos\,\theta_G\right)$$

$$\frac{d}{dt}\left(\frac{\partial T^*}{\partial \dot{\theta}}\right) = m_1 r_G\left(\ddot{y}\sin\theta_G - \ddot{z}\cos\theta_G + \dot{y}\dot{\theta}\cos\theta_G + \dot{z}\dot{\theta}\sin\theta_G\right) + m_1 r_G^2\ddot{\theta} + J\ddot{\theta}$$

$$\frac{\partial T^*}{\partial z} = \frac{\partial T^*}{\partial y} = 0$$

$$\frac{\partial T^*}{\partial \theta} = m_1\dot{\theta} r_G\left(\dot{y}\dot{\theta} cos\,\theta_G + \dot{z}\dot{\theta}\sin\theta_G\right)$$

Potential Energy Partial Differential Derivations

The potential energy partial differential energy equation derivations are presented in the following sets of equations. Equation (3.142) is used to derive these equations.

Three significant equation solution specific changes occur between Phases I and II, which are solved via direct methods, and Phases III and IV, which are solved via Lagrangian energy methods. First the Lagrangian energy method requires magnetic air gap differentials for the potential energy. Recall that the magnetic spring constants are air gap distance dependent variable values and therefore are not constant values for the Lagrangian potential energy partial differential solutions. Fortunately the spring constant equations are readily differentiable, as shown in the differential equations for G_3, equations (3.98) and (3.99), and the solutions of the B_T, B_N, and J_x, equations (3.102), (3.103), and (3.107), from Chapters 3.3.a.ii and 3.3.a.iii.

Second the magnetic air gaps are no longer uniquely in the z coordinate direction. Instead the air gaps are in the z and y coordinate directions. The components of the body force equations solved must reflect this change. Third the linear varying magnetic air gap has both linear and rotational components, as mentioned previously in this Phase III solution and shown in equation (3.142), which must also be expressed in the body force equation solution. The second change noted here effects all parts of the Lagrangian. The first and third changes effect, and only effect, the potential energy components of the Lagrangian energy method. None of these changes pose a significant challenge but they do require good equation bookkeeping which must be observed.

The z and y coordinate direction air gap lengths, which replace the body force equation air gap distance values, are shown in equation (3.142). Referring to equation (3.110), the body force equation constant component differentials for the magnetic spring constant variables are solved through the functional dependencies of the following equations. Note that these equations are for each respective normal repulsive force produced by each solenoid's tangential magnetic component, B_T, only. The normal magnetic component, B_N, is also solved in this analysis but it is not required for the damping stability criteria under analysis. This B_N component only produces a drag force on the secondary's propulsive motion.

Repulsive Force:

$$\left\langle F_z(\xi,z,\theta)\right\rangle \rightarrow \left\langle F_z\left\{J_x\left[G_3(\xi,z,\theta)\right],B_y\left[G_3'(\xi,z,\theta)\right]\right\}\right\rangle$$
$$\left\langle F_y(\xi,y,\theta)\right\rangle \rightarrow \left\langle F_y\left\{J_z\left[G_3(\xi,y,\theta)\right],B_x\left[G_3'(\xi,y,\theta)\right]\right\}\right\rangle$$

Drag Force:

$$\left\langle F_{zDrag}(\xi,z,\theta)\right\rangle \rightarrow \left\langle F_{zDrag}\left\{J_x\left[G_3(\xi,z,\theta)\right],B_z\left[G_3(\xi,z,\theta)\right]\right\}\right\rangle$$
$$\left\langle F_{yDrag}(\xi,y,\theta)\right\rangle \rightarrow \left\langle F_{yDrag}\left\{J_z\left[G_3(\xi,y,\theta)\right],B_y\left[G_3(\xi,y,\theta)\right]\right\}\right\rangle$$

Noting these body force equation functional dependencies, all other values are considered constant, the body force equation differentials are provided in equation set (3.143). These body force equation differentials are required for the potential energy differentials.

Repulsive Force:

$$\left\langle F_z'(\xi,z,\theta)\right\rangle \rightarrow \left\langle F_z'\left\{J_x\left[G_3'(\xi,z,\theta)\right],B_y\left[G_3''(\xi,z,\theta)\right],J_x\left[G_3(\xi,z,\theta)\right],B_y\left[G_3'(\xi,z,\theta)\right]\right\}\right\rangle$$
$$\left\langle F_y'(\xi,y,\theta)\right\rangle \rightarrow \left\langle F_y'\left\{J_z\left[G_3'(\xi,y,\theta)\right],B_x\left[G_3''(\xi,y,\theta)\right],J_z\left[G_3(\xi,y,\theta)\right],B_x\left[G_3'(\xi,y,\theta)\right]\right\}\right\rangle \quad (3.143)$$

Drag Force:

$$\left\langle F_{zDrag}'(\xi,z,\theta)\right\rangle \rightarrow \left\langle F_{zDrag}'\left\{J_x\left[G_3'(\xi,z,\theta)\right],B_z\left[G_3'(\xi,z,\theta)\right],J_x\left[G_3(\xi,z,\theta)\right],B_z\left[G_3(\xi,z,\theta)\right]\right\}\right\rangle$$
$$\left\langle F_{yDrag}'(\xi,y,\theta)\right\rangle \rightarrow \left\langle F_{yDrag}'\left\{J_z\left[G_3'(\xi,y,\theta)\right],B_y\left[G_3'(\xi,y,\theta)\right],J_z\left[G_3(\xi,y,\theta)\right],B_y\left[G_3(\xi,y,\theta)\right]\right\}\right\rangle$$

The magnetic spring constants, as outlined in equation (3.117), assume the forms of equation set (3.144).

Repulsive Force:

$$k_z = \frac{\left[\frac{1}{2}\mathrm{Re}\left(J_x B_y^*\right)\right]\bullet\begin{pmatrix}\text{Magnetic}\\ \text{Volume}\end{pmatrix}}{z_g} = \frac{1}{2}\bullet\begin{pmatrix}\text{Magnetic}\\ \text{Volume}\end{pmatrix}\bullet\left[\frac{\mathrm{Re}\left(J_x B_{Ty}^*\right)}{z_g}\right]$$
$$k_y = \frac{\left[\frac{1}{2}\mathrm{Re}\left(J_z B_x^*\right)\right]\bullet\begin{pmatrix}\text{Magnetic}\\ \text{Volume}\end{pmatrix}}{y_g} = \frac{1}{2}\bullet\begin{pmatrix}\text{Magnetic}\\ \text{Volume}\end{pmatrix}\bullet\left[\frac{\mathrm{Re}\left(J_z B_{Tx}^*\right)}{y_g}\right] \quad (3.144)$$

Drag Force:

$$k_{zDrag} = \frac{\left[\frac{1}{2}\mathrm{Re}\left(J_x B_z^*\right)\right] \bullet \begin{pmatrix}\text{Magnetic}\\ \text{Volume}\end{pmatrix}}{z_g} = \frac{1}{2} \bullet \begin{pmatrix}\text{Magnetic}\\ \text{Volume}\end{pmatrix} \bullet \left[\frac{\mathrm{Re}\left(J_x B_z^*\right)}{z_g}\right]$$

$$k_{yDrag} = \frac{\left[\frac{1}{2}\mathrm{Re}\left(J_z B_y^*\right)\right] \bullet \begin{pmatrix}\text{Magnetic}\\ \text{Volume}\end{pmatrix}}{y_g} = \frac{1}{2} \bullet \begin{pmatrix}\text{Magnetic}\\ \text{Volume}\end{pmatrix} \bullet \left[\frac{\mathrm{Re}\left(J_z B_y^*\right)}{y_g}\right]$$

In order to properly solve the partial derivatives for the air gap distance dependent magnetic spring constants, substitutions and differentials must be performed on the air gap distance denominator values of equation (3.144) and the air gap distance dependent force components provided in equation (3.98) for G_3.

k_z Derivations:

The following solve for the air gap distance component from the denominator of the magnetic spring constant equation.

$$\frac{\partial\left[z_g^{-1}(z,\theta)\right]}{\partial z} = z_g'(z,\theta) = \frac{1}{z_g^2}$$

$$\frac{\partial\left[z_g^{-1}(z,\theta)\right]}{\partial \theta} = z_g'(z,\theta) = \frac{-\ell_z \cos(\theta)}{z_g^2}$$

Now solve for the G_3 component of the repulsive magnetic force equation. Note that the G_3 equation exponential substitutions provide the following output for the z directed magnetic spring constants.

For C_{GA}: $e^{\left\{z-\left[\left(z_{g\_init}-z\right)+\ell_z \sin\theta\right]\right\}\xi} = e^{\left(2z-z_{g\_init}-\ell_z \sin\theta\right)\xi}$

For C_{GB}: $e^{\left\{\left[\left(z_{g\_init}-z\right)+\ell_z \sin\theta\right]-z\right\}\xi} = e^{\left(z_{g\_init}-2z+\ell_z \sin\theta\right)\xi}$

This substitution provides the following equations for $G_3(\xi, z, \theta)$ and all of its derivatives. Note that for brevity the applicable range of $0 \le z \le z_g$ is removed from these and all subsequent equations.

$$G_3(\xi,z,\theta)=\left[C_{GA}e^{\left(2z-z_{g\_init}-\ell_z\sin\theta\right)\xi}+C_{GB}e^{\left(z_{g\_init}-2z+\ell_z\sin\theta\right)\xi}\right]$$

$$\frac{\partial\left[G_3(\xi,z,\theta)\right]}{\partial z}=G_3'(\xi,z,\theta)=2\xi\left[\begin{matrix}C_{GA}e^{\left(2z-z_{g\_init}-\ell_z\sin\theta\right)\xi}-\\-C_{GB}e^{\left(z_{g\_init}-2z+\ell_z\sin\theta\right)\xi}\end{matrix}\right]$$

$$\frac{\partial^2\left[G_3(\xi,z,\theta)\right]}{\partial z^2}=G_3''(\xi,z,\theta)=4\xi^2\left[\begin{matrix}C_{GA}e^{\left(2z-z_{g\_init}-\ell_z\sin\theta\right)\xi}+\\+C_{GB}e^{\left(z_{g\_init}-2z+\ell_z\sin\theta\right)\xi}\end{matrix}\right]$$

$$\frac{\partial\left[G_3(\xi,z,\theta)\right]}{\partial\theta}=G_3'(\xi,z,\theta)=\xi\ell_z\cos\theta\left[\begin{matrix}C_{GB}e^{\left(z_{g\_init}-2z+\ell_z\sin\theta\right)\xi}-\\-C_{GA}e^{\left(2z-z_{g\_init}-\ell_z\sin\theta\right)\xi}\end{matrix}\right]$$

$$\frac{\partial^2\left[G_3(\xi,z,\theta)\right]}{\partial\theta^2}=G_3''(\xi,z,\theta)=\xi^2\ell_z^2\cos^2\theta\left[\begin{matrix}C_{GA}e^{\left(2z-z_{g\_init}-\ell_z\sin\theta\right)\xi}+\\+C_{GB}e^{\left(z_{g\_init}-2z+\ell_z\sin\theta\right)\xi}\end{matrix}\right]$$

This produces the desired functional dependency equations for the magnetic spring constant derivatives. These equations are used to solve the nonlinear magnetic spring constant component of the potential energy partial differential equation via the summation of the partial derivative components. This form of summation will follow each remaining spring constant derivation section of Phases III and IV.

$$\sum z_g'(z,\theta)=\frac{1-\ell_z\cos(\theta)}{z_g^2} \tag{3.145}$$

$$\sum G_3'(\xi,z,\theta)=\left(2\xi+\xi\ell_z\cos\theta\right)\left[\begin{matrix}C_{GB}e^{\left(z_{g\_init}-2z+\ell_z\sin\theta\right)\xi}-\\-C_{GA}e^{\left(2z-z_{g\_init}-\ell_z\sin\theta\right)\xi}\end{matrix}\right] \tag{3.146}$$

$$\sum G_3''(\xi,z,\theta)=\left(4\xi^2+\xi^2\ell_z^2\cos^2\theta\right)\left[\begin{matrix}C_{GA}e^{\left(2z-z_{g\_init}-\ell_z\sin\theta\right)\xi}+\\+C_{GB}e^{\left(z_{g\_init}-2z+\ell_z\sin\theta\right)\xi}\end{matrix}\right] \tag{3.147}$$

k_y Derivations:

The following equations solve for the air gap distance component from the denominator of the magnetic spring constant equation.

$$\frac{\partial\left[y_g^{-1}(y,\theta)\right]}{\partial y} = y_g'(y,\theta) = \frac{1}{y_g^2}$$

$$\frac{\partial\left[y_g^{-1}(y,\theta)\right]}{\partial \theta} = y_g'(y,\theta) = \frac{\ell_y \cos(\theta)}{y_g^2}$$

Now solve for the G_3 component of the repulsive magnetic force equation. Now perform the exponential substitutions for the y directed magnetic spring constants for the G_3 equation.

$$\text{For } C_{GA}\text{: } e^{\left\{y-\left[\left(y_{g\_init}-y\right)-\ell_y \sin\theta\right]\right\}\xi} = e^{\left(2y-y_{g\_init}+\ell_y \sin\theta\right)\xi}$$

$$\text{For } C_{GB}\text{: } e^{\left\{\left[\left(y_{g\_init}-y\right)-\ell_y \sin\theta\right]-y\right\}\xi} = e^{\left(y_{g\_init}-2y-\ell_y \sin\theta\right)\xi}$$

This substitution provides the following equations for $G_3(\xi, y, \theta)$ and all of its derivatives.

$$G_3(\xi,y,\theta) = \left[C_{GA}e^{\left(2y-y_{g\_init}+\ell_y \sin\theta\right)\xi} + C_{GB}e^{\left(y_{g\_init}-2y-\ell_y \sin\theta\right)\xi}\right]$$

$$\frac{\partial\left[G_3(\xi,y,\theta)\right]}{\partial y} = G_3'(\xi,y,\theta) = 2\xi\left[\begin{matrix}C_{GA}e^{\left(2y-y_{g\_init}+\ell_y \sin\theta\right)\xi} - \\ -C_{GB}e^{\left(y_{g\_init}-2y-\ell_y \sin\theta\right)\xi}\end{matrix}\right]$$

$$\frac{\partial^2\left[G_3(\xi,y,\theta)\right]}{\partial y^2} = G_3''(\xi,y,\theta) = 4\xi^2\left[\begin{matrix}C_{GA}e^{\left(2y-y_{g\_init}+\ell_y \sin\theta\right)\xi} + \\ +C_{GB}e^{\left(y_{g\_init}-2y-\ell_y \sin\theta\right)\xi}\end{matrix}\right]$$

$$\frac{\partial\left[G_3(\xi,y,\theta)\right]}{\partial \theta} = G_3'(\xi,y,\theta) = \xi\ell_y \cos\theta\left[\begin{matrix}C_{GA}e^{\left(2y-y_{g\_init}+\ell_y \sin\theta\right)\xi} - \\ -C_{GB}e^{\left(y_{g\_init}-2y-\ell_y \sin\theta\right)\xi}\end{matrix}\right]$$

$$\frac{\partial^2\left[G_3(\xi,y,\theta)\right]}{\partial \theta^2} = G_3''(\xi,y,\theta) = \xi^2\ell_y^2 \cos^2\theta\left[\begin{matrix}C_{GA}e^{\left(2y-y_{g\_init}+\ell_y \sin\theta\right)\xi} + \\ +C_{GB}e^{\left(y_{g\_init}-2y-\ell_y \sin\theta\right)\xi}\end{matrix}\right]$$

This produces the desired functional dependency equations for the magnetic spring constant derivatives. These equations are used to solve the nonlinear magnetic

spring constant component of the potential energy partial differential equation via the summation of the partial derivative components.

$$\sum y_g'(y,\theta) = \frac{1+\ell_y\cos(\theta)}{y_g^2} \tag{3.148}$$

$$\sum G_3'(\xi,y,\theta) = \left(2\xi+\xi\ell_y\cos\theta\right)\begin{bmatrix} C_{GA}e^{\left(2y-y_{g\_init}+\ell_y\sin\theta\right)\xi} - \\ -C_{GB}e^{\left(y_{g\_init}-2y-\ell_y\sin\theta\right)\xi}\end{bmatrix} \tag{3.149}$$

$$\sum G_3''(\xi,y,\theta) = \left(4\xi^2+\xi^2\ell_y^2\cos^2\theta\right)\begin{bmatrix} C_{GA}e^{\left(2y-y_{g\_init}+\ell_y\sin\theta\right)\xi} + \\ +C_{GB}e^{\left(y_{g\_init}-2y-\ell_y\sin\theta\right)\xi}\end{bmatrix} \tag{3.150}$$

Magnetic Spring Constant Derivation Solutions – Repulsive Force:

Referring only to the air gap distance dependent values of the air gap distance itself and the G_3 components of the spring force equation (3.144), the air gap distance dependent components assume the abbreviated form shown in equation (3.151). Note that the z axis air gap is used for reference but this equation applies to any air gap direction.

$$\frac{G_3G_3'}{z_g} = \frac{2G_3'}{z_g} + \frac{G_3G_3''}{z_g} + \frac{G_3G_3'}{z_g'} = \overbrace{\frac{2G_3'+G_3G''}{z_g}}^{\text{Body Force Component}} + \overbrace{\frac{G_3G_3'}{z_g'}}^{\text{Denominator Air Gap Component}} \tag{3.151}$$

Equation (3.151) is now used to solve for the appropriate forms of the magnetic spring constant derivatives.

$$k_z' = \frac{1}{2}\bullet\begin{pmatrix}\text{Magnetic}\\ \text{Volume}\end{pmatrix}\left\{\begin{bmatrix}\text{Re}\left(J_x\left[\sum G_3'(\xi,z,\theta)\right]B_y^*\left[\sum G_3'(\xi,z,\theta)\right]\right)+ \\ +\text{Re}\left(J_x\left[\sum G_3(\xi,z,\theta)\right]B_y^*\left[\sum G_3''(\xi,z,\theta)\right]\right)\end{bmatrix}\frac{}{z_g}+ \right.$$
$$\left. +\text{Re}\left(J_x\left[\sum G_3(\xi,z,\theta)\right]B_y^*\left[\sum G_3'(\xi,z,\theta)\right]\right)\sum z_g'(z,\theta)\right\} \tag{3.152}$$

$$k'_y = \frac{1}{2}\bullet\begin{pmatrix}\text{Magnetic}\\ \text{Volume}\end{pmatrix}\left\{\begin{array}{l}\text{Re}\left(J_z\left[\sum G'_3(\xi,y,\theta)\right]B^*_x\left[\sum G'_3(\xi,y,\theta)\right]\right)+\\ \dfrac{+\text{Re}\left(J_z\left[\sum G_3(\xi,y,\theta)\right]B^*_x\left[\sum G''_3(\xi,y,\theta)\right]\right)}{y_g}+\\ +\text{Re}\left(J_z\left[\sum G_3(\xi,y,\theta)\right]B^*_x\left[\sum G'_3(\xi,y,\theta)\right]\right)\sum y'_g(y,\theta)\end{array}\right\} \quad (3.153)$$

Magnetic Spring Constant Derivation Solutions – Drag Force:

$$k'_{zDrag} = \frac{1}{2}\bullet\begin{pmatrix}\text{Magnetic}\\ \text{Volume}\end{pmatrix}\left\{\begin{array}{l}\text{Re}\left(J_x\left[\sum G'_3(\xi,z,\theta)\right]B^*_z\left[\sum G'_3(\xi,z,\theta)\right]\right)+\\ \dfrac{+\text{Re}\left(J_x\left[\sum G_3(\xi,z,\theta)\right]B^*_z\left[\sum G_3(\xi,z,\theta)\right]\right)}{z_g}+\\ +\text{Re}\left(J_x\left[\sum G_3(\xi,z,\theta)\right]B^*_z\left[\sum G'_3(\xi,z,\theta)\right]\right)\sum z'_g(z,\theta)\end{array}\right\}$$

$$k'_{yDrag} = \frac{1}{2}\bullet\begin{pmatrix}\text{Magnetic}\\ \text{Volume}\end{pmatrix}\left\{\begin{array}{l}\text{Re}\left(J_z\left[\sum G'_3(\xi,y,\theta)\right]B^*_y\left[\sum G'_3(\xi,y,\theta)\right]\right)+\\ \dfrac{+\text{Re}\left(J_z\left[\sum G_3(\xi,y,\theta)\right]B^*_y\left[\sum G_3(\xi,y,\theta)\right]\right)}{y_g}+\\ +\text{Re}\left(J_z\left[\sum G_3(\xi,y,\theta)\right]B^*_y\left[\sum G'_3(\xi,y,\theta)\right]\right)\sum y'_g(y,\theta)\end{array}\right\}$$

Potential Energy Derivation Solutions:

Finally the potential energy partial derivatives are solved in the following equations. Note that the appropriate forms of equations (3.145) through (3.147) for the G_3 equation and all of the appropriate derivatives must be inserted for the z dependent linear and rotational magnetic spring constant values in equation (3.152). The same is true for including the appropriate forms of equations (3.148) through (3.150) for the y dependent linear and rotational magnetic spring constant values in equation (3.153). For example, in equation (3.153) for the magnetic spring variable k'_y, the appropriate forms of the functions G_3, G'_3, and G''_3 come from the superposition equations (3.149) and (3.150). This superposition is mathematically performed by superimposing each respective G_3, G'_3, and G''_3 component inside of

the respective J_z and B_x^* equations being solved and then taking a single multiplication of the J_z and B_x^* in each respective potential energy partial derivative equations. The air gap partial differential superposition comes from equation (3.148).

Only the repulsive force potential energy partial differentials are solved since this is the area of interest in this analysis. The propulsive drag component could also be determined in a similar fashion along the propulsion vector.

$$\frac{\partial U}{\partial z} = \left[\frac{k_z' z_g^2}{2} - \left(k_z + k_{HA} \right) z_g \right] + g\left(m_1 + m_2 \right) - \left(k_{mechz} \right)\left(z_{g\_init} - z \right)$$

$$\frac{\partial U}{\partial y} = \left(\frac{k_y' y_g^2}{2} - k_y y_g \right) - k_{mechy}\left(y_{g\_init} - y \right)$$

$$\frac{\partial U}{\partial \theta} = \left[\frac{k_z' z_g^2}{2} + \left(k_z + k_{HA} \right) \ell_z z_g \cos\theta \right] + \left[\frac{k_y' y_g^2}{2} - k_y \ell_y y_g \cos\theta \right] - g m_1 \ell_z \cos\theta$$

Lagrange Equations of Motion

Use the partial differential kinetic and potential energy equation derivations to solve Lagrange's equation of motion, equation (3.154), and the subsequent equations of motion for each generalized coordinate. Then solve for the generalized coordinate equation form suitable for numerical state space solution. This numerical solution equation form always isolates the highest differentials of the single respective generalized coordinate under analysis. The generalized force, Q, is zero for this homogeneous system. $Q \neq 0$ when a disturbing force is introduced to provide the particular solution.

$$\frac{d}{dt}\left(\frac{\partial T^*}{\partial \dot{q}_i} \right) - \frac{\partial T^*}{\partial q_i} + \frac{\partial U}{\partial q_i} + \overbrace{\cancelto{0}{\frac{\partial D}{\partial \dot{q}_i}}}^{\text{System Natural Damping Component}} = Q_i \qquad (3.154)$$

Generalized Coordinate $q = z$:

Equation (3.155) solves for $q = z$.

$$\left(m_1 + m_2\right)\ddot{z} - m_1 r_G\left(\ddot{\theta}\cos\theta_G - \dot{\theta}^2\sin\theta_G\right) +$$
$$+\left[\frac{k_z' z_g^2}{2} - \left(k_z + k_{HA}\right)z_g\right] + g\left(m_1 + m_2\right) - \left(k_{mechz}\right)\left(z_{g\_init} - z\right) = 0$$

$$\ddot{z} = \frac{\left\{\begin{array}{l} m_1 r_G\left(\ddot{\theta}\cos\theta_G - \dot{\theta}^2\sin\theta_G\right) - \left[\dfrac{k_z' z_g^2}{2} - \left(k_z + k_{HA}\right)z_g\right] - \\ -g\left(m_1 + m_2\right) + \left(k_{mechz}\right)\left(z_{g\_init} - z\right) \end{array}\right\}}{\left(m_1 + m_2\right)} \qquad (3.155)$$

Generalized Coordinate $q = y$:

Equation (3.156) solves for $q = y$.

$$\left(m_1 + m_2\right)\ddot{y} + m_1 r_G\left(\ddot{\theta}\sin\theta_G + \dot{\theta}^2 cos\,\theta_G\right) +$$
$$+\left(\frac{k_y' y_g^2}{2} - k_y y_g\right) - k_{mechy}\left(y_{g\_init} - y\right) = 0$$

$$\ddot{y} = \frac{\left[k_{mechy}\left(y_{g\_init} - y\right) - m_1 r_G\left(\ddot{\theta}\sin\theta_G + \dot{\theta}^2 cos\,\theta_G\right) - \left(\dfrac{k_y' y_g^2}{2} - k_y y_g\right)\right]}{\left(m_1 + m_2\right)} \qquad (3.156)$$

Generalized Coordinate $q = \theta$:

Equation (3.157) solves for $q = \theta$.

$$m_1 r_G\left(\ddot{y}\sin\theta_G - \ddot{z}\cos\theta_G + \dot{y}\dot{\theta}\cos\theta_G + \dot{z}\dot{\theta}\sin\theta_G\right) + m_1 r_G^2\ddot{\theta} + J\ddot{\theta} -$$
$$-m_1\dot{\theta}r_G\left(\dot{y}\dot{\theta}cos\,\theta_G + \dot{z}\dot{\theta}\sin\theta_G\right) +$$
$$+\left[\frac{k_z' z_g^2}{2} + \left(k_z + k_{HA}\right)\ell_z z_g\cos\theta\right] + \left[\frac{k_y' y_g^2}{2} - k_y\ell_y y_g\cos\theta\right] - gm_1\ell_z\cos\theta = 0$$

$$\ddot{\theta} = \frac{\left\{ \begin{array}{l} m_1 \dot{\theta} r_G \left(\dot{y}\dot{\theta} \cos\theta_G + \dot{z}\dot{\theta}\sin\theta_G \right) - m_1 r_G \left(\begin{array}{l} \ddot{y}\sin\theta_G - \ddot{z}\cos\theta_G + \\ + \dot{y}\dot{\theta}\cos\theta_G + \dot{z}\dot{\theta}\sin\theta_G \end{array} \right) - \\ - \left[\frac{k_z' z_g^2}{2} + \left(k_z + k_{HA} \right) \ell_z z_g \cos\theta \right] - \left[\frac{k_y' y_g^2}{2} - k_y \ell_y y_g \cos\theta \right] + g m_1 \ell_z \cos\theta \end{array} \right\}}{m_1 r_G^2 + J} \quad (3.157)$$

The three Phase III homogenous equations of motion forms as presented in equations (3.155), (3.156), and (3.157) are suitable for solving a numerical state space solution. Observe that the equations of motion are highly nonlinear. Nonlinearities are based on geometric or material nonlinearities. This system is geometrically nonlinear as well as materially nonlinear in the primary iron core of both the principal and control solenoids until complete magnetic saturation occurs. Matrix format is only applicable for linear systems and therefore not employed in this analysis. Linearization approximations such as small angle approximations or assuming appropriate lumped generalized coordinates allow determining approximate vibration response through matrix format utilization. This technique helps understand the basics of system response, but answers quickly lose validity with greater linearization approximations. Geometric linearization approximations are currently not used for the reasons mentioned in the Phase IV small angle approximation equation of (3.159), but noted as a possible future tool.

3.5.b Computational Analysis

A Phase III computational analysis would follow a similar pattern as Phase I and described in Chapter 3.3.b. No Phase II specific computational analyses are performed.

3.5.c Control and Optimization Analysis

3.5.c.i Soft Computing Control Theory

Phase III would implement a similar soft computing method as Phase I which is described in Chapter 3.3.c.ii. No Phase III specific soft computing control methods are implemented.

3.6 PHASE IV

3.6.a Analytical Equation Derivation

3.6.a.i Plant Dynamics

Plant Equation of Motion

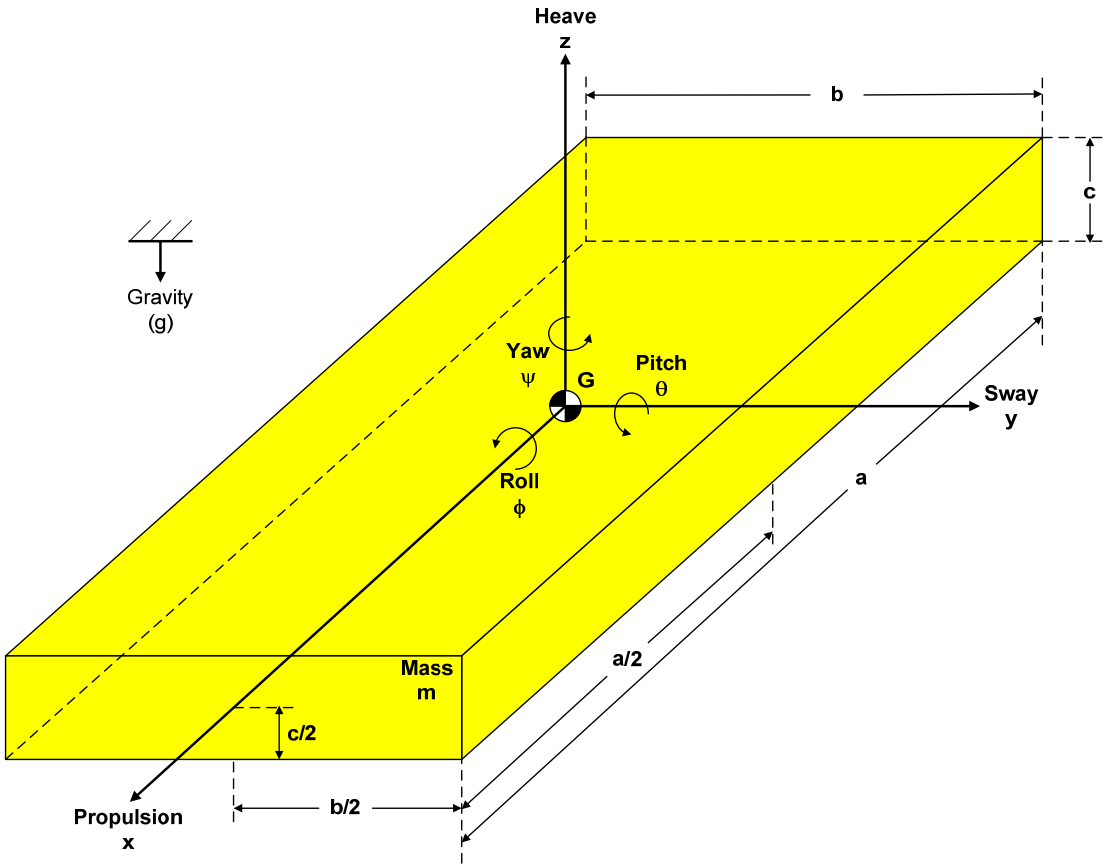

Figure 3.6-1: Phase IV System Equivalent Levitated 6 D.O.F. Vehicle

The Phase IV plant levitated six D.O.F. mechanical relations are provided in Figure 3.6-1. The x, y, and z parameter definitions are provided in Chapter 3.1.b. All Phase IV energy elements are sized equivalently to Phase II and III. As globally described in Chapter 2.3.e, the main mathematical differences between Phase III and Phase IV are the nonlinearities introduced through the extra coupled degrees of freedom. By assuming rigid body motion of a basic polar moment shape such as the perfect rectangular mass shown in Figure 3.6-1 where the C.O.M. location is the same as the body reference frame center and the geometric center, J, the angular mass moment of inertia, may be solved with an uncoupled diagonal mass moment of inertia matrix without the complexity of a coupled mass moment of inertia matrix solution. Here the body reference frame origin is taken where all magnetic springs cancel with respect to one another and the gravitational body force. As stated in Phase III, unless the angular coupling of the mass moment of inertia from either a complex shape or a C.O.M. location differing from the geometric center is the focus of analysis, this perfect rectangular body approximation or equivalent is a common first step. After the basic performance is understood then the use of C.A.D. models and eventually test performance data will provide any necessary modifications for the simulation model and corresponding analysis.

In Figure 3.6-1 the roll and pitch y axis lateral side height c interference of the secondary on the stator guidance system is ignored by assuming that although the C.O.M. and geometric center are fixed, the secondary height corners along the length c remain orthogonal to the primary regardless of actual secondary orientation. As equivalent assumption occurs for the vehicle rotation with respect to the guideway bottom. These assumptions to ignore the changing aspect of the vehicle edges with respect to the guideway lateral side walls and base as the vehicle rotates is satisfactory for a proof of concept model since a vehicle disturbance which causes the vehicle to approach these boundary limitation is considered a failure, but these assumptions must be rectified prior to implementing a final system model.

All prime mover, control, and disturbance perturbation forces for all axes are discretely lumped onto the vehicle's Halbach array full wavelength locations. For this analysis this approximation is taken one step further by only using the Halbach array full wavelength node locations at the extreme ends of the levitated vehicle. Principal coil lateral and vertical entities then assume the superposition of all Halbach array forces located at the end of vehicle nodes. On top of the Halbach array coil location approximation, control coil lateral and vertical entities are placed at the same end of vehicle nodes. Therefore, as shown in Figure 3.6-2, each bottom corner node of the six D.O.F. vehicle locates a vertical and lateral coil which represents the superposition of the Halbach array magnetic force values as well as the control coil force values. This Phase IV node organization differs from Phase III where the magnetic control coil nodes, k_z and k_y, the Halbach array node, k_{HA}, and the mechanical spring nodes, k_{mechz} and k_{mechy}, are identified independently as depicted in Figure 3.5-1. The equation $k_{yBS} = k_{yBS\_\text{Lateral Principal Coil}} + k_{yBS\_\text{Lateral Control Coil}}$ is provided as an example of the Phase IV dual control and principle coil location concept. This approximation provides a manageable simulation model while maintaining the complex D.O.F. coupling. This approximation may also be used for any E.D.R. maglev system. The coil subscripts of Figure 3.6-2 refer to the various control and principle solenoid coil bow, aft, starboard, and port locations.

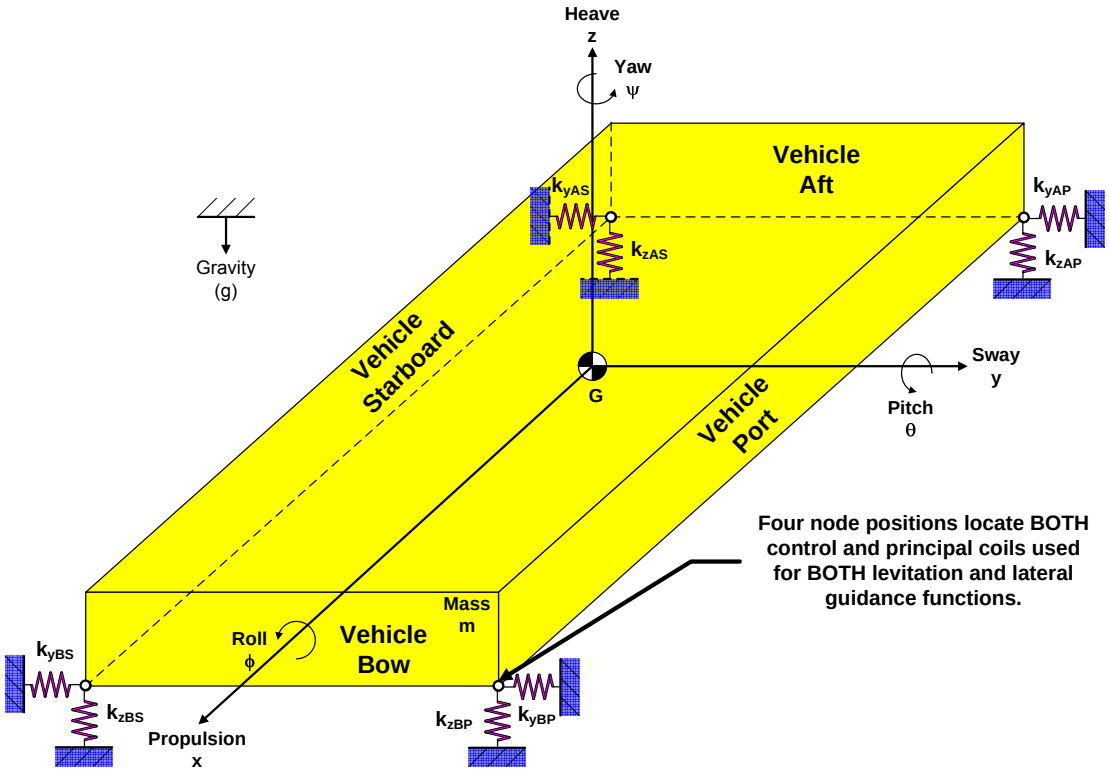

Figure 3.6-2: Phase IV Electromagnetic Spring Model

As Figure 3.6-2 indicates, the Phase IV vehicle is held aloft and guided entirely through electromagnetic means unlike Phase I which uses mechanical guides with the potential of additional vertical mechanical springs and Phases II and III which use mechanical guides as well as vertical mechanical springs. Each Phase IV node locates the lateral guidance and vertical levitation electromagnetic spring control and principle coil combinations.

System Kinematics

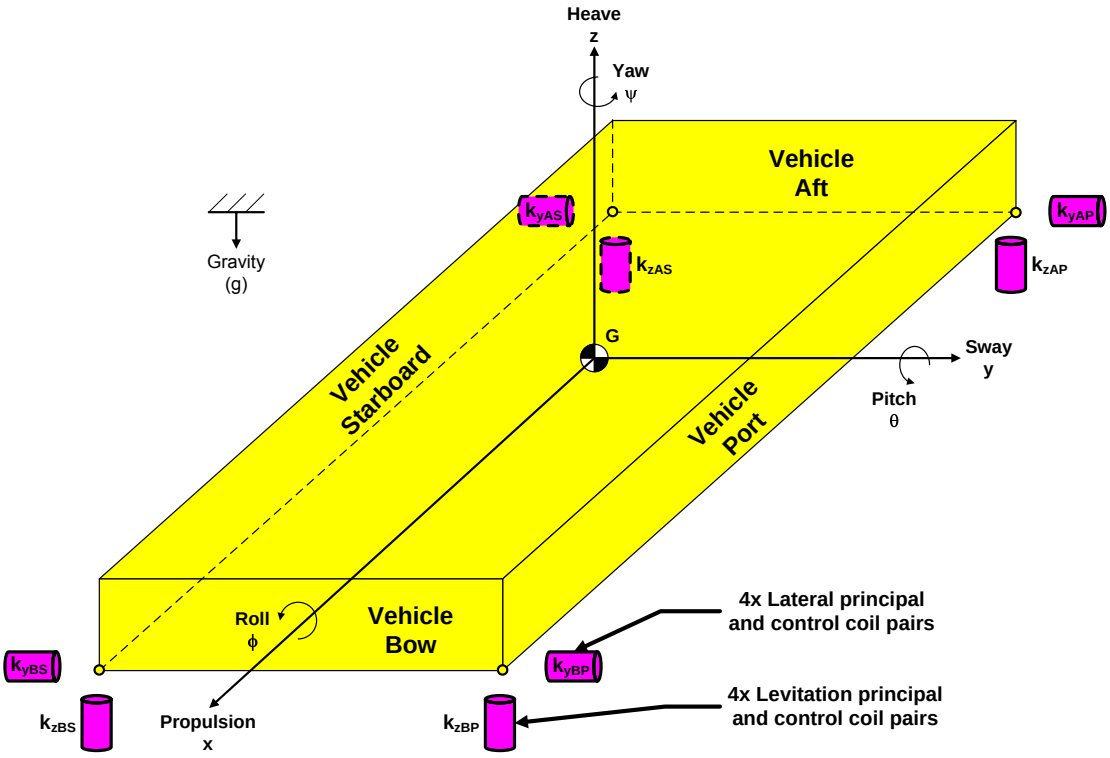

Figure 3.6-3: Phase IV Electromagnetic Coil Model

The coil locations used for analysis are provided in Figure 3.6-3. It should be noted that the shape of the vehicle and corresponding coil locations in Figure 3.6-3 are different than Figure 2.3-3. The change is made to provide for a perfectly rectangular primary. Everything else being equal, coil primary and secondary

locations may be mathematically interchanged between the vehicle and the guideway as long as they have the same magnetic interactions across the air gap, in the primary, and in the secondary as well as follow the vehicle motion such that they are always interacting through the same vehicle nodes and corresponding guideway locations at all times. This perfectly rectangular rigid body where the C.O.M. location is the same as the body reference frame center and the geometric center assumes the polar mass moment of inertia equation set (3.158) applies.

$$\begin{aligned} J_{xx} &= \frac{m}{12}\left(b^2 + c^2\right) \\ J_{yy} &= \frac{m}{12}\left(a^2 + c^2\right) \\ J_{zz} &= \frac{m}{12}\left(a^2 + b^2\right) \end{aligned} \tag{3.158}$$

Small angle approximations are often used by assuming the overall translational body motions dominate the linear translation of rotational motions. This is particularly true in many large six D.O.F. systems where the body dimensions are appreciably greater than the overall body motions of heave, sway, roll, pitch, or yaw under analysis. Principle acceleration values then typically apply equation (3.159) as a second part of the small angle approximation since it is expected that the translational motions from the angular displacements are negligible.

$$\begin{pmatrix} \text{Small Angle} \\ \text{Approximation} \end{pmatrix}: \ \theta \simeq 0 \rightarrow \begin{cases} \sin\theta \simeq 0 \simeq \theta \\ \cos\theta \simeq 1 \end{cases} \tag{3.159}$$

In this analysis small angle approximations are not used for two important reasons. First, referring to Figure 2.4-1, the small perturbations of the body under analysis are meant to be controlled and not dismissed. The control hardware itself focuses on controlling the air gap magnetic spring constant value, the root of the plant analysis, which is non-linearly dependent on the air gap distance. In this case where the smallest angular motion of a vehicle with large dimensions strongly effects the control variable, the magnetic spring constant, fidelity of the angular generalized coordinates is required. This is especially true for the pitch generalized coordinate

since the vehicle geometry is greatest in the length direction and hence any pitch D.O.F. perturbation causes the greatest vehicle translation from an angular motion origin. This fact is witnessed in the Phase IV angular outputs in comparison to the accompanying translational outputs of Chapter 5.3.c. Second, although this analysis is focused on developing a large mass control scheme for full scale implementation, this analysis is also meant to accept a wide range of general cases for subscale through full scale analysis and testing purposes such that the body dimensions may approach similar magnitudes as the body motion.

Eulerian angles are required to allow the three rotational Cartesian coordinates to specify the rotational position of the body as well as the time derivatives of that rotational position through the relation $\vec{\omega} = \dot{\vec{\phi}} + \dot{\vec{\theta}} + \dot{\vec{\psi}}$ as discussed in Greenwood [3]. Since the small angle approximation is not used, small angle body rotations define components of the magnetic spring potential energy translations. Therefore the Euler angles need to transform from the body generalized rotational coordinates in the body reference frame to the inertial reference frame. This places $\vec{\omega}$ in the inertial reference frame as presented in a similar transformation in Dukkipati [1].

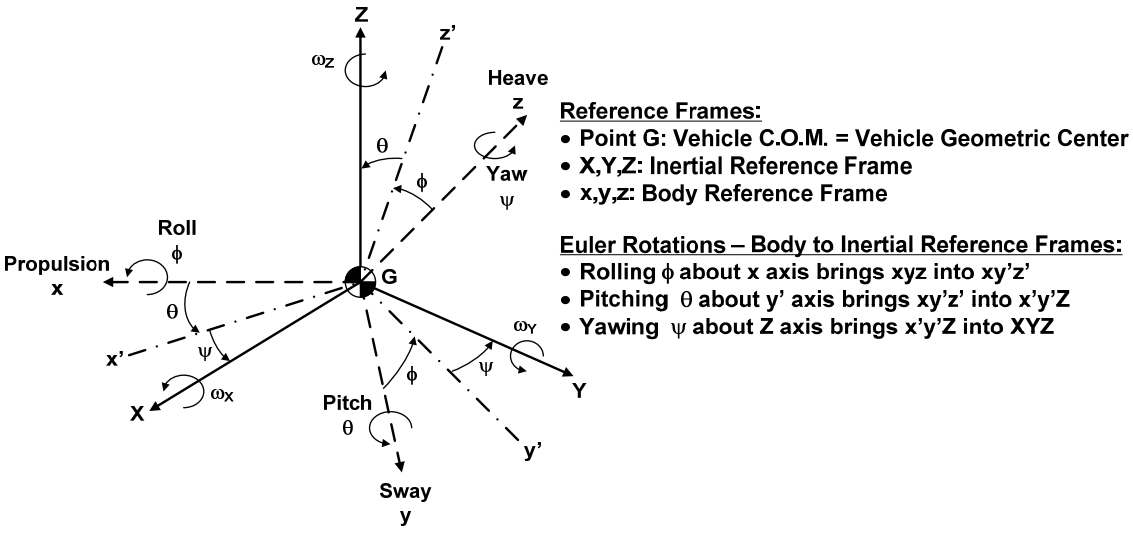

Figure 3.6-4: Phase IV Electromagnetic Coil Model – Front View

There are multiple ways to perform this Euler angle transformation. Figure 3.6-4 shows the Euler angle definitions used in the Phase IV analysis. The angular velocities associated with the Euler angles that represent the body reference frame roll, pitch, and yaw motions in the inertial reference frame are detailed in equation set (3.160).

$$\begin{aligned} &\text{X axis: } \omega_X = \dot{\phi}\cos\theta\cos\psi + \dot{\theta}\sin\psi \\ &\text{Y axis: } \omega_Y = \dot{\theta}\cos\psi - \dot{\phi}\cos\theta\sin\psi \\ &\text{Z axis: } \omega_Z = \dot{\psi} + \dot{\phi}\sin\theta \end{aligned} \tag{3.160}$$

Which leads to the equation set (3.161).

$$\begin{aligned} \omega_X^2 &= \dot{\phi}^2\cos^2\theta\cos^2\psi + 2\dot{\phi}\dot{\theta}\cos\theta\cos\psi\sin\psi + \dot{\theta}^2\sin^2\psi \\ \omega_Y^2 &= \dot{\theta}^2\cos^2\psi - 2\dot{\phi}\dot{\theta}\cos\theta\cos\psi\sin\psi + \dot{\phi}^2\cos^2\theta\sin^2\psi \\ \omega_Z^2 &= \dot{\psi}^2 + 2\dot{\phi}\dot{\psi}\sin\theta + \dot{\phi}^2\sin^2\theta \end{aligned} \tag{3.161}$$

Energy Derivations

For a simple method of maintaining desired accuracy for this six D.O.F. system, the Phase IV nonlinear equations of motion are solved in detail via Lagrange's energy method instead of direct methods. Basic examples of six D.O.F. maglev bodies that assume the small angle approximation are presented in Jayawant [10] via the direct method and Sinha [20] via the direct method and a small treatise on a general holonomic energy method. The generalized coordinates used for the Lagrangian analysis are $q = (x, y, z, \phi, \theta, \psi)$. Now that the generalized coordinates for this six D.O.F. system are set, the equations of motion can by determined by employing the Lagrangian equation in a manner similar to Phase III. Again note, as outlined Phase III, that the problem's physics and geometry defines the unidirectional potential energy sign convention.

$$T^* = \frac{1}{2}m\left(\dot{x}^2 + \dot{y}^2 + \dot{z}^2\right) + \frac{1}{2}\left(J_{xx}\omega_X^2 + J_{yy}\omega_Y^2 + J_{zz}\omega_Z^2\right) \tag{3.162}$$

$$U = mgz_g + \frac{1}{2}\left[\sum_j \left(k_{yj} y_{gj}^2\right)_j + \sum_k \left(k_{zk} z_{gk}^2\right)_k\right] \tag{3.163}$$

As originally introduced and defined in Chapter 3.1.b and reintroduced in more detail in Phase III, the linear varying magnetic air gap has both linear and rotational components, shown in the linear gap distance equations $z_g = \left\{z_{g\_init} + \left[z + \sum f_z\left(angle\right)\right]\right\}$ and $y_g = \left\{y_{g\_init} + \left[y + \sum f_y\left(angle\right)\right]\right\}$, which must be expressed in the body force equation solution through the potential energy component of the Lagrangian. Therefore an air gap effective distance per each coil solution similar to the one using Figure 3.5-2 of Phase III is required. Multiple two dimensional views of Figure 3.6-3, which are Figure 3.6-5, Figure 3.6-6, and Figure 3.6-7, are used to solve for the effective air gaps for each lateral and vertical coil pair.

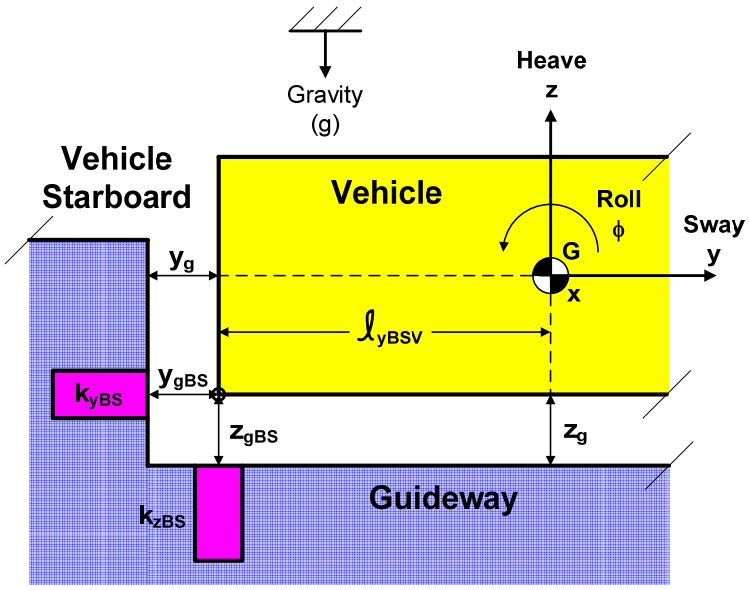

Figure 3.6-5: Phase IV Electromagnetic Coil Model – Front View

The front view of the bow, starboard levitation control module is shown in Figure 3.6-5. The new coil subscripts V and L within these two dimensional views refer to the various vertical and lateral coil locations respectively.

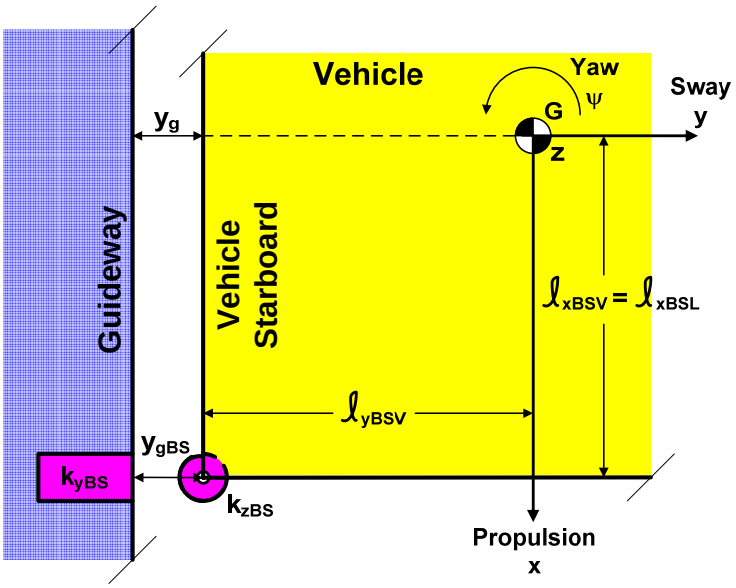

Figure 3.6-6: Phase IV Electromagnetic Coil Model – Plan View

The plan view of the bow, starboard levitation control module is shown in Figure 3.6-6.

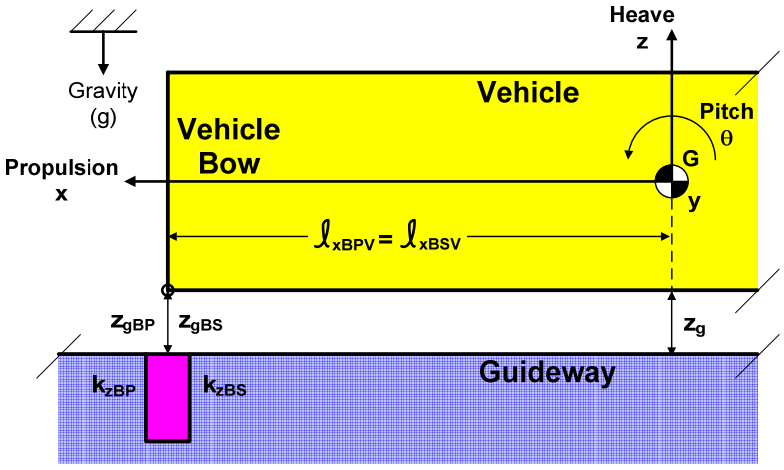

Figure 3.6-7: Phase IV Electromagnetic Coil Model – Side View

The side view of the bow, port and starboard levitation control modules are shown in Figure 3.6-7.

As described in more detail in Chapter 3.5.a.i of Phase III, the sign convention taken is that each respective variable magnetic spring constant, k, increases with a decrease in each respective air gap, but the gravitational dependent potential energy decreases with a decrease in z_g. This sign convention along with Figure 3.6-5, Figure 3.6-6, and Figure 3.6-7 provide Table 3.6-1. In this table the sign indicates the angular displacement direction with respect to the sign convention for increasing or decreasing potential energy.

Table 3.6-1: Potential Energy Angular Displacement Trigonometric Relations

AIR GAP LINEAR DISPLACEMENTS		
y Coordinate Axis Lateral Displacements	**z Coordinate Axis Vertical Displacements**	
ψ **Yaw Based**	ϕ **Roll Based**	θ **Pitch Based**
$\ell_{xBSL} = -\left(\frac{a}{2}\right)\sin\psi$	$\ell_{yBSV} = \left(\frac{b}{2}\right)\sin\phi$	$\ell_{xBSV} = \left(\frac{a}{2}\right)\sin\theta$
$\ell_{xBPL} = \left(\frac{a}{2}\right)\sin\psi$	$\ell_{yBPV} = -\left(\frac{b}{2}\right)\sin\phi$	$\ell_{xBPV} = \left(\frac{a}{2}\right)\sin\theta$
$\ell_{xAPL} = -\left(\frac{a}{2}\right)\sin\psi$	$\ell_{yAPV} = -\left(\frac{b}{2}\right)\sin\phi$	$\ell_{xAPV} = -\left(\frac{a}{2}\right)\sin\theta$
$\ell_{xASL} = \left(\frac{a}{2}\right)\sin\psi$	$\ell_{yASV} = \left(\frac{b}{2}\right)\sin\phi$	$\ell_{xASV} = -\left(\frac{a}{2}\right)\sin\theta$

Using Table 3.6-1 rewrite the potential energy equation, equation (3.163), by substituting in for the gap length variables. This provides equation (3.164) for the potential energy. Note that in this equation the various air gap distances are identified for each respective coil as well as the gravitational center.

$$U = mg\left(\overbrace{z_{g\_init}+z}^{=z_g}\right)+\frac{1}{2}\left\{\left[k_{yBS}\left(\overbrace{y_{g\_init}-y-\frac{a}{2}\sin\psi}^{=y_{gBS}}\right)^2+k_{yBP}\left(\overbrace{y_{g\_init}+y+\frac{a}{2}\sin\psi}^{=y_{gBP}}\right)^2+\right.\right.$$
$$\left.+k_{yAS}\left(\overbrace{y_{g\_init}-y+\frac{a}{2}\sin\psi}^{=y_{gAS}}\right)^2+k_{yAP}\left(\overbrace{y_{g\_init}+y-\frac{a}{2}\sin\psi}^{=y_{gAP}}\right)^2\right]+$$
$$+\left[k_{zBS}\left(\overbrace{z_{g\_init}-z+\frac{b}{2}\sin\phi+\frac{a}{2}\sin\theta}^{=z_{gBS}}\right)^2+k_{zBP}\left(\overbrace{z_{g\_init}-z-\frac{b}{2}\sin\phi+\frac{a}{2}\sin\theta}^{=z_{gBP}}\right)^2+\right.$$
$$\left.\left.+k_{zAS}\left(\overbrace{z_{g\_init}-z+\frac{b}{2}\sin\phi-\frac{a}{2}\sin\theta}^{=z_{gAS}}\right)^2+k_{zAP}\left(\overbrace{z_{g\_init}-z-\frac{b}{2}\sin\phi-\frac{a}{2}\sin\theta}^{=z_{gAP}}\right)^2\right]\right\} \quad (3.164)$$

Kinetic Energy Partial Differential Derivations

The kinetic co-energy partial differential energy equation derivations are presented in the following sets of equations. Equations (3.158), (3.161), and (3.162) are used to derive these equations.

$$\frac{\partial T^*}{\partial \dot{x}} = m\dot{x}$$

$$\frac{\partial T^*}{\partial \dot{y}} = m\dot{y}$$

$$\frac{\partial T^*}{\partial \dot{z}} = m\dot{z}$$

$$\frac{\partial T^*}{\partial \dot{\phi}} = J_{xx}\left(\dot{\phi}\cos^2\theta\cos^2\psi + \dot{\theta}\cos\theta\cos\psi\sin\psi\right) +$$
$$+ J_{yy}\left(-\dot{\theta}\cos\theta\cos\psi\sin\psi + \dot{\phi}\cos^2\theta\sin^2\psi\right) + J_{zz}\left(\dot{\psi}\sin\theta + \dot{\phi}\sin^2\theta\right)$$

$$\frac{\partial T^*}{\partial \dot{\theta}} = J_{xx}\left(\dot{\phi}\cos\theta\cos\psi\sin\psi + \dot{\theta}\sin^2\psi\right) + J_{yy}\left(\dot{\theta}\cos^2\psi - \dot{\phi}\cos\theta\cos\psi\sin\psi\right)$$

$$\frac{\partial T^*}{\partial \dot{\psi}} = J_{zz}\left(\dot{\psi} + \dot{\phi}\sin\theta\right)$$

$$\frac{d}{dt}\left(\frac{\partial T^*}{\partial \dot{x}}\right) = m\ddot{x}$$

$$\frac{d}{dt}\left(\frac{\partial T^*}{\partial \dot{y}}\right) = m\ddot{y}$$

$$\frac{d}{dt}\left(\frac{\partial T^*}{\partial \dot{z}}\right) = m\ddot{z}$$

$$\frac{d}{dt}\left(\frac{\partial T^*}{\partial \dot{\phi}}\right) = J_{xx}\left[\left(\ddot{\phi}\cos^2\theta\cos^2\psi - 2\dot{\phi}\dot{\theta}\cos\theta\sin\theta\cos^2\psi - 2\dot{\phi}\dot{\psi}\cos^2\theta\sin\psi\cos\psi\right) +\right.$$
$$\left. + \left(\ddot{\theta}\cos\theta\cos\psi\sin\psi - \dot{\theta}^2\sin\theta\cos\psi\sin\psi - \dot{\theta}\dot{\psi}\cos\theta\sin^2\psi + \dot{\theta}\dot{\psi}\cos\theta\cos^2\psi\right)\right] +$$
$$+ J_{yy}\left[\left(-\ddot{\theta}\cos\theta\cos\psi\sin\psi + \dot{\theta}^2\sin\theta\cos\psi\sin\psi + \dot{\theta}\dot{\psi}\cos\theta\sin^2\psi - \dot{\theta}\dot{\psi}\cos\theta\cos^2\psi\right) +\right.$$
$$\left. + \left(\ddot{\phi}\cos^2\theta\sin^2\psi - 2\dot{\phi}\dot{\theta}\cos\theta\sin\theta\sin^2\psi + 2\dot{\phi}\dot{\psi}\cos^2\theta\sin\psi\cos\psi\right)\right] +$$
$$+ J_{zz}\left[\left(\ddot{\psi}\sin\theta + \dot{\psi}\dot{\theta}\cos\theta\right) + \left(\ddot{\phi}\sin^2\theta + 2\dot{\phi}\dot{\theta}\sin\theta\cos\theta\right)\right]$$

$$\frac{d}{dt}\left(\frac{\partial T^*}{\partial \dot{\theta}}\right) = J_{xx}\left[\begin{pmatrix}\ddot{\phi}\cos\theta\cos\psi\sin\psi - \dot{\phi}\dot{\theta}\sin\theta\cos\psi\sin\psi - \\ -\dot{\phi}\dot{\psi}\cos\theta\sin^2\psi + \dot{\phi}\dot{\psi}\cos\theta\cos^2\psi\end{pmatrix}+\right.$$
$$\left.+\left(\ddot{\theta}\sin^2\psi + 2\dot{\theta}\dot{\psi}\sin\psi\cos\psi\right)\right] + J_{yy}\left[\left(\ddot{\theta}\cos^2\psi - 2\dot{\theta}\dot{\psi}\cos\psi\sin\psi\right)-\right.$$
$$\left.-\left(\ddot{\phi}\cos\theta\cos\psi\sin\psi - \dot{\phi}\dot{\theta}\sin\theta\cos\psi\sin\psi - \dot{\phi}\dot{\psi}\cos\theta\sin^2\psi + \dot{\phi}\cos\theta\cos^2\psi\right)\right]$$

$$\frac{d}{dt}\left(\frac{\partial T^*}{\partial \dot{\psi}}\right) = J_{zz}\left[\ddot{\psi} + \left(\ddot{\phi}\sin\theta + \dot{\phi}\dot{\theta}\cos\theta\right)\right]$$

$$\frac{\partial T^*}{\partial x} = \frac{\partial T^*}{\partial y} = \frac{\partial T^*}{\partial z} = \frac{\partial T^*}{\partial \phi} = 0$$

$$\frac{\partial T^*}{\partial \theta} = J_{xx}\left(-\dot{\phi}^2\dot{\theta}\cos\theta\sin\theta\cos^2\psi - \dot{\phi}\dot{\theta}^2\sin\theta\cos\psi\sin\psi\right)+$$
$$+J_{yy}\left(\dot{\phi}\dot{\theta}^2\sin\theta\cos\psi\sin\psi - \dot{\phi}^2\dot{\theta}\cos\theta\sin\theta\sin^2\psi\right)+$$
$$+J_{zz}\left(\dot{\phi}\dot{\theta}\dot{\psi}\cos\theta + \dot{\phi}^2\dot{\theta}\sin\theta\cos\theta\right)$$

$$\frac{\partial T^*}{\partial \psi} = J_{xx}\left[-\dot{\phi}^2\dot{\psi}\cos^2\theta\cos\psi\sin\psi + \dot{\phi}\dot{\theta}\dot{\psi}\cos\theta\left(\cos^2\psi - \sin^2\psi\right) + \dot{\theta}^2\dot{\psi}\sin\psi\cos\psi\right]+$$
$$+J_{yy}\left[-\dot{\theta}^2\dot{\psi}\cos\psi\sin\psi - \dot{\phi}\dot{\theta}\dot{\psi}\cos\theta\left(\cos^2\psi - \sin^2\psi\right) + \dot{\phi}^2\dot{\psi}\cos^2\theta\sin\psi\cos\psi\right]$$

Potential Energy Partial Differential Derivations

In the potential energy partial differential derivations the magnetic spring constants assume the form of equation (3.117) in both the y and z axis directions which is rewritten in a more useful form in Phase III equation set (3.144). Equation set (3.144) for the tangential magnetic component repulsive spring constant as well as normal magnetic component drag spring constant equation set is rewritten here in abbreviated form for convenience.

Repulsive Force:

$$k_z = \frac{1}{2} \bullet \begin{pmatrix} \text{Magnetic} \\ \text{Volume} \end{pmatrix} \bullet \left[\frac{\text{Re}\left(J_x B_y^* \right)}{z_g} \right]$$

$$k_y = \frac{1}{2} \bullet \begin{pmatrix} \text{Magnetic} \\ \text{Volume} \end{pmatrix} \bullet \left[\frac{\text{Re}\left(J_z B_x^* \right)}{y_g} \right]$$

Drag Force:

$$k_{zDrag} = \frac{1}{2} \bullet \begin{pmatrix} \text{Magnetic} \\ \text{Volume} \end{pmatrix} \bullet \left[\frac{\text{Re}\left(J_x B_z^* \right)}{z_g} \right]$$

$$k_{yDrag} = \frac{1}{2} \bullet \begin{pmatrix} \text{Magnetic} \\ \text{Volume} \end{pmatrix} \bullet \left[\frac{\text{Re}\left(J_z B_y^* \right)}{y_g} \right]$$

As in Phase III, the body force equation differentials for the magnetic spring constants are provided in equation set (3.143). These body force equation differentials are required for the potential energy differentials and are attained via the differential solutions of G_3, equations (3.98) and (3.99), and the solutions of the B_T, B_N, and J_x, equations (3.102), (3.103), and (3.107), from Chapters 3.3.a.ii and 3.3.a.iii. Following the same procedure as set in Chapter 3.5.a.i of Phase III the partial differential solutions for the air gap distance denominator values of the repulsive spring constant equations are provided for each particular air gap. The G_3 parameters from the force component of the spring constant equations start by substituting the applicable air gap variables into the G_3 exponential. Note that for simplicity the Cartesian coordinate directions of B_T, B_N, and J_x in equations (3.102), (3.103), and (3.107) are not used in Phase IV unlike in Phase III. Instead only the general forms B_T, B_N, and J are used without a Cartesian coordinate direction subscript. Note that for brevity the applicable ranges of $0 \le z \le z_g$ and $0 \le y \le y_g$ are removed from these and all subsequent equations as they are in Phase III.

k_{yBS} Derivations:

The following equations solve for the air gap distance component from the denominator of the magnetic spring constant equation.

$$\frac{\partial\left[y_g{}^{-1}(y,\psi)\right]}{\partial y} = y'_{gBS}(y,\psi) = \frac{1}{y_{gBS}^2}$$

$$\frac{\partial\left[y_g{}^{-1}(y,\psi)\right]}{\partial \psi} = y'_{gBS}(y,\psi) = \frac{a\cos(\psi)}{2y_{gBS}^2}$$

Now solve for the G_3 component of the repulsive magnetic force equation. The G_3 equation exponential substitutions provide the following output for the y directed magnetic spring constants.

$$\text{For } C_{GA}\text{: } e^{\left\{y-\left[y_{g\_init}-y-\frac{a}{2}\sin\psi\right]\right\}\xi} = e^{\left(2y-y_{g\_init}+\frac{a}{2}\sin\psi\right)\xi}$$

$$\text{For } C_{GB}\text{: } e^{\left\{\left[y_{g\_init}-y-\frac{a}{2}\sin\psi\right]-y\right\}\xi} = e^{\left(y_{g\_init}-2y-\frac{a}{2}\sin\psi\right)\xi}$$

This substitution provides the following equations for $G_{3yBS}(\xi,y,\psi)$ and all of its derivatives.

$$G_{3yBS}(\xi,y,\psi) = \left[C_{GA}e^{\left(2y-y_{g\_init}+\frac{a}{2}\sin\psi\right)\xi} + C_{GB}e^{\left(y_{g\_init}-2y-\frac{a}{2}\sin\psi\right)\xi}\right] \tag{3.165}$$

$$\frac{\partial\left[G_{3yBS}(\xi,y,\psi)\right]}{\partial y} = G'_{3yBS}(\xi,y,\psi) = 2\xi\left[\begin{matrix}C_{GA}e^{\left(2y-y_{g\_init}+\frac{a}{2}\sin\psi\right)\xi} - \\ -C_{GB}e^{\left(y_{g\_init}-2y-\frac{a}{2}\sin\psi\right)\xi}\end{matrix}\right]$$

$$\frac{\partial^2\left[G_{3yBS}(\xi,y,\psi)\right]}{\partial y^2} = G''_{3yBS}(\xi,y,\psi) = 4\xi^2\left[\begin{matrix}C_{GA}e^{\left(2y-y_{g\_init}+\frac{a}{2}\sin\psi\right)\xi} + \\ +C_{GB}e^{\left(y_{g\_init}-2y-\frac{a}{2}\sin\psi\right)\xi}\end{matrix}\right]$$

$$\frac{\partial\left[G_{3yBS}(\xi,y,\psi)\right]}{\partial \psi} = G'_{3yBS}(\xi,y,\psi) = \frac{a\xi}{2}\cos\psi\left[\begin{matrix}C_{GA}e^{\left(2y-y_{g\_init}+\frac{a}{2}\sin\psi\right)\xi} - \\ -C_{GB}e^{\left(y_{g\_init}-2y-\frac{a}{2}\sin\psi\right)\xi}\end{matrix}\right]$$

$$\frac{\partial^2\left[G_{3yBS}\left(\xi,y,\psi\right)\right]}{\partial\psi^2}=G''_{3yBS}\left(\xi,y,\psi\right)=\frac{a^2\xi^2}{4}\cos^2\psi\left[\begin{matrix}C_{GA}e^{\left(2y-y_{g\_init}+\frac{a}{2}\sin\psi\right)\xi}+\\+C_{GB}e^{\left(y_{g\_init}-2y-\frac{a}{2}\sin\psi\right)\xi}\end{matrix}\right]$$

$$\sum y'_{gBS}\left(y,\psi\right)=\frac{1}{y_{gBS}^2}+\frac{a\cos\left(\psi\right)}{2y_{gBS}^2} \tag{3.166}$$

$$\sum G'_{3yBS}\left(\xi,y,\psi\right)=\left(2\xi+\frac{a\xi}{2}\cos\psi\right)\left[\begin{matrix}C_{GA}e^{\left(2y-y_{g\_init}+\frac{a}{2}\sin\psi\right)\xi}-\\-C_{GB}e^{\left(y_{g\_init}-2y-\frac{a}{2}\sin\psi\right)\xi}\end{matrix}\right] \tag{3.167}$$

$$\sum G''_{3yBS}\left(\xi,y,\psi\right)=\left(4\xi^2+\frac{a^2\xi^2}{4}\cos^2\psi\right)\left[\begin{matrix}C_{GA}e^{\left(2y-y_{g\_init}+\frac{a}{2}\sin\psi\right)\xi}+\\+C_{GB}e^{\left(y_{g\_init}-2y-\frac{a}{2}\sin\psi\right)\xi}\end{matrix}\right] \tag{3.168}$$

k_{yBP} Derivations:

The following equations solve for the air gap distance component from the denominator of the magnetic spring constant equation.

$$\frac{\partial\left[y_g{}^{-1}\left(y,\psi\right)\right]}{\partial y}=y'_{gBP}\left(y,\psi\right)=-\frac{1}{y_{gBP}^2}$$

$$\frac{\partial\left[y_g{}^{-1}\left(y,\psi\right)\right]}{\partial\psi}=y'_{gBP}\left(y,\psi\right)=-\frac{a\cos\left(\psi\right)}{2y_{gBP}^2}$$

Now solve for the G_3 component of the repulsive magnetic force equation. The G_3 equation exponential substitutions provide the following output for the y directed magnetic spring constants.

For C_{GA}: $e^{\left\{y-\left[y_{g\_init}+y+\frac{a}{2}\sin\psi\right]\right\}\xi}=e^{\left(-y_{g\_init}-\frac{a}{2}\sin\psi\right)\xi}$

For C_{GB}: $e^{\left\{\left[y_{g\_init}+y+\frac{a}{2}\sin\psi\right]-y\right\}\xi}=e^{\left(y_{g\_init}+\frac{a}{2}\sin\psi\right)\xi}$

This substitution provides the following equations for $G_{3yBP}\left(\xi,y,\psi\right)$ and all of its derivatives.

$$G_{3yBP}\left(\xi,y,\psi\right)=\left[C_{GA}e^{\left(-y_{g\_init}-\frac{a}{2}\sin\psi\right)\xi}+C_{GB}e^{\left(y_{g\_init}+\frac{a}{2}\sin\psi\right)\xi}\right] \tag{3.169}$$

$$\frac{\partial\left[G_{3yBP}\left(\xi,y,\psi\right)\right]}{\partial y}=G'_{3yBP}\left(\xi,y,\psi\right)=0$$

$$\frac{\partial^2\left[G_{3yBP}\left(\xi,y,\psi\right)\right]}{\partial y^2}=G''_{3yBP}\left(\xi,y,\psi\right)=0$$

$$\frac{\partial\left[G_{3yBP}\left(\xi,y,\psi\right)\right]}{\partial\psi}=G'_{3yBP}\left(\xi,y,\psi\right)=\frac{a\xi}{2}\cos\psi\left[\begin{matrix}C_{GB}e^{\left(y_{g\_init}+\frac{a}{2}\sin\psi\right)\xi}-\\-C_{GA}e^{\left(-y_{g\_init}-\frac{a}{2}\sin\psi\right)\xi}\end{matrix}\right]$$

$$\frac{\partial^2\left[G_{3yBP}\left(\xi,y,\psi\right)\right]}{\partial\psi^2}=G''_{3yBP}\left(\xi,y,\psi\right)=\frac{a^2\xi^2}{4}\cos^2\psi\left[\begin{matrix}C_{GB}e^{\left(y_{g\_init}+\frac{a}{2}\sin\psi\right)\xi}+\\+C_{GA}e^{\left(-y_{g\_init}-\frac{a}{2}\sin\psi\right)\xi}\end{matrix}\right]$$

$$\sum y'_{gBP}\left(y,\psi\right)=-\frac{1}{y_{gBP}^2}-\frac{a\cos\left(\psi\right)}{2y_{gBP}^2} \tag{3.170}$$

$$\sum G'_{3yBP}\left(\xi,y,\psi\right)=-\frac{a\xi}{2}\cos\psi\left[\begin{matrix}C_{GA}e^{\left(-y_{g\_init}-\frac{a}{2}\sin\psi\right)\xi}-\\-C_{GB}e^{\left(y_{g\_init}+\frac{a}{2}\sin\psi\right)\xi}\end{matrix}\right] \tag{3.171}$$

$$\sum G''_{3yBP}\left(\xi,y,\psi\right)=\frac{a^2\xi^2}{4}\cos^2\psi\left[\begin{matrix}C_{GA}e^{\left(-y_{g\_init}-\frac{a}{2}\sin\psi\right)\xi}+\\+C_{GB}e^{\left(y_{g\_init}+\frac{a}{2}\sin\psi\right)\xi}\end{matrix}\right] \tag{3.172}$$

k_{yAS} Derivations:

The following equations solve for the air gap distance component from the denominator of the magnetic spring constant equation.

$$\frac{\partial\left[y_g{}^{-1}\left(y,\psi\right)\right]}{\partial y}=y'_{gAS}\left(y,\psi\right)=\frac{1}{y_{gAS}^2}$$

$$\frac{\partial\left[y_g{}^{-1}(y,\psi)\right]}{\partial\psi} = y'_{gAS}(y,\psi) = -\frac{a\cos(\psi)}{2y_{gAS}^2}$$

Now solve for the G_3 component of the repulsive magnetic force equation. The G_3 equation exponential substitutions provide the following output for the y directed magnetic spring constants.

$$\text{For } C_{GA}\text{: } e^{\left\{y-\left[y_{g\_init}-y+\frac{a}{2}\sin\psi\right]\right\}\xi} = e^{\left(2y-y_{g\_init}-\frac{a}{2}\sin\psi\right)\xi}$$

$$\text{For } C_{GB}\text{: } e^{\left\{\left[y_{g\_init}-y+\frac{a}{2}\sin\psi\right]-y\right\}\xi} = e^{\left(y_{g\_init}-2y+\frac{a}{2}\sin\psi\right)\xi}$$

This substitution provides the following equations for $G_{3yAS}(\xi,y,\psi)$ and all of its derivatives.

$$G_{3yAS}(\xi,y,\psi) = \left[C_{GA}e^{\left(2y-y_{g\_init}-\frac{a}{2}\sin\psi\right)\xi} + C_{GB}e^{\left(y_{g\_init}-2y+\frac{a}{2}\sin\psi\right)\xi}\right] \tag{3.173}$$

$$\frac{\partial\left[G_{3yAS}(\xi,y,\psi)\right]}{\partial y} = G'_{3yAS}(\xi,y,\psi) = 2\xi\left[\begin{matrix}C_{GA}e^{\left(2y-y_{g\_init}-\frac{a}{2}\sin\psi\right)\xi} - \\ -C_{GB}e^{\left(y_{g\_init}-2y+\frac{a}{2}\sin\psi\right)\xi}\end{matrix}\right]$$

$$\frac{\partial^2\left[G_{3yAS}(\xi,y,\psi)\right]}{\partial y^2} = G''_{3yAS}(\xi,y,\psi) = 4\xi^2\left[\begin{matrix}C_{GA}e^{\left(2y-y_{g\_init}-\frac{a}{2}\sin\psi\right)\xi} + \\ +C_{GB}e^{\left(y_{g\_init}-2y+\frac{a}{2}\sin\psi\right)\xi}\end{matrix}\right]$$

$$\frac{\partial\left[G_{3yAS}(\xi,y,\psi)\right]}{\partial\psi} = G'_{3yAS}(\xi,y,\psi) = \frac{a\xi}{2}\cos\psi\left[\begin{matrix}C_{GB}e^{\left(y_{g\_init}-2y+\frac{a}{2}\sin\psi\right)\xi} - \\ -C_{GA}e^{\left(2y-y_{g\_init}-\frac{a}{2}\sin\psi\right)\xi}\end{matrix}\right]$$

$$\frac{\partial^2\left[G_{3yAS}(\xi,y,\psi)\right]}{\partial\psi^2} = G''_{3yAS}(\xi,y,\psi) = \frac{a^2\xi^2}{4}\cos^2\psi\left[\begin{matrix}C_{GB}e^{\left(y_{g\_init}-2y+\frac{a}{2}\sin\psi\right)\xi} + \\ +C_{GA}e^{\left(2y-y_{g\_init}-\frac{a}{2}\sin\psi\right)\xi}\end{matrix}\right]$$

$$\sum y'_{gAS}(y,\psi) = \frac{1}{y_{gAS}^2} - \frac{a\cos(\psi)}{2y_{gAS}^2} \tag{3.174}$$

$$\sum G'_{3yAS}(\xi,y,\psi)=\left(2\xi-\frac{a\xi}{2}\cos\psi\right)\left[\begin{matrix}C_{GA}e^{\left(2y-y_{g\_init}-\frac{a}{2}\sin\psi\right)\xi}-\\-C_{GB}e^{\left(y_{g\_init}-2y+\frac{a}{2}\sin\psi\right)\xi}\end{matrix}\right] \tag{3.175}$$

$$\sum G''_{3yAS}(\xi,y,\psi)=\left(4\xi^2+\frac{a^2\xi^2}{4}\cos^2\psi\right)\left[\begin{matrix}C_{GA}e^{\left(2y-y_{g\_init}-\frac{a}{2}\sin\psi\right)\xi}+\\+C_{GB}e^{\left(y_{g\_init}-2y+\frac{a}{2}\sin\psi\right)\xi}\end{matrix}\right] \tag{3.176}$$

k_{yAP} Derivations:

The following equations solve for the air gap distance component from the denominator of the magnetic spring constant equation.

$$\frac{\partial\left[y_g{}^{-1}(y,\psi)\right]}{\partial y}=y'_{gAP}(y,\psi)=-\frac{1}{y_{gAP}^2}$$

$$\frac{\partial\left[y_g{}^{-1}(y,\psi)\right]}{\partial \psi}=y'_{gAP}(y,\psi)=\frac{a\cos(\psi)}{2y_{gAP}^2}$$

Now solve for the G_3 component of the repulsive magnetic force equation. The G_3 equation exponential substitutions provide the following output for the y directed magnetic spring constants.

For C_{GA}: $e^{\left\{y-\left[y_{g\_init}+y-\frac{a}{2}\sin\psi\right]\right\}\xi}=e^{\left(-y_{g\_init}+\frac{a}{2}\sin\psi\right)\xi}$

For C_{GB}: $e^{\left\{\left[y_{g\_init}+y-\frac{a}{2}\sin\psi\right]-y\right\}\xi}=e^{\left(y_{g\_init}-\frac{a}{2}\sin\psi\right)\xi}$

This substitution provides the following equations for $G_{3yAP}(\xi,y,\psi)$ and all of its derivatives.

$$G_{3yAP}(\xi,y,\psi)=\left[C_{GA}e^{\left(-y_{g\_init}+\frac{a}{2}\sin\psi\right)\xi}+C_{GB}e^{\left(y_{g\_init}-\frac{a}{2}\sin\psi\right)\xi}\right] \tag{3.177}$$

$$\frac{\partial\left[G_{3yAP}(\xi,y,\psi)\right]}{\partial y}=G'_{3yAP}(\xi,y,\psi)=0$$

$$\frac{\partial^2\left[G_{3yAP}\left(\xi,y,\psi\right)\right]}{\partial y^2}=G''_{3yAP}\left(\xi,y,\psi\right)=0$$

$$\frac{\partial\left[G_{3yAP}\left(\xi,y,\psi\right)\right]}{\partial \psi}=G'_{3yAP}\left(\xi,y,\psi\right)=\frac{a\xi}{2}\cos\psi\left[\begin{matrix}C_{GA}e^{\left(-y_{g\_init}+\frac{a}{2}\sin\psi\right)\xi}-\\-C_{GB}e^{\left(y_{g\_init}-\frac{a}{2}\sin\psi\right)\xi}\end{matrix}\right]$$

$$\frac{\partial^2\left[G_{3yAP}\left(\xi,y,\psi\right)\right]}{\partial \psi^2}=G''_{3yAP}\left(\xi,y,\psi\right)=\frac{a^2\xi^2}{4}\cos^2\psi\left[\begin{matrix}C_{GA}e^{\left(-y_{g\_init}+\frac{a}{2}\sin\psi\right)\xi}+\\+C_{GB}e^{\left(y_{g\_init}-\frac{a}{2}\sin\psi\right)\xi}\end{matrix}\right]$$

$$\sum y'_{gAP}\left(y,\psi\right)=-\frac{1}{y_{gAP}^2}+\frac{a\cos\left(\psi\right)}{2y_{gAP}^2} \tag{3.178}$$

$$\sum G'_{3yAP}\left(\xi,y,\psi\right)=\frac{a\xi}{2}\cos\psi\left[\begin{matrix}C_{GA}e^{\left(-y_{g\_init}+\frac{a}{2}\sin\psi\right)\xi}-\\-C_{GB}e^{\left(y_{g\_init}-\frac{a}{2}\sin\psi\right)\xi}\end{matrix}\right] \tag{3.179}$$

$$\sum G''_{3yAP}\left(\xi,y,\psi\right)=\frac{a^2\xi^2}{4}\cos^2\psi\left[\begin{matrix}C_{GA}e^{\left(-y_{g\_init}+\frac{a}{2}\sin\psi\right)\xi}+\\+C_{GB}e^{\left(y_{g\_init}-\frac{a}{2}\sin\psi\right)\xi}\end{matrix}\right] \tag{3.180}$$

k_{zBS} Derivations:

The following equations solve for the air gap distance component from the denominator of the magnetic spring constant equation.

$$\frac{\partial\left[z_g{}^{-1}\left(z,\phi,\theta\right)\right]}{\partial z}=z'_{gBS}\left(z,\phi,\theta\right)=\frac{1}{z_{gBS}^2}$$

$$\frac{\partial\left[z_g{}^{-1}\left(z,\phi,\theta\right)\right]}{\partial \phi}=z'_{gBS}\left(z,\phi,\theta\right)=-\frac{b\cos\left(\phi\right)}{2z_{gBS}^2}$$

$$\frac{\partial\left[z_g{}^{-1}\left(z,\phi,\theta\right)\right]}{\partial \theta}=z'_{gBS}\left(z,\phi,\theta\right)=-\frac{a\cos\left(\theta\right)}{2z_{gBS}^2}$$

Now solve for the G_3 component of the repulsive magnetic force equation. The G_3 equation exponential substitutions provide the following output for the z directed magnetic spring constants.

$$\text{For } C_{GA}\text{: } e^{\left\{z-\left[z_{g\_init}-z+\frac{b}{2}\sin\phi+\frac{a}{2}\sin\theta\right]\right\}\xi} = e^{\left(2z-z_{g\_init}-\frac{b}{2}\sin\phi-\frac{a}{2}\sin\theta\right)\xi}$$

$$\text{For } C_{GB}\text{: } e^{\left\{\left[z_{g\_init}-z+\frac{b}{2}\sin\phi+\frac{a}{2}\sin\theta\right]-z\right\}\xi} = e^{\left(z_{g\_init}-2z+\frac{b}{2}\sin\phi+\frac{a}{2}\sin\theta\right)\xi}$$

This substitution provides the following equations for $G_{3zBS}(\xi,z,\phi,\theta)$ and all of its derivatives.

$$G_{3zBS}(\xi,z,\phi,\theta) = \left[C_{GA}e^{\left(2z-z_{g\_init}-\frac{b}{2}\sin\phi-\frac{a}{2}\sin\theta\right)\xi} + C_{GB}e^{\left(z_{g\_init}-2z+\frac{b}{2}\sin\phi+\frac{a}{2}\sin\theta\right)\xi}\right] \quad (3.181)$$

$$\frac{\partial\left[G_{3zBS}(\xi,z,\phi,\theta)\right]}{\partial z} = G'_{3zBS}(\xi,z,\phi,\theta) = 2\xi\left[\begin{matrix}C_{GA}e^{\left(2z-z_{g\_init}-\frac{b}{2}\sin\phi-\frac{a}{2}\sin\theta\right)\xi} - \\ -C_{GB}e^{\left(z_{g\_init}-2z+\frac{b}{2}\sin\phi+\frac{a}{2}\sin\theta\right)\xi}\end{matrix}\right]$$

$$\frac{\partial^2\left[G_{3zBS}(\xi,z,\phi,\theta)\right]}{\partial z^2} = G''_{3zBS}(\xi,z,\phi,\theta) = 4\xi^2\left[\begin{matrix}C_{GA}e^{\left(2z-z_{g\_init}-\frac{b}{2}\sin\phi-\frac{a}{2}\sin\theta\right)\xi} + \\ +C_{GB}e^{\left(z_{g\_init}-2z+\frac{b}{2}\sin\phi+\frac{a}{2}\sin\theta\right)\xi}\end{matrix}\right]$$

$$\frac{\partial\left[G_{3zBS}(\xi,z,\phi,\theta)\right]}{\partial \phi} = G'_{3zBS}(\xi,z,\phi,\theta) = \frac{b\xi}{2}\cos\phi\left[\begin{matrix}C_{GB}e^{\left(z_{g\_init}-2z+\frac{b}{2}\sin\phi+\frac{a}{2}\sin\theta\right)\xi} - \\ -C_{GA}e^{\left(2z-z_{g\_init}-\frac{b}{2}\sin\phi-\frac{a}{2}\sin\theta\right)\xi}\end{matrix}\right]$$

$$\frac{\partial^2\left[G_{3zBS}(\xi,z,\phi,\theta)\right]}{\partial \phi^2} = G''_{3zBS}(\xi,z,\phi,\theta) = \frac{b^2\xi^2}{4}\cos^2\phi\left[\begin{matrix}C_{GB}e^{\left(z_{g\_init}-2z+\frac{b}{2}\sin\phi+\frac{a}{2}\sin\theta\right)\xi} + \\ +C_{GA}e^{\left(2z-z_{g\_init}-\frac{b}{2}\sin\phi-\frac{a}{2}\sin\theta\right)\xi}\end{matrix}\right]$$

$$\frac{\partial\left[G_{3zBS}(\xi,z,\phi,\theta)\right]}{\partial \theta} = G'_{3zBS}(\xi,z,\phi,\theta) = \frac{a\xi}{2}\cos\theta\left[\begin{matrix}C_{GB}e^{\left(z_{g\_init}-2z+\frac{b}{2}\sin\phi+\frac{a}{2}\sin\theta\right)\xi} - \\ -C_{GA}e^{\left(2z-z_{g\_init}-\frac{b}{2}\sin\phi-\frac{a}{2}\sin\theta\right)\xi}\end{matrix}\right]$$

$$\frac{\partial^2\left[G_{3zBS}\left(\xi,z,\phi,\theta\right)\right]}{\partial\theta^2}=G''_{3zBS}\left(\xi,z,\phi,\theta\right)=\frac{a^2\xi^2}{4}\cos^2\theta\left[\begin{matrix}C_{GB}e^{\left(z_{g\_init}-2z+\frac{b}{2}\sin\phi+\frac{a}{2}\sin\theta\right)\xi}+\\+C_{GA}e^{\left(2z-z_{g\_init}-\frac{b}{2}\sin\phi-\frac{a}{2}\sin\theta\right)\xi}\end{matrix}\right]$$

$$\sum z'_{gBS}\left(z,\phi,\theta\right)=\frac{1}{z_{gBS}^2}+\frac{-b\cos\left(\phi\right)-a\cos\left(\theta\right)}{2z_{gBS}^2} \tag{3.182}$$

$$\sum G'_{3zBS}\left(\xi,y,\psi\right)=\left(2\xi-\frac{b\xi}{2}\cos\phi-\frac{a\xi}{2}\cos\theta\right)\left[\begin{matrix}C_{GA}e^{\left(2z-z_{g\_init}-\frac{b}{2}\sin\phi-\frac{a}{2}\sin\theta\right)\xi}-\\-C_{GB}e^{\left(z_{g\_init}-2z+\frac{b}{2}\sin\phi+\frac{a}{2}\sin\theta\right)\xi}\end{matrix}\right] \tag{3.183}$$

$$\sum G''_{3zBS}\left(\xi,y,\psi\right)=\left(4\xi^2+\frac{b^2\xi^2}{4}\cos^2\phi+\frac{a^2\xi^2}{4}\cos^2\theta\right)\left[\begin{matrix}C_{GA}e^{\left(2z-z_{g\_init}-\frac{b}{2}\sin\phi-\frac{a}{2}\sin\theta\right)\xi}+\\+C_{GB}e^{\left(z_{g\_init}-2z+\frac{b}{2}\sin\phi+\frac{a}{2}\sin\theta\right)\xi}\end{matrix}\right] \tag{3.184}$$

k_{zBP} Derivations:

The following equations solve for the air gap distance component from the denominator of the magnetic spring constant equation.

$$\frac{\partial\left[z_g^{-1}\left(z,\phi,\theta\right)\right]}{\partial z}=z'_{gBP}\left(z,\phi,\theta\right)=\frac{1}{z_{gBP}^2}$$

$$\frac{\partial\left[z_g^{-1}\left(z,\phi,\theta\right)\right]}{\partial\phi}=z'_{gBP}\left(z,\phi,\theta\right)=\frac{b\cos\left(\phi\right)}{2z_{gBP}^2}$$

$$\frac{\partial\left[z_g^{-1}\left(z,\phi,\theta\right)\right]}{\partial\theta}=z'_{gBP}\left(z,\phi,\theta\right)=-\frac{a\cos\left(\theta\right)}{2z_{gBP}^2}$$

Now solve for the G_3 component of the repulsive magnetic force equation. G_3 equation exponential substitutions provide the following output for the z directed magnetic spring constants.

For C_{GA}: $e^{\left\{z-\left[z_{g\_init}-z-\frac{b}{2}\sin\phi+\frac{a}{2}\sin\theta\right]\right\}\xi}=e^{\left(2z-z_{g\_init}+\frac{b}{2}\sin\phi-\frac{a}{2}\sin\theta\right)\xi}$

For C_{GB}: $e^{\left\{\left[z_{g\_init}-z-\frac{b}{2}\sin\phi+\frac{a}{2}\sin\theta\right]-z\right\}\xi}=e^{\left(z_{g\_init}-2z-\frac{b}{2}\sin\phi+\frac{a}{2}\sin\theta\right)\xi}$

This substitution provides the following equations for $G_{3zBP}(\xi,z,\phi,\theta)$ and all of its derivatives.

$$G_{3zBP}(\xi,z,\phi,\theta)=\left[C_{GA}e^{\left(2z-z_{g\_init}+\frac{b}{2}\sin\phi-\frac{a}{2}\sin\theta\right)\xi}+C_{GB}e^{\left(z_{g\_init}-2z-\frac{b}{2}\sin\phi+\frac{a}{2}\sin\theta\right)\xi}\right] \quad (3.185)$$

$$\frac{\partial\left[G_{3zBP}(\xi,z,\phi,\theta)\right]}{\partial z}=G'_{3zBP}(\xi,z,\phi,\theta)=2\xi\left[\begin{matrix}C_{GA}e^{\left(2z-z_{g\_init}+\frac{b}{2}\sin\phi-\frac{a}{2}\sin\theta\right)\xi}-\\-C_{GB}e^{\left(z_{g\_init}-2z-\frac{b}{2}\sin\phi+\frac{a}{2}\sin\theta\right)\xi}\end{matrix}\right]$$

$$\frac{\partial^2\left[G_{3zBP}(\xi,z,\phi,\theta)\right]}{\partial z^2}=G''_{3zBP}(\xi,z,\phi,\theta)=4\xi^2\left[\begin{matrix}C_{GA}e^{\left(2z-z_{g\_init}+\frac{b}{2}\sin\phi-\frac{a}{2}\sin\theta\right)\xi}+\\+C_{GB}e^{\left(z_{g\_init}-2z-\frac{b}{2}\sin\phi+\frac{a}{2}\sin\theta\right)\xi}\end{matrix}\right]$$

$$\frac{\partial\left[G_{3zBP}(\xi,z,\phi,\theta)\right]}{\partial\phi}=G'_{3zBP}(\xi,z,\phi,\theta)=\frac{b\xi}{2}\cos\phi\left[\begin{matrix}C_{GA}e^{\left(2z-z_{g\_init}+\frac{b}{2}\sin\phi-\frac{a}{2}\sin\theta\right)\xi}-\\-C_{GB}e^{\left(z_{g\_init}-2z-\frac{b}{2}\sin\phi+\frac{a}{2}\sin\theta\right)\xi}\end{matrix}\right]$$

$$\frac{\partial^2\left[G_{3zBP}(\xi,z,\phi,\theta)\right]}{\partial\phi^2}=G''_{3zBP}(\xi,z,\phi,\theta)=\frac{b^2\xi^2}{4}\cos^2\phi\left[\begin{matrix}C_{GA}e^{\left(2z-z_{g\_init}+\frac{b}{2}\sin\phi-\frac{a}{2}\sin\theta\right)\xi}+\\+C_{GB}e^{\left(z_{g\_init}-2z-\frac{b}{2}\sin\phi+\frac{a}{2}\sin\theta\right)\xi}\end{matrix}\right]$$

$$\frac{\partial\left[G_{3zBP}(\xi,z,\phi,\theta)\right]}{\partial\theta}=G'_{3zBP}(\xi,z,\phi,\theta)=\frac{a\xi}{2}\cos\theta\left[\begin{matrix}C_{GB}e^{\left(z_{g\_init}-2z-\frac{b}{2}\sin\phi+\frac{a}{2}\sin\theta\right)\xi}-\\-C_{GA}e^{\left(2z-z_{g\_init}+\frac{b}{2}\sin\phi-\frac{a}{2}\sin\theta\right)\xi}\end{matrix}\right]$$

$$\frac{\partial^2\left[G_{3zBP}(\xi,z,\phi,\theta)\right]}{\partial\theta^2}=G''_{3zBP}(\xi,z,\phi,\theta)=\frac{a^2\xi^2}{4}\cos^2\theta\left[\begin{matrix}C_{GB}e^{\left(z_{g\_init}-2z-\frac{b}{2}\sin\phi+\frac{a}{2}\sin\theta\right)\xi}+\\+C_{GA}e^{\left(2z-z_{g\_init}+\frac{b}{2}\sin\phi-\frac{a}{2}\sin\theta\right)\xi}\end{matrix}\right]$$

$$\sum z'_{gBP}\left(z,\phi,\theta\right)=\frac{1}{z_{gBP}^{2}}+\frac{b\cos\left(\phi\right)-a\cos\left(\theta\right)}{2z_{gBP}^{2}} \tag{3.186}$$

$$\sum G'_{3zBP}\left(\xi,y,\psi\right)=\left(2\xi+\frac{b\xi}{2}\cos\phi-\frac{a\xi}{2}\cos\theta\right)\begin{bmatrix}C_{GA}e^{\left(2z-z_{g\_init}+\frac{b}{2}\sin\phi-\frac{a}{2}\sin\theta\right)\xi}-\\-C_{GB}e^{\left(z_{g\_init}-2z-\frac{b}{2}\sin\phi+\frac{a}{2}\sin\theta\right)\xi}\end{bmatrix} \tag{3.187}$$

$$\sum G''_{3zBP}\left(\xi,y,\psi\right)=\left(4\xi^{2}+\frac{b^{2}\xi^{2}}{4}\cos^{2}\phi+\frac{a^{2}\xi^{2}}{4}\cos^{2}\theta\right)\begin{bmatrix}C_{GA}e^{\left(2z-z_{g\_init}+\frac{b}{2}\sin\phi-\frac{a}{2}\sin\theta\right)\xi}+\\+C_{GB}e^{\left(z_{g\_init}-2z-\frac{b}{2}\sin\phi+\frac{a}{2}\sin\theta\right)\xi}\end{bmatrix} \tag{3.188}$$

k_{zAS} Derivations:

The following equations solve for the air gap distance component from the denominator of the magnetic spring constant equation.

$$\frac{\partial\left[z_{g}^{-1}\left(z,\phi,\theta\right)\right]}{\partial z}=z'_{gAS}\left(z,\phi,\theta\right)=\frac{1}{z_{gAS}^{2}}$$

$$\frac{\partial\left[z_{g}^{-1}\left(z,\phi,\theta\right)\right]}{\partial\phi}=z'_{gAS}\left(z,\phi,\theta\right)=-\frac{b\cos\left(\phi\right)}{2z_{gAS}^{2}}$$

$$\frac{\partial\left[z_{g}^{-1}\left(z,\phi,\theta\right)\right]}{\partial\theta}=z'_{gAS}\left(z,\phi,\theta\right)=\frac{a\cos\left(\theta\right)}{2z_{gAS}^{2}}$$

Now solve for the G_3 component of the repulsive magnetic force equation. G_3 equation exponential substitutions provide the following output for the z directed magnetic spring constants.

For C_{GA}: $e^{\left\{z-\left[z_{g\_init}-z+\frac{b}{2}\sin\phi-\frac{a}{2}\sin\theta\right]\right\}\xi}=e^{\left(2z-z_{g\_init}-\frac{b}{2}\sin\phi+\frac{a}{2}\sin\theta\right)\xi}$

For C_{GB}: $e^{\left\{\left[z_{g\_init}-z+\frac{b}{2}\sin\phi-\frac{a}{2}\sin\theta\right]-z\right\}\xi}=e^{\left(z_{g\_init}-2z+\frac{b}{2}\sin\phi-\frac{a}{2}\sin\theta\right)\xi}$

This substitution provides the following equations for $G_{3zAS}\left(\xi,z,\phi,\theta\right)$ and all of its derivatives.

$$G_{3zAS}\left(\xi,z,\phi,\theta\right)=\left[C_{GA}e^{\left(2z-z_{g\_init}-\frac{b}{2}\sin\phi+\frac{a}{2}\sin\theta\right)\xi}+C_{GB}e^{\left(z_{g\_init}-2z+\frac{b}{2}\sin\phi-\frac{a}{2}\sin\theta\right)\xi}\right] \quad (3.189)$$

$$\frac{\partial\left[G_{3zAS}\left(\xi,z,\phi,\theta\right)\right]}{\partial z}=G'_{3zAS}\left(\xi,z,\phi,\theta\right)=2\xi\left[\begin{matrix}C_{GA}e^{\left(2z-z_{g\_init}-\frac{b}{2}\sin\phi+\frac{a}{2}\sin\theta\right)\xi}-\\-C_{GB}e^{\left(z_{g\_init}-2z+\frac{b}{2}\sin\phi-\frac{a}{2}\sin\theta\right)\xi}\end{matrix}\right]$$

$$\frac{\partial^2\left[G_{3zAS}\left(\xi,z,\phi,\theta\right)\right]}{\partial z^2}=G''_{3zAS}\left(\xi,z,\phi,\theta\right)=4\xi^2\left[\begin{matrix}C_{GA}e^{\left(2z-z_{g\_init}-\frac{b}{2}\sin\phi+\frac{a}{2}\sin\theta\right)\xi}+\\+C_{GB}e^{\left(z_{g\_init}-2z+\frac{b}{2}\sin\phi-\frac{a}{2}\sin\theta\right)\xi}\end{matrix}\right]$$

$$\frac{\partial\left[G_{3zAS}\left(\xi,z,\phi,\theta\right)\right]}{\partial\phi}=G'_{3zAS}\left(\xi,z,\phi,\theta\right)=\frac{b\xi}{2}\cos\phi\left[\begin{matrix}C_{GB}e^{\left(z_{g\_init}-2z+\frac{b}{2}\sin\phi-\frac{a}{2}\sin\theta\right)\xi}-\\-C_{GA}e^{\left(2z-z_{g\_init}-\frac{b}{2}\sin\phi+\frac{a}{2}\sin\theta\right)\xi}\end{matrix}\right]$$

$$\frac{\partial^2\left[G_{3zAS}\left(\xi,z,\phi,\theta\right)\right]}{\partial\phi^2}=G''_{3zAS}\left(\xi,z,\phi,\theta\right)=\frac{b^2\xi^2}{4}\cos^2\phi\left[\begin{matrix}C_{GB}e^{\left(z_{g\_init}-2z+\frac{b}{2}\sin\phi-\frac{a}{2}\sin\theta\right)\xi}+\\+C_{GA}e^{\left(2z-z_{g\_init}-\frac{b}{2}\sin\phi+\frac{a}{2}\sin\theta\right)\xi}\end{matrix}\right]$$

$$\frac{\partial\left[G_{3zAS}\left(\xi,z,\phi,\theta\right)\right]}{\partial\theta}=G'_{3zAS}\left(\xi,z,\phi,\theta\right)=\frac{a\xi}{2}\cos\theta\left[\begin{matrix}C_{GA}e^{\left(2z-z_{g\_init}-\frac{b}{2}\sin\phi+\frac{a}{2}\sin\theta\right)\xi}-\\-C_{GB}e^{\left(z_{g\_init}-2z+\frac{b}{2}\sin\phi-\frac{a}{2}\sin\theta\right)\xi}\end{matrix}\right]$$

$$\frac{\partial^2\left[G_{3zAS}\left(\xi,z,\phi,\theta\right)\right]}{\partial\theta^2}=G''_{3zAS}\left(\xi,z,\phi,\theta\right)=\frac{a^2\xi^2}{4}\cos^2\theta\left[\begin{matrix}C_{GA}e^{\left(2z-z_{g\_init}-\frac{b}{2}\sin\phi+\frac{a}{2}\sin\theta\right)\xi}+\\+C_{GB}e^{\left(z_{g\_init}-2z+\frac{b}{2}\sin\phi-\frac{a}{2}\sin\theta\right)\xi}\end{matrix}\right]$$

$$\sum z'_{gAS}\left(z,\phi,\theta\right)=\frac{1}{z_{gAS}^2}+\frac{-b\cos\left(\phi\right)+a\cos\left(\theta\right)}{2z_{gAS}^2} \quad (3.190)$$

$$\sum G'_{3zAS}\left(\xi,y,\psi\right)=\left(2\xi-\frac{b\xi}{2}\cos\phi+\frac{a\xi}{2}\cos\theta\right)\left[\begin{matrix}C_{GA}e^{\left(2z-z_{g\_init}-\frac{b}{2}\sin\phi+\frac{a}{2}\sin\theta\right)\xi}-\\-C_{GB}e^{\left(z_{g\_init}-2z+\frac{b}{2}\sin\phi-\frac{a}{2}\sin\theta\right)\xi}\end{matrix}\right] \quad (3.191)$$

$$\sum G''_{3zAS}\left(\xi,y,\psi\right)=\left(4\xi^2+\frac{b^2\xi^2}{4}\cos^2\phi+\frac{a^2\xi^2}{4}\cos^2\theta\right)\left[\begin{matrix}C_{GA}e^{\left(2z-z_{g\_init}-\frac{b}{2}\sin\phi+\frac{a}{2}\sin\theta\right)\xi}+\\+C_{GB}e^{\left(z_{g\_init}-2z+\frac{b}{2}\sin\phi-\frac{a}{2}\sin\theta\right)\xi}\end{matrix}\right] \quad (3.192)$$

k_{zAP} Derivations:

The following equations solve for the air gap distance component from the denominator of the magnetic spring constant equation.

$$\frac{\partial\left[z_g^{-1}\left(z,\phi,\theta\right)\right]}{\partial z}=z'_{gAP}\left(z,\phi,\theta\right)=\frac{1}{z_{gAP}^2}$$

$$\frac{\partial\left[z_g^{-1}\left(z,\phi,\theta\right)\right]}{\partial \phi}=z'_{gAP}\left(z,\phi,\theta\right)=\frac{b\cos\left(\phi\right)}{2z_{gAP}^2}$$

$$\frac{\partial\left[z_g^{-1}\left(z,\phi,\theta\right)\right]}{\partial \theta}=z'_{gAP}\left(z,\phi,\theta\right)=\frac{a\cos\left(\theta\right)}{2z_{gAP}^2}$$

Now solve for the G_3 component of the repulsive magnetic force equation. G_3 equation exponential substitutions provide the following output for the z directed magnetic spring constants.

For C_{GA}: $e^{\left\{z-\left[z_{g\_init}-z-\frac{b}{2}\sin\phi-\frac{a}{2}\sin\theta\right]\right\}\xi}=e^{\left(2z-z_{g\_init}+\frac{b}{2}\sin\phi+\frac{a}{2}\sin\theta\right)\xi}$

For C_{GB}: $e^{\left\{\left[z_{g\_init}-z-\frac{b}{2}\sin\phi-\frac{a}{2}\sin\theta\right]-z\right\}\xi}=e^{\left(z_{g\_init}-2z-\frac{b}{2}\sin\phi-\frac{a}{2}\sin\theta\right)\xi}$

This substitution provides the following equations for $G_{3zAP}\left(\xi,z,\phi,\theta\right)$ and all of its derivatives.

$$G_{3zAP}\left(\xi,z,\phi,\theta\right)=\left[C_{GA}e^{\left(2z-z_{g\_init}+\frac{b}{2}\sin\phi+\frac{a}{2}\sin\theta\right)\xi}+C_{GB}e^{\left(z_{g\_init}-2z-\frac{b}{2}\sin\phi-\frac{a}{2}\sin\theta\right)\xi}\right] \quad (3.193)$$

$$\frac{\partial\left[G_{3zAP}\left(\xi,z,\phi,\theta\right)\right]}{\partial z}=G'_{3zAP}\left(\xi,z,\phi,\theta\right)=2\xi\left[\begin{matrix}C_{GA}e^{\left(2z-z_{g\_init}+\frac{b}{2}\sin\phi+\frac{a}{2}\sin\theta\right)\xi}-\\-C_{GB}e^{\left(z_{g\_init}-2z-\frac{b}{2}\sin\phi-\frac{a}{2}\sin\theta\right)\xi}\end{matrix}\right]$$

$$\frac{\partial^2\left[G_{3zAP}\left(\xi,z,\phi,\theta\right)\right]}{\partial z^2}=G''_{3zAP}\left(\xi,z,\phi,\theta\right)=4\xi^2\left[\begin{matrix}C_{GA}e^{\left(2z-z_{g\_init}+\frac{b}{2}\sin\phi+\frac{a}{2}\sin\theta\right)\xi}+\\+C_{GB}e^{\left(z_{g\_init}-2z-\frac{b}{2}\sin\phi-\frac{a}{2}\sin\theta\right)\xi}\end{matrix}\right]$$

$$\frac{\partial\left[G_{3zAP}\left(\xi,z,\phi,\theta\right)\right]}{\partial\phi}=G'_{3zAP}\left(\xi,z,\phi,\theta\right)=\frac{b\xi}{2}\cos\phi\left[\begin{matrix}C_{GA}e^{\left(2z-z_{g\_init}+\frac{b}{2}\sin\phi+\frac{a}{2}\sin\theta\right)\xi}-\\-C_{GB}e^{\left(z_{g\_init}-2z-\frac{b}{2}\sin\phi-\frac{a}{2}\sin\theta\right)\xi}\end{matrix}\right]$$

$$\frac{\partial^2\left[G_{3zAP}\left(\xi,z,\phi,\theta\right)\right]}{\partial\phi^2}=G''_{3zAP}\left(\xi,z,\phi,\theta\right)=\frac{b^2\xi^2}{4}\cos^2\phi\left[\begin{matrix}C_{GA}e^{\left(2z-z_{g\_init}+\frac{b}{2}\sin\phi+\frac{a}{2}\sin\theta\right)\xi}+\\+C_{GB}e^{\left(z_{g\_init}-2z-\frac{b}{2}\sin\phi-\frac{a}{2}\sin\theta\right)\xi}\end{matrix}\right]$$

$$\frac{\partial\left[G_{3zAP}\left(\xi,z,\phi,\theta\right)\right]}{\partial\theta}=G'_{3zAP}\left(\xi,z,\phi,\theta\right)=\frac{a\xi}{2}\cos\theta\left[\begin{matrix}C_{GA}e^{\left(2z-z_{g\_init}+\frac{b}{2}\sin\phi+\frac{a}{2}\sin\theta\right)\xi}-\\-C_{GB}e^{\left(z_{g\_init}-2z-\frac{b}{2}\sin\phi-\frac{a}{2}\sin\theta\right)\xi}\end{matrix}\right]$$

$$\frac{\partial^2\left[G_{3zAP}\left(\xi,z,\phi,\theta\right)\right]}{\partial\theta^2}=G''_{3zAP}\left(\xi,z,\phi,\theta\right)=\frac{a^2\xi^2}{4}\cos^2\theta\left[\begin{matrix}C_{GA}e^{\left(2z-z_{g\_init}+\frac{b}{2}\sin\phi+\frac{a}{2}\sin\theta\right)\xi}+\\+C_{GB}e^{\left(z_{g\_init}-2z-\frac{b}{2}\sin\phi-\frac{a}{2}\sin\theta\right)\xi}\end{matrix}\right]$$

$$\sum z'_{gAP}\left(z,\phi,\theta\right)=\frac{1}{z_{gAP}^2}+\frac{b\cos\left(\phi\right)+a\cos\left(\theta\right)}{2z_{gAP}^2}\tag{3.194}$$

$$\sum G'_{3zAP}\left(\xi,y,\psi\right)=\left(2\xi+\frac{b\xi}{2}\cos\phi+\frac{a\xi}{2}\cos\theta\right)\left[\begin{matrix}C_{GA}e^{\left(2z-z_{g\_init}+\frac{b}{2}\sin\phi+\frac{a}{2}\sin\theta\right)\xi}-\\-C_{GB}e^{\left(z_{g\_init}-2z-\frac{b}{2}\sin\phi-\frac{a}{2}\sin\theta\right)\xi}\end{matrix}\right]\tag{3.195}$$

$$\sum G''_{3zAP}\left(\xi,y,\psi\right)=\left(4\xi^2+\frac{b^2\xi^2}{4}\cos^2\phi+\frac{a^2\xi^2}{4}\cos^2\theta\right)\left[\begin{matrix}C_{GA}e^{\left(2z-z_{g\_init}+\frac{b}{2}\sin\phi+\frac{a}{2}\sin\theta\right)\xi}+\\+C_{GB}e^{\left(z_{g\_init}-2z-\frac{b}{2}\sin\phi-\frac{a}{2}\sin\theta\right)\xi}\end{matrix}\right]\tag{3.196}$$

This produces the desired functional dependency equations for the magnetic spring constant derivatives. These equations are used to solve the nonlinear magnetic spring constant component of the potential energy partial differential equation.

Potential Energy Derivation Solutions – Repulsive Force:

The potential energy magnetic spring derivations of equations (3.197) through (3.204) follow a similar format as the Phase III solutions shown in equations (3.152) and (3.153) where equation (3.151) is now used to solve for the appropriate forms of the magnetic spring constant derivatives. Only the repulsive force spring constant partial differentials are solved since this is the area of interest in this analysis. The propulsive drag component could also be determined in a similar fashion along the propulsion vector.

$$k'_{yBS}=\frac{1}{2}\bullet\begin{pmatrix}\text{Magnetic}\\ \text{Volume}\end{pmatrix}\left\{\begin{array}{l}\dfrac{\begin{array}{l}\text{Re}\left(J\left[\sum G'_{3yBS}(\xi,y,\psi)\right]B_T^*\left[\sum G'_{3yBS}(\xi,y,\psi)\right]\right)+\\ +\text{Re}\left(J\left[\sum G_{3yBS}(\xi,y,\psi)\right]B_T^*\left[\sum G''_{3yBS}(\xi,y,\psi)\right]\right)\end{array}}{y_{gBS}}+\\ +\text{Re}\left(J\left[\sum G_{3yBS}(\xi,y,\psi)\right]B_T^*\left[\sum G'_{3yBS}(\xi,y,\psi)\right]\right)\sum y'_{gBS}(y,\psi)\end{array}\right\} \tag{3.197}$$

$$k'_{yBP}=\frac{1}{2}\bullet\begin{pmatrix}\text{Magnetic}\\ \text{Volume}\end{pmatrix}\left\{\begin{array}{l}\dfrac{\begin{array}{l}\text{Re}\left(J\left[\sum G'_{3yBP}(\xi,y,\psi)\right]B_T^*\left[\sum G'_{3yBP}(\xi,y,\psi)\right]\right)+\\ +\text{Re}\left(J\left[\sum G_{3yBP}(\xi,y,\psi)\right]B_T^*\left[\sum G''_{3yBP}(\xi,y,\psi)\right]\right)\end{array}}{y_{gBP}}+\\ +\text{Re}\left(J\left[\sum G_{3yBP}(\xi,y,\psi)\right]B_T^*\left[\sum G'_{3yBP}(\xi,y,\psi)\right]\right)\sum y'_{gBP}(y,\psi)\end{array}\right\} \tag{3.198}$$

$$k'_{yAS}=\frac{1}{2}\bullet\begin{pmatrix}\text{Magnetic}\\ \text{Volume}\end{pmatrix}\left\{\begin{array}{l}\dfrac{\begin{array}{l}\mathrm{Re}\left(J\left[\sum G'_{3yAS}(\xi,y,\psi)\right]B_T^*\left[\sum G'_{3yAS}(\xi,y,\psi)\right]\right)+\\ +\mathrm{Re}\left(J\left[\sum G_{3yAS}(\xi,y,\psi)\right]B_T^*\left[\sum G''_{3yAS}(\xi,y,\psi)\right]\right)\end{array}}{y_{gAS}}+\\ +\mathrm{Re}\left(J\left[\sum G_{3yAS}(\xi,y,\psi)\right]B_T^*\left[\sum G'_{3yAS}(\xi,y,\psi)\right]\right)\sum y'_{gAS}(y,\psi)\end{array}\right\} \tag{3.199}$$

$$k'_{yAP}=\frac{1}{2}\bullet\begin{pmatrix}\text{Magnetic}\\ \text{Volume}\end{pmatrix}\left\{\begin{array}{l}\dfrac{\begin{array}{l}\mathrm{Re}\left(J\left[\sum G'_{3yAP}(\xi,y,\psi)\right]B_T^*\left[\sum G'_{3yAP}(\xi,y,\psi)\right]\right)+\\ +\mathrm{Re}\left(J\left[\sum G_{3yAP}(\xi,y,\psi)\right]B_T^*\left[\sum G''_{3yAP}(\xi,y,\psi)\right]\right)\end{array}}{y_{gAP}}+\\ +\mathrm{Re}\left(J\left[\sum G_{3yAP}(\xi,y,\psi)\right]B_T^*\left[\sum G'_{3yAP}(\xi,y,\psi)\right]\right)\sum y'_{gAP}(y,\psi)\end{array}\right\} \tag{3.200}$$

$$k'_{zBS}=\frac{1}{2}\bullet\begin{pmatrix}\text{Magnetic}\\ \text{Volume}\end{pmatrix}\left\{\begin{array}{l}\dfrac{\begin{array}{l}\mathrm{Re}\left(J\left[\sum G'_{3zBS}(\xi,z,\phi,\theta)\right]B_T^*\left[\sum G'_{3zBS}(\xi,z,\phi,\theta)\right]\right)+\\ +\mathrm{Re}\left(J\left[\sum G_{3zBS}(\xi,z,\phi,\theta)\right]B_T^*\left[\sum G''_{3zBS}(\xi,z,\phi,\theta)\right]\right)\end{array}}{z_{gBS}}+\\ +\mathrm{Re}\left(J\left[\sum G_{3zBS}(\xi,z,\phi,\theta)\right]B_T^*\left[\sum G'_{3zBS}(\xi,z,\phi,\theta)\right]\right)\sum z'_{gBS}(z,\phi,\theta)\end{array}\right\} \tag{3.201}$$

$$k'_{zBP}=\frac{1}{2}\bullet\begin{pmatrix}\text{Magnetic}\\ \text{Volume}\end{pmatrix}\left\{\begin{array}{l}\dfrac{\begin{array}{l}\mathrm{Re}\left(J\left[\sum G'_{3zBP}(\xi,z,\phi,\theta)\right]B_T^*\left[\sum G'_{3zBP}(\xi,z,\phi,\theta)\right]\right)+\\ +\mathrm{Re}\left(J\left[\sum G_{3zBP}(\xi,z,\phi,\theta)\right]B_T^*\left[\sum G''_{3zBP}(\xi,z,\phi,\theta)\right]\right)\end{array}}{z_{gBP}}+\\ +\mathrm{Re}\left(J\left[\sum G_{3zBP}(\xi,z,\phi,\theta)\right]B_T^*\left[\sum G'_{3zBP}(\xi,z,\phi,\theta)\right]\right)\sum z'_{gBP}(z,\phi,\theta)\end{array}\right\} \tag{3.202}$$

$$k'_{zAS}=\frac{1}{2}\bullet\begin{pmatrix}\text{Magnetic}\\ \text{Volume}\end{pmatrix}\left\{\begin{array}{l}\operatorname{Re}\left(J\left[\sum G'_{3zAS}\left(\xi,z,\phi,\theta\right)\right]B_T^*\left[\sum G'_{3zAS}\left(\xi,z,\phi,\theta\right)\right]\right)+\\ +\operatorname{Re}\left(J\left[\sum G_{3zAS}\left(\xi,z,\phi,\theta\right)\right]B_T^*\left[\sum G''_{3zAS}\left(\xi,z,\phi,\theta\right)\right]\right)\\ \hline z_{gAS}\\ +\operatorname{Re}\left(J\left[\sum G_{3zAS}\left(\xi,z,\phi,\theta\right)\right]B_T^*\left[\sum G'_{3zAS}\left(\xi,z,\phi,\theta\right)\right]\right)\sum z'_{gAS}\left(z,\phi,\theta\right)\end{array}\right\} \tag{3.203}$$

$$k'_{zAP}=\frac{1}{2}\bullet\begin{pmatrix}\text{Magnetic}\\ \text{Volume}\end{pmatrix}\left\{\begin{array}{l}\operatorname{Re}\left(J\left[\sum G'_{3zAP}\left(\xi,z,\phi,\theta\right)\right]B_T^*\left[\sum G'_{3zAP}\left(\xi,z,\phi,\theta\right)\right]\right)+\\ +\operatorname{Re}\left(J\left[\sum G_{3zAP}\left(\xi,z,\phi,\theta\right)\right]B_T^*\left[\sum G''_{3zAP}\left(\xi,z,\phi,\theta\right)\right]\right)\\ \hline z_{gAP}\\ +\operatorname{Re}\left(J\left[\sum G_{3zAP}\left(\xi,z,\phi,\theta\right)\right]B_T^*\left[\sum G'_{3zAP}\left(\xi,z,\phi,\theta\right)\right]\right)\sum z'_{gAP}\left(z,\phi,\theta\right)\end{array}\right\} \tag{3.204}$$

Finally the potential energy partial derivatives are solved in the following equations. Note that the appropriate forms of equations (3.165) through (3.180) for the G_3 equation and all of the appropriate derivatives must be inserted for the y dependent linear and rotational magnetic spring constant values in equations (3.197) through (3.200). The same is true for including the appropriate forms of equations (3.181) through (3.196) for the z dependent linear and rotational magnetic spring constant values in equations (3.201) through (3.204). For example, in equation (3.204) for the magnetic spring variable k'_{zAP}, the appropriate forms of the functions G_{3zAP}, G'_{3zAP}, and G''_{3zAP} come from equation (3.193) and the superposition equations (3.195) and (3.196). This superposition is mathematically performed by superimposing each respective G_3, G'_3, and G''_3 component inside of the respective J, B_T^*, and B_N^* equation being solved and then finally taking a single multiplication of the total J, B_T^*, and B_N^* values in each respective potential energy partial derivative equation. The air gap partial differential superposition comes from equation (3.194).

$$\frac{\partial U}{\partial y}=\left[\begin{array}{l}\left(\frac{k'_{yBS}y_{gBS}^2}{2}-k_{yBS}y_{gBS}\right)+\left(\frac{k'_{yBP}y_{gBP}^2}{2}+k_{yBP}y_{gBP}\right)+\\+\left(\frac{k'_{yAP}y_{gAP}^2}{2}+k_{yAP}y_{gAP}\right)+\left(\frac{k'_{yAS}y_{gAS}^2}{2}-k_{yAS}y_{gAS}\right)\end{array}\right]$$

$$\frac{\partial U}{\partial z}=\left[\begin{array}{l}mg+\left(\frac{k'_{zBS}z_{gBS}^2}{2}-k_{zBS}z_{gBS}\right)+\left(\frac{k'_{zBP}z_{gBP}^2}{2}-k_{zBP}z_{gBP}\right)+\\+\left(\frac{k'_{zAS}z_{gAS}^2}{2}-k_{zAS}z_{gAS}\right)+\left(\frac{k'_{zAP}z_{gAP}^2}{2}-k_{zAP}z_{gAP}\right)\end{array}\right]$$

$$\frac{\partial U}{\partial \phi}=\left[\begin{array}{l}\left(\frac{k'_{zBS}z_{gBS}^2}{2}+\frac{b}{2}k_{zBS}z_{gBS}\cos\phi\right)+\left(\frac{k'_{zBP}z_{gBP}^2}{2}-\frac{b}{2}k_{zBP}z_{gBP}\cos\phi\right)+\\+\left(\frac{k'_{zAS}z_{gAS}^2}{2}+\frac{b}{2}k_{zAS}z_{gAS}\cos\phi\right)+\left(\frac{k'_{zAP}z_{gAP}^2}{2}-\frac{b}{2}k_{zAP}z_{gAP}\cos\phi\right)\end{array}\right]$$

$$\frac{\partial U}{\partial \theta}=\left[\begin{array}{l}\left(\frac{k'_{zBS}z_{gBS}^2}{2}+\frac{a}{2}k_{zBS}z_{gBS}\cos\theta\right)+\left(\frac{k'_{zBP}z_{gBP}^2}{2}+\frac{a}{2}k_{zBP}z_{gBP}\cos\theta\right)+\\+\left(\frac{k'_{zAS}z_{gAS}^2}{2}-\frac{a}{2}k_{zAS}z_{gAS}\cos\theta\right)+\left(\frac{k'_{zAP}z_{gAP}^2}{2}-\frac{a}{2}k_{zAP}z_{gAP}\cos\theta\right)\end{array}\right]$$

$$\frac{\partial U}{\partial \psi}=\left[\begin{array}{l}\left(\frac{k'_{yBS}y_{gBS}^2}{2}-\frac{a}{2}k_{yBS}y_{gBS}\cos\psi\right)+\left(\frac{k'_{yBP}y_{gBP}^2}{2}+\frac{a}{2}k_{yBP}y_{gBP}\cos\psi\right)+\\+\left(\frac{k'_{yAP}y_{gAP}^2}{2}-\frac{a}{2}k_{yAP}y_{gAP}\cos\psi\right)+\left(\frac{k'_{yAS}y_{gAS}^2}{2}+\frac{a}{2}k_{yAS}y_{gAS}\cos\psi\right)\end{array}\right]$$

Lagrange Equations of Motion

Use the partial differential kinetic and potential energy equation derivations to solve Lagrange's equation of motion, equation (3.205), and the subsequent equations of motion for each generalized coordinate. Then solve for the generalized coordinate equation form suitable for numerical state space solution. This numerical solution equation form always isolates the highest differentials of the single respective

generalized coordinate under analysis. The generalized force, Q, is zero for this homogeneous system. $Q \neq 0$ when a disturbing force is introduced to provide the particular solution.

$$\frac{d}{dt}\left(\frac{\partial T^*}{\partial \dot{q}_i}\right) - \frac{\partial T^*}{\partial q_i} + \frac{\partial U}{\partial q_i} + \overbrace{\cancel{\frac{\partial D}{\partial \dot{q}_i}}^{0}}^{\text{System Natural Damping Component}} = Q_i \tag{3.205}$$

Generalized Coordinate $q = x$:

Equation (3.206) solves for $q = x$.

$$m\ddot{x} = 0 \tag{3.206}$$

Generalized Coordinate $q = y$:

Equation (3.207) solves for $q = y$.

$$m\ddot{y} + \left[\begin{array}{l} \left(\frac{k'_{yBS} y_{gBS}^2}{2} - k_{yBS} y_{gBS}\right) + \left(\frac{k'_{yBP} y_{gBP}^2}{2} + k_{yBP} y_{gBP}\right) + \\ + \left(\frac{k'_{yAS} y_{gAS}^2}{2} - k_{yAS} y_{gAS}\right) + \left(\frac{k'_{yAP} y_{gAP}^2}{2} + k_{yAP} y_{gAP}\right) \end{array}\right] = 0$$

$$\ddot{y} = -\frac{\left[\begin{array}{l} \left(\frac{k'_{yBS} y_{gBS}^2}{2} - k_{yBS} y_{gBS}\right) + \left(\frac{k'_{yBP} y_{gBP}^2}{2} + k_{yBP} y_{gBP}\right) + \\ + \left(\frac{k'_{yAS} y_{gAS}^2}{2} - k_{yAS} y_{gAS}\right) + \left(\frac{k'_{yAP} y_{gAP}^2}{2} + k_{yAP} y_{gAP}\right) \end{array}\right]}{m} \tag{3.207}$$

Generalized Coordinate $q = z$:

Equation (3.208) solves for $q = z$.

$$m\ddot{z} + \left[\begin{array}{l} mg + \left(\frac{k'_{zBS} z_{gBS}^2}{2} - k_{zBS} z_{gBS}\right) + \left(\frac{k'_{zBP} z_{gBP}^2}{2} - k_{zBP} z_{gBP}\right) + \\ + \left(\frac{k'_{zAS} z_{gAS}^2}{2} - k_{zAS} z_{gAS}\right) + \left(\frac{k'_{zAP} z_{gAP}^2}{2} - k_{zAP} z_{gAP}\right) \end{array}\right] = 0$$

$$\ddot{z} = -\frac{\left[\begin{array}{l} mg + \left(\frac{k'_{zBS} z_{gBS}^2}{2} - k_{zBS} z_{gBS}\right) + \left(\frac{k'_{zBP} z_{gBP}^2}{2} - k_{zBP} z_{gBP}\right) + \\ + \left(\frac{k'_{zAS} z_{gAS}^2}{2} - k_{zAS} z_{gAS}\right) + \left(\frac{k'_{zAP} z_{gAP}^2}{2} - k_{zAP} z_{gAP}\right) \end{array}\right]}{m} \qquad (3.208)$$

Generalized Coordinate $q = \phi$:

Equation (3.209) solves for $q = \phi$.

$$\left\{\begin{array}{l} J_{xx}\left[\left(\ddot{\phi}\cos^2\theta\cos^2\psi - 2\dot{\phi}\dot{\theta}\cos\theta\sin\theta\cos^2\psi - 2\dot{\phi}\dot{\psi}\cos^2\theta\sin\psi\cos\psi\right) + \right. \\ \left. + \left(\ddot{\theta}\cos\theta\cos\psi\sin\psi - \dot{\theta}^2\sin\theta\cos\psi\sin\psi - \dot{\theta}\dot{\psi}\cos\theta\sin^2\psi + \dot{\theta}\dot{\psi}\cos\theta\cos^2\psi\right)\right] + \\ + J_{yy}\left[\left(-\ddot{\theta}\cos\theta\cos\psi\sin\psi + \dot{\theta}^2\sin\theta\cos\psi\sin\psi + \dot{\theta}\dot{\psi}\cos\theta\sin^2\psi - \dot{\theta}\dot{\psi}\cos\theta\cos^2\psi\right) + \right. \\ \left. + \left(\ddot{\phi}\cos^2\theta\sin^2\psi - 2\dot{\phi}\dot{\theta}\cos\theta\sin\theta\sin^2\psi + 2\dot{\phi}\dot{\psi}\cos^2\theta\sin\psi\cos\psi\right)\right] + \\ + J_{zz}\left[\left(\ddot{\psi}\sin\theta + \dot{\psi}\dot{\theta}\cos\theta\right) + \left(\ddot{\phi}\sin^2\theta + 2\dot{\phi}\dot{\theta}\sin\theta\cos\theta\right)\right] \end{array}\right\} +$$

$$+ \left[\begin{array}{l} \left(\frac{k'_{zBS} z_{gBS}^2}{2} + \frac{b}{2} k_{zBS} z_{gBS}\cos\phi\right) + \left(\frac{k'_{zBP} z_{gBP}^2}{2} - \frac{b}{2} k_{zBP} z_{gBP}\cos\phi\right) + \\ + \left(\frac{k'_{zAS} z_{gAS}^2}{2} + \frac{b}{2} k_{zAS} z_{gAS}\cos\phi\right) + \left(\frac{k'_{zAP} z_{gAP}^2}{2} - \frac{b}{2} k_{zAP} z_{gAP}\cos\phi\right) \end{array}\right] = 0$$

$$\ddot{\phi} = -\frac{\left\{\begin{array}{l} J_{xx}\left(\begin{array}{l}\ddot{\theta}\cos\theta\cos\psi\sin\psi - 2\dot{\phi}\dot{\psi}\cos^2\theta\sin\psi\cos\psi - \\ -\dot{\theta}^2\sin\theta\cos\psi\sin\psi - \dot{\theta}\dot{\psi}\cos\theta\sin^2\psi + \\ +\dot{\theta}\dot{\psi}\cos\theta\cos^2\psi - 2\dot{\phi}\dot{\theta}\cos\theta\sin\theta\cos^2\psi\end{array}\right) + \\ +J_{yy}\left(\begin{array}{l}-\ddot{\theta}\cos\theta\cos\psi\sin\psi + 2\dot{\phi}\dot{\psi}\cos^2\theta\sin\psi\cos\psi + \\ +\dot{\theta}^2\sin\theta\cos\psi\sin\psi + \dot{\theta}\dot{\psi}\cos\theta\sin^2\psi - \\ -\dot{\theta}\dot{\psi}\cos\theta\cos^2\psi - 2\dot{\phi}\dot{\theta}\cos\theta\sin\theta\sin^2\psi\end{array}\right) + \\ +J_{zz}\left(\ddot{\psi}\sin\theta + \dot{\psi}\dot{\theta}\cos\theta + 2\dot{\phi}\dot{\theta}\sin\theta\cos\theta\right) + \\ +\left[\begin{array}{l}\left(\frac{k'_{zBS}z_{gBS}^2}{2} + \frac{b}{2}k_{zBS}z_{gBS}\cos\phi\right) + \left(\frac{k'_{zBP}z_{gBP}^2}{2} - \frac{b}{2}k_{zBP}z_{gBP}\cos\phi\right) + \\ +\left(\frac{k'_{zAS}z_{gAS}^2}{2} + \frac{b}{2}k_{zAS}z_{gAS}\cos\phi\right) + \left(\frac{k'_{zAP}z_{gAP}^2}{2} - \frac{b}{2}k_{zAP}z_{gAP}\cos\phi\right)\end{array}\right]\end{array}\right\}}{J_{xx}\left(\cos^2\theta\cos^2\psi\right) + J_{yy}\left(\cos^2\theta\sin^2\psi\right) + J_{zz}\left(\sin^2\theta\right)}$$

(3.209)

Generalized Coordinate $q = \theta$:

Equation (3.210) solves for $q = \theta$.

$$\left\{\begin{array}{l} J_{xx}\left[\left(\begin{array}{l}\ddot{\phi}\cos\theta\cos\psi\sin\psi-\dot{\phi}\dot{\theta}\sin\theta\cos\psi\sin\psi-\\ -\dot{\phi}\dot{\psi}\cos\theta\sin^2\psi+\dot{\phi}\dot{\psi}\cos\theta\cos^2\psi\end{array}\right)+\right. \\ \left.+\left(\ddot{\theta}\sin^2\psi+2\dot{\theta}\dot{\psi}\sin\psi\cos\psi\right)\right]+J_{yy}\left[\left(\ddot{\theta}\cos^2\psi-2\dot{\theta}\dot{\psi}\cos\psi\sin\psi\right)-\right. \\ \left.-\left(\ddot{\phi}\cos\theta\cos\psi\sin\psi-\dot{\phi}\dot{\theta}\sin\theta\cos\psi\sin\psi-\dot{\phi}\dot{\psi}\cos\theta\sin^2\psi+\dot{\phi}\cos\theta\cos^2\psi\right)\right] \end{array}\right\}- $$

$$-\left[\begin{array}{l} J_{xx}\left(-\dot{\phi}^2\dot{\theta}\cos\theta\sin\theta\cos^2\psi-\dot{\phi}\dot{\theta}^2\sin\theta\cos\psi\sin\psi\right)+ \\ +J_{yy}\left(\dot{\phi}\dot{\theta}^2\sin\theta\cos\psi\sin\psi-\dot{\phi}^2\dot{\theta}\cos\theta\sin\theta\sin^2\psi\right)+ \\ +J_{zz}\left(\dot{\phi}\dot{\theta}\dot{\psi}\cos\theta+\dot{\phi}^2\dot{\theta}\sin\theta\cos\theta\right) \end{array}\right]+$$

$$+\left[\begin{array}{l}\left(\frac{k'_{zBS}z_{gBS}^2}{2}+\frac{a}{2}k_{zBS}z_{gBS}\cos\theta\right)+\left(\frac{k'_{zBP}z_{gBP}^2}{2}+\frac{a}{2}k_{zBP}z_{gBP}\cos\theta\right)+ \\ +\left(\frac{k'_{zAS}z_{gAS}^2}{2}-\frac{a}{2}k_{zAS}z_{gAS}\cos\theta\right)+\left(\frac{k'_{zAP}z_{gAP}^2}{2}-\frac{a}{2}k_{zAP}z_{gAP}\cos\theta\right)\end{array}\right]=0$$

$$\ddot{\theta}=-\frac{\left\{\begin{array}{l} J_{xx}\left(\begin{array}{l}\ddot{\phi}\cos\theta\cos\psi\sin\psi-\dot{\phi}\dot{\theta}\sin\theta\cos\psi\sin\psi-\\ -\dot{\phi}\dot{\psi}\cos\theta\sin^2\psi+2\dot{\theta}\dot{\psi}\sin\psi\cos\psi+\\ +\dot{\phi}^2\dot{\theta}\cos\theta\sin\theta\cos^2\psi+\dot{\phi}\dot{\theta}^2\sin\theta\cos\psi\sin\psi+\\ +\dot{\phi}\dot{\psi}\cos\theta\cos^2\psi\end{array}\right)+ \\ +J_{yy}\left(\begin{array}{l}-\ddot{\phi}\cos\theta\cos\psi\sin\psi+\dot{\phi}\dot{\theta}\sin\theta\cos\psi\sin\psi+\\ +\dot{\phi}\dot{\psi}\cos\theta\sin^2\psi-2\dot{\theta}\dot{\psi}\sin\psi\cos\psi+\\ +\dot{\phi}^2\dot{\theta}\cos\theta\sin\theta\cos^2\psi-\dot{\phi}\dot{\theta}^2\sin\theta\cos\psi\sin\psi-\\ -\dot{\phi}\cos\theta\cos^2\psi\end{array}\right)- \\ -J_{zz}\left(\dot{\phi}\dot{\theta}\dot{\psi}\cos\theta+\dot{\phi}^2\dot{\theta}\sin\theta\cos\theta\right)+ \\ +\left[\begin{array}{l}\left(\frac{k'_{zBS}z_{gBS}^2}{2}+\frac{a}{2}k_{zBS}z_{gBS}\cos\theta\right)+\left(\frac{k'_{zBP}z_{gBP}^2}{2}+\frac{a}{2}k_{zBP}z_{gBP}\cos\theta\right)+ \\ +\left(\frac{k'_{zAS}z_{gAS}^2}{2}-\frac{a}{2}k_{zAS}z_{gAS}\cos\theta\right)+\left(\frac{k'_{zAP}z_{gAP}^2}{2}-\frac{a}{2}k_{zAP}z_{gAP}\cos\theta\right)\end{array}\right] \end{array}\right\}}{J_{xx}\left(\sin^2\psi\right)+J_{yy}\left(\cos^2\psi\right)} \quad (3.210)$$

Generalized Coordinate $q = \psi$:

Equation (3.211) solves for $q = \psi$.

$$\ddot{\psi} = -\frac{\left\{\begin{array}{l} \left\{J_{zz}\left[\ddot{\psi} + \left(\ddot{\phi}\sin\theta + \dot{\phi}\dot{\theta}\cos\theta\right)\right]\right\} - \\ -\left\{\begin{array}{l} J_{xx}\left[-\dot{\phi}^2\dot{\psi}\cos^2\theta\cos\psi\sin\psi + \dot{\phi}\dot{\theta}\dot{\psi}\cos\theta\left(\cos^2\psi - \sin^2\psi\right) + \dot{\theta}^2\dot{\psi}\sin\psi\cos\psi\right] + \\ + J_{yy}\left[-\dot{\theta}^2\dot{\psi}\cos\psi\sin\psi - \dot{\phi}\dot{\theta}\dot{\psi}\cos\theta\left(\cos^2\psi - \sin^2\psi\right) + \dot{\phi}^2\dot{\psi}\cos^2\theta\sin\psi\cos\psi\right] \end{array}\right\} + \\ + \left[\begin{array}{l} \left(\frac{k'_{yBS}y_{gBS}^2}{2} - \frac{a}{2}k_{yBS}y_{gBS}\cos\psi\right) + \left(\frac{k'_{yBP}y_{gBP}^2}{2} + \frac{a}{2}k_{yBP}y_{gBP}\cos\psi\right) + \\ + \left(\frac{k'_{yAS}y_{gAS}^2}{2} + \frac{a}{2}k_{yAS}y_{gAS}\cos\psi\right) + \left(\frac{k'_{yAP}y_{gAP}^2}{2} - \frac{a}{2}k_{yAP}y_{gAP}\cos\psi\right) \end{array}\right] = 0 \end{array}\right.}{J_{zz}}$$

$$\left\{\begin{array}{l} J_{zz}\left(\ddot{\phi}\sin\theta + \dot{\phi}\dot{\theta}\cos\theta\right) - \\ -J_{xx}\left[\begin{array}{l} \dot{\phi}^2\dot{\psi}\cos^2\theta\cos\psi\sin\psi - \dot{\phi}\dot{\theta}\dot{\psi}\cos\theta\left(\cos^2\psi - \sin^2\psi\right) - \\ -\dot{\theta}^2\dot{\psi}\sin\psi\cos\psi \end{array}\right] - \\ -J_{yy}\left[\begin{array}{l} -\dot{\phi}^2\dot{\psi}\cos^2\theta\cos\psi\sin\psi + \dot{\phi}\dot{\theta}\dot{\psi}\cos\theta\left(\cos^2\psi - \sin^2\psi\right) + \\ +\dot{\theta}^2\dot{\psi}\sin\psi\cos\psi \end{array}\right] + \\ + \left[\begin{array}{l} \left(\frac{k'_{yBS}y_{gBS}^2}{2} - \frac{a}{2}k_{yBS}y_{gBS}\cos\psi\right) + \left(\frac{k'_{yBP}y_{gBP}^2}{2} + \frac{a}{2}k_{yBP}y_{gBP}\cos\psi\right) + \\ + \left(\frac{k'_{yAS}y_{gAS}^2}{2} + \frac{a}{2}k_{yAS}y_{gAS}\cos\psi\right) + \left(\frac{k'_{yAP}y_{gAP}^2}{2} - \frac{a}{2}k_{yAP}y_{gAP}\cos\psi\right) \end{array}\right] \end{array}\right\}$$

(3.211)

The Phase IV homogeneous equations of motion forms as presented as equations (3.206) through (3.211) are suitable for numerical state space solution. As at the end of Phase III analysis, observe that the equations of motion are geometrically highly nonlinear as well as materially nonlinear in the primary iron core of both the principal and control solenoids until complete magnetic saturation occurs.

3.6.b Computational Analysis

A Phase IV computational analysis would follow a similar pattern as Phase I and described in Chapter 3.3.b. No Phase II specific computational analyses are performed.

3.6.c Control and Optimization Analysis

3.6.c.i Soft Computing Control Theory

Phase IV implements a similar soft computing method as Phase I which is described in Chapter 3.3.c.ii. Besides a few gain changes between Phase I and Phase IV soft computing methods, such as the maximum output control voltage level, the main difference between Phase I and IV is the area of implementation. In essence the Phase I control method is applied to each and every Phase IV solenoid separately as an individual controller.

CHAPTER 4 TESTING

4.1 TESTING OVERVIEW

As mentioned at the end of Chapter 2.3.a, only Phase I is tested and hence produces results. Phases II through IV are still provided for outlining a logical test schedule.

4.2 PHASE I: STATIC TRANSLATIONAL 1 D.O.F. SOL. E.D.S. SYSTEM

4.2.a Overall Purpose

Phase I statically isolates a single D.O.F. E.D.S. system for analysis and damping control. This simplified system allows a basis for statically governed E.D.S. damping theory, modeling accuracy determination for a rudimentary static system model, and a measure of effectiveness for each control scheme. Every E.D.S. system initiates from this principle.

In general the tested translational motion models any one of the three maglev system's translational D.O.F., although this test is listed as a vertical D.O.F. motion of a static maglev system test because of the system's secondary motion relative to the gravity body force vector.

4.2.b Governing Physical Parameters

As shown in Chapter 3.3.a the z directed vertical motion is the state variable of interest. This position vector provides the solenoid force on the secondary for a fixed solenoid current. The z directed acceleration determines the secondary's inertial force. The z directed velocity is observed and used for damping control. Both solenoids' geometries and currents provide their output forcing functions.

4.2.c Phase I Testing

4.2.c.i Test Apparatus

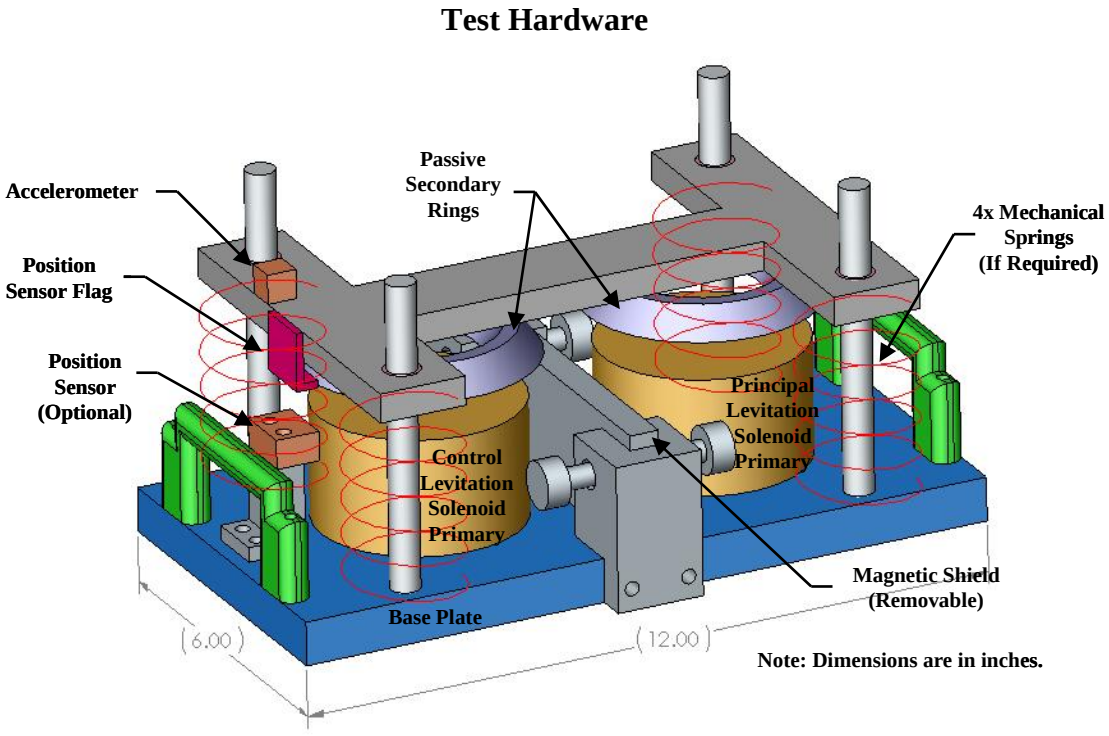

Figure 4.2-1: Phase I Test Apparatus – Initial Concept

The initial concept test article shown in Figure 4.2-1 provides the basis for the final test article. It consists of a pair of solenoid primaries magnetically interacting with an underdamped mechanical secondary system. The test apparatus consists of a single solenoid as the principal levitation prime mover solenoid. This principal solenoid is designed to levitate a coaxial secondary of similar diameter via the connected AC source. Note that the solenoid diameter is not the same dimension as the secondary diameter. The control solenoid is also held fixed next to the principal levitation solenoid and below the conducting secondary plate. The secondary is a conducting plate held above the principal and control solenoid primaries with respect to gravity. The test restricts secondary motion in y axis translating direction. Bearings

provide z axis motion for the secondary. Each secondary covers their respective primary solenoids and are slightly thicker than the skin depth of the levitation magnetic flux density produced in the primaries. An accelerometer is placed on the secondary to monitor accelerations in a direction parallel to the forced secondary motion. Accelerometers are inherently electronically noisy output data instruments, but the required velocity and position data is often unaffected due to natural filtering of the output acceleration signal when vigilantly integrating to attain reasonably accurate observed signals.

Figure 4.2-1 includes extra elements previously not discussed. An optional position sensor is fixed to the solenoid base plate to monitor the secondary position relative to the solenoids. The position sensor is desired but listed as optional due to difficulty of readily attaining one. A removable magnetic shield is used to magnetically isolate the principal and control coils. This shield is not considered necessary in Phase I, but may be required for isolating the magnetic control coils in later phases in order to reduce eddy currently being produced in the lower power control coils from the more powerful principal levitation, guidance, and propulsion systems. The figure also indicates the potential use of four axial, y axis directed mechanical springs which are affixed between the plate and support rods. These are provided as an option when attached to the base plate and secondary connector bar. The springs allow either a higher spring constant in the air gap or a mock principal levitation system which allows the principal solenoid to act as a second control solenoid.

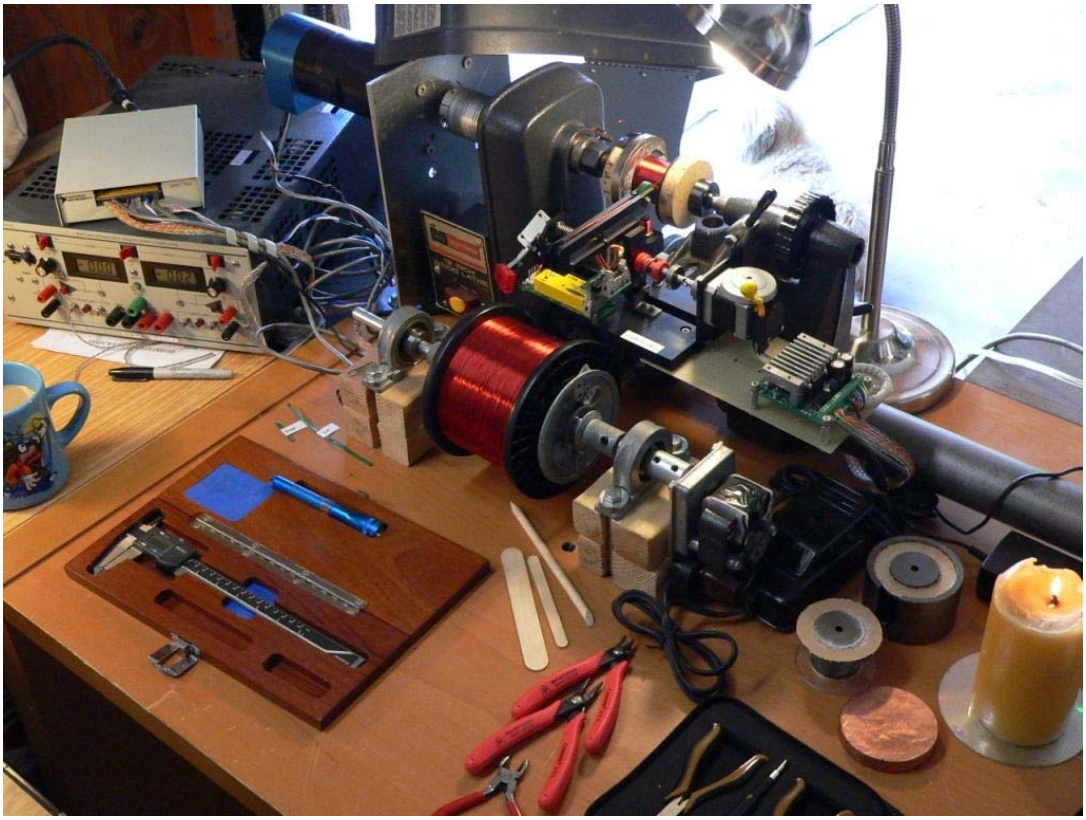

Figure 4.2-2: Solenoid Coil Winding Machine – Winding Hardware

Both the principal and control solenoids require a means of fabricating the various coils as per set analytical and computational specifications. A numerically controlled, dual axis winding machine with integrated wire tensiometer was designed and built for this purpose. A servo controlled induction motor turned the solenoid axis and a stepper motor provided the linear follower axis. The final machine produced reasonably high packing factor coils at a solenoid axis turn rate up to 500 rpm. Limit switches position A picture of this machine is provided in Figure 4.2-2. Supplemental pictures of this machine are provided in Appendix E.3.

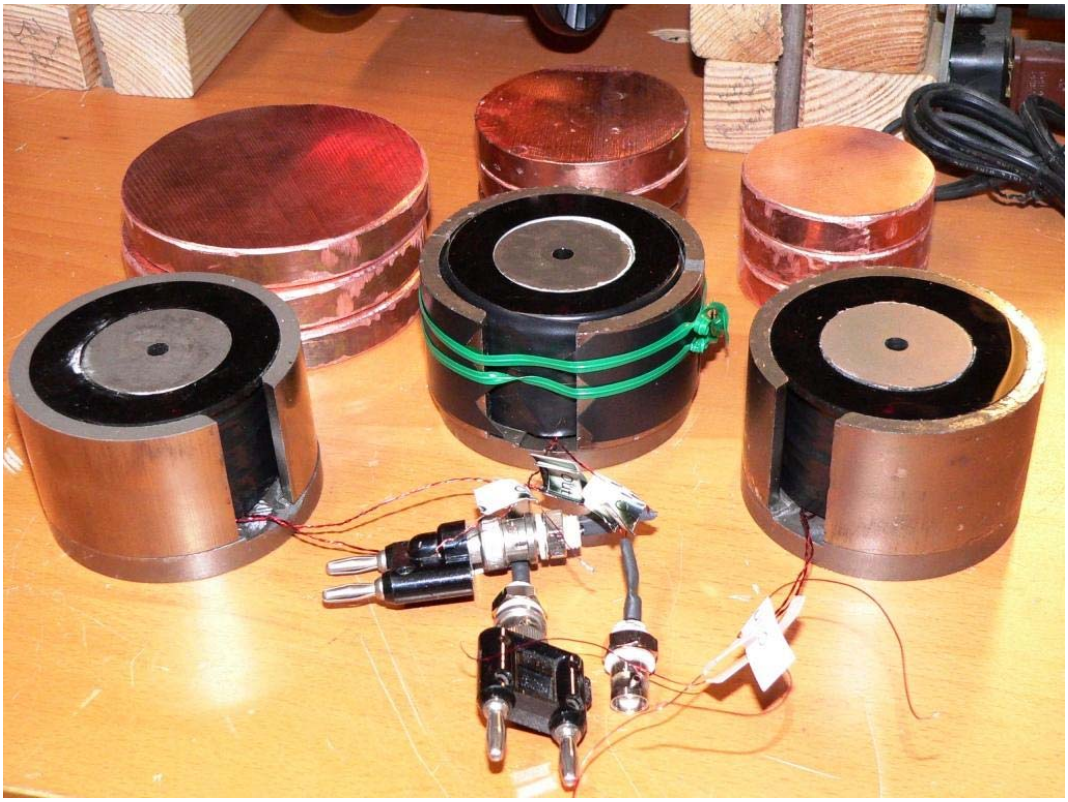

Figure 4.2-3: Phase I Test Solenoids & Secondaries

A picture of the three wound solenoid cores used for final testing and multiple ½" thick copper secondaries with diameters of 2.5", 3", and 4" is presented in Figure 4.2-3. Additional solenoid core pictures and drawings are provided in Appendix E.2.

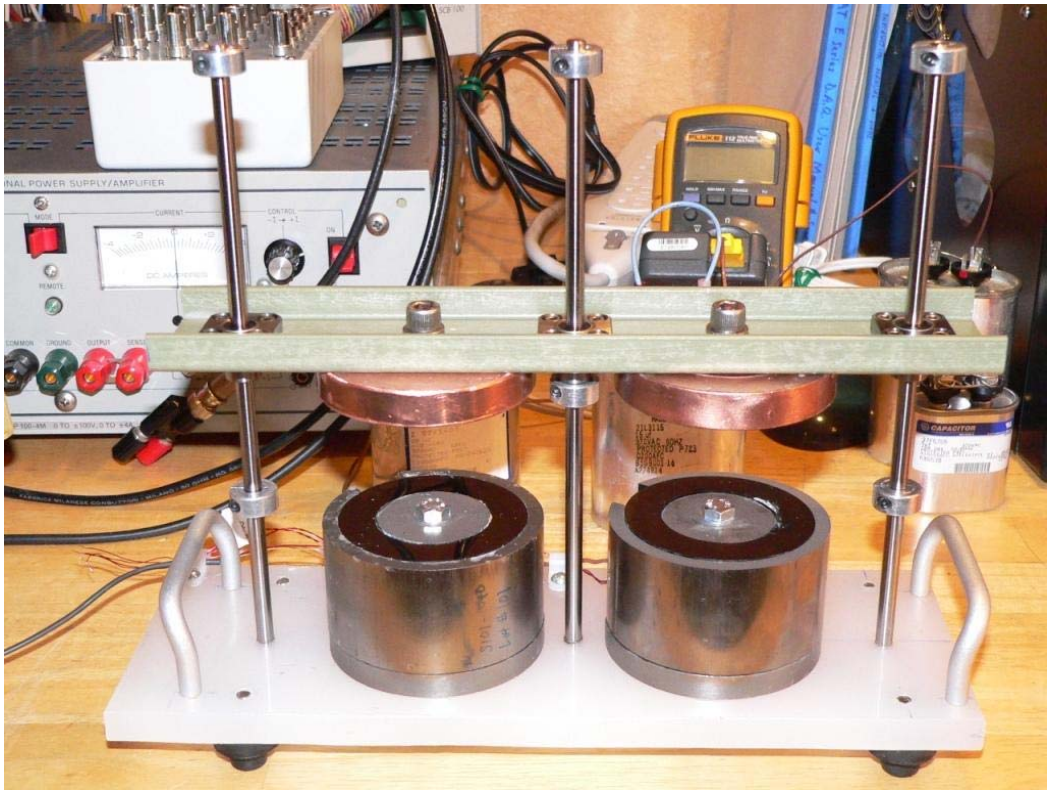

Figure 4.2-4: Phase I Test Apparatus – Roller Bearing Concept

Figure 4.2-4 shows a picture of a modified version incarnate of the initial test apparatus presented in Figure 4.2-1. Although extreme care was given to linear bearing rod alignment and the linear bearing friction was minimized through the addition of a light machine oil on the linear rods, the bearing friction still proved too great to allow multiple oscillations. A next level concept to provide true levitation with outer diameter constraint is provided in Appendix D.2.

The final test apparatus used is provided in Figure 4.2-5 and Figure 4.2-8. Simplicity achieved the final desired goal. Wooden sticks pressed into thick foam and constrained by pipe clamps around the solenoid core provide a reasonable measure of 1 D.O.F. confinement while allowing true secondary levitation.

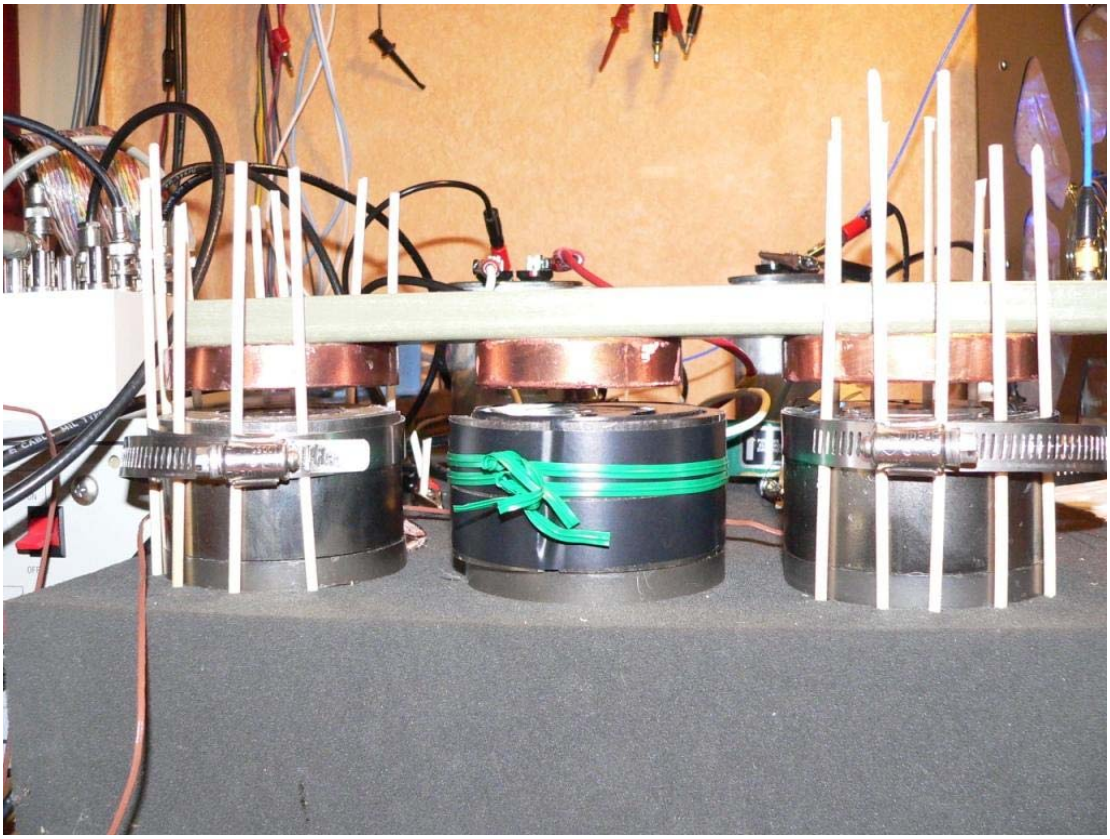

Figure 4.2-5: Phase I Test Apparatus – Final Design Close Up

A component layout of Phase I is provided in Figure 4.2-6 and an electrical schematic of Phase I is provided in Figure 4.2-7. The final overall Phase I test apparatus setup is presented in Figure 4.2-8. Phase I test sensor and control parameters are listed and described in Table 4.2-1. Electrically the Phase I system includes the use of a series capacitor called the resonant capacitor on both the principal and control solenoid systems. Each resonant capacitor is impedance matched with the inductance of the connected solenoid circuit. A parallel impedance matched capacitor assists a current limited source by lowering the source current for an equivalent load current. A series impedance matched capacitor, the configuration used here, assists an impedance limited load by allowing a higher source and load current for the same amount of load impedance.

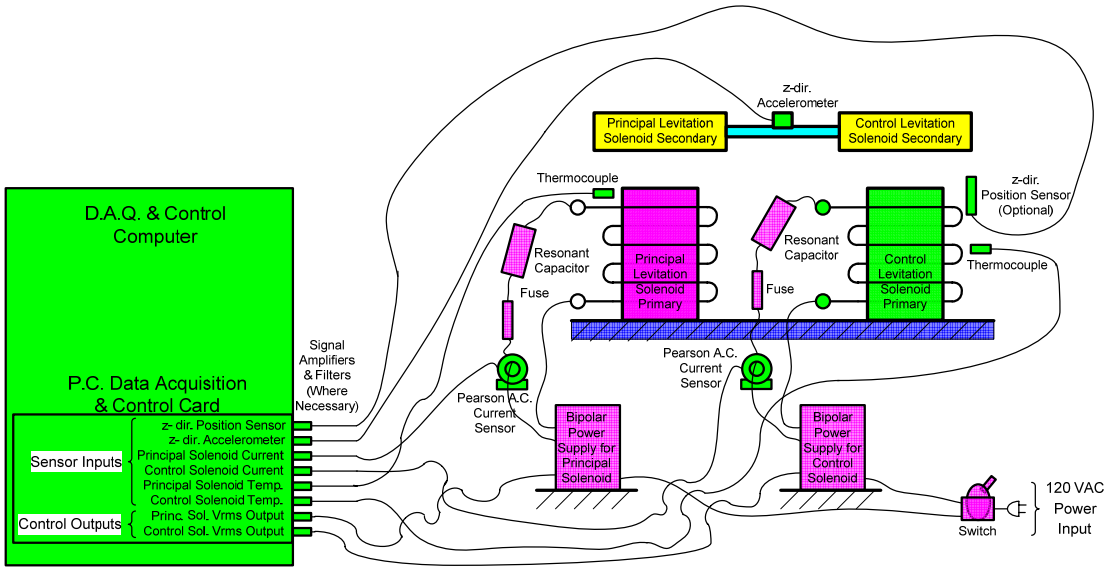

Figure 4.2-6: Phase I Test Layout

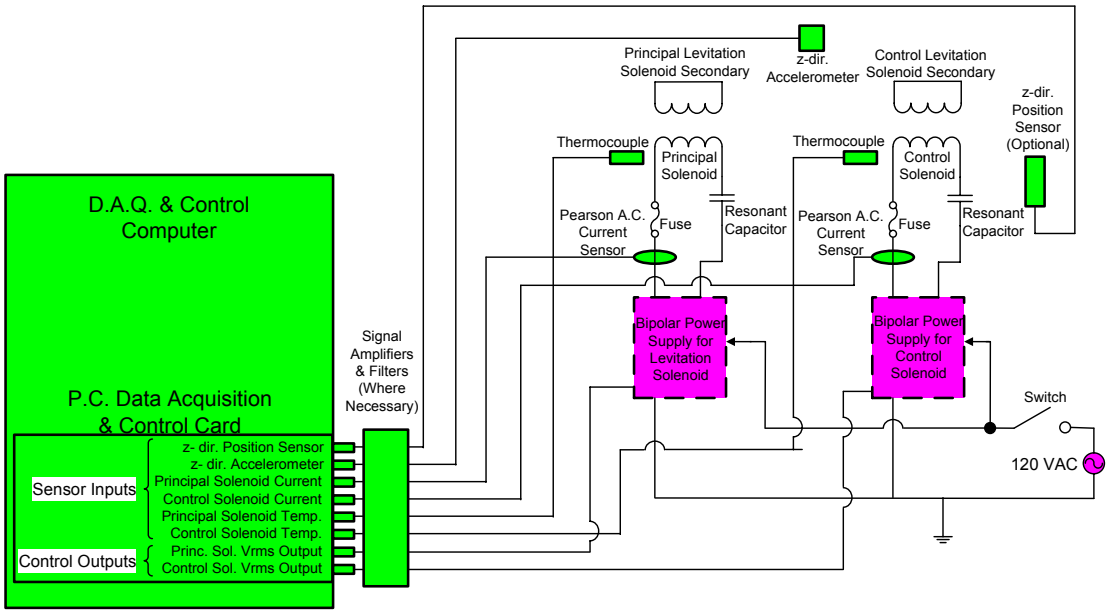

Figure 4.2-7: Phase I Test Electrical Schematic

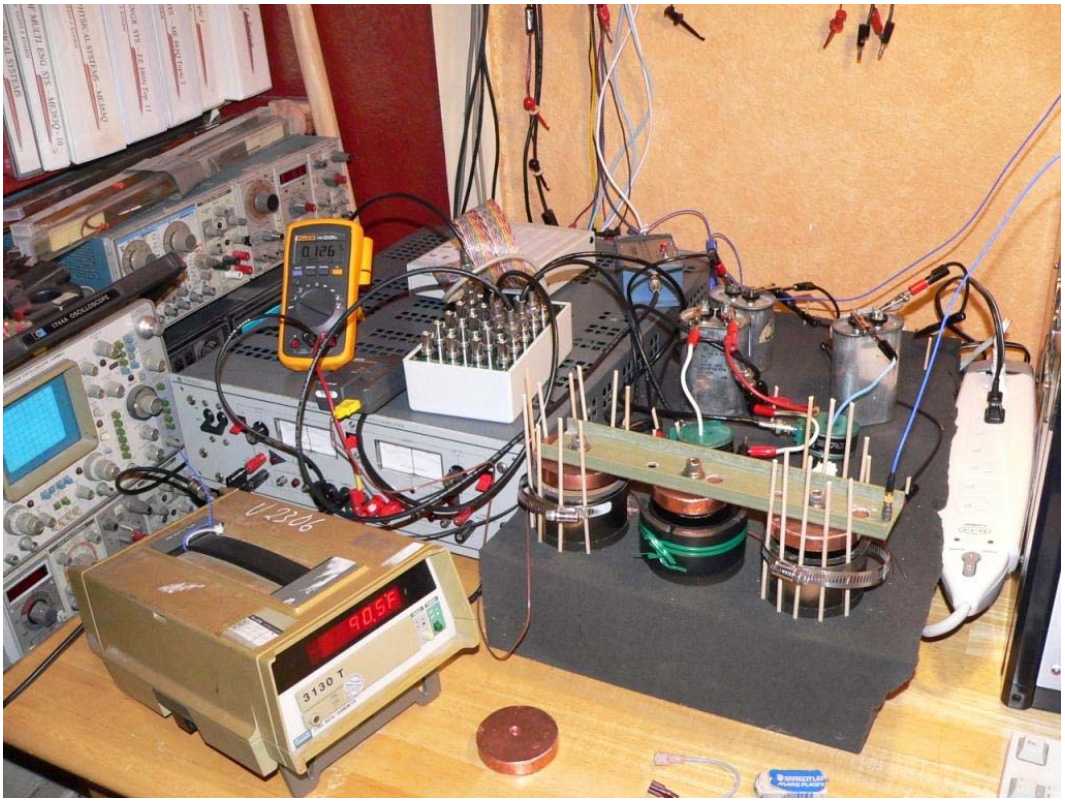

Figure 4.2-8: Phase I Test Apparatus – Final Design Overall

Table 4.2-1: Phase I Test Sensor & Control Parameter List

ANALYSIS AND CONTROL PARAMETERS			
Param. Type	**Item #**	**Param. Name**	**Parameter Description**
SENSOR INPUTS	1	z	(Optional) z coordinate direction distance between solenoid primaries and secondary plate. State variable.
	2	$\ddot{z}$	z coordinate direction acceleration of secondary plate. State variable second derivative.
	3	I_{prin}	Principal solenoid coil current.
	4	I_{cntl}	Control solenoid coil current.
	5	T_{prin}	Principal solenoid coil temperature.
	6	T_{cntl}	Control solenoid coil temperature.

CONTROL OUTPUTS	7	V_{prin}	Principal solenoid coil voltage. Prime mover for secondary levitation and set electrical perturbation force.
	8	V_{cntl}	Control solenoid coil voltage. Controls secondary oscillations from perturbation forces.

Test Software

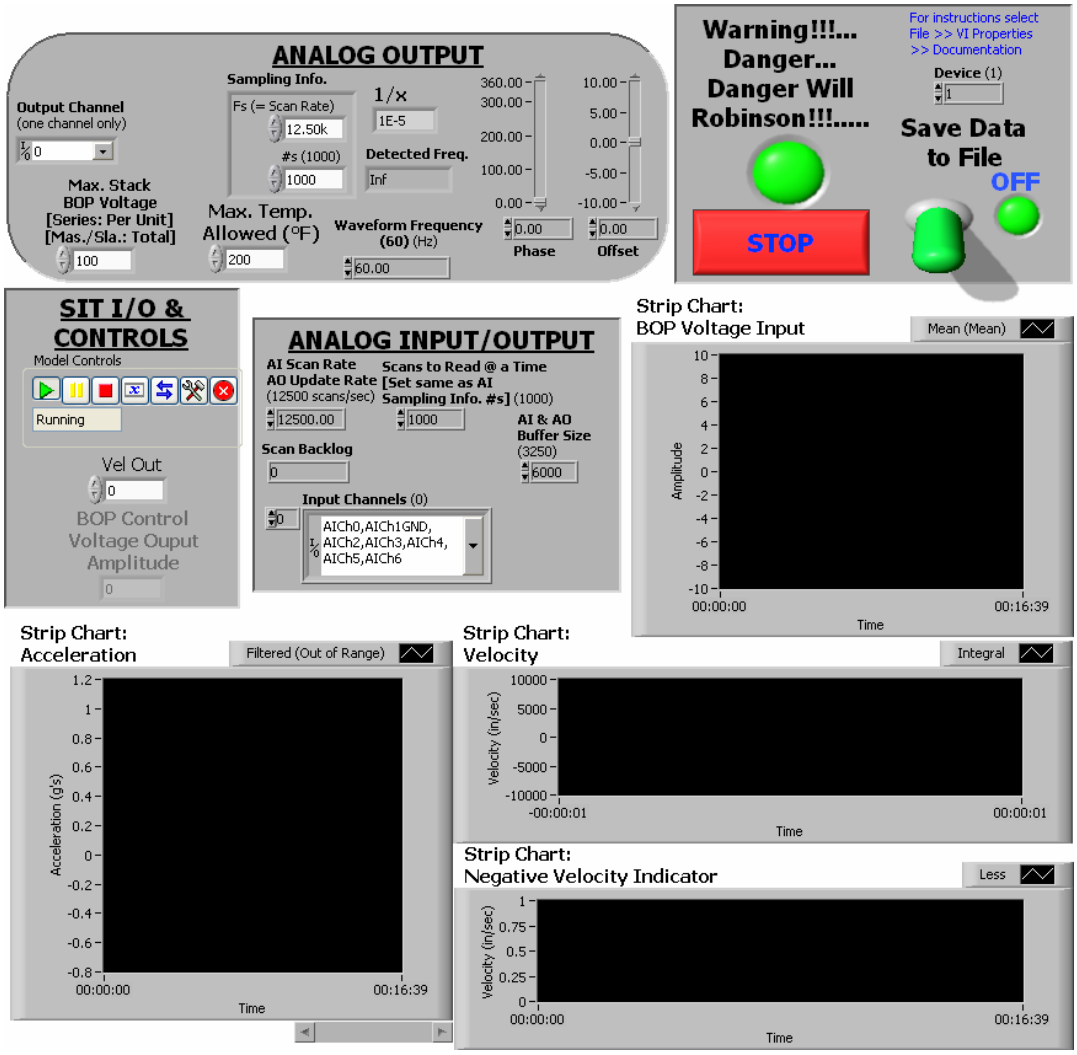

Figure 4.2-9: Phase I Test Front Panel

The Phase I test debugging front panel is presented in Figure 4.2-9. The block diagrams for this front panel are presented in Figure 4.2-10 and Figure 4.2-11. Final

test results are produced from subsets of this front panel and subsequent block diagrams. In these subsets the computer screen charting information which updates in situ with the D.A.Q. are removed from the final system tests since this functionality requires valuable computational time.

A software based 25 Hz low pass filter was originally placed on the accelerometer data to help filter out Gaussian white noise as well as any high frequency secondary motions that are not part of the fundamental perturbation oscillation. This filter was eventually removed to assist in speeding up computer processing time and mollify accelerometer offsets that served to magnify observed velocity and position integration errors.

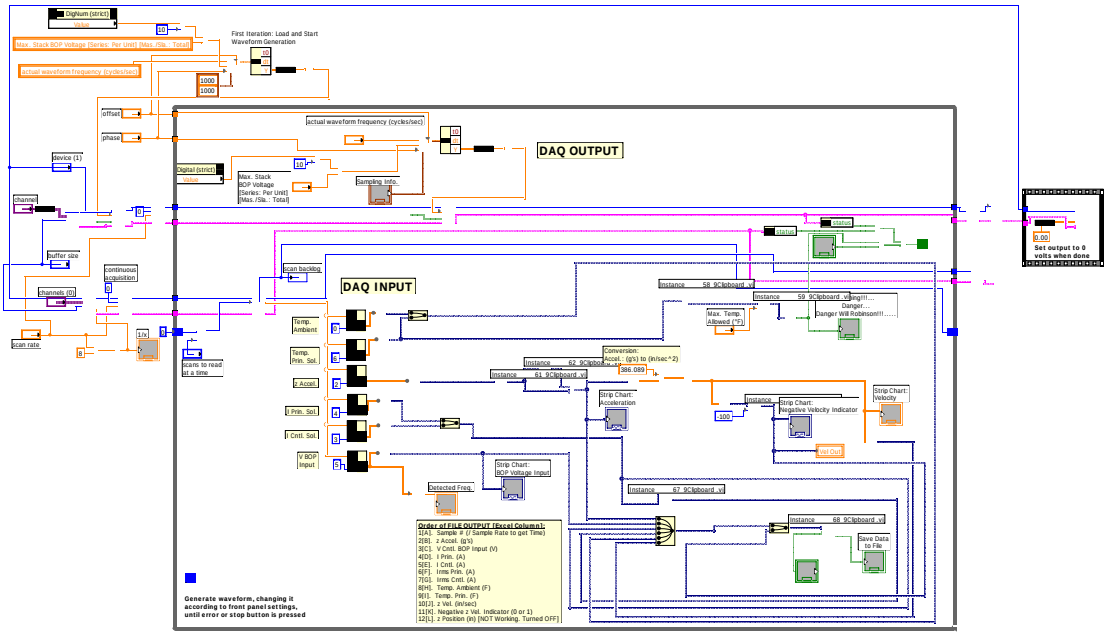

Figure 4.2-10: Phase I Test D.A.Q. I/O Block Diagram

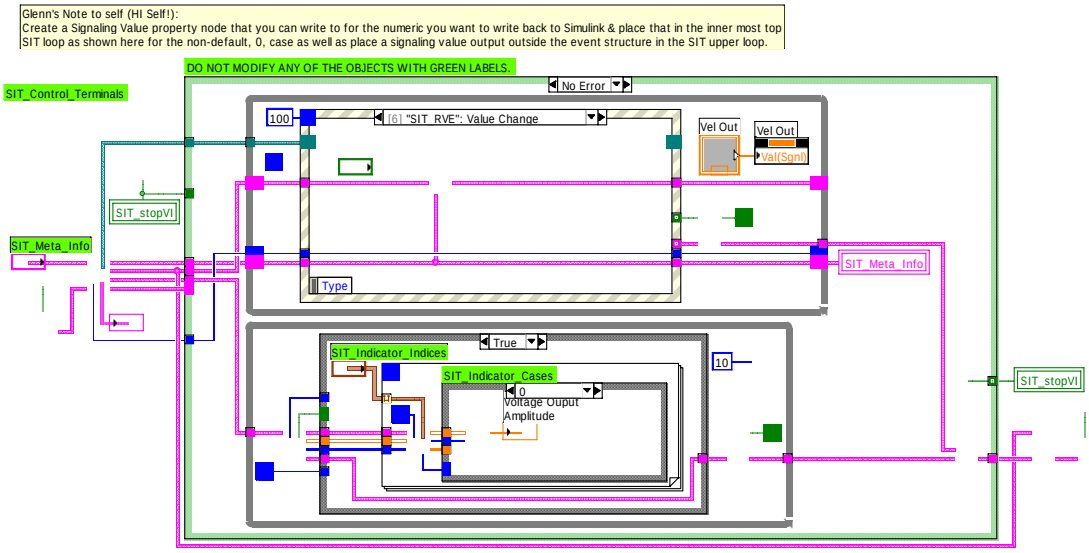

Figure 4.2-11: Phase I Test Simulation Interface Toolkit Block Diagram

4.2.c.ii Phase I, Test #1: Solenoid Parameter Determination

In the first part of this experiment the solenoid electrical parameters are determined for all principal and control solenoids used. This data is acquired for solenoids with and without a secondary present as well as open and closed circuited opposing coils in multiple coil solenoids in order to account for the mutual inductance components.

In the second part of this experiment each solenoid is individually powered at both the individual coil level as well as coils in parallel. This test is performed for a variety of voltage amplitudes and frequencies with and without a secondary present which corresponds to the analytical and computational tests performed. The set test voltage amplitudes are 50 VAC, 100 VAC, 120 VAC, and 150 VAC. The set test frequencies are 0 Hz, 60 Hz, 100 Hz, 250 Hz, 500 Hz, and 1000 Hz.

The final empirical test data is compared with analytical and computational output as listed in the Appendix. The results of this test are discussed in Chapter 5.2.e.ii and the hardware used in this test is presented in Appendix D.1.

4.2.c.iii Phase I, Test #2: Uncontrolled Response Test

In this experiment the principal response parameters are determined with the principal solenoids energized and not magnetically isolated from other solenoids. Therefore the principal solenoids are energized, the control solenoid is not energized, forcing functions are applied to the secondary from the principal solenoids, and data is acquired.

The controlled principal solenoid current provides a set levitation force and disturbing forcing function. The z directed acceleration and potentially the position are directly sensed. This feedback provides an observed z directed velocity and z directed position if the position is not sensed. The results and conclusion of this test are provided in Chapters 5.2.e.iii and 6.2.d.i respectively.

4.2.c.iv Phase I, Test #3: Controlled Response Test

This series of experiments follows the exact same format as the experiments run in Chapter 4.2.c.iii except that the control solenoid is also active and using the secondary motion data to provide damping control. The controller itself determines and varies the control solenoid's output voltage to achieve secondary damping without the extended oscillations witnessed in the Chapter 4.2.c.iii test. The results and conclusion of this test are provided in Chapters 5.2.e.iv and 6.2.d.ii respectively.

4.3 PHASE II: DYNAMIC TRANSLATIONAL AND ROTATIONAL COUPLED 1 D.O.F. ROTATING WHEEL E.D.S. SYSTEM

4.3.a Overall Purpose

Phase II dynamically isolates a single D.O.F. E.D.S. system for analysis and damping control. This simplified system allows a basis for dynamically governed E.D.S. damping theory, modeling accuracy determination for a rudimentary dynamic system model, and a measure of effectiveness for each control scheme. Every dynamic E.D.S. system initiates from this principle.

The tested single translational motion models the vertical D.O.F. motion of a dynamic maglev system due to the solenoid positions relative to the moving secondary.

4.3.b Governing Physical Parameters

4.3.c Phase II Testing

4.3.c.i Test Apparatus

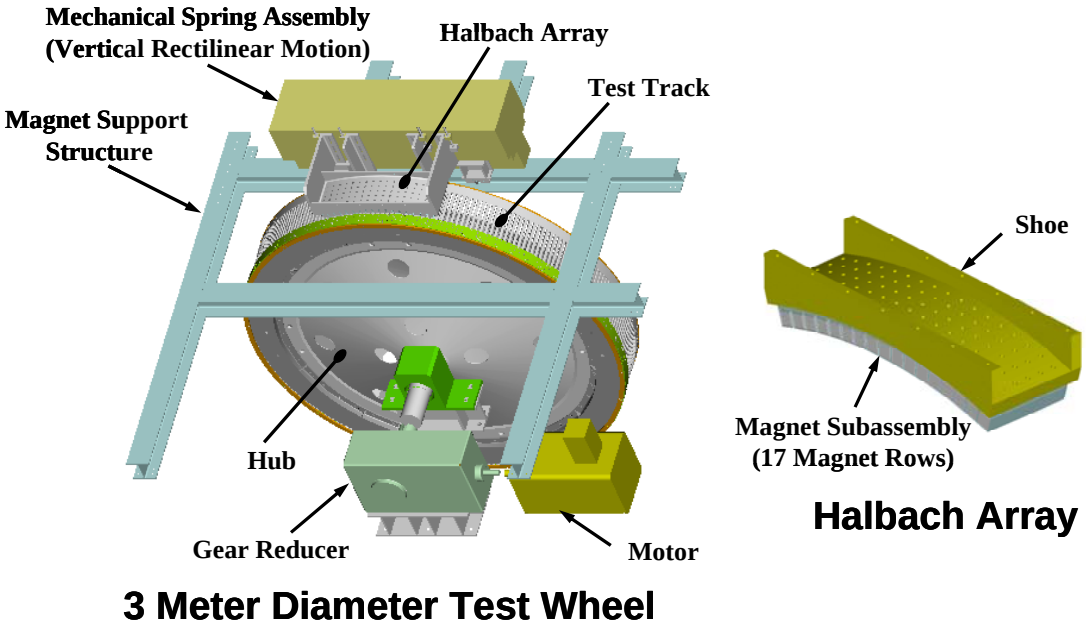

Figure 4.3-1: Phase II Dynamic Test Facility

Figure 4.3-1, provided courtesy of General Atomics low speed maglev technology program, shows an above view of the existing dynamic test facility which houses the Phase II proposed test apparatus. The control system is not depicted in this figure. The vertical levitation system consists of a Halbach array permanent magnetic source primary. This Halbach array assembly is termed the Halbach primary. The dynamic secondary is a large, rotary wheel containing a Litz wire ladder track. This

wheel is acts as the passive secondary for both principal and control primary systems. The Halbach primary is only allowed to vibrate in an axis orthogonal relative to the secondary surface. A set of control solenoids is held fixed in the same plane as the Halbach primary. A position sensor is fixed next to the Halbach primary to monitor the secondary position relative to the Halbach primary. An accelerometer is placed on the Halbach primary to monitor the Halbach primary accelerations in a direction parallel to this primary's axis.

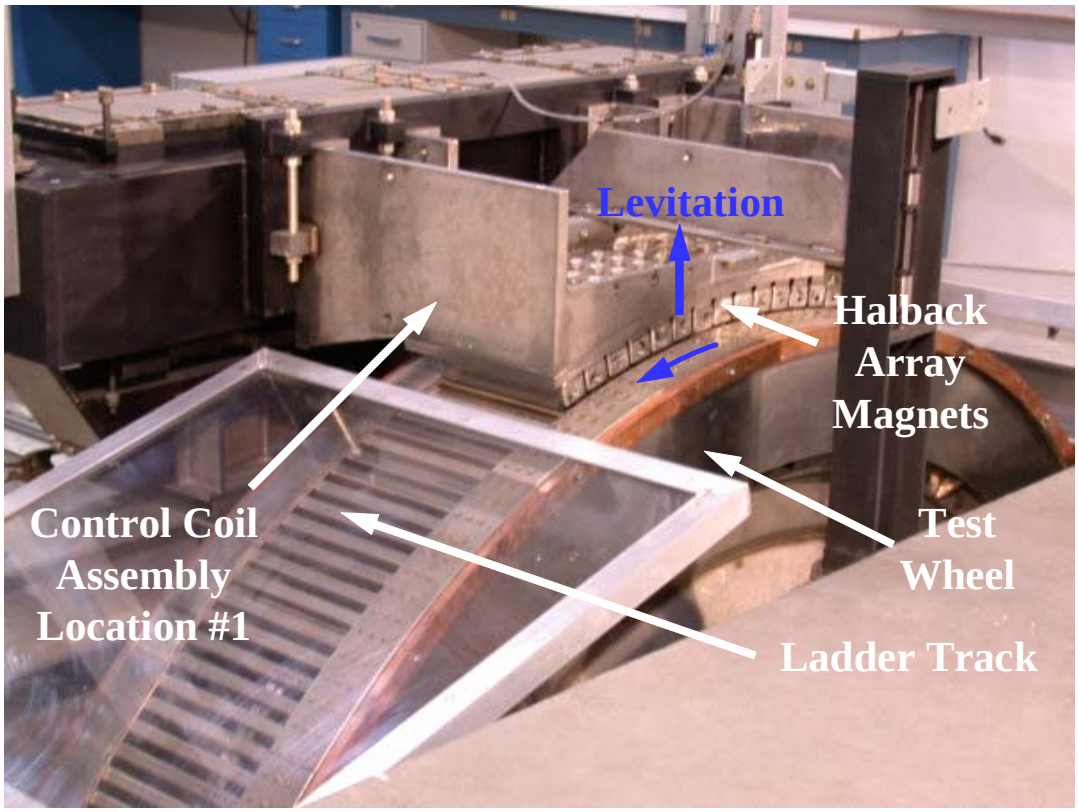

Figure 4.3-2: Phase II Dynamic Test Facility Picture

The dynamic test facility demonstrates levitation in Figure 4.3-2, provided courtesy of General Atomics low speed maglev technology program. In this figure the levitation lift off occurred during a localized propulsive velocity of 2.5 $\left(\frac{\text{m}}{\text{sec}}\right)$ to

achieve an air gap of greater than 25 mm with 900 kg levitated weight. The control system is not depicted in this figure, but the location of one of the control coil assemblies is indicated in the figure. The second control coil assembly location attaches to a similar plate on the other side of the Halbach array. The secondary wheel's radius is extremely large to provide an approximation of a linear maglev system response. The control solenoids' radii are much smaller than the secondary's radius. This allows all of the solenoids to exist in essentially the same rim velocity location on the secondary and therefore approximate linear conditions. Both the secondary wheel and the implemented control coils are sized to allow a close approximation to a true, linear maglev system. Phase II test sensor and control parameters are listed and described in Table 4.3-1.

Table 4.3-1: Phase II Test Sensor & Control Parameter List

ANALYSIS & CONTROL PARAMETERS			
Param. Type	**Item #**	**Param. Name**	**Parameter Description**
SENSOR INPUTS	1	z	z coordinate vertical direction distance between Halbach array assembly primary and rotating wheel secondary. State variable.
	2	$\ddot{z}$	z coordinate direction acceleration of Halbach array assembly. State variable second derivative.
	3	ω	Wheel radial velocity.
	4	I_{cntl}	Control solenoid coil current per coil.
	5	T_{cntl}	z coordinate direction control coil temperature.
CONTROL OUTPUTS	6	ω	Wheel radial velocity. Principal levitation system prime mover. Mechanical perturbation force when propulsive velocity feeds energy into vertical levitation oscillations.
	7	V_{cntl}	Control coil voltage per coil assembly. Controls secondary oscillations from perturbation forces.

4.3.c.ii Phase II, Test #1: Control Solenoid Parameter Determination

In the first part of this experiment the solenoid electrical parameters are determined for all control solenoids used. This data is acquired for solenoids with and

without a secondary present as well as open and closed circuited opposing coils in multiple coil solenoids in order to account for the mutual inductance components.

In the second part of this experiment each solenoid is individually powered at both the individual coil level as well as coils in parallel. This test is performed for a variety of voltage amplitudes and frequencies with and without a secondary present and the output data is compared to equivalent analytical and computational analyses.

4.3.c.iii Phase II, Test #2: Uncontrolled Response Test

In this experiment the principal response parameters are determined with the principal system energized. Therefore the secondary spins to acquire vertical oscillation data versus propulsive velocity via the position and acceleration sensors, the control solenoids are not energized but are closed circuited, and data is acquired.

4.3.c.iv Phase II, Test #3: Controlled Response Test

This series of experiments follows the exact same format as the experiments run in Chapter 4.3.c.iii except that the control solenoids are also active and using the secondary motion data to provide damping control. The controller determines and varies the control solenoid's output voltage to achieve secondary damping without the extended oscillations witnessed in the uncontrolled response test.

4.4 PHASE III: DYNAMIC TRANSLATIONAL AND ROTATIONAL 3 D.O.F. COUPLED SOLENOIDAL E.D.S. SYSTEM

4.4.a Overall Purpose

Phase III dynamically couples three D.O.F. of an E.D.S. system for analysis and damping control as demonstrated in Table 4.4-1. Two D.O.F. are translational and one D.O.F. is rotational as shown in Figure 3.5-1. Energy is also inputted into the system from the propulsion D.O.F., but this D.O.F. is not controlled and hence excluded from this table. This complex system allows insight into determining the governing E.D.S. damping theory for a three D.O.F. system, modeling accuracy

determination for the coupled system model, and a measure of effectiveness for each control scheme. As described in Chapter 2.3, the three D.O.F. system chosen is a quarter component model of the six D.O.F. maglev E.D.S. system in Phase IV. This three D.O.F. E.D.S. system allows one last logical step before investigating six D.O.F. E.D.S. system in Phase IV.

Table 4.4-1: Phases III D.O.F. with D.O.F. Coupling

Controlled Coupled and Uncoupled, Translational and Rotational D.O.F. [(X) = an active D.O.F.; (Grey Box) = non-applicable or repetitive case]							
Type of D.O.F.		**Translational**			**Rotational**		
	D.O.F. Description	Propulsion	Vertical	Lateral	Roll	Yaw	Pitch
Translational	Propulsion						
	Vertical		**X**		**X**		
	Lateral			**X**	**X**		
Rotational	Roll				**X**		
	Yaw						
	Pitch						

The vertical motion from Phase II is modeled again in Phase III. The additional translational motion models the lateral D.O.F. motion of a dynamic maglev system due to the secondary rim solenoid positions relative to the moving secondary. The additional rotational motion models the roll D.O.F. motion of a dynamic maglev system due to the mechanical coupling between the solenoid pairs. This mechanical coupling between the solenoid pairs also provides the mode coupling between the three modeled D.O.F.

4.4.b Governing Physical Parameters

4.4.c Phase III Testing

4.4.c.i Test Apparatus

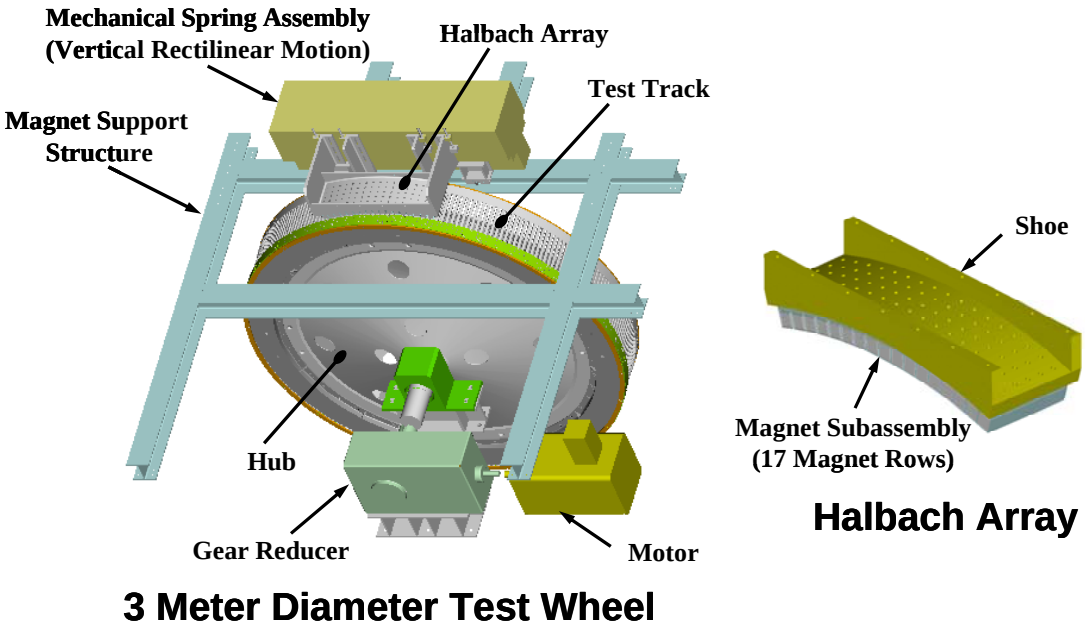

Figure 4.4-1: Phase III Test Apparatus

The proposed test apparatus shown in Figure 4.4-1, provided courtesy of General Atomics low speed maglev technology program, consists of the same initial test apparatus used in Phase II testing as described in Chapter 4.3.c.i. The control system is not depicted in this figure. The only control difference is two added lateral control solenoid sets on the outside rim of the secondary. These rim solenoid pairs are mechanically coupled to the solenoid pair from Phase II. Additional accelerometers and a position sensor are fixed next to the added lateral control solenoid sets in the same solenoid respective orientation as the sensor components in Phase II. Phase III test sensor and control parameters are listed and described in Table 4.4-2.

Table 4.4-2: Phase III Test Sensor & Control Parameter List

ANALYSIS & CONTROL PARAMETERS			
Param. Type	**Item #**	**Param. Name**	**Parameter Description**
SENSOR INPUTS	1	z	z coordinate vertical direction distance between Halbach array assembly primary and rotating wheel secondary. State variable.
	2	y	y coordinate lateral direction distance between Halbach array assembly primary and rotating wheel secondary. State variable.
	3	$\ddot{z}$	z coordinate direction acceleration of Halbach array assembly. State variable second derivative.
	4	$\ddot{y}$	y coordinate direction acceleration of Halbach array assembly. State variable second derivative.
	5	ω	Wheel radial velocity.
	6	I_{z_cntl}	z coordinate direction control coil current per coil.
	7	I_{y_cntl}	y coordinate direction control coil current per coil.
	8	T_{z_cntl}	z coordinate direction control coil temperature.
	9	T_{y_cntl}	y coordinate direction control coil temperature.
CONTROL OUTPUTS	10	ω	Wheel radial velocity. Principal system prime mover. Mechanical perturbation force when propulsive velocity feeds energy into vertical levitation oscillations.
	11	V_{z_cntl}	z coordinate direction control coil voltage per coil assembly. Controls secondary oscillations from perturbation forces.

	12	V_{y_cntl}	z coordinate direction control coil voltage per coil assembly. Controls secondary oscillations from perturbation forces.

4.4.c.ii Phase III, Test #1: Control Solenoid Parameter Determination

In the first part of this experiment the solenoid electrical parameters are determined for all control solenoids used. This data is acquired for solenoids with and without a secondary present as well as open and closed circuited opposing coils in multiple coil solenoids in order to account for the mutual inductance components.

In the second part of this experiment each solenoid is individually powered at both the individual coil level as well as coils in parallel. This test is performed for a variety of voltage amplitudes and frequencies with and without a secondary present and the output data is compared to equivalent analytical and computational analyses.

4.4.c.iii Phase III, Test #2: Uncontrolled Response Test

In this experiment the principal response parameters are determined with the principal system energized. Therefore the secondary spins to acquire vertical and lateral oscillation data via the position and acceleration sensors, the control solenoids are not energized but are closed circuited, and data is acquired.

4.4.c.iv Phase III, Test #3: Controlled Response Test

This series of experiments follows the exact same format as the experiments run in Chapter 4.4.c.iii except that the control solenoids are also active and using the secondary motion data to provide damping control. The controller determines and varies the control solenoid's output voltage to achieve secondary damping without the extended oscillations witnessed in the uncontrolled response test.

The levitation force, lateral force, and propulsive to vertical energy coupling depends on the wheel's rotational velocity. The vertical heave and lateral guidance directed acceleration and position are directly sensed. This feedback provides an

observed z, y, and θ directed velocity. The controller determines and varies the control solenoids output currents necessary for secondary damping.

4.5 PHASE IV: DYNAMIC TRANSLATIONAL AND ROTATIONAL COUPLED 6 D.O.F. FULL VEHICLE E.D.S. MAGLEV SYSTEM

4.5.a Overall Purpose

Phase IV analyzes all six D.O.F. of the E.D.S. system shown in Figure 2.3-1 for analysis and damping control as demonstrated in Table 4.5-1. This extremely complex system allows insight into determining the governing E.D.S. damping theory for a six D.O.F. system, modeling accuracy determination for the coupled system model, and a measure of effectiveness for each control scheme. Quantifying and controlling a six D.O.F., E.D.S. maglev system is the goal of this dissertation.

Table 4.5-1: Phases IV D.O.F. with D.O.F. Coupling

Controlled Coupled and Uncoupled, Translational and Rotational D.O.F. [(X) = an active D.O.F.; (Grey Box) = non-applicable or repetitive case]							
Type of D.O.F.		**Translational**			**Rotational**		
	D.O.F. Description	Propulsion	Vertical	Lateral	Roll	Yaw	Pitch
Translational	Propulsion	**X**					**X**
	Vertical		**X**		**X**		**X**
	Lateral			**X**	**X**	**X**	
Rotational	Roll				**X**		
	Yaw					**X**	
	Pitch						**X**

4.5.b Governing Physical Parameters

4.5.c Phase IV Testing

4.5.c.i Test Apparatus

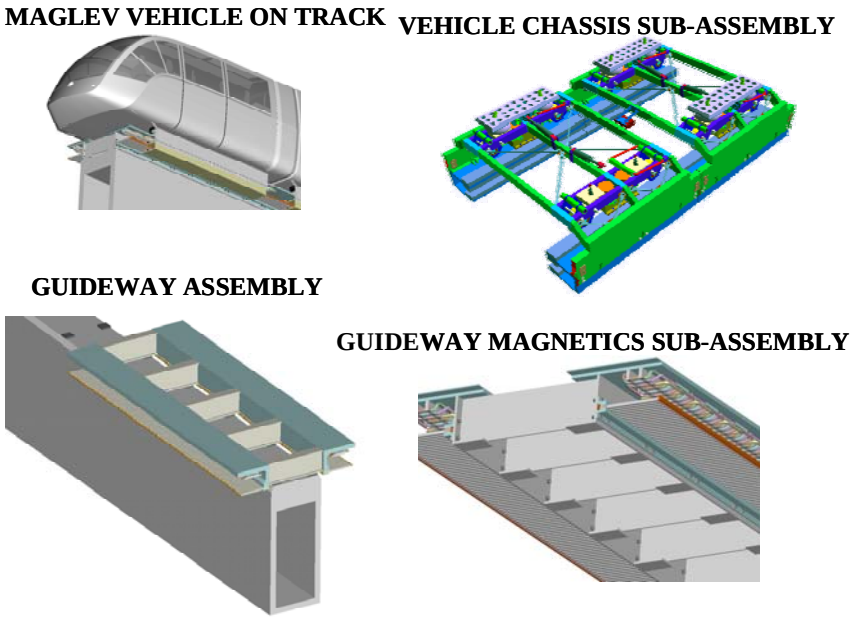

Figure 4.5-1: Phase IV Test Apparatus

The complete Phase IV proposed test apparatus consists of retrofitting multiple test apparatus systems, a minimum of four, from Phase III as described in Chapter 4.4.c.i to a linear maglev chassis system. Figure 4.5-1 shows multiple views of the Phase IV test apparatus. Figure 4.5-2 shows a detailed view of the Phase IV magnetics module. Figure 4.5-1 and Figure 4.5-2 are provided courtesy of General Atomics low speed maglev technology program. Only the maglev vehicle chassis and not the complete maglev vehicle body is included in this test. The control system is not depicted in this figure. This proposed system involves a full scale, L.S.M. propelled, commercial application maglev chassis. Phase IV test sensor and control parameters are listed and described in Table 4.5-2.

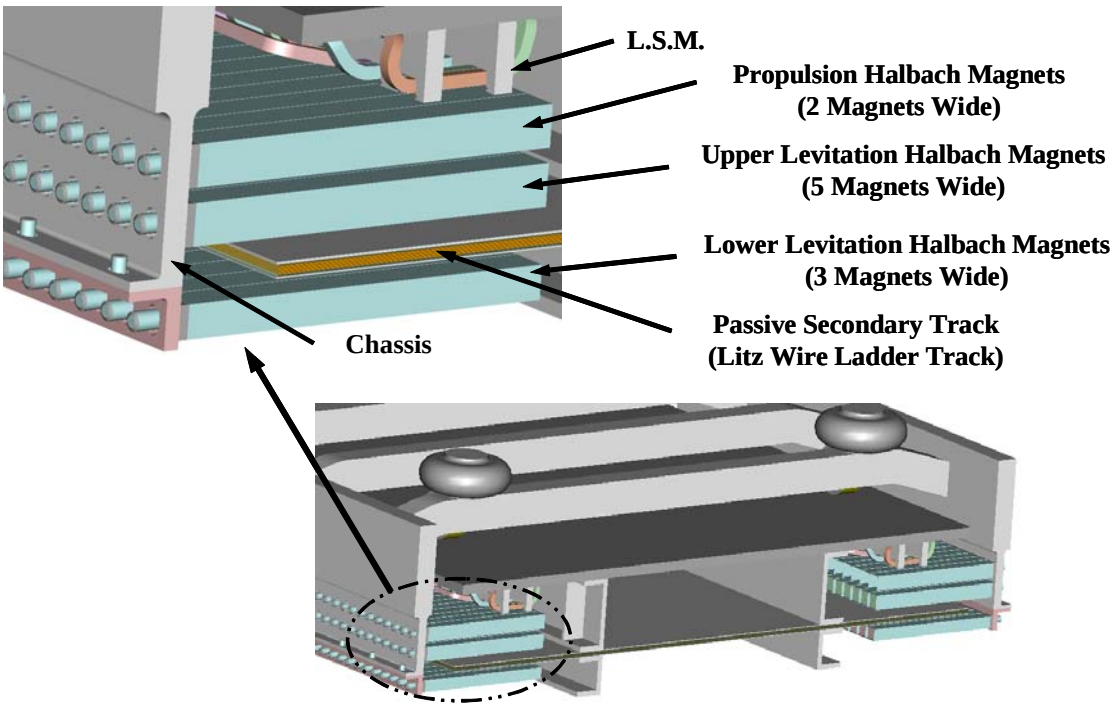

Figure 4.5-2: Phase IV Test Apparatus Magnetics Module

Table 4.5-2: Phase IV Test Sensor & Control Parameter List

ANALYSIS & CONTROL PARAMETERS			
Param. Type	**Item #**	**Param. Name**	**Parameter Description**
SENSOR INPUTS	1	z	z coordinate vertical direction distance between vehicle Halbach primary and ladder track secondary. State variable.
	2	y	y coordinate lateral direction distance between vehicle Halbach primary and ladder track secondary. State variable.
	3	$\ddot{z}$	z coordinate direction acceleration of vehicle. State variable second derivative.
	4	$\ddot{y}$	y coordinate direction acceleration of vehicle. State variable second derivative.
	5	$\dot{x}$	Vehicle propulsive velocity. Vehicle sensor input.
	6	$\ddot{x}$	Vehicle propulsive acceleration. Vehicle sensor input.
	7	I_{z_cntl}	z coordinate direction control coil current per coil.
	8	I_{y_cntl}	y coordinate direction control coil current per coil.
	9	T_{z_cntl}	z coordinate direction control coil temperature.
	10	T_{y_cntl}	y coordinate direction control coil temperature.
CONTROL OUTPUTS	11	$\dot{x}$	Vehicle propulsive velocity. Principal system prime mover. Mechanical perturbation force when propulsive velocity feeds energy into vertical levitation oscillations.
	12	V_{z_cntl}	z coordinate direction control coil voltage per coil assembly. Controls secondary oscillations from perturbation forces.
	13	V_{y_cntl}	z coordinate direction control coil voltage per coil assembly. Controls secondary oscillations from perturbation forces.

4.5.c.ii Phase IV, Test #1: Control Solenoid Parameter Determination

In the first part of this experiment the solenoid electrical parameters are determined for all control solenoids used. This data is acquired for solenoids with and without a secondary present as well as open and closed circuited opposing coils in multiple coil solenoids in order to account for the mutual inductance components.

In the second part of this experiment each solenoid is individually powered at both the individual coil level as well as coils in parallel. This test is performed for a variety of voltage amplitudes and frequencies with and without a secondary present and the output data is compared to equivalent analytical and computational analyses.

4.5.c.iii Phase IV, Test #2: Uncontrolled Response Test

In this experiment the principal response parameters are determined with the principal system energized. Therefore the maglev's propulsion system is set in motion, levitation is achieved via the Halbach primary system, the control solenoids are not energized but are closed circuited, and data is acquired.

4.5.c.iv Phase IV, Test #3: Controlled Response Test

This series of experiments follows the exact same format as the experiments run in Chapter 4.5.c.iii except that the control solenoids are also active and using the secondary motion data to provide damping control. The controller determines and varies the control solenoid's output voltage to achieve secondary damping without the extended oscillations witnessed in the uncontrolled response test.

The controlled principal primary solenoid currents provide set levitation and lateral forces and disturbing forcing functions. The levitation and lateral forces also depend on the vehicle's propulsive velocity. The z, y, and x directed accelerations and positions are directly sensed. This feedback provides an observed z, y, and x directed velocity. The controller determines and varies the control solenoids output currents necessary for vehicle damping.

CHAPTER 5 RESULTS

5.1 OVERALL SYSTEM SOLUTION

All modeling and control algorithms derived in Chapter 3 are modeled in the appendices, the salient results are presented in Chapter 5, and final conclusions are presented in Chapter 6. Phase I numerical analysis results are summarized in Table 5.2-1 and Phase IV numerical analysis results are summarized in Table 5.3-1.

As mentioned at the end of Chapter 2.3.a, all phases are analyzed and simulated and hence produce analytical results. Only Phase I is tested, but the groundwork is laid towards future Phases II, III, & IV building and testing for producing empirical results. The numerically simulated and equivalent computationally simulated Phase I and numerically simulated Phase IV system parameters are briefed in Table 5.1-1. The Phase I dimensions correspond to Figure 3.3-1. The Phase IV dimensions correspond to Figure 3.6-1. All systems are developed around readily available single phase voltage, current, and frequency power sources in order to limit the use of specialized power conditioning equipment.

Table 5.1-1: Phase I & IV Numerically Simulated System Parameters

MAIN SOLENOID DESIGN PARAMETERS				
Component	**Item #**	**Parameter Name**	**Phase I**	**Phase IV**
SECONARY	1	Secondary Shape	Disk	Rectangular Parallelepiped
	2	Conducting Material	Electrolytic Tough Pitch Copper	Electrolytic Tough Pitch Copper
	3	x Axis Propulsive Velocity	0	80 m/sec
	4	Mass & Weight	0.207 kg 2.031 N = 0.457 lbf	267.3 kg 2622 N = 589.4 lbf
	5	Dimensions	Radius = 1.166 in Height = 0.331 in	a = 3.2 m = 126 in b = 0.8 m = 31.5 in c = 0.0084 m = 0.331 in

	6	Simulation Control Hold Distance	z Axis: 0.6 in	z Axis: 1 in y Axis: 1 in
PRIMARY	7	Magnetic Spring Constant Ratios	k_{Cntl}:k_{Prin} ≈ 1:10	k_{Cntl}:k_{Prin} ≈ 1:10 k_{yCntl}:k_{zCntl} ≈ 1:1.6
	8	Core Material	Ferrite	Ferrite
	9	Number of Solenoids per System	1	1
	10	Number of Coils per Solenoid	Principal: 2 Control: 1	Principal: 2 Control: 1
	11	Wire Size	30 AWG	18 AWG
	12	Height	1.615 in	7 in
	13	Solenoid Outside Core Radius	1.6 in	4.5 in
	14	Source RMS Voltage	120 V_{rms}	280 V_{rms}
	15	Source Frequency	60 Hz	60 Hz
	16	Series Resonant Capacitor	Yes	Yes
	17	External Resistor	No	No

In the numerical simulations the principal solenoids are essentially simple complete on or off system with no other external control. This often unrealistic scenario requires an even more robust control solenoid control kernel than an actual maglev system but provides even greater challenges for this control solution. At the start of any simulation, prior to allowing secondary mechanical motion, these simple on and off principal coils are allowed to charge up to full on voltage and magnetic flux in the air gap. This initialization time, which is governed by the electrical time

constants of each system and should not be confused with a control coil turn on delay time, simulates a specified operational condition by removing the initial turn on transients. After this initialization period has passed the secondary is released from the set starting point and allowed to move in any D.O.F. specified by the simulation.

The simulation assumes an isolated electric source assumption. Since in reality the electrical load experiences a changing mutual inductance due to the motion of the secondary with respect to the primary, the current supplying the load changes respectively. In an electrical simulation this change is accounted for by either varying the load electrical parameters or introducing a varying voltage drop on the source voltage. This variation both changes the supply current level and hence the magnetic spring constant values as well as set up an oscillation in the primary electrical circuit itself which could be seen in the secondary mechanical motion. This complexity is deemed unnecessary for this level of analysis and hence is ignored in this paper. A final system design must include this complexity.

There are many ways to analyze the functionality of the control system that is developed in this paper. Specifics for each analysis step taken are presented throughout Chapter 5.2 for Phase I and Chapter 5.3 for Phase IV. In general the analysis steps across Phase I to the final Phase IV are provide an example of a magnetic air gap underdamped system oscillatory motion, compare the introduced linear to nonlinear controlled magnetic damping, then numerically test the chosen nonlinear control damping system through extreme cases such as perturbations at the system natural frequency as well as stochastic perturbations. All periodic perturbation forces and offset values assume relatively high amplitude compared to what is expected during actual operations. Such high amplitudes provide a more rigorous test of the proposed control scheme. Table 5.1-2 outlines the various sets of control system analysis options which eventually developed and are hard coded into the numerical input file as permanent run options.

Table 5.1-2: Phase I & IV Numerical Analysis Hard Coded Run Options

SIMULATION RUN OPTIONS				
Option Category	**Item #**	**Option Name**	**Phase I**	**Phase IV**
			"X" = Option Provided	
SOLENOID DESIGN	1	Similar or dissimilar principal and control solenoid automatic setting	X	X
	2	1, 2, or 3 coils per solenoid	X	X
	3	Wire Gage: 18 to 32 AWG	X	X
	4	External Series Resonant Capacitor	X	X
	5	External Series Resistor	X	X
PRINCIPAL COIL WAVEFORM	6	None	X	X
	7	Constant V_{rms}	X	X
	8	Constant V_{rms} with a Single 0 V_{rms} Down Pulse	X	X
	9	Constant V_{rms} with a Double 0 V_{rms} Down Pulse	X	X
CONTROL	10	None	X	X
	11	I.-P.D.	X	-
	12	Fuzzy Control	X	X
	13	Neuro-Fuzzy Control	X	X
INITIAL SECONDARY OFFSET	14	0 Offset	X	X
	15	Set Offset Distance for Every Free D.O.F.	X	X
PERTURBATION FORCE	16	Perturbation Start Time	X	X
	17	Off	X	X
	18	Set	X	X
	19	Sinusoidal	X	X
	20	Stochastic	X	X

5.2 PHASE I

5.2.a Governing Physical Laws

Solenoid Design

The computational results provided in Appendix B.1 indicate that as long as the concentration of the $\vec{B}$ is focused away from the solenoid central axis then a primary and secondary ring design develops over a plain disk where the secondary ring is sized to capture the maximum primary $\vec{B}$ for this circular system. A larger overall ring diameter while maintaining the same ring radial length produces more overall area for the energy interaction between the primary and secondary, but also more system reactance which lowers the primary current allowable for an otherwise fixed configuration. The solenoid secondary magnetic area design is therefore considered optimum for the largest diameter ring allowable from primary coil heating limitations when the external source resistance is set to zero. The secondary magnetic volume design is governed by considering the skin depth penetration in a repulsive force to weight ratio. The optimum secondary height consistently appears to be a depth just in excess of the skin depth. A final small diameter primary solenoid optimum performance versus material cost analysis is briefed in Appendix B.1.b.

A solenoid primary design balance also occurs with the number of solenoid wire turns for a given input source voltage when all else is considered equal. As the number of turns increases the system has more inductance but less allowable current for control. The opposite is also true when the number of turns decreases the system inductance but provides more allowable current for control. Inserting a series resonant capacitor provided increased current with increased inductance which allowed the possibility of accepting a solenoid which is otherwise a high inductive current choked solenoid. Therefore the new limits were bounded by source current capability, solenoid coil current thermal limits, acceptable limits with the increased transient times, and the capacitor sizing limits.

Another study shows the design balance between the number of coils within the solenoid primary itself as well as whether or not the primary coils are magnetically isolated from one another within the primary. The benefit of parallel multiple primary coils allows for a lower impedance and hence a lower current per coil than in an equivalent single or lesser number of coils system. This can be crucial in a small wire gage, thermally limited system. A single series resonant capacitor can then be sized for multiple impedance matched primary coils in parallel to raise the coil currents that drop below a desired level. The troubles of splitting a solenoid into multiple coils comes from proper balancing of the current densities in each coil in a single solenoid coil configuration, comparison of the current densities between solenoid coil configurations, and transformer action between the coils. Transformer action occurs in non-magnetically isolated coils where the overall reactance of a coil is raised from the mutual coupling with every other closed circuit coil. This transformer action naturally lowers the current in each affected coil in the solenoid. A series resonant capacitor can again be used to mitigate this transformer effect as in the case of the designs in this paper.

These balances allow a quick optimum magnitude of weighted parameters optimization study. A sample of which is shown in Appendix A.1.a for wire sizes of a small diameter primary solenoid. In the wire size comparison table in this appendix it is assumed that the optimum current density is 15 mega ampere turns per square meter.

5.2.b Analytical Component Modeling

The basic analytic analysis which fed the numerical and computational analysis as well as the test apparatus specific analysis is presented in Appendix A.1. The only main difference between Phase I and IV is the magnitude of inputs and outputs. The first order analytical solenoid design approximation produced proper parameter trends but lower than actual magnitudes. An example of the Phase I closed form analytic solution secondary radius dependent magnetic flux density tangential

and normal real component values are provided in Figure 5.2-1 for the numerical simulation equivalent analysis and Figure 5.2-3 for the test apparatus equivalent analysis. An example of the Phase I closed form analytic solution secondary radius dependent control solenoid levitation force, F_z and F_{lev}, and gravitational force, F_g, versus air gap distance, z_g, is provided in Figure 5.2-2 for the numerical simulation equivalent analysis and Figure 5.2-4 for the test apparatus equivalent analysis.

The primary and secondary values for the numerical simulation equivalent computational analysis model are provided in the Phase I section of Table 5.1-1. The primary of the test apparatus computational model is geometrically similar to the numerical simulation equivalent computational model except that the winding consists of 28 AWG wire. The secondary of the test apparatus computational model is geometrically similar to the numerical simulation equivalent computational model except that the radius is 1.5 inches and thickness is 0.5 inches. The numerical simulation equivalent computational model geometric dimensions are chosen from an initial optimum performance versus material cost analysis which is briefed in Appendix B.1.a and Appendix B.1.b. The test apparatus computational model geometric dimensions are chosen from readily available materials that are analyzed and compared in Appendix A.1.a for primary wire sizes and Appendix B.1.b for secondary geometries which expanded upon the initial secondary computational analysis.

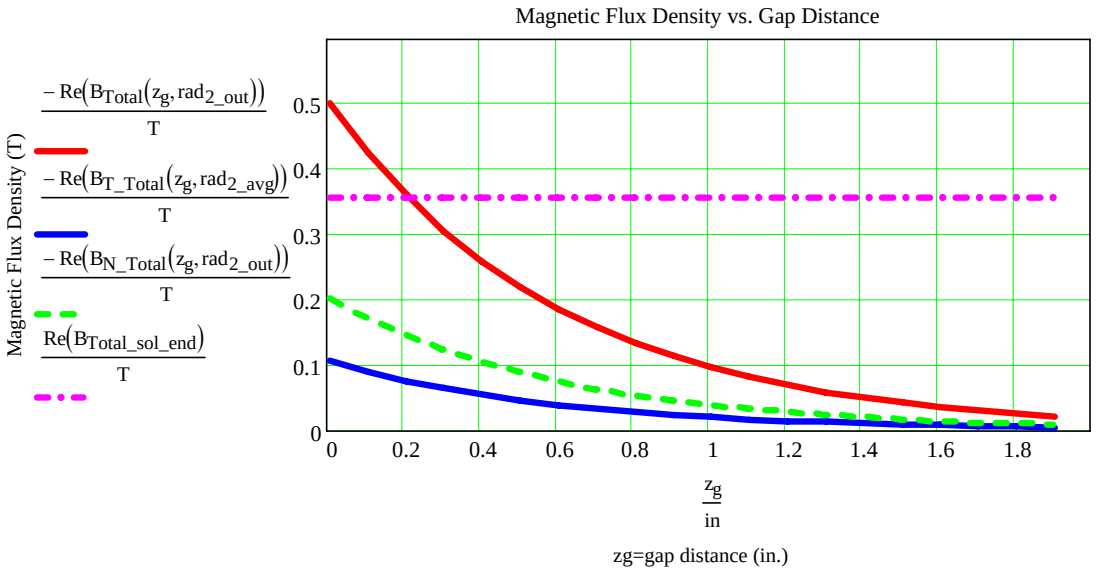

Figure 5.2-1: Num. Equiv. Analytic Model Control Sol. B_T & B_N vs. Gap Dist.

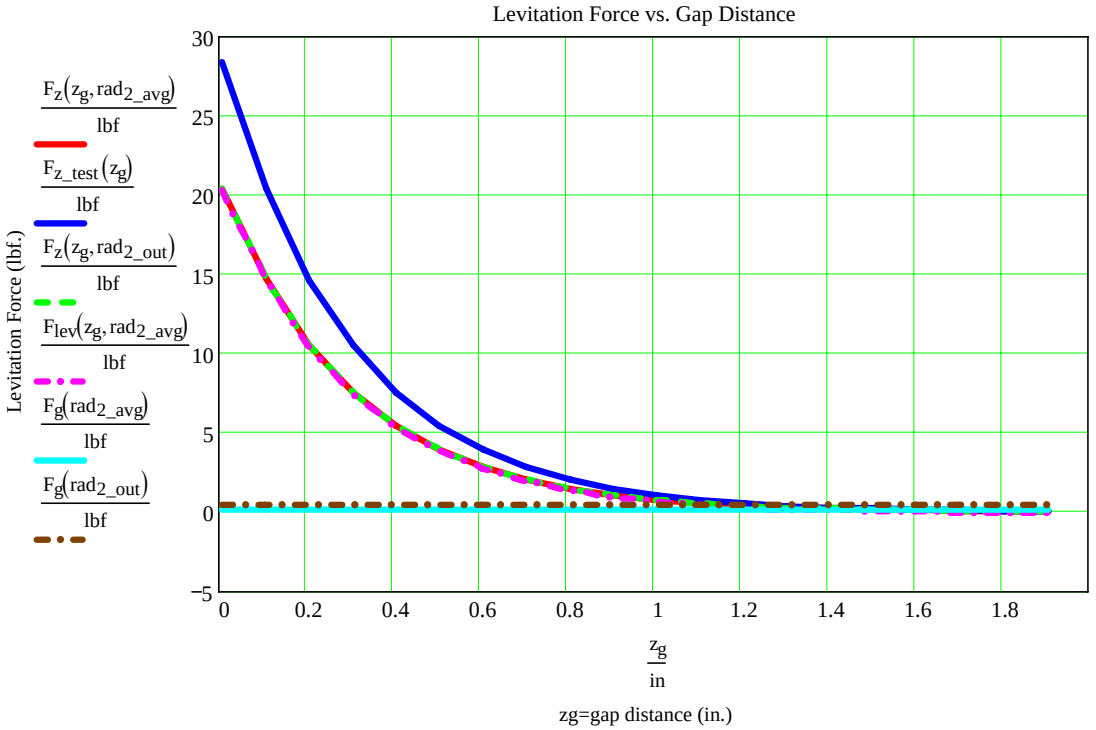

Figure 5.2-2: Num. Equiv. Analytic Model Control Sol. Vert. Force vs. Gap Dist.

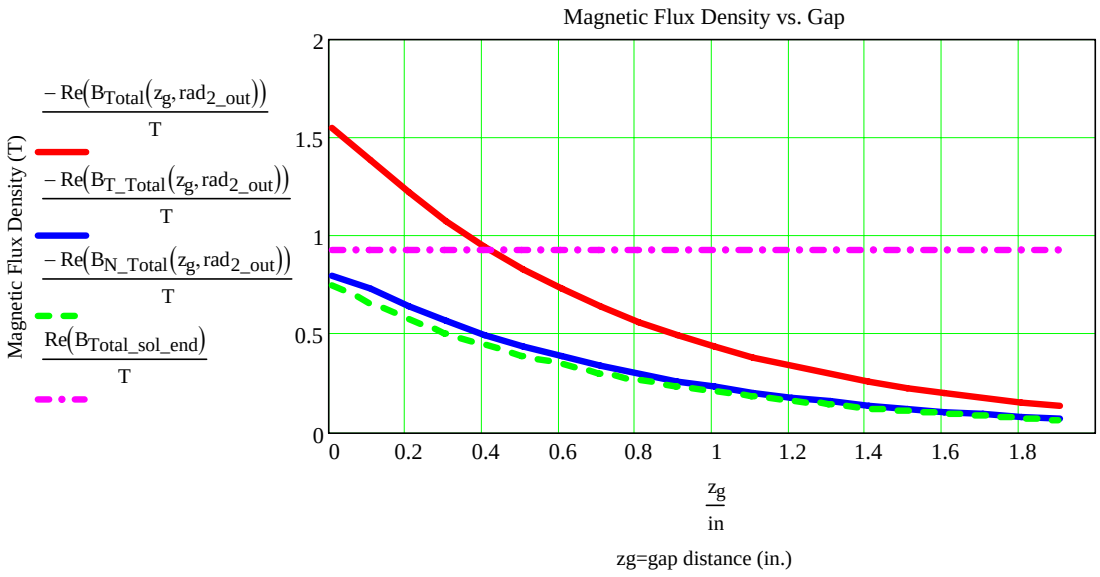

Figure 5.2-3: Test Apparatus Anal. Model Control Sol. B_T & B_N vs. Gap Dist.

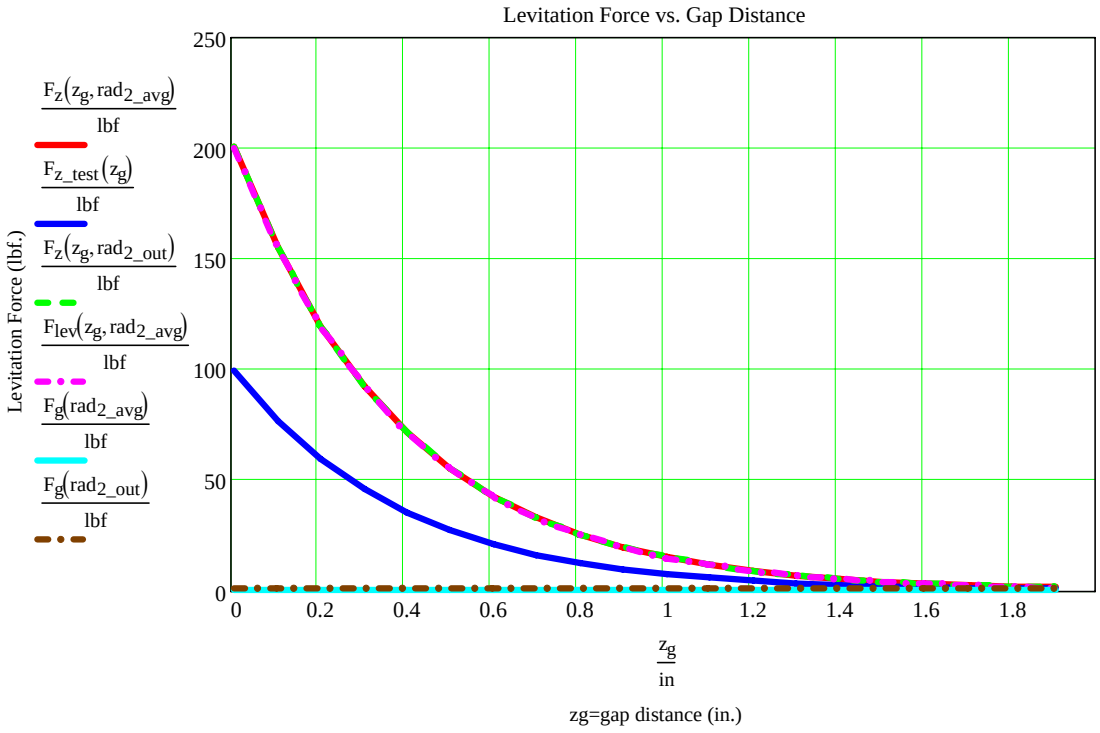

Figure 5.2-4: Test Apparatus Anal. Model Control Sol. Vert. Force vs. Gap Dist.

5.2.c Computational Component Modeling

The final non-linear time average computational results for the numerical simulation Phase I 0.6 inch air gap system modeled analytically in Chapter 5.2.b and numerically in Chapter 5.2.d lists a 1.145 lbf = 5.093 N secondary repulsive force. This final computational repulsive force value corresponds to the numerical analysis damped oscillation principal solenoid repulsive force value for the 0.6 inch air gap levitation hold position provided in Figure 5.2-13. The magnetic potential, magnetic flux density, and secondary current density plots for this system are provided in Figure 5.2-5, Figure 5.2-6, and Figure 5.2-7 respectively.

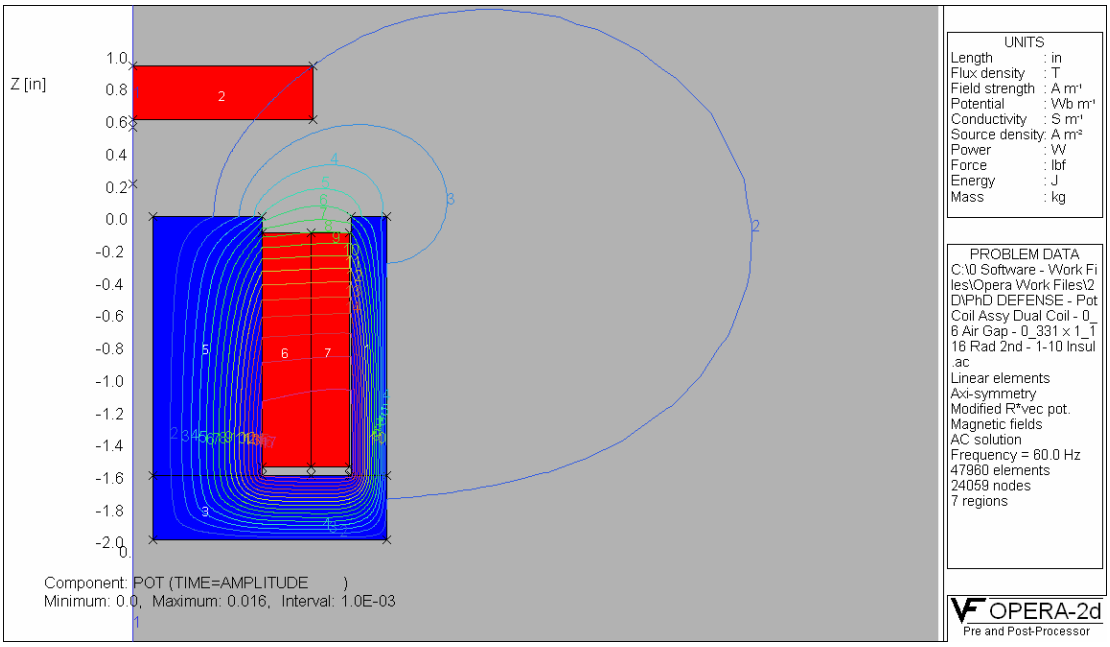

Figure 5.2-5: Numerical Solution Equivalent Computational Potential Solution

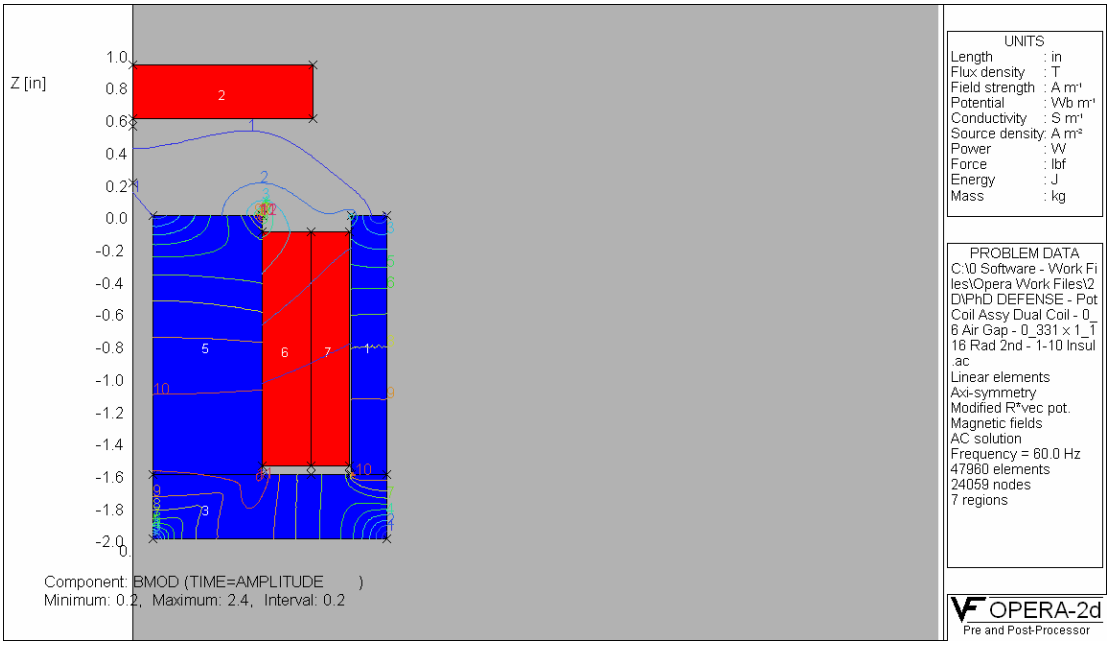

Figure 5.2-6: Numerical Solution Equivalent Computational $\vec{B}$ Solution

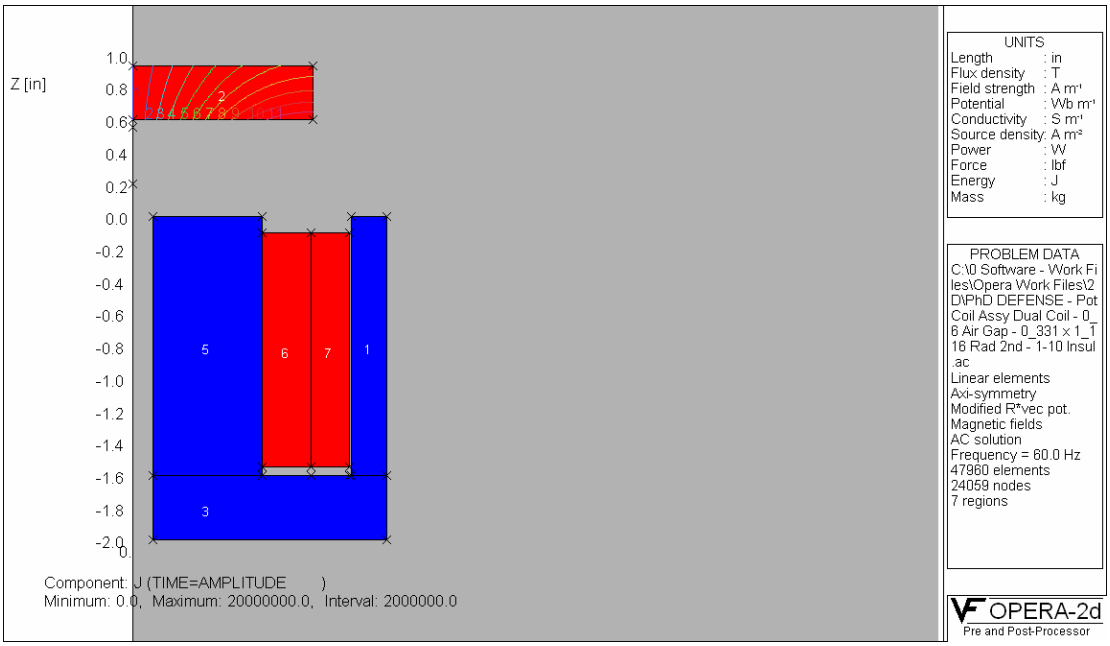

Figure 5.2-7: Numerical Solution Equivalent Comp. Secondary $\vec{J}$ Solution

The final non-linear time average computational results for the test apparatus Phase I 0.6 inch air gap system modeled analytically in Chapter 5.2.b lists a 2.801 lbf = 12.459 N secondary repulsive force. The magnetic potential, magnetic flux density, and secondary current density plots for this system are provided in Figure 5.2-8, Figure 5.2-9, and Figure 5.2-10 respectively.

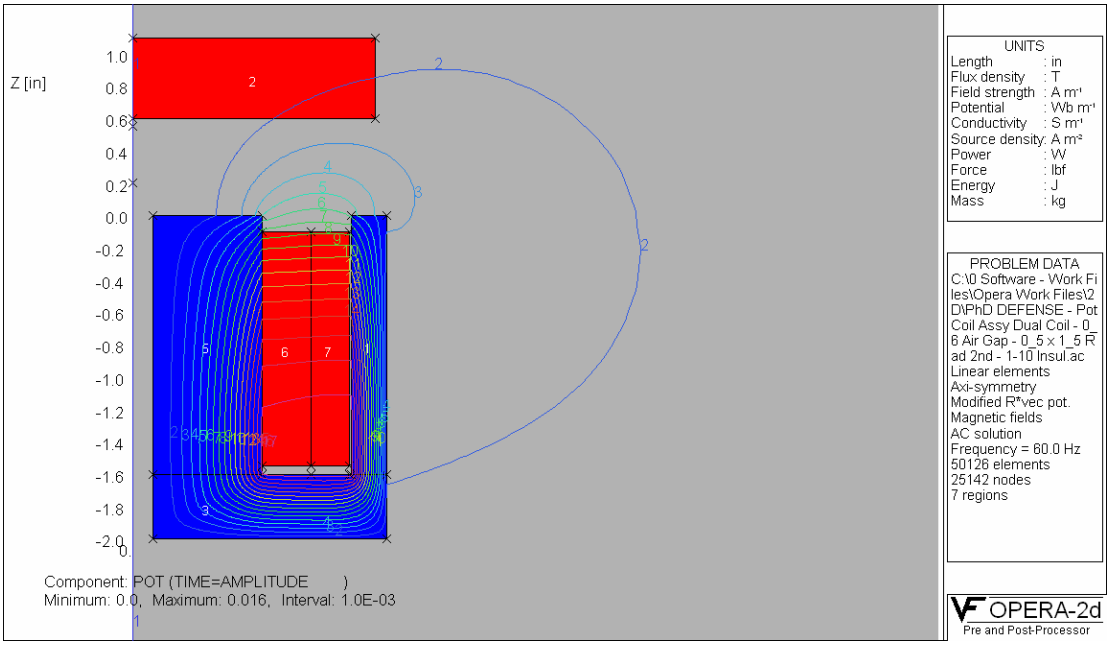

Figure 5.2-8: Test Apparatus Equivalent Computational Potential Solution

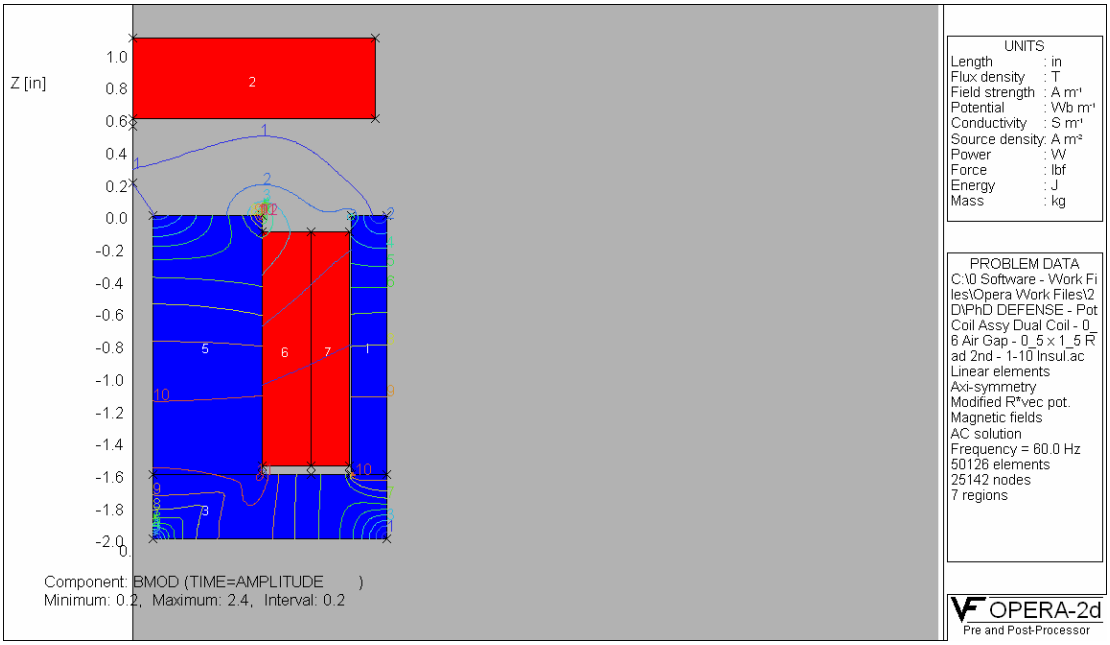

Figure 5.2-9: Test Apparatus Equivalent Computational $\vec{B}$ Solution

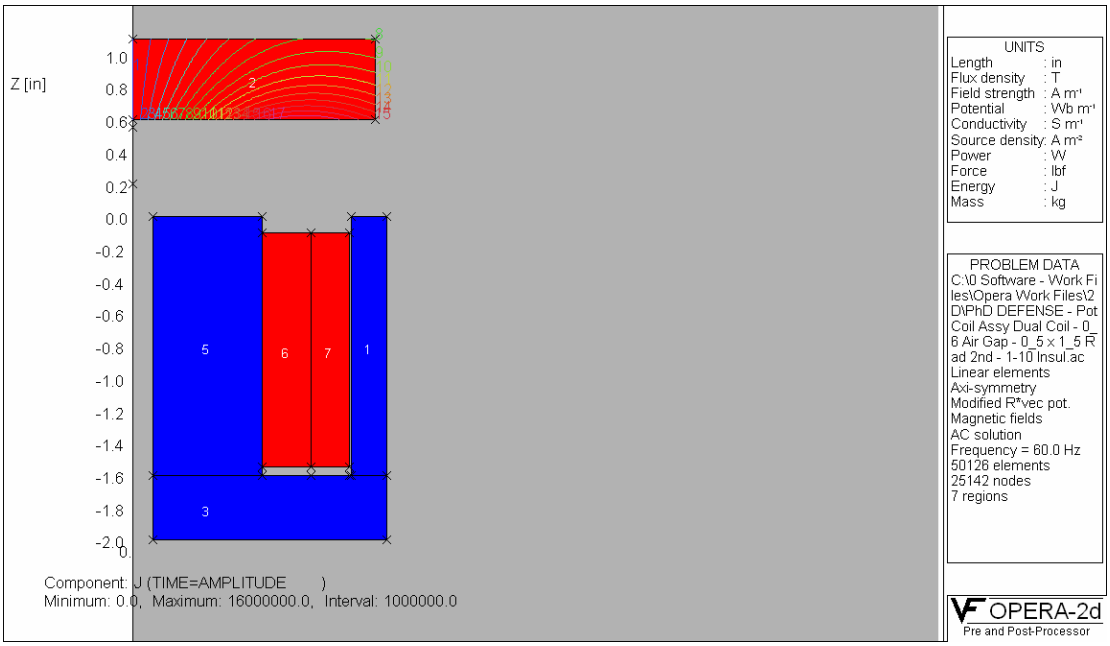

Figure 5.2-10: Test Apparatus Equivalent Comp. Secondary $\vec{J}$ Solution

5.2.d Numerical System Modeling

5.2.d.i Overall

The Simulink® model shown in Figure 5.2-11 provides the top level model of the Phase I numerical simulation. The multitudes of lower level Simulink® models are provided in Appendix C.1.a. This model implements the Phase I simulation dynamics and control equations outlined in Chapter 3.3.a. The supplemental Matlab® solenoid design, Phase I input, and Phase I output function files that are called by this Simulink® model are listed in Appendix C.2.a, C.2.b.i, and C.2.b.ii respectively.

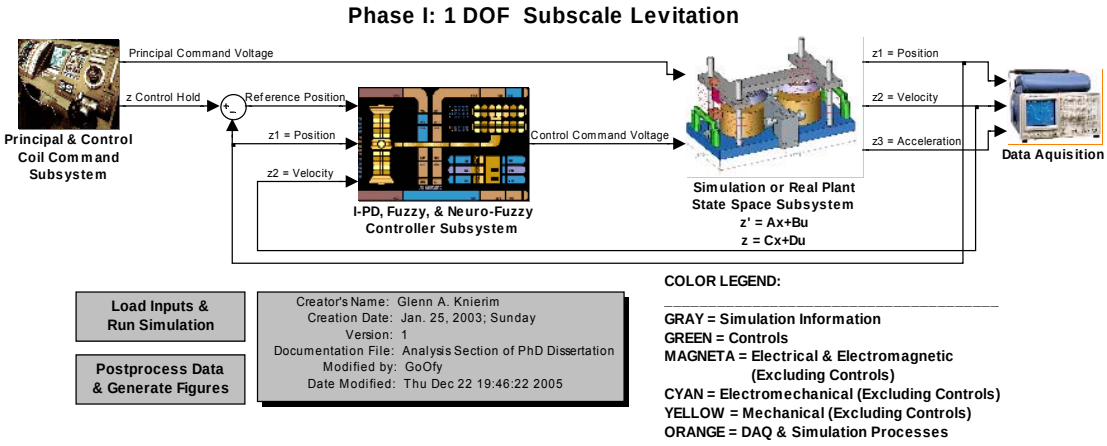

Figure 5.2-11: Phase I Numerical Simulation - Top Level Model

5.2.d.ii Initial Mechanical Offset

Since this is the first presentation of Phase I output, this opportunity is used to show plots that demonstrate general system performance. Future Phase I sections only produce plots that illustrate the point discussed in that particular section and it is understood that the general system performance trends do not change.

Solenoid Setup – Typical Operation

The following set of plots is for a principal solenoid with two coils wound with 30 AWG wire and operated with a constant AC voltage and a control solenoid

with one coil wound with 30 AWG wire where all other parameters between the solenoids are equal. As the plots in this section demonstrate for this type of system, the control solenoid has an order of magnitude less available energy than the principal solenoid. Therefore the control solenoid is meant for damping control only and cannot act as a back up principal solenoid.

Numerical Modeling with Soft Computing Fuzzy Control

The implemented top level fuzzy logic control model inside of the Simulink® program assumes the form of Figure 5.2-12. The fuzzy inference system structure and discussion of this model is provided in Chapter 3.3.c.ii.

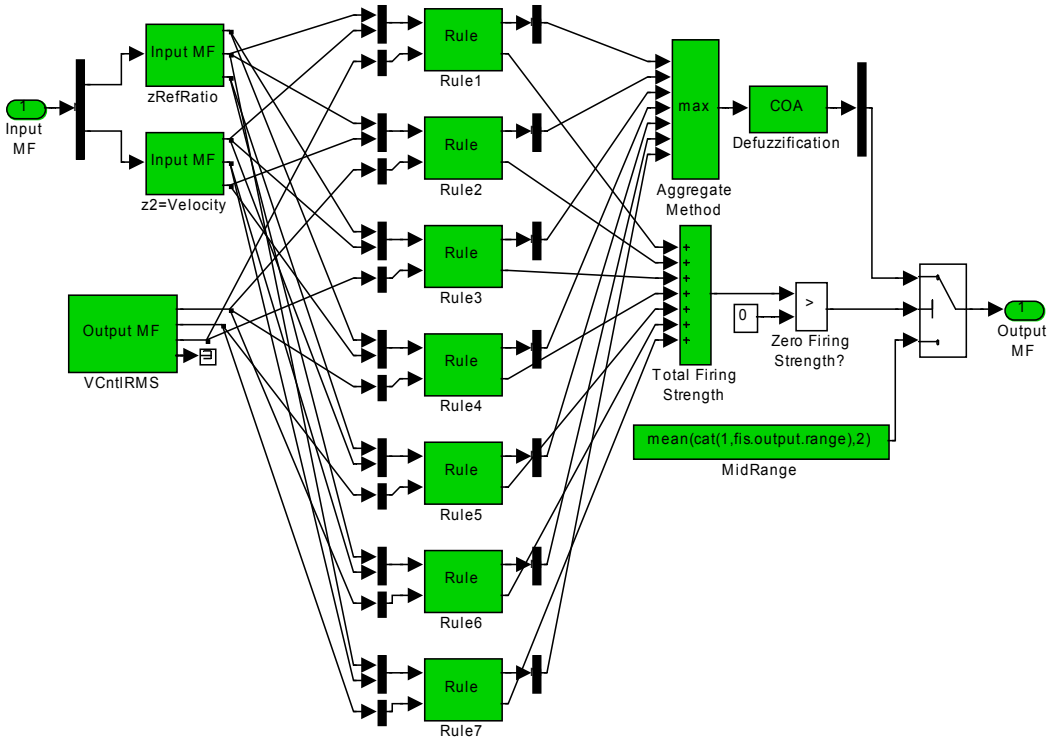

Figure 5.2-12: Phase I Fuzzy Logic Control Simulink Model

The secondary mechanical outputs are provided in Figure 5.2-13. The first plot of the z axis mechanical motion indicates that the system initially experiences an

increasingly large z axis amplitude oscillation. When 1 second has passed the controller turns on and successfully dampens the oscillation down to a relatively low amplitude level within 2 more seconds. This damping rate is readily increased by increasing the control coil repulsive force. The second plot provides the secondary z axis velocity. The third plot provides the principal and control solenoid forces acting on the secondary with reference to the weight or gravitational force of the secondary.

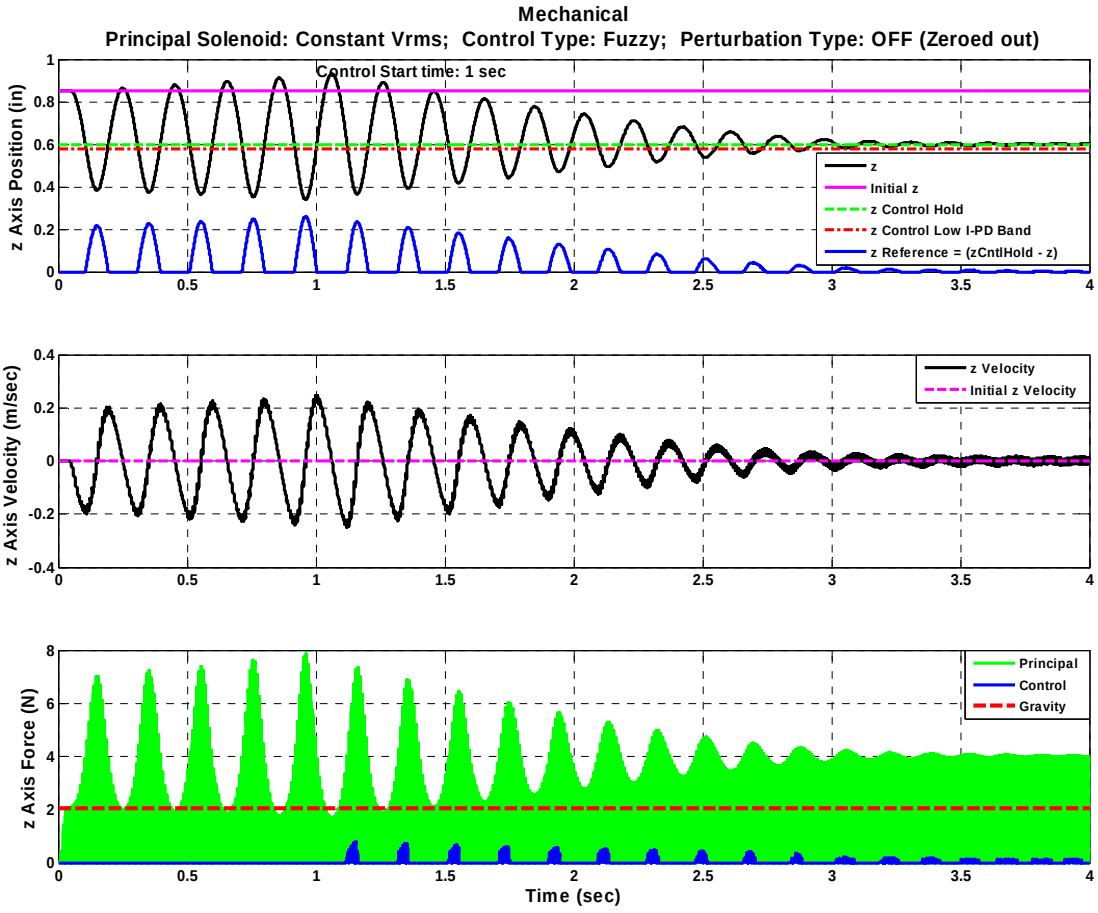

Figure 5.2-13: Mechanical Plots with Offset Initial Conditions

The energy and power output of Figure 5.2-14 indicates that the amount of oscillation energy and power in the system which includes to the amount of energy required to maintain the desired air gap superimposed with the secondary oscillation

energy. The first plot of control magnetic spring energy corresponds to the amount of energy removed from the secondary motion for each control oscillation period. The control energy works to remove the secondary kinetic energy. The maximum kinetic energy occurs during the secondary mechanical half stroke position where the velocity is maximized. The gravitational potential energy peaks and valleys occur in an opposing sequence to the principal solenoid magnetic spring energy. This chosen control solenoid has less than half the available energy of the principal solenoid. Therefore the control solenoid is meant for damping control only and cannot act as a back up principal solenoid. The second power plot has the same general trends as the energy plot. Besides trends the power plot also has a sign convention where positive principal power indicates an increasing secondary potential energy as principal power flows into the secondary, negative principal power indicates a decreasing secondary potential energy as the secondary approaches the minimum oscillation point, and negative control power indicates the flow of energy being removed from the secondary oscillation.

The energy components are listed as instantaneous energies compared to a running sum of each energy component. The instantaneous energies provide the instantaneous and periodic energy magnitudes and trends but not the total component energy summation which is the required energy form if an energy balance calculation is desire. The instantaneous energy output is adequate for the purposes of this paper.

As introduced in Chapter 1.2.c, the energy and power plots are for the secondary motion viewpoint only. The total system energy and power, which includes the primary electrical source and electromagnetic transmission across the air gap, are not considered since this paper is a proof of system concept only and not a final design effort.

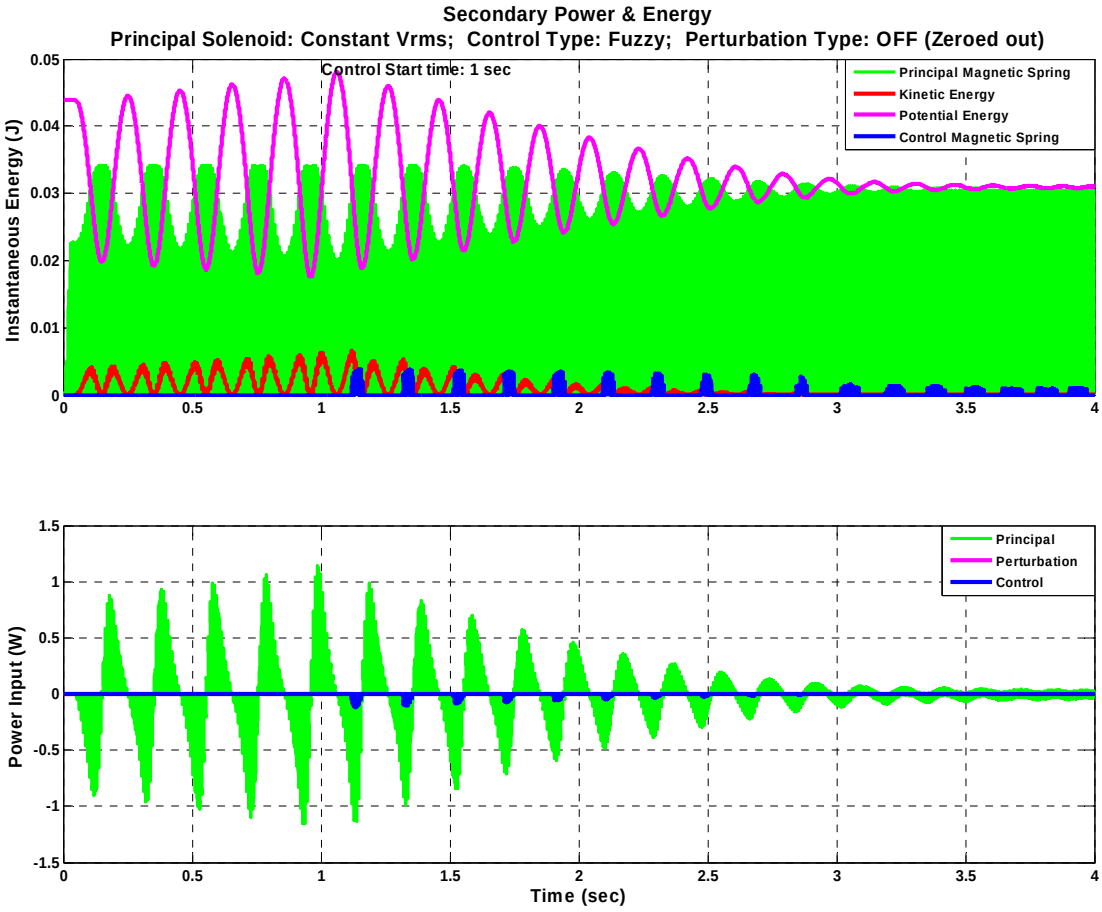

Figure 5.2-14: Power & Energy with Offset Initial Conditions

Figure 5.2-15 provides the time constants and spring constants of the system modeled. The oscillations are evident of the magnetic spring constant dependency on the secondary position with respect to the primary. This trend is also evident in the Phase I test output result plots presented in Chapter 5.2.e. The first system response output plot indicates that the electrical time constants are orders of magnitude lower than the mechanical time constants. Therefore the electrical system time response is fast enough to achieve the required secondary principal and control force values. The second plot compares the principal to control magnetic spring constants. As expected in this system the principal magnetic spring constant is approximately an order of magnitude larger than the control magnetic spring constant. The final plot provides

the mechanical system natural resonant frequency for the combined principal and control coil system.

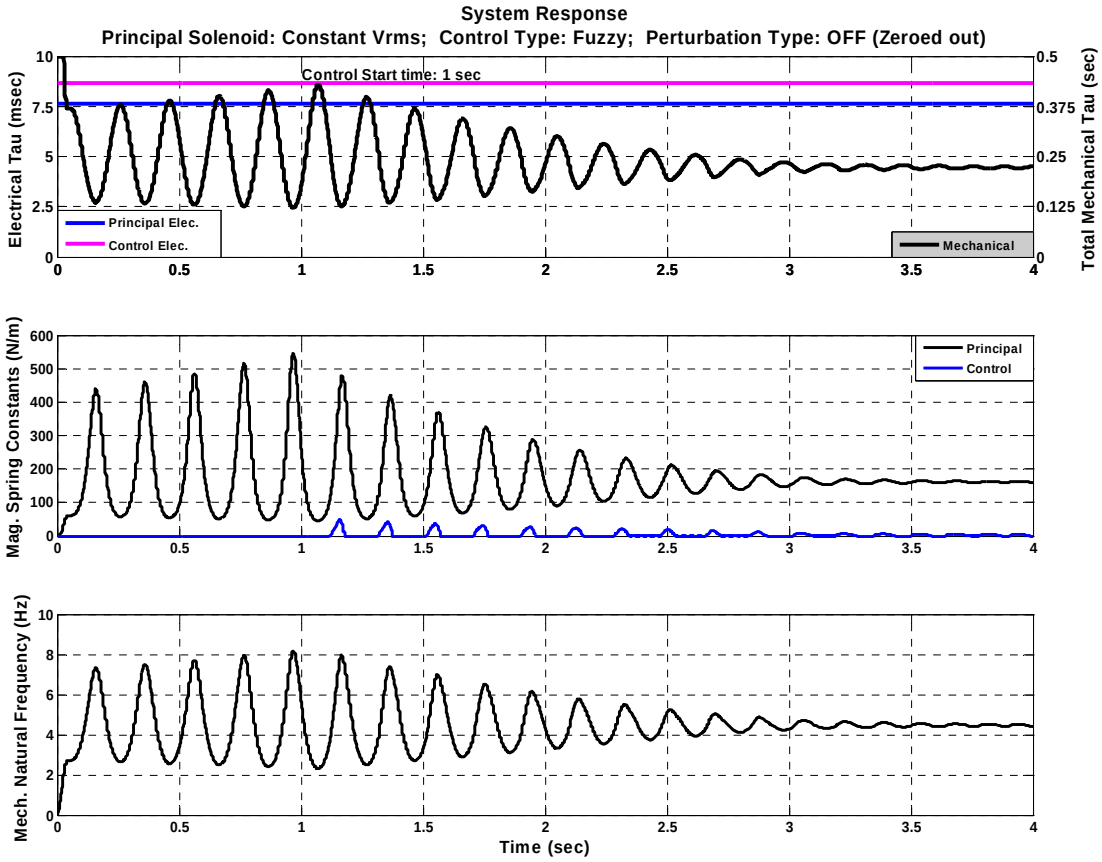

Figure 5.2-15: System Response with Offset Initial Conditions

The electrical output of Figure 5.2-16 indicates that the system initially experiences only the principal coil response. The first plot of source voltages indicates that when 1 second has passed the controller turns on and continues to operate by energizing the control coils whereas the principal coils remains on throughout the simulation. The second plot provides the solenoid source currents and control voltage turn on times. This plot shows the 2 times difference between the principal and control solenoid currents as well as the control current turn on and turn off lag with respect to the control voltage turn on times. The final plot provides the

control coil currents in the control coils with respect to a naturally cooled, steady state safe wire current value. Note that the coil wire currents exceed the typical safe continuous duty currents of the wire. This basic comparison shows that the control coils are acceptable for the short term operation required for this feasibility study. There is no need to perform a similar comparison of the principal coil currents since this type of principal system is only used for simulation purposes here and is far too inefficient to ever implement in a final design.

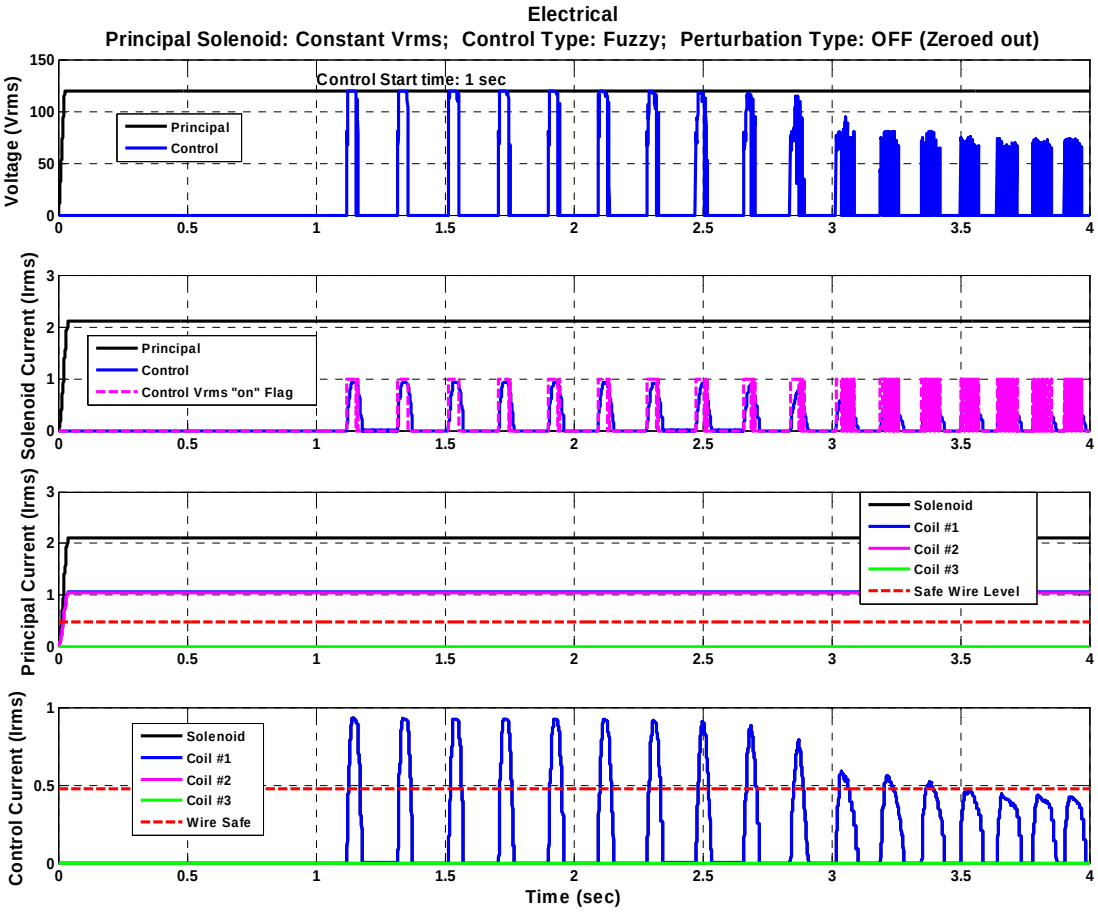

Figure 5.2-16: Electrical Plots with Offset Initial Conditions

The first order thermal output analysis of the solenoid coils is provided in Figure 5.2-17. The first plot, which provides the solenoid heat generation, also

indicates the system initially experiences only the principal coil response. When 1 second has passed the controller turns on and the controller continues to intermittently inject a thermal load into the control coils. The control solenoid and control coil #1 plots are the same here since the control solenoid is comprised of only one coil. The second plot shows the various coil temperature rises due to internal heat generation minus free convective and radiative cooling. This plot shows that the inefficient principal coil wire temperatures are elevating faster then 2°C every second whereas the intermittently power control coils are ratcheting up in temperature at a slower rate. For a demonstration setup of this system this principal and control solenoid temperature rises are acceptable for the short term operation required for this feasibility study, but both temperature rises must be monitored closely during actual tests.

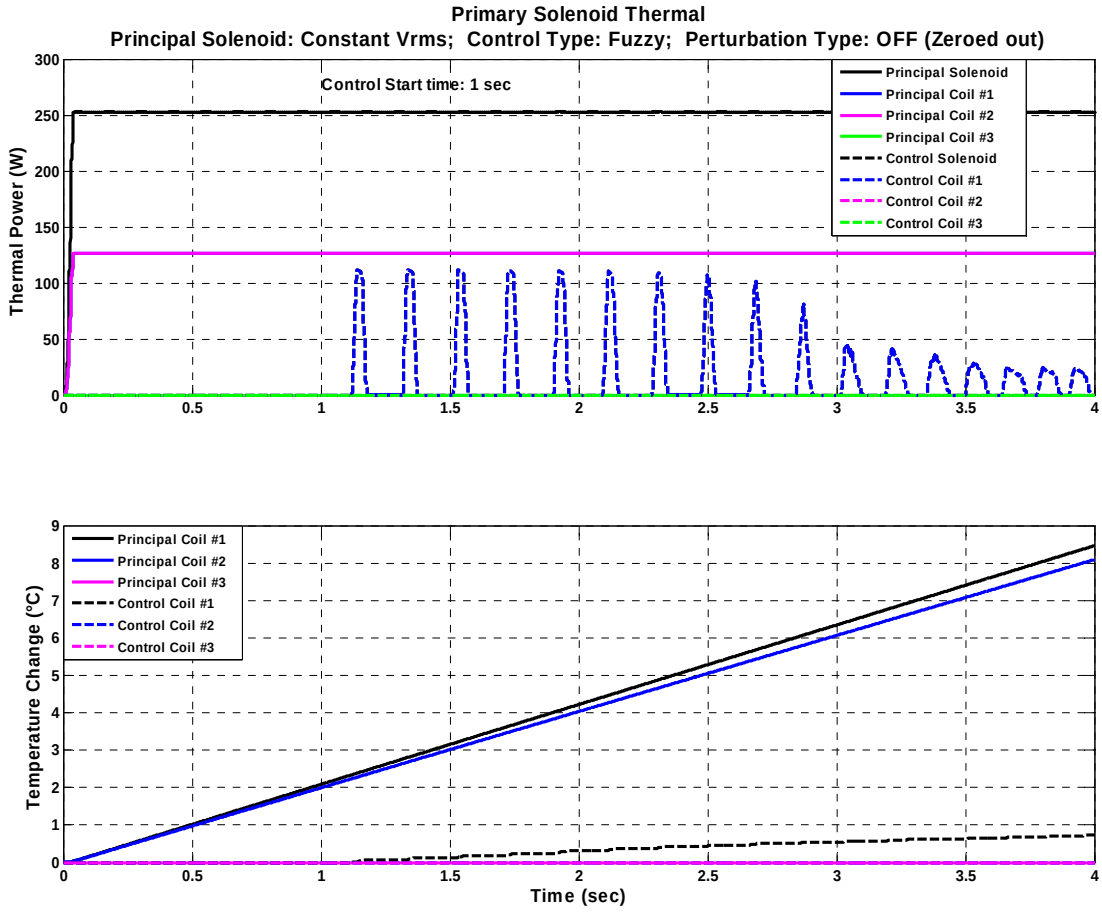

Figure 5.2-17: Thermal Plots with Offset Initial Conditions

Numerical Modeling with Linear State Space Control

The mechanical output of Figure 5.2-18 indicates that the system initially experiences a relatively large z axis amplitude oscillation. When 1 second has passed the I.-P.D. controller turns on and successfully dampens the oscillation down to a relatively low amplitude level within a subsequent 2 seconds. This control response is similar to the fuzzy control response presented in Figure 5.2-13.

Note the added complexity of a low I.-P.D. band line which is incorporated into this system as represented by the position plot of Figure 5.2-18. This band line is used to help increase I.-P.D. damping control by lowering the position where the

control coils are energized. Without this low I.-P.D. band line the control coil acts to force the secondary past the desired position when the secondary damping approaches the desired position value and therefore maintain higher than desired oscillations about the desired position. A brief sensitivity analysis indicated that the I.-P.D. controller performance in the low oscillation amplitude domain relies somewhat heavily on the location of this band line.

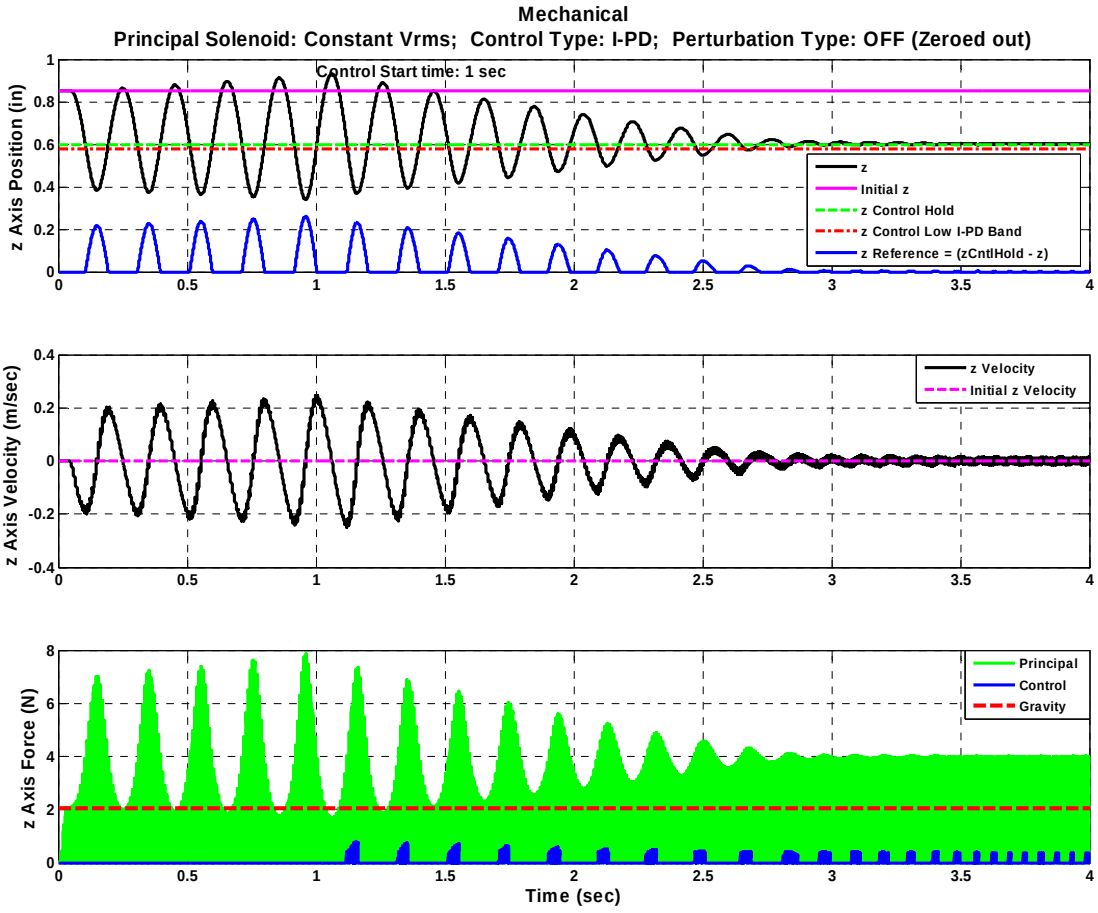

Figure 5.2-18: Mech. Plots with Offset Initial Conditions & I.-P.D. Control

The energy and power output of Figure 5.2-19 indicates that the amount of oscillation energy and power in the system which includes to the amount of energy required to maintain the desired air gap as well as the energy required to remove the

oscillation of the wire. This I.-P.D. control response is similar to the fuzzy control response presented in Figure 5.2-14.

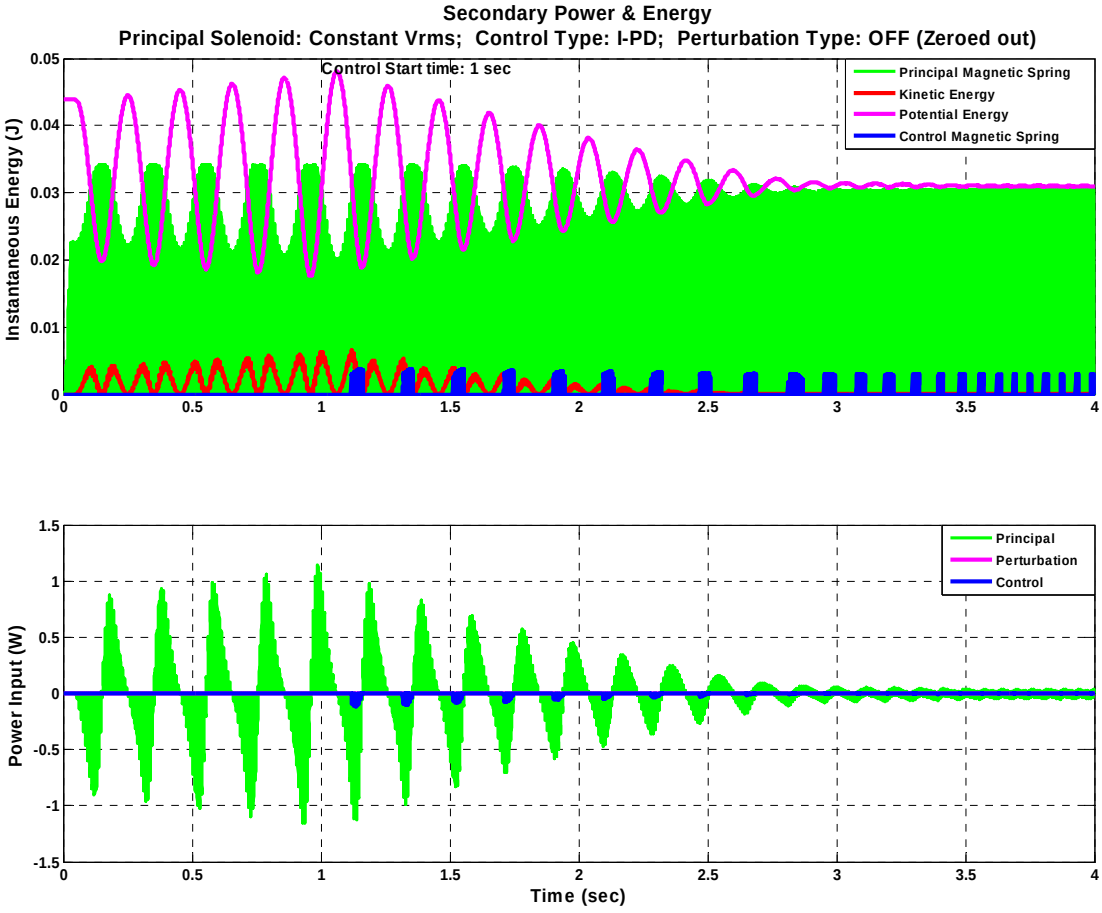

Figure 5.2-19: Power & Energy with Offset Initial Conditions & I.-P.D. Control

5.2.d.iii Initial Mechanical Offset with 2x Vrms Down Pulses

Solenoid Setup – Extreme Operation

The following set of plots is for identical principal and control solenoids both with two coils wound with 30 AWG wire found only in Chapter 5.2.d.iii. The principal solenoid is operated with a constant AC voltage that experiences two voltage down pulses from full voltage to 0 voltage for 0.25 seconds each and occurs

at 0.25 seconds and 1.25 seconds. The control solenoid has the same available energy as the principal solenoid and therefore the control solenoid is meant for damping control as well as a back up principal solenoid during the two voltage down pulses.

Numerical Modeling with Linear State Space Control

The mechanical output of Figure 5.2-20 indicates that the I.-P.D. controller could not maintain a stable system control response during either the first or second voltage down pulses which occur at 0.25 and 1.25 seconds respectively as indicated in the energy and power plots of Figure 5.2-21 and the electrical plots of Figure 5.2-22. Therefore this is not an acceptable controller for this type of extreme disturbance.

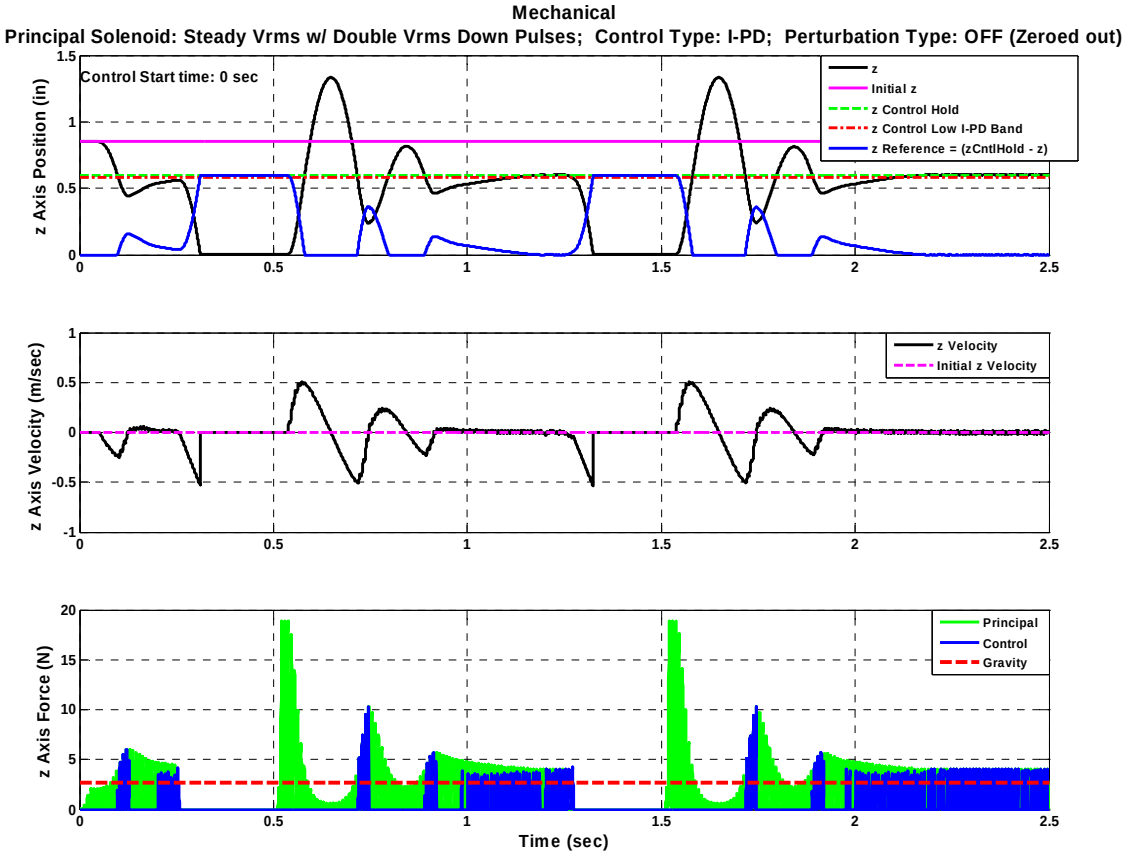

Figure 5.2-20: Mech. Plots with 2x Vrms Down Pulses & I.-P.D. Control

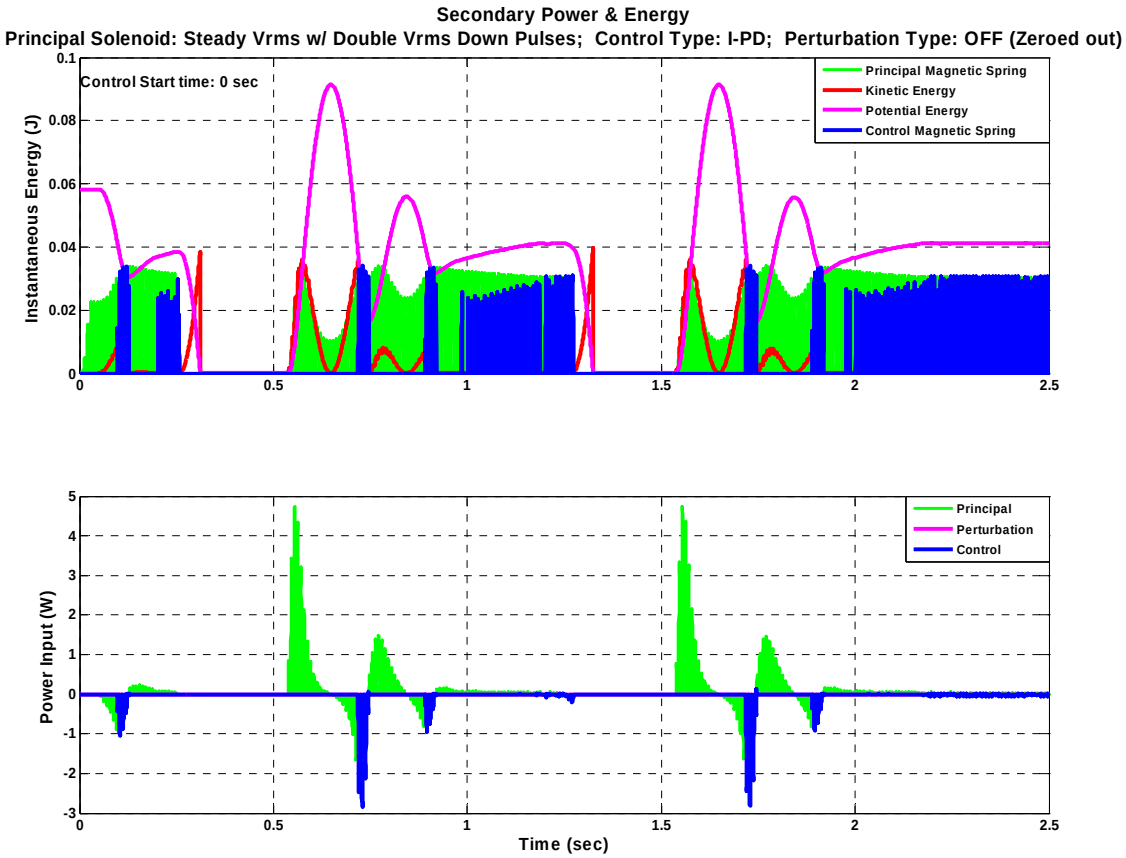

Figure 5.2-21: Power & Energy with 2x Vrms Down Pulses & I.-P.D. Control

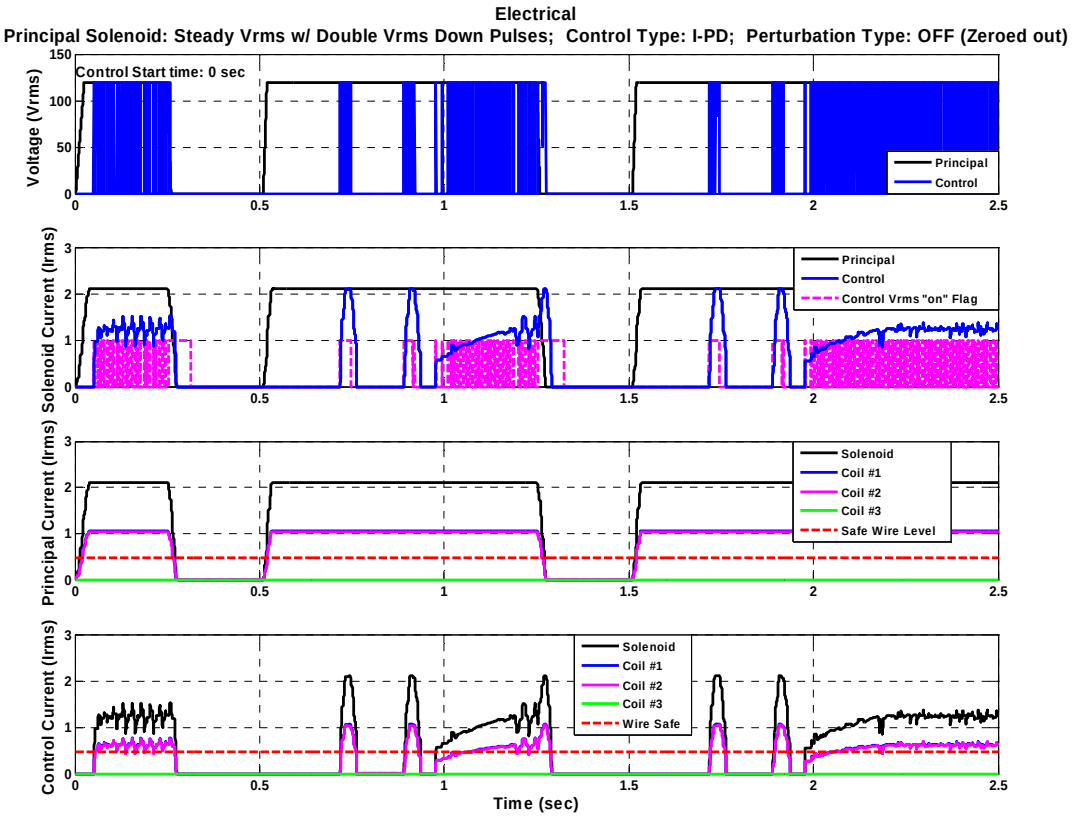

Figure 5.2-22: Elec. Plots with 2x Vrms Down Pulses & I.-P.D. Control

Numerical Modeling with Soft Computing Fuzzy Control

The mechanical output of Figure 5.2-23 indicates that the fuzzy controller maintains an extremely stable system control response during both the first and second voltage down pulses which occur at 0.25 and 1.25 seconds respectively as indicated in the energy and power plots of Figure 5.2-24 and the electrical plots of Figure 5.2-25. In this case the control coil completely assumed the roll of the principal coil with no extra control rule allocation than the original control rules. Upon reinstatement of the principal coil after each down pulse the mechanical oscillation damped out and approached the optimum value within 0.5 seconds. Therefore this is an acceptable controller for this type of extreme disturbance and will no longer be analyzed.

I.-P.D. control for basic linear cases and nonlinear cases where piecewise linear rules dominate in general respond similarly to nonlinear based control systems. Linear control with a large enough conditional rule set or at least a rule set focused on a particular disturbance should also work acceptably well under set extreme conditions. The shortcoming of linear control is when an unexpected nonlinear disturbance occurs as is often the case in reality. Without a large linear control rule set the linear controller either turns unstable or is at least more sensitive to the disturbance than an equivalent soft computing nonlinear control scheme with a more robust response generated from a comparatively mild rule set.

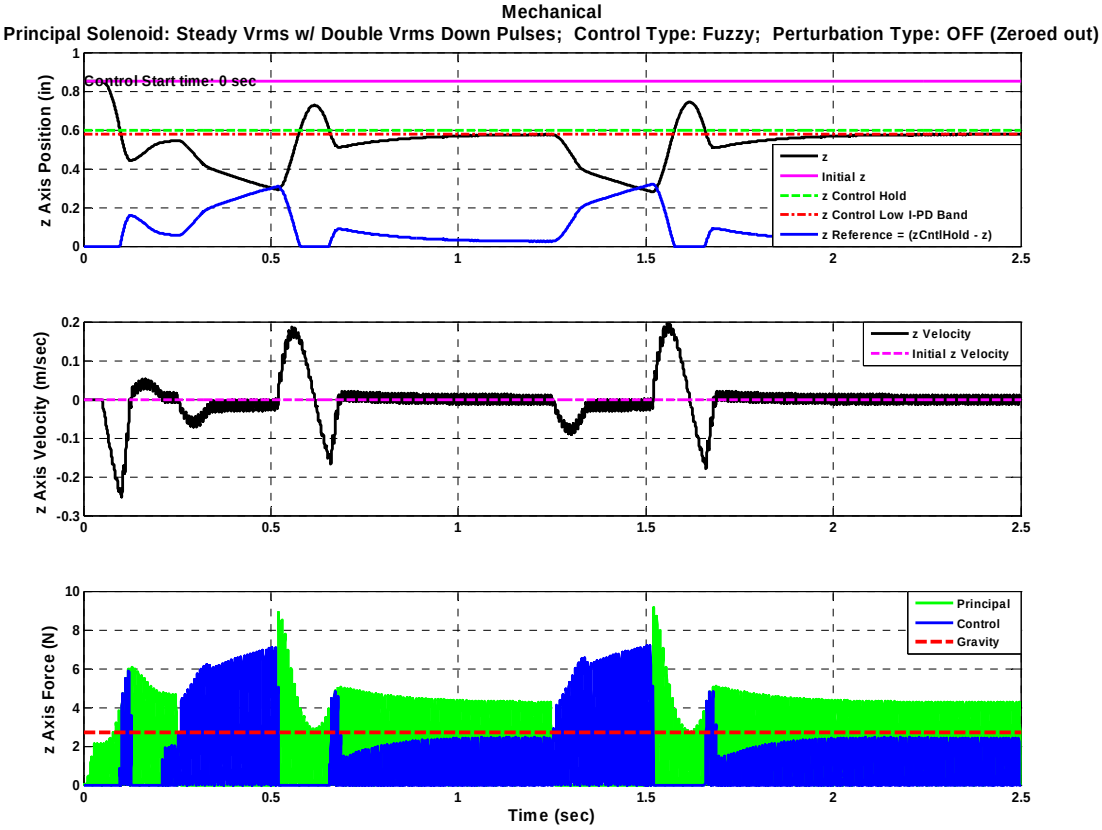

Figure 5.2-23: Mech. Plots with 2x Vrms Down Pulses & Fuzzy Control

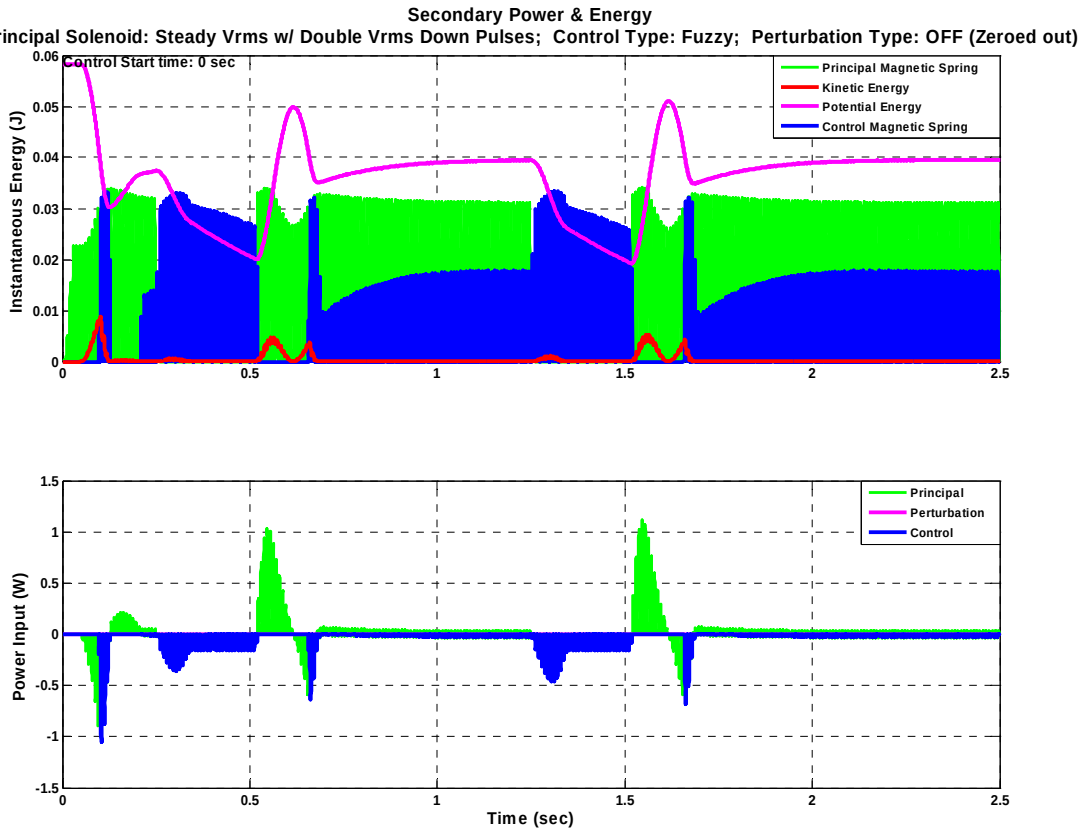

Figure 5.2-24: Power & Energy with 2x Vrms Down Pulses & Fuzzy Control

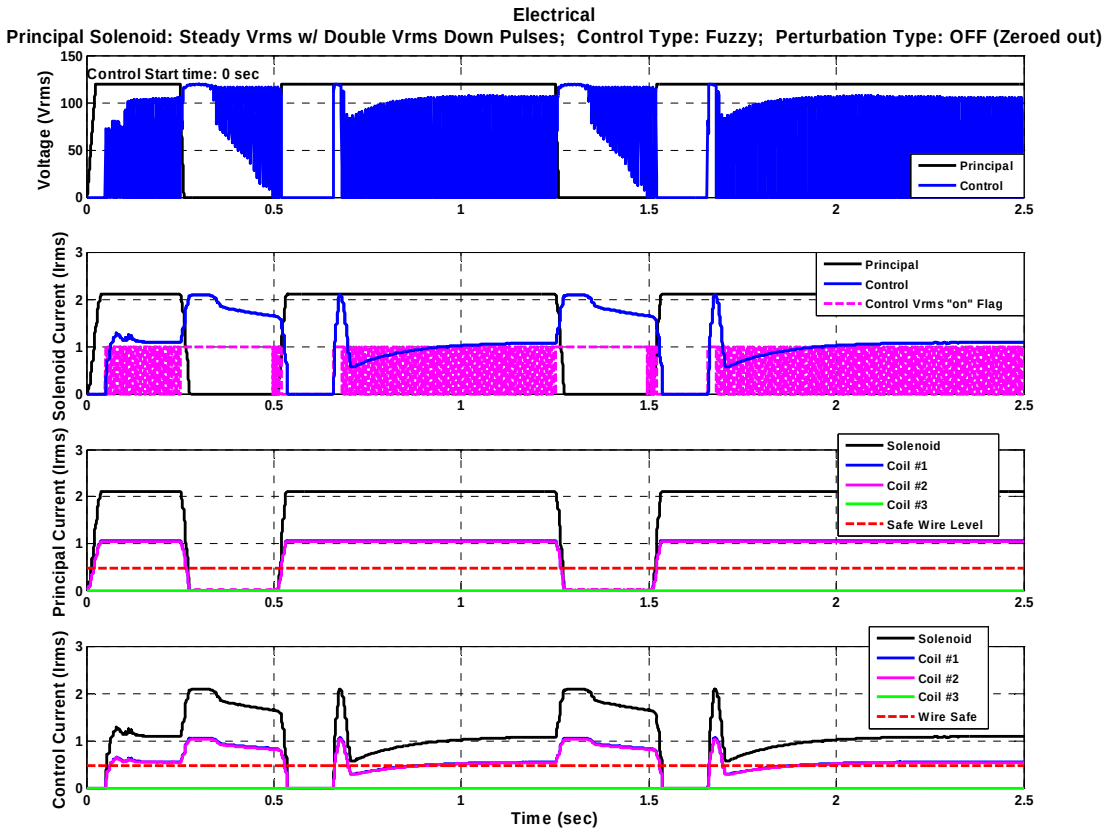

Figure 5.2-25: Elec. Plots with 2x Vrms Down Pulses & Fuzzy Control

5.2.d.iv Step Response with No Control

The uncontrolled unit step response determines the magnetic spring constant system resonant frequency value. The system resonant frequency varies with the nonlinearly changing magnetic spring constant as shown in Figure 5.2-28. The step response finds an approximate median natural frequency value, but true resonance is never achieved unless the perturbation frequency is allowed to vary and track the changing resonant frequency. The median resonant frequency value is the sinusoidal perturbation frequency input. The mechanical motion is presented in Figure 5.2-26. The power and energy plot is presented in Figure 5.2-27.

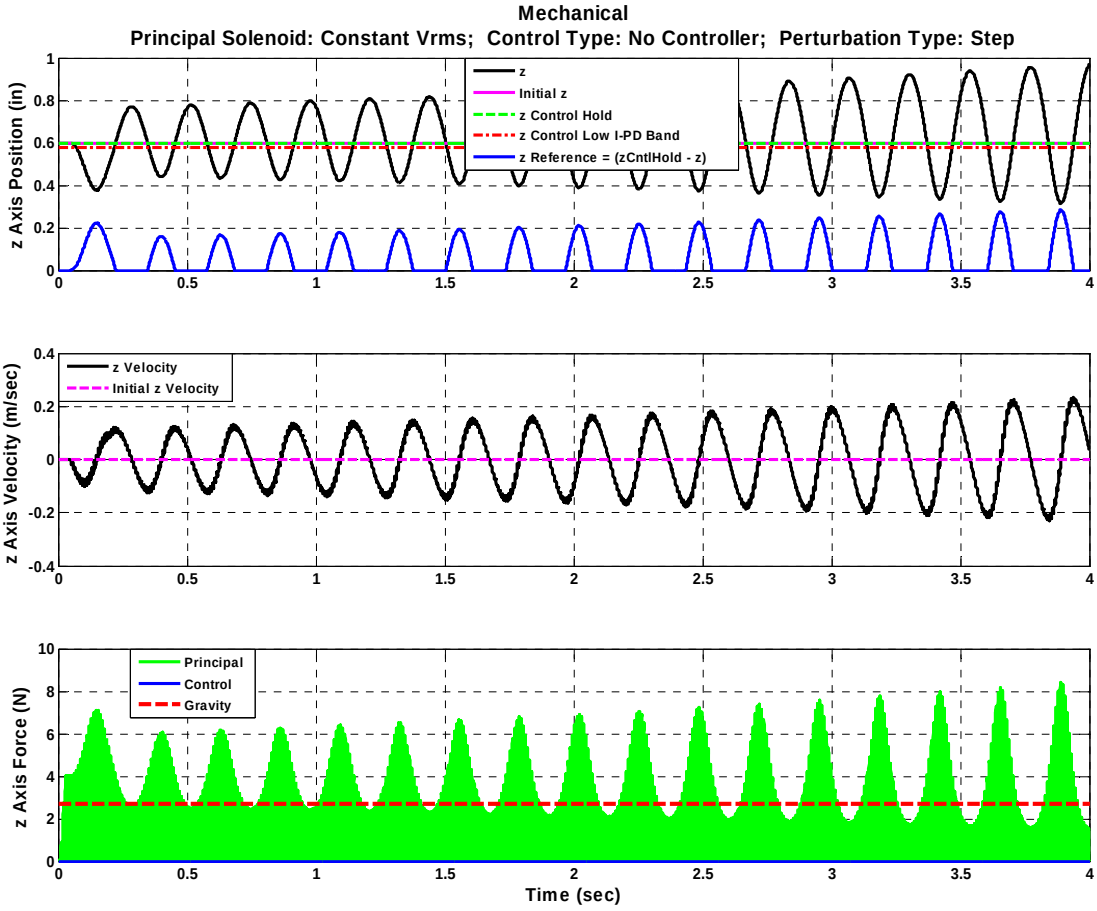

Figure 5.2-26: Mechanical Plot with Step Perturbation & No Control

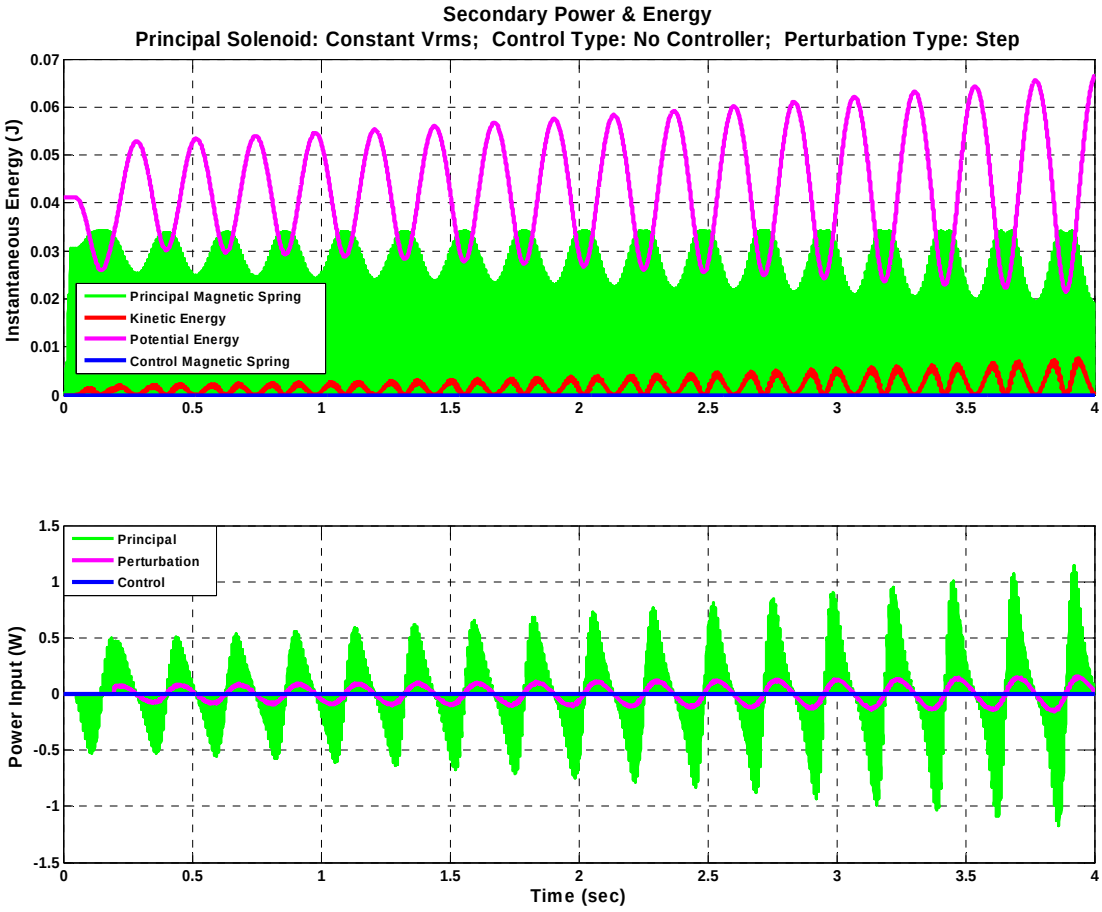

Figure 5.2-27: Power & Energy with Step Perturbation & No Control

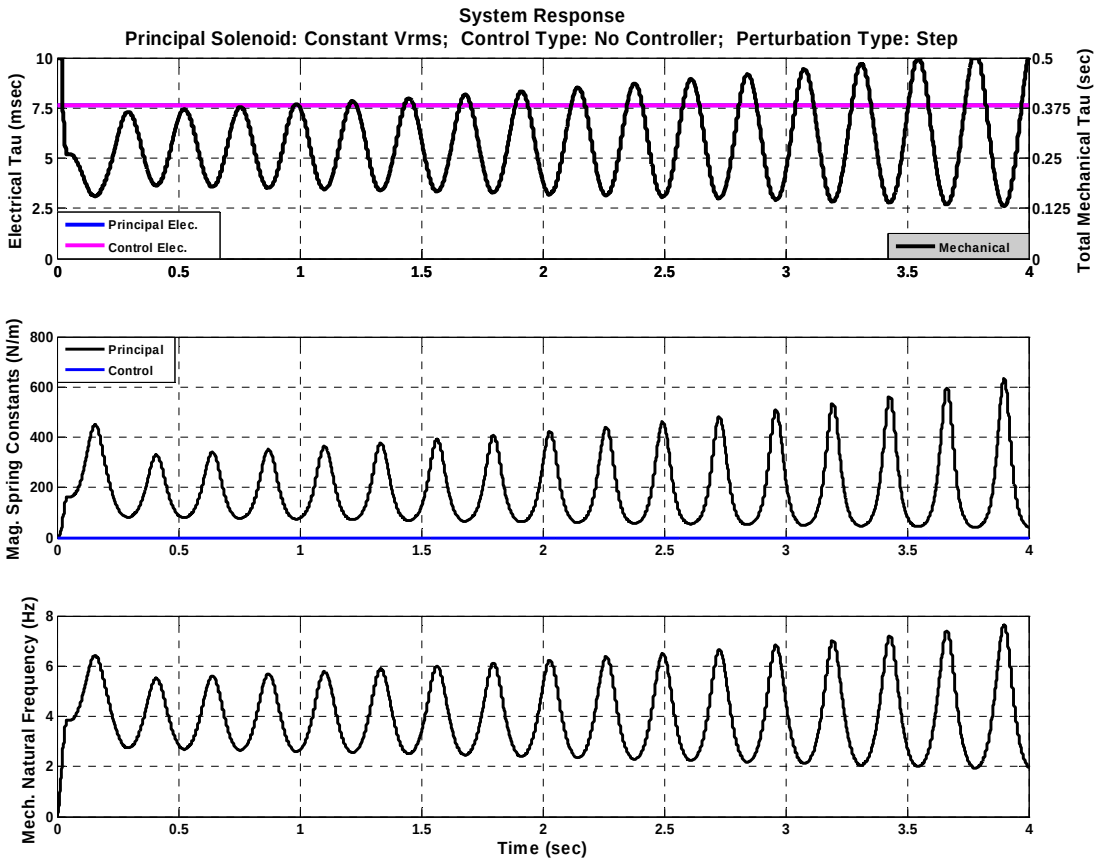

Figure 5.2-28: System Response with Step Perturbation & No Control

5.2.d.v Sinusoidal Response

The sinusoidal perturbation frequency value comes from the step response median resonant frequency. A common sinusoidal frequency witnessed in maglev system operation is a mechanical variation in the guideway track. An example is this track variation is the track to track set distance interface. Such mechanical variations produce a propulsive velocity dependent, vertical periodic disturbance into the system. This sinusoidal perturbation is meant to represent the worse case scenario of the periodic disturbance occurring at the magnetic air gap natural frequency. The mechanical motion is presented in Figure 5.2-29. The power and energy plot is presented in Figure 5.2-30.

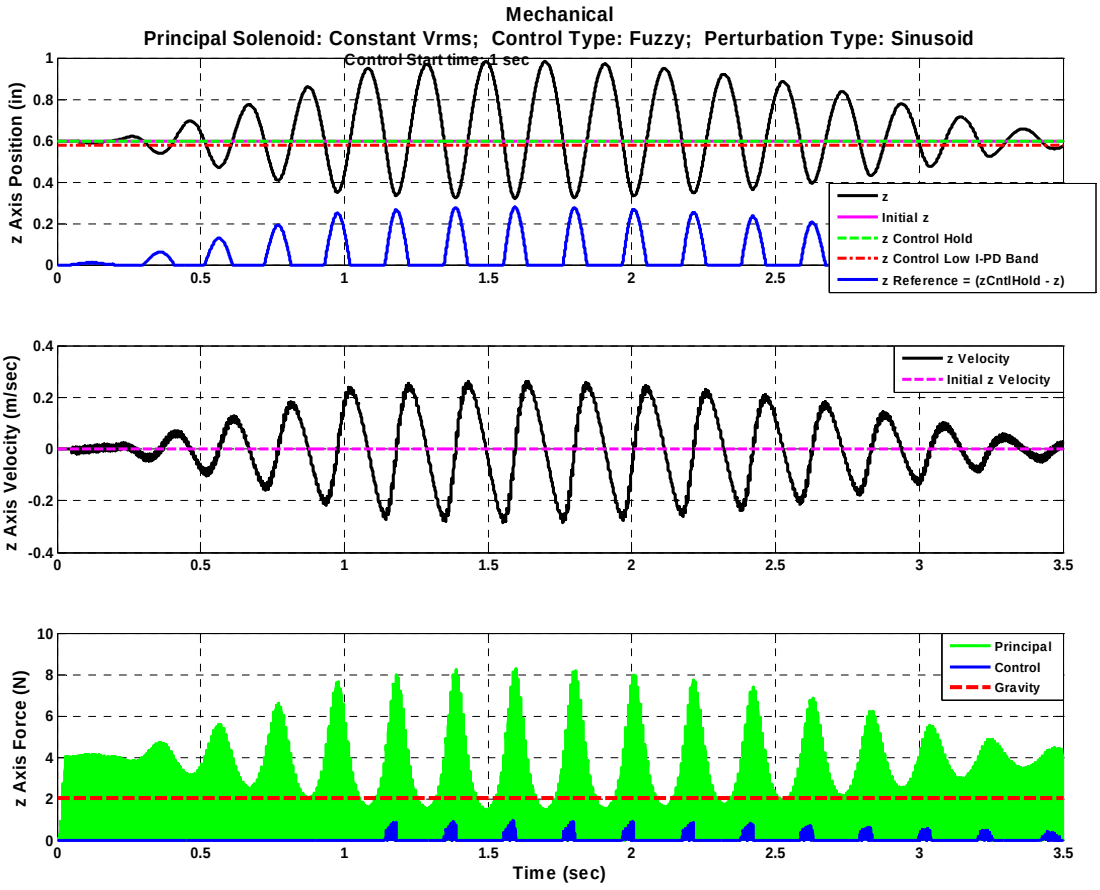

Figure 5.2-29: Mechanical Plots with Sinusoidal Perturbation

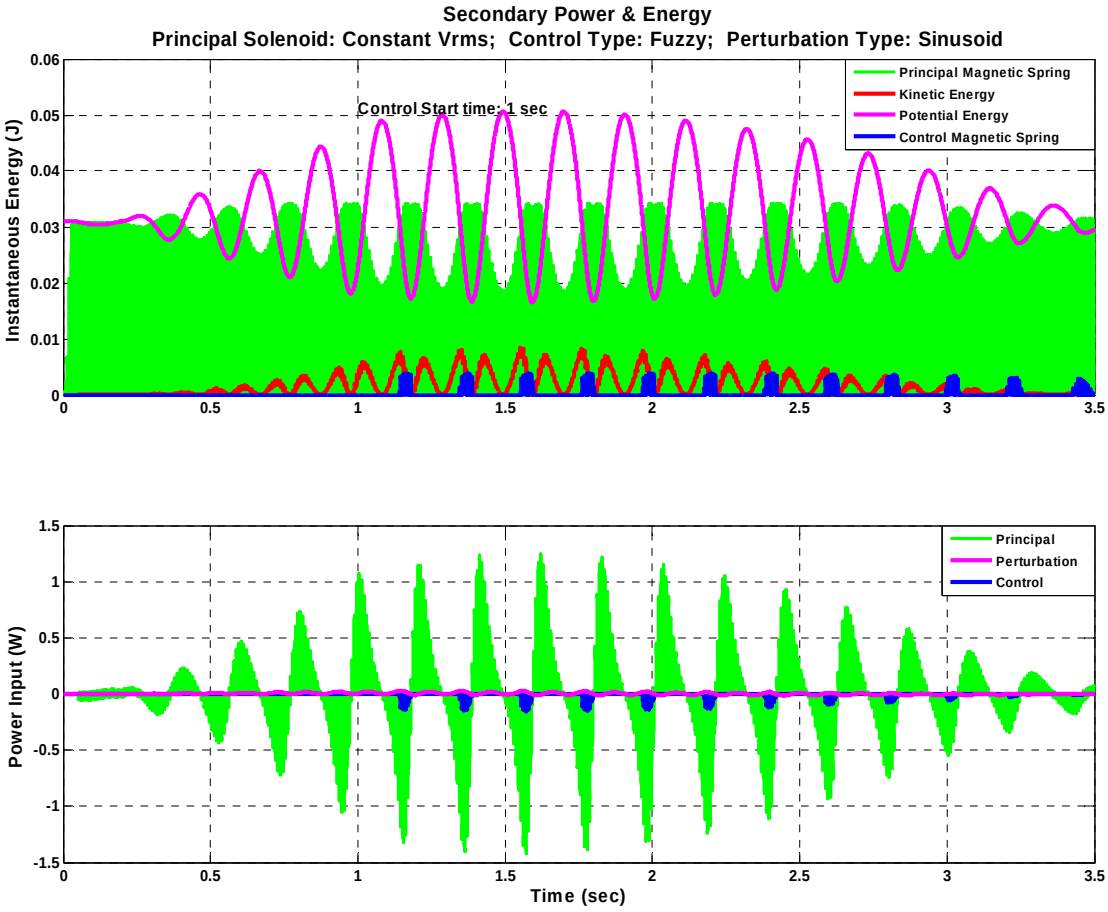

Figure 5.2-30: Power & Energy with Sinusoidal Perturbation

5.2.d.vi Stochastic Response

The stochastic response, which is often the most realistic perturbation case during a real system operation, provides a random response input. The mechanical motion is presented in Figure 5.2-31. The power plot in Figure 5.2-32 provides the power input fluxations for this disturbance.

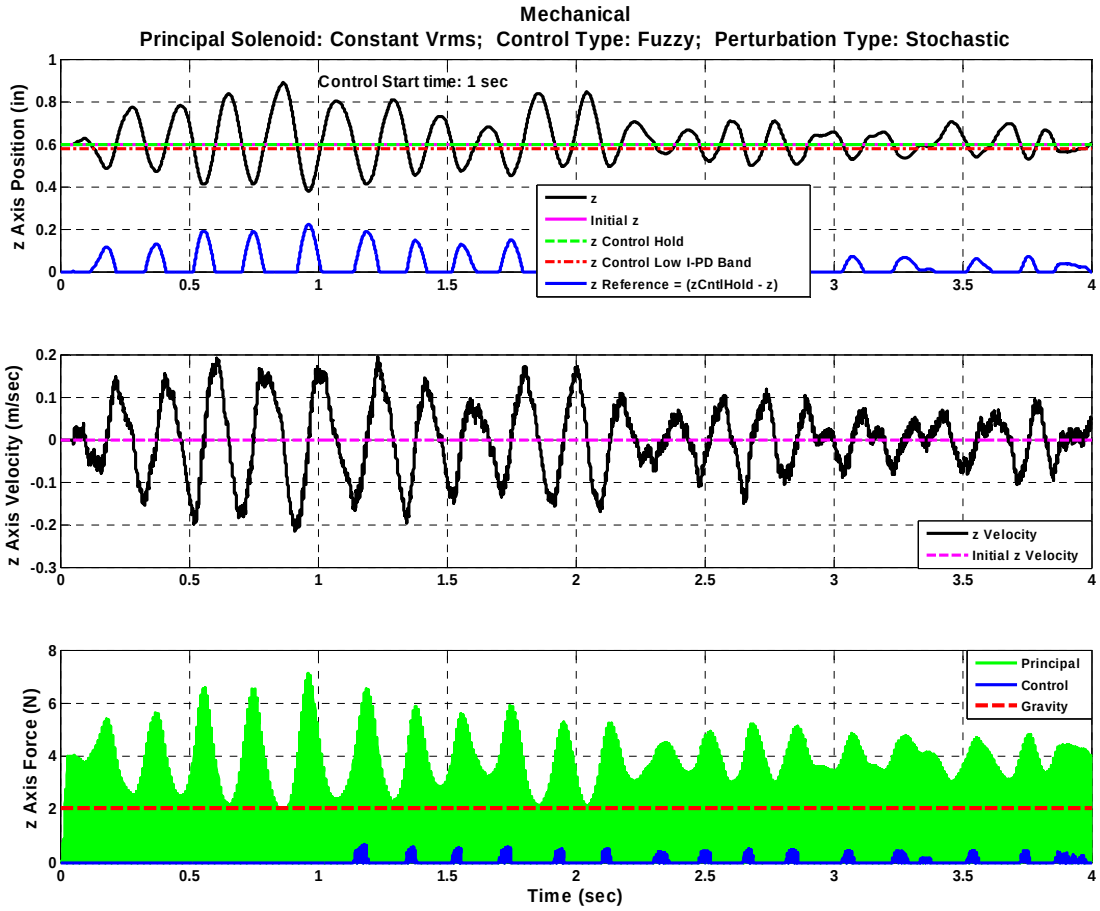

Figure 5.2-31: Mechanical Plots with Stochastic Perturbation

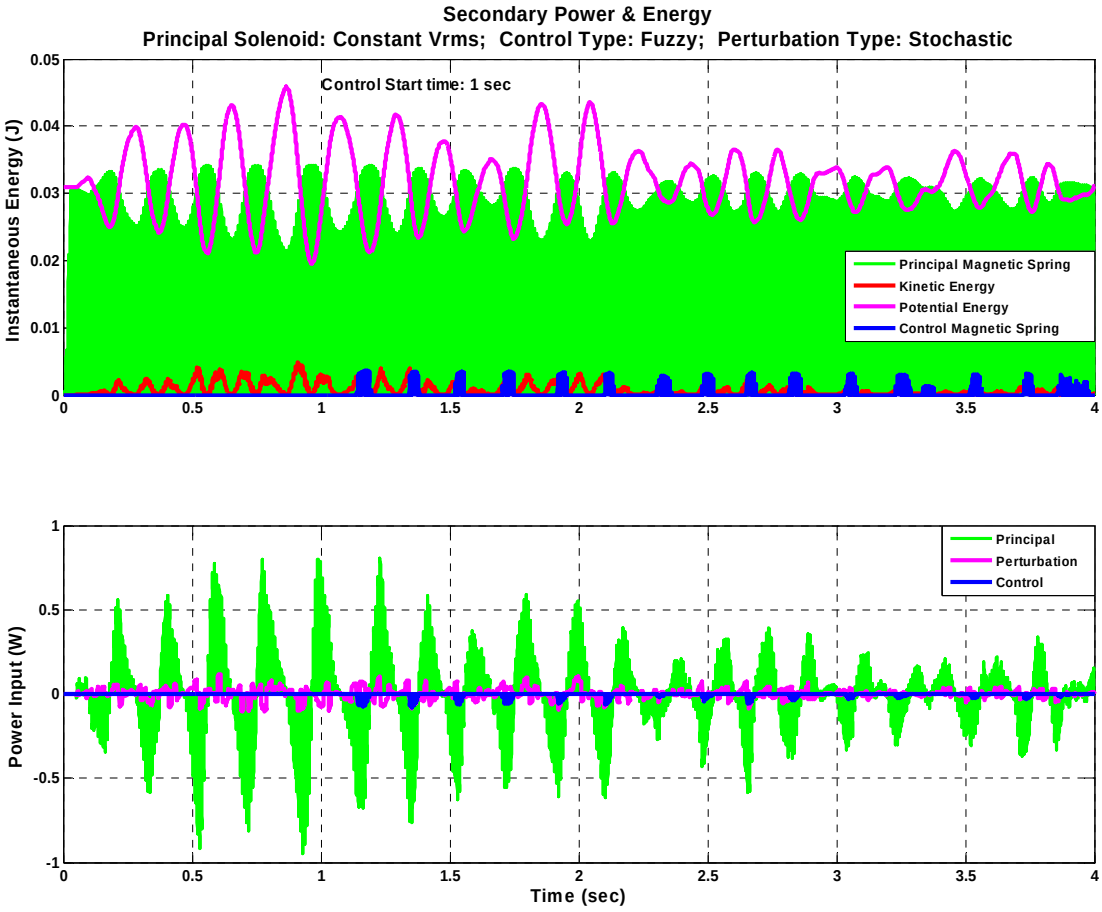

Figure 5.2-32: Power & Energy with Stochastic Perturbation

5.2.d.vii Stochastic & Offset Response with Equivalent Solenoid Systems

Even though the extreme stochastic perturbation response presented in Chapter 5.2.d.vi did not dampen the oscillation down to the desired levels, it did maintain a somewhat dampened oscillation level. This led to an even more extreme case where a stochastic perturbation is superimposed on an already offset system. This perturbation case is applied to a system where the control solenoid is the same design and hence the same force and energy output as the principal solenoid. As Figure 5.2-33 and Figure 5.2-34 show the system was approaching an unstable failure

prior to the control system initialization at 1 second. Then the added controller completely damped the oscillation within 1 second.

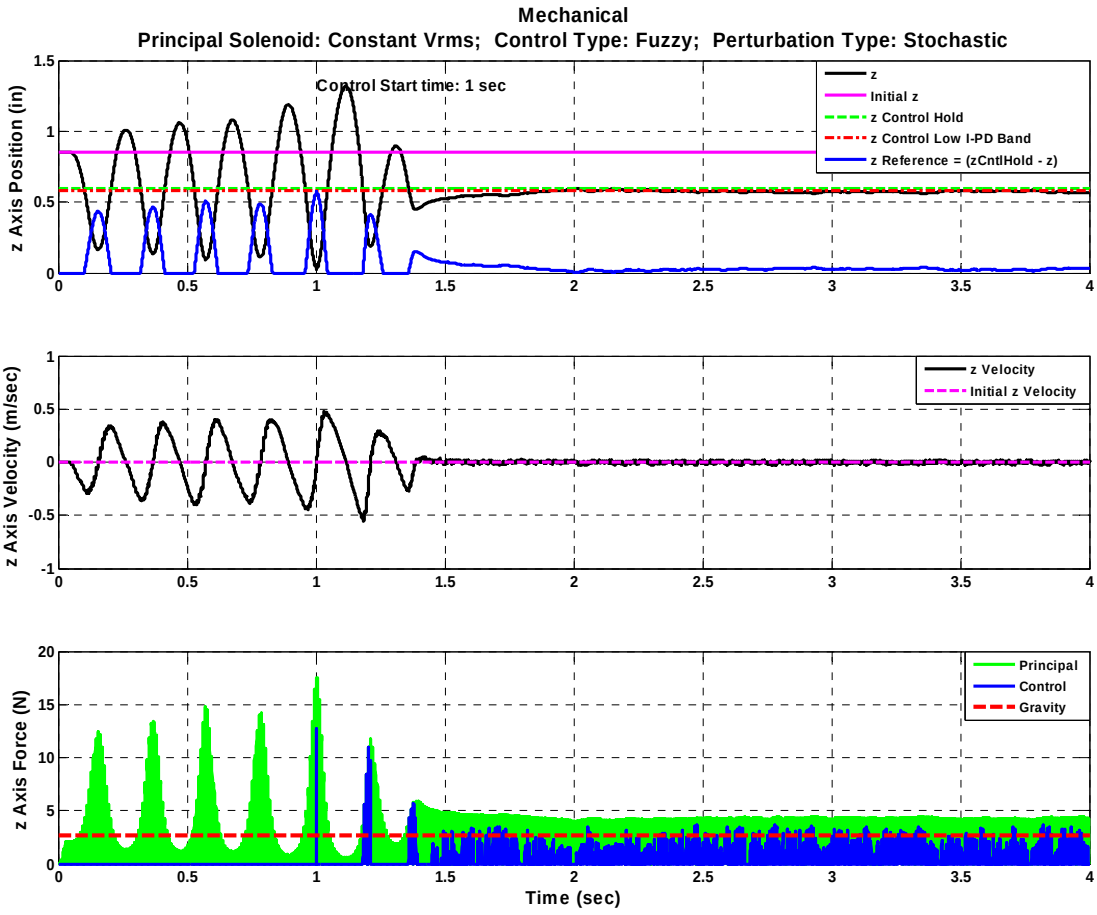

Figure 5.2-33: Mech. Plots with Stochastic Perturbation & Offset Initial Cond.

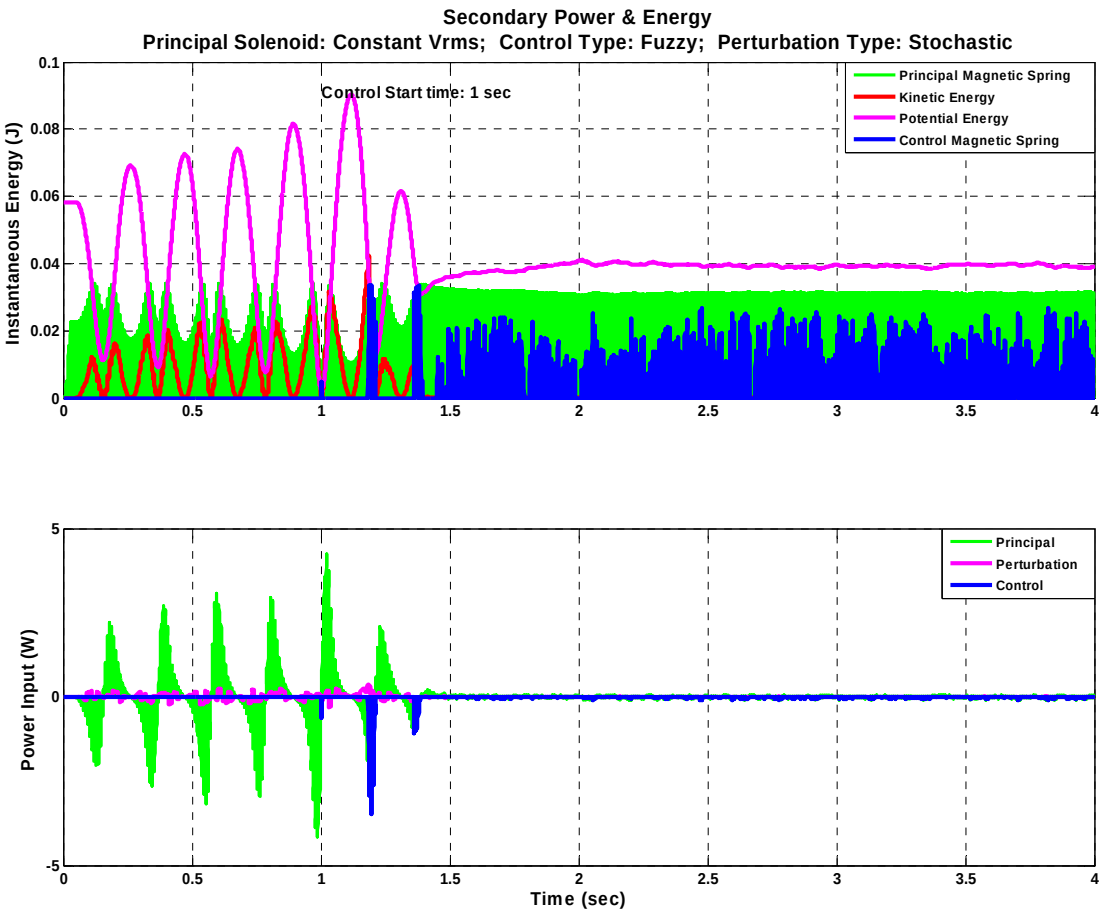

Figure 5.2-34: Power & Energy with Stochastic Pert. & Offset Initial Cond.

Figure 5.2-35 shows that even though the control solenoid is capable of equivalent power output as the principal solenoid, it only draws that much current and hence power during extreme offset conditions. The majority of the control system power draw is much lower than the principal solenoid. The forth plot even shows the control coils themselves maintaining a safe continuous duty current level.

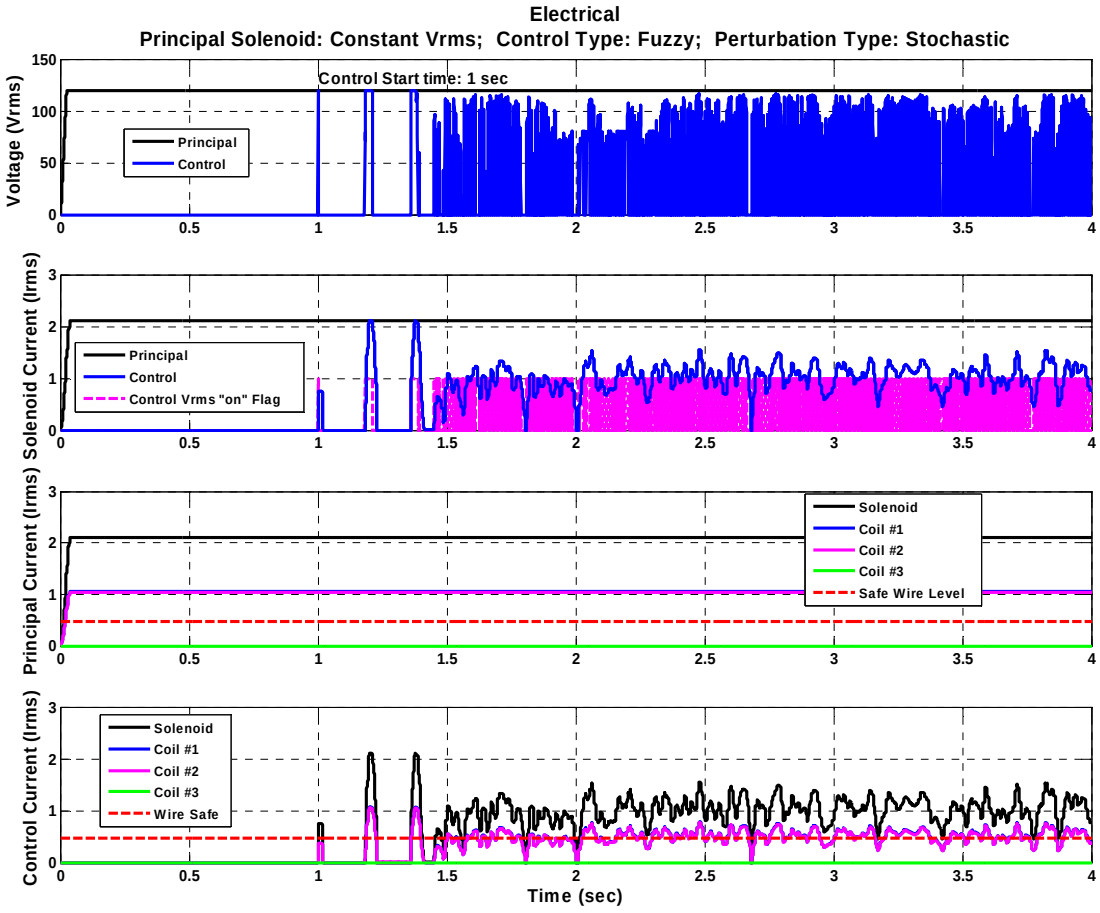

Figure 5.2-35: Elec. Plots with Stochastic Perturbation & Offset Initial Cond.

5.2.d.viii Numerical Simulation Results Summary

Phase I numerical analysis results are summarized in Table 5.2-1. In this table the green cells indicate desired output values that are achieved and red cells indicate desired output values that are not achieved. These desired damping levels are listed in

the table headings in blue font inside of yellow cells. The final oscillation magnitude values are chosen as values which retain relative accuracy with this model while approaching what is considered an acceptable damping level of this system by the author.

A control start energy column is added to Table 5.2-1 to provide a sense of the levels of perturbation energy that the control system must dampen in the translational D.O.F. This list does not encompass all of the perturbation energy, but instead only provides the major components experienced by the z and y axis control solenoids.

Table 5.2-1: Phase I Numerical Analysis Results Summary

Simulation #	INPUTS					OUTPUTS			
	Principal Solenoid Input Waveform	**Control to Principal Solenoid Power Sizing Ratio**	**Control Type**	**Initial Offset**	**Perturbation Type**	**Control Damping Time**	**Control Start Peak to Peak Mechanical Oscillation Value**	**Control End Peak to Peak Oscillation Value**	**Maximum Control Potential Energy**
				(Yes/ No)		**Desired: 2 sec**		**Desired: 0.1 in.**	
						(sec)	(in.)	(in.)	(mJ)
1	Steady V_{rms}	≈ 1:10	Fuzzy	Yes	None	1.75	0.7	0.1	48
2			I.-P.D.			1.75	0.7		48
3	Steady V_{rms} with Double V_{rms} Down Pulses	1:1				**I.-P.D. CONTROLLER FAILED**			90
4			Fuzzy			0.3	0.4	0.1	52
5	Steady V_{rms}	≈ 1:10		No	Sinusoidal	2	0.6		50
6					Stochastic	2.75	0.5		47
7		1:1		Yes		0.5	1.25		90

5.2.e System Testing

5.2.e.i Overall

During Phase I testing only an accelerometer directly presented secondary motion. Therefore both the position and velocity required integrating observers.

All test data was taken with ambient and all solenoid temperatures between 68°F and 71°F.

5.2.e.ii Phase I, Test #1: Solenoid Parameter Determination

The only result of this test is a slight modification to the solenoid coil inductance component analytical equation. The approximated relative permeability term was slightly increased from the initial value used. This test is described in Chapter 4.2.c.ii and the hardware used in this test is presented in Appendix D.1.

5.2.e.iii Phase I, Test #2: Uncontrolled Response Test

The accelerometer raw sampled data is presented in Figure 5.2-36, the observed velocity is presented in Figure 5.2-37, and the observed position is presented in Figure 5.2-38. The inherent integration filtering effects are witnessed in the velocity and position plots. The observed position data is incorrect due to initial accelerometer offset errors which increase with the double integration. The position plot is still valuable for indicating the proper oscillation trend, period, a coarse range of oscillation amplitudes, and approximated final damped levitation height. The mechanical response period is approximately 0.2 seconds and the maximum acceleration is approximately 9.5 g’s. Approximately seven perturbation periods are experienced prior to complete damping of the perturbation force. The D.A.Q. hardware for all data channels in this test is set to sample input data at 10,000 samples per second per channel or 10 kHz which translates to a 0.1 milli second sampling period. This test is described in Chapter 4.2.c.iii and the test conclusions are presented in Chapter 6.2.d.i.

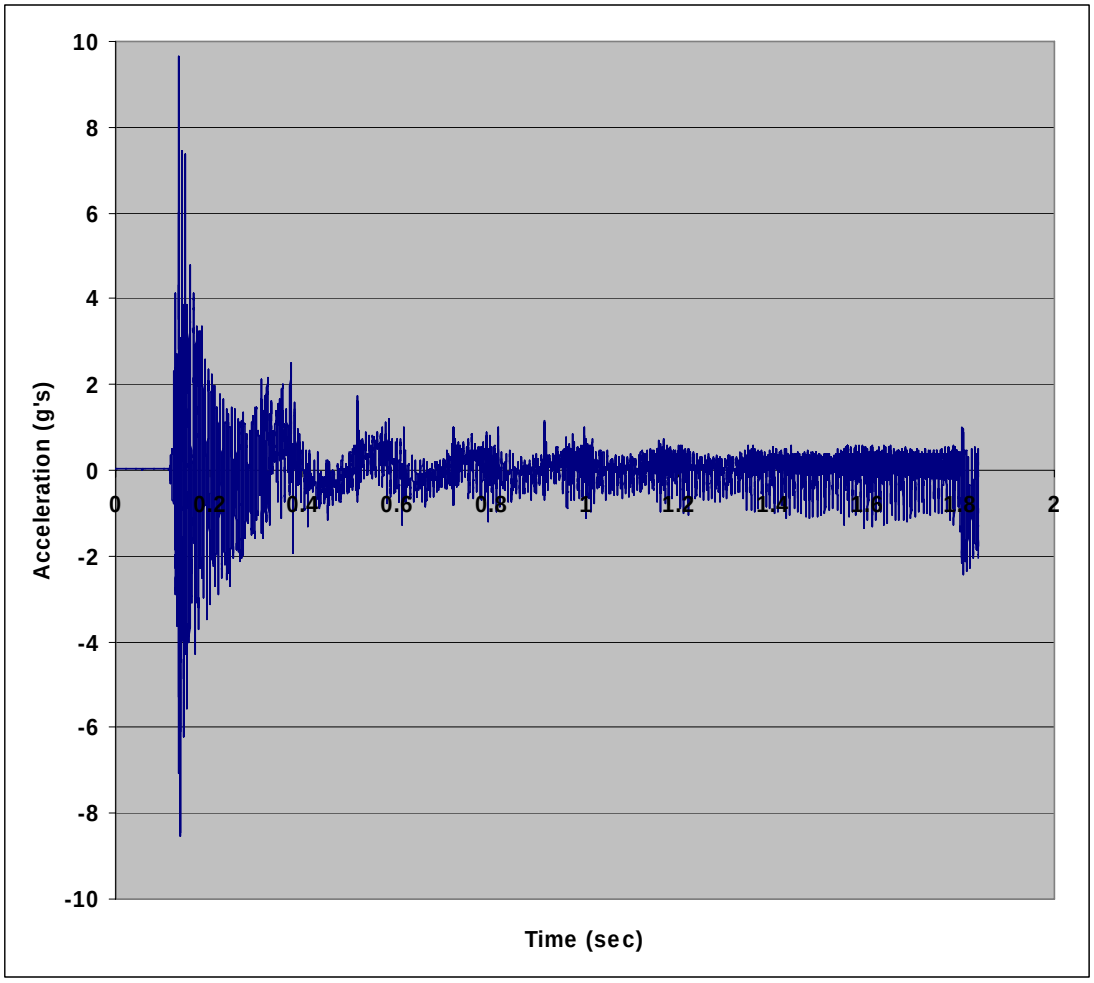

Figure 5.2-36: Phase I No Control Test Acceleration

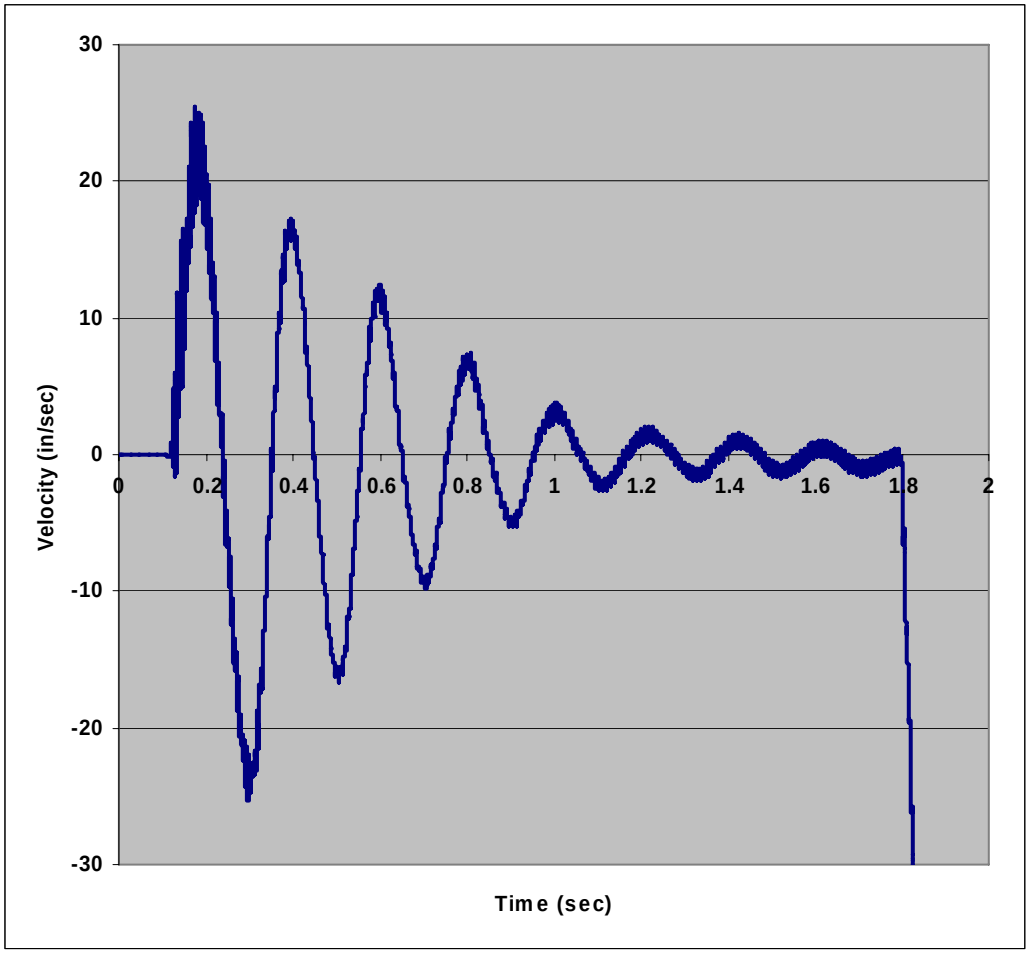

Figure 5.2-37: Phase I No Control Test Velocity

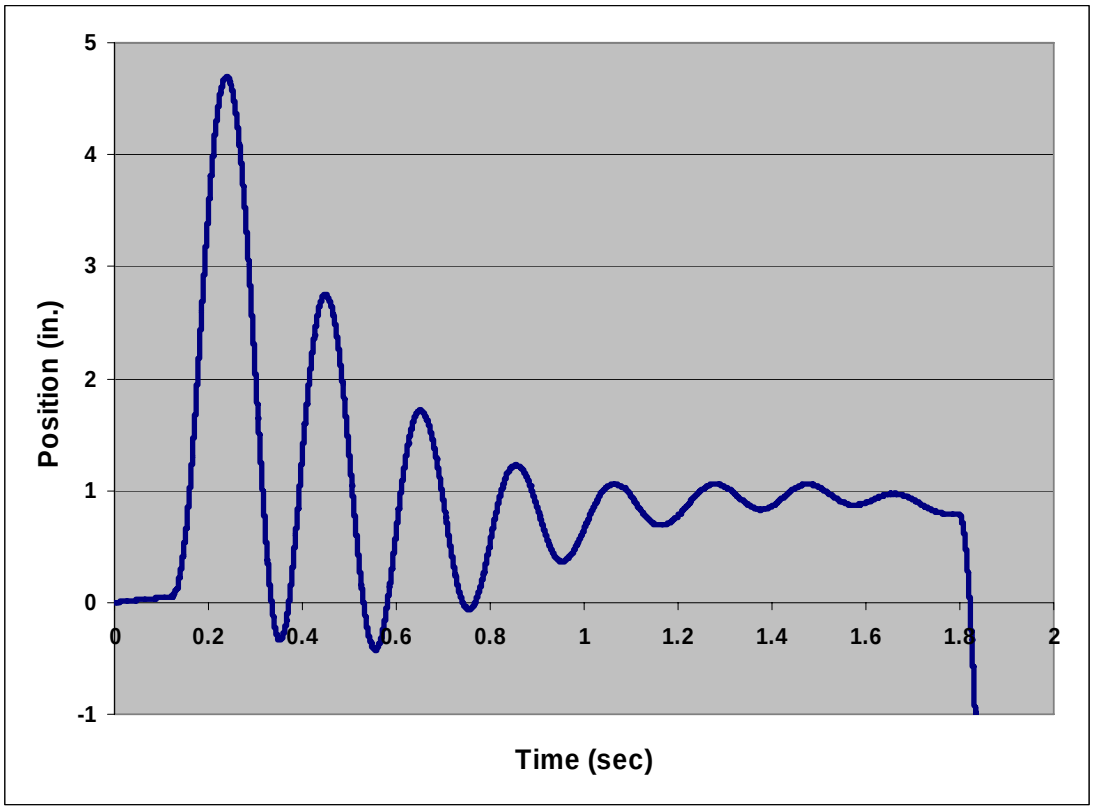

Figure 5.2-38: Phase I No Control Test Position

A noise damping limitation of the mechanical components is witnessed in all uncontrolled response test secondary motion plots around 1.6 seconds onwards due to both accelerometer and overall test hardware limitations. The accelerometer is an extremely low weight unit chosen to minimize the secondary weight while maintaining reasonable accuracy about the system response frequency. Accelerometers are commonly known for their superposition of Gaussian white noise with their output fundamental frequency signals, but unfortunately the unit used is slightly more sensitive than desired. Therefore observer numerical integration of the output signal for control system use and presentation is limited. Magnetically the overall test hardware itself is comprised of simple solenoids and corresponding secondaries which does not allow for the typical parasitic damping of small oscillations witnessed in full scale maglev systems. The secondary also consists of an

extremely low inertia structure which readily allows the introduction of a small disturbance motion from equilibrium oscillations in comparison to a full scale, large inertial maglev system. These accelerometer and overall test hardware factors do not greatly effect a large secondary oscillation such as the types of perturbations introduced for numerical simulation and testing, but the combination of these limiting mechanical factors produces a constant low oscillating noise around 0.5 g's in the accelerometer output signal. The accelerometer component of this noise is not generated from a real motion. The overall test hardware component of this noise is generated from real motion but is only an artifact of this test apparatus and not experienced in a large inertial maglev system. This noise strongly effects the controlled response data as discussed in Chapter 5.2.e.iv.

Observation of Figure 5.2-36, Figure 5.2-37, and Figure 5.2-38 indicates an inherent system damping. It is readily recognized from Figure 4.2-5 and Figure 4.2-8 that the mechanical secondary contact with the retaining sticks used in the final test apparatus introduces this retarding friction force. It is believed that the retarding force is solely based on mechanical friction and the stick to secondary clearance and secondary design itself do not allow a retarding force through an angular jamming of the secondary between the sticks. Figure 5.2-39 provides a schematic of the test geometry used to determine an approximate normal and friction force value for input into numerical simulations.

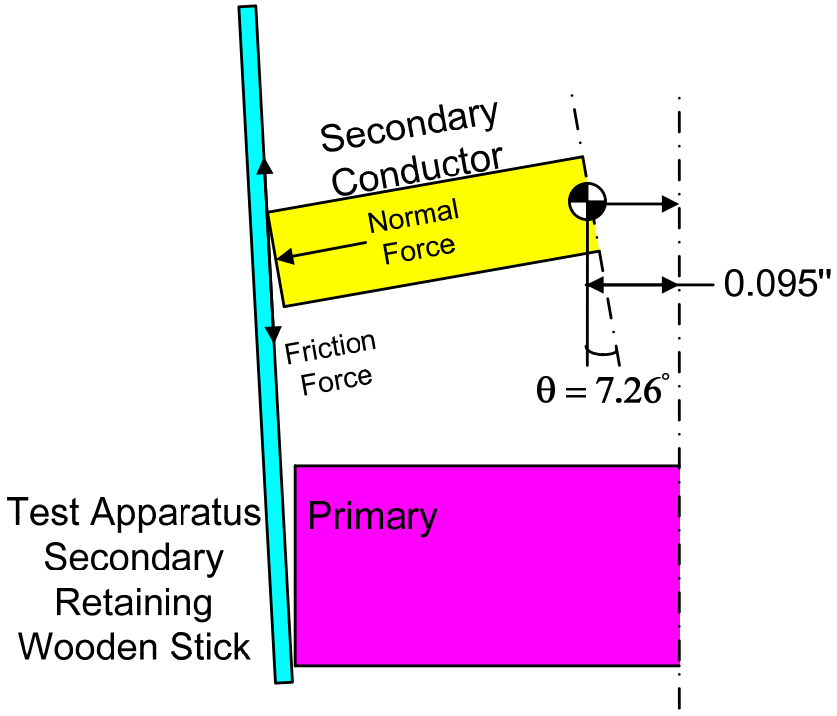

Figure 5.2-39: Phase I Test Apparatus Friction Force

Figure 5.2-40 presents the principal solenoid current for one of the identical solenoids used in this test. This information is useful for acquiring current amplitudes, current densities, approximate principal solenoid electrical time constants indicated by the signal rise and fall time from 0 A, and witnessing the primary to secondary magnetic flux linkage response or mutual inductance response to the secondary motion as indicated by the peak current oscillation.

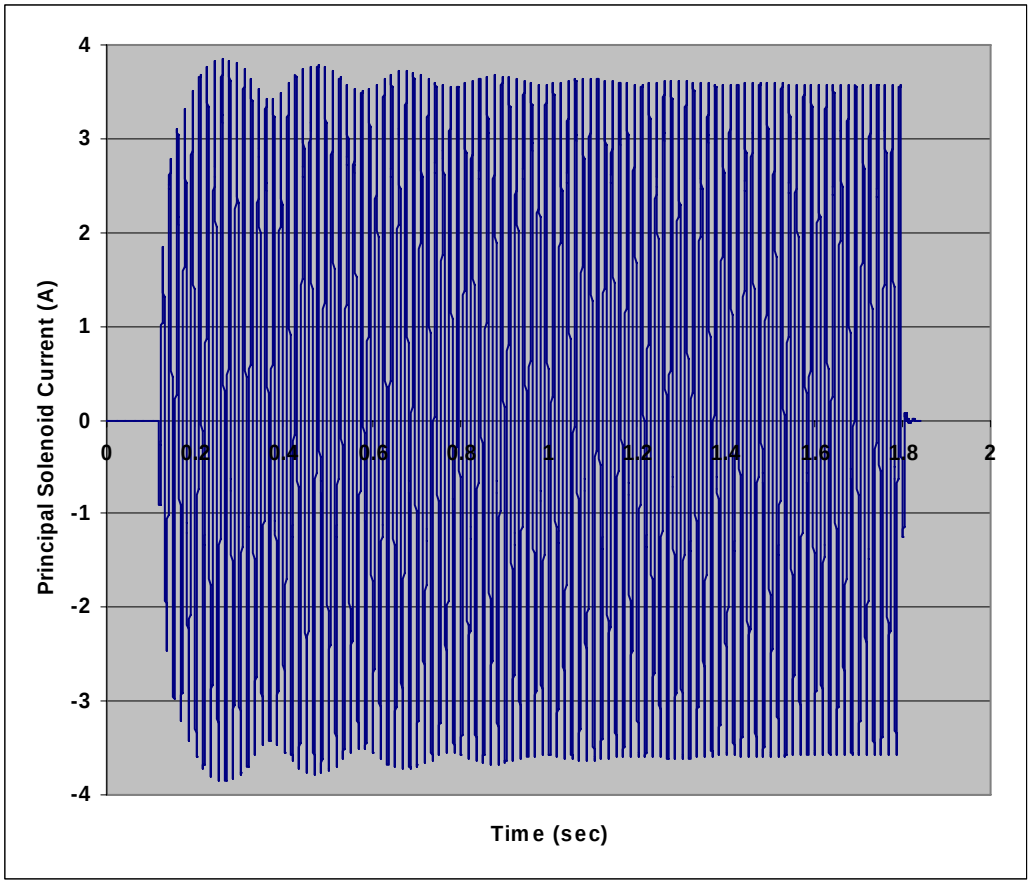

Figure 5.2-40: Phase I No Control Test Principal Solenoid Current

5.2.e.iv Phase I, Test #3: Controlled Response Test

The accelerometer, bipolar amplifier or B.O.P. control voltage input, and control solenoid current sampled raw data values are all presented in Figure 5.2-41.

The mechanical response period is approximately 10 milli seconds and the maximum acceleration is approximately 3 g's. Approximately three perturbation periods are experienced prior to complete damping of the perturbation force. The same approximate 0.5 g constant low oscillating noise in the accelerometer output signal as witnessed in the uncontrolled response test of Chapter 5.2.e.iii is also present in this controlled response test. The D.A.Q. hardware for all data channels in this test is set to sample input data at 50,000 samples per second per channel or 50 kHz which translates to a 0.02 milli second sampling period. This test is described in Chapter 4.2.c.iv and the test conclusions are presented in Chapter 6.2.d.ii.

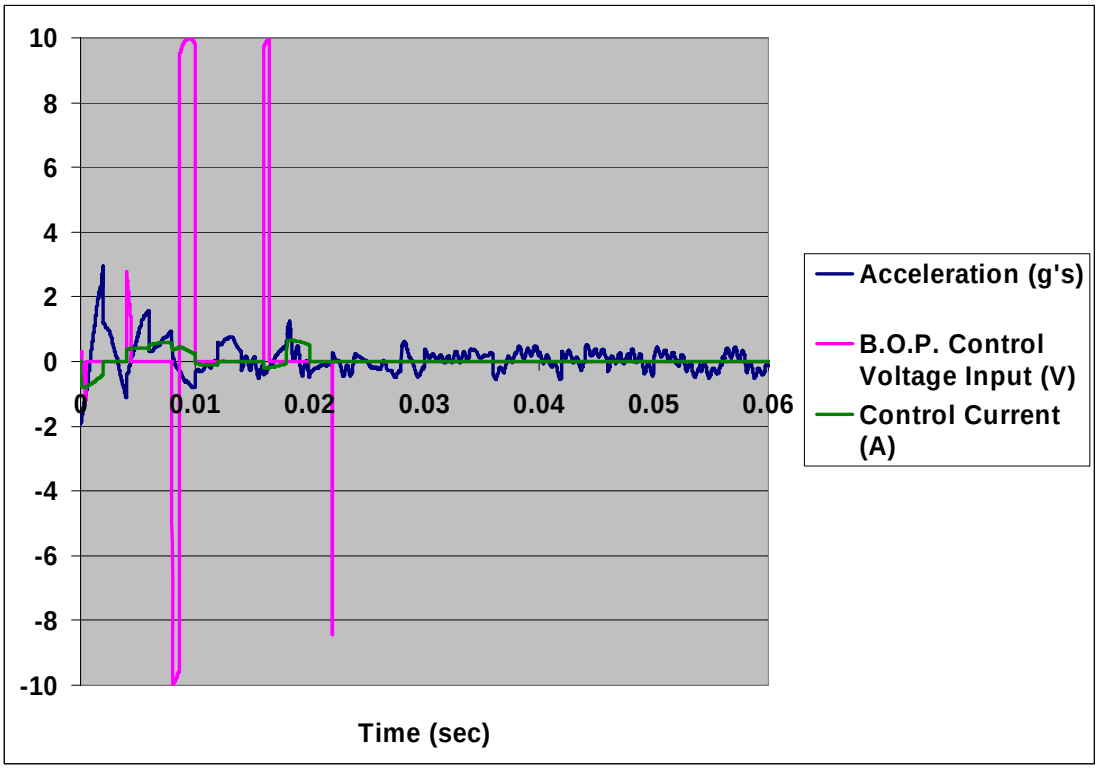

Figure 5.2-41: Phase I Control Test Accel. & Control Solenoid V & I

The introduction of the control solenoid periodically increased the secondary position dependent fundamental mechanical response frequency of the overall system by raising the system spring constant as demonstrated previously in the numerical

results of Figure 5.2-15. This increase is readily witnessed in the mechanical response period reduction from 200 milli seconds for the uncontrolled response test to 10 milli seconds for the controlled response test. Although a large portion of this 20 times increase is considered real since the control solenoid used provides a slightly greater magnetic pressure than a single principal solenoid, a portion is considered erroneous since the perturbation mechanical oscillation amplitude is rapidly approaching the Gaussian white noise amplitude which operates at a much higher frequency than the system mechanical motion frequency. A comparison of the Phase I uncontrolled to controlled response test is provided in Table 5.2-2.

Table 5.2-2: Phase I Uncontrolled to Controlled Response Test Comparisons

Phase I Response Test	Input and Test Apparatus Constants			Output		
	D.A.Q. Sampling Period	**Tested Solenoid Electrical (L/R) Time Constant**	**Accel. Output Signal Noise Level**	**# of Pert. Periods**	**Mechanical Perturbation Response Period**	**Max. Accel.**
	(msec)	**(msec)**	**(g's)**	**#**	**(msec)**	**(g's)**
Uncontrolled	0.1	Principal: 9.4 Control: 8.6	±0.5	7	200	9.5
Controlled	0.02		±0.5	3	10	3
Factor Decrease	5			2.33	20	3.17
Note: The Controlled Response test data has known limitations which leads to potential errors as discussed throughout Chapter 5.2.e.iv.						

The author must note that the controlled test output is not as accurate as the uncontrolled test output due to the author's home laboratory accelerometer limitations mentioned in Chapter 5.2.e.iii, control response test electrical hardware limitations, D.A.Q. limitations, and computer hardware limitations as suggested in Chapter 2.6.a.ii. Due to a lack of apparatus, a complete and proper test solution can only be acquired through a notion of ingenuity. Therefore careful examination of the control response test apparatus and results is now provided. At this lower amplitude the perturbation mechanical motion quickly damps away and only leaves the disturbance

motion from equilibrium oscillations which reside at a higher frequency than the original oscillating frequency. In this frequency range the accelerometer cannot properly distinguish between the accelerated motion and the Gaussian white noise. The control response test electrical hardware itself experiences an electrical response time limitation since the principal and control solenoid electrical time constants are both only slightly lower than the mechanical perturbation response period. Since the solenoid electrical time constants are not much lower than the perturbation response period a time lag will exist between the desired and actual solenoid full current times. Although the D.A.Q. hardware does not experience channel sweep limitations since the D.A.Q. board sweeps across all channels at 500,000 samples per second, the D.A.Q. hardware internal buffer does experience overflow issues which are due to both the D.A.Q. hardware and computer processor read rates allowable. Finally the control computer experiences processing speed limitations which delays the control response time beyond the desired control response time. These computer processing limitations are encountered due to both this increase in system response frequency as well as the need to maintain proper closed loop control.

A proper D.A.Q. and closed loop feedback control system would typically run a real time operating system processor kernel to help solve these limitation problems. Unfortunately a real time operating system setup is not available at the author's home laboratory at this time due to hardware limitations. Since the real time operating system processor kernel is not available and the existing system experiences control response lag time issues, the author tricked the control system into a desired response cycle. Referring to the fuzzy logic control inference system surface plot Figure 3.3-17, the controller demands a constant full voltage for the majority of secondary reference positions away from the desired nominal position as well as for the majority of negative or downward sloping secondary velocities. Noting these control triggers, the reference position is set to a constant full turn on value. Therefore the remaining trigger is the velocity direction and magnitude. In the control response test reported the author provided an extremely small downward mechanical impulse, just enough

to trigger the control system turn on state, moments prior to energizing the principal and control solenoids. When timed properly the final result, as indicated in Figure 5.2-41, is a rising control current amplitude approximately corresponding to the first negative secondary velocity motion. The inherent time lag of the system then provided the control turn on state approximately corresponding to each subsequent negative secondary velocity motion. Although this desired control trigger timing does not provide an optimized control output, it still has the desired effect of providing a high electromagnetic damping coefficient. Theoretically a real time operating system and corresponding control kernel would achieve an even better electromagnetic damping system response.

These accelerometer, electrical hardware, and processing limitation difficulties stemming from the increased system frequency produces control data with assumed aliasing issues. The author believes that this aliasing produced control test data output potentially missed a few signal amplitudes. This affects the maximum amplitude value, the oscillation period, and the final settling times. These restrictions unfortunately did not allow a proper comparison of simulation and test data. This being stated, the position amplitude, the oscillation period, and final settling times witnessed between the controlled and uncontrolled response tests still undeniably differed by multiplicative factors although perhaps not as great as the factors presented in Table 5.2-2. Therefore, although the control response test data potentially missed a few key points, the overall output oscillation maximum amplitude, oscillation period, and final settling time trends are generally correct and identify that the controlled system responds much more favorably than the uncontrolled system by quickly dampening the perturbation oscillation within a much shorter settling time and a lowered overall oscillation amplitude.

5.3 PHASE IV

5.3.a Governing Physical Laws

The same governing physical laws outlined in Chapter 5.2.a for Phase I apply to this analysis.

5.3.b Analytical & Computational Component Modeling

The same basic analytic analysis which fed the numerical analysis is presented in Appendix A.1. The only main difference between Phase I and IV is the magnitude of inputs and outputs. An example of the Phase IV closed form analytic solution secondary radius dependent magnetic flux density tangential and normal real component values are provided in Figure 5.3-1. An example of the Phase IV closed form analytic solution secondary radius dependent control solenoid levitation forces, F_z and F_{lev}, and gravitational force, F_g, versus air gap distance, z_g, is provided in Figure 5.3-2.

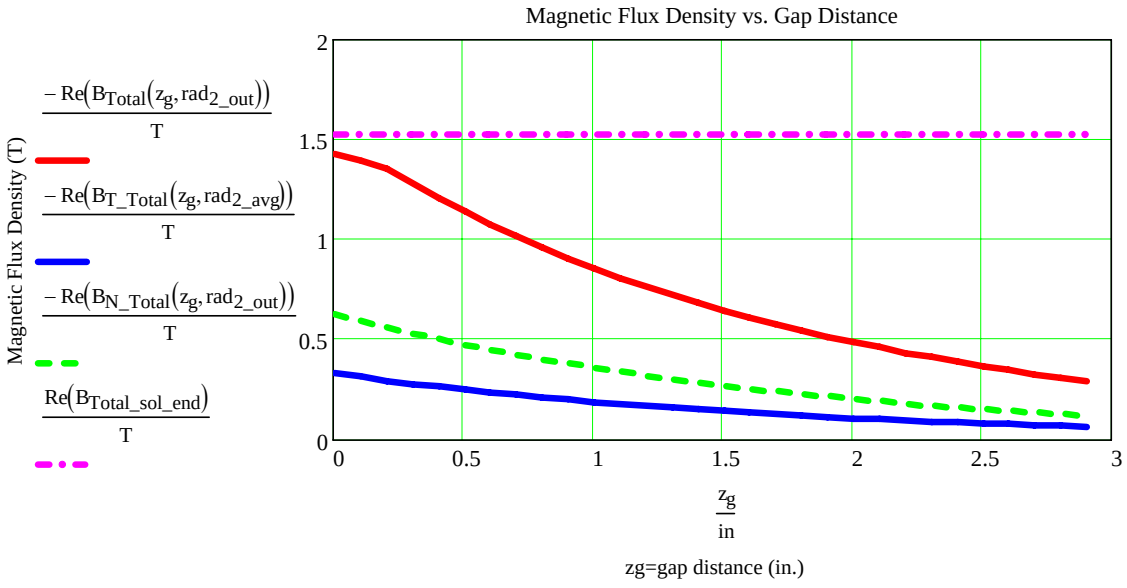

Figure 5.3-1: Phase IV Analytic Model Control Sol. B_T & B_N vs. Gap Dist.

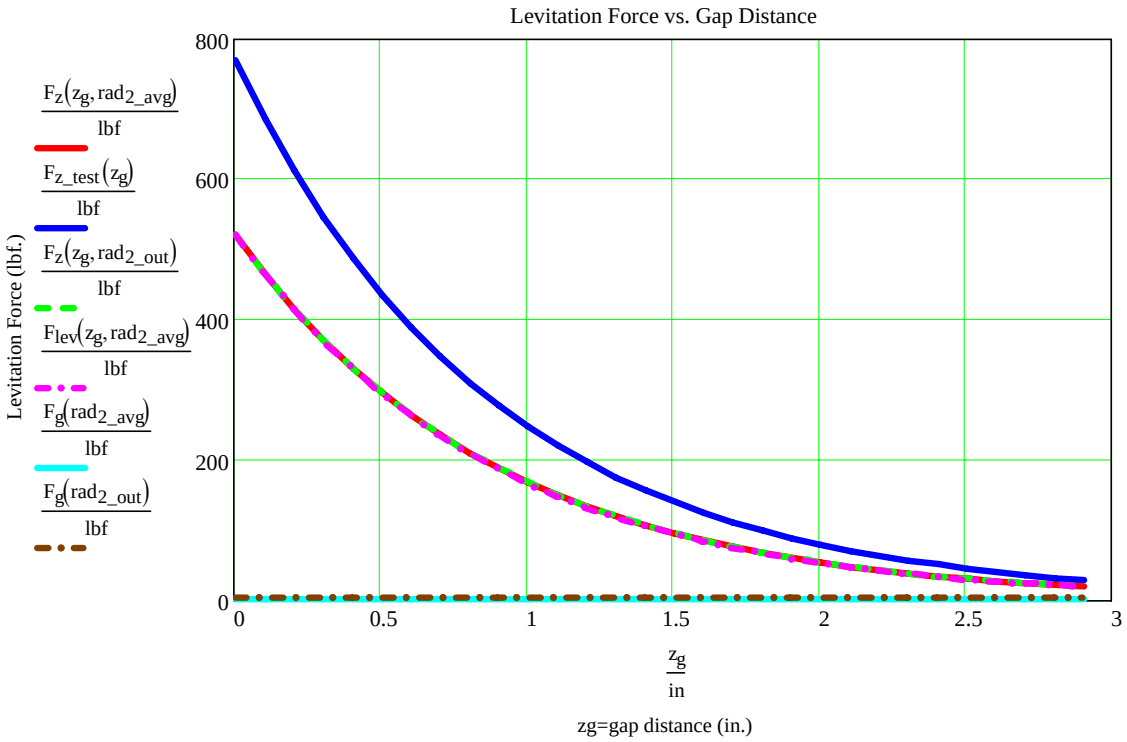

Figure 5.3-2: Phase IV Analytic Model Control Sol. Vertical Force vs. Gap Dist.

No detailed computational component modeling occurred for Phase IV directly. Phase I computational values along with scaling laws are adequate for the purposes of this paper.

5.3.c Numerical System Modeling

5.3.c.i Overall

The Simulink® model shown in Figure 5.3-3 provides the top level model of the Phase IV numerical simulation. The multitudes of lower level Simulink® models are provided in Appendix C.1.b. This model implements the Phase IV simulation dynamics and control equations outlined in Chapter 3.6. The supplemental Matlab® solenoid design, Phase I input, and Phase I output function files that are called by this Simulink® model are listed in Appendix C.2.a, C.2.c.i, and C.2.c.ii respectively.

Phase IV simulations assume that the maglev vehicle has attained a steady state propulsive velocity 80 $\frac{m}{\sec}$ prior to the onset of each analysis and maintains this steady state propulsion throughout the analysis. The principal magnetic spring constants and total system mass of this system are chosen to maintain a 1 inch air gap in both the z and y axis directions. This air gap choice is small enough to allow a reasonably good system forcing function with enough range of motion to witness the underdamped oscillations and the effects of the introduced magnetic air gap damping control solenoids.

Besides the vertical levitation and lateral guidance principal and control coil options used for simulating and controlling this system, there is also a z axis only principal and control coil active option. This option removes the y axis constraints and acts as if the z axis of the maglev vehicle sits upon a perfectly conducting plane with free motion in the x and y axis plane. Therefore the vehicle will levitate and rotate freely, but the absence of lateral coils removes the guidance complexity and

concern. This z axis active only simulation and control permutation is used for model debugging and verification purposes.

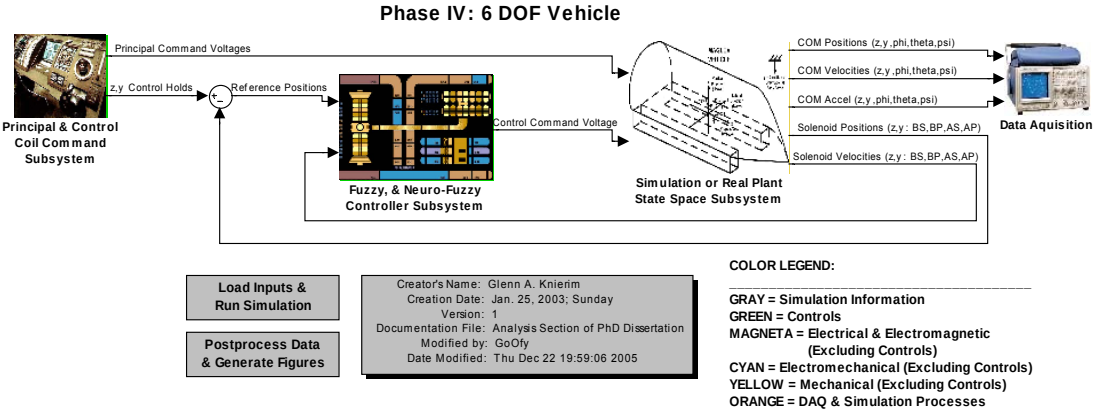

Figure 5.3-3: Phase IV Numerical Simulation - Top Level Model

In this analysis the principal and control coil pairs have individual control algorithms. This level of control is acceptable for this proof of concept analysis, but fine tuning the overall secondary vehicle body oscillations via the secondary's C.O.M. acceleration are also required for a final maglev control system.

5.3.c.ii Initial Mechanical Offset

Since this is the first presentation of Phase IV output, this opportunity is used to show plots that demonstrate general system performance. Future Phase IV sections only produce plots that illustrate the point discussed in that particular section and it is understood that the general system performance trends do not change.

Solenoid Setup – Typical Operation

The following set of plots is for a principal solenoid with two coils wound with 18 AWG wire and operated with a constant AC voltage and a control solenoid with one coil wound with 18 AWG wire where all other parameters between the solenoids are equal. As in Phase I the plots in this section demonstrate for this type of system, the control solenoid has an order of magnitude less available energy than the

principal solenoid. Therefore the control solenoid is meant for damping control only and cannot act as a back up principal solenoid.

Numerical Modeling with Soft Computing Fuzzy Control

The secondary z axis center of mass mechanical outputs are provided in Figure 5.3-4. The first plot of the z axis mechanical motion indicates that the system initially experiences an increasingly large z axis amplitude oscillation. When 1.5 seconds has passed the controller turns on and successfully dampens the oscillation down to a relatively low amplitude level within 1 more second. This damping rate is readily increased by increasing the control coil repulsive force. The second plot provides the secondary z axis velocity. The third plot provides the principal and control solenoid forces acting on the secondary with reference to the weight or gravitational force of the secondary.

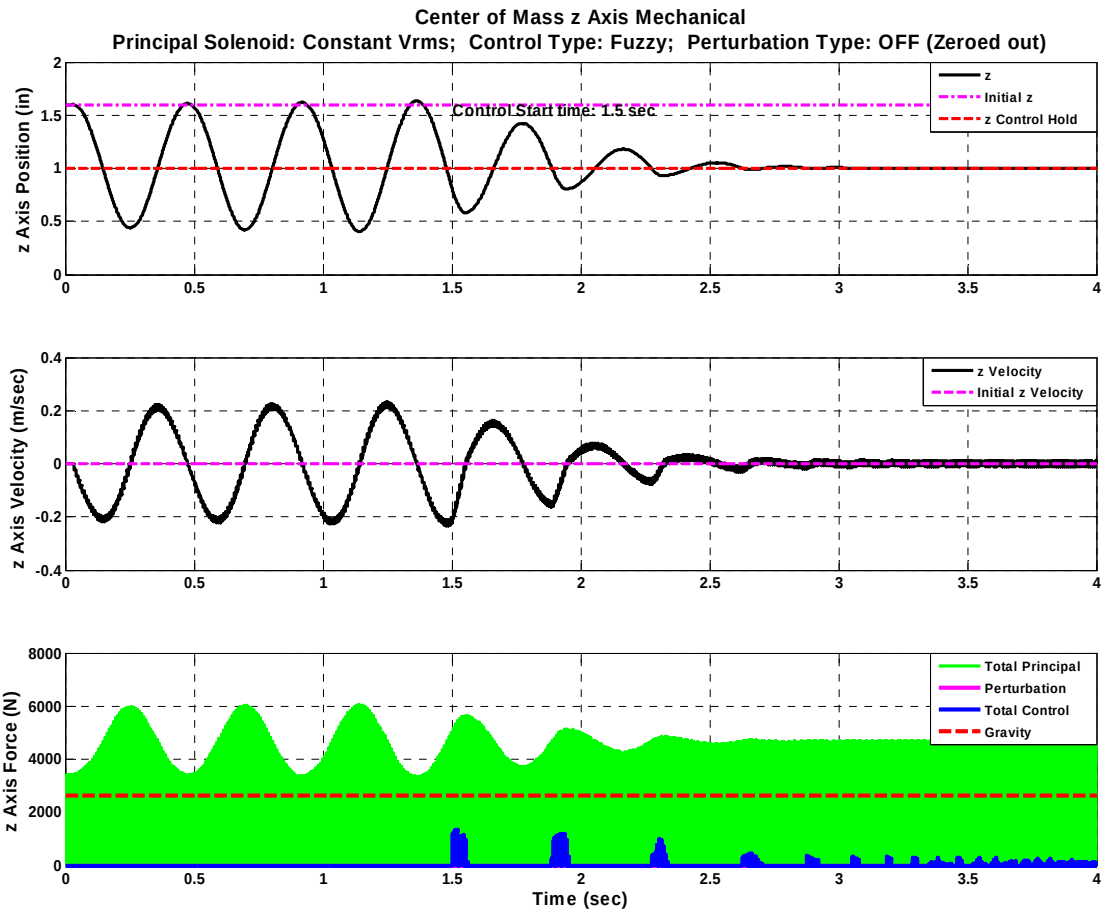

Figure 5.3-4: z Axis C.O.M. Mechanical Plots with Offset Initial Conditions

The secondary y axis center of mass mechanical outputs are provided in Figure 5.3-5. The first plot of the y axis mechanical motion indicates that the system initially also experiences an increasingly large y axis amplitude oscillation. When 1.5 seconds has passed the controller turns on and successfully dampens the oscillation down to a relatively low amplitude level within 1.5 more seconds. This damping rate is readily increased by increasing the control coil repulsive force. The second plot provides the secondary y axis velocity. The third plot provides the principal and control solenoid forces acting on the secondary. Since the lateral guidance y axis does not contend with gravity, it typically operates with a much lower magnetic force value than the vertical levitation z axis. In Phase IV system presented throughout this

paper, the lateral guidance force output is approximately 1.6 times lower than the vertical levitation force output for the same gap distance value.

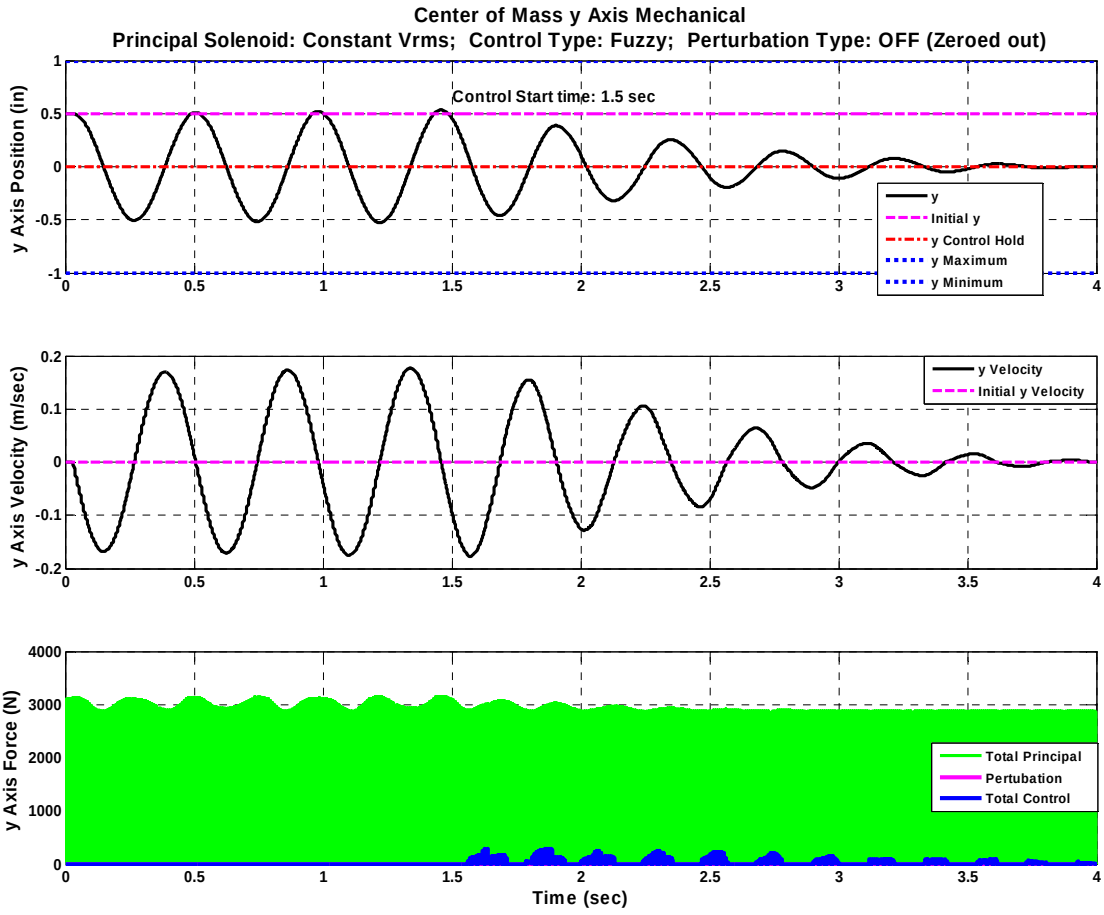

Figure 5.3-5: y Axis C.O.M. Mechanical Plots with Offset Initial Conditions

The secondary angular axes center of mass mechanical outputs are provided in Figure 5.3-6. The first plot of the angular axes mechanical motion indicates that the system initially also experiences a steady to increasingly large angular axes amplitude oscillation. When 1.5 seconds has passed the controller turns on and successfully dampens the oscillation down to a relatively low amplitude level within 1 more second. This damping rate is readily increased by increasing the control coil repulsive

force. The second plot provides angular perturbation torques where for this case are set to zero.

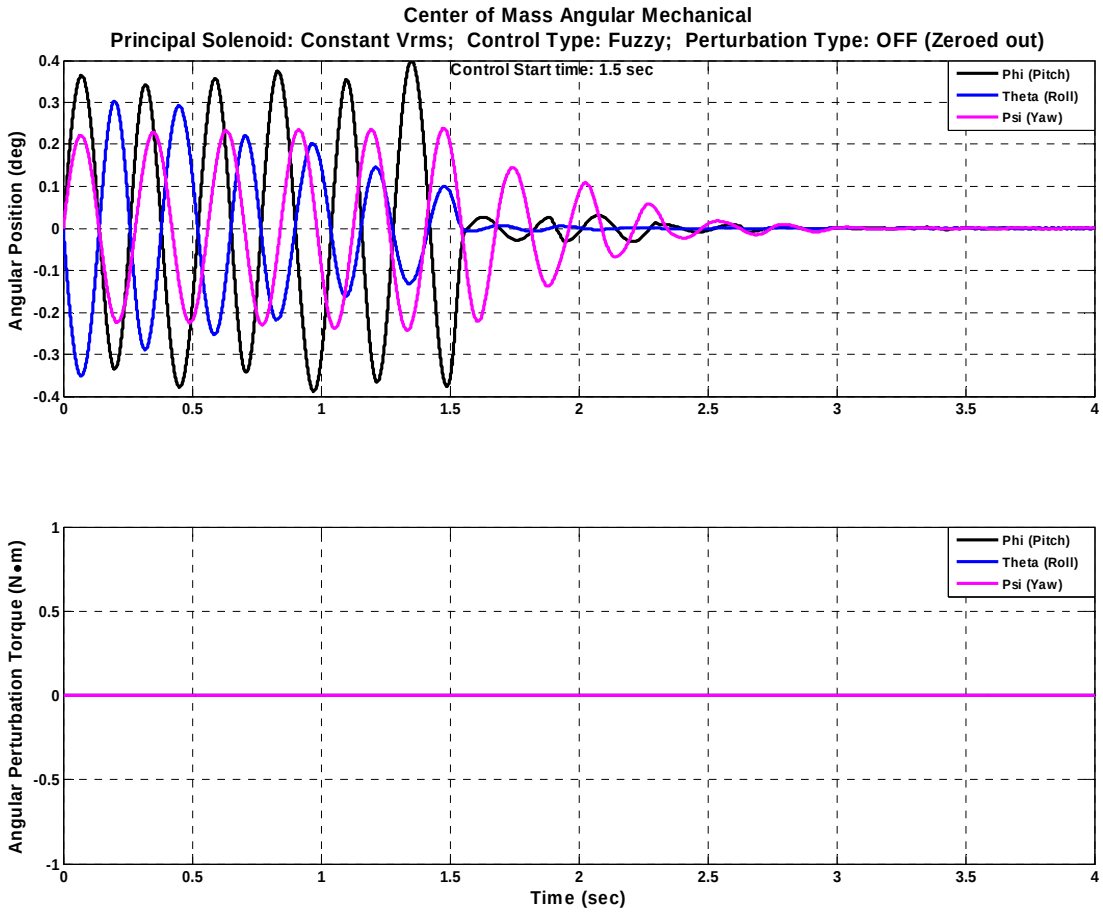

Figure 5.3-6: Angular Axes C.O.M. Mech. Plots with Offset Initial Conditions

The BS, bow and starboard, vehicle solenoid position z and y axis mechanical outputs are provided in Figure 5.3-7. The first plot of the z axis and the third plot of the y axis mechanical motion indicate that these solenoids initially experience an erratically large z and y axis amplitude oscillation. When 1.5 seconds has passed the controller turns on and successfully dampens the oscillations down to a relatively low amplitude level within 1 more seconds for the z axis and 1.5 more seconds for the y axis. This damping rate is readily increased by increasing the control coil repulsive

force. The second and forth plots provide the respective secondary z and y axis principal and control forces. Figure 5.3-8, Figure 5.3-9, and Figure 5.3-10 provide the z and y axis values for the BP, AS, and AP vehicle solenoid positions respectively. A composite plot of the z and y axis position values for all solenoid vehicle positions is provided in Figure 5.3-11. A comparison of the vehicle solenoid position plots to the various C.O.M. plots above illustrates how both the translational and rotational D.O.F. effect the vehicle body motion. In future chapters only the composite position plot is provided for the individual solenoid mechanical displacements.

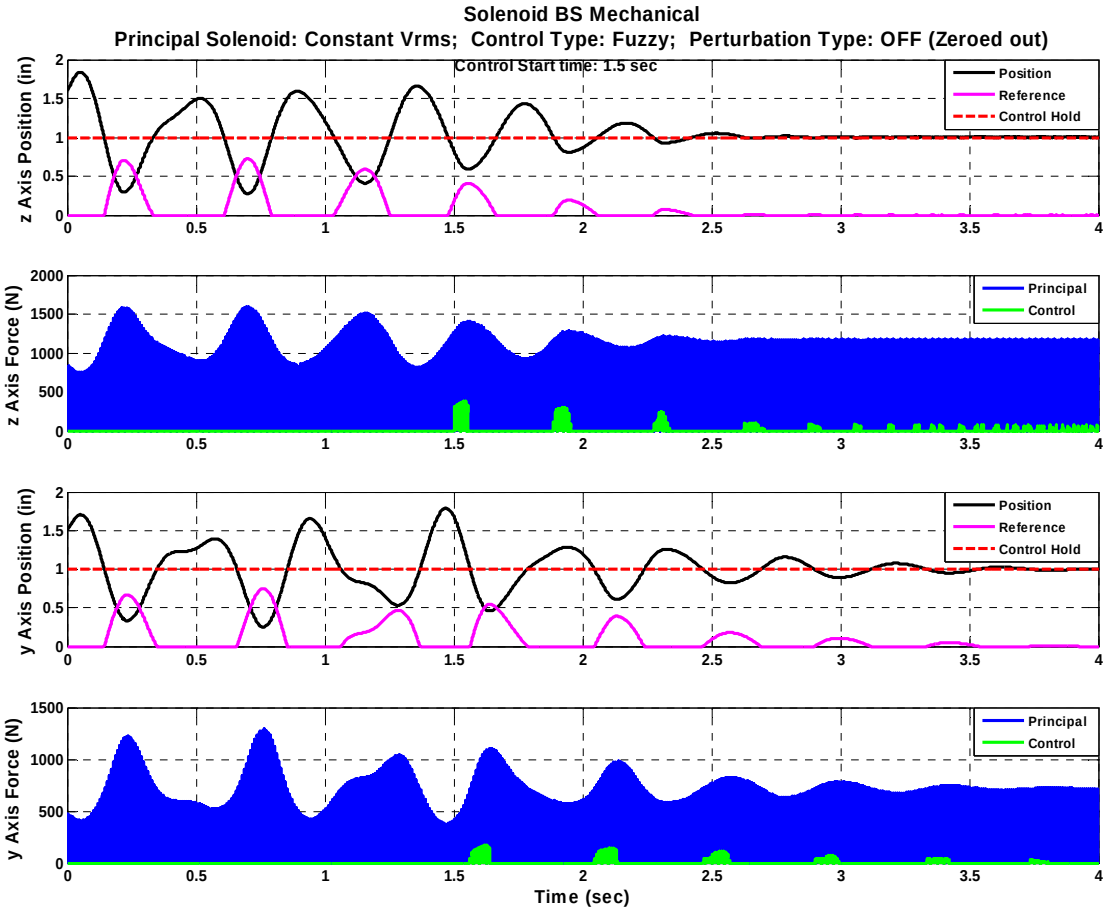

Figure 5.3-7: z & y Axis BS Mechanical Plots with Offset Initial Conditions

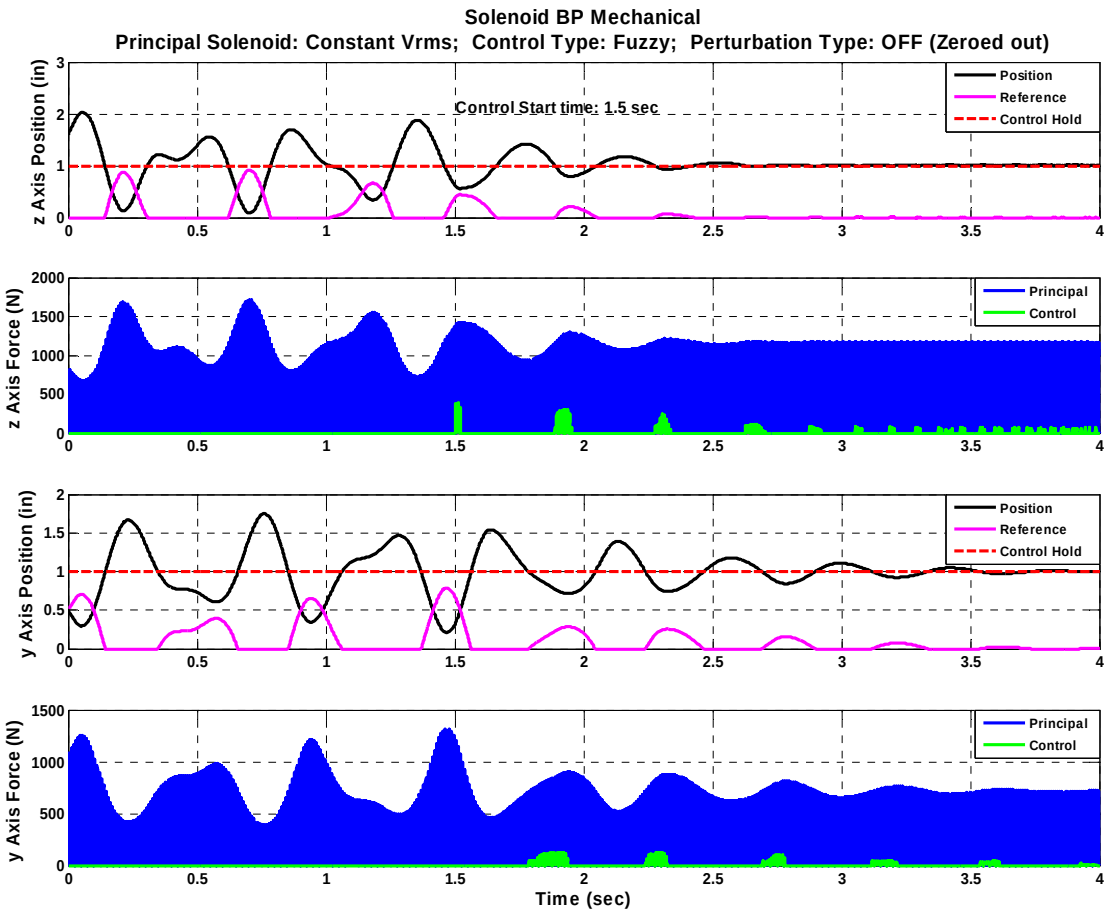

Figure 5.3-8: z & y Axis BP Mechanical Plots with Offset Initial Conditions

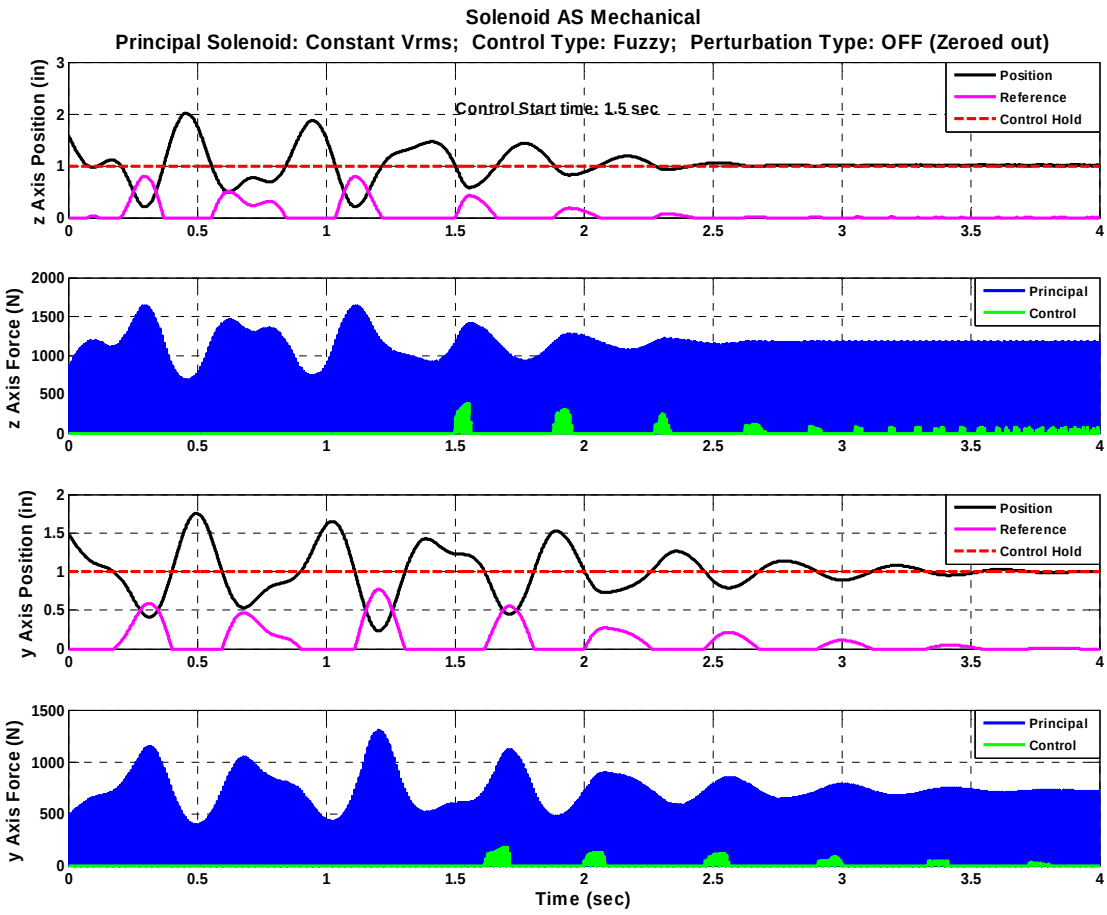

Figure 5.3-9: z & y Axis AS Mechanical Plots with Offset Initial Conditions

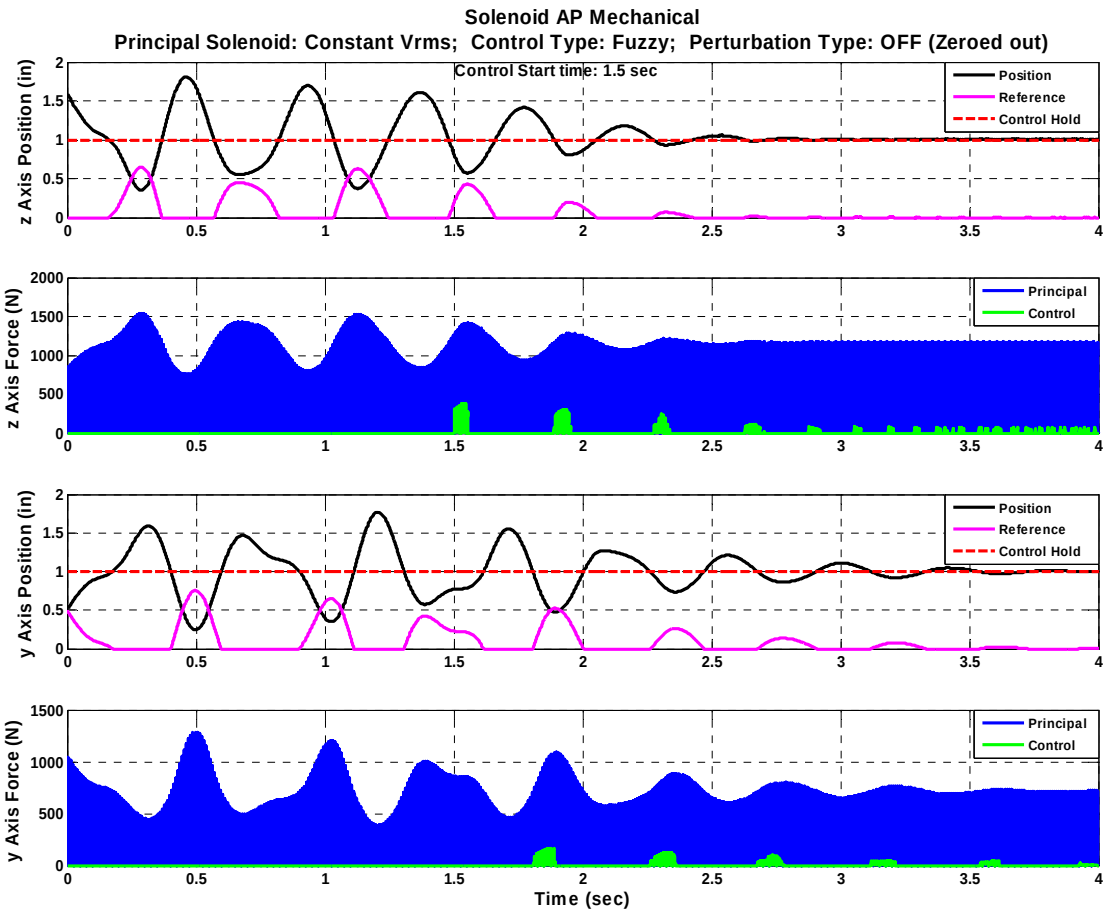

Figure 5.3-10: z & y Axis AP Mechanical Plots with Offset Initial Conditions

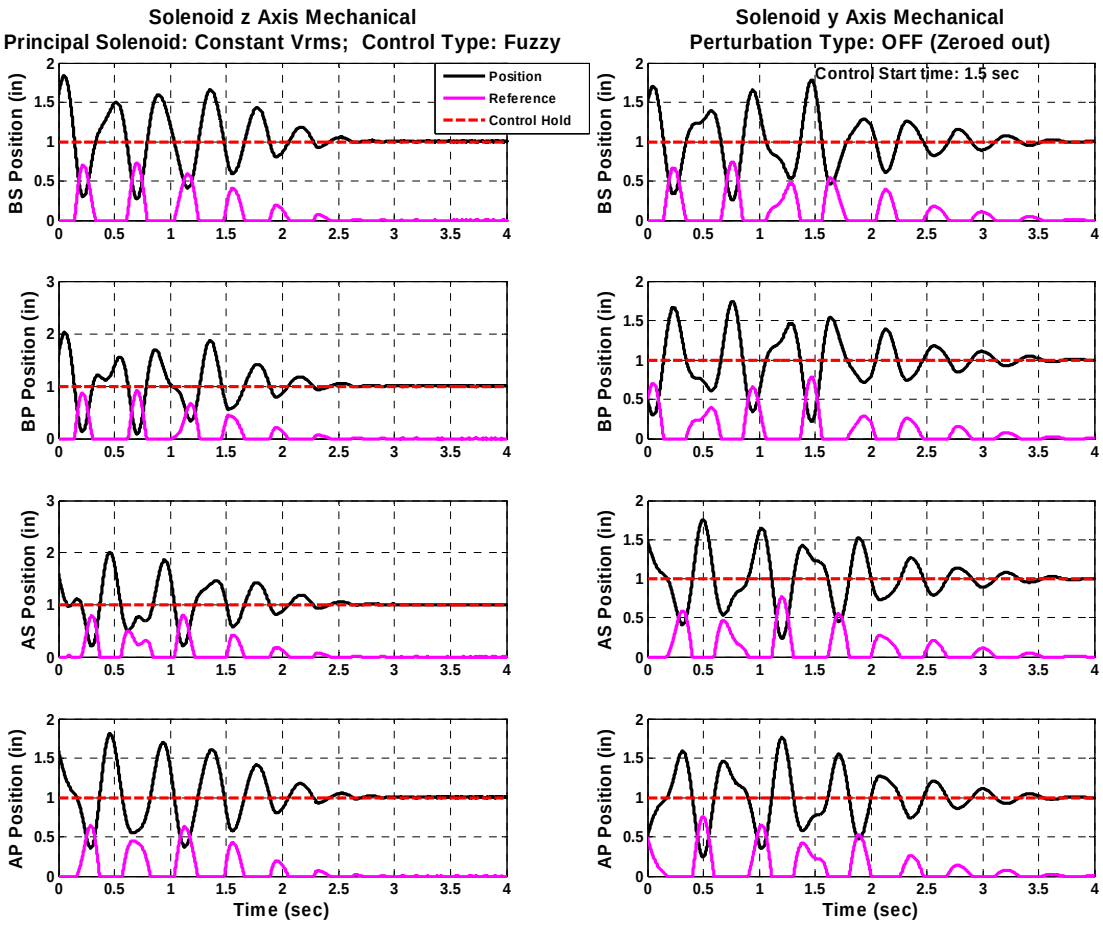

Figure 5.3-11: z & y Axis Mechanical Plots with Offset Initial Conditions

The energy and power output of Figure 5.3-12 indicates that the amount of oscillation energy and power in the system which includes to the amount of energy required to maintain the desired air gap superimposed with the secondary oscillation energy. The first and third plots of control magnetic spring energy correspond to the amount of energy removed from the secondary motion for each control oscillation period. The control energy works to remove the secondary kinetic energy. The maximum kinetic energy occurs during the secondary mechanical half stroke position where the velocity is maximized. For the first plot of the z axis the gravitational potential energy peaks and valleys occur in an opposing sequence to the principal

solenoid magnetic spring energy. This chosen control solenoid has less than half the available energy of the principal solenoid. Therefore the control solenoid is meant for damping control only and cannot act as a back up principal solenoid. The second and forth power plots have the same general trends as their respective energy plots. Besides trends the power plots also have a sign convention where positive principal power indicates an increasing secondary potential energy as principal power flows into the secondary, negative principal power indicates a decreasing secondary potential energy as the secondary approaches the minimum oscillation point, positive control power indicates the flow of every being removed from the starboard side secondary oscillation, and negative control power indicates the flow of energy being removed from the port side secondary oscillation.

The energy components are listed as instantaneous energies compared to a running sum of each energy component. The instantaneous energies provide the instantaneous and periodic energy magnitudes and trends but not the total component energy summation which is the required energy form if an energy balance calculation is desire. The instantaneous energy output is adequate for the purposes of this paper.

As introduced in Chapter 1.2.c, the energy and power plots are for the secondary motion viewpoint only. The total system energy and power, which includes the primary electrical source and electromagnetic transmission across the air gap, are not considered since this paper is a proof of system concept only and not a final design effort.

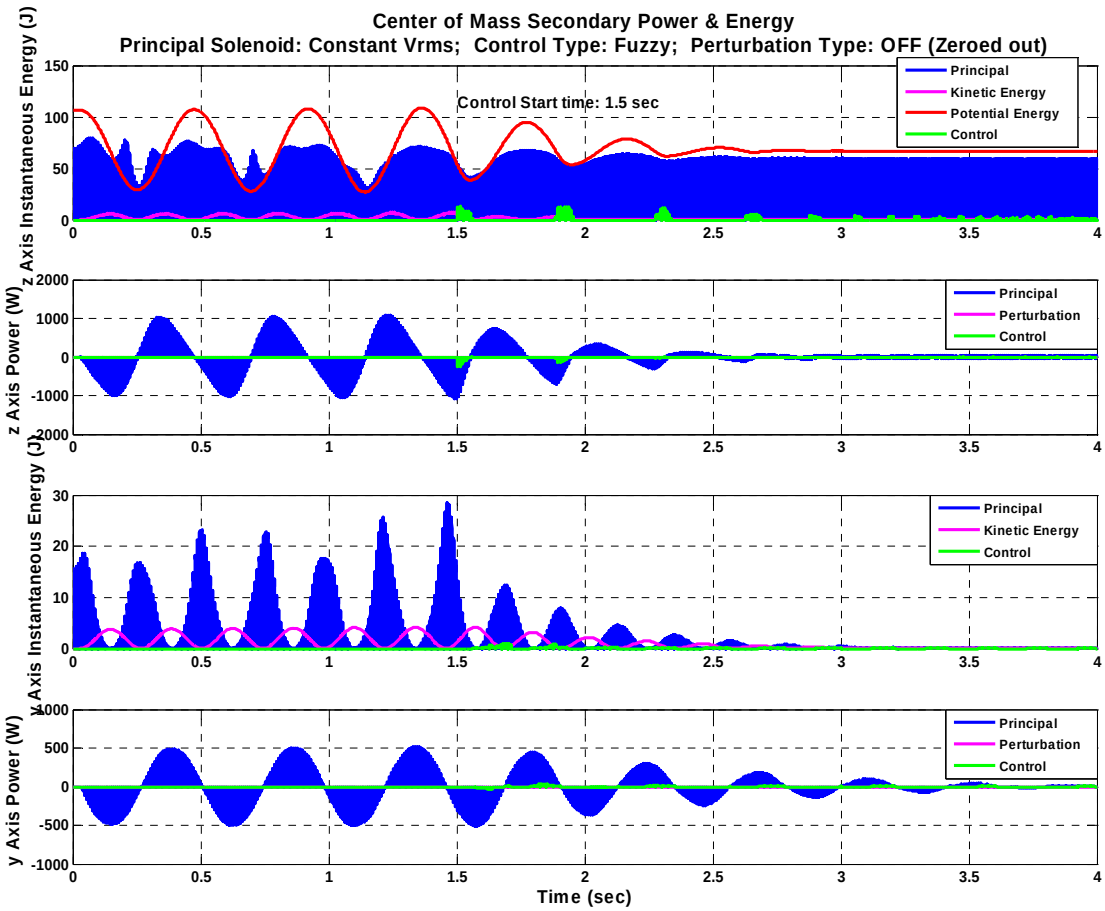

Figure 5.3-12: Power & Energy with Offset Initial Conditions

The first system response output plot of Figure 5.3-13 indicates that the electrical time constants are approaching the mechanical time constants, but they are still 2 to 3 times lower than the mechanical time constants. Therefore the electrical system time response is still fast enough to achieve the required secondary principal and control force values, but caution must be maintained in this area. The second plot compares the principal to control magnetic spring constants. As expected in this system the principal magnetic spring constant is approximately an order of magnitude larger than the control magnetic spring constant. The final plot provides the mechanical system natural resonant frequency for the combined principal and control coil system.

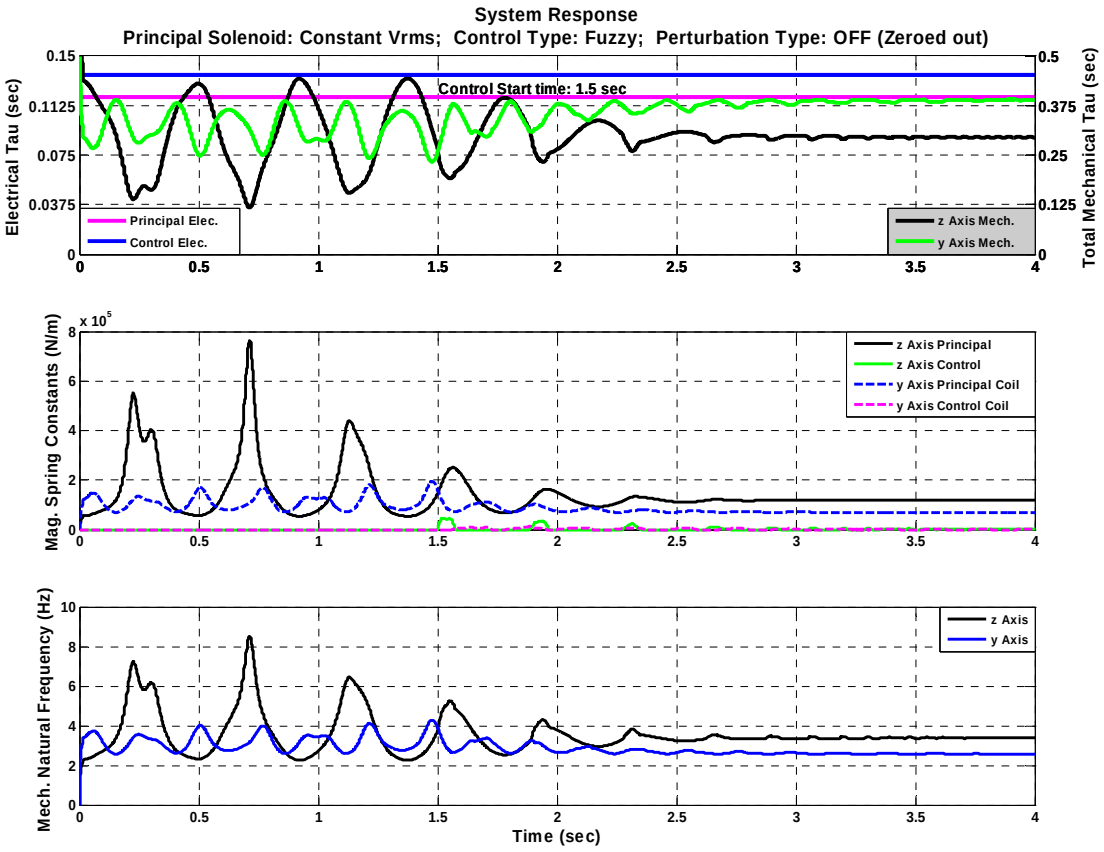

Figure 5.3-13: System Response with Offset Initial Conditions

The electrical output of Figure 5.3-14 for both the z and y axis BS principal and control solenoids indicates that the system initially experiences only the principal coil response on each axis. The first plot of source voltages indicates that when 1.5 seconds has passed the controller turns on and continues to operate by energizing the control coils whereas the principal coils remains on throughout the simulation. The second plot provides the z axis solenoid source currents and control voltage turn on times. The third plot provides the same information for the y axis. These current plots show the 2 times difference between the principal and control solenoid currents as well as the control current turn on and turn off lag with respect to the control voltage turn on times. These plots also provide the control coil currents in the control coils with respect to a naturally cooled, steady state safe wire current value. Note that the coil wire currents exceed the typical safe continuous duty currents of the wire. This basic comparison shows that the control coils are acceptable for the short term operation required for this feasibility study. There is no need to perform a similar comparison of the principal coil currents since this type of principal system is only used for simulation purposes here and is far too inefficient to ever implement in a final design.

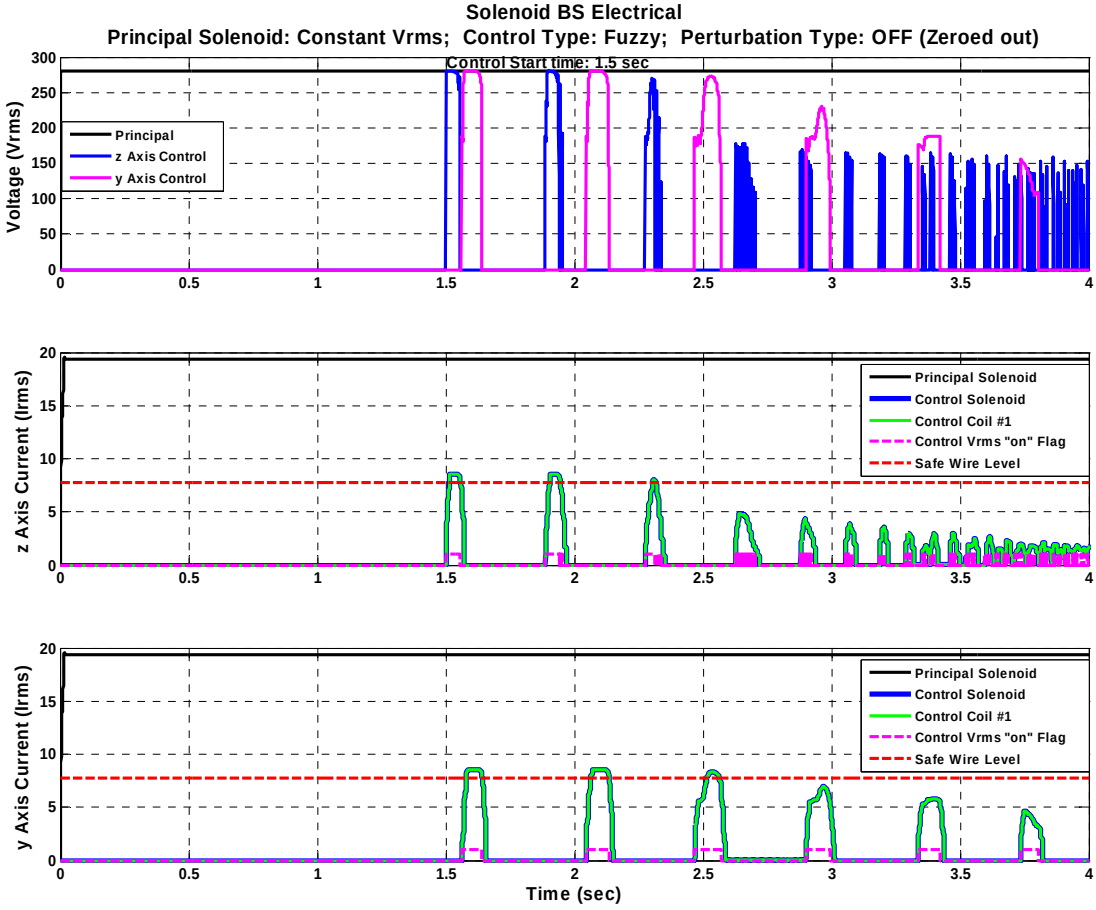

Figure 5.3-14: Electrical Plots with Offset Initial Conditions

The magnetic flux density tangential component for both the z and y axis BS principal and control solenoids is provided in Figure 5.3-15. The first plot provides the z axis values. The second plot provides the y axis values. Only the tangential B which interacts with the secondary J to produce the repulsive force is shown. The peak saturation value approximation, where the magnetic flux density suddenly changes from no saturation to completely saturated, is exceeded on the principal coil z axis peak plot but not the y axis plot. Since the relative permeability of the primary iron is only slightly above unity, the value used here is 4.673, the effects of complete saturation are not severe.

The magnetic flux density tangential component magnitudes are presented below. The magnetically based magnetomechanical values such as force, pressure, and spring constant are all derived directly from complex number manipulation of the Lorentz force equation real component $\left[\text{Real}\left(J \times B^{*}\right)\right]$ as indicated in equation (3.104), but both the J and B components are complex as they enter this cross product and hence it is the total complex components that are multiplied to form the magnetomechanical outputs prior to truncation of the imaginary component. Therefore instead of retaining convention which focuses uniquely on the real form of the B to achieve a feel for the B, the simulation in this paper tracks both the real and magnitude components and chooses to report the magnitude component of the B in the plots below.

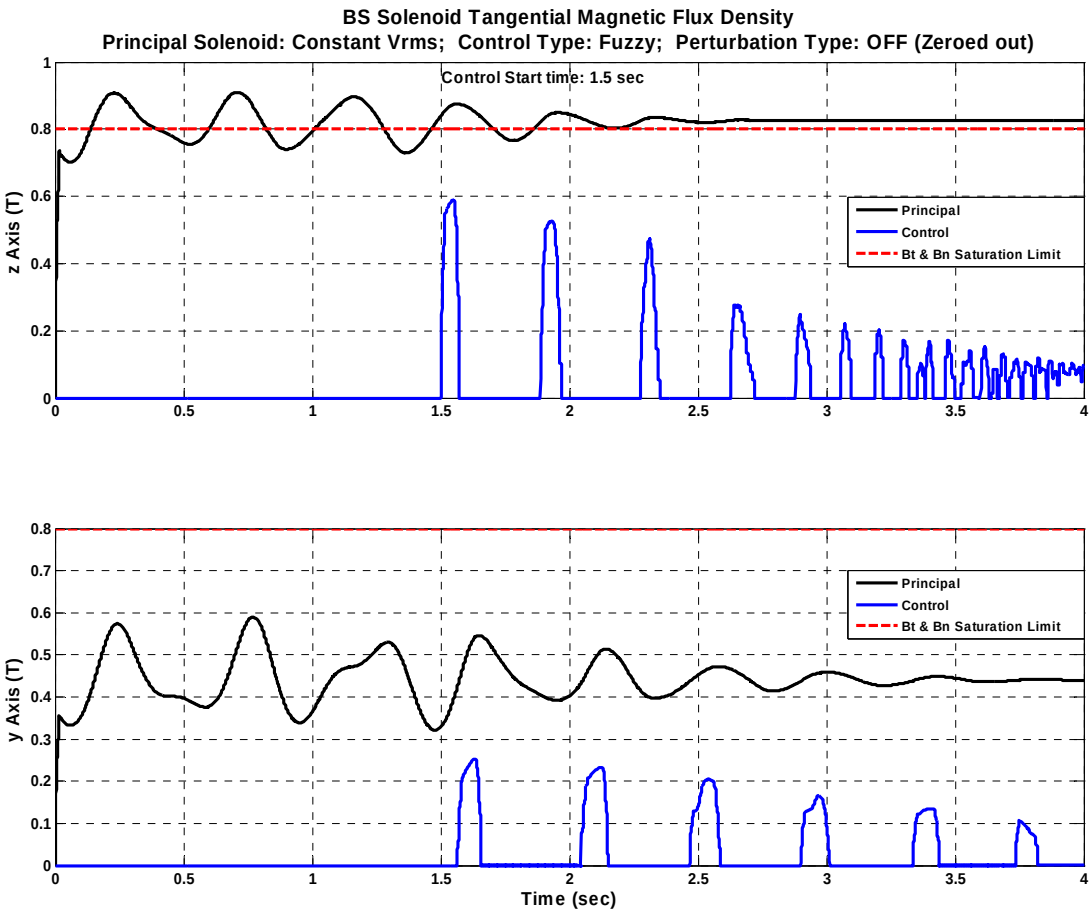

Figure 5.3-15: Tangential Magnetic Flux Density Plots with Offset Initial Cond.

The first order z and y axis thermal output analysis of the solenoid coils is provided in Figure 5.3-16. The first plot, which provides the solenoid heat generation, also indicates the system initially experiences only the principal coil response. When 1.5 seconds has passed the controller turns on and the controller continues to intermittently inject a thermal load into the control coils. The second plot shows the various coil temperature rises due to internal heat generation minus free convective and radiative cooling. This plot shows that the inefficient principal coil wire temperatures are elevating faster then 0.75°C every second whereas the intermittently power control coils are ratcheting up in temperature at a slower rate. For a

demonstration setup of this system this principal and control solenoid temperature rises are acceptable for the short term operation required for this feasibility study, but both temperature rises must be monitored closely during actual tests.

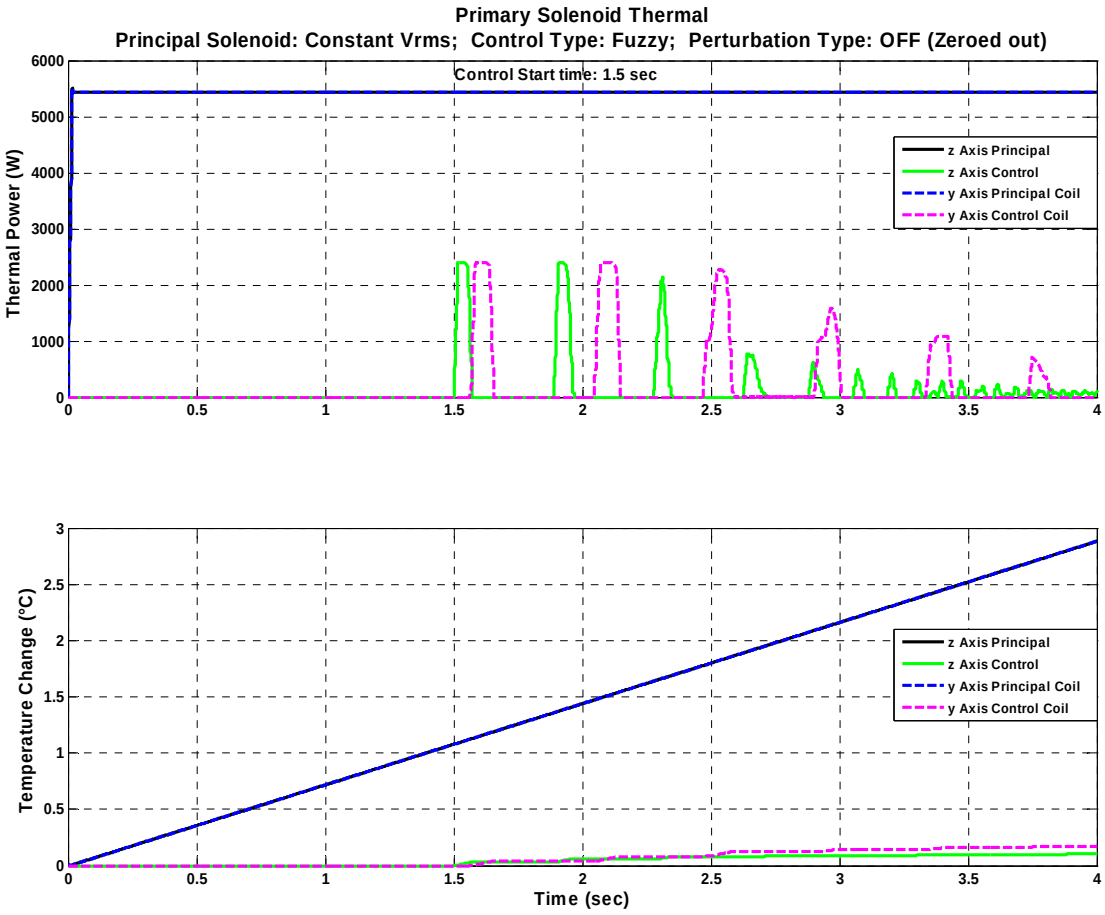

Figure 5.3-16: Primary Solenoid Thermal Plots with Offset Initial Conditions

5.3.c.iii Initial Mechanical Offset with 2x Vrms Down Pulses

Solenoid Setup – Extreme Operation

The following set of plots is for identical principal and control solenoids both with two coils wound with 18 AWG wire found only in Chapters 5.3.c.iii and 5.3.c.vii for Phase IV. The principal solenoid is operated with a constant AC voltage that

experiences two voltage down pulses from full voltage to 0 voltage for 0.25 seconds each and occurs at 0.5 seconds and 1.5 seconds. The control solenoid has the same available energy as the principal solenoid and therefore the control solenoid is meant for damping control as well as a back up principal solenoid during the two voltage down pulses.

Numerical Modeling with Soft Computing Fuzzy Control

The mechanical outputs of Figure 5.3-17, Figure 5.3-18, Figure 5.3-19, and Figure 5.3-20 indicate that the fuzzy controller maintains an extremely stable system control response during both the first and second voltage down pulses which occur at 0.25 and 1.25 seconds respectively as indicated in the energy and power plots of Figure 5.3-21 and the electrical plots of Figure 5.3-22. In this case the control coil completely assumed the roll of the principal coil with no extra control rule allocation than the original control rules. Upon reinstatement of the principal coil after each down pulse the mechanical oscillations damped out and approached the optimum values within 0.5 seconds for the z axis and under 0.25 seconds for the y and rotational axes. Therefore this is an acceptable controller for this type of extreme disturbance.

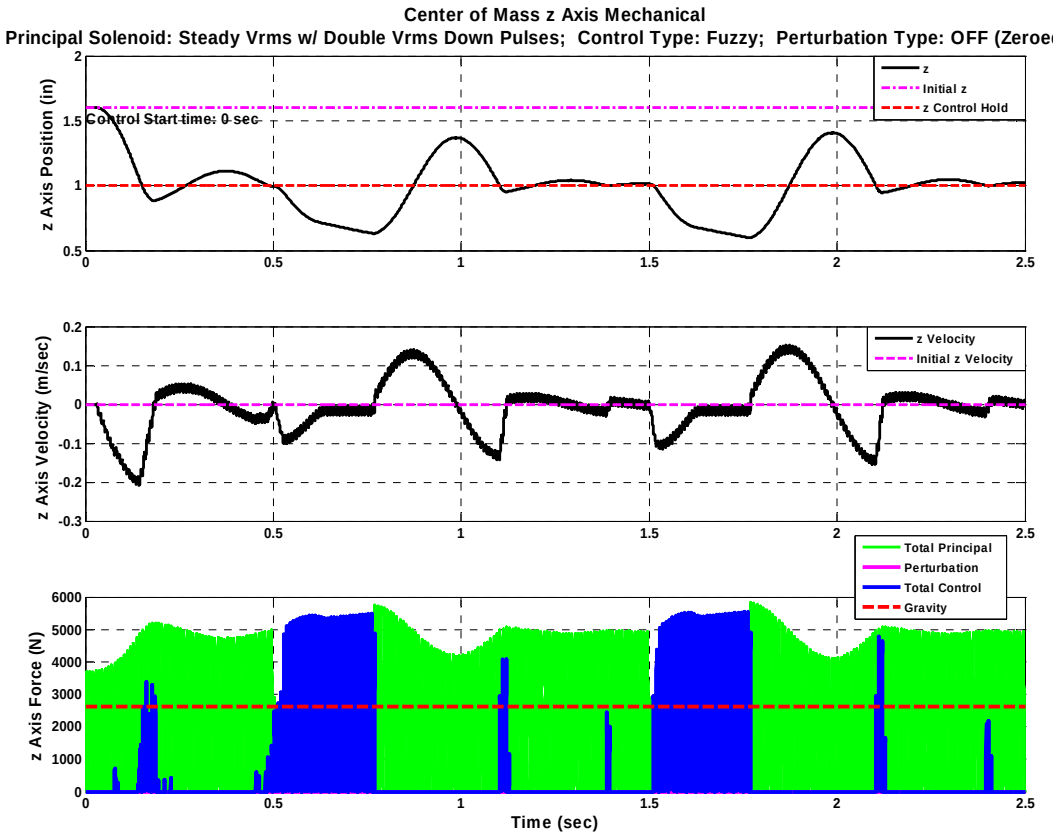

Figure 5.3-17: z Axis C.O.M. with 2x Vrms Down Pulses & Fuzzy Control

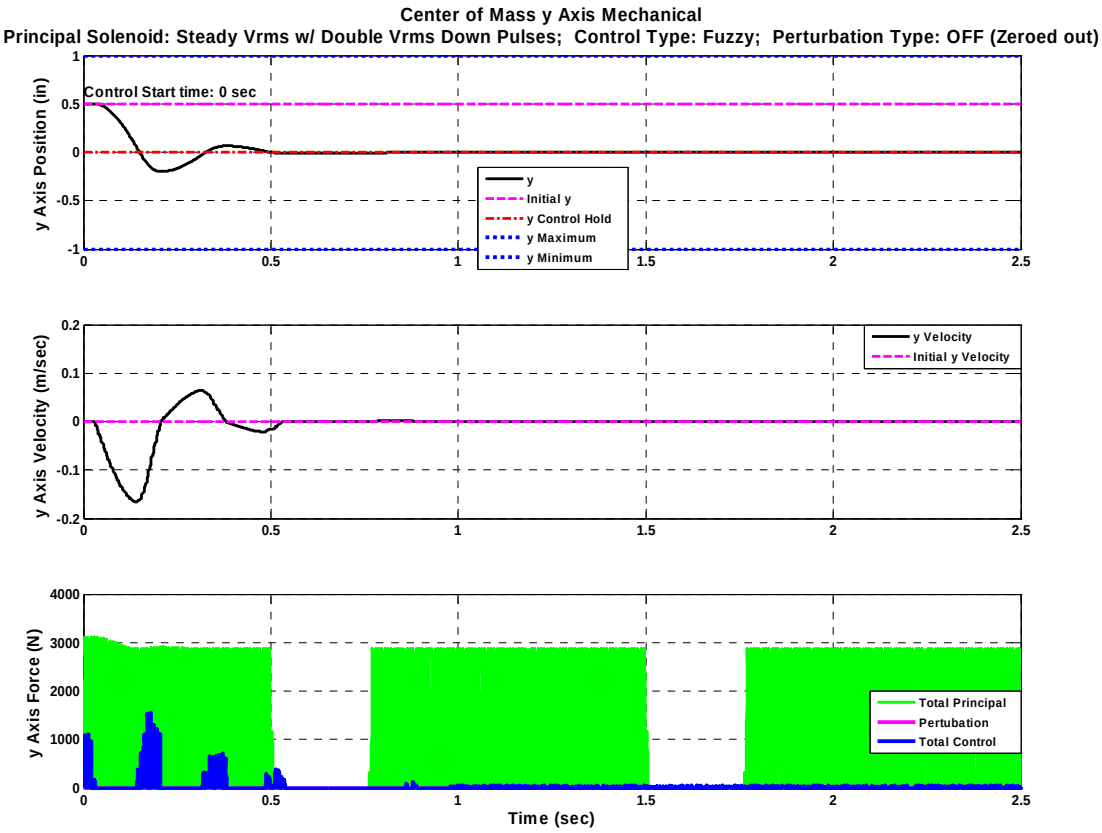

Figure 5.3-18: y Axis C.O.M. with 2x Vrms Down Pulses & Fuzzy Control

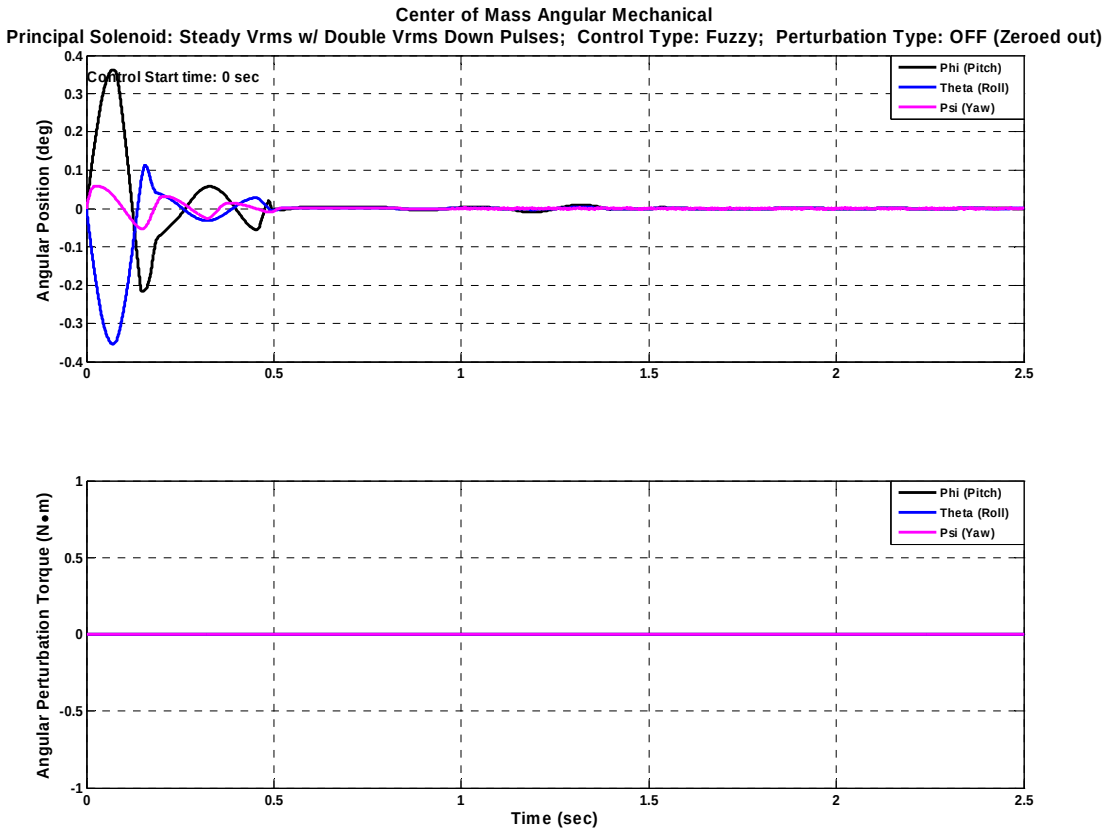

Figure 5.3-19: Angular Axes C.O.M. w/ 2x Vrms Down Pulses & Fuzzy Control

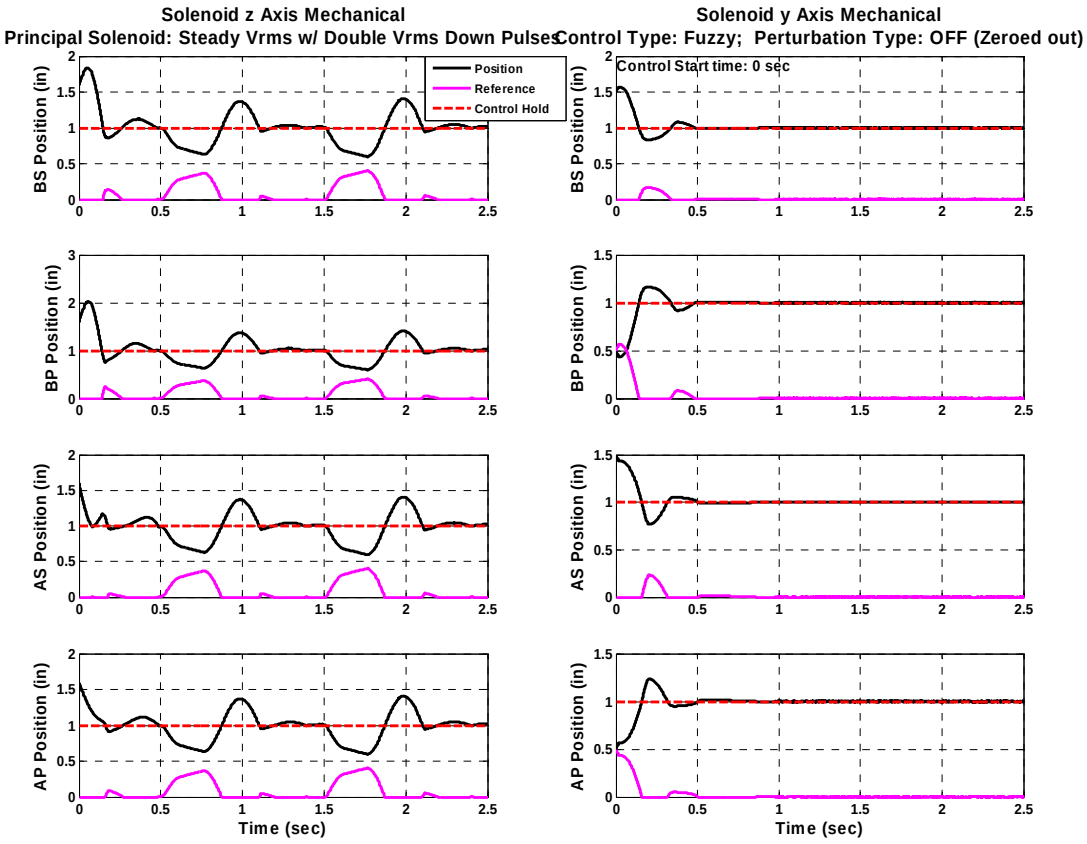

Figure 5.3-20: z & y Axis Mech. with 2x Vrms Down Pulses & Fuzzy Control

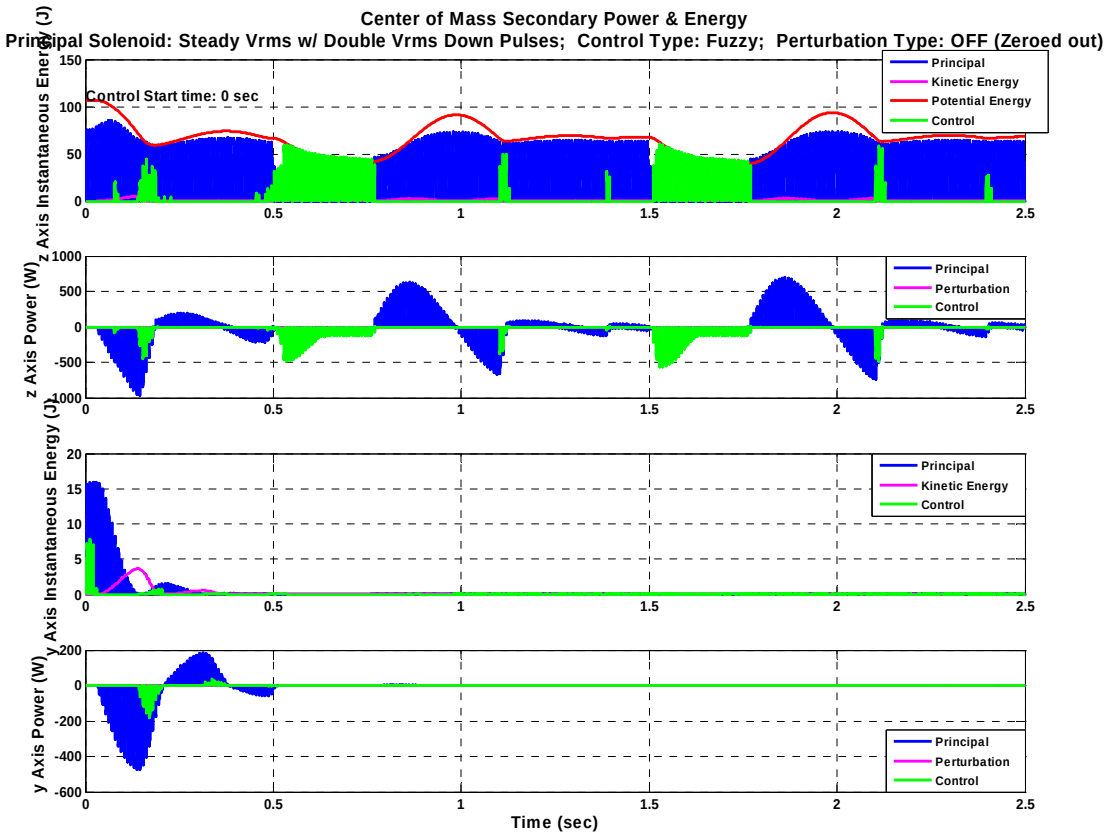

Figure 5.3-21: Power & Energy with 2x Vrms Down Pulses & Fuzzy Control

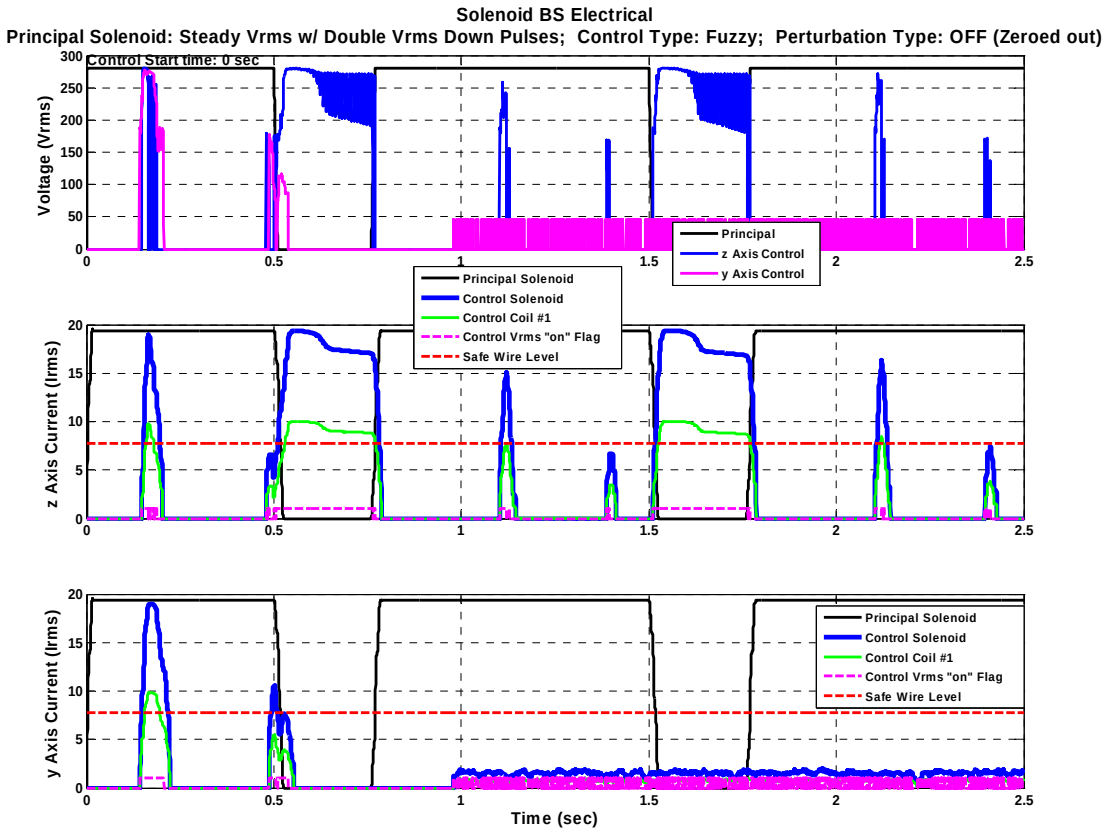

Figure 5.3-22: Elec. Plots with 2x Vrms Down Pulses & Fuzzy Control

5.3.c.iv Sinusoidal Response

The sinusoidal perturbation frequency values come from the step response median resonant frequencies for each D.O.F. which are provided in Chapter 6.3.a.iii. A common sinusoidal frequency witnessed in maglev system operation is a mechanical variation in the guideway track. An example is this track variation is the track to track set distance interface. Such mechanical variations produce a propulsive velocity dependent, vertical periodic disturbance into the system. This sinusoidal perturbation is meant to represent the worse case scenario of the periodic disturbance occurring at the magnetic air gap natural frequency.

In this study Figure 5.3-23, Figure 5.3-24, Figure 5.3-25, and Figure 5.3-26 indicate that although the control system dampens the sinusoidal perturbations, the

oscillations still retain a relatively high magnitude. The power and energy effects of these oscillations are witnessed in Figure 5.3-27 . The z axis, which experiences a higher translational oscillation than the y axis, peak to peak oscillation amplitudes are still in the range of 0.5 inches 4.5 seconds after the onset of the control system. Although this type of worst case sinusoidal oscillation in every control D.O.F. at a high perturbation magnitude should never sustain itself in actual operation, this case still identifies the potential need for a higher force control solenoid.

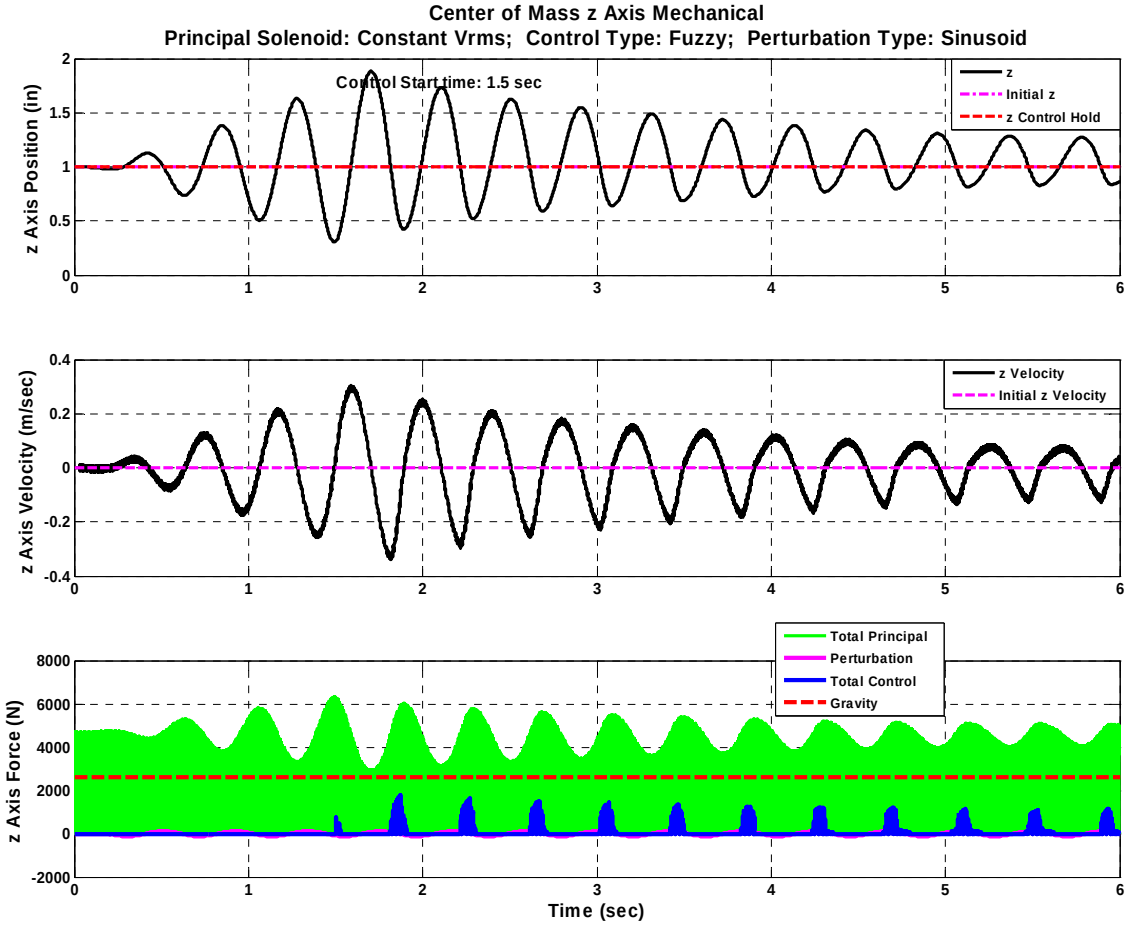

Figure 5.3-23: z Axis C.O.M. Mechanical Plots with Sinusoidal Perturbation

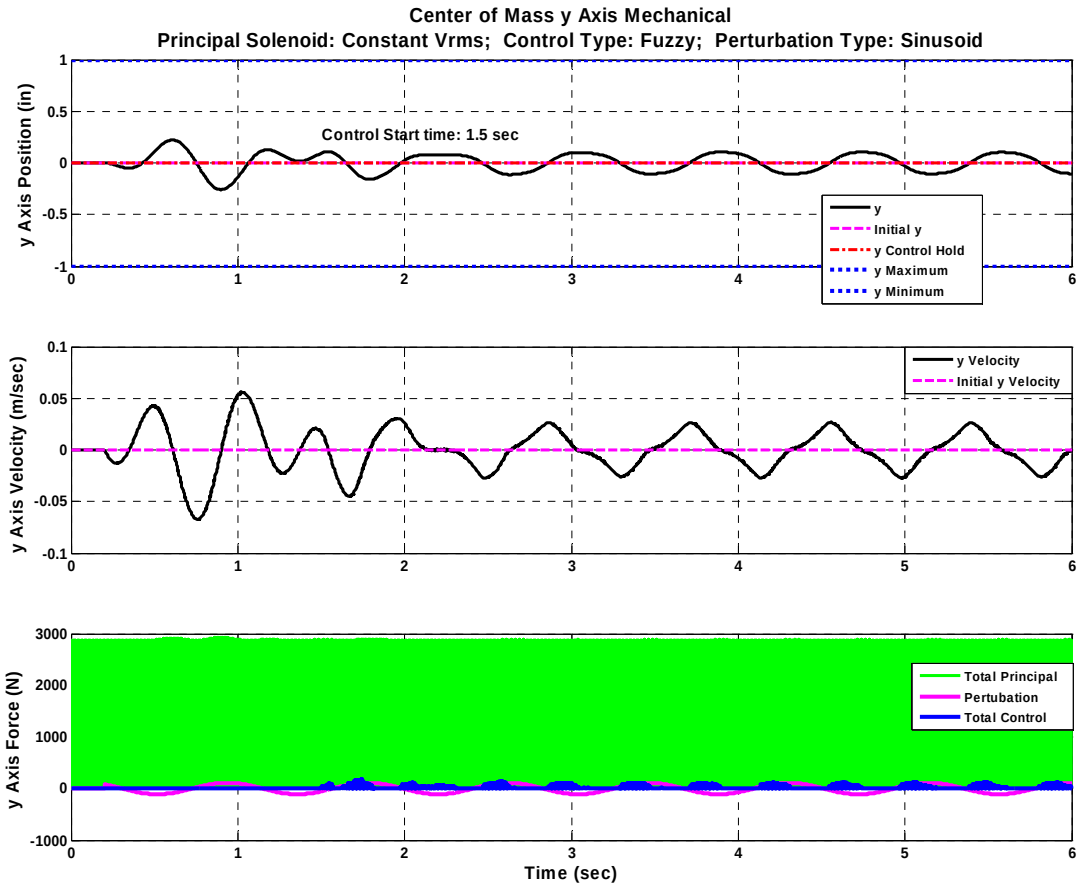

Figure 5.3-24: y Axis C.O.M. Mechanical Plots with Sinusoidal Perturbation

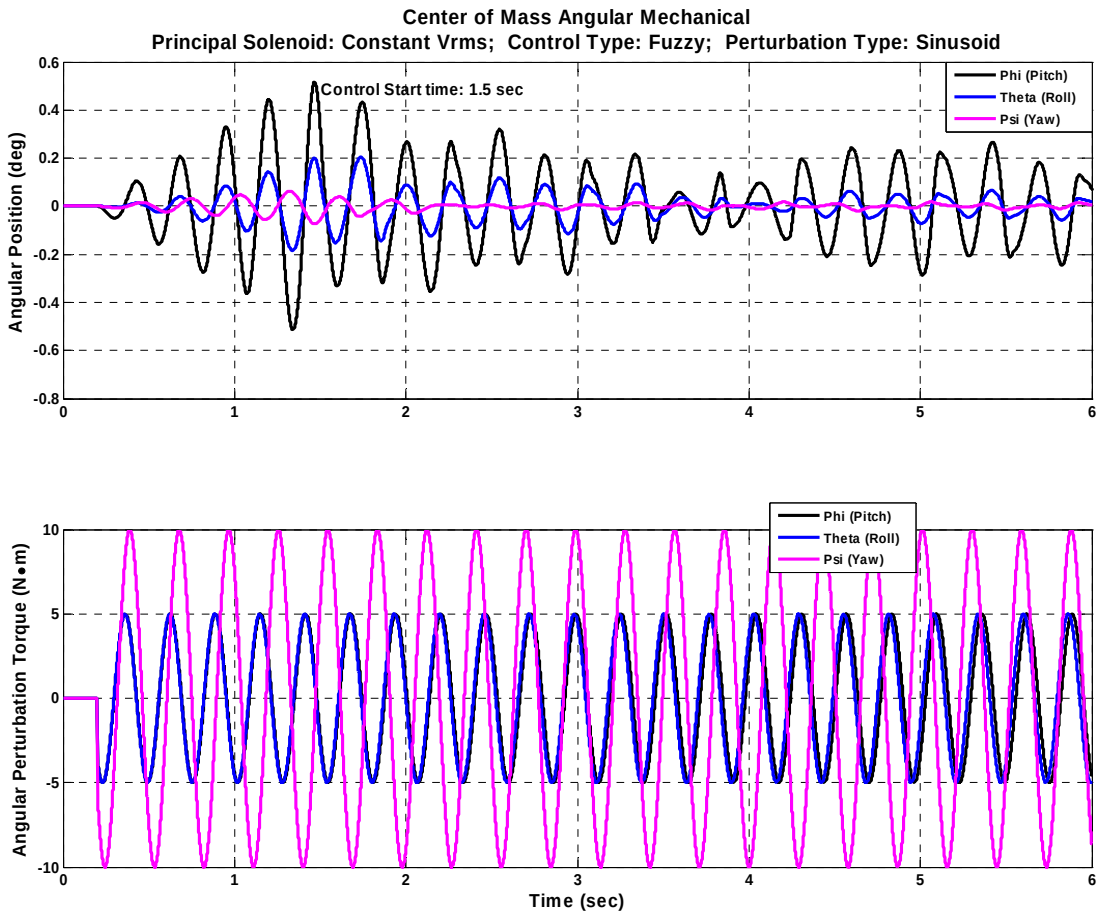

Figure 5.3-25: Angular Axes C.O.M. Mech. Plots with Sinusoidal Perturbation

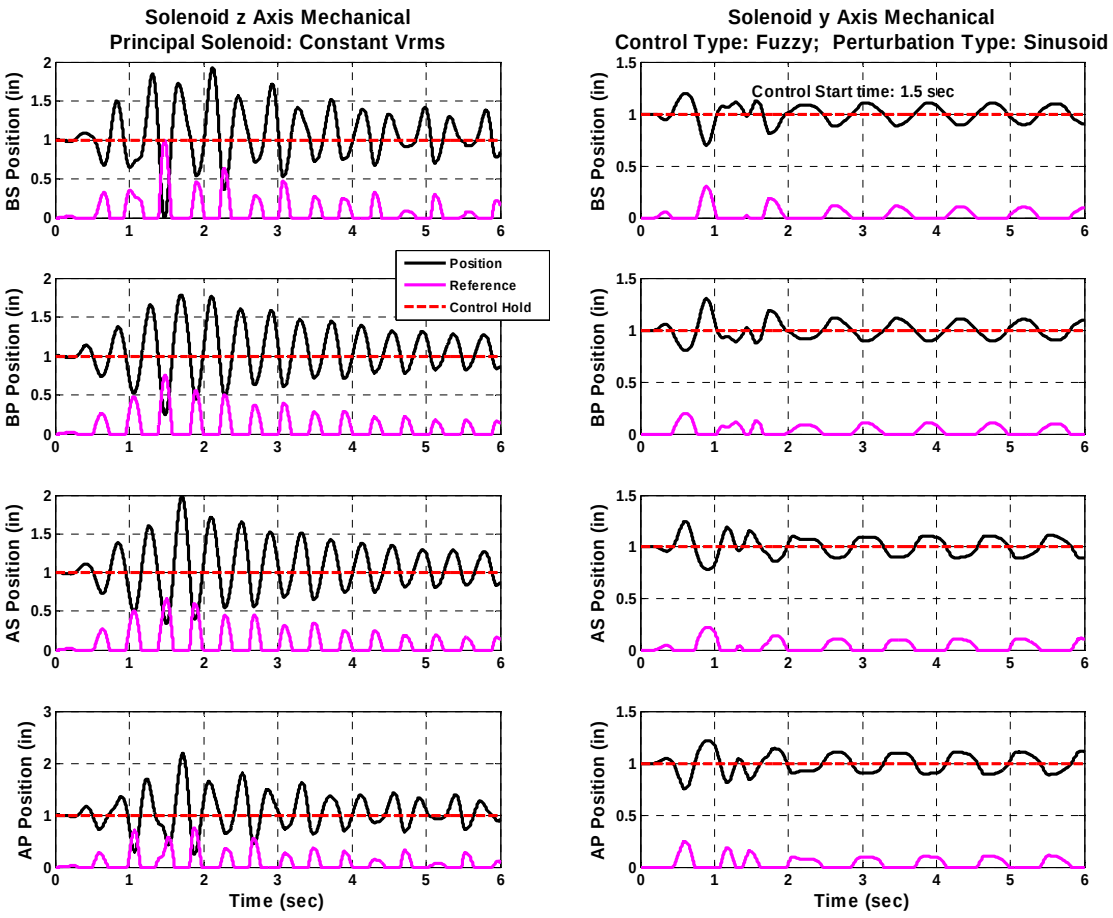

Figure 5.3-26: z & y Axis Mechanical Plots with Sinusoidal Perturbation

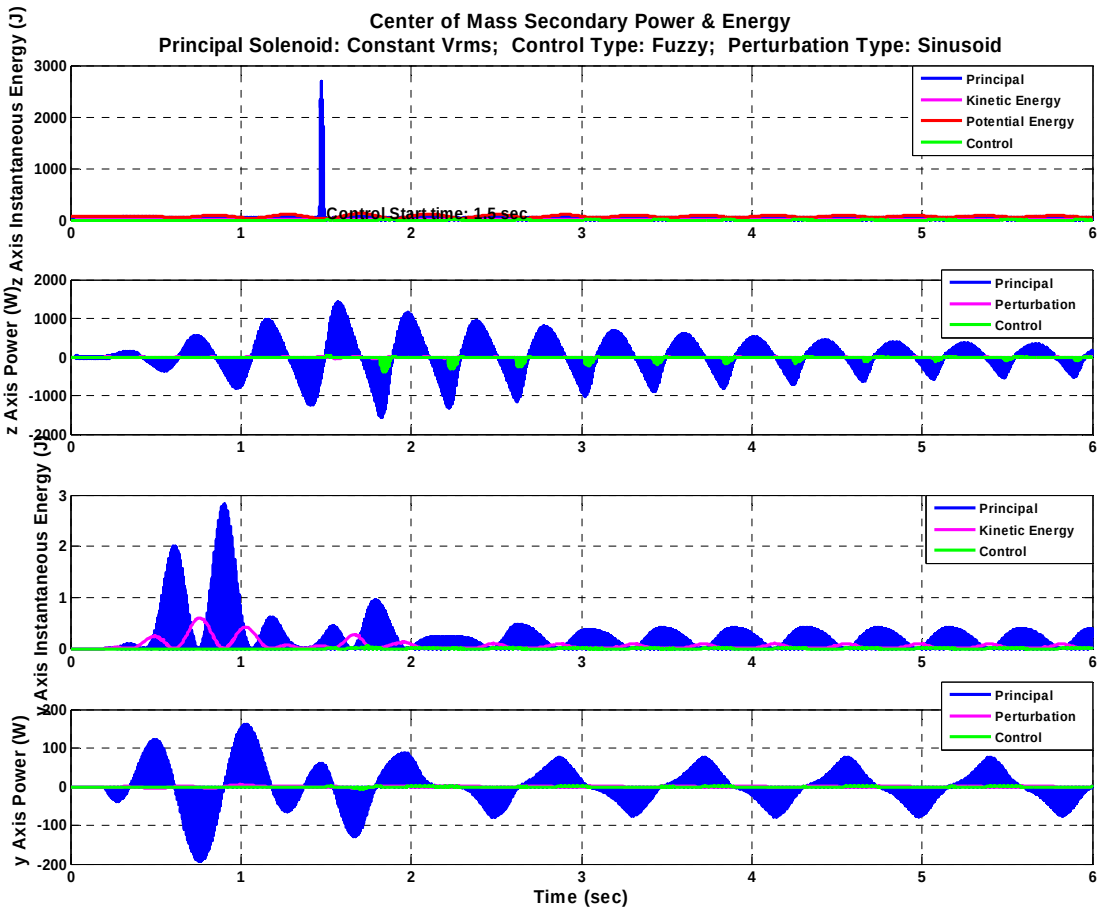

Figure 5.3-27: Power & Energy with Sinusoidal Perturbation

5.3.c.v Sinusoidal & Offset Response with Equivalent Sol. Systems

Even though the extreme sinusoidal perturbation response presented in Chapter 5.3.c.iv did not dampen the oscillation down to the desired levels, it did maintain a somewhat dampened oscillation level. Searching for an acceptable control response with a sinusoidal based perturbation led to an even more extreme case where a sinusoidal perturbation is superimposed on an already offset system. This perturbation case is applied to a system where the control solenoid is the same design and hence the same force and energy output as the principal solenoid as originally presented in Chapter 5.3.c.iii for Phase IV. As Figure 5.3-28, Figure 5.3-29, Figure 5.3-30, and Figure 5.3-31 show the system was approaching an unstable failure prior

to the control system initialization at 1.5 seconds. Then the added controller completely damped the oscillation within a maximum of 1 second for the worst case z axis and around 0.5 seconds for the y and rotational axes. The power and energy plots of this system are provided in Figure 5.3-32.

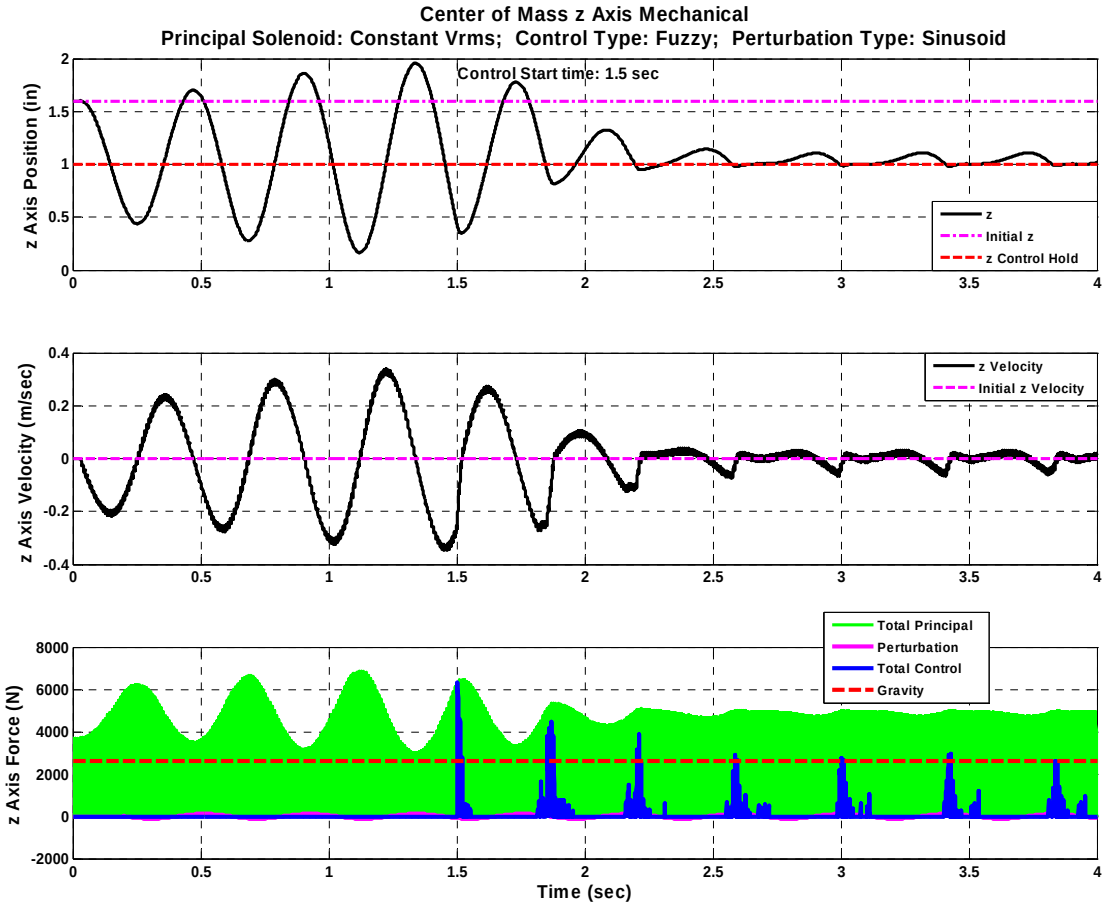

Figure 5.3-28: z Axis C.O.M. Mech. with Sinusoidal Pert. & Offset Initial Cond.

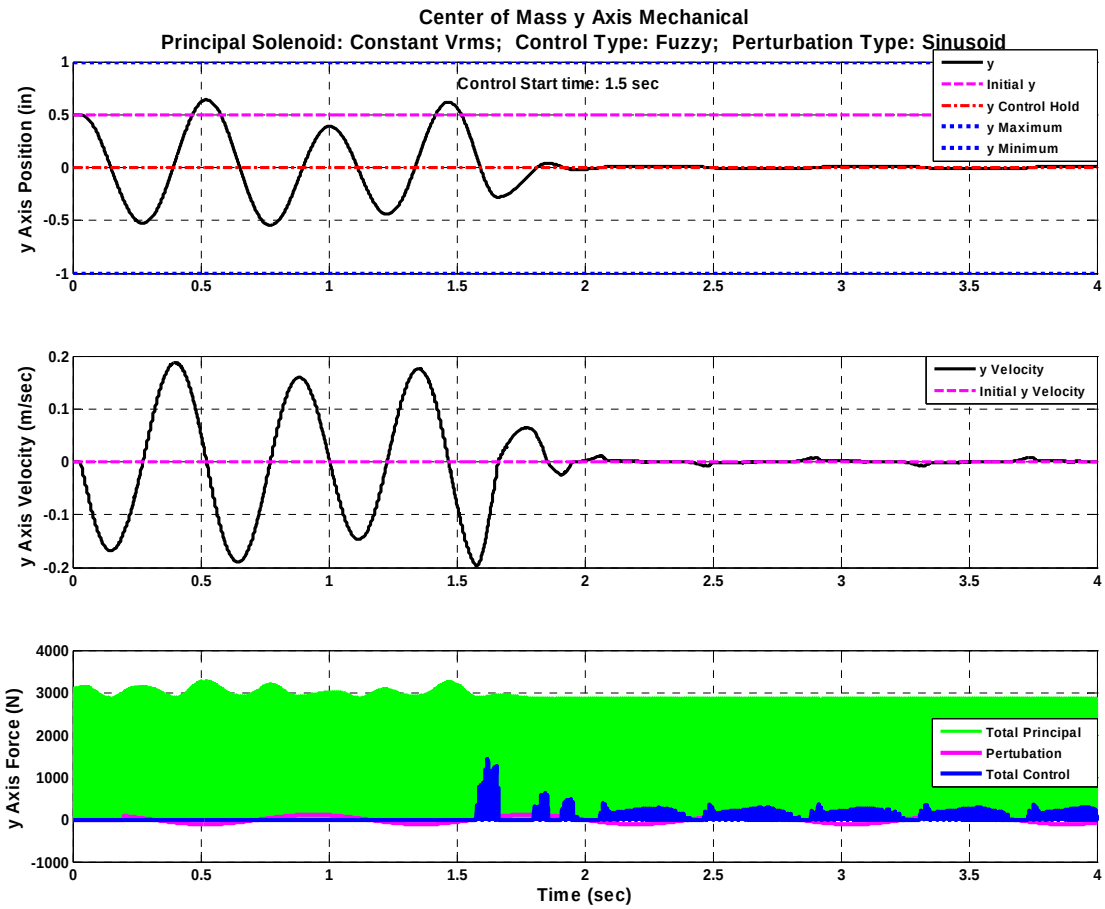

Figure 5.3-29: y Axis C.O.M. Mech. with Sinusoidal Pert. & Offset Init. Cond.

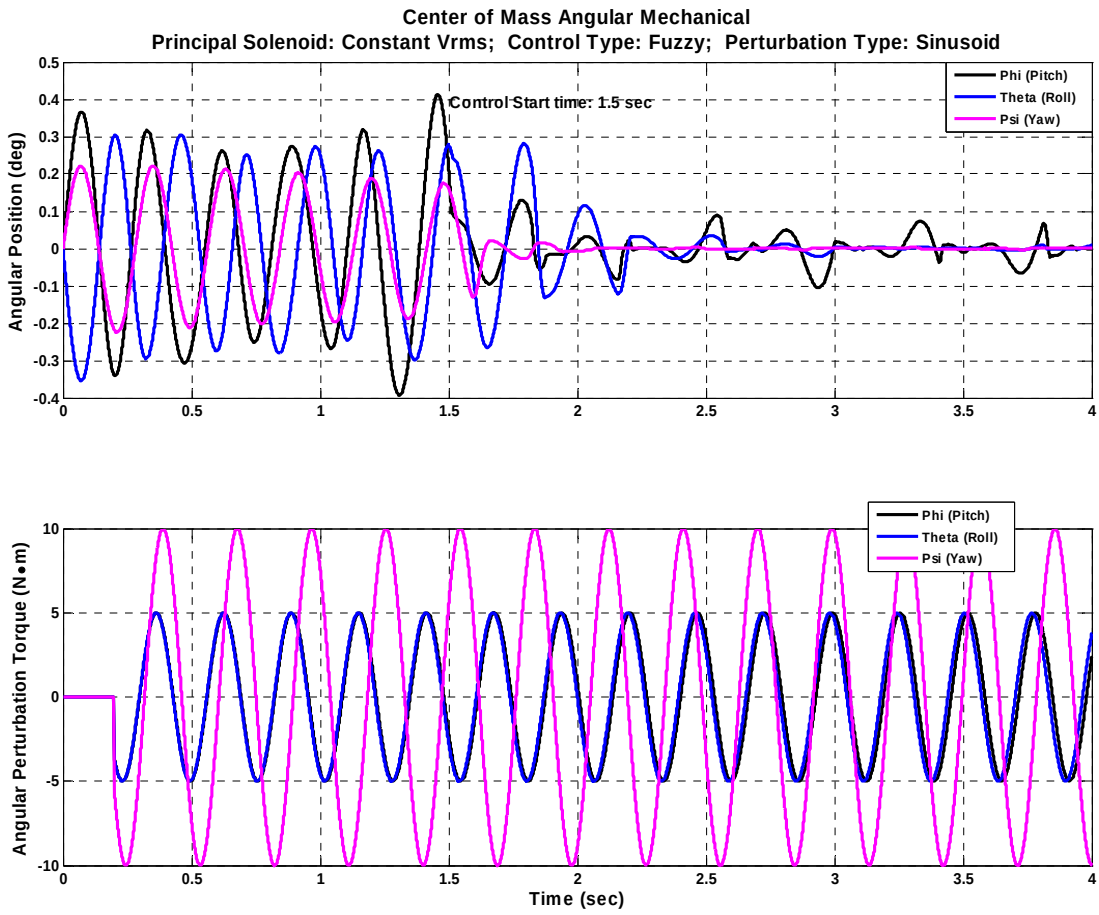

Figure 5.3-30: Angular Axes C.O.M. with Sinusoidal Pert. & Offset Init. Cond.

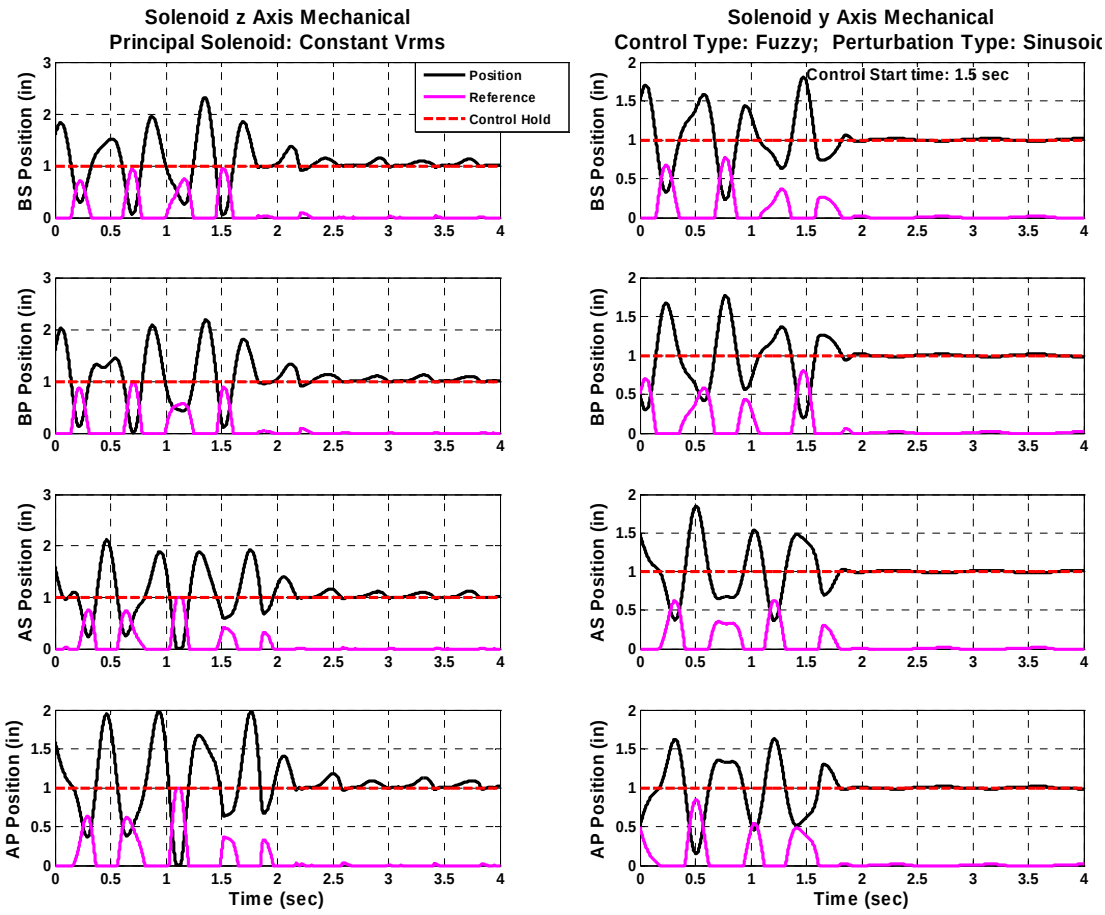

Figure 5.3-31: z & y Axis Mech. Plots with Sinusoidal Pert. & Offset Init. Cond.

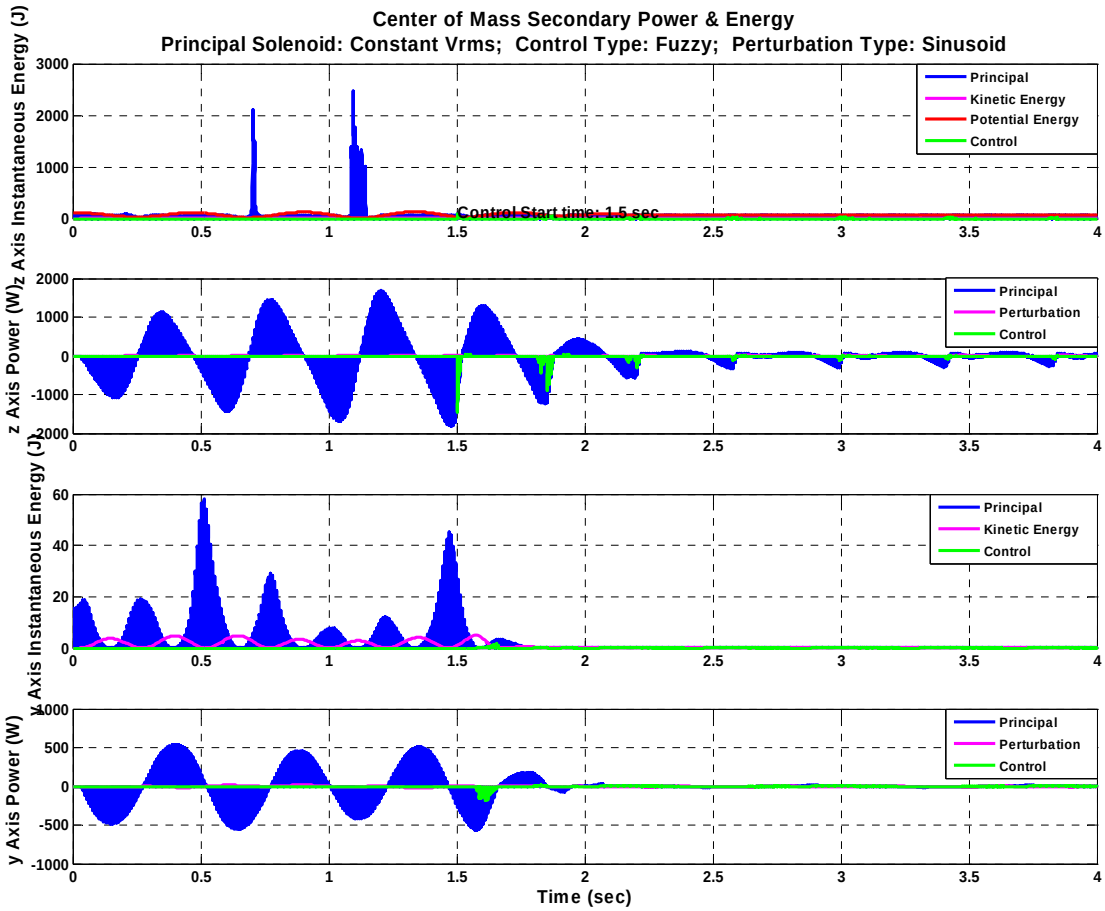

Figure 5.3-32: Power & Energy with Sinusoidal Pert. & Offset Initial Cond.

Figure 5.3-33 for the BS solenoid principal and control systems shows that even though the control solenoid is capable of equivalent power output as the principal solenoid, it only draws that much current and hence power during extreme offset conditions. The majority of the control system power draw is much lower than the principal solenoid. The second and third plots even show the control coils themselves maintaining a safe continuous duty current level.

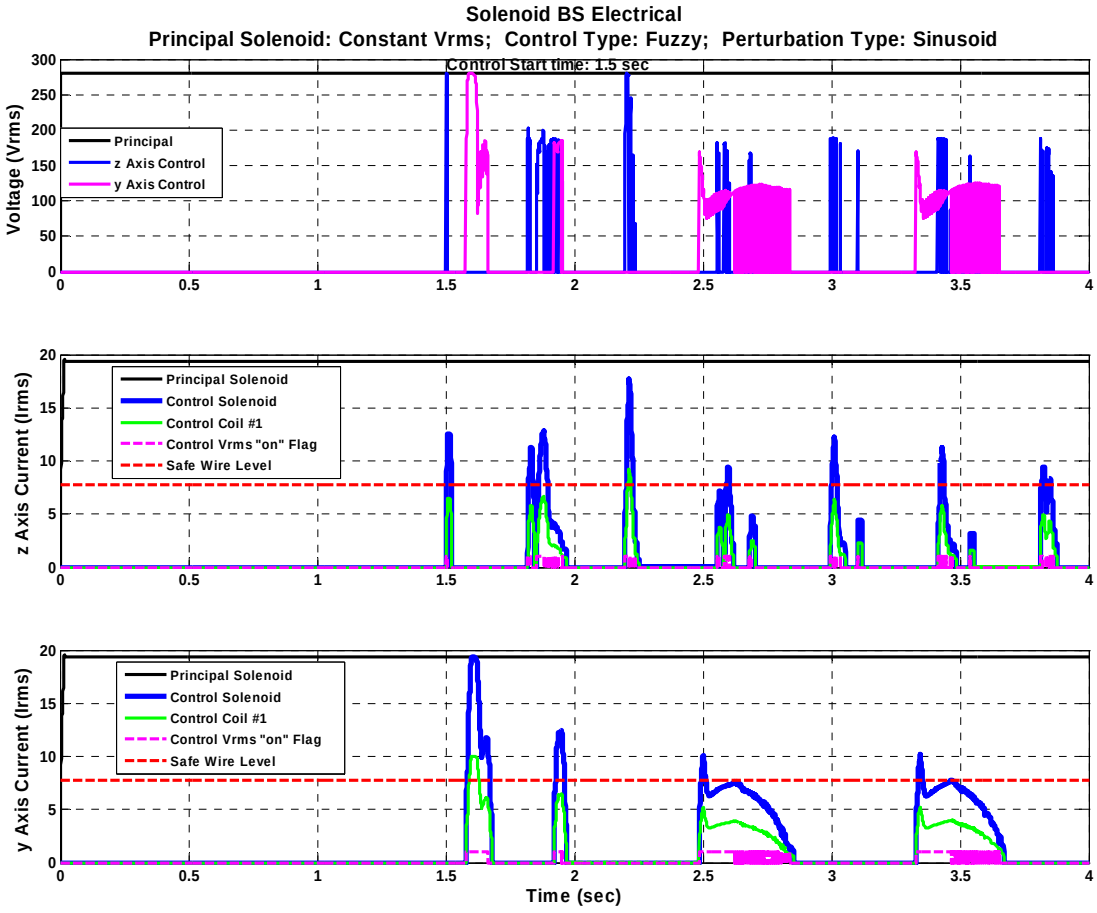

Figure 5.3-33: Elec. Plots with Sinusoidal Perturbation & Offset Initial Cond.

5.3.c.vi Stochastic Response

The stochastic response, which is often the most realistic perturbation case during a real system operation, provides a random response input. In this study the

mechanical motion plots presented in Figure 5.3-34, Figure 5.3-35, Figure 5.3-36, and Figure 5.3-37 indicate that the control system dampens the stochastic perturbations to a reasonably low level, but a better response is still desired. The z axis, which experiences a higher translational oscillation than the y axis, peak to peak oscillation amplitudes are still in the range of 0.15 inches 2.5 seconds after the onset of the control system. The power and energy effects of these oscillations are witnessed in Figure 5.3-38. Much like the sinusoidal case of Chapter 5.3.c.iv, this case also still identifies the potential need for a higher force control solenoid.

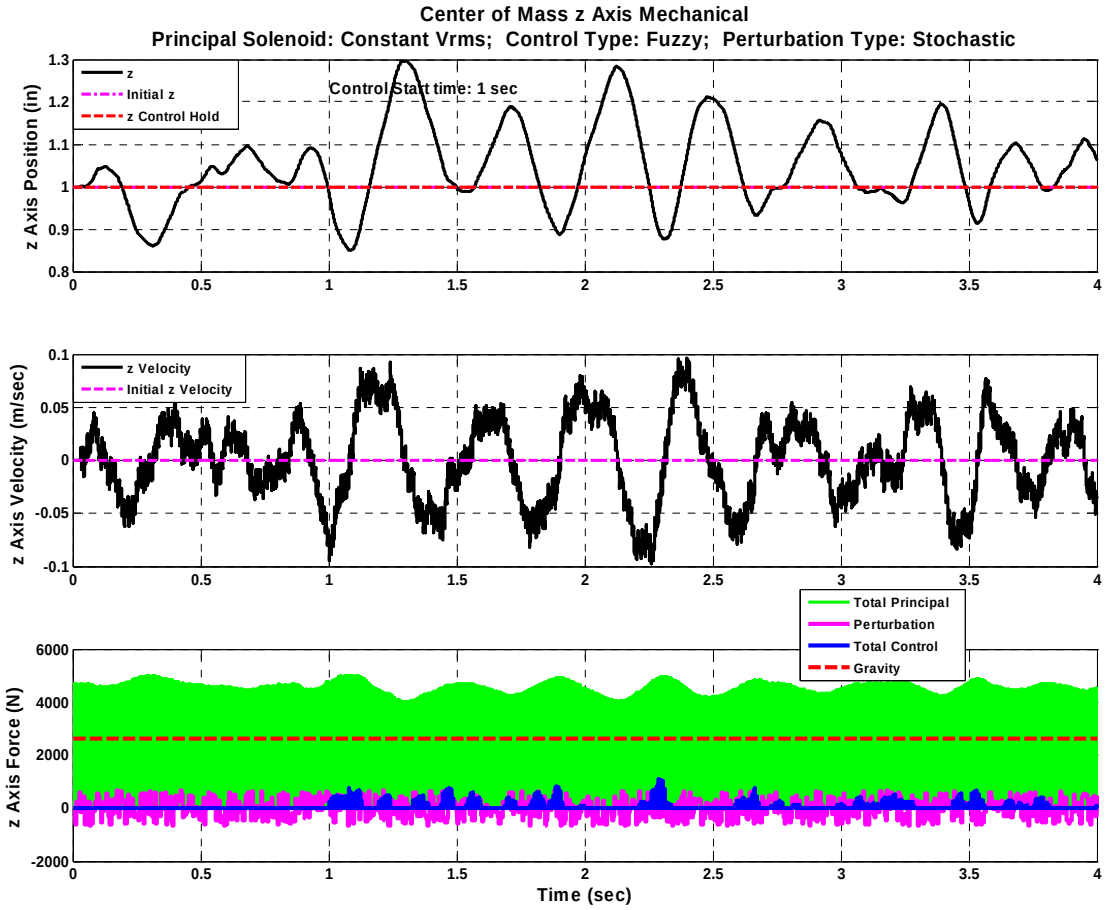

Figure 5.3-34: z Axis C.O.M. Mechanical Plots with Stochastic Perturbation

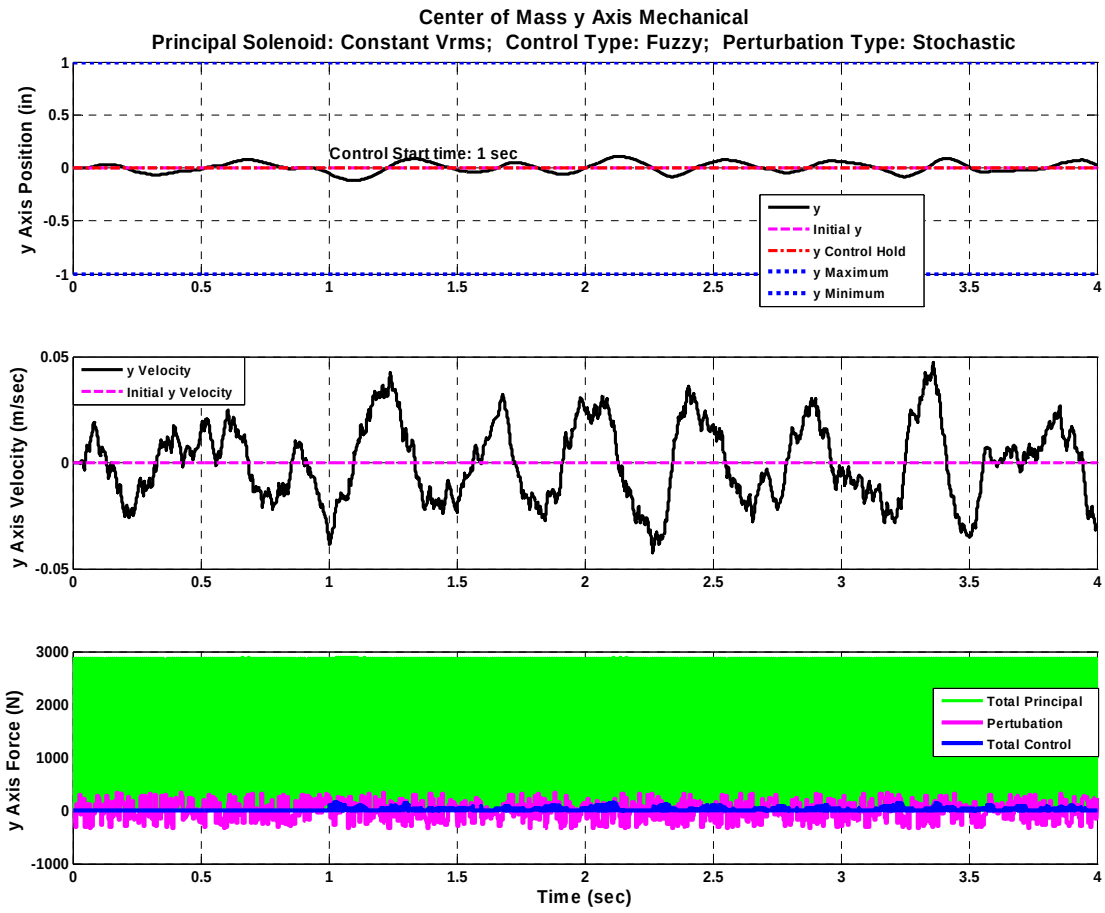

Figure 5.3-35: y Axis C.O.M. Mechanical Plots with Stochastic Perturbation

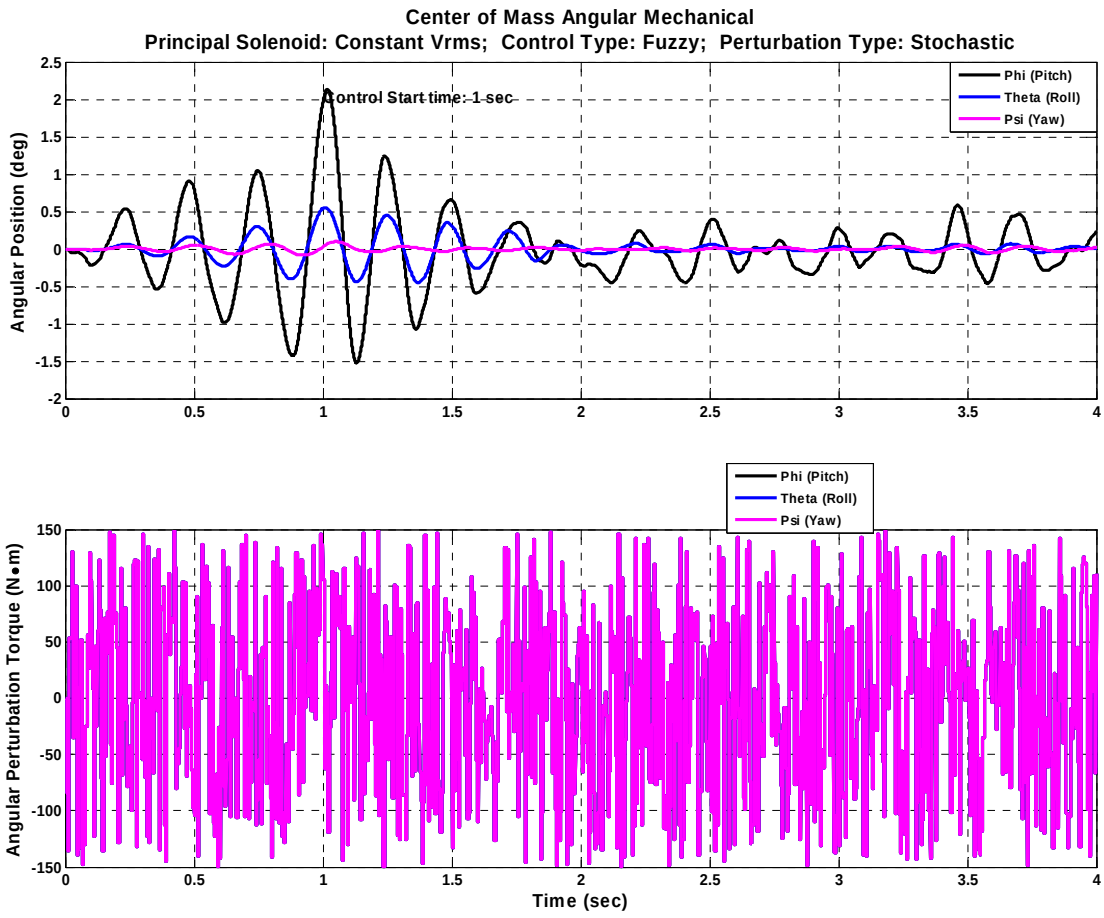

Figure 5.3-36: Angular Axes C.O.M. Mech. Plots with Stochastic Perturbation

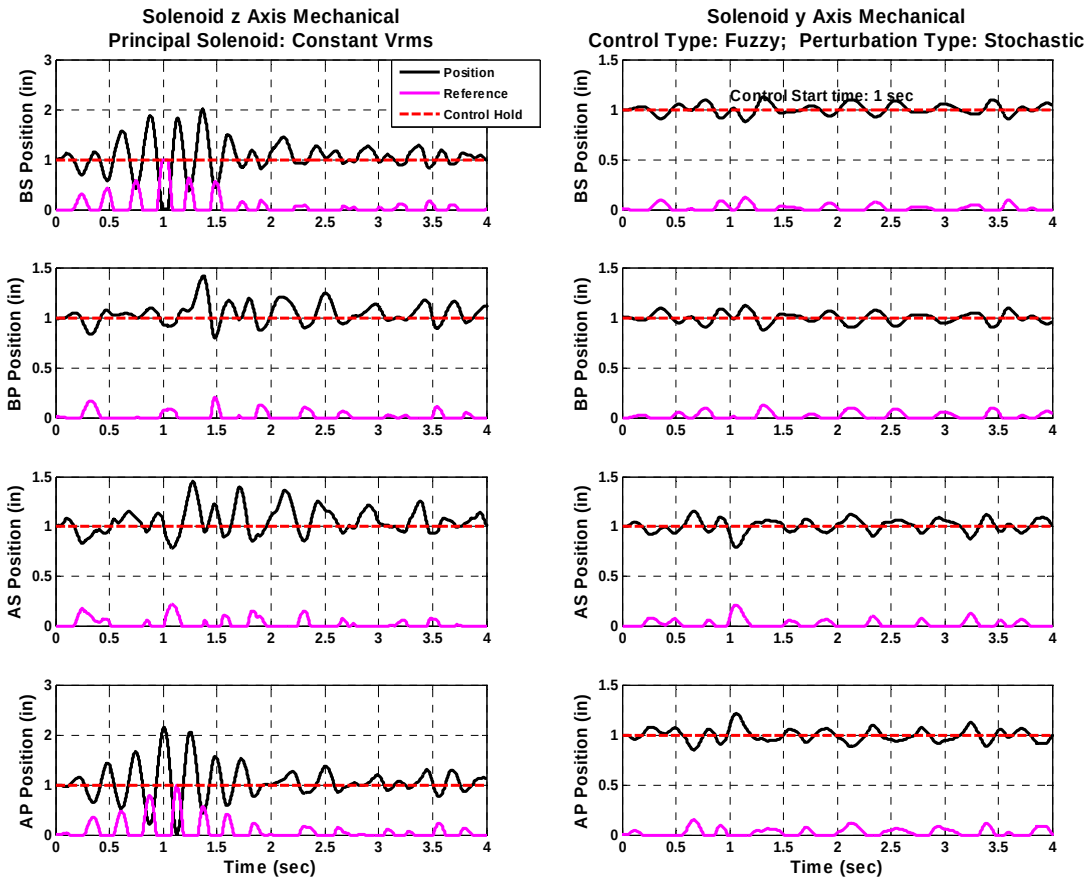

Figure 5.3-37: z & y Axis Mechanical Plots with Stochastic Perturbation

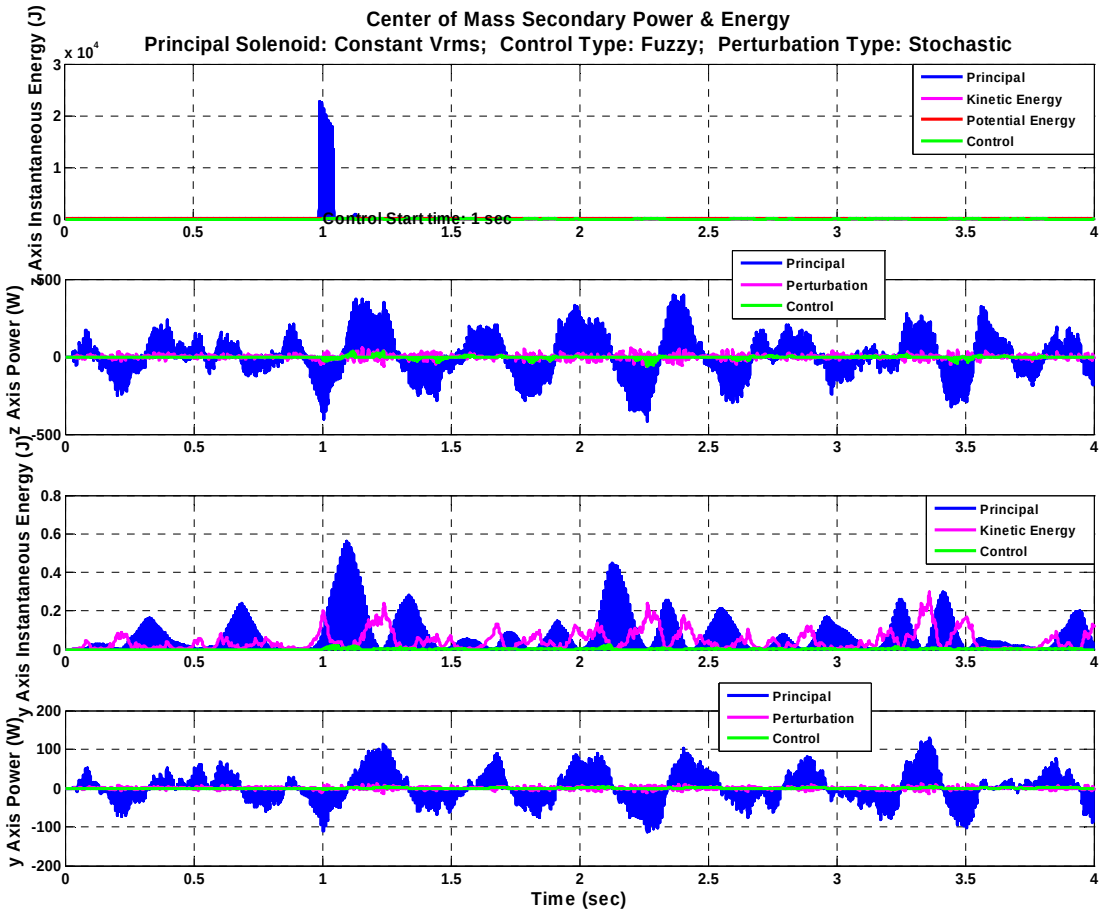

Figure 5.3-38: Power & Energy with Stochastic Perturbation

5.3.c.vii Stochastic & Offset Response with Equivalent Sol. Systems

Even though the extreme stochastic perturbation response presented in Chapter 5.3.c.vi did not dampen the oscillation down to the desired levels, it did maintain a somewhat dampened oscillation level. Searching for an acceptable control response with a stochastic based perturbation led to an even more extreme case where a stochastic perturbation is superimposed on an already offset system. This perturbation case is applied to a system where the control solenoid is the same design and hence the same force and energy output as the principal solenoid as originally presented in Chapter 5.3.c.iii for Phase IV. As Figure 5.3-39, Figure 5.3-40, Figure

5.3-41, and Figure 5.3-42 show the system was maintaining a large oscillation prior to the control system initialization at 1 second. Then the added controller completely damped the oscillation within a maximum of 1.5 seconds for the worst case z axis and 0.5 seconds for the y and rotational axes. The power and energy plots of this system are provided in Figure 5.3-43.

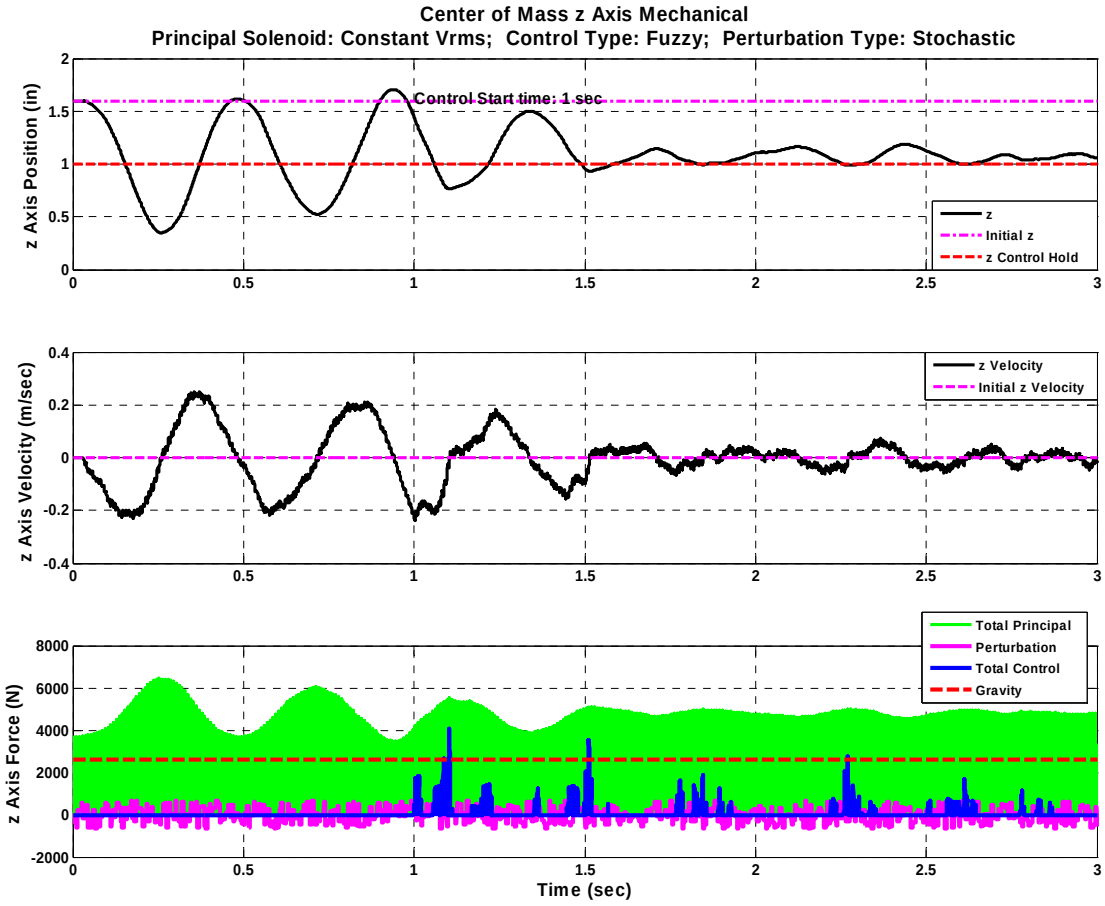

Figure 5.3-39: z Axis C.O.M. Mech. with Stochastic Pert. & Offset Initial Cond.

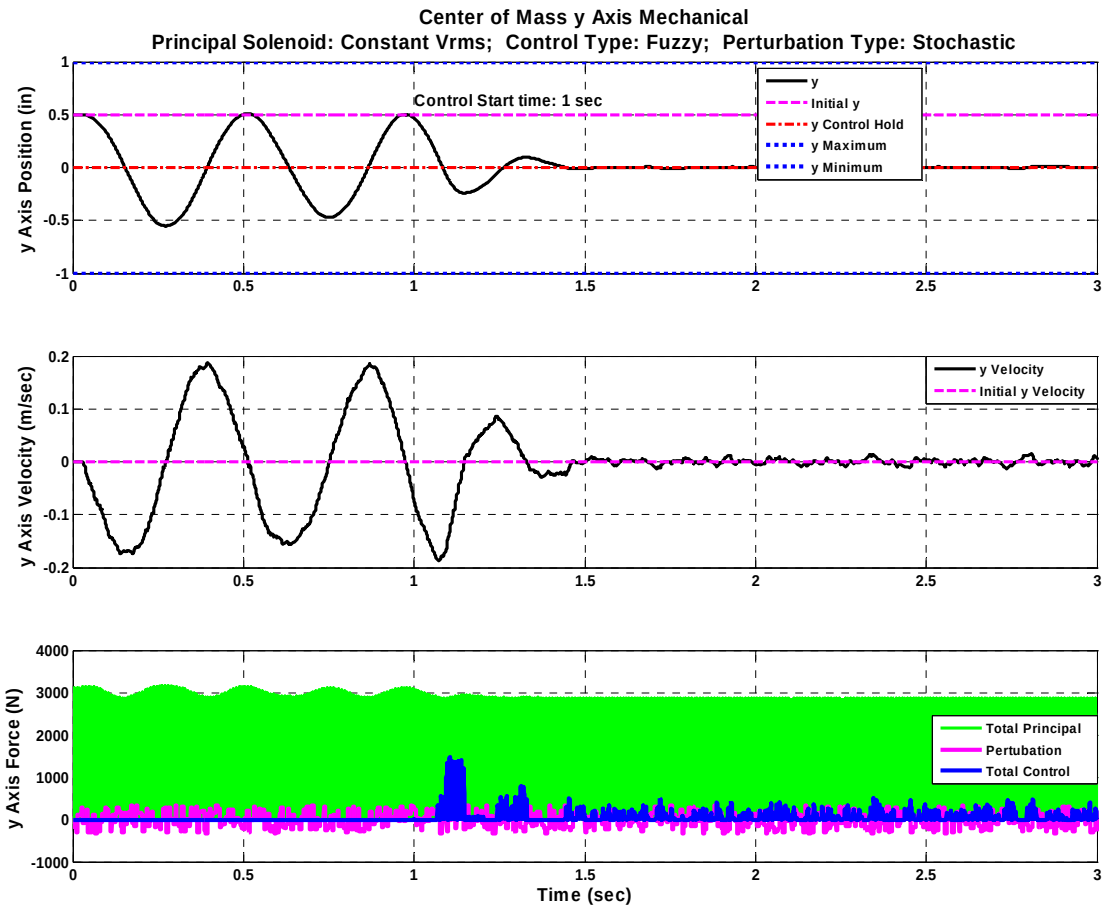

Figure 5.3-40: y Axis C.O.M. Mech. with Stochastic Pert. & Offset Init. Cond.

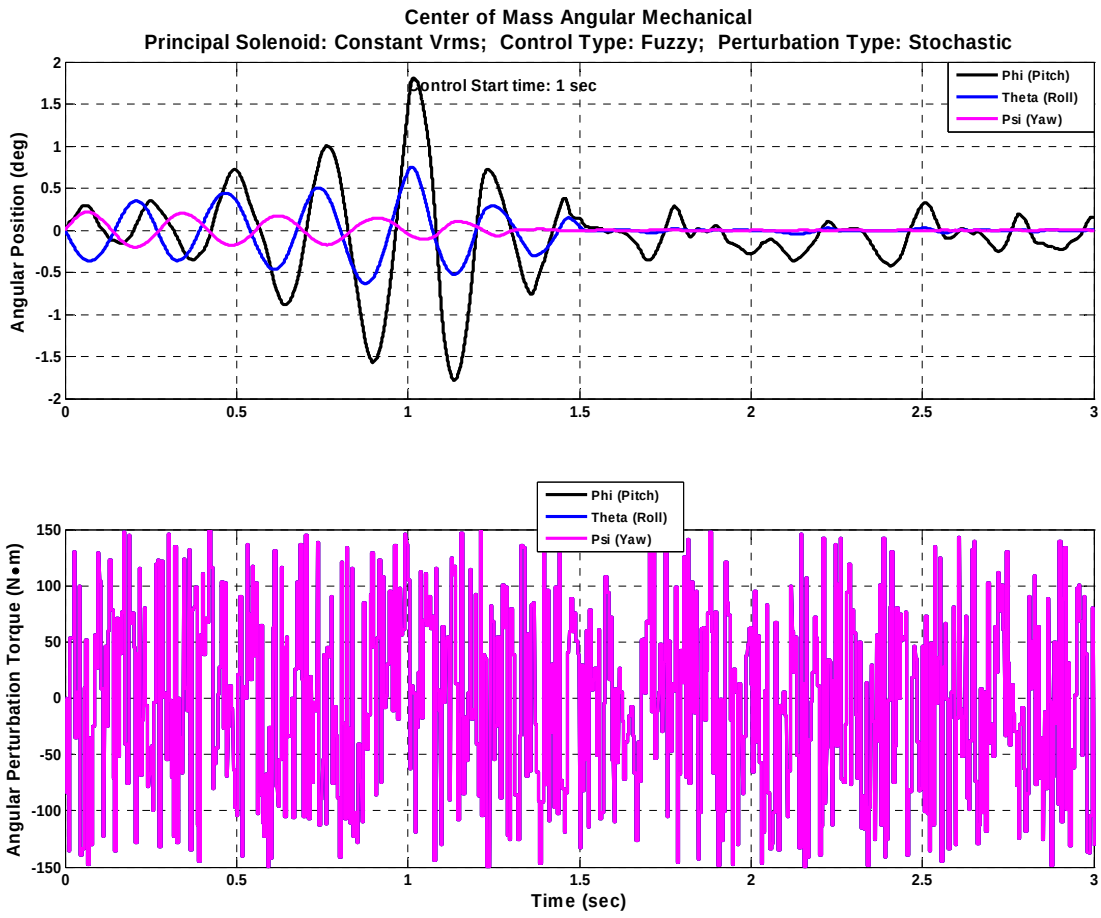

Figure 5.3-41: Angular Axes C.O.M. with Stochastic Pert. & Offset Init. Cond.

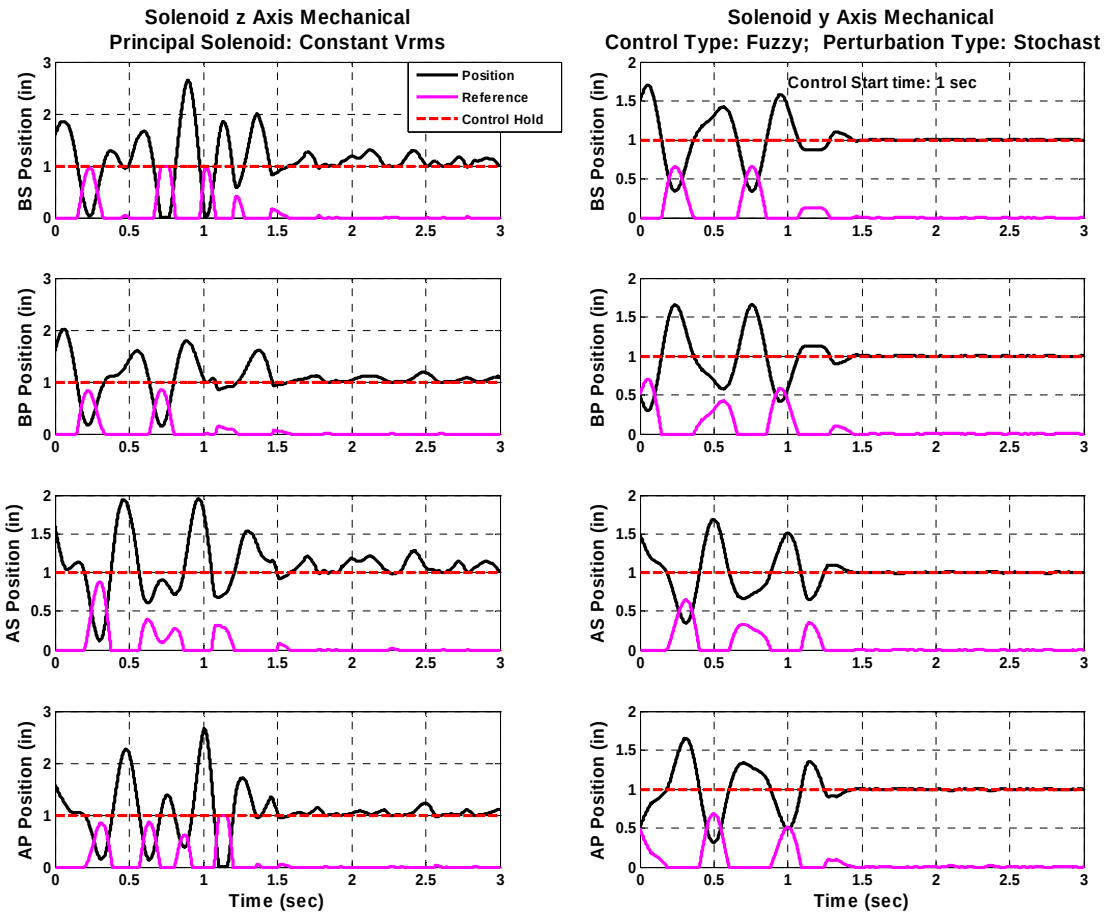

Figure 5.3-42: z & y Axis Mech. Plots with Stochastic Pert. & Offset Init. Cond.

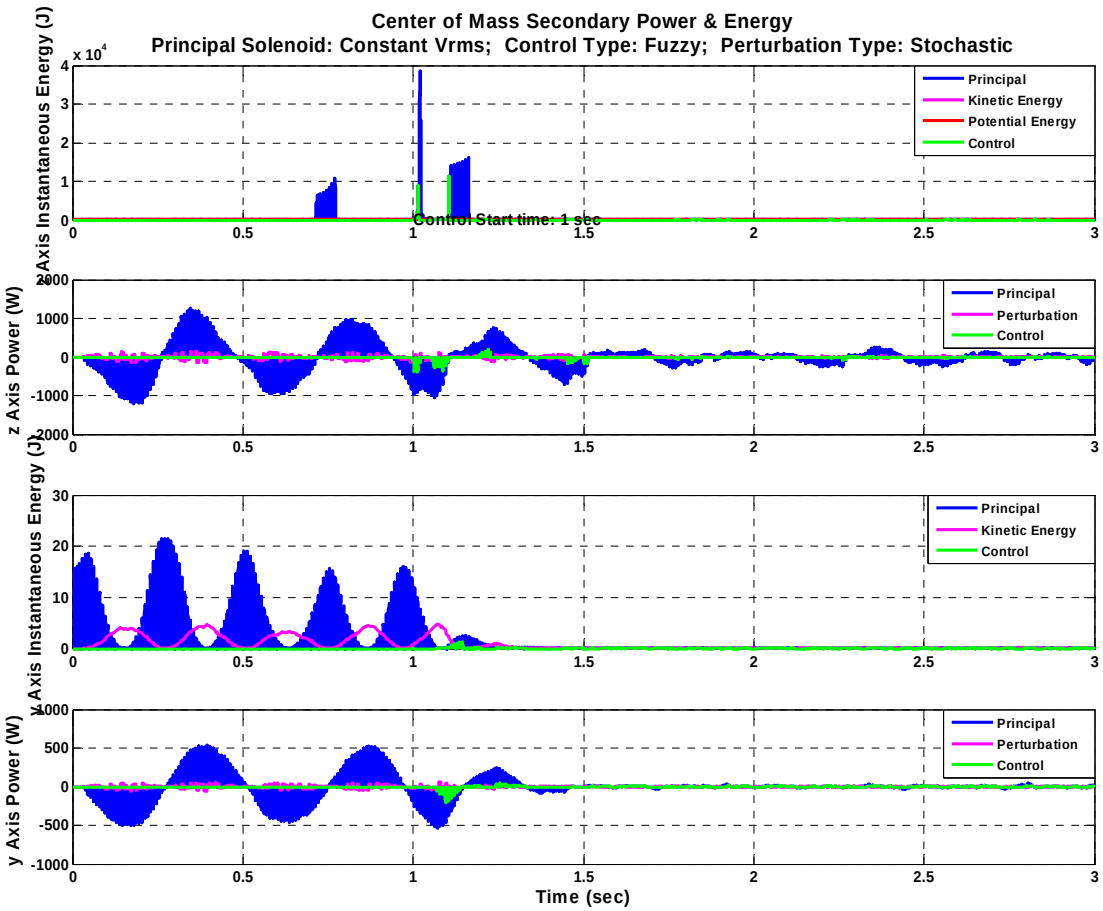

Figure 5.3-43: Power & Energy with Stochastic Pert. & Offset Initial Cond.

Figure 5.3-44 for the BS solenoid principal and control systems shows that even though the control solenoid is capable of equivalent power output as the principal solenoid, it only draws that much current and hence power during extreme offset conditions. The majority of the control system power draw is much lower than the principal solenoid. The second and third plots even show the control coils themselves maintaining a safe continuous duty current level.

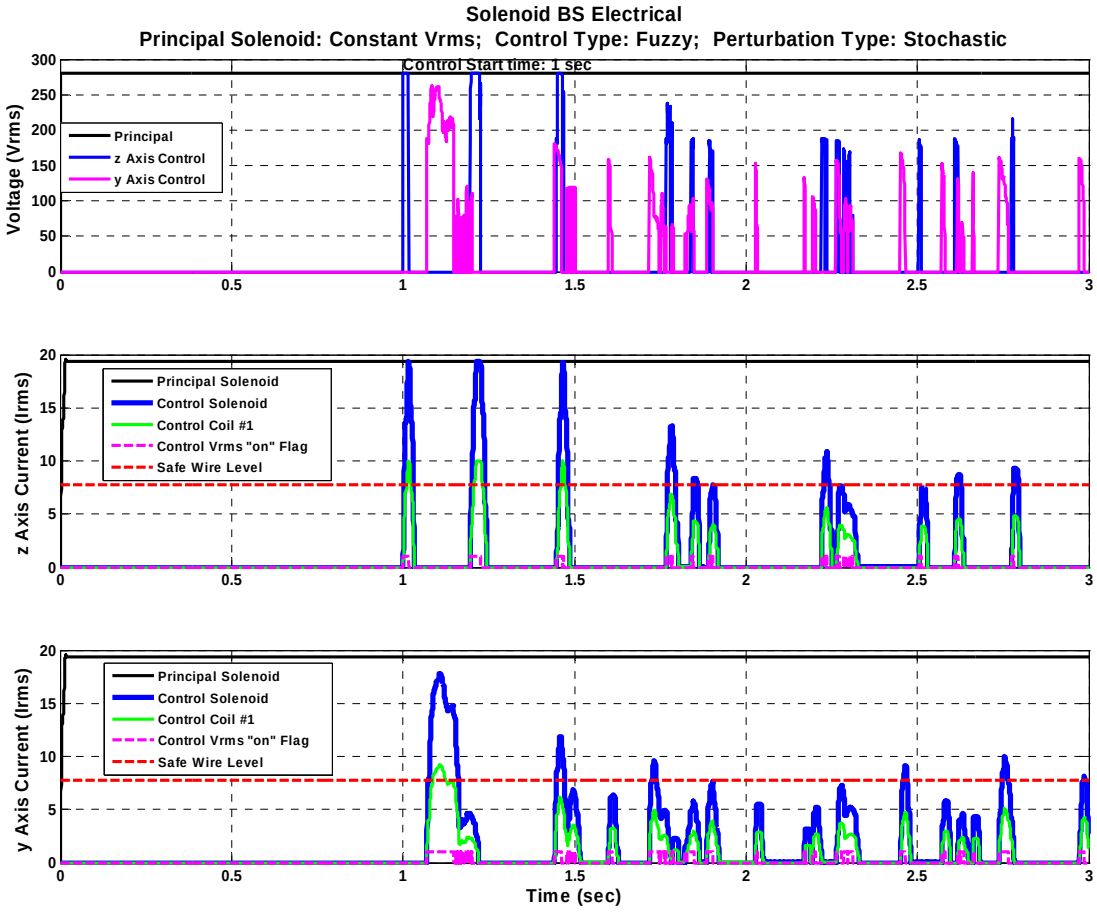

Figure 5.3-44: Elec. Plots with Stochastic Perturbation & Offset Initial Cond.

5.3.c.viii Numerical Simulation Results Summary

Phase IV numerical analysis results are summarized in Table 5.3-1. In this table the green cells indicate desired output values that are achieved and red cells

indicate desired output values that are not achieved. These desired damping levels are listed in the table headings in blue font inside of yellow cells. The final oscillation magnitude values are chosen as values which retain relative accuracy with this model while approaching the low oscillation energy parasitic damping levels of an actual maglev system. This real maglev system parasitic damping effect is not modeled by this analysis. Therefore at this low oscillation level the parasitic damping of the system should finalize the oscillation energy removal.

The ϕ angular value experiences the lowest torque and hence the largest angular deflection due to the short secondary width in comparison to the secondary length.

The y and ψ axis desired values are readily achieved in comparison to the other axis values due to the continual bi-directional damping across the y axis alone.

A control start energy column is added to Table 5.3-1 to provide a sense of the levels of perturbation energies that the control system must dampen in the translational D.O.F. This list does not encompass all of the perturbation energy, but instead only provides the major components experienced by the z and y axis control solenoids.

Simulation numbers 4 and 6 for the respective sinusoidal and stochastic high amplitude and continual perturbation inputs across all free D.O.F. experience large final z and ϕ axis output values. These output values exceed the desired values and hence the output cells are shaded red. This seems to indicate that the 1:1 principal to control solenoid system ratio does not help dampen the oscillations. In fact this output is deceiving. By referring to the output plots of these simulations one quickly sees that all of the oscillations dampen out extremely fast, experiencing much lower times and oscillation magnitudes than the desired value limits, but the extremely high perturbation amplitudes continue to periodically push these axis values past their desired final oscillation level. Therefore if these extreme types of perturbations continue, then the system does not achieve the desired limit value. In a real system

these extremely high amplitude perturbation oscillations are avoided by avoiding the mechanical resonant frequency in the operational design as well as other high amplitude continuous perturbation frequencies. In this case in which diminishing high amplitude periodic perturbations are the worse case periodic perturbations, or a single extreme disturbance offset such as the case outlined in Chapter 5.3.c.ii, the system performs reasonably well.

Table 5.3-1: Phase IV Numerical Analysis Results Summary

Simulation #	INPUTS					OUTPUTS							
	Principal Solenoid Input Waveform	Control to Principal & Control y to z Solenoid Power Sizing Ratios	Control Type	Initial Offset for Every Free DOF	Pert. Type	Control Damping Time		Control Start C.O.M. Peak to Peak Mechanical Oscillation Value		Control End C.O.M. Peak to Peak Value		Maximum Control Start Energy	
						Desired: 1 sec				Desired z & y: 0.1 in. Angles: 0.05 °		P.E.	K.E.
						z & y	Angles	z & y	Angles	z & y	Angles	z	y
				(Yes/ No)		(sec)		(in.)	(deg.)	(in.)	(deg.)	(J)	
1	Steady V_{rms}	≈ 1:10 ≈ 1:1.6	Fuzzy	Yes	None	**z: 0.75 y: 1.5**	ϕ: 0.1 θ: 0.05 ψ: 0.75	z: 1.5 y: 1.1	ϕ: 0.7 θ: 0.22 ψ: 0.5	z: 0.1 y: 0.1	ϕ: 0.05 θ: 0.05 ψ: 0.05	z: 110 y: 5	
2	Steady V_{rms} with Double V_{rms} Down Pulses	1:1 ≈ 1:1.6				z: 0.35 y: 0.35	ϕ: 0.4 θ: 0.35 ψ: 0.25	z: 0.8 y: 0.8	ϕ: 0.8 θ: 0.8 ψ: 0.2	z: 0.1 y: 0.1	ϕ: 0.05 θ: 0.05 ψ: 0.05	z: 110 y: 5	
3	Steady V_{rms}	≈ 1:10 ≈ 1:1.6		No	Sine	**z: 3 y: 0.5**	**ϕ: 1.5 θ: 1.5 ψ: 0.5**	z: 1.5 y: 0.4	ϕ: 0.1 θ: 0.4 ψ: 0.15	**z: 0.5 y: 0.2**	**ϕ: 0.35 θ: 0.2 ψ: 0.05**	z: 125 y: 0.5	
4		1:1 ≈ 1:1.6		Yes		z: 1 y: 0.3	ϕ: 0.4 θ: 0.7 ψ: 0.2	z: 1.8 y: 1	ϕ: 0.8 θ: 0.6 ψ: 0.35	z: 0.1 y: 0.1	**ϕ: 0.15 θ: 0.05 ψ: 0.05**	z: 130 y: 5	

5		≈ 1:10 ≈ 1:1.6		No	Stoch.	**z: 2.75** **y: 0.4**	**ϕ: 3.5** **θ: 0.8** **ψ: 0.1**	z: 0.45 y: 0.2	ϕ: 3.5 θ: 1 ψ: 0.1	z: 0.1 y: 0.1	**ϕ: 0.8** **θ: 0.05** **ψ: 0.05**	z: 85 y: 0.2
6		1:1 ≈ 1:1.6		Yes		**z: 1.6** **y: 0.3**	**ϕ: 1.5** **θ: 0.5** **ψ: 0.25**	z: 1.25 y: 1	ϕ: 3.4 θ: 1.4 ψ: 0.4	z: 0.1 y: 0.1	**ϕ: 0.35** **θ: 0.05** **ψ: 0.05**	z: 115 y: 5

CHAPTER 6 FINAL CONCLUSIONS

6.1 OVERALL SYSTEM SOLUTION

All modeling and control algorithms derived in Chapter 3 are modeled in the appendices, the salient results are presented in Chapter 5, and final conclusions are presented in Chapter 6. Chapter 6 conclusions refer to each corresponding area in Chapter 5.

6.2 PHASE I

6.2.a Analytical Component Modeling

The analytical repulsive force output is acceptable for the Phase I experiment principal and control solenoid lift requirements. This output is described in Chapter 5.2.b.

6.2.b Computational Component Modeling

The numerical simulation equivalent computational analysis output indicates a good correlation between the respective repulsive lift force values. The computational simulation that analyzes the Phase I test apparatus indicates that the computational repulsive force output is acceptable for the Phase I experiment principal and control solenoid lift requirements.. These output are described in Chapter 5.2.c.

6.2.c Numerical System Modeling

6.2.c.i Initial Mechanical Offset

Chapter 5.2.d.ii clearly indicates that both the linear I.-P.D. controller and nonlinear fuzzy controller respond similarly and acceptably for this basic system test.

6.2.c.ii Initial Mechanical Offset with 2x Vrms Down Pulses

The I.-P.D. linear to fuzzy nonlinear control response comparison presented in Chapter 5.2.d.iii, where the system is still quite basic in comparison to the final complex nonlinear maglev system of Phase IV, dictates that linear control is not adequate for the final maglev system. Therefore only nonlinear soft computing methods are analyzed in future chapters.

6.2.c.iii Step Response with No Control

The step response presented in Chapter 5.2.d.iv provided the median system natural frequency value of 4.74 Hz. Note that without control the step response input produces a continually increasing secondary oscillation amplitude. This type of system response is also witnessed in all runs during the uncontrolled region when the onset of the controller is delayed.

6.2.c.iv Sinusoidal Response

The soft programming fuzzy control system responded acceptably for the sinusoidal response test presented in Chapter 5.2.d.v.

6.2.c.v Stochastic Response

The soft programming fuzzy control system responded acceptably for the stochastic response test presented in Chapter 5.2.d.vi.

6.2.c.vi Stochastic & Offset Response with Equivalent Sol. Systems

Chapter 5.2.d.vii illustrated that increasing the control system power output provided a very good damping response to an unstable system with extreme disturbance conditions.

6.2.c.vii Phase I Numerical Simulation Conclusions

Phase I numerical analysis results are summarized in Table 5.2-1.

Phase I begs the question of what level of damping power is required for a proper maglev system implementation. The answer lies somewhere between the low control energy case implemented for the majority of the simulations in this paper and the high control energy case where the control solenoids are on the same order of power output as the principal solenoids. As introduced as a general statement in Chapter 1.2.c, the final system design choice must account for a specific maglev system implementation design requirements such as maximum oscillations allowable, maximum period to dampen oscillations, maximum overshoot, and maximum control system power and sizing allowable. Such systems have such a wide range of maglev implementation schemes. The author is maintaining this paper as a general maglev scheme proof of concept work. Therefore no further specific maglev scheme design work is performed.

It was initially assumed that the principal and control solenoid systems required segregation due to time constant issues. Phase I output with extremely low electrical transient times in comparison to the mechanical transient times indicates that if a particular maglev scheme is determined where principal and control system separation is not required for controlling the magnetic air gap spring constants with enough power for the required motion, then this type of magnetically active suspension control should perform wonderfully without the complexity of the added control hardware. An example of such a system is superimposing both the principal and control voltages onto the same prime mover for both the vertical and lateral systems. In the case of this paper this union entails combining the principal and control solenoids and incorporating the control voltage superimposed on top of the principal voltage signal.

6.2.d System Testing

6.2.d.i Phase I, Test #2: Uncontrolled Response Test

Chapters 4.2.c.iii and 5.2.e.iii provide the uncontrolled response test setup and results respectively. The results indicate that although magnetic levitation oscillations are achieved, the mechanical contacts in the test apparatus provided a high friction damping force. This test apparatus is still considered useful for Phase I test purposes since the observed seven perturbation periods prior to damping down to the low oscillation noise level are enough for providing controlled response.

6.2.d.ii Phase I, Test #2: Controlled Response Test

Chapters 4.2.c.iv and 5.2.e.iv provide the controlled response test setup and results respectively. As stated in Chapter 5.2.e.iv and presented in Table 5.2-2, the controlled system responds much more favorably than the uncontrolled system by quickly dampening the perturbation system oscillation within a much shorter settling time and a lowered overall oscillation amplitude.

6.2.d.iii Phase I Testing Conclusions

Comparing the uncontrolled response test to the controlled response test not only validates the numerical simulation trends, but empirically proves the entire premise of introduced electromagnetic damping.

6.3 PHASE IV

6.3.a Numerical System Modeling

6.3.a.i Initial Mechanical Offset

The soft programming fuzzy control system responded acceptably for the basic initial mechanical offset response test presented in Chapter 5.3.c.ii. Although, as indicated in Figure 5.3-13, the electrical time constants are approaching mechanical

time constants with values only 2 to 3 times less. As discussed in that chapter, this range is almost unacceptable. Also, as shown in Figure 5.3-15, the principal solenoid z axis magnetic flux density exceeds the saturation limits. Slightly exceeding the magnetic saturation limit is acceptable for this analysis, but in a final design effort this fact would require more scrutiny in the form of core material selection, simulating saturation levels, and saturation effects of system performance.

6.3.a.ii Initial Mechanical Offset with 2x Vrms Down Pulses

The soft programming fuzzy control system responded acceptably for the extreme case of an initial mechanical offset with two principal source voltage down pulses response test with equivalent principal and control solenoid hardware presented in Chapter 5.3.c.iii.

6.3.a.iii Step Response with No Control

Two simulations are required to isolate the median step response resonant frequency values for each D.O.F. Since orthogonality provides non-coupled motion, the two orthogonal translational D.O.F. and three orthogonal rotational D.O.F. comprise the two simulation groupings required. Since the only outcome of these runs was the median resonant frequency values, these runs are not presented in the Results section and only the median resonant frequency values are provided. The median system natural frequency values of the z, y, ϕ, θ, and ψ axes are 2.41, 1.19, 3.80, 3.82, and 3.46 Hz respectively. Note that without control the step response input produces continually increasing secondary oscillation amplitude. This type of system response is also witnessed in all runs during the uncontrolled region when the onset of the controller is delayed.

6.3.a.iv Sinusoidal Response

The soft programming fuzzy control system dampened the sinusoidal response test presented in Chapter 5.3.c.iv, but this case identified the potential need for a higher force control solenoid.

6.3.a.v Sinusoidal & Offset Response with Equivalent Sol. Systems

The soft programming fuzzy control system responded acceptably for the extreme case of sinusoidal response with initial offset conditions test with equivalent principal and control solenoid hardware presented in Chapter 5.3.c.v. This system shows that by increasing the control solenoid force output, even an extreme perturbation and initial offset case can be controlled within reasonable operational limits.

6.3.a.vi Stochastic Response

The soft programming fuzzy control system dampened the stochastic response test presented in Chapter 5.3.c.v, but much like the sinusoidal case of Chapter 5.3.c.iv, this case identified the potential need for a higher force control solenoid.

6.3.a.vii Stochastic & Offset Response with Equivalent Sole. Systems

The soft programming fuzzy control system responded acceptably for the extreme case of stochastic response with initial offset conditions test with equivalent principal and control solenoid hardware presented in Chapter 5.3.c.vii. This system shows that by increasing the control solenoid force output, yet another extreme perturbation and initial offset case can be controlled within reasonable operational limits.

6.3.a.viii Phase IV Numerical Simulation Conclusions

Phase IV numerical analysis results are summarized in Table 5.3-1. Phase IV numerical simulation conclusions builds upon Phase I numerical simulation conclusions discussed in Chapter 6.2.c.vii.

Both Phase I and Phase IV simulations ranged from small to large mass secondary bodies, from which a sampling is represented in the Results section of this paper, to determine applicability of this control hardware and math kernel scheme to various motional magnitude and frequency application levels of inertial, potential, and dissipative energy maglev systems. This Phase IV proof of concept analysis proves that mechanical oscillations can indeed be removed from a maglev system in an acceptable fashion exclusively through magnetic air gap interaction, although in some extreme cases rarely seen during actual operating conditions a higher control force ratio than the 1 to 10 control to principal solenoid force sized system is required to achieve acceptable performance. A proper control system design study for a particular maglev system with set operational requirements will define final control solenoid sizing.

6.4 OVERALL CONCLUSION

This paper provides an outline for a working model of solely electromagnetic air gap suspension damping control technique. This outline is formed by quantifying the dilemma in the Chapter 1.2.a problem statement and attaining the general Chapter 1.2.b original achievement statement through means of the specific goal assigned in Chapter 1.2.c. Although the exact control system design for a final maglev system is intentionally never chosen, the general control hardware power sizing and the roots of final soft computing optimal fuzzy and adaptive neuro-fuzzy control kernels are specified through the small and large mass systems simulated in Phase I and IV and tested through the Phase I test program.

APPENDIX A MATHCAD EXACT SOLUTION PROGRAMS

A.1 SYSTEM SOLENOID DESIGNS

A.1.a General Solenoid Design for All Phases

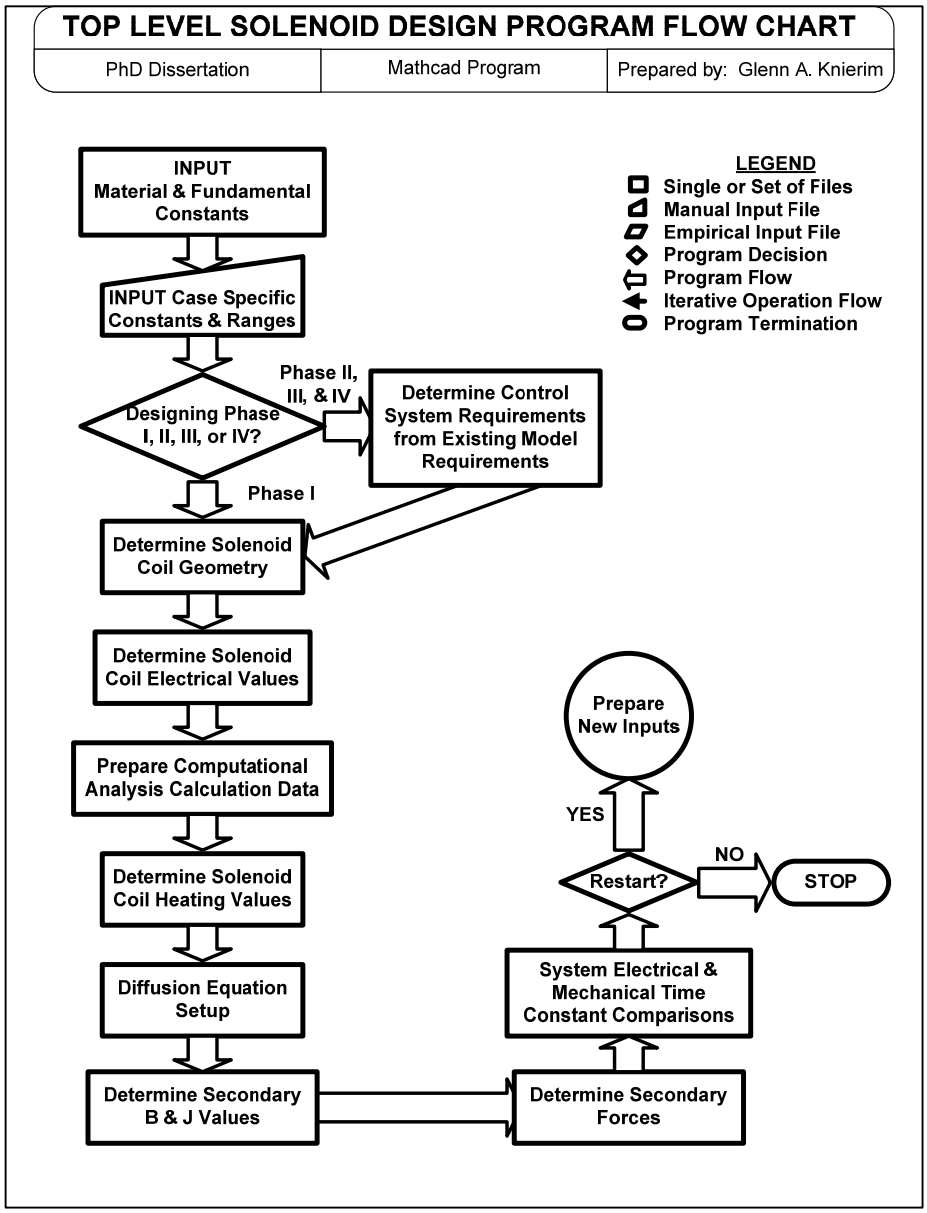

Figure A-1: Mathcad Solenoid Design Flow Chart

SOLENOID TEST SETUP VALUES

Item #	Solenoid Core	# of Coils	Wire Height	Wire Gage	I Wire Safe	Coil #1 Wire Layers	Coil #2 Wire Layers	Coil #1 Total # of Turns	Coil #2 Total # of Turns	# of Turns per Layer	Source Vrms	Source Freq.	Coil #2 Outside Radius w/ Insul. Core Inside: 1.35"	Coil #1 Resistance	Coil #2 Resistance	Coil #1 Inductance	Coil #2 Inductance	Total Inductance (Coils in Parallel)	Total Solenoid Resistance (Coils In Parallel)	Total Solenoid Reactance (Coils In Parallel)	Optimized Capacitance vs. Set Test Capacitance	I Source	I Coil #1	I Coil #2	Amp x Turns Coil #1	Amp x Turns Coil #2	Internal Heat Gen. (BOTH Sols.)	J Coil #1	J Coil #2
			in		mA						Vrms	Hz	in	Ω	Ω	H	H	H	Ω	Ω	μF	A	A	A	A-turns	A-turns	W	A-turns/in²	Aiming for 15 or less
1			1.442			16.75	13.25	1541	1219				1.336	47.089	48.340	4.782	4.873	2.363	23.853	890.994		0.135	0.067	0.068	103.25	82.892	0.43	1.17	1.197
			1.46			15.5	12.5	1534.5	1237.5	99			1.283	46.434	47.729	0.360	0.365	0.179	23.536	887.384	0	1.851	0.836	0.846	1282.8	1048.9	66.61	14.69	14.86
2			1.442	28	761	16.75	13.25	1541	1219					47.089	47.089	0.372	0.364	0.184	23.545	69.358		1.635	0.81	0.825	1248.2	1005.7	62.85	14.25	14.5
3						17	14	1479	1218				1.336	45.279	48.514	0.356	0.376	2.363	23.853	890.994	38.45	5.214	2.635	2.689	3997.2	3031.6	614.93	45.22	43.75
4																					0	1.647	0.847	0.8	1252.7	974.4	63.53	14.89	14.06
5						16.25	12.75	1414	1109				1.32	43.03	43.98	0.326	0.311	0.159	21.721	60.003	0	1.881	0.923	0.959	1365.1	1168.1	83.19	16.22	16.85
6																					25.38	3.373	1.668	1.705	3074.1	24808	404.73	38.45	37.28
7				29	611	19	15	1843	1455				1.331	70.236	72.003	0.552	0.536	2.363	23.853	890.994	0	3.106	0.547	0.559	1008.1	813.35	43.51	11.95	12.22
8																					20	2.575	1.273	1.302	2346.1	1894.4	236.88	27.52	28.45
9																					18.63	2.348	1.16	1.188	2132	24328	1974.2	299.77	31.16
10	Micro. Base	2				20	16	2180	1744				1.304	105.221	108.254	0.763	0.749	0.378	53.358	142.490	16.47	2.248	1.045	1.141	2132	24328	1974.2	299.77	31.16
11																					10	2.705	1.365	1.341	2472.8	6422.88	258.06	9.91	9.89
12				30	477	21	17	2289	1853		120	60	1.33	111.182	116.832	0.846	0.863	2.363	23.853	890.994	10	1.012	0.511	0.5	1169.7	926.5	58.24	14.26	13.94
13			1.369																		20	1.884	0.953	0.931	2181.4	1726.1	202.24	26.59	26
14																					25	1.516	0.766	0.749	1753.4	1387.9	130.78	21.39	20.91
15																					10.4	1.32	0.657	0.664	1907.9	1526.5	156.60	23.14	23.38
16																					0	0.443	0.22	0.223	638.88	512.68	17.84	7.77	7.85
17				31	377	24	19	2904	2289				1.342	178.887	184.587	1.364	1.342	2.363	23.853	890.994	7.5	0.895	0.445	0.45	1292.3	1034.6	72.80	15.68	15.85
18																					10	1.312	0.653	0.659	1896.3	1515	156.44	22.99	23.24
19																					15	1.001	0.498	0.503	1446.2	1156.4	91.07	17.54	17.73
20																					20	0.787	0.391	0.396	1135.5	910.4	56.29	13.79	13.94
21																					7.14	0.884	0.447	0.437	1557.3	1239.7	108.09	19.49	19.05
22				32	304	26	21	3484	2814				1.336	264.903	278.357	1.953	1.991	2.363	23.853	890.994	0	0.303	0.153	0.15	533.05	422.1	12.46	6.69	6.54
23																					10	0.696	0.352	0.344	1226.4	968.02	65.76	15.34	14.99

Important Outputs to Monitor
Optimum Capacitance Values
Best: Potential Outputs to Use
Good: 2nd Level Potential Outputs to Use

Figure A-2: Phase I Primary Wire Sizing Comparisons

PhD DISSERTATION
LEVITATION SOLENOID DESIGN
- PARAMETRIC STUDY -

Notes:
1. This document is comprised of many approximations and assumptions to achieve the closed form solution.
2. This document is ONLY meant to give rough order values for the true case.
3. This document provides a quick parametric study of the Phase I simplified case of the state equation to verify the equations & provide approx. parameters.
4. Matlab is used to simulate & wrap numerical simulation & control around these equations.
5. Ansys & Opera are used to computationally verify the state equation outputs under certain conditions.
6. Labview is used to control a prototype system demonstration and compare test to simulation data.
7. Subscript (1) is for the solenoid primary. Subscript (C1), (C2), & (C3) are solenoid inside to outside coils 1, 2, & 3.
8. Subscript (2) is for the levitated disk secondary.
9. The multiple coils are assumed co-axial.

Highlighter Notes:	Yellow = Input Values
	Green = Output Values
	Blue = Governing Equations
	Purple = Important Input or Output Notes

CONSTANTS & VARIABLES (ALL PHASES)

Constants - Material & Fundamental:

$\mu_0 = 1.257 \times 10^{-6} \frac{H}{m}$

$\sigma_{Cu} := \frac{1}{1.673 \cdot 10^{-6} \cdot ohm \cdot cm}$

$density_{Cu} := 8.934 \cdot 10^{3} \frac{kg}{m^3}$

$C_{p\_Cu} := 0.0922 \cdot \frac{cal}{gm \cdot K}$

Note: Cp = Specific Heat

$Coef_{temp\_Cu} := 0.0043 \cdot \frac{1}{K}$

$\sigma_{Al} := \frac{1}{2.655 \cdot 10^{-6} \cdot ohm \cdot cm}$

$density_{Al} := 2.692 \cdot 10^{3} \frac{kg}{m^3}$

$C_{p\_Al} := 0.23 \cdot \frac{cal}{gm \cdot K}$

$Coef_{temp\_Al} := 0.004 \cdot \frac{1}{K}$

$\sigma_{Cu} = 5.977 \times 10^{7} \frac{S}{m}$

$\sigma_{Al} = 3.766 \times 10^{7} \frac{S}{m}$

$g = 9.807 \frac{m}{s^2}$

Note: Opera conductivity input is in (Siemens/meter) when in S.I.

Constants - Material & Geometry:

Design to a maximum perturbation oscillation zero to peak amplitude of this ratio of the normal air gap.

$Ratio_{0toPeak\_gap\_design} := \frac{1}{3}$

$Ratio_{gap\_design} := 2 \cdot Ratio_{0toPeak\_gap\_design}$

Note: z_0 represents the boundary condition distance between regions 1, the primary, and 3, the air gap b/w the primary and secondary.

$z_0 := 0 \cdot in$

$Coef_{temp\_wire} := Coef_{temp\_Cu}$

$density_{wire} := density_{Cu}$

$\sigma_1 := \sigma_{Cu}$

$\sigma_2 := \sigma_{Cu}$

$C_{p\_wire} := C_{p\_Cu}$

$density_2 := density_{Cu}$

$B_{sat}(z_g, rad_2) := 0.8 \cdot T$

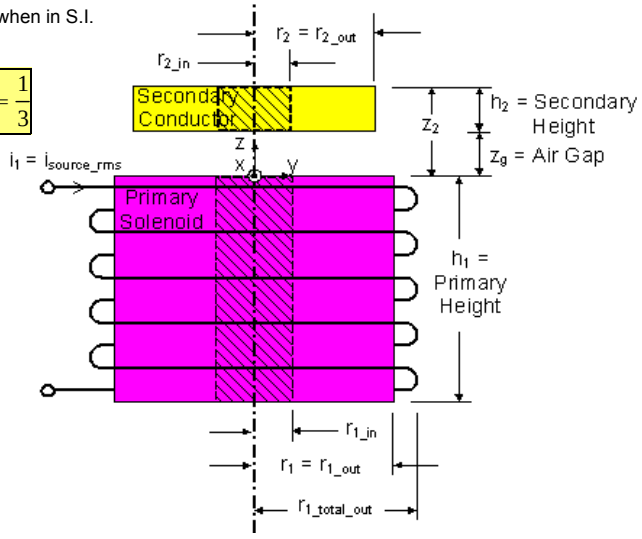

B SATURATION Notes (Refer to diss. Write-up):

- The magnetic equations in this analysis do not provide for a gap distance dependent coupling of the mutual inductance for either the principal or control solenoids. Instead the mutual inductance is set to a typical operational cc value
- Now what is presented is INCORRECT. The magnetic equations in this analysis also do not provide for the primary iron B-H curve in either the principal or control solenoid. Instead the magnetic flux density, B, is set with a step function to purely saturate at a constant value. Although only the real component of the B is used in physical outputs such as force and current density, but this saturating value is applied to both the real and imaginary B components for numerical purposes. This magnetic saturation is only placed upon the B and not upon the inductance of each coil and thereby uncoupling the saturating magnetic flux density from the primary current. This is incorrect since in reality as the primary iron saturates the inductance will lower at that state and allow more current into the coils for a unit voltage increase compared to a unit voltage increase of an unsaturated core. Assuming no resonant capacitor, this will raise the coil temperatures as well as B in an increasingly linear fashion with the increased current which in turn saturates the iron even more yet only providing an increasingly linear output force. This process continues with increased current until the primary iron is completely saturated and linear. This incorrect uncoupling of the saturating magnetic flux density from the primary current is acceptable for this analysis for the following two specific reasons. The first is due to the introduced series resonance capacitor used with each solenoid as discussed in Chapter . As the coil primary iron saturates the introduced resonance capacitor will no longer be in resonance with the solenoid. Therefore as the solenoid coil inductances vary the capacitor will restrict the source current and in turn the B through its' own reactive losses. The second is that for best performance it is desired to operate in a resonant capacitor to coil inductor condition with maximum B and as low a primary current per coil as possible due to thermal limitations. Therefore even though taking the saturation of the B and not coupling this value with the coil inductance provides an incorrect result, it also provides the combined effective material, geometric, and electrical operational bandwidths to avoid. Therefore the proper system operation should naturally avoid these operational bandwidth areas by designing a system that experiences only a low saturation during peak performance.

A.1.b Phase I Solenoid Design

PHASE I - SOLENOID DESIGN

Solenoid Core & Magnet Wire Materials Readily Available @ Home Lab (ALL Round Wire):

18 gage Cu wire: Diam. 0.0403" commonly handles 7.75A safely. Heavy Build Diam. = 0.0431"	20 gage Cu wire: Diam. 0.032" commonly handles 4.89A safely. Heavy Build Diam. = 0.0346"	22 gage Cu wire: Diam. 0.0253" commonly handles 3.04A safely. Heavy Build Diam. = 0.0276"
26 gage Cu wire: Diam. 0.0159" commonly handles 1.2 A safely. Heavy Build Diam. = 0.0178"	28 gage Cu wire: Diam. 0.0126" commonly handles 761mA safely. Heavy Build Diam. = 0.0144"	30 gage Cu wire: Diam. 0.0100" commonly handles 477mA safely. Heavy Build Diam. = 0.0116"
31 gage Cu wire: Diam. 0.0089" commonly handles 377mA safely. Heavy Build Diam. = 0.0105"	32 gage Cu wire: Diam. 0.008" commonly handles 304mA safely. Heavy Build Diam. = 0.0095"	37 gage Cu wire: Diam. 0.0045" commonly handles 94.3mA safely. Heavy Build Diam. = 0.0055"

Initial solenoid Core Empirical Measurements (VERY loose packing factor for 1 layer):

Note: As specific coils are wound with exact material and geometry, update this area and the mu used.

ϕ4.1" (16 turns, height 1")

Core:	Air	Fe
D:	0.0243	0.159
R (Ω):	0.058	0.059
L (μH):	38.5	58.9
C (μF):	634	426

ϕ2.25 " (27 turns, height 1.25")

Core:	Air	Fe
D:	0.196	0.113
R (Ω):	0.059	0.059
L (μH):	47.9	82.2
C (μF):	517	309

L Ratios (Iron/Air): $\frac{58.9}{38.5} = 1.53$ $\frac{82.2}{47.9} = 1.716$

Constants - Material (from Empirical Data):

Relative Permeability for Iron Used: $\mu_{r1} = 4.673$

$\mu_{r1} := 4.673$ Relative permeability of primary iron. Determined below from test data plugged into L analysis.

$\mu_1 := \mu_{r1} \cdot \mu_0$ $\mu_2 := \mu_0$ $\mu_3 := \mu_0$ $\mu_4 := \mu_0$

Constants - Primary Solenoid Geometry:

$\phi_{1\_out} := 2 \cdot 0.8 \cdot in$ $\quad rad_{1\_in} := 0.125 \cdot in$ Inside radius of a single solenoid. Primary hole is probably never used since it's a financial burden without an immediate analytical gain..

$rad_{1\_out} := \frac{\phi_{1\_out}}{2}$ **Vary Sol. Fe O.D. for Solutions** Outside radius of a single solenoid $\quad rad_{1\_out} = 0.8\,in$

$area_1 := \pi \cdot \left(rad_{1\_out}^2 - rad_{1\_in}^2\right)$ Solenoid core magnet area $\quad area_1 = 1.962\,in^2 \quad area_1 = 12.655\,cm^2$

Constants - Primary Solenoid Wire Geometry

$AWG := 28$

$$\phi_{C1wire\_elec} := \begin{cases} 0.0403 \cdot in & \text{if } AWG = 18 \\ 0.032 \cdot in & \text{if } AWG = 20 \\ 0.0253 \cdot in & \text{if } AWG = 22 \\ 0.0201 \cdot in & \text{if } AWG = 24 \\ 0.0159 \cdot in & \text{if } AWG = 26 \\ 0.0126 \cdot in & \text{if } AWG = 28 \\ 0.0113 \cdot in & \text{if } AWG = 29 \\ 0.01 \cdot in & \text{if } AWG = 30 \\ 0.0089 \cdot in & \text{if } AWG = 31 \\ 0.008 \cdot in & \text{if } AWG = 32 \\ 0.0045 \cdot in & \text{if } AWG = 37 \end{cases} \quad \phi_{C1wire\_mech} := \begin{cases} 0.0431 \cdot in & \text{if } AWG = 18 \\ 0.0346 \cdot in & \text{if } AWG = 20 \\ 0.0276 \cdot in & \text{if } AWG = 22 \\ 0.0223 \cdot in & \text{if } AWG = 24 \\ 0.0178 \cdot in & \text{if } AWG = 26 \\ 0.0144 \cdot in & \text{if } AWG = 28 \\ 0.0130 \cdot in & \text{if } AWG = 29 \\ 0.0116 \cdot in & \text{if } AWG = 30 \\ 0.0105 \cdot in & \text{if } AWG = 31 \\ 0.0095 \cdot in & \text{if } AWG = 32 \\ 0.0055 \cdot in & \text{if } AWG = 37 \end{cases}$$

$\phi_{C1wire\_elec} = 0.013\,in$

$\phi_{C1wire\_mech} = 0.014\,in$

$\phi_{C2wire\_elec} := \phi_{C1wire\_elec}$

$\phi_{C2wire\_mech} := \phi_{C1wire\_mech}$

$\phi_{C3wire\_elec} := \phi_{C1wire\_elec}$

$\phi_{C3wire\_mech} := \phi_{C1wire\_mech}$

$$I_{AWG\_safe} := \begin{cases} 7.75 \cdot A & \text{if } AWG = 18 \\ 4.89 \cdot A & \text{if } AWG = 20 \\ 3.04 \cdot A & \text{if } AWG = 22 \\ 1.93 \cdot A & \text{if } AWG = 24 \\ 1.2 \cdot A & \text{if } AWG = 26 \\ 0.761 \cdot A & \text{if } AWG = 28 \\ 0.611 \cdot A & \text{if } AWG = 29 \\ 0.477 \cdot A & \text{if } AWG = 30 \\ 0.377 \cdot A & \text{if } AWG = 31 \\ 0.304 \cdot A & \text{if } AWG = 32 \\ 0.0943 \cdot A & \text{if } AWG = 37 \end{cases}$$

$rad_{C1wire\_elec} := \frac{\phi_{C1wire\_elec}}{2}$ $\quad rad_{C2wire\_elec} := \frac{\phi_{C1wire\_elec}}{2}$

$rad_{C3wire\_elec} := \frac{\phi_{C1wire\_elec}}{2}$

$I_{AWG\_safe} = 0.761\ A$

IMPORTANT NOTE: To turn ***"ON"*** a coil, just set the coil flag ***= 1.*** To turn ***"OFF"*** a coil, just set the coil flag ***= 0,*** *BUT* only turn ***"OFF"*** coils in highest to lowest numerical sequence.

$flag_{C1} := 1$ $\quad flag_{C2} := 1$ $\quad flag_{C3} := 0$ $\quad N_{Core\_Pedestals\_for\_Layers} := 1$ $\quad height_{single\_pedestal} := 1.615 \cdot in$

Height Allowed: [(% of Wound Center Pedestal)-(Pedestal Groove)-(Polymer Cover)-(Approx. Winding End Tol.)]

$height_{pedestal} := N_{Core\_Pedestals\_for\_Layers} \cdot height_{single\_pedestal}$ $\quad \%Height_{PedestalAvailableWound} := 100$

$$height_{C1wire} := \left[\left(\frac{\%Height_{PedestalAvailableWound}}{100} \cdot height_{pedestal} - 0.03 \cdot in\right) - 0.1 \cdot in - \left(5 \cdot \phi_{C1wire\_mech}\right)\right]$$

$$height_{C1pedestal\_unused} := \left(1 - \frac{\%Height_{PedestalAvailableWound}}{100}\right) \cdot height_{pedestal}$$

$height_{C2wire} := height_{C1wire}$

$height_{C3wire} := height_{C1wire}$

$pf_{turn} := 1.1$ Estimated packing factor per turn. Wire diam. to wire diam.

$$N_{C1wire\_height} := ceil\left(\frac{height_{C1wire}}{pf_{turn} \cdot \phi_{C1wire\_mech}}\right)$$

Note: Approx. # of solenoid wires per laying winding height.

$N_{C2wire\_height} := N_{C1wire\_height} \cdot flag_{C2}$ $\quad N_{C3wire\_height} := N_{C1wire\_height} \cdot flag_{C3}$

$height_{C1wire} = 1.413\,in$ $\quad height_{C1pedestal\_unused} = 0\,in$

$N_{C1wire\_height} = 90$ $\quad N_{C2wire\_height} = 90$ $\quad N_{C3wire\_height} = 0$

$area_{C1wire\_elec} := \pi \cdot rad_{C1wire\_elec}^2$ $area_{C2wire\_elec} := \pi \cdot rad_{C2wire\_elec}^2$ $area_{C3wire\_elec} := \pi \cdot rad_{C3wire\_elec}^2$

$rad_{C1wire\_mech} := \frac{\phi_{C1wire\_mech}}{2}$ $rad_{C2wire\_mech} := \frac{\phi_{C1wire\_mech}}{2}$ $rad_{C3wire\_mech} := \frac{\phi_{C1wire\_mech}}{2}$

$area_{C1wire\_mech} := \pi \cdot rad_{C1wire\_mech}^2$ $area_{C2wire\_mech} := \pi \cdot rad_{C2wire\_mech}^2$ $area_{C3wire\_mech} := \pi \cdot rad_{C3wire\_mech}^2$

$N_{C1wire\_layers} := 16.75 \cdot flag_{C1}$ $N_{C1wireRatio} := (N_{C1wire\_layers} - floor(N_{C1wire\_layers}))$

$N_{C1wireExtra} := \begin{cases} 0 & \text{if } N_{C1wireRatio} = 0 \\ N_{C1wireRatio} & \text{otherwise} \end{cases}$ $N_{C2wireExtra} := \begin{cases} 0 & \text{if } N_{C1wireRatio} = 0 \\ 1 - N_{C1wireRatio} & \text{otherwise} \end{cases}$

$N_{C1wireExtra} = 0.75$

$N_{C2wireExtra} = 0.25$

$N_{C2wire\_layers} := flag_{C2} \cdot (round(0.78 \cdot N_{C1wire\_layers}) + N_{C2wireExtra})$

$N_{C3wire\_layers} := flag_{C3} \cdot (round(0.5 \cdot N_{C1wire\_layers}))$

$N_{C1turns} := round(N_{C1wire\_layers} \cdot N_{C1wire\_height})$

$N_{C2turns} := round(N_{C2wire\_layers} \cdot N_{C2wire\_height})$

$N_{C3turns} := round(N_{C3wire\_layers} \cdot N_{C3wire\_height})$

$N_{C1turns} = 1508$ $N_{C2turns} = 1193$ $N_{C3turns} = 0$

$N_{C1wire\_layers} = 16.75$ $N_{C2wire\_layers} = 13.25$ $N_{C3wire\_layers} = 0$

$length_{C1wire\_layers} := pf_{turn} \cdot ceil(N_{C1wire\_layers}) \cdot \phi_{C1wire\_mech}$ $length_{C2wire\_layers} := pf_{turn} \cdot ceil(N_{C2wire\_layers}) \cdot \phi_{C2wire\_mech}$

$length_{C3wire\_layers} := pf_{turn} \cdot ceil(N_{C3wire\_layers}) \cdot \phi_{C3wire\_mech}$ $length_{C1wire\_layers} = 0.269\,in$ $length_{C2wire\_layers} = 0.222\,in$

$rad_{coil\_insul} := 0.015 \cdot in$ $length_{C3wire\_layers} = 0\,in$

ADDED INSULATION
(For length layers build)
Inside Coil: 0.017"
Outside Coil: 0.012"
Min. Shell inside: 1.308"

Note: Shell inside radius is approximately 1.35".

$rad_{C1\_out} := rad_{1\_out} + length_{C1wire\_layers} + 2 \cdot rad_{coil\_insul}$

$rad_{C2\_out} := rad_{C1\_out} + length_{C2wire\_layers} + rad_{coil\_insul}$

$rad_{C3\_out} := rad_{C2\_out} + length_{C3wire\_layers} + rad_{coil\_insul}$ $rad_{C1\_out} = 1.099\,in$ $rad_{C2\_out} = 1.336\,in$ $rad_{C3\_out} = 1.351\,in$

$area_{C1X} := length_{C1wire\_layers} \cdot height_{C1wire}$ $area_{C1X} = 0.38\,in^2$

$area_{C2X} := length_{C2wire\_layers} \cdot height_{C2wire}$ $area_{C2X} = 0.313\,in^2$

$area_{C3X} := length_{C2wire\_layers} \cdot height_{C3wire}$ $area_{C3X} = 0.313\,in^2$

Note: Total radial direction, cross sectional solenoid current density area for Computational Mag. runs & Mech. radius approx.

$pf_{C1} := \frac{N_{C1turns} \cdot area_{C1wire\_elec}}{area_{C1X}}$ $pf_{C1} = 0.494$

$pf_{C2} := \frac{N_{C2turns} \cdot area_{C2wire\_elec}}{area_{C2X}}$ $pf_{C2} = 0.475$

pf = Total packing factor; Used with both the ampere turn area for the volume current density and length for the surface current density. NOT including external coil insulation in this calc.

$pf_{C3} := \frac{N_{C2turns} \cdot area_{C2wire\_elec}}{area_{C2X}}$ $pf_{C3} = 0.475$

$length_{C1wire} := \sum_{nlay=0}^{floor(N_{C1wire\_layers})-1} \left[N_{C1wire\_height} \cdot 2 \cdot \pi \cdot (rad_{1\_out} + rad_{C1wire\_mech} + nlay \cdot \phi_{C1wire\_mech}) \right]$

$length_{C2wire} := \sum_{nlay=0}^{floor(N_{C2wire\_layers})-1} \left[N_{C2wire\_height} \cdot 2 \cdot \pi \cdot (rad_{C1\_out} + rad_{C2wire\_mech} + nlay \cdot \phi_{C2wire\_mech}) \right]$

$length_{C3wire} := \sum_{nlay=0}^{floor(N_{C3wire\_layers})-1} \left[N_{C3wire\_height} \cdot 2 \cdot \pi \cdot (rad_{C2\_out} + rad_{C3wire\_mech} + nlay \cdot \phi_{C3wire\_mech}) \right]$

$length_{C1wireExtra} := \begin{cases} 0 & \text{if } N_{C1wireRatio} = 0 \\ N_{C1wireExtra} \cdot N_{C1wire\_height} \cdot 2 \cdot \pi \cdot \left[rad_{1\_out} + rad_{C1wire\_mech} + (ceil(N_{C1wire\_layers}) - 1) \cdot \phi_{C1wire\_mech} \right] & \text{otherwise} \end{cases}$

$length_{C2wireExtra} := \begin{cases} 0 & \text{if } N_{C1wireRatio} = 0 \\ N_{C2wireExtra} \cdot N_{C2wire\_height} \cdot 2 \cdot \pi \cdot \left[rad_{C1\_out} + rad_{C2wire\_mech} + (ceil(N_{C2wire\_layers}) - 1) \cdot \phi_{C2wire\_mech} \right] & \text{otherwise} \end{cases}$

$length_{C1wireExtra} = 36.672\,ft$ $length_{C2wireExtra} = 15.241\,ft$

Constants - Control Solenoid Electrical Source & Secondary Magnetic:

$freq := 60 \cdot Hz$ $\omega := 2 \cdot \pi \cdot freq$ $v_{rms} := 120 \cdot V$

$v_{peak} := \sqrt{2} \cdot v_{rms}$ $v_{peak} = 169.706\ V$

Note: $flag_{Cres}$ above turns the capatitor "ON" (1) or "OFF" (0).

$flag_{Cres} := 0$ $R_{external\_R} := 0 \cdot ohm$

Effective wavelength: $\lambda_{eff} := 2 \cdot (2 \cdot rad_{mag\_max})$

$\lambda_{eff} = 4.711\ in$

Pole pitch: $\tau_p := \frac{\lambda_{eff}}{2}$ $\tau_p = 2.355\ in$

Wave number: $\beta := \frac{2 \cdot \pi}{\lambda_{eff}}$ $\beta = 1.334 \frac{1}{in}$

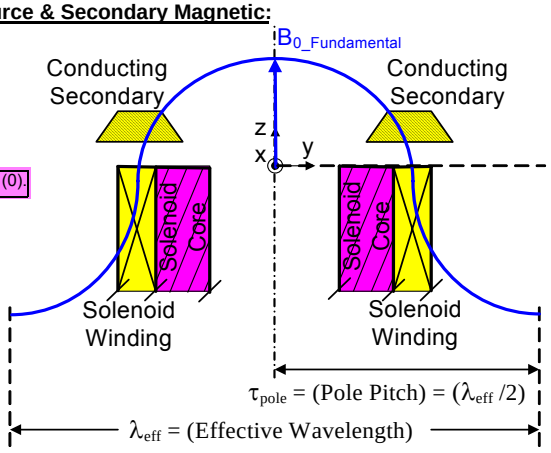

Constants - Mechanical - Secondary (Initially assuming a flat disc secondary):

Note: Use volume 2 for the secondary mass and weight, but use volume magnetic for the magnetic pressure volume.

$\delta := \sqrt{\frac{2}{\omega \cdot \mu_0 \cdot \sigma_2}}$ $\delta = 0.331\ in$

Note: The skin depth is used to determine the secondary's thickness.

$vel := 0 \frac{m}{s}$

$area_2(rad_2) := \pi \cdot (rad_2^2 - rad_{2\_in}^2)$ $area_{2\_max} := 2 \cdot \pi \cdot \int_{rad_{2\_in}}^{rad_{2\_out}} r\ dr$ $area_{2\_max} = 5.297\ in^2$

$area_{mag} := \pi \cdot (rad_{mag\_max}^2 - rad_{mag\_min}^2)$

$rad_{mag\_min} = 0.338\ in$

$rad_{mag\_max} = 1.178\ in$

$vol_2(rad_2) := \delta \cdot area_2(rad_2)$ $vol_{2max} := \delta \cdot area_{2\_max}$

$mass_2(rad_2) := vol_2(rad_2) \cdot density_2$ $mass_{2max} := vol_{2max} \cdot density_2$ $mass_{2max} = 0.257\ kg$

$F_g(rad_2) := mass_2(rad_2) \cdot g$ $F_{gmax} := mass_{2max} \cdot g$

Air Gap Magnetic Volume:

$vol_{mag} := \delta \cdot area_{mag}$

Note: The subscript "Actual" is meant to represent the actual secondary sizing used.

$thk_{2Actual} := 0.375 \cdot in$ $rad_{2Actual} := 1.5 \cdot in$ $rad_{2ActualIn} := 0 \cdot in$ $area_{2Actual} := \pi \cdot (rad_{2Actual}^2 - rad_{2ActualIn}^2)$

$vol_{2Actual} := thk_{2Actual} \cdot area_{2Actual}$ $mass_{2Actual} := density_2 \cdot vol_{2Actual}$ $F_{gActual} := mass_{2Actual} \cdot g$

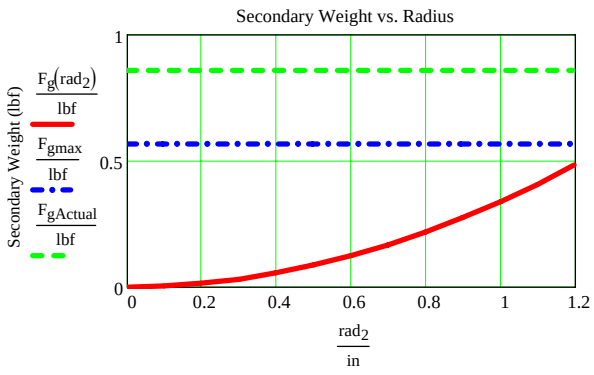

$F_g(rad_2) =$

0	lbf
3.355·10-3	
0.013	
0.03	
0.054	
0.084	
0.121	
0.164	
0.215	
0.272	
0.335	
0.406	
0.483	

$F_g(rad_{2\_out}) = 0.566\ lbf$

$F_{gActual} = 0.856\ lbf$

Note: The magnetic volume solution used for the magnetic analysis is the **air gap magnetic volume** .

Solenoid Electrical R & L Values:

$R_{C1sol} := \frac{length_{C1wire}}{\sigma_1 \cdot area_{C1wire\_elec}}$ $R_{C2sol} := \frac{length_{C2wire}}{\sigma_1 \cdot area_{C2wire\_elec}}$

$R_{C3sol} := \frac{length_{C3wire}}{\sigma_1 \cdot area_{C3wire\_elec}}$

$R_{C1sol} = 46.434\ \Omega$ $R_{C2sol} = 47.729\ \Omega$ $R_{C3sol} = 0$

Note: These equations directly assume that only the self inductance of the iron core of the primary coil affects the reactive component of the impedance. The MUTUAL component is accounted for by the experimental adjustment terms.

Inductance Tests:

Constants - Mechanical - Secondary (Initially assuming a flat disc secondary):

Note: Use volume 2 for the secondary mass and weight, but use volume magnetic for the magnetic pressure volume.

$\delta := \sqrt{\frac{2}{\omega \cdot \mu_0 \cdot \sigma_2}}$ $\delta = 0.331\,in$

Note: The skin depth is used to determine the secondary's thickness.

$vel := 0\,\frac{m}{s}$

$area_2(rad_2) := \pi \cdot \left(rad_2^2 - rad_{2\_in}^2\right)$ $area_{2\_max} := 2 \cdot \pi \cdot \int_{rad_{2\_in}}^{rad_{2\_out}} r\,dr$ $area_{2\_max} = 5.297\,in^2$

$area_{mag} := \pi \cdot \left(rad_{mag\_max}^2 - rad_{mag\_min}^2\right)$

$rad_{mag\_min} = 0.338\,in$

$rad_{mag\_max} = 1.178\,in$

$vol_2(rad_2) := \delta \cdot area_2(rad_2)$ $vol_{2max} := \delta \cdot area_{2\_max}$

$mass_2(rad_2) := vol_2(rad_2) \cdot density_2$ $mass_{2max} := vol_{2max} \cdot density_2$ $mass_{2max} = 0.257\ kg$

Air Gap Magnetic Volume:

$vol_{mag} := \delta \cdot area_{mag}$

$F_g(rad_2) := mass_2(rad_2) \cdot g$ $F_{gmax} := mass_{2max} \cdot g$

Note: The subscript "Actual" is meant to represent the actual secondary sizing used.

$thk_{2Actual} := 0.375 \cdot in$ $rad_{2Actual} := 1.5 \cdot in$ $rad_{2ActualIn} := 0 \cdot in$ $area_{2Actual} := \pi \cdot \left(rad_{2Actual}^2 - rad_{2ActualIn}^2\right)$

$vol_{2Actual} := thk_{2Actual} \cdot area_{2Actual}$ $mass_{2Actual} := density_2 \cdot vol_{2Actual}$ $F_{gActual} := mass_{2Actual} \cdot g$

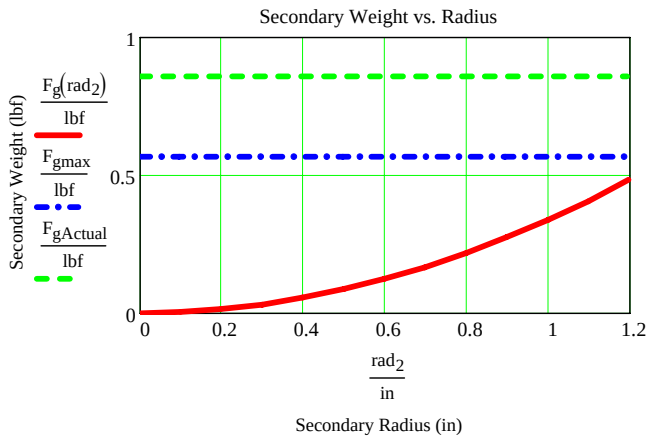

$F_g(rad_2) =$

0	lbf
$3.355 \cdot 10^{-3}$	
0.013	
0.03	
0.054	
0.084	
0.121	
0.164	
0.215	
0.272	
0.335	
0.406	
0.483	

$F_g(rad_{2\_out}) = 0.566\,lbf$

$F_{gActual} = 0.856\,lbf$

Note: The magnetic volume solution used for the magnetic analysis is the **air gap magnetic volume** .

Solenoid Electrical R & L Values:

$R_{C1sol} := \frac{length_{C1wire}}{\sigma_1 \cdot area_{C1wire\_elec}}$ $R_{C2sol} := \frac{length_{C2wire}}{\sigma_1 \cdot area_{C2wire\_elec}}$ $R_{C3sol} := \frac{length_{C3wire}}{\sigma_1 \cdot area_{C3wire\_elec}}$

$R_{C1sol} = 46.434\ \Omega$ $R_{C2sol} = 47.729\ \Omega$ $R_{C3sol} = 0$

Note: These equations directly assume that only the self inductance of the iron core of the primary coil affects the reactive component of the impedance. The MUTUAL component is accounted for by the experimental adjustment terms.

Inductance Tests:

adjustment terms.

Inductance Tests:

$$L_{sol\_LongSol} := \frac{\mu_1 \cdot N_{C1turns}^{2} \cdot area_1}{height_{C1wire}} \qquad L_{sol\_LongSol} = 0.464\,H$$

Note: NO Coil #3 Experimental Adjustment since no such coil fabricated to date.

$$L_{C1\_AdjustFromExp} := \frac{0.406}{0.36} \qquad L_{C2\_AdjustFromExp} := \frac{0.269}{0.355}$$

$L_{C1\_AdjustFromExp} = 1.128$ $\quad L_{C1\_AdjustFromExp} \cdot \mu_{r1} = 5.27$

$L_{C2\_AdjustFromExp} = 0.758$ $\quad L_{C2\_AdjustFromExp} \cdot \mu_{r1} = 3.541$

$\mu_{r1} = 4.673$

$$L_{C1solCheck1} := L_{C1\_AdjustFromExp} \cdot \mu_{r1} \cdot \frac{0.8 \cdot \left(\frac{r_{C1\_winding\_avg}}{in} \cdot N_{C1turns} \right)^2}{6 \cdot \frac{r_{C1\_winding\_avg}}{in} + 9 \cdot \frac{height_{C1wire}}{in} + 10 \cdot \frac{length_{C1wire\_layers}}{in}} \cdot \left(10^{-6} \cdot H\right) \qquad L_{C1solCheck1} = 0.406\ H$$

$$L_{C2solCheck1} := L_{C2\_AdjustFromExp} \cdot \mu_{r1} \cdot \frac{0.8 \cdot \left(\frac{r_{C2\_winding\_avg}}{in} \cdot N_{C2turns} \right)^2}{6 \cdot \frac{r_{C2\_winding\_avg}}{in} + 9 \cdot \frac{height_{C2wire}}{in} + 10 \cdot \frac{length_{C2wire\_layers}}{in}} \cdot \left(10^{-6} \cdot H\right) \qquad L_{C2solCheck1} = 0.269\ H$$

$$L_{C3solCheck1} := \mu_{r1} \cdot \frac{0.8 \cdot \left(\frac{r_{C3\_winding\_avg}}{in} \cdot N_{C3turns} \right)^2}{6 \cdot \frac{r_{C3\_winding\_avg}}{in} + 9 \cdot \frac{height_{C3wire}}{in} + 10 \cdot \frac{length_{C3wire\_layers}}{in}} \cdot \left(10^{-6} \cdot H\right) \qquad L_{C3solCheck1} = 0$$

$$\frac{length_{C1wire\_layers}}{height_{C1wire}} = 0.163$$

$$L_{solCheck2} := \mu_{r1} \cdot \frac{r_{C1\_winding\_avg} \cdot N_{C1turns}^{2}}{13.5} \cdot \log(10) \cdot \frac{3.6 \cdot r_{C1\_winding\_avg}}{length_{C1wire\_layers}^{2} + height_{C1wire}^{2}} \cdot 10^{-6} \cdot H \qquad L_{solCheck2} = 1.135\ H$$

Note [Compare empirical L to analytical L]: $L_{solCheck1}$ of the three inductance methods used above provides the solution closest empirical data and hence is used for all calcs.

$$L_{C1sol} := L_{C1solCheck1} \qquad L_{C2sol} := \begin{cases} 0 \cdot H & \text{if } N_{C2wire\_height} = 0 \\ L_{C2solCheck1} & \text{otherwise} \end{cases} \qquad L_{C3sol} := \begin{cases} 0 \cdot H & \text{if } N_{C3wire\_height} = 0 \\ L_{C3solCheck1} & \text{otherwise} \end{cases}$$

$L_{C1sol} = 0.406\ H$ $\quad L_{C2sol} = 0.269\ H$ $\quad L_{C3sol} = 0$

$$\tau_{C1sol} := \frac{L_{C1sol}}{R_{C1sol}} \qquad \tau_{C2sol} := \frac{L_{C2sol}}{R_{C2sol}} \qquad \tau_{C3sol} := \frac{L_{C3sol}}{R_{C3sol}}$$

$\tau_{C1sol} = 8.752 \times 10^{-3}\ s$ $\quad \tau_{C2sol} = 5.629 \times 10^{-3}\ s$ $\quad \tau_{C3sol} = 0$

$$\mu_{r1\_TestData} := \frac{0.313 \cdot H}{\frac{0.8 \cdot \left(\frac{r_{C1\_winding\_avg}}{in} \cdot N_{C1turns} \right)^2}{6 \cdot \frac{r_{C1\_winding\_avg}}{in} + 9 \cdot \frac{height_{C1wire}}{in} + 10 \cdot \frac{length_{C1wire\_layers}}{in}} \cdot \left(10^{-6} \cdot H\right)}$$

$\mu_{r1\_TestData} = 4.059$

POT COIL TEST:
16 layer coil w/ 86 turns per layer (as per L Method #1):
Fe center post only: mu_r = 2.463
Fe core: mu_r = 4.673

SOLENOID CIRCUIT ANALYSIS:

Note: Set up and use a series resonant capacitor that removes the imaginary impedance component. This is preferred here since winding area is limited and hence counterbalances the increased current choke as the number of turns is increased for a smaller wire gage. Essentially it allows a higher current for the same impedance.

$$Z_{C1sol} := R_{C1sol} + j \cdot \omega \cdot L_{C1sol} \qquad |Z_{C1sol}| = 160.088\ \Omega \qquad Z_{C1sol} = (46.434 + 153.206i)\ \Omega$$

$$Z_{C2sol} := R_{C2sol} + j \cdot \omega \cdot L_{C2sol} \qquad |Z_{C2sol}| = 111.961\ \Omega \qquad Z_{C2sol} = (47.729 + 101.278i)\ \Omega$$

$$Z_{C3sol} := R_{C3sol} + j \cdot \omega \cdot L_{C3sol} \qquad |Z_{C3sol}| = 0 \qquad Z_{C3sol} = 0$$

$$Z_{sol\_parallel} := \begin{cases} \left(\frac{Z_{C1sol} \cdot Z_{C2sol}}{Z_{C1sol} + Z_{C2sol}}\right) + R_{external\_R} & \text{if } N_{C3wire\_height} = 0 \\ Z_{C1sol} + R_{external\_R} & \text{if } N_{C2wire\_height} = 0 \\ \left(\frac{1}{\frac{1}{Z_{C1sol}} + \frac{1}{Z_{C2sol}} + \frac{1}{Z_{C3sol}}}\right) + R_{external\_R} & \text{otherwise} \end{cases}$$

$$Z_{sol\_parallel} = (56.98 + 161.08i)\ \Omega$$

$$L_{CapRes\_parallel} := \begin{cases} \frac{L_{C1sol} \cdot L_{C2sol}}{L_{C1sol} + L_{C2sol}} & \text{if } N_{C3wire\_height} = 0 \\ L_{C1sol} & \text{if } N_{C2wire\_height} = 0 \\ \frac{1}{\frac{1}{L_{C1sol}} + \frac{1}{L_{C2sol}} + \frac{1}{L_{C3sol}}} & \text{otherwise} \end{cases}$$

Note: $L_{CapRes\_parallel}$ is the equivalent parallel inductance used for sizing the resonant capacitor IF one is placed in the circuit.

$$L_{CapRes\_parallel} = 0.427\ H$$

$$C_{res} := \begin{cases} 0 & \text{if } flag_{Cres} = 0 \cdot F \\ \frac{1}{(2 \cdot \pi \cdot freq)^2 \cdot L_{CapRes\_parallel}} & \text{otherwise} \end{cases}$$

Note: Use Cres for sizing the resonant capacitor to place in series with solenoid.
$flag_{Cres}$ above turns the capatitor "ON" (1) or "OFF" (0).

$$C_{res} = 1.647 \times 10^{-5}\ F$$

$$Z_{sol\_circuit\_total} := \begin{cases} Z_{sol\_parallel} & \text{if } C_{res} = 0 \cdot F \\ \frac{1}{j \cdot \omega \cdot C_{res}} + Z_{sol\_parallel} & \text{otherwise} \end{cases}$$

$$Z_{sol\_circuit\_total} = (56.98 + 4.092i \times 10^{-3})\ \Omega$$

$$i_{source\_rms} := \frac{v_{rms}}{Z_{sol\_circuit\_total}} \qquad i_{source\_peak} := \sqrt{2} \cdot i_{source\_rms}$$

$$i_{C1\_rms} := \begin{cases} \left(\frac{Z_{C2sol}}{Z_{C1sol} + Z_{C2sol}}\right) \cdot i_{source\_rms} & \text{if } N_{C3wire\_height} = 0 \\ i_{source\_rms} & \text{if } N_{C2wire\_height} = 0 \\ \left(\frac{\frac{1}{Z_{C1sol}}}{\frac{1}{Z_{C1sol}} + \frac{1}{Z_{C2sol}} + \frac{1}{Z_{C3sol}}}\right) \cdot i_{source\_rms} & \text{otherwise} \end{cases}$$

$$i_{C1\_peak} := \sqrt{2} \cdot i_{C1\_rms}$$

$$i_{C1\_rms} = (1.065 - 5.08i \times 10^{-3})\ A$$

$$i_{C2\_rms} := \begin{cases} \left(\frac{Z_{C1sol}}{Z_{C1sol} + Z_{C2sol}}\right) \cdot i_{source\_rms} & \text{if } N_{C3wire\_height} = 0 \\ 0 \cdot A & \text{if } N_{C2wire\_height} = 0 \\ \left(\frac{\frac{1}{Z_{C2sol}}}{\frac{1}{Z_{C1sol}} + \frac{1}{Z_{C2sol}} + \frac{1}{Z_{C3sol}}}\right) \cdot i_{source\_rms} & \text{otherwise} \end{cases}$$

$$i_{C2\_rms} = (1.041 + 4.929i \times 10^{-3})\ A$$

$$i_{C3\_rms} := \begin{cases} 0\cdot A & \text{if } N_{C3wire\_height} = 0 \\ \left(\frac{\frac{1}{Z_{C3sol}}}{\frac{1}{Z_{C1sol}} + \frac{1}{Z_{C2sol}} + \frac{1}{Z_{C3sol}}} \right) \cdot i_{source\_rms} & \text{otherwise} \end{cases}$$

$i_{C3\_rms} = 0\ A$

Monitor Wire Max. RMS Current Values

$|i_{source\_rms}| = 2.106\ A$ $|i_{source\_peak}| = 2.978\ A$

$I_{AWG\_safe} = 0.477\ A$ $|i_{C1\_peak}| = 1.506\ A$ $|i_{C1\_rms}| = 1.065\ A$ $|i_{C2\_rms}| = 1.041\ A$ $|i_{C3\_rms}| = 0\ A$

$Amp\_Turns_{C1} := N_{C1turns} \cdot \sqrt{2} \cdot i_{C1\_rms}$ $Amp\_Turns_{C2} := N_{C2turns} \cdot \sqrt{2} \cdot i_{C2\_rms}$ $|Amp\_Turns_{C1}| = 3.447 \times 10^3\ A$

$Amp\_Turns_{C3} := N_{C3turns} \cdot \sqrt{2} \cdot i_{C3\_rms}$ $|Amp\_Turns_{C2}| = 2.728 \times 10^3\ A$ $|Amp\_Turns_{C3}| = 0\ A$

$$J_{C1wire\_rms} := \frac{i_{C1\_rms}}{area_{C1wire\_elec}} \quad J_{C2wire\_rms} := \frac{i_{C2\_rms}}{area_{C2wire\_elec}} \quad J_{C3wire\_rms} := \frac{i_{C3\_rms}}{area_{C3wire\_elec}}$$

$|J_{C1wire\_rms}| = 2.102 \times 10^7\ \frac{A}{m^2}$ $|J_{C2wire\_rms}| = 2.055 \times 10^7\ \frac{A}{m^2}$ $|J_{C3wire\_rms}| = 0\ \frac{A}{m^2}$

$$J_{C1total\_peak} := \frac{Amp\_Turns_{C1}}{pf_{C1} \cdot area_{C1X}} \quad K_{C1total\_peak} := \frac{Amp\_Turns_{C1}}{pf_{C1} \cdot length_{C1wire\_layers}}$$

$$J_{C2total\_peak} := \frac{Amp\_Turns_{C2}}{pf_{C2} \cdot area_{C2X}} \quad K_{C2total\_peak} := \frac{Amp\_Turns_{C2}}{pf_{C2} \cdot length_{C2wire\_layers}}$$

$$J_{C3total\_peak} := \frac{Amp\_Turns_{C3}}{pf_{C3} \cdot area_{C3X}} \quad K_{C3total\_peak} := \frac{Amp\_Turns_{C3}}{pf_{C3} \cdot length_{C3wire\_layers}}$$

Use these J & K values for Closed Form Solution Anslysis below & Computational Magnetic Analysis Runs

$|J_{C1total\_peak}| = 2.972 \times 10^7\ \frac{A}{m^2}$ $|J_{C2total\_peak}| = 2.906 \times 10^7\ \frac{A}{m^2}$ $|J_{C3total\_peak}| = 0\ \frac{A}{m^2}$

$|K_{C1total\_peak}| = 1.046 \times 10^6\ \frac{A}{m}$ $|K_{C2total\_peak}| = 1.022 \times 10^6\ \frac{A}{m}$ $|K_{C3total\_peak}| = 0\ \frac{A}{m}$

$K_{Tot\_peak} := K_{C1total\_peak} + K_{C2total\_peak} + K_{C3total\_peak}$ $|K_{Tot\_peak}| = 2.068 \times 10^6\ \frac{A}{m}$

$Re(J_{C1total\_peak}) = 2.972 \times 10^7\ \frac{A}{m^2}$ $Re(J_{C2total\_peak}) = 2.906 \times 10^7\ \frac{A}{m^2}$ $Re(J_{C3total\_peak}) = 0\ \frac{A}{m^2}$

$Re(K_{C1total\_peak}) = 1.046 \times 10^6\ \frac{A}{m}$ $Re(K_{C2total\_peak}) = 1.022 \times 10^6\ \frac{A}{m}$ $Re(K_{C3total\_peak}) = 0\ \frac{A}{m}$

Note: The Opera Computational model accepts the REAL current density PEAK value (Peak is to find the Bpeak value). The final lift force is of couse propotional to (NI)^2 or (Amp_Turns)^2. Most other current based equations require the RMS or amplitude, absolute, value of the current.

Mathcad & Opera Inductance & Energy Comparisons (Single Coil only):

$$L_{sol\_air1} := 1 \cdot \frac{0.8 \cdot \left(\frac{r_{C1\_winding\_avg}}{in} \cdot N_{C1turns} \right)^2}{6 \cdot \frac{r_{C1\_winding\_avg}}{in} + 9 \cdot \frac{height_{C1wire}}{in} + 10 \cdot \frac{length_{C1wire\_layers}}{in}} \cdot \left(10^{-6} \cdot H \right)$$

$L_{sol\_air1} = 0.181\ H$

$Z_{sol\_air} := R_{C1sol} + j \cdot \omega \cdot L_{sol\_air1}$ $Z_{sol\_air\_circuit\_total} := Z_{sol\_air} + R_{external\_R}$ $|Z_{sol\_air}| = 130.474\ \Omega$

$|Z_{sol\_air\_circuit\_total}| = 130.474\ \Omega$

$$i_{source\_air\_rms} := \frac{v_{rms}}{Z_{sol\_air\_circuit\_total}} \qquad i_{source\_air\_peak} := \sqrt{2} \cdot i_{source\_air\_rms}$$

Monitor Wire Max. RMS Current Values

$|i_{source\_air\_rms}| = 0.92\ A$

$$Amp\_Turns\_air := N_{C1turns} \cdot i_{source\_air\_peak}$$

$$J_{total\_air\_peak} := \frac{Amp\_Turns\_air}{pf_{C1} \cdot area_{C1X}}$$

Use this value for single coil Opera Runs with AIR CORE

$$|J_{total\_air\_peak}| = 2.567 \times 10^{7}\ \frac{A}{m^2}$$

Solenoid Heat Generation & Temperature Rise (Lumped Capacitance Method):

Note: The Lumped Capacitance Method is ONLY used to get a quick idea for the heat generation and associated temperature rise in the primary for the applied thermal transient.

Adiabatic Stored Power & Associated Temps.

$$q_{C1sol} := \left|i_{C1\_rms}^{2} \cdot R_{C1sol}\right| \qquad q_{C2sol} := \left|i_{C2\_rms}^{2} \cdot R_{C2sol}\right| \qquad q_{C3sol} := \left|i_{C3\_rms}^{2} \cdot R_{C3sol}\right|$$

$q_{C1sol} = 126.097\ W$

$q_{C2sol} = 126.623\ W$

$q_{C3sol} = 0$

$$q_{R\_external} := \left|i_{source\_rms}^{2} \cdot R_{external\_R}\right|$$

$q_{R\_external} = 0$

$$vol_{C1wire} := length_{C1wire} \cdot area_{C1wire\_elec} \qquad vol_{C2wire} := length_{C2wire} \cdot area_{C2wire\_elec} \qquad vol_{C3wire} := length_{C3wire} \cdot area_{C3wire\_elec}$$

$$q_{C1wire\_vol} := \frac{q_{C1sol}}{vol_{C1wire}} \qquad q_{C2wire\_vol} := \frac{q_{C2sol}}{vol_{C2wire}} \qquad q_{C3wire\_vol} := \frac{q_{C3sol}}{vol_{C3wire}}$$

$$\Delta Temp_{C1wire}(t_{temp}) := \frac{q_{C1wire\_vol}}{density_{wire} \cdot C_{p\_wire}} \cdot t_{temp}$$

$$\Delta Temp_{C2wire}(t_{temp}) := \frac{q_{C2wire\_vol}}{density_{wire} \cdot C_{p\_wire}} \cdot t_{temp} \qquad \Delta Temp_{C3wire}(t_{temp}) := \frac{q_{C3wire\_vol}}{density_{wire} \cdot C_{p\_wire}} \cdot t_{temp}$$

Note: J equal or greater than 15 Amp/mm^2 typically requires direct water cooling.

$$J_{C1wire\_rms} = 21.017 - 0.1i\ \frac{A}{mm^2}$$

$$J_{C2wire\_rms} = 20.545 + 0.097i\ \frac{A}{mm^2}$$

$$J_{C3wire\_rms} = 0\ \frac{A}{mm^2}$$

$|J_{C1wire\_rms}| = 21.017\ \frac{A}{mm^2}$

$|J_{C2wire\_rms}| = 20.546\ \frac{A}{mm^2}$

$|J_{C3wire\_rms}| = 0\ \frac{A}{mm^2}$

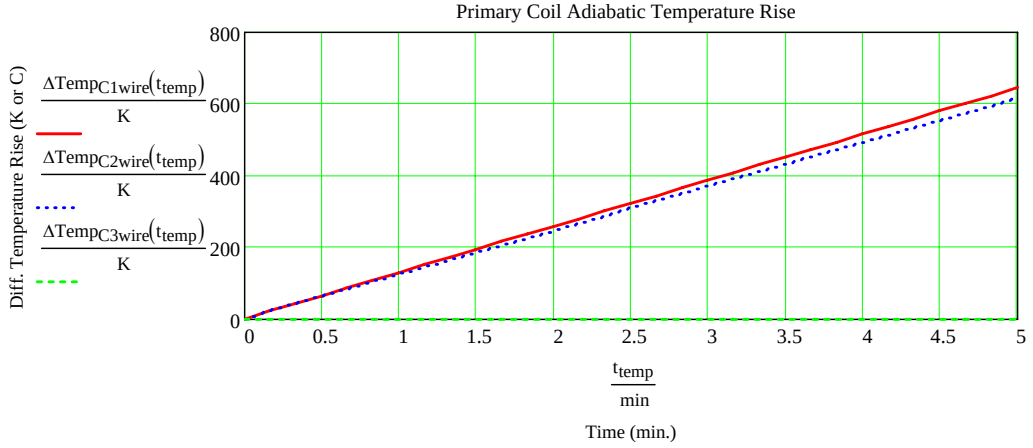

$$\rho_{C1\_new}(t_{temp}) := \frac{1}{\sigma_1}\cdot\left(1 + Coef_{temp\_wire}\cdot\Delta Temp_{C1wire}(t_{temp})\right)$$

$$\rho_{C2\_new}(t_{temp}) := \frac{1}{\sigma_1}\cdot\left(1 + Coef_{temp\_wire}\cdot\Delta Temp_{C2wire}(t_{temp})\right)$$

$$\rho_{C3\_new}(t_{temp}) := \frac{1}{\sigma_1}\cdot\left(1 + Coef_{temp\_wire}\cdot\Delta Temp_{C3wire}(t_{temp})\right)$$

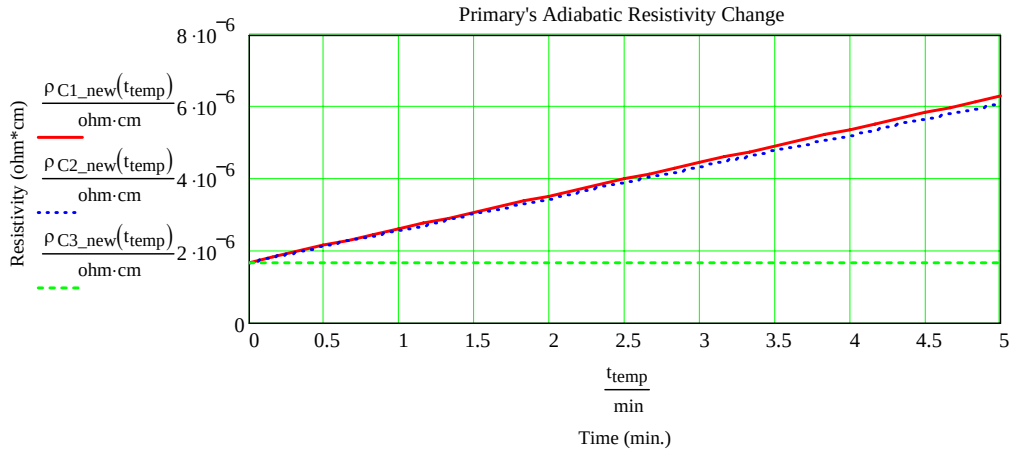

Convective Power & Associated Temps. (Ignoring Radiation and Conductive Powers):

$$h_{heat\_trans\_coef} := 15\cdot\frac{W}{m^2\cdot K}$$

Note: Approximated free or natural gas convective coefficient

$$area_{sol\_outside\_surface} := height_{C1wire}\cdot\left(2\cdot\pi\cdot rad_{mag\_max}\right) + 2\cdot\left(\pi\cdot rad_{mag\_max}^{2} - \pi\cdot rad_{mag\_min}^{2}\right)$$

$$q_{conv}(t_{temp}) := h_{heat\_trans\_coef}\cdot area_{sol\_outside\_surface}\cdot\left(\Delta Temp_{C1wire}(t_{temp}) + \Delta Temp_{C2wire}(t_{temp}) + \Delta Temp_{C3wire}(t_{temp})\right)$$

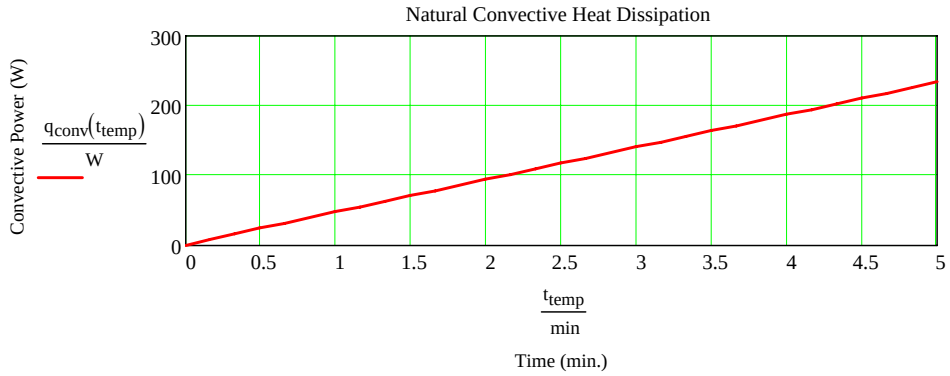

Note: C_T = (Thermal Capacitance)

$$C_{T\_solC1} := density_{wire}\cdot C_{p\_wire}\cdot vol_{C1wire} \qquad C_{T\_solC1} = 58.845\,\frac{joule}{K}$$

$$C_{T\_solC2} := density_{wire}\cdot C_{p\_wire}\cdot vol_{C2wire} \qquad C_{T\_solC2} = 61.836\,\frac{joule}{K}$$

$$C_{T\_solC3} := density_{wire}\cdot C_{p\_wire}\cdot vol_{C3wire} \qquad C_{T\_solC3} = 0\,\frac{joule}{K}$$

Note: τ_t = (Thermal Time Constant)

$$\tau_{tC1} := \frac{C_{T\_solC1}}{h_{heat\_trans\_coef} \cdot area_{sol\_outside\_surface}} \qquad \tau_{tC1} = 318.194\ s$$

$$\tau_{tC2} := \frac{C_{T\_solC2}}{h_{heat\_trans\_coef} \cdot area_{sol\_outside\_surface}} \qquad \tau_{tC2} = 334.364\ s$$

$$\tau_{tC3} := \frac{C_{T\_solC3}}{h_{heat\_trans\_coef} \cdot area_{sol\_outside\_surface}} \qquad \tau_{tC3} = 0$$

$$Temp\_rise_{C1steady\_state} := \frac{q_{C1sol}}{h_{heat\_trans\_coef} \cdot area_{sol\_outside\_surface}}$$

$Temp\_rise_{C1steady\_state} = 681.842\ K$

$Temp\_rise_{C1steady\_state} = 1.227 \times 10^3\ R$

$$Temp\_rise_{C2steady\_state} := \frac{q_{C2sol}}{h_{heat\_trans\_coef} \cdot area_{sol\_outside\_surface}}$$

$Temp\_rise_{C2steady\_state} = 684.686\ K$

$Temp\_rise_{C2steady\_state} = 1.232 \times 10^3\ R$

$$Temp\_rise_{C3steady\_state} := \frac{q_{C3sol}}{h_{heat\_trans\_coef} \cdot area_{sol\_outside\_surface}}$$

$Temp\_rise_{C3steady\_state} = 0\ K$

$Temp\_rise_{C3steady\_state} = 0\ R$

$T_{init} := 300 \cdot K$

$T_{infC1} := Temp\_rise_{C1steady\_state} + T_{init}$ $\quad T_{infC1} = 981.842\ K$

$T_{infC2} := Temp\_rise_{C2steady\_state} + T_{init}$ $\quad T_{infC2} = 984.686\ K$

$T_{infC3} := Temp\_rise_{C3steady\_state} + T_{init}$ $\quad T_{infC3} = 300\ K$

$T_{C1C2C3rise} := T_{init}, T_{init} + 1 \cdot K .. T_{infC1}$

$$t_{C1rise}(T_{C1C2C3rise}) := \tau_{tC1} \cdot \ln\left(\frac{T_{init} - T_{infC1}}{T_{C1C2C3rise} - T_{infC1}}\right)$$

$$t_{C2rise}(T_{C1C2C3rise}) := \tau_{tC2} \cdot \ln\left(\frac{T_{init} - T_{infC2}}{T_{C1C2C3rise} - T_{infC2}}\right)$$

$$t_{C3rise}(T_{C1C2C3rise}) := \tau_{tC3} \cdot \ln\left(\frac{T_{init} - T_{infC3}}{T_{C1C2C3rise} - T_{infC3}}\right)$$

Note: As a good rule of thumb, the Temp. initial value is set to the S.T.P. value of 300 K and the Temp. infinity value approaches this initial Temp. value plus the Temp rise value.

Rise Time to Reach Steady State Temp.

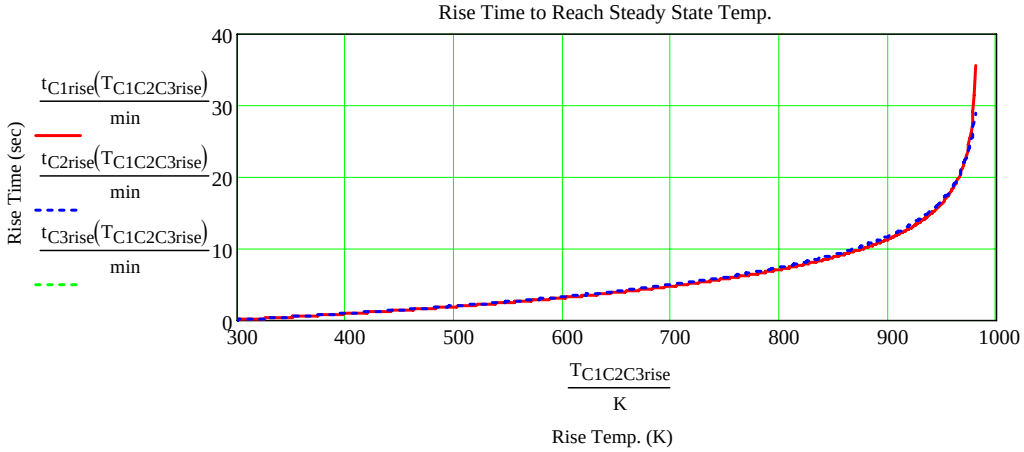

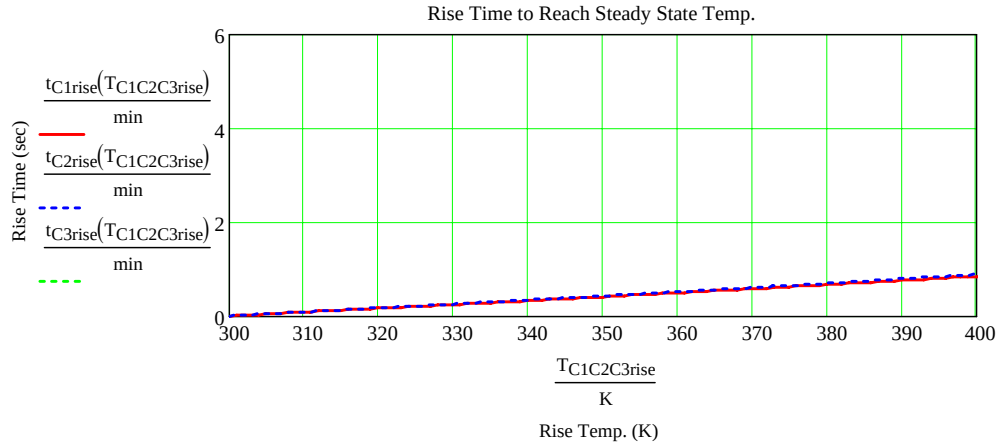

$Temp_{OFHC\_yield} :=$

20
200
400
600
650
750

$\sigma_y :=$

5000
5000
4000
2800
2000
1800

Melting temperature of OFHC copper = 1981 degrees F.
Melting temperature of ETP copper = 1949 to 1981 degrees F.

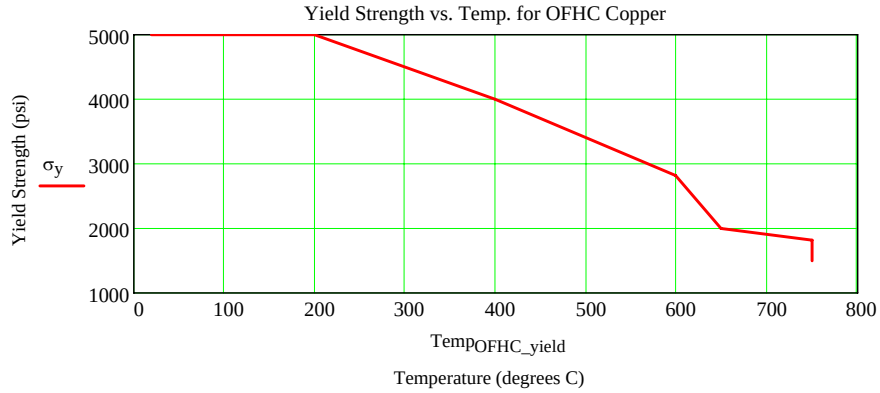

Note: The Thermal equations are only used to get a "feel" for the magnitude of heat generation and dissipation. They are NOT intended for an in depth thermal analysis. Instead the equations are being used to roughly "tweak" the soleniod into a proper range of size and operation as well as help determine if an external resistor or reactance of some sort is required. The temp. rise is used to not only compare with the melting temp. of the wire, but also compare with the yield vs. temperature curve of the wire. The linear curve fit above indicates that only over 200 degrees C does one start to see significant yield. Since the temp. rise equation above is a delta temperature, the degrees C and K are the same delta and the degrees F and R are the same delta and hence a direct comparison is allowed.

Diffusion Equation Setup - Determining Equation Constants:

$$\xi_1 := \frac{-j\cdot\mu_2\cdot\sigma_2\cdot\nu_2 + \sqrt{\left(j\cdot\mu_2\cdot\sigma_2\cdot\nu_2\right)^2 - 4\cdot j\cdot\mu_2\cdot\sigma_2\cdot\omega}}{2} \qquad \xi_2 := \frac{-j\cdot\mu_2\cdot\sigma_2\cdot\nu_2 - \sqrt{\left(j\cdot\mu_2\cdot\sigma_2\cdot\nu_2\right)^2 - 4\cdot j\cdot\mu_2\cdot\sigma_2\cdot\omega}}{2}$$

$$\xi_1 = (118.989 - 118.989i)\ \frac{1}{m} \qquad \xi_2 = (-118.989 + 118.989i)\ \frac{1}{m} \qquad \beta = 50.944\ \frac{1}{m}$$

$$\gamma_{\xi 1} := \sqrt{\xi_1^{\,2} + j\cdot\nu_2\cdot\mu_2\cdot\sigma_2\cdot\xi_1 + j\cdot\omega\cdot\mu_2\cdot\sigma_2}$$

$$\gamma_{\xi 2} := \sqrt{\xi_2^{\,2} + j\cdot\nu_2\cdot\mu_2\cdot\sigma_2\cdot\xi_2 + j\cdot\omega\cdot\mu_2\cdot\sigma_2}$$

$$\gamma_{\xi 1} = \left(1.349\times 10^{-6} + 1.349i\times 10^{-6}\right)\frac{1}{m}$$

$$\gamma_{\xi 2} = \left(1.349\times 10^{-6} + 1.349i\times 10^{-6}\right)\frac{1}{m}$$

$$\gamma_{neg\beta} := \sqrt{(-\beta)^2 - j\cdot\nu_2\cdot\mu_2\cdot\sigma_2\cdot\beta + j\cdot\omega\cdot\mu_2\cdot\sigma_2}$$

$$\gamma_{neg\beta\_Check} := \sqrt{(-\beta - \xi_1)\cdot(-\beta - \xi_2)}$$

$$\gamma_{neg\beta\_Check} = (124.561 + 113.667i)\frac{1}{m}$$

$$\gamma_{neg\beta} = (124.561 + 113.667i)\frac{1}{m}$$

$$C_{5\_\xi 1} := \frac{\gamma_{\xi 1}\cdot\mu_4 - \xi_1\cdot\mu_2}{\gamma_{\xi 1}\cdot\mu_4 + \xi_1\cdot\mu_2}$$

$$C_{5\_\xi 2} := \frac{\gamma_{\xi 2}\cdot\mu_4 - \xi_2\cdot\mu_2}{\gamma_{\xi 2}\cdot\mu_4 + \xi_2\cdot\mu_2}$$

$$C_{5\_neg\beta} := \frac{\gamma_{neg\beta}\cdot\mu_4 + \beta\cdot\mu_2}{\gamma_{neg\beta}\cdot\mu_4 - \beta\cdot\mu_2}$$

$$H_0 := \sqrt{\xi_1\cdot\xi_2} \qquad H_{neg\beta} := \sqrt{(\beta + \xi_1)\cdot(\beta + \xi_2)} \qquad H_{pr\_\xi 1} := (\xi_1 - \xi_2) \qquad H_{pr\_\xi 2} := (\xi_2 - \xi_1)$$

$$H_0 = (118.989 + 118.989i)\frac{1}{m}$$

$$H_{neg\beta} = (124.561 + 113.667i)\frac{1}{m}$$

$$H_{pr\_\xi 1} = (237.978 - 237.978i)\frac{1}{m}$$

$$H_{pr\_\xi 2} = (-237.978 + 237.978i)\frac{1}{m}$$

$$C_{GA\_\xi 1} := (\xi_1 + \gamma_{\xi 1})\cdot\left[C_{5\_\xi 1}\cdot\left(1 + \frac{\mu_3\cdot\gamma_{\xi 1}}{\mu_2\cdot\xi_1}\right) \ldots + e^{2\cdot\delta\cdot\gamma_{\xi 1}}\cdot\left(1 - \frac{\mu_3\cdot\gamma_{\xi 1}}{\mu_2\cdot\xi_1}\right)\right]$$

$$C_{GB\_\xi 1} := (\xi_1 + \gamma_{\xi 1})\cdot\left[C_{5\_\xi 1}\cdot\left(1 - \frac{\mu_3\cdot\gamma_{\xi 1}}{\mu_2\cdot\xi_1}\right) \ldots + e^{2\cdot\delta\cdot\gamma_{\xi 1}}\cdot\left(1 + \frac{\mu_3\cdot\gamma_{\xi 1}}{\mu_2\cdot\xi_1}\right)\right]$$

$$C_{GA\_\xi 2} := (\xi_2 + \gamma_{\xi 2})\cdot\left[C_{5\_\xi 2}\cdot\left(1 + \frac{\mu_3\cdot\gamma_{\xi 2}}{\mu_2\cdot\xi_2}\right) \ldots + e^{2\cdot\delta\cdot\gamma_{\xi 2}}\cdot\left(1 - \frac{\mu_3\cdot\gamma_{\xi 2}}{\mu_2\cdot\xi_2}\right)\right]$$

$$C_{GB\_\xi 2} := (\xi_2 + \gamma_{\xi 2})\cdot\left[C_{5\_\xi 2}\cdot\left(1 - \frac{\mu_3\cdot\gamma_{\xi 2}}{\mu_2\cdot\xi_2}\right) \ldots + e^{2\cdot\delta\cdot\gamma_{\xi 2}}\cdot\left(1 + \frac{\mu_3\cdot\gamma_{\xi 2}}{\mu_2\cdot\xi_2}\right)\right]$$

$$C_{GA\_neg\beta} := \frac{-\beta + \gamma_{neg\beta}}{K_{3neg\beta\_NEW}}\cdot\left[C_{5\_neg\beta}\cdot\left(1 + \frac{\gamma_{neg\beta}\cdot\mu_3}{-\beta\cdot\mu_2}\right) \ldots + K_{3neg\beta\_Replace}\cdot\left(1 - \frac{\gamma_{neg\beta}\cdot\mu_3}{-\beta\cdot\mu_2}\right)\right]$$

$$C_{GB\_neg\beta} := \frac{-\beta + \gamma_{neg\beta}}{K_{3neg\beta\_NEW}}\cdot\left[C_{5\_neg\beta}\cdot\left(1 - \frac{\gamma_{neg\beta}\cdot\mu_3}{-\beta\cdot\mu_2}\right) \ldots + K_{3neg\beta\_Replace}\cdot\left(1 + \frac{\gamma_{neg\beta}\cdot\mu_3}{-\beta\cdot\mu_2}\right)\right]$$

$$G_{3\xi 1}(z_g) := C_{GA\_\xi 1}\cdot e^{(z_0 - z_g)\cdot\xi_1} + C_{GB\_\xi 1}\cdot e^{(z_g - z_0)\cdot\xi_1}$$

$$G_{3\xi 2}(z_g) := C_{GA\_\xi 2}\cdot e^{(z_0 - z_g)\cdot\xi_2} + C_{GB\_\xi 2}\cdot e^{(z_g - z_0)\cdot\xi_2}$$

$$G_{3neg\beta}(z_g) := C_{GA\_neg\beta}\cdot e^{(z_0 - z_g)\cdot(-\beta)} + C_{GB\_neg\beta}\cdot e^{(z_g - z_0)\cdot(-\beta)}$$

Diffusion Equation Setup - Providing G'() Equation Solutions:

$$G_{pr\_30}(z_g) := 0\cdot\frac{1}{m^2}$$

$$G_{pr\_3\xi 1}(z_g) := \xi_1\cdot\left[C_{GA\_\xi 1}\cdot e^{(z_0 - z_g)\cdot\xi_1} - C_{GB\_\xi 1}\cdot e^{(z_g - z_0)\cdot\xi_1}\right]$$

$$G_{pr\_3\xi 2}(z_g) := \xi_2\cdot\left[C_{GA\_\xi 2}\cdot e^{(z_0 - z_g)\cdot\xi_2} - C_{GB\_\xi 2}\cdot e^{(z_g - z_0)\cdot\xi_2}\right]$$

$$G_{pr\_3neg\beta}(z_g) := -\beta\cdot\left[C_{GA\_neg\beta}\cdot e^{(z_0 - z_g)\cdot(-\beta)} - C_{GB\_neg\beta}\cdot e^{(z_g - z_0)\cdot(-\beta)}\right]$$

Magnetic Flux Density Component Set Up:

$$E_1(rad_2) := \frac{e^{j\cdot(rad_2 - rad_{2\_out})\cdot\xi_1}\cdot e^{-j\cdot\beta\cdot rad_{2\_out}}}{\xi_1\cdot(\xi_1+\beta)} \qquad E_2(rad_2) := \frac{e^{j\cdot(rad_2 - rad_{2\_in})\cdot\xi_2}\cdot e^{-j\cdot\beta\cdot rad_{2\_in}}}{\xi_2\cdot(\xi_2+\beta)}$$

$$E_{3A}(rad_2) := \frac{e^{-j\cdot\beta\cdot rad_{2\_out}}}{2\cdot\beta} \qquad E_{3B}(rad_2) := \frac{e^{-j\cdot\beta\cdot rad_{2\_in}}}{2\cdot\beta}$$

Secondary Diffused Magnetic Flux Density & Secondary Current Density Equations:

Note: Time average Force, <F> uses PEAK values to calculate the <F> from the AC Steady State current and B. Therefore Bpeak and Jpeak are required for all <F> inputs.

$$B_{N\_magC1}(z_g, rad_2) := -j\cdot\mu_3\cdot\left|K_{C1total\_peak}\right|\cdot\left(\begin{array}{l}\xi_1\cdot E_1(rad_2)\cdot\frac{\gamma_{\xi1}\cdot G_{3\xi1}(z_g)}{H_{pr\_\xi1}} \ ... \\ +\xi_2\cdot E_2(rad_2)\cdot\frac{\gamma_{\xi2}\cdot G_{3\xi2}(z_g)}{H_{pr\_\xi2}} - e^{-j\cdot\beta\cdot rad_2}\cdot\frac{G_{3neg\beta}(z_g)}{H_{neg\beta}}\end{array}\right)$$

$$B_{N\_magC2}(z_g, rad_2) := -j\cdot\mu_3\cdot\left|K_{C2total\_peak}\right|\cdot\left(\begin{array}{l}\xi_1\cdot E_1(rad_2)\cdot\frac{\gamma_{\xi1}\cdot G_{3\xi1}(z_g)}{H_{pr\_\xi1}} \ ... \\ +\xi_2\cdot E_2(rad_2)\cdot\frac{\gamma_{\xi2}\cdot G_{3\xi2}(z_g)}{H_{pr\_\xi2}} - e^{-j\cdot\beta\cdot rad_2}\cdot\frac{G_{3neg\beta}(z_g)}{H_{neg\beta}}\end{array}\right)$$

$$B_{N\_magC3}(z_g, rad_2) := -j\cdot\mu_3\cdot\left|K_{C3total\_peak}\right|\cdot\left(\begin{array}{l}\xi_1\cdot E_1(rad_2)\cdot\frac{\gamma_{\xi1}\cdot G_{3\xi1}(z_g)}{H_{pr\_\xi1}} \ ... \\ +\xi_2\cdot E_2(rad_2)\cdot\frac{\gamma_{\xi2}\cdot G_{3\xi2}(z_g)}{H_{pr\_\xi2}} - e^{-j\cdot\beta\cdot rad_2}\cdot\frac{G_{3neg\beta}(z_g)}{H_{neg\beta}}\end{array}\right)$$

$$B_{T\_magC1}(z_g, rad_2) := \mu_3\cdot(K_{C1total\_peak})\cdot\left[\begin{array}{l}E_1(rad_2)\cdot\frac{\gamma_{\xi1}\cdot G_{pr\_3\xi1}(z_g)}{H_{pr\_\xi1}} + E_2(rad_2)\cdot\frac{\gamma_{\xi2}\cdot G_{pr\_3\xi2}(z_g)}{H_{pr\_\xi2}} \ ... \\ +-\left(E_{3A}(rad_2) + E_{3B}(rad_2)\right)\cdot\frac{G_{pr\_30}(z_g)}{H_0} + \frac{e^{-j\cdot\beta\cdot rad_2}}{\beta}\cdot\frac{G_{pr\_3neg\beta}(z_g)}{H_{neg\beta}}\end{array}\right]$$

$$B_{T\_magC2}(z_g, rad_2) := \mu_3\cdot\left|K_{C2total\_peak}\right|\cdot\left[\begin{array}{l}E_1(rad_2)\cdot\frac{\gamma_{\xi1}\cdot G_{pr\_3\xi1}(z_g)}{H_{pr\_\xi1}} + E_2(rad_2)\cdot\frac{\gamma_{\xi2}\cdot G_{pr\_3\xi2}(z_g)}{H_{pr\_\xi2}} \ ... \\ +-\left(E_{3A}(rad_2) + E_{3B}(rad_2)\right)\cdot\frac{G_{pr\_30}(z_g)}{H_0} + \frac{e^{-j\cdot\beta\cdot rad_2}}{\beta}\cdot\frac{G_{pr\_3neg\beta}(z_g)}{H_{neg\beta}}\end{array}\right]$$

$$B_{T\_magC3}(z_g, rad_2) := \mu_3\cdot\left|K_{C3total\_peak}\right|\cdot\left[\begin{array}{l}E_1(rad_2)\cdot\frac{\gamma_{\xi1}\cdot G_{pr\_3\xi1}(z_g)}{H_{pr\_\xi1}} + E_2(rad_2)\cdot\frac{\gamma_{\xi2}\cdot G_{pr\_3\xi2}(z_g)}{H_{pr\_\xi2}} \ ... \\ +-\left(E_{3A}(rad_2) + E_{3B}(rad_2)\right)\cdot\frac{G_{pr\_30}(z_g)}{H_0} + \frac{e^{-j\cdot\beta\cdot rad_2}}{\beta}\cdot\frac{G_{pr\_3neg\beta}(z_g)}{H_{neg\beta}}\end{array}\right]$$

$$J_{xC1}(z_g, rad_2) := \frac{1}{\mu_2}\cdot\frac{d}{drad_2}\left[B_{N\_magC1}(z_g, rad_2)\cdot e^{j\cdot(\omega\cdot t - \beta\cdot rad_2)}\right] \qquad J_{xC2}(z_g, rad_2) := \frac{1}{\mu_2}\cdot\frac{d}{drad_2}\left[B_{N\_magC2}(z_g, rad_2)\cdot e^{j\cdot(\omega\cdot t - \beta\cdot rad_2)}\right]$$

$$J_{xC3}(z_g, rad_2) := \frac{1}{\mu_2}\cdot\frac{d}{drad_2}\left[B_{N\_magC3}(z_g, rad_2)\cdot e^{j\cdot(\omega\cdot t - \beta\cdot rad_2)}\right]$$

$$J_{xTest1}(z_g, rad_2) := \frac{-j\cdot\mu_3\cdot\left|K_{C1total\_peak}\right|\cdot e^{j\cdot(\omega\cdot t)}}{\mu_2}\cdot\left[\begin{array}{l}j\cdot(\xi_1-\beta)\cdot\frac{\xi_1\cdot e^{j\cdot(rad_2 - rad_{2\_out})\cdot\xi_1}\cdot e^{-j\cdot\beta\cdot rad_{2\_out}}\cdot e^{-j\cdot(\beta\cdot rad_2)}}{\xi_1\cdot(\xi_1+\beta)}\cdot\frac{\gamma_{\xi1}\cdot G_{3\xi1}(z_g)}{H_{pr\_\xi1}} \ ... \\ +j\cdot(\xi_2-\beta)\cdot\frac{\xi_2\cdot e^{j\cdot(rad_2 - rad_{2\_in})\cdot\xi_2}\cdot e^{-j\cdot\beta\cdot rad_{2\_in}}\cdot e^{-j\cdot(\beta\cdot rad_2)}}{\xi_2\cdot(\xi_2+\beta)}\cdot\frac{\gamma_{\xi2}\cdot G_{3\xi2}(z_g)}{H_{pr\_\xi2}} \ ... \\ +j\cdot 2\cdot\beta^2\cdot\left(\frac{e^{-j\cdot 2\cdot\beta\cdot rad_2}}{\beta}\cdot\frac{G_{3neg\beta}(z_g)}{H_{neg\beta}}\right)\end{array}\right]$$

Note: The induced current density should never exceed the total source current density. In this case the all values are on a per source coil basis.

$$\left|J_{C1total\_peak}\right| = 2.972 \times 10^{7}\ \frac{A}{m^2} \qquad \left|J_{C2total\_peak}\right| = 2.906 \times 10^{7}\ \frac{A}{m^2} \qquad \left|J_{C3total\_peak}\right| = 0\ \frac{A}{m^2}$$

$$J_{xC1}\left(z_{g\_min}, rad_{2\_out}\right) = \left(-2.737 \times 10^{7} + 9.648i \times 10^{6}\right)\ \frac{A}{m^2}$$

Note: This current density tests at the boundary b/w regions 1 and 3 indicate that the Mathcad derivations are working properly.

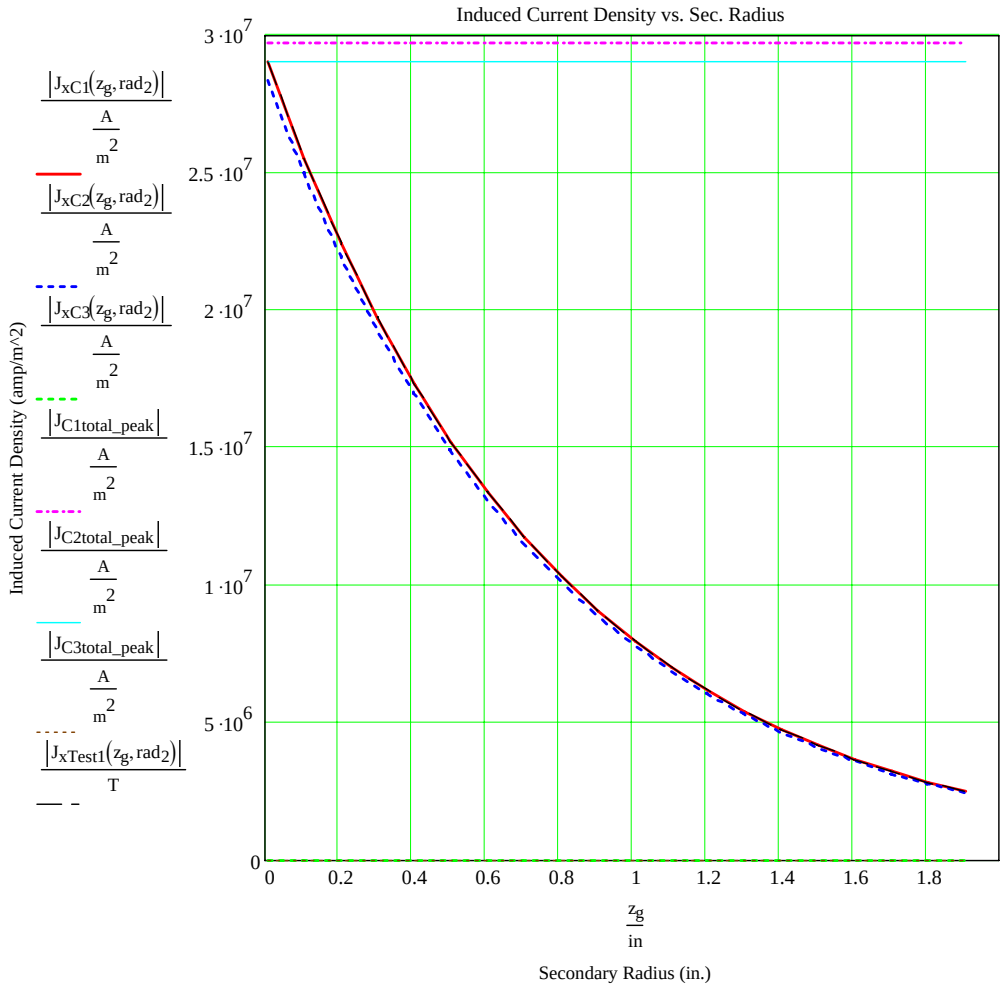

Secondary Diffused Magnetic Flux Density & Secondary Current Density Equations:

$$B_{NC1}(z_g, rad_2) := B_{N\_magC1}(z_g, rad_2)\cdot e^{j\cdot(\omega\cdot t-\beta\cdot rad_2)} \qquad B_{TC1}(z_g, rad_2) := B_{T\_magC1}(z_g, rad_2)\cdot e^{j\cdot(\omega\cdot t-\beta\cdot rad_2)}$$

$$B_{C1}(z_g, rad_2) := B_{NC1}(z_g, rad_2) + B_{TC1}(z_g, rad_2) \qquad B_{prC1}(z_g, rad_2) := B_{N\_magC1}(z_g, rad_2) + B_{T\_magC1}(z_g, rad_2)$$

$$B_{NC2}(z_g, rad_2) := B_{N\_magC2}(z_g, rad_2)\cdot e^{j\cdot(\omega\cdot t-\beta\cdot rad_2)} \qquad B_{TC2}(z_g, rad_2) := B_{T\_magC2}(z_g, rad_2)\cdot e^{j\cdot(\omega\cdot t-\beta\cdot rad_2)}$$

$$B_{C2}(z_g, rad_2) := B_{NC2}(z_g, rad_2) + B_{TC2}(z_g, rad_2) \qquad B_{prC2}(z_g, rad_2) := B_{N\_magC2}(z_g, rad_2) + B_{T\_magC2}(z_g, rad_2)$$

$$B_{NC3}(z_g, rad_2) := B_{N\_magC3}(z_g, rad_2)\cdot e^{j\cdot(\omega\cdot t-\beta\cdot rad_2)} \qquad B_{TC3}(z_g, rad_2) := B_{T\_magC3}(z_g, rad_2)\cdot e^{j\cdot(\omega\cdot t-\beta\cdot rad_2)}$$

$$B_{C3}(z_g, rad_2) := B_{NC3}(z_g, rad_2) + B_{TC3}(z_g, rad_2) \qquad B_{prC3}(z_g, rad_2) := B_{N\_magC3}(z_g, rad_2) + B_{T\_magC3}(z_g, rad_2)$$

$$B_{T\_Total\_Material}(z_g, rad_2) := B_{TC1}(z_g, rad_2) + B_{TC2}(z_g, rad_2) + B_{TC3}(z_g, rad_2)$$

$$B_{N\_Total\_Material}(z_g, rad_2) := B_{NC1}(z_g, rad_2) + B_{NC2}(z_g, rad_2) + B_{NC3}(z_g, rad_2)$$

Taking B Saturation into account:

$$B_{T\_Total\_Real}(z_g, rad_2) := \begin{cases} \text{if } Re(B_{T\_Total\_Material}(z_g, rad_2)) > 0 \\ \quad \begin{cases} Re(B_{T\_Total\_Material}(z_g, rad_2)) & \text{if } Re(B_{T\_Total\_Material}(z_g, rad_2)) < B_{sat}(z_g, rad_2)\cdot sign(Re(B_{T\_Total\_Material}(z_g, rad_2))) \\ B_{sat}(z_g, rad_2)\cdot sign(Re(B_{T\_Total\_Material}(z_g, rad_2))) & \text{otherwise} \end{cases} \\ \text{if } Re(B_{T\_Total\_Material}(z_g, rad_2)) < 0 \\ \quad \begin{cases} Re(B_{T\_Total\_Material}(z_g, rad_2)) & \text{if } Re(B_{T\_Total\_Material}(z_g, rad_2)) > B_{sat}(z_g, rad_2)\cdot sign(Re(B_{T\_Total\_Material}(z_g, rad_2))) \\ B_{sat}(z_g, rad_2)\cdot sign(Re(B_{T\_Total\_Material}(z_g, rad_2))) & \text{otherwise} \end{cases} \end{cases}$$

$$B_{T\_Total\_Imag}(z_g, rad_2) := \begin{cases} \text{if } Im(B_{T\_Total\_Material}(z_g, rad_2)) > 0 \\ \quad \begin{cases} Im(B_{T\_Total\_Material}(z_g, rad_2)) & \text{if } Im(B_{T\_Total\_Material}(z_g, rad_2)) < B_{sat}(z_g, rad_2)\cdot sign(Im(B_{T\_Total\_Material}(z_g, rad_2))) \\ B_{sat}(z_g, rad_2)\cdot sign(Im(B_{T\_Total\_Material}(z_g, rad_2))) & \text{otherwise} \end{cases} \\ \text{if } Im(B_{T\_Total\_Material}(z_g, rad_2)) < 0 \\ \quad \begin{cases} Im(B_{T\_Total\_Material}(z_g, rad_2)) & \text{if } Im(B_{T\_Total\_Material}(z_g, rad_2)) > B_{sat}(z_g, rad_2)\cdot sign(Im(B_{T\_Total\_Material}(z_g, rad_2))) \\ B_{sat}(z_g, rad_2)\cdot sign(Im(B_{T\_Total\_Material}(z_g, rad_2))) & \text{otherwise} \end{cases} \end{cases}$$

$$B_{N\_Total\_Real}(z_g, rad_2) := \begin{cases} \text{if } Re(B_{N\_Total\_Material}(z_g, rad_2)) > 0 \\ \quad \begin{cases} Re(B_{N\_Total\_Material}(z_g, rad_2)) & \text{if } Re(B_{N\_Total\_Material}(z_g, rad_2)) < B_{sat}(z_g, rad_2)\cdot sign(Re(B_{N\_Total\_Material}(z_g, rad_2))) \\ B_{sat}(z_g, rad_2)\cdot sign(Re(B_{N\_Total\_Material}(z_g, rad_2))) & \text{otherwise} \end{cases} \\ \text{if } Re(B_{N\_Total\_Material}(z_g, rad_2)) < 0 \\ \quad \begin{cases} Re(B_{N\_Total\_Material}(z_g, rad_2)) & \text{if } Re(B_{N\_Total\_Material}(z_g, rad_2)) > B_{sat}(z_g, rad_2)\cdot sign(Re(B_{N\_Total\_Material}(z_g, rad_2))) \\ B_{sat}(z_g, rad_2)\cdot sign(Re(B_{N\_Total\_Material}(z_g, rad_2))) & \text{otherwise} \end{cases} \end{cases}$$

$$B_{N\_Total\_Imag}(z_g, rad_2) := \begin{cases} \text{if } Im(B_{N\_Total\_Material}(z_g, rad_2)) > 0 \\ \quad \begin{cases} Im(B_{N\_Total\_Material}(z_g, rad_2)) & \text{if } Im(B_{N\_Total\_Material}(z_g, rad_2)) < B_{sat}(z_g, rad_2)\cdot sign(Im(B_{N\_Total\_Material}(z_g, rad_2))) \\ B_{sat}(z_g, rad_2)\cdot sign(Im(B_{N\_Total\_Material}(z_g, rad_2))) & \text{otherwise} \end{cases} \\ \text{if } Im(B_{N\_Total\_Material}(z_g, rad_2)) < 0 \\ \quad \begin{cases} Im(B_{N\_Total\_Material}(z_g, rad_2)) & \text{if } Im(B_{N\_Total\_Material}(z_g, rad_2)) > B_{sat}(z_g, rad_2)\cdot sign(Im(B_{N\_Total\_Material}(z_g, rad_2))) \\ B_{sat}(z_g, rad_2)\cdot sign(Im(B_{N\_Total\_Material}(z_g, rad_2))) & \text{otherwise} \end{cases} \end{cases}$$

$$B_{T\_Total}(z_g, rad_2) := B_{T\_Total\_Real}(z_g, rad_2) + j\cdot B_{T\_Total\_Imag}(z_g, rad_2)$$

$$B_{N\_Total}(z_g, rad_2) := B_{N\_Total\_Real}(z_g, rad_2) + j\cdot B_{N\_Total\_Imag}(z_g, rad_2)$$

$$B_{Total}(z_g, rad_2) := B_{T\_Total}(z_g, rad_2) + B_{N\_Total}(z_g, rad_2)$$

Units Check:

$B_{N\_magC1}(z_{g\_avg}, rad_{2\_out}) = 0.097 - 0.017iT$

$B_{T\_magC1}(z_{g\_avg}, rad_{2\_out}) = -0.017 - 0.097iT$

$B_{N\_magC2}(z_{g\_avg}, rad_{2\_out}) = 0.095 - 0.016iT$

$B_{T\_magC2}(z_{g\_avg}, rad_{2\_out}) = -0.016 - 0.095iT$

$B_{N\_magC3}(z_{g\_avg}, rad_{2\_out}) = 0\,T$

$B_{T\_magC3}(z_{g\_avg}, rad_{2\_out}) = 0\,T$

$B_{T\_Total}(z_{g\_avg}, rad_{2\_out}) = (-0.184 + 0.065i)\ T$

$B_{N\_Total}(z_{g\_avg}, rad_{2\_out}) = (-0.065 - 0.184i)\ T$

$J_{xC1}(z_{g\_avg}, rad_{2\_out}) = \left(-7.553 \times 10^6 + 2.663i \times 10^6\right) \frac{A}{m^2}$

$J_{xC2}(z_{g\_avg}, rad_{2\_out}) = \left(-7.383 \times 10^6 + 2.603i \times 10^6\right) \frac{A}{m^2}$

$J_{xC3}(z_{g\_avg}, rad_{2\_out}) = 0 \frac{A}{m^2}$

$rad_{mag\_min} = 0.338\,in$

$rad_{mag\_max} = 1.214\,in$

$rad_{2\_out} = 1.345\,in$ $z_{g\_avg} = 1.005\,in$

B Order of Magnitude Check via Quick Solenoid Equations:

$$B_{C1sol\_end} := \frac{\mu_1 \cdot Amp\_Turns_{C1}}{2 \cdot \sqrt{rad_{C1\_out}^2 + length_{C1wire\_layers}^2}}$$

$$B_{C1sol\_middle} := \frac{\mu_1 \cdot Amp\_Turns_{C1}}{\sqrt{4 \cdot rad_{C1\_out}^2 + length_{C1wire\_layers}^2}}$$

$$B_{C2sol\_end} := \frac{\mu_1 \cdot Amp\_Turns_{C2}}{2 \cdot \sqrt{rad_{C2\_out}^2 + length_{C2wire\_layers}^2}}$$

$$B_{C2sol\_middle} := \frac{\mu_1 \cdot Amp\_Turns_{C2}}{\sqrt{4 \cdot rad_{C2\_out}^2 + length_{C2wire\_layers}^2}}$$

$$B_{C3sol\_end} := \frac{\mu_1 \cdot Amp\_Turns_{C3}}{2 \cdot \sqrt{rad_{C2\_out}^2 + length_{C2wire\_layers}^2}}$$

$$B_{C3sol\_middle} := \frac{\mu_1 \cdot Amp\_Turns_{C3}}{\sqrt{4 \cdot rad_{C3\_out}^2 + length_{C3wire\_layers}^2}}$$

$B_{Total\_sol\_end} := B_{C1sol\_end} + B_{C2sol\_end} + B_{C3sol\_end}$

$B_{Total\_sol\_middle} := B_{C1sol\_middle} + B_{C2sol\_middle} + B_{C3sol\_middle}$

$|B_{C1sol\_end}| = 0.353\ T$ $|B_{C2sol\_end}| = 0.234\ T$ $|B_{C3sol\_end}| = 0\ T$ $|B_{Total\_sol\_end}| = 0.587\ T$

$|B_{C1sol\_middle}| = 0.36\ T$ $|B_{C2sol\_middle}| = 0.236\ T$ $|B_{C3sol\_middle}| = 0\ T$ $|B_{Total\_sol\_middle}| = 0.597\ T$

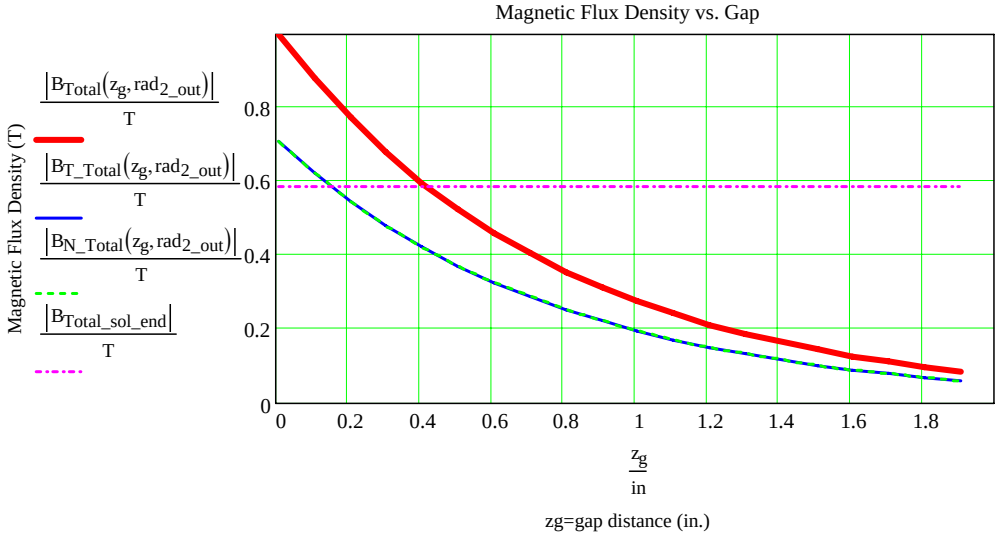

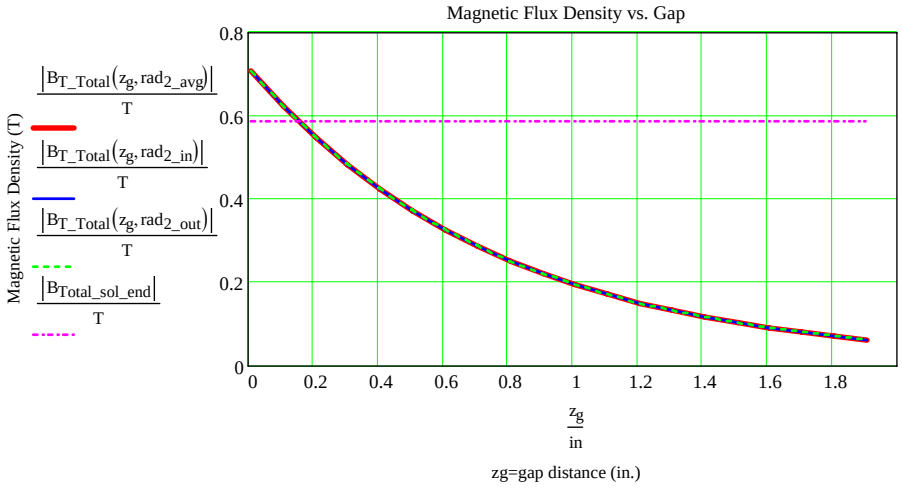
Magnetic Flux Density vs. Gap
Magnetic Flux Density (T)
|BT_Total(zg, rad2_avg)| / T
|BT_Total(zg, rad2_in)| / T
|BT_Total(zg, rad2_out)| / T
|BTotal_sol_end| / T
0.8
0.6
0.4
0.2
0
0 0.2 0.4 0.6 0.8 1 1.2 1.4 1.6 1.8
zg / in
zg=gap distance (in.)

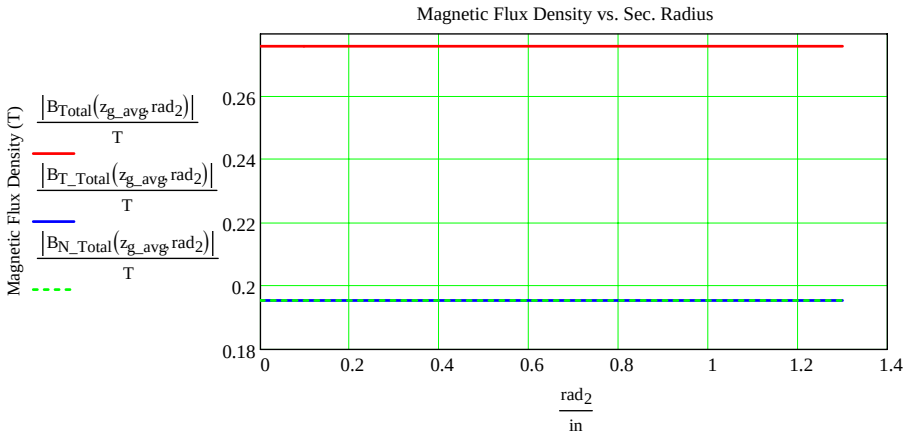
Magnetic Flux Density vs. Sec. Radius
Magnetic Flux Density (T)
|BTotal(zg_avg, rad2)| / T
|BT_Total(zg_avg, rad2)| / T
|BN_Total(zg_avg, rad2)| / T
0.26
0.24
0.22
0.2
0.18
0 0.2 0.4 0.6 0.8 1 1.2 1.4
rad2 / in
Secondary Radius (in.)

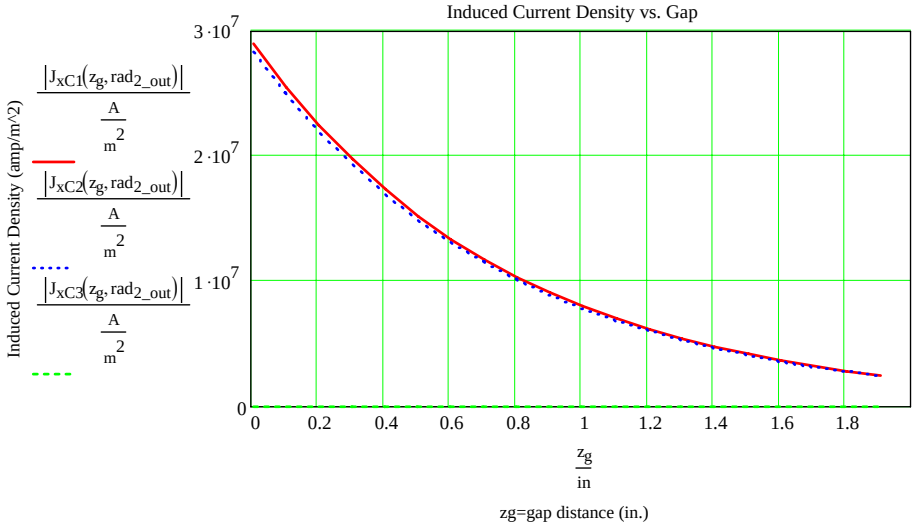
Induced Current Density vs. Gap
Induced Current Density (amp/m^2)
|JxC1(zg, rad2_out)| / A/m^2
|JxC2(zg, rad2_out)| / A/m^2
|JxC3(zg, rad2_out)| / A/m^2
3·10^7
2·10^7
1·10^7
0
0 0.2 0.4 0.6 0.8 1 1.2 1.4 1.6 1.8
zg / in
zg=gap distance (in.)

Force Equations:

Note: The force may be detemined via either maintaining the radius as a variable which represents the maximum secondary radius or by setting the maximum secondary radius and integrating to remove this variable from the equation. Here the secondary radius is maintained as a parametric value, but a radius removing test variable is established to verify that the radius parameter is actually the maximum radius value. The parametric analysis is performed here is Mathcad to assist the non-parametric simulation performed in Matlab/Simulink.

$$F_{C1z\_test}(z_g) := \frac{2\cdot\pi\cdot\delta}{2}\cdot\left[\int_{rad_{mag\_min}}^{rad_{C1\_out}} rad_2\cdot\left(Re\left(J_{xC1}(z_g, rad_2)\cdot\overline{B_{TC1}(z_g, rad_2)}\right)\right) drad_2\right]$$

$$F_{C2z\_test}(z_g) := \frac{2\cdot\pi\cdot\delta}{2}\cdot\left[\int_{rad_{C1\_out}}^{rad_{C2\_out}} rad_2\cdot\left(Re\left(J_{xC2}(z_g, rad_2)\cdot\overline{B_{TC2}(z_g, rad_2)}\right)\right) drad_2\right]$$

$$F_{C3z\_test}(z_g) := \frac{2\cdot\pi\cdot\delta}{2}\cdot\left[\int_{rad_{C2\_out}}^{rad_{mag\_max}} rad_2\cdot\left(Re\left(J_{xC2}(z_g, rad_2)\cdot\overline{B_{TC2}(z_g, rad_2)}\right)\right) drad_2\right]$$

Units Check:

$F_{C1z\_test}(z_{g\_max}) = 0.126\,lbf$

$F_{C2z\_test}(z_{g\_max}) = 0.062\,lbf$

$F_{C3z\_test}(z_{g\_max}) = -0.033\,lbf$

$$F_{z\_test}(z_g) := F_{C1z\_test}(z_g) + F_{C2z\_test}(z_g) + F_{C3z\_test}(z_g)$$

Horizontal (y) Centering Force

$$F_{C1y\_density}(z_g, rad_2) := \frac{1}{2}\cdot Re\left(J_{xC1}(z_g, rad_2)\cdot\overline{B_{NC1}(z_g, rad_2)}\right)$$

$$F_{C2y\_density}(z_g, rad_2) := \frac{1}{2}\cdot Re\left(J_{xC2}(z_g, rad_2)\cdot\overline{B_{NC2}(z_g, rad_2)}\right)$$

$$F_{C3y\_density}(z_g, rad_2) := \frac{1}{2}\cdot Re\left(J_{xC3}(z_g, rad_2)\cdot\overline{B_{NC3}(z_g, rad_2)}\right)$$

Vertical (z) Lifting Force

$$F_{C1z\_density}(z_g, rad_2) := \frac{1}{2}\cdot Re\left(J_{xC1}(z_g, rad_2)\cdot\overline{B_{TC1}(z_g, rad_2)}\right)$$

$$F_{C2z\_density}(z_g, rad_2) := \frac{1}{2}\cdot Re\left(J_{xC2}(z_g, rad_2)\cdot\overline{B_{TC2}(z_g, rad_2)}\right)$$

$$F_{C3z\_density}(z_g, rad_2) := \frac{1}{2}\cdot Re\left(J_{xC3}(z_g, rad_2)\cdot\overline{B_{TC3}(z_g, rad_2)}\right)$$

$$F_y(z_g, rad_2) := \left(F_{C1y\_density}(z_g, rad_2) + F_{C2y\_density}(z_g, rad_2) + F_{C3y\_density}(z_g, rad_2)\right)\cdot vol_{mag}$$

$$F_z(z_g, rad_2) := \left(F_{C1z\_density}(z_g, rad_2) + F_{C2z\_density}(z_g, rad_2) + F_{C3z\_density}(z_g, rad_2)\right)\cdot vol_{mag}$$

$$F_{lev}(z_g, rad_2) := F_z(z_g, rad_2) - F_g(rad_2)$$

Units Check:

$F_y(z_{g\_avg}, rad_{2\_avg}) = 3.106\times10^{-14}\,lbf$

$F_z(z_{g\_avg}, rad_{2\_avg}) = 4.027\,lbf$

$rad_{mag\_min} = 0.338\,in$

$rad_{mag\_max} = 1.214\,in$

$rad_{2\_in} = 0\,in$ $rad_{1\_out} = 0.8\,in$ $rad_{2\_avg} = 0.672\,in$ $rad_{2\_out} = 1.345\,in$ $rad_{1\_in} = 0.125\,in$ $z_{g\_avg} = 1.005\,in$

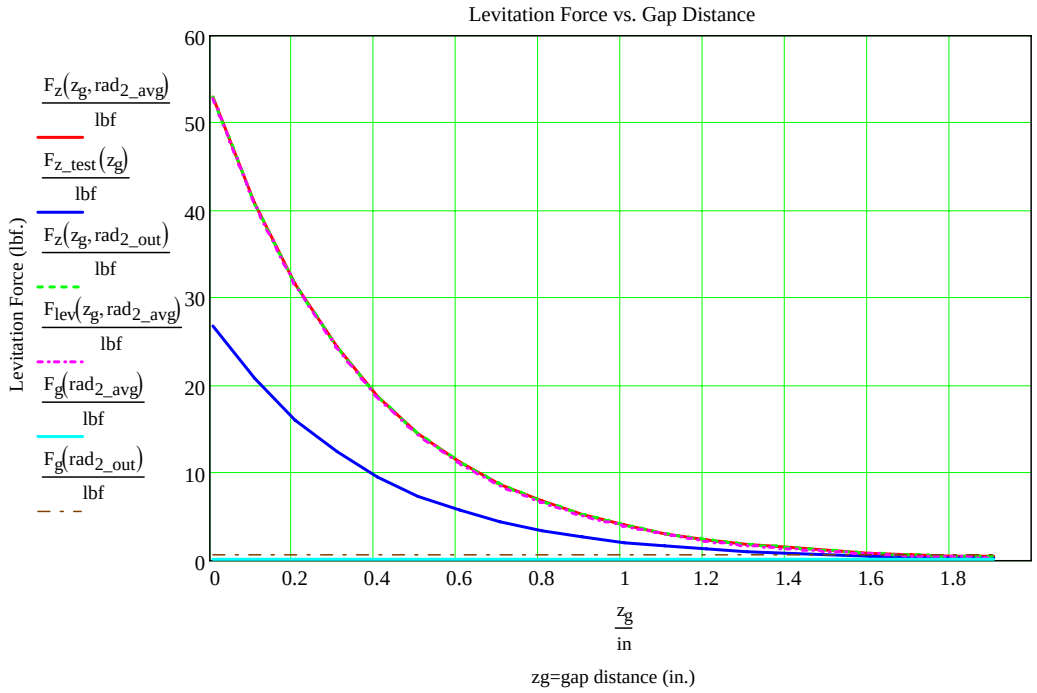
Levitation Force vs. Gap Distance
$F_z(z_g, rad_{2\_avg})$ lbf
$F_{z\_test}(z_g)$ lbf
$F_z(z_g, rad_{2\_out})$ lbf
$F_{lev}(z_g, rad_{2\_avg})$ lbf
$F_g(rad_{2\_avg})$ lbf
$F_g(rad_{2\_out})$ lbf
Levitation Force (lbf.)
60
50
40
30
20
10
0
0
0.2
0.4
0.6
0.8
1
1.2
1.4
1.6
1.8
z_g in
zg=gap distance (in.)

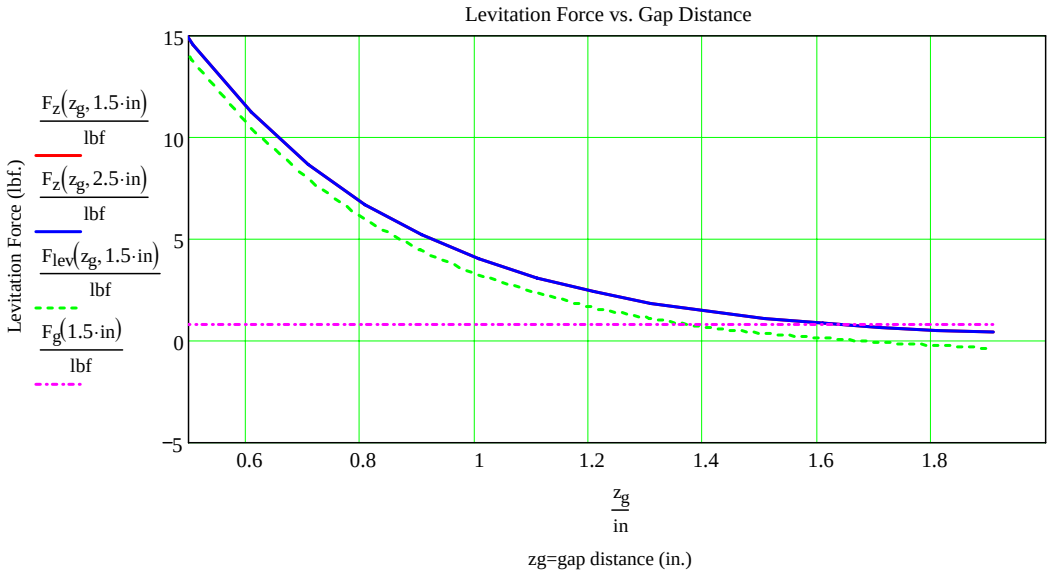
Levitation Force vs. Gap Distance
$F_z(z_g, 1.5 \cdot in)$ lbf
$F_z(z_g, 2.5 \cdot in)$ lbf
$F_{lev}(z_g, 1.5 \cdot in)$ lbf
$F_g(1.5 \cdot in)$ lbf
Levitation Force (lbf.)
15
10
5
0
−5
0.6
0.8
1
1.2
1.4
1.6
1.8
z_g in
zg=gap distance (in.)

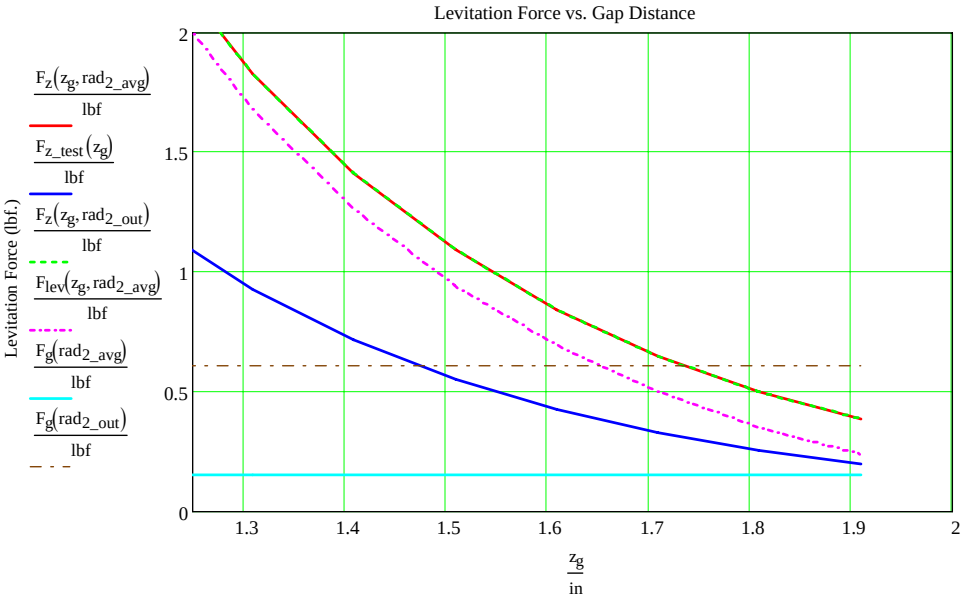
Levitation Force vs. Gap Distance
Levitation Force (lbf.)
$F_z(z_g, rad2\_avg)$ lbf
$F_{z\_test}(z_g)$ lbf
$F_z(z_g, rad2\_out)$ lbf
$F_{lev}(z_g, rad2\_avg)$ lbf
$F_g(rad2\_avg)$ lbf
$F_g(rad2\_out)$ lbf
2
1.5
1
0.5
0
1.3
1.4
1.5
1.6
1.7
1.8
1.9
2
z_g in
zg=gap distance (in.)

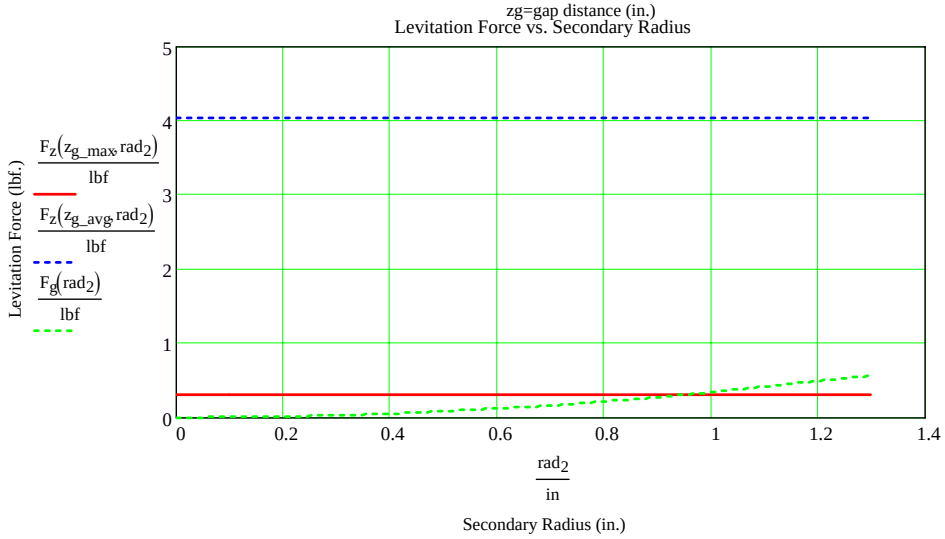
Levitation Force vs. Secondary Radius
Levitation Force (lbf.)
$F_z(z_{g\_max}, rad2)$ lbf
$F_z(z_{g\_avg}, rad2)$ lbf
$F_g(rad2)$ lbf
5
4
3
2
1
0
0
0.2
0.4
0.6
0.8
1
1.2
1.4
$rad2$ in
Secondary Radius (in.)

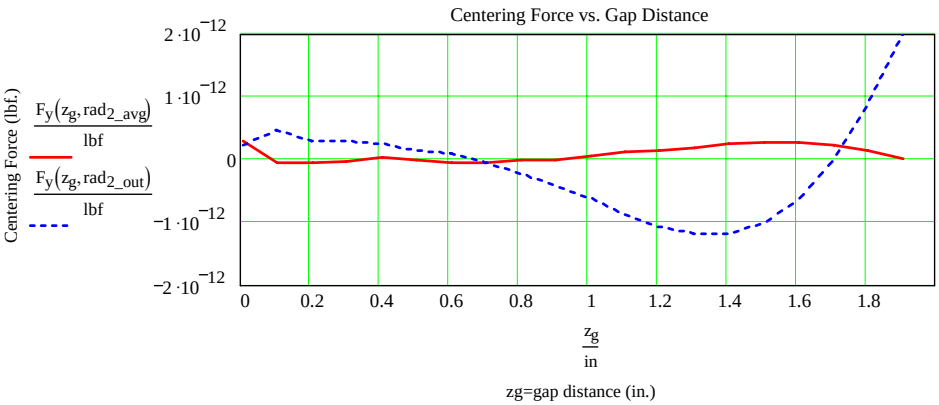
Centering Force vs. Gap Distance
Centering Force (lbf.)
$F_y(z_g, rad2\_avg)$ lbf
$F_y(z_g, rad2\_out)$ lbf
$2 \cdot 10^{-12}$
$1 \cdot 10^{-12}$
0
$-1 \cdot 10^{-12}$
$-2 \cdot 10^{-12}$
0
0.2
0.4
0.6
0.8
1
1.2
1.4
1.6
1.8
z_g in
zg=gap distance (in.)

Analysis - Approximated Plant Natural Oscillation Values:

$k_{plant}(z_g, rad_2) := \frac{F_z(z_g, rad_2)}{z_{g\_avg}}$

Primary plant system spring constant approx.

$k_{plant}(z_{g\_avg}, rad_{2\_avg}) = 701.717 \frac{kg}{s^2}$

$\omega_n(z_g, rad_2) := \sqrt{\frac{k_{plant}(z_g, rad_2)}{mass_2(rad_2)}}$

Primary plant natural radial frequency (assuming a harmonic oscillator). Right now only account for a single secondary per solenoid.

$\omega_n(z_{g\_avg}, rad_{2\_avg}) = 100.983 \frac{1}{s}$

$freq_n(z_g, rad_2) := \frac{\omega_n(z_g, rad_2)}{2\pi}$

Primary plant natural frequency.

$freq_n(z_{g\_avg}, rad_{2\_avg}) = 16.072 \frac{1}{s}$

$num_{oscillations}(z_g, rad_2) := time_{stop\_pert} \cdot freq_n(z_g, rad_2)$

Number of oscillations to stop the perturbation.

$num_{oscillations}(z_{g\_avg}, rad_{2\_avg}) = 16.072$

Note: This plant may be naturally too stiff to continue oscillations of its' own accord and hence an external force will possibly be applied to induce oscillations.

Analysis - Time Constant Comparison:

Note: The solenoid's (L/R) electrical time constant must be appreciably faster than plant's mechanical time constant for a system to operate properly.

$z_{g\_avg} = 1.005\,in$

$\tau_n(z_g, rad_2) := \frac{1}{freq_n(z_g, rad_2)}$

Primary plant natural period.

$\tau_n(z_{g\_avg}, rad_{2\_out}) = 0.124\ s$

$\tau_{C1elec} := \frac{L_{C1sol}}{R_{C1sol}}$

Solenoid electrical time constants.

$\tau_{C1elec} = 7.612 \times 10^{-3}\ s$

$\tau_{C2elec} := \frac{L_{C2sol}}{R_{C2sol}}$

$\frac{\tau_{C1elec}}{\tau_n(z_{g\_avg}, rad_{2\_out})} = 0.061$

$\frac{\tau_{C2elec}}{\tau_n(z_{g\_avg}, rad_{2\_out})} = 0.059$

$\tau_{C2elec} = 7.386 \times 10^{-3}\ s$

Note: The Data Acquisition System time constant must be equivalent or faster than the electrical and mechanical time constant for a system to operate properly. This requirement is satisfied here.

$freq_{DAQ\_min} := 500 \cdot Hz$

$\tau_{DAQ\_min} := \frac{1}{freq_{DAQ\_min}}$

$\tau_{DAQ\_min} = 2 \times 10^{-3}\ s$

A.1.c Phase II & III Solenoid Levitation Design Setup

PHASE II & III - LEVITATION REQUIREMENTS (Single Sided Halbach Array)

Constants - Primary:

$\lambda := 0.432 \cdot m$ $\quad width_{HB\_array} := 0.25 \cdot m$

$A_z := \left[\left(2 \cdot \lambda\right) + 0.05 \cdot m\right] \cdot width_{HB\_array}$

$A_z = 0.229\ m^2$ Equivalent magnetic lift area. This constant is set in Phase II & III.

$z_{g\_lev} := 2.5 \cdot cm$ Normal air gap. Zero oscillation amplitude position. This constant is set in Phase IV.

$weight_{upper\_HB\_array} := 695 \cdot lbf$ $\quad weight_{Ormond\_device} := 319 \cdot lbf$

$weight_{total} := weight_{upper\_HB\_array} + weight_{Ormond\_device}$ $\quad mass := \frac{weight_{total}}{g}$

$weight_{total} = 1.014 \times 10^3\ lbf$

$mass = 459.943\ kg$ VERTICAL mass to lift. This constant is set in Phase II & III.
Horizontal mass is: [(825-319)+695+20]/g

Constants - Secondary:

$density_2 := density_{Al}$ Secondary density.

$\sigma_2 := \sigma_{Al}$ Secondary conductivity.

NOTE: An aluminum secondary is chosen.

$n_{sol} := 20$ Number of control solenoids.

$rad_{1\_in} := 4 \cdot in$ Radius of a single control solenoid.

$A_{core} := \pi \cdot rad_{1\_in}^2$ Core area of a single control solenoid. $A_{core} = 0.032\ m^2$

$time_{stop\_pert} := 2 \cdot sec$ Time to stop the perturbation.

Analysis - Plant Perturbation Input Values (Force, Pressure, B, & Energy):

$F_z := mass \cdot g$ Secondary force required on secondary surface at nominal air gap. $F_z = 4.51 \times 10^3\ N$

$Pressure_z := \frac{F_z}{A_z}$ Secondary pressure required on secondary surface at nominal air gap. $Pressure_z = 1.974 \times 10^4\ Pa$

$B := \sqrt{2 \cdot \mu_0 \cdot Pressure_z}$ Magnetic flux density required on secondary surface at nomial air gap from Maxwell Stress Tensor equation. $B = 0.223\ T$

Note: Here B output is in the range expected for Urban Maglev. Data from other sources.

$d_{pert} := Ratio_{gap\_design} \cdot z_{g\_lev}$ Perturbation peak to peak amplitude. $d_{pert} = 16.667\ mm$

Note: Assuming constant magnetic flux density, B, equipotential lines across the air gap. This assumption assumed valid when using the zero amplitude position for all B calcs. The negative and positive B and hence forces around the zero amplitude position assume to average out to this zero amplitude B and force value.

$E_z := F_z \cdot d_{pert}$ Perturbation peak to peak energy. $E_z = 75.175\ J$

Analysis - Plant Natural Oscillation Values:

$k_{plant} := \frac{F_z}{z_{g\_lev}}$ Primary plant system spring constant. $k_{plant} = 1.804 \times 10^5\ \frac{kg}{s^2}$

$\omega_n := \sqrt{\frac{k_{plant}}{mass}}$ Primary plant natural radial frequency (assuming a harmonic oscillator). $\omega_n = 19.806\ \frac{1}{s}$

$freq_n := \frac{\omega_n}{2\pi}$ Primary plant natural frequency. $freq_n = 3.152\ \frac{1}{s}$

$num_{oscillations} := time_{stop\_pert} \cdot freq_n$ Number of oscillations to stop the perturbation. $num_{oscillations} = 6.304$

Analysis - Control System Force Values (from Conservation of Energy):

Note: Assuming each peak to peak oscillation removes an equal amount of energy throughout the entire repulsion half stroke of the secondary.

$F_{control} := \frac{E_z}{\frac{d_{pert} \cdot num_{oscillations}}{2}}$ Total control force required. $F_{control} = 1.431 \times 10^3\ N$

$Force_{control\_ratio} := \frac{F_{control}}{F_z}$ Ratio of Levitation Force to Levitation Control Force $Force_{control\_ratio} = 0.317$

Note: It is important to note that the control force required is a fraction of the prime mover levitation force. Such a relation MUST hold true for a control system of this type to operate.

$F_{sol} := \frac{F_{control}}{n_{sol}}$ Force required per solenoid. $F_{sol} = 71.546\ N$

$Pressure_{sol} := \frac{F_{sol}}{A_{core}}$ Secondary pressure required on secondary surface at nominal air gap. $Pressure_{sol} = 2.206 \times 10^3\ Pa$

$B_{sol} := \sqrt{2 \cdot \mu_0 \cdot Pressure_{sol}}$ Magnetic flux density required on secondary surface at nomial air gap from Maxwell Stress Tensor equation. $B_{sol} = 0.074\ T$

A.1.d Phase IV Solenoid Levitation Design Setup

PHASE IV - LEVITATION REQUIREMENTS

Constants - Primary:

$\lambda := 0.432 \cdot m$ $\quad width_{HB\_array} := 0.25 \cdot m$

$num_{lev\_ski\_sets} := 2$ $\quad width_{HB\_array\_bottom} := 0.15 \cdot m$

$A_{z\_top} := \left[\left[(9 \cdot \lambda) + 0.05 \cdot m\right] \cdot width_{HB\_array}\right] \cdot num_{lev\_ski\_sets}$

$A_{z\_bottom} := \left[\left[(9 \cdot \lambda) + 0.05 \cdot m\right] \cdot width_{HB\_array\_bottom}\right] \cdot num_{lev\_ski\_sets}$

$A_z := A_{z\_top} + A_{z\_bottom}$

$A_z = 3.15\ m^2$ Equivalent magnetic lift area. This constant is set in Phase IV.

$z_{g\_lev} := 2.5 \cdot cm$ Normal air gap. Zero oscillation amplitude position. This constant is set in Phase IV.

$mass := 18000 \cdot kg$ Mass to lift. This constant is set in Phase IV.

Constants - Secondary:

$density_2 := density_{Al}$ Secondary density.

NOTE: An aluminum secondary is chosen.

$\sigma_2 := \sigma_{Al}$ Secondary conductivity.

$n_{sol} := 20$ Number of control solenoids.

$rad_{1\_in} := 4 \cdot in$ Radius of a single control solenoid.

$A_{core} := \pi \cdot rad_{1\_in}^2$ Core area of a single control solenoid. $A_{core} = 0.032\ m^2$

$time_{stop\_pert} := 2 \cdot sec$ Time to stop the perturbation.

Analysis - Plant Perturbation Input Values (Force, Pressure, B, & Energy):

$F_z := mass \cdot g$ Secondary force required on secondary surface at nominal air gap. $F_z = 1.765 \times 10^5\ N$

$Pressure_z := \frac{F_z}{A_z}$ Secondary pressure required on secondary surface at nominal air gap. $Pressure_z = 5.603 \times 10^4\ Pa$

$B := \sqrt{2 \cdot \mu_0 \cdot Pressure_z}$ Magnetic flux density required on secondary surface at nomial air gap from Maxwell Stress Tensor equation. $B = 0.375\ T$

Note: Here B output is in the range expected for Urban Maglev. Data from other sources.

$d_{pert} := Ratio_{gap\_design} \cdot z_{g\_lev}$ Perturbation peak to peak amplitude. $d_{pert} = 16.667\ mm$

Note: Assuming constant magnetic flux density, B, equipotential lines across the air gap. This assumption assumed valid when using the zero amplitude position for all B calcs. The negative and positive B and hence forces around the zero amplitude position assume to average out to this zero amplitude B and force value.

$E_z := F_z \cdot d_{pert}$ Perturbation peak to peak energy. $E_z = 2.942 \times 10^3\ J$

Analysis - Plant Natural Oscillation Values:

$k_{plant} := \frac{F_z}{z_{g\_lev}}$ Primary plant system spring constant. $k_{plant} = 7.061 \times 10^6 \ \frac{kg}{s^2}$

$\omega_n := \sqrt{\frac{k_{plant}}{mass}}$ Primary plant natural radial frequency (assuming a harmonic oscillator). $\omega_n = 19.806 \ \frac{1}{s}$

$freq_n := \frac{\omega_n}{2\pi}$ Primary plant natural frequency. $freq_n = 3.152 \ \frac{1}{s}$

$num_{oscillations} := time_{stop\_pert} \cdot freq_n$ Number of oscillations to stop the perturbation. $num_{oscillations} = 6.304$

Analysis - Control System Force Values (from Conservation of Energy):

Note: Assuming each peak to peak oscillation removes an equal amount of energy throughout the entire repulsion half stroke of the secondary.

$F_{control} := \frac{E_z}{\frac{d_{pert} \cdot num_{oscillations}}{2}}$ Total control force required. $F_{control} = 5.6 \times 10^4 \ N$

$Force_{control\_ratio} := \frac{F_{control}}{F_z}$ Ratio of Levitation Force to Levitation Control Force $Force_{control\_ratio} = 0.317$

Note: It is important to note that the control force required is a fraction of the prime mover levitation force. Such a relation MUST hold true for a control system of this type to operate.

$F_{sol} := \frac{F_{control}}{n_{sol}}$ Force required per solenoid. $F_{sol} = 2.8 \times 10^3 \ N$

$Pressure_{sol} := \frac{F_{sol}}{A_{core}}$ Secondary pressure required on secondary surface at nominal air gap. $Pressure_{sol} = 8.634 \times 10^4 \ Pa$

$B_{sol} := \sqrt{2 \cdot \mu_0 \cdot Pressure_{sol}}$ Magnetic flux density required on secondary surface at nomial air gap from Maxwell Stress Tensor equation. $B_{sol} = 0.466 \ T$

A.2 LINEAR STATE SPACE CONTROL CLOSED LOOP POLES

STATE SPACE SERVO CONTROL SYSTEM CLOSED LOOP POLES

Desired Damping Parameters:

$t_{2\%\_settling} := 2 \cdot sec$ Settling Time $\qquad M_p := 0.15$ Maximum Overshoot

Pole (x) & (y) Positions & Damping Constant:

$$x := \frac{4}{t_{2\%\_settling}} \qquad x = 2\,Hz$$

$$M_p = e^{-\pi \cdot \left(\frac{\zeta}{\sqrt{1-\zeta^2}}\right)} \qquad \frac{-\ln(M_p)}{\left(\ln(M_p)^2 + \pi^2\right)^{\frac{1}{2}}}$$

$$\zeta := \frac{-\ln(M_p)}{\left(\ln(M_p)^2 + \pi^2\right)^{\frac{1}{2}}}$$

Note: (ζ) = Damping Ratio.

$\zeta = 0.517$

$$y := \left(\frac{4}{\zeta \cdot t_{2\%\_settling}}\right) \cdot \sqrt{1-\zeta^2}$$

$y = 3.312\,Hz$

Natural Angular Frequency & Natural Frequency:

$$\omega_n := \frac{x}{\zeta} \cdot \frac{1}{Hz} \qquad \omega_n = 3.869$$

$$f_n := \frac{\omega_n}{2 \cdot \pi} \cdot Hz \qquad f_n = 0.616\,Hz$$

Butterworth Pattern for Closed Loop Control System Poles:

$$radius := \sqrt{\left(\frac{x}{Hz}\right)^2 + \left(\frac{y}{Hz}\right)^2} \qquad radius = 3.869$$

Note: Radius value indicates optimum position for Real Axis closed loop control system pole.

Solved Characteristic Equation:

$\mu_{pole1} := x + j \cdot y \qquad \mu_{pole2} := x - j \cdot y \qquad (s - \mu_{pole1}) \cdot (s - \mu_{pole2}) \cdot (s - radius)$

Note: Plug in all numerical values.

$$(s - 2 - j \cdot 3.312) \cdot (s - 2 + j \cdot 3.312) \cdot (s - 3.869)$$

$$s^3 - 7.869 \cdot s^2 + 30.445344 \cdot s - 57.916391936$$

Matrix Manipulation:

$$\begin{bmatrix} \left(\frac{1}{m}\right) & \left(\frac{1}{m}\right) & 0 \\ \left(\frac{k_c + k_p}{m^2}\right) & 0 & \left(\frac{1}{m}\right) \\ 0 & 0 & 0 \end{bmatrix}^{-1}$$

APPENDIX B COMPUTATIONAL SOLUTIONS

B.1 PHASE I SOLENOID DESIGN TRIALS

B.1.a Opera Solenoid Design - Initial

Phase I - Preliminary Opera Run Output Trends Table

	Input										Output					
Run #	Gap Distance (in.)	Iron Relative Permeability	Primary Current Density (A/m^2)	Secondary Outside Radius (in.)	Secondary Inside Radius (in.)	Secondary Thickness (in.)	Primary Outside Radius (in.)	Primary Inside Radius (in.)	Solenoid Height (in.)	Secondary Weight (N)	Coil Type Description	Forces in (N) for 60 Hz Source Frequency		Forces in (N) for 500 Hz Source Frequency		Forces in (N) for 1 KHz Source Frequency	
	z_g	μ_r	J_1	rad_2	rad_1	thk	rad_{1_out}	rad_{1_in}	h			Radius Dir.	Lift Dir.	Radius Dir.	Lift Dir.	Radius Dir.	Lift Dir.
1	0.02	1000	8.66E+06	3	0	0.5	2.62	2.5	2	-	Solenoid w/ Disk	-1.967	2.503	-1.587	3.953	-1.532	4.176
2	0.02	1000	8.66E+06	3	0	0.2	2.62	2.5	2	-	Solenoid w/ Thinner Disk Secondary	-1.988	1.790	-1.782	4.050	-1.624	4.236
3	0.02	1000	8.66E+06	3	1.5	0.5	2.62	2.5	2	-	Sol. w/ Ring Secondary	-1.978	2.494	-1.573	3.956	-1.509	4.182
4	0.02	1000	8.66E+06	3	1.5	0.5	2.62	2.5	2	-	E-Core Sol. w/ Ring Secondary	-0.763	3.487	-0.123	5.234	-0.097	5.767
5	0.02	1000	8.66E+06	2.25	0.75	0.5	1.62	1.5	2	-	E-Core Sol. w/ Smaller Ring Secondary	-0.104	1.896	-0.050	2.995	-0.042	3.344
6	0.02	1000	8.66E+06	4	2.5	0.5	3.62	3.5	2	-	E-Core Sol. w/ Larger Ring Secondary	-1.147	5.002	-0.183	7.417	-0.147	8.153
7	0.02	1000	8.66E+06	4	2.5	0.5	3.62	3.5	2	-	Same as 6 but Two Coils w/ Opposite J_1 w/ Half per Coil	-0.697	1.538	-0.999	4.023	-0.993	4.539
8	0.02	1000	8.66E+06	4	2.5	0.5	3.62	3.5	2	-	Same as 6 but Two Coils w/ Same Dir. J_1 w/ Half per Coil	-1.151	3.431	-1.352	4.787	-1.340	5.293
9	0.02	1000	8.66E+06	-	-	0.5	-	-	0.12	-	Small Radius Pancake Ring	-0.280	1.669	-0.165	2.340	-0.148	2.467
10	0.02	1000	9.03E+06	4	2.5	0.5	3.62	3.5	2	6.626	E-Core Sol. w/ Larger Ring Secondary & more J_1	-1.248	5.443	-0.199	8.072	-0.160	8.873
11	0.02	1000	8.66E+06	4.5	3.25	0.5	5.5	3.5	0.12	6.583	Large Radius Pancake Ring	-6.053	8.945	-5.236	10.407	-5.207	10.593
12	0.02	1000	9.03E+06	4.5	3.25	0.5	5.5	3.5	0.12	6.583	Large Radius Pancake Ring & more J_1	-6.587	9.735	-5.698	11.325	-5.666	11.528
13	0.02	1000	9.03E+06	5.5	3.25	0.5	5.5	3.5	0.120	13.378	Trapazoidal Pancake	-	12.700	-	-	-	-
14	0.02	1000	9.03E+06	5.5 & 4.5	4.25 & 3.25	0.5	5.5	3.5	0.120	7.432	Trapazoidal Pancake	-1.773	12.931	-0.782	14.046	-0.616	14.223

Notes:
1. All preliminary cases listed were run in chronological order in an attempt to "bound" the problem from intuition. Case #14 provides the best results to date.
2. The solenoid dimension change form between various run types. The coil dimensions depicted represent similar dimension locations between coil types.
3. The primary coil and secondary conductor cross sectional area are maintained between computational runs.
4. The secondary weight is only determined for cases involving a possible final design.
5. All current densities used are within allowable primary heating. The lower current desity includes an external primary resistor.
   The higher current density does not include an external resistor.

Figure B-1: Opera Computational Solution Test Matrix @ 60 Hz

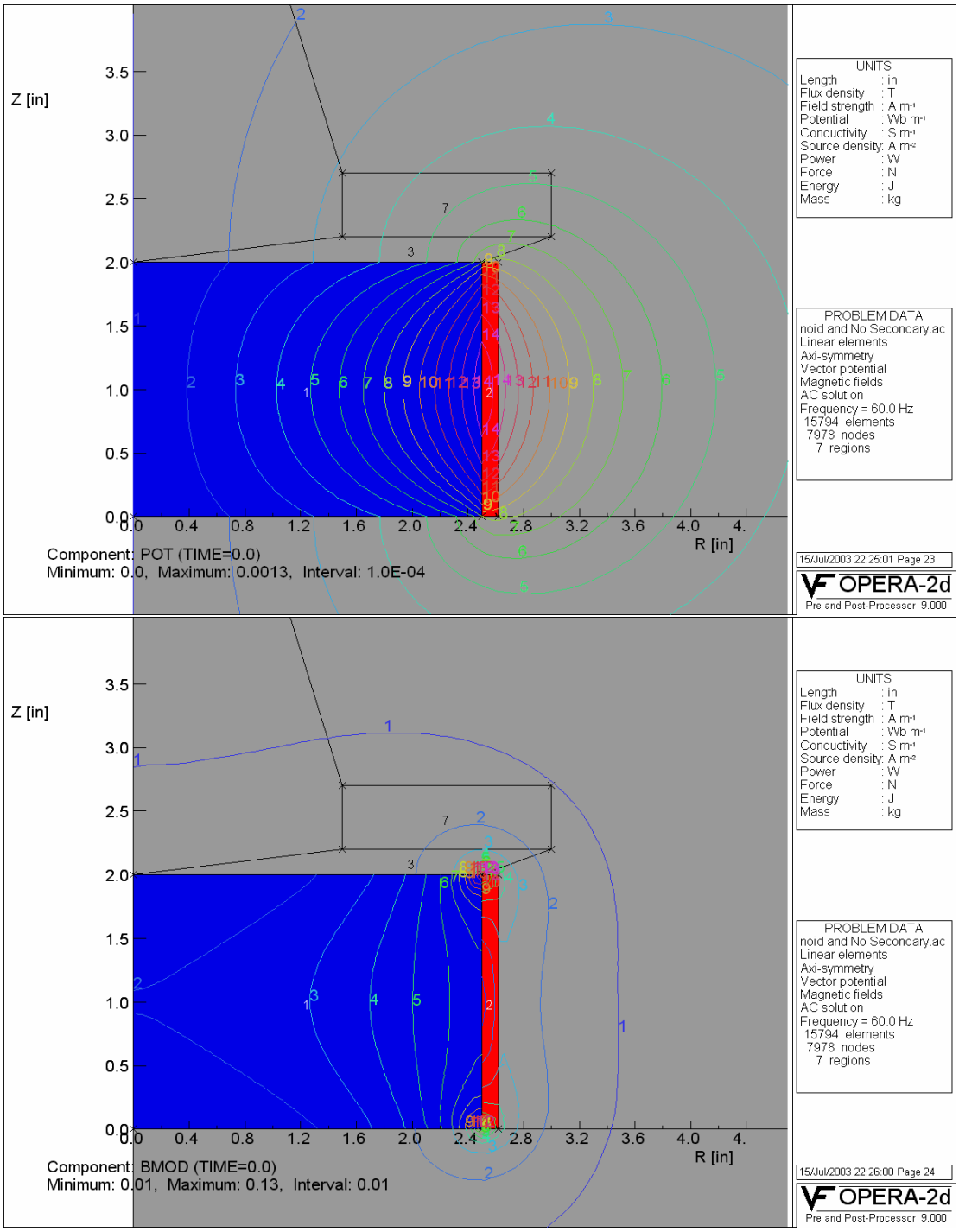

Figure B-2: Phase I Solenoid Without Secondary

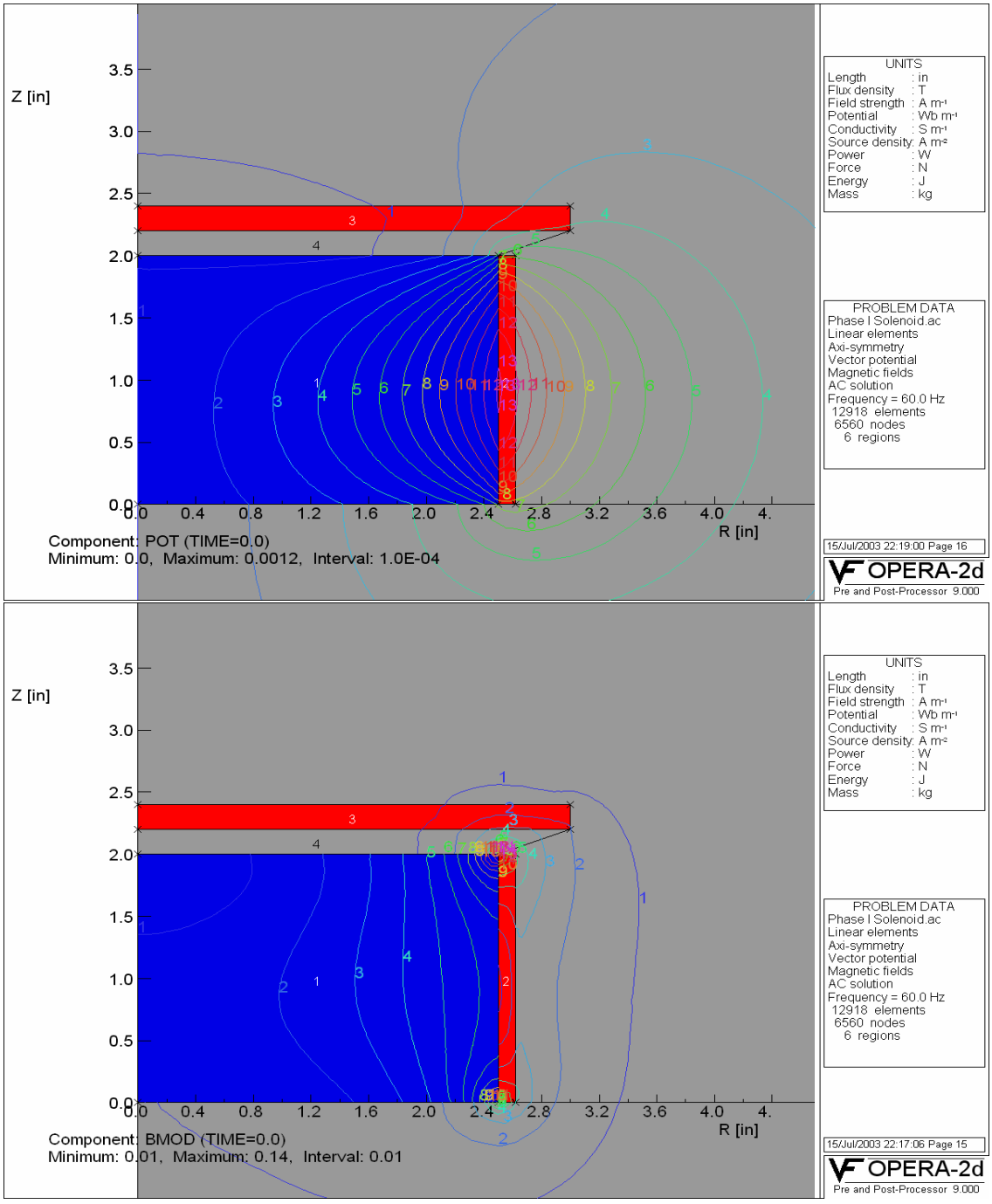

Figure B-3: Phase I Solenoid with Thin Disk Secondary

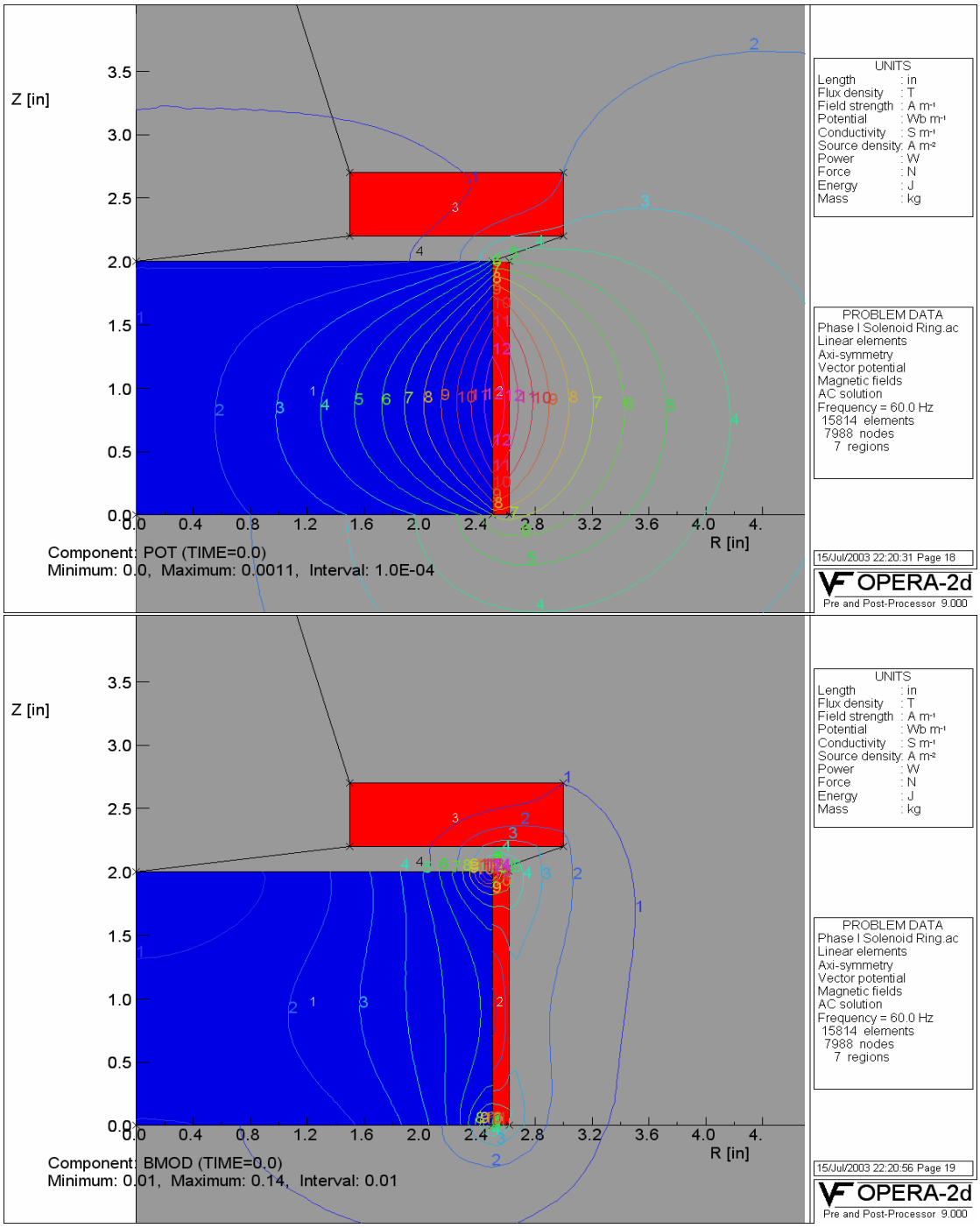

Figure B-4: Phase I Solenoid with Ring Secondary

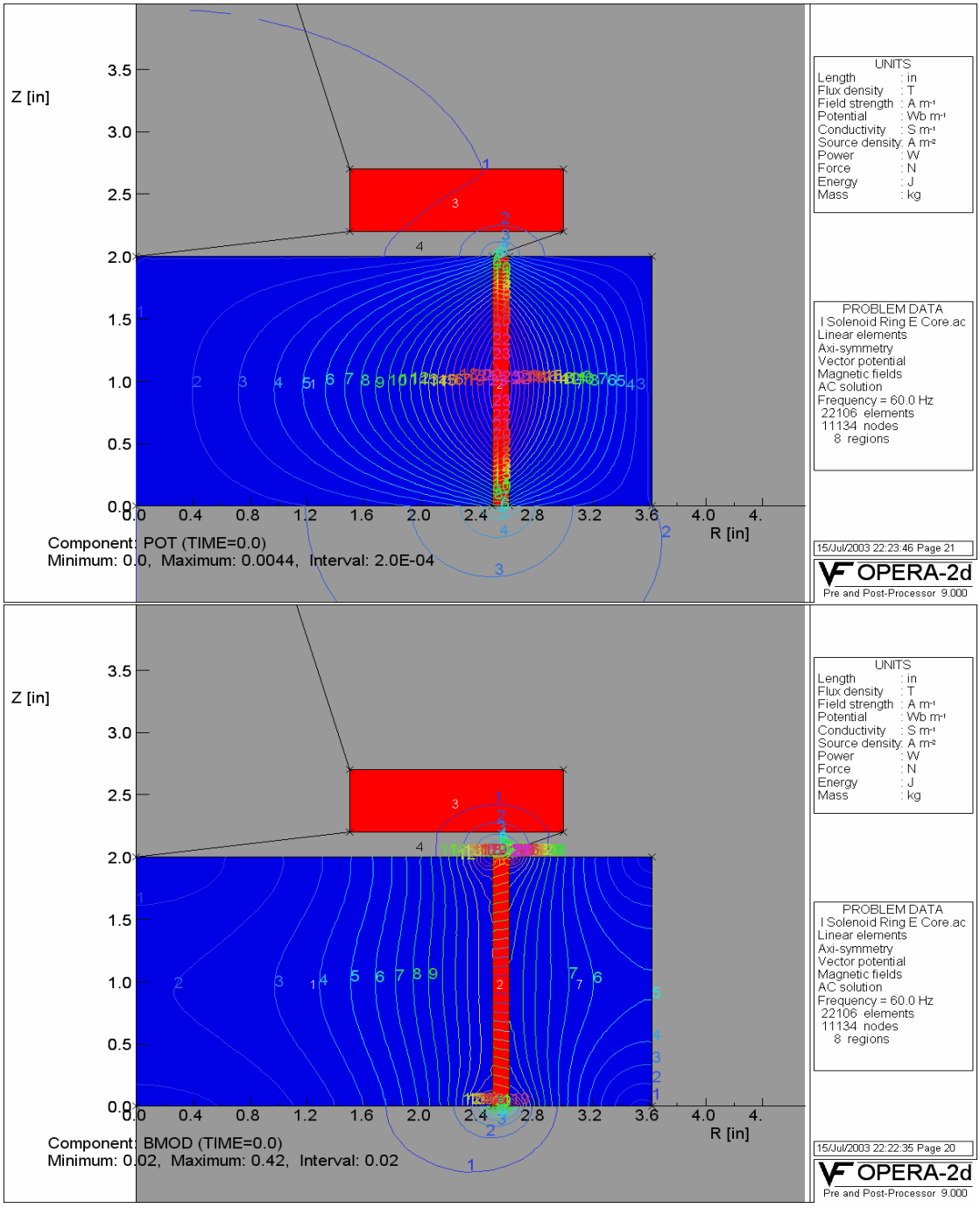

Figure B-5: Phase I E-Core Solenoid with Ring Secondary

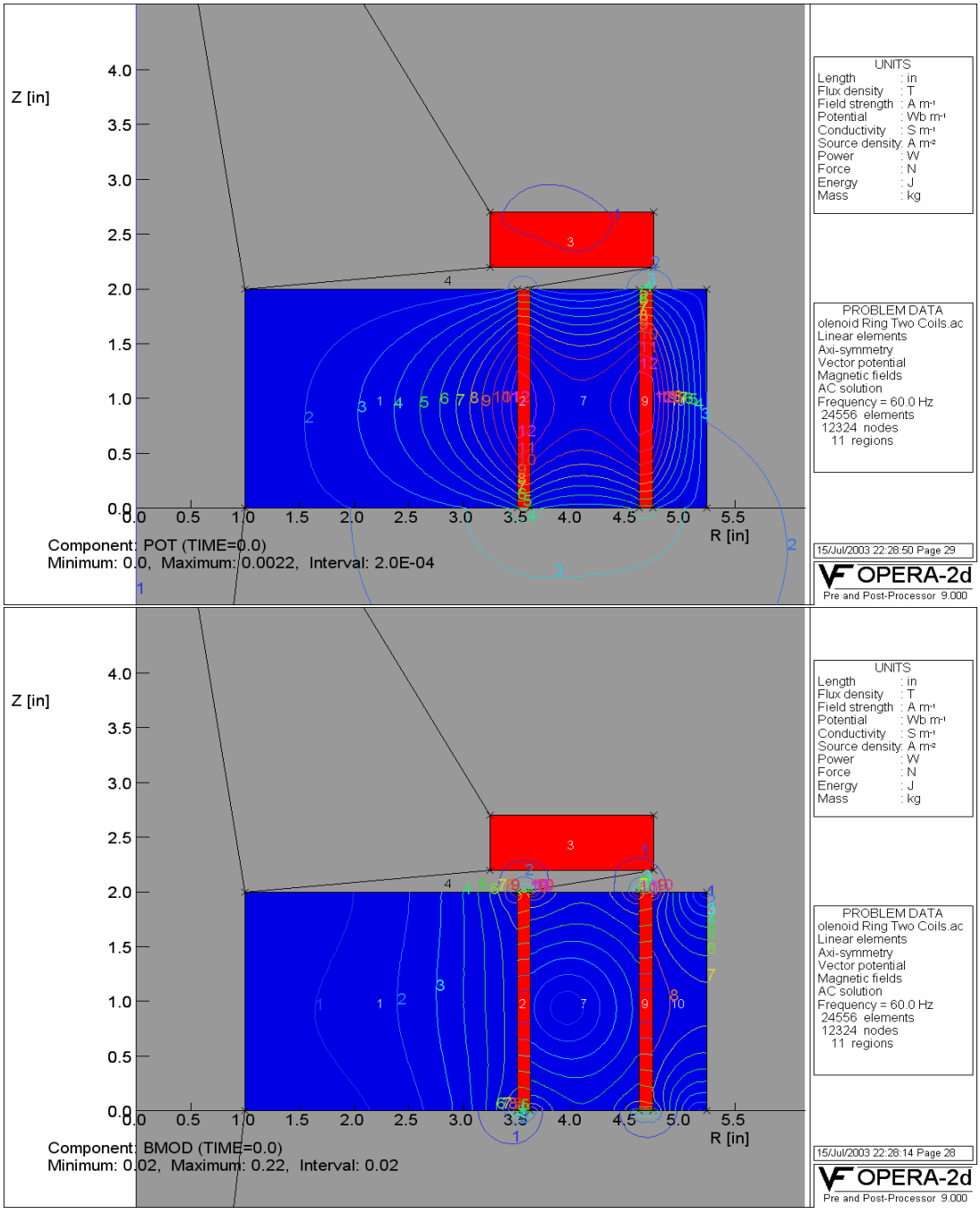

Figure B-6: Phase I E-Core Solenoid, 2 Windings with Ring Secondary

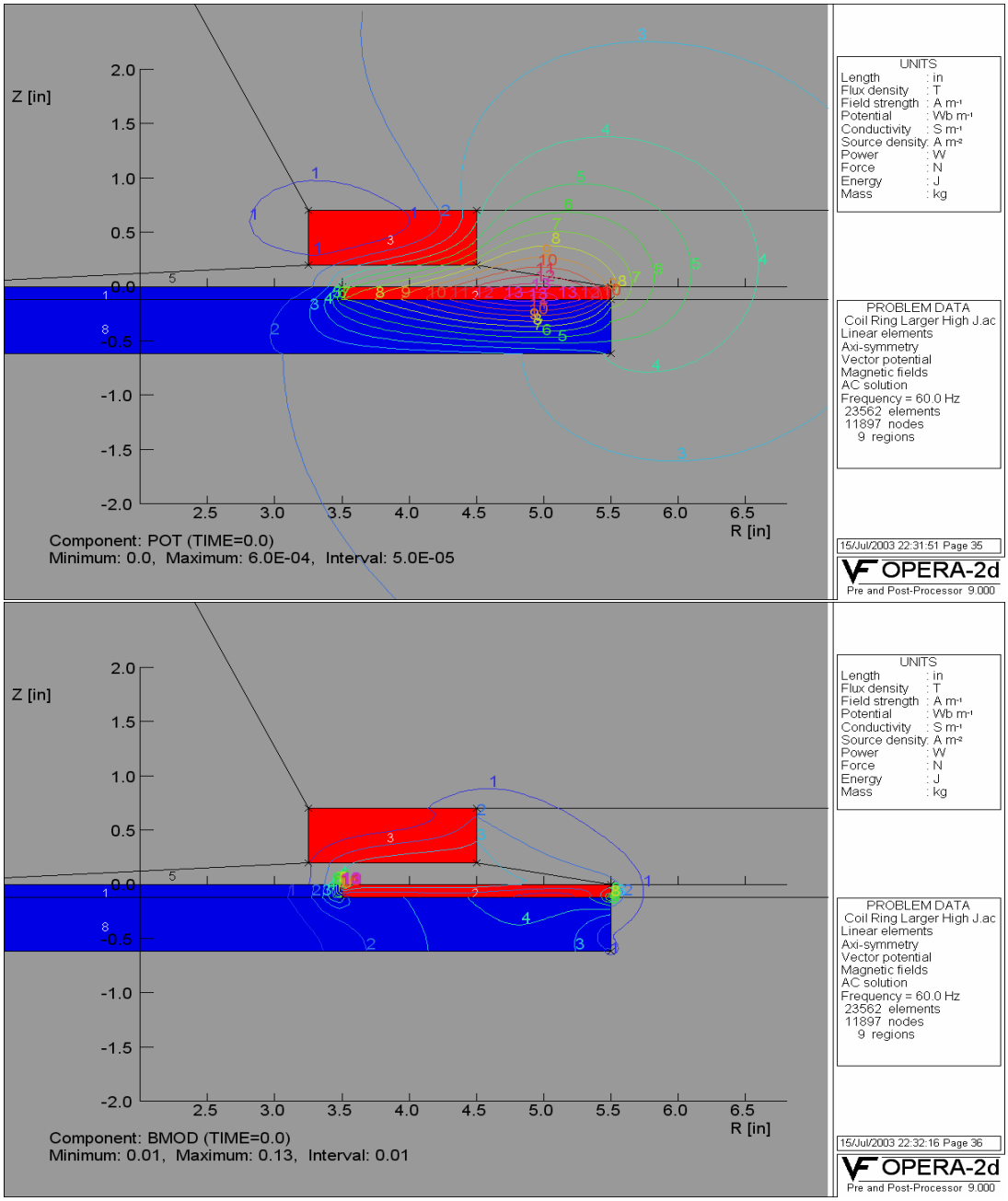

Figure B-7: Phase I Pancake Coil with Ring Secondary

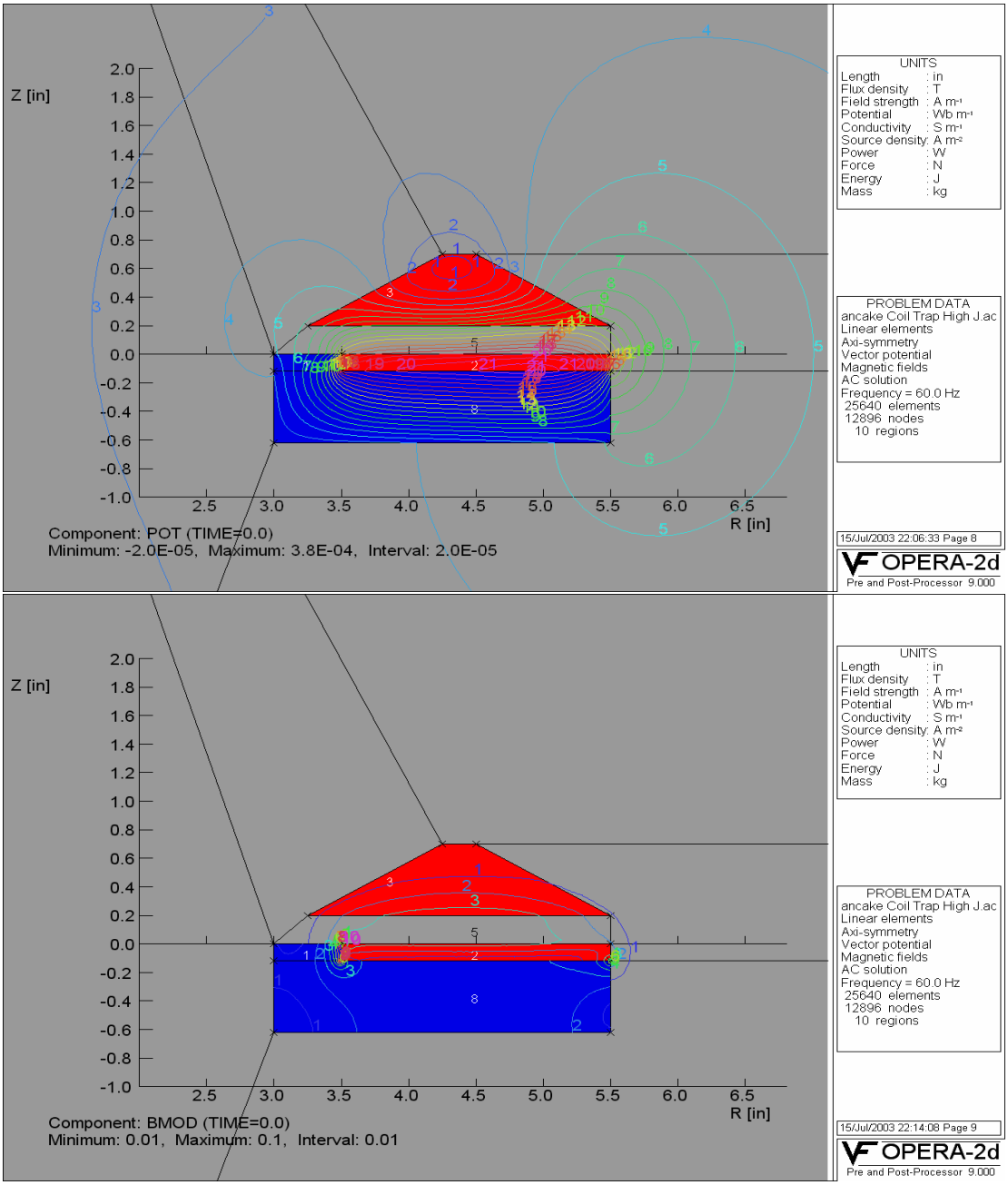

Figure B-8: Phase I Pancake Coil with Trapezoidal Ring Secondary

B.1.b Opera Solenoid Design - Final

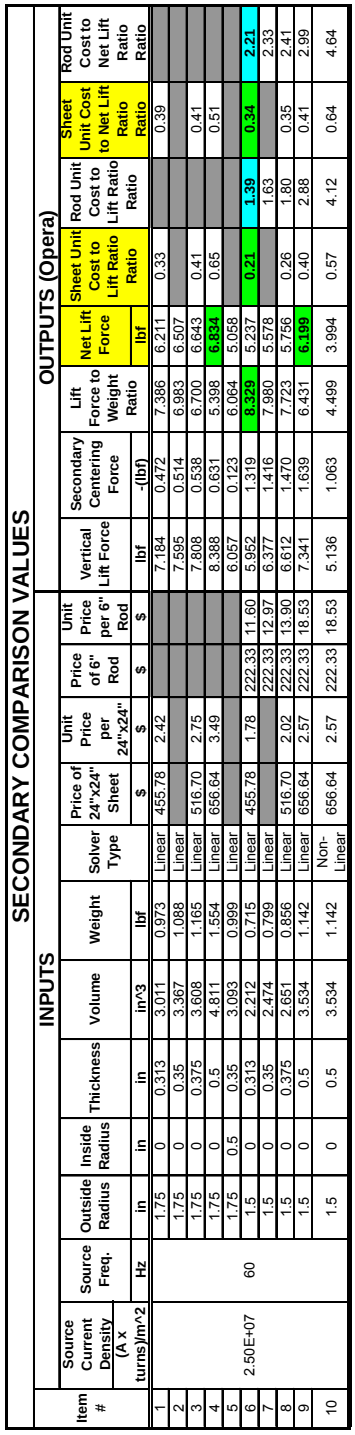

SECONDARY COMPARISON VALUES

Item #	INPUTS: Source Current Density (A-x turns)/in^2	Source Freq. Hz	Outside Radius in	Inside Radius in	Thickness in	Volume in^3	Weight lbf	Solver Type	Price of 24"x24" Sheet $	Unit Price per 24"x24" $	Price of 6" Rod $	Unit Price per 6" Rod $	OUTPUTS (Opera): Vertical Lift Force lbf	Secondary Centering Force -(lbf)	Lift Force to Weight Ratio	Net Lift Force lbf	Sheet Unit Cost to Lift Ratio Ratio	Rod Unit Cost to Lift Ratio Ratio	Sheet Unit Cost to Net Lift Ratio Ratio	Rod Unit Cost to Net Lift Ratio Ratio
1			1.75	0	0.313	3.011	0.973	Linear	455.78	2.42			7.184	0.472	7.386	6.211	0.33		0.39	
2			1.75	0	0.35	3.367	1.088	Linear					7.595	0.514	6.983	6.507				
3			1.75	0	0.375	3.608	1.165	Linear	516.70	2.75			7.808	0.538	6.700	6.643	0.41		0.41	
4			1.75	0	0.5	4.811	1.554	Linear	656.64	3.49			8.388	0.631	5.398	**6.834**	0.65		0.51	
5			1.75	0.5	0.35	3.093	0.999	Linear					6.057	0.123	6.064	5.058				
6	2.50E+07	60	1.5	0	0.313	2.212	0.715	Linear	455.78	1.78	222.33	11.60	5.952	1.319	**8.329**	5.237	**0.21**	**1.39**	**0.34**	**2.21**
7			1.5	0	0.35	2.474	0.799	Linear			222.33	12.97	6.377	1.416	7.980	5.578		1.63		2.33
8			1.5	0	0.375	2.651	0.856	Linear	516.70	2.02	222.33	13.90	6.612	1.470	7.723	5.756	0.26	1.80	0.35	2.41
9			1.5	0	0.5	3.534	1.142	Linear	656.64	2.57	222.33	18.53	7.341	1.639	6.431	**6.199**	0.40	2.88	0.41	2.99
10			1.5	0	0.5	3.534	1.142	Non-Linear	656.64	2.57	222.33	18.53	5.136	1.063	4.499	3.994	0.57	4.12	0.64	4.64

(Density of Cu) x (Grav. 0.323 lbf/in^3

NOTES:
- Pricing is per McMaster-Carr stock for Alloy 110 on 2/14/06.
- Thermal effects NOT accounted for in chart yet a major factor in final
- Plate stock pricing may be low enough to only consider best
- Costing sets a standard plant stock for all and assumes no loss of material across sheet or rod sizing per secondary diam. Also machining cost differences not accounted for in chart.

Figure B-9: Phase I Secondary Geometry Comparisons @ 60 Hz

APPENDIX C MATLAB & SIMULINK NUMERICAL SOLUTION PROGRAMS

C.1 SIMULINK FILES

C.1.a Main Simulink Operational Files – Phase I

Due to the vast amount of numerical simulation files, only the main Simulink® operational files required for the Phase I input, numerical simulation, and output are represented in this appendix.

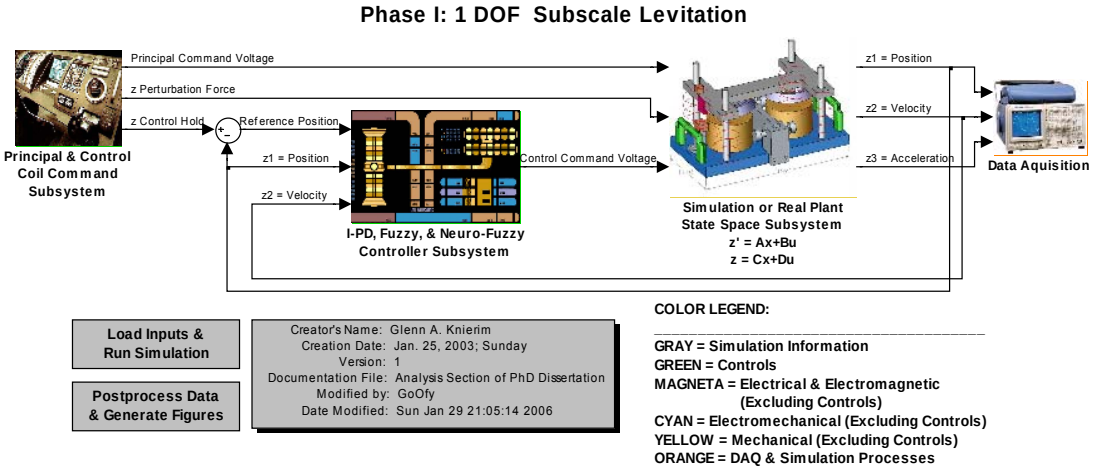

Figure C-1: Phase I - Main Top Level Simulation Level

C.1.a.i Command Inputs Subsystem

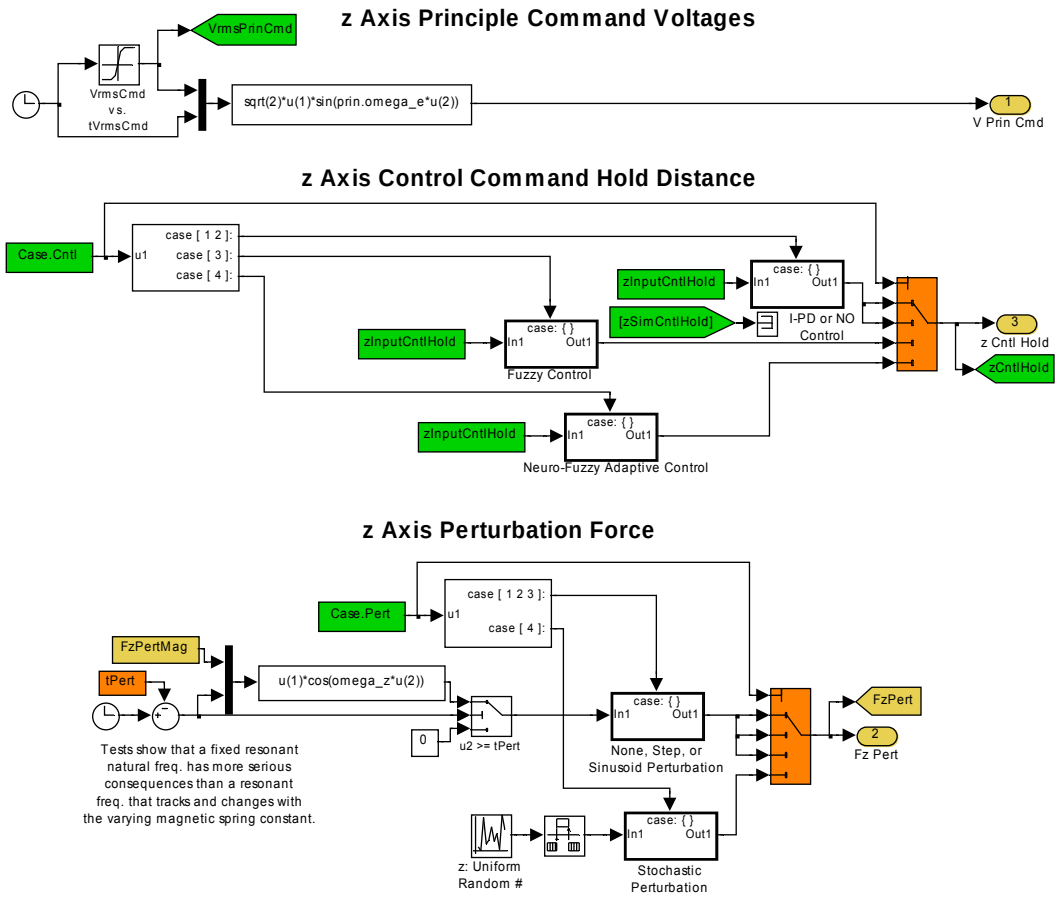

Figure C-2: Phase I – Principal & Control Coil Command

C.1.a.ii Control Subsystem

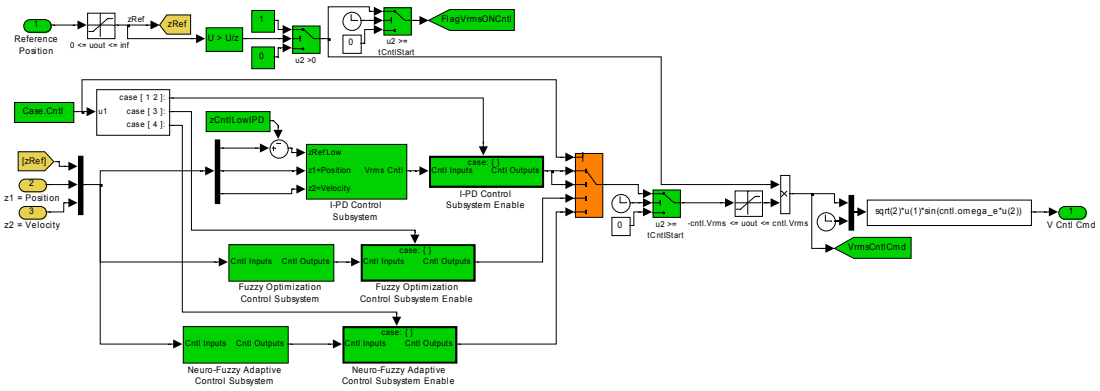

Figure C-3: Phase I – I.-P.D., Fuzzy, & Neuro-Fuzzy Controller

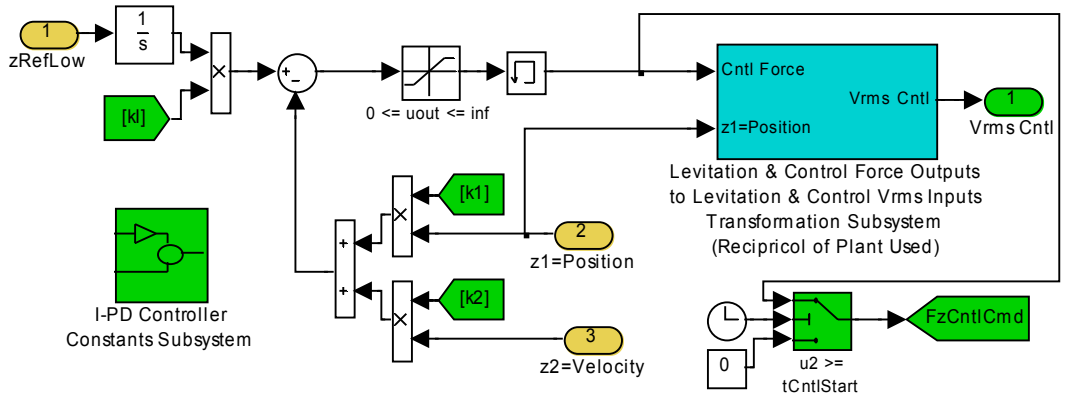

Figure C-4: Phase I – I.-P.D. Controller

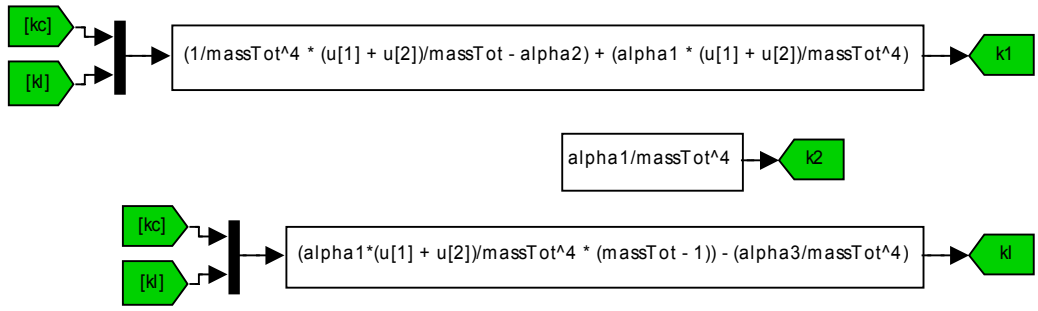

Figure C-5: Phase I – I.-P.D. Controller Gains

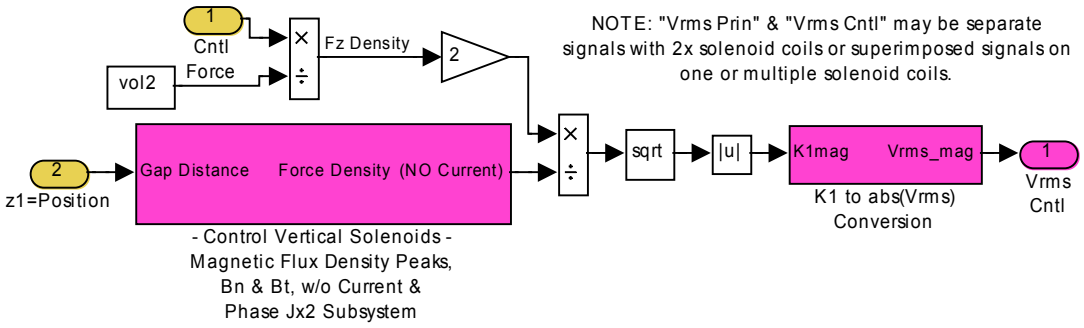

Figure C-6: Phase I – I.-P.D. Controller Transformation

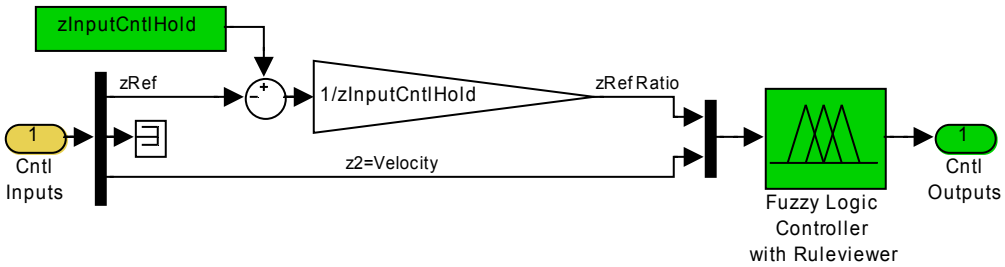

Figure C-7: Phase I – Fuzzy Controller

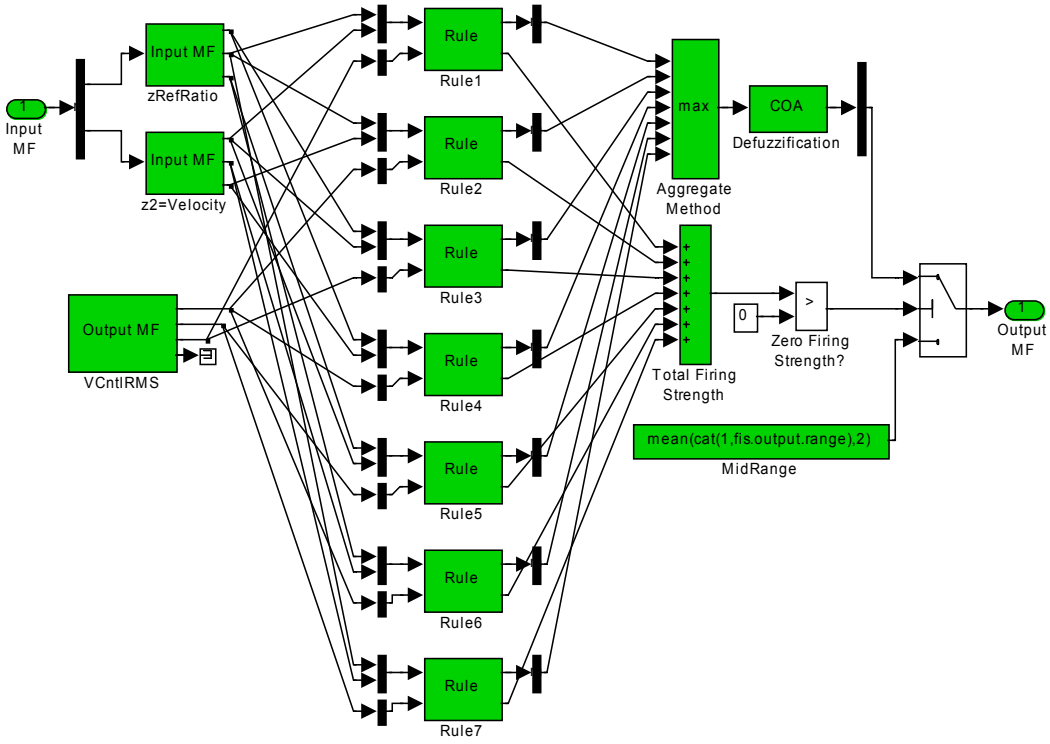

Figure C-8: Phase I – Fuzzy Logic Controller Simulink Model

C.1.a.iii Plant Subsystem

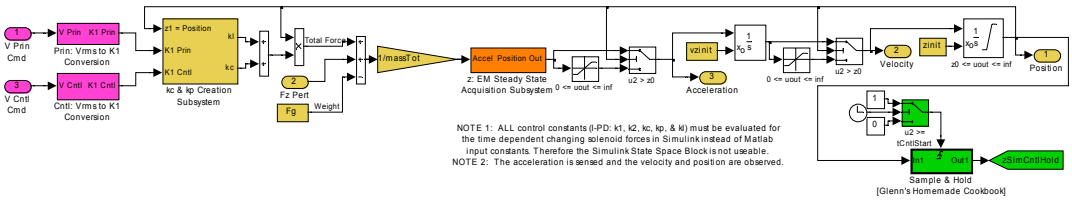

Figure C-9: Phase I – Plant

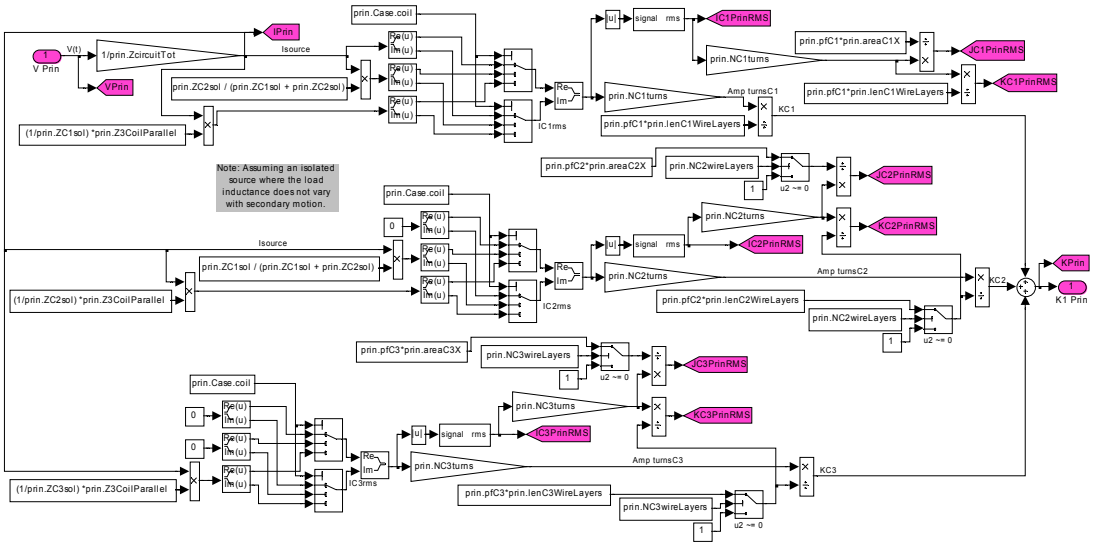

Figure C-10: Phase I – Principal Coil Vrms to K1 Conversion

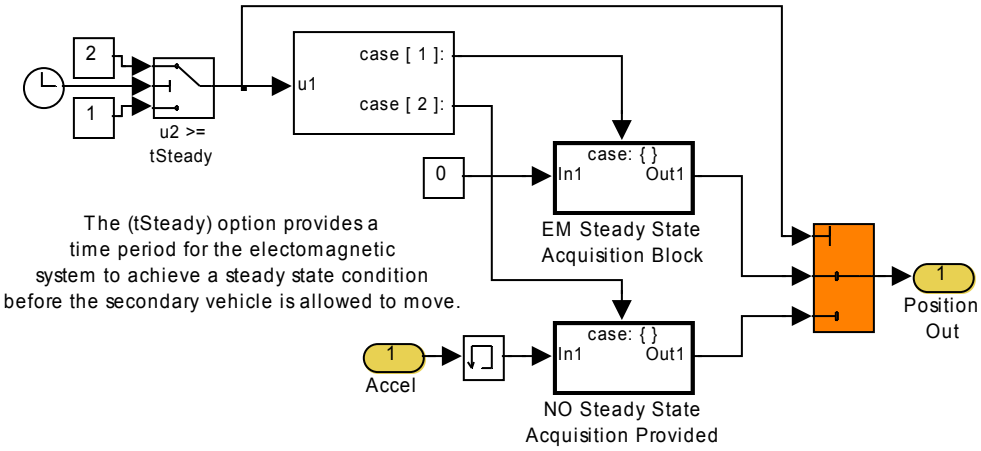

Figure C-11: Phase I – E.M. Steady State Acquisition

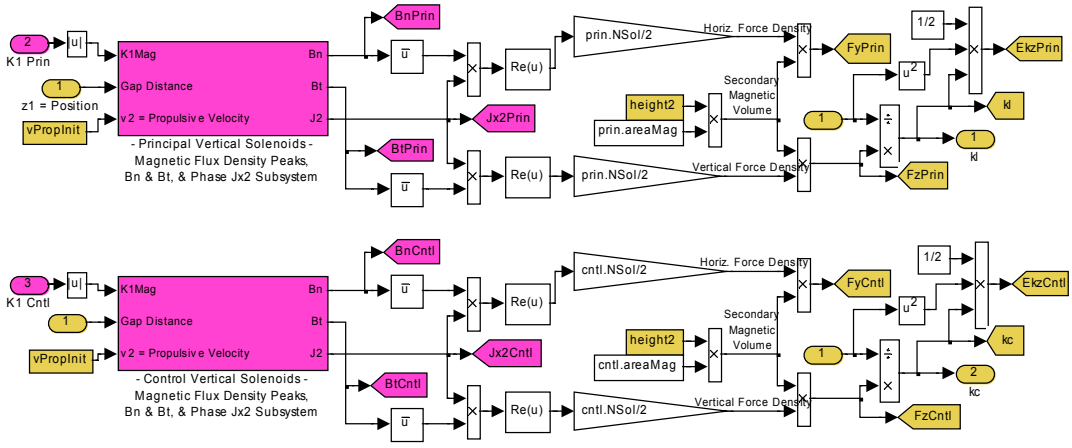

Figure C-12: Phase I – Magnetic Spring Constant Creation

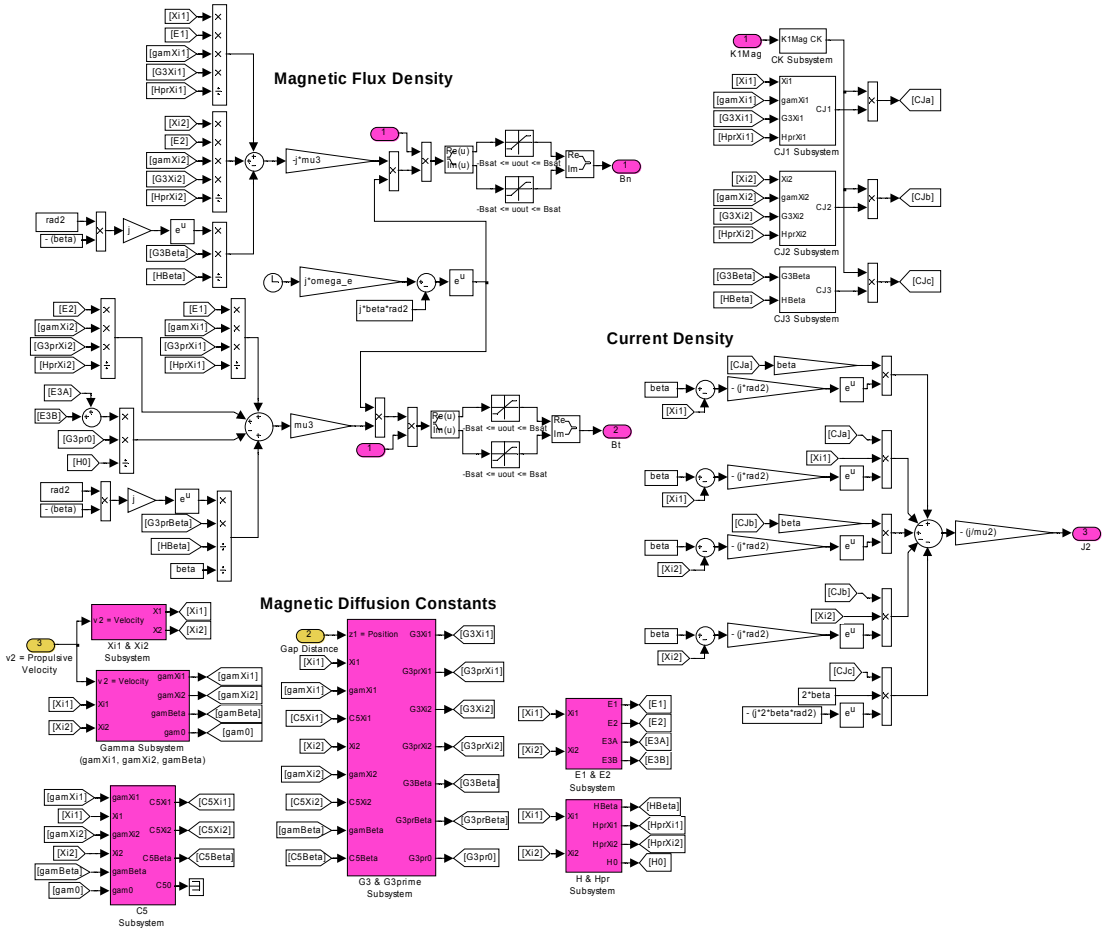

Figure C-13: Phase I – Principal B_N, B_T, & Phase J_{x2}

C.1.a.iv Data Acquisition Output Subsystem

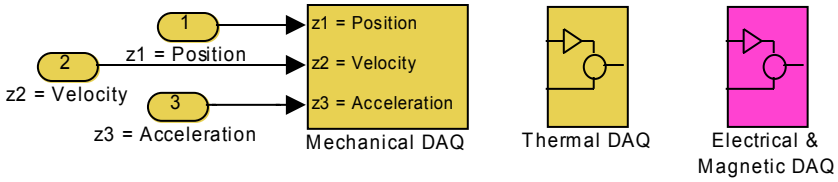

Figure C-14: Phase I – Data Acquisition

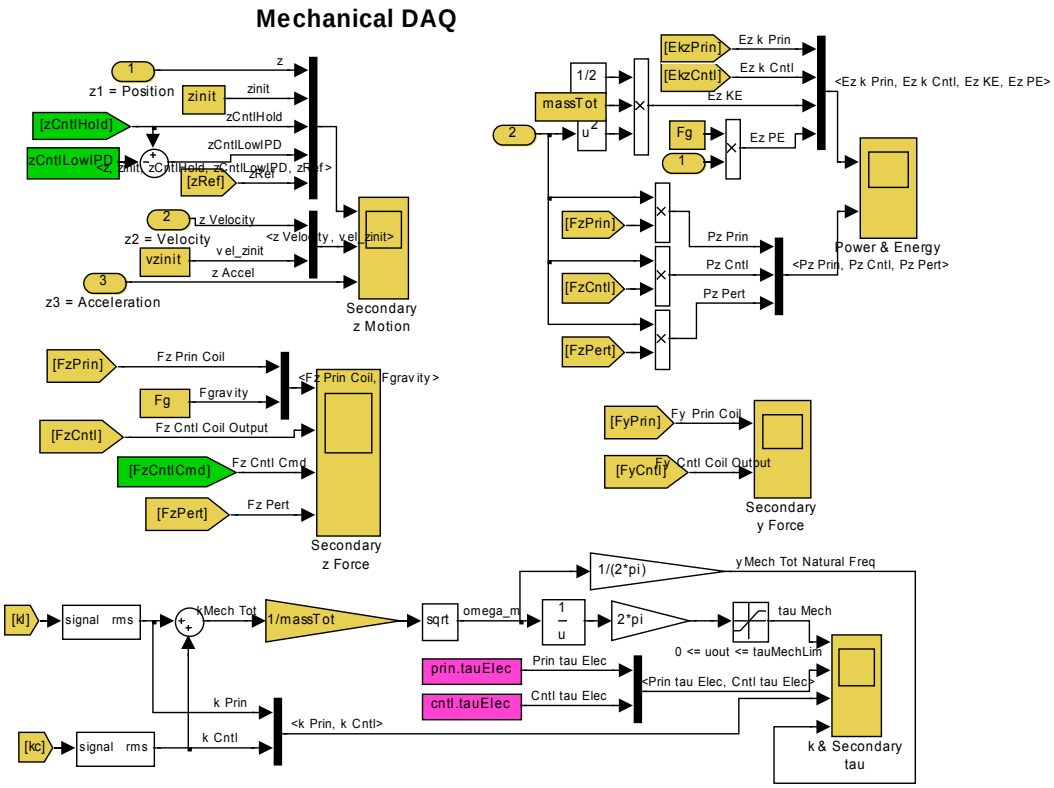

Figure C-15: Phase I – Mechanical D.A.Q.

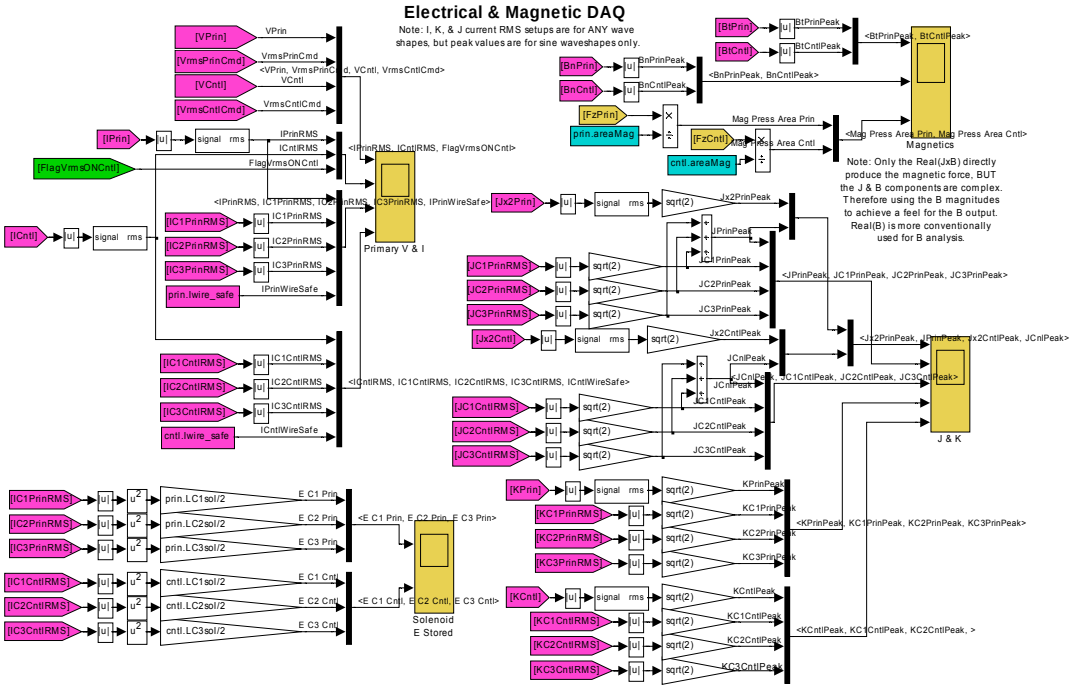

Figure C-16: Phase I – Electrical & Magnetic D.A.Q.

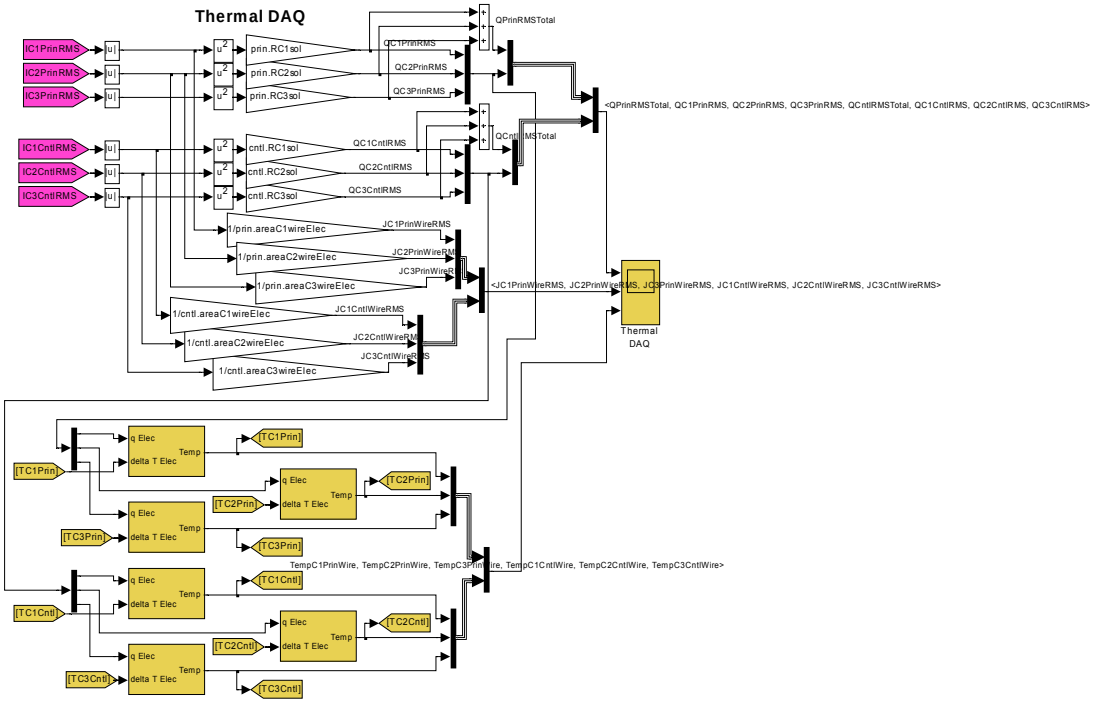

Figure C-17: Phase I – Thermal D.A.Q.

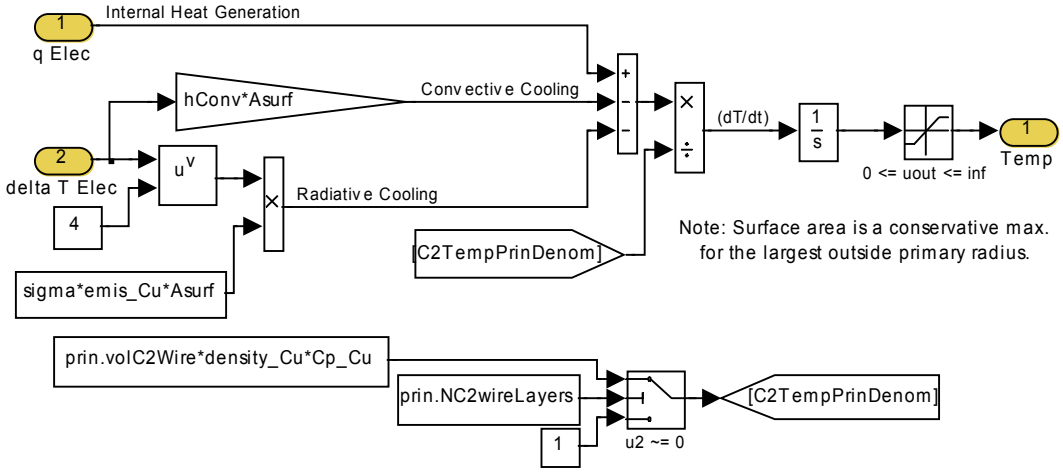

Figure C-18: Phase I – Thermal D.A.Q. Temperature Rise

C.1.b Main Simulink Operational Files – Phase IV

Due to the vast amount of numerical simulation files, only the main Simulink® operational files required for the Phase IV input, numerical simulation, and output are represented in this appendix.

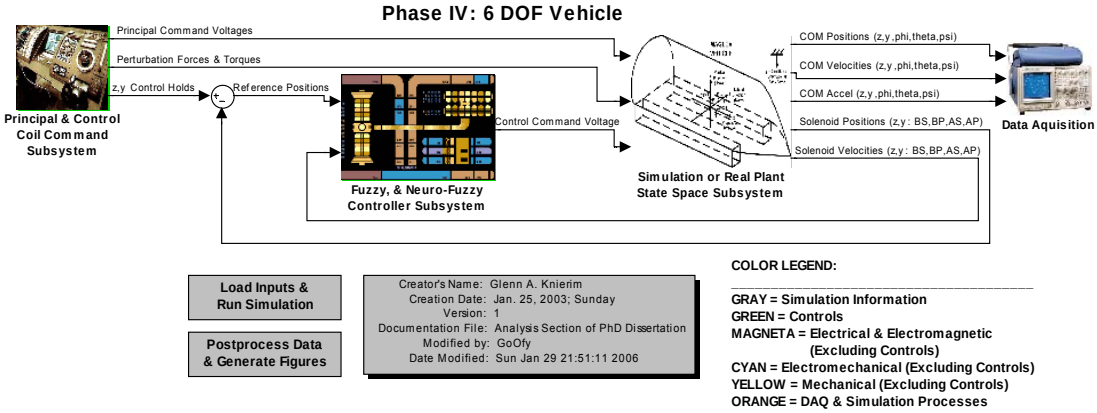

Figure C-19: Phase IV - Main Top Level Simulation Level

C.1.b.i Command Inputs Subsystem

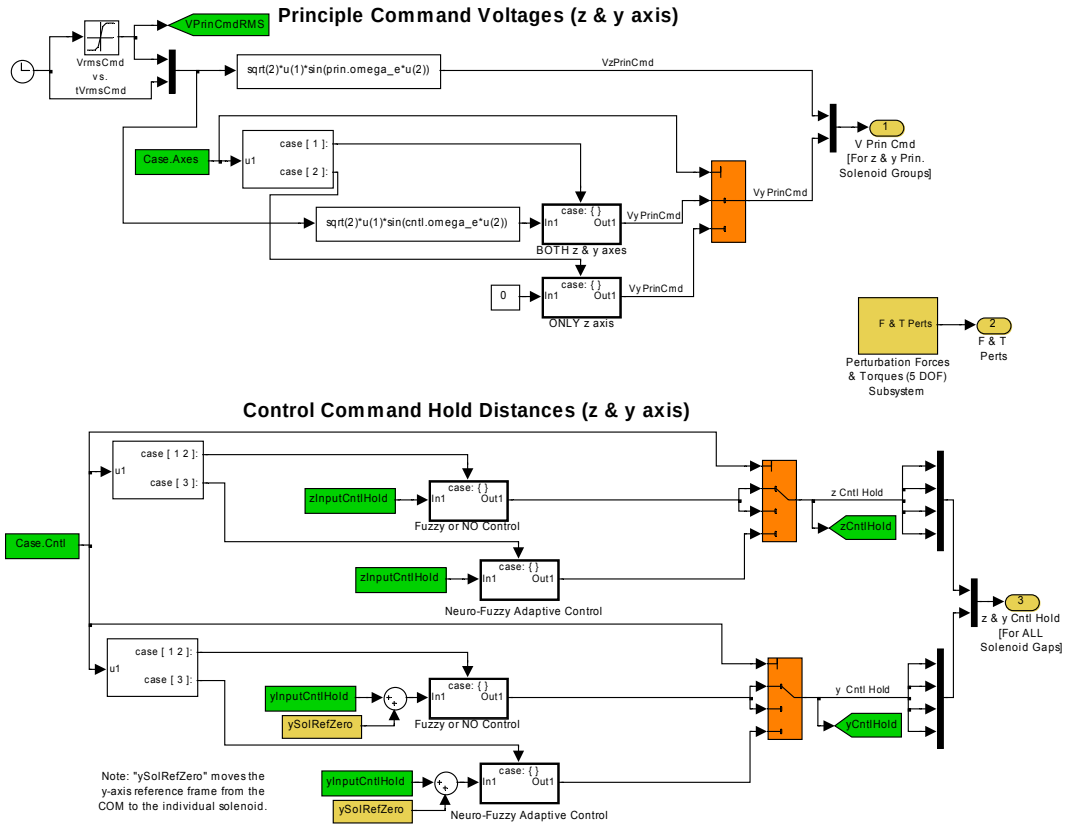

Figure C-20: Phase IV – Principal & Control Coil Command

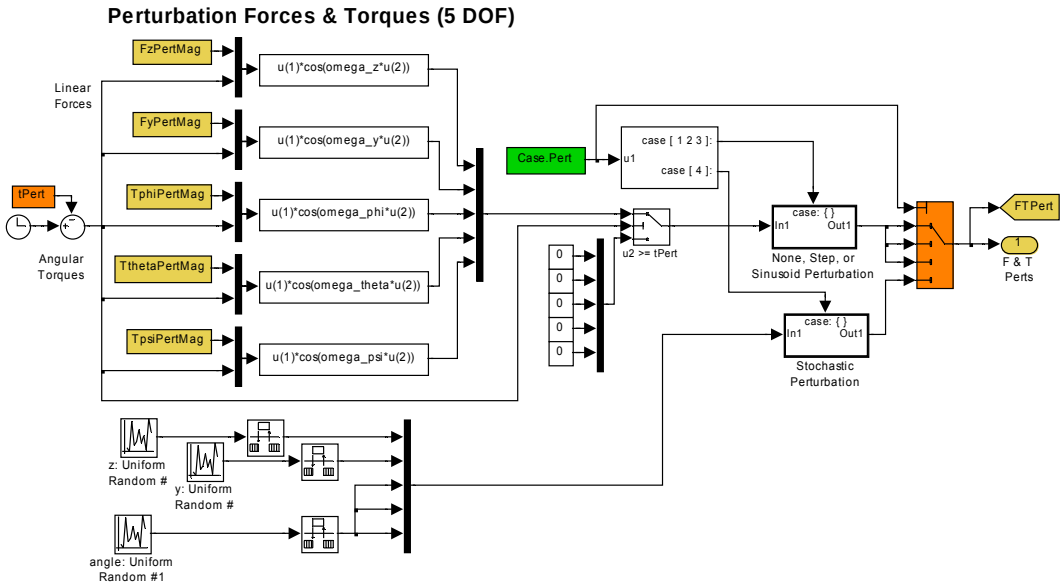

Figure C-21: Phase IV – Perturbation Forces & Torques (5 D.O.F.)

C.1.b.ii Control Subsystem

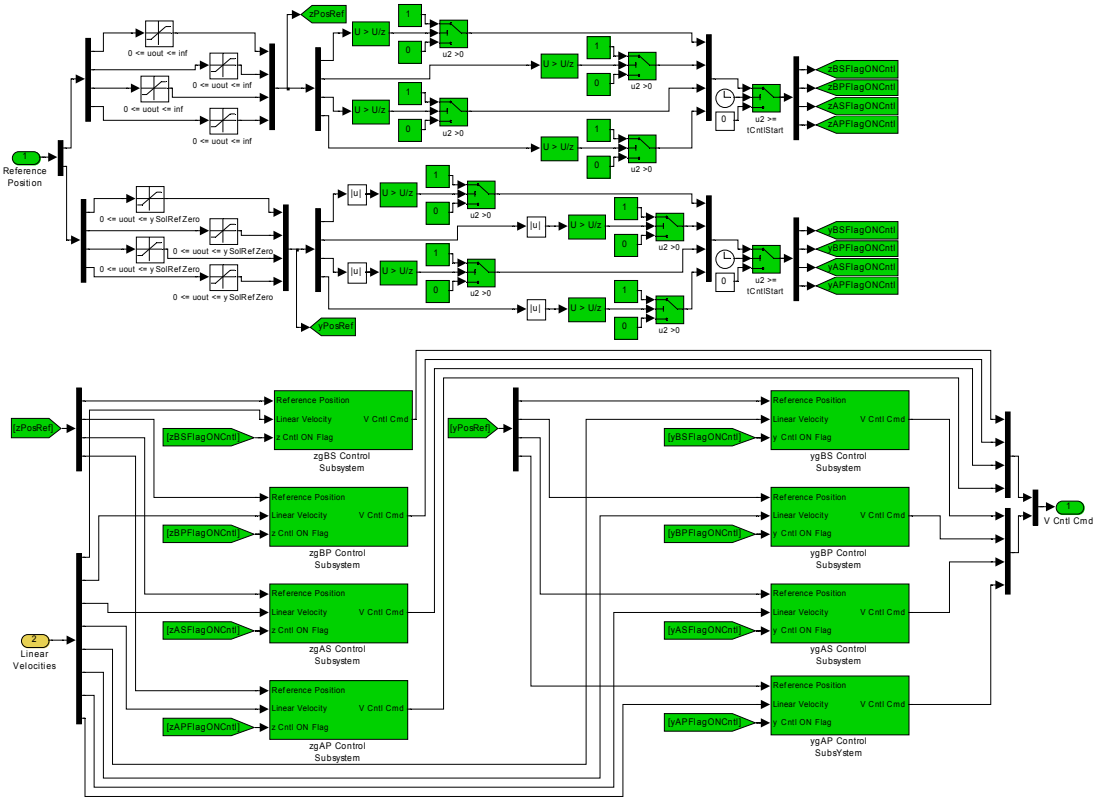

Figure C-22: Phase IV –Fuzzy & Neuro-Fuzzy Controller

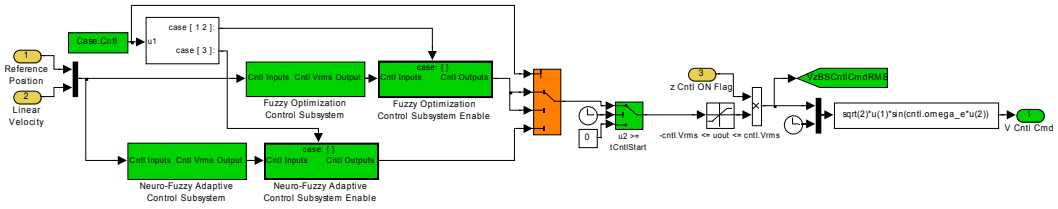

Figure C-23: Phase IV – z_{gBS} Control

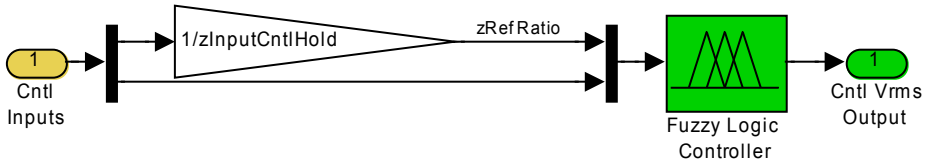

Figure C-24: Phase IV – Fuzzy Controller

C.1.b.iii Plant Subsystem

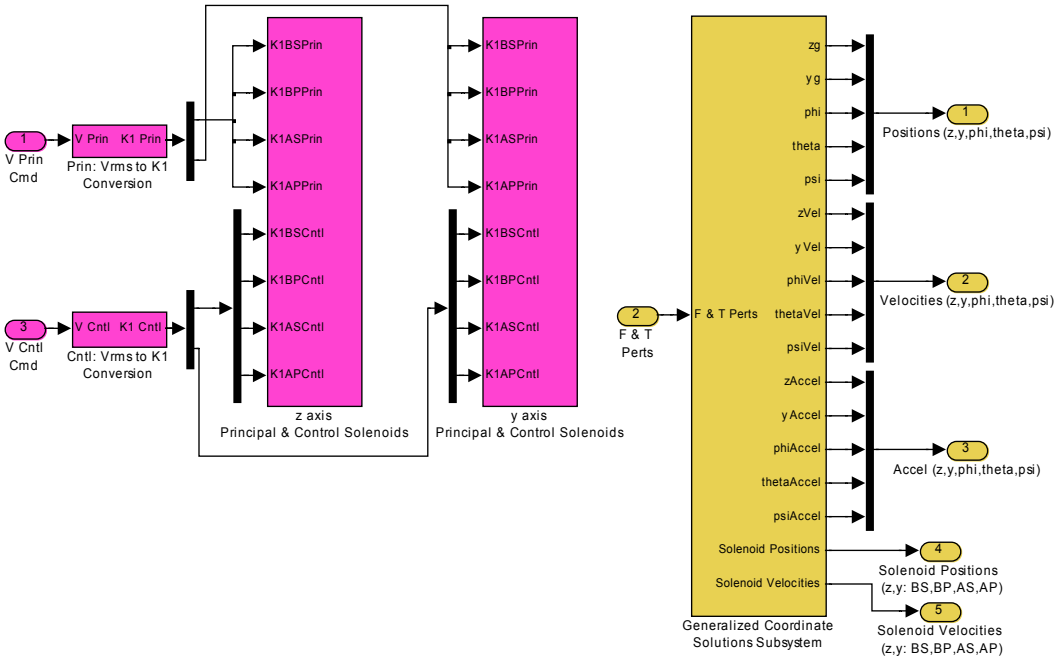

Figure C-25: Phase IV – Plant

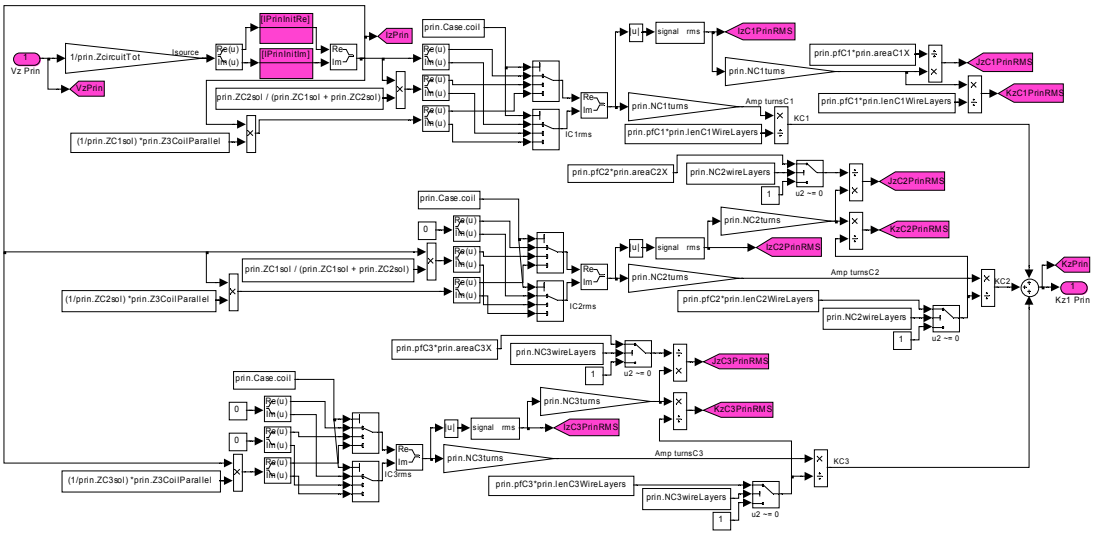

Figure C-26: Phase IV – z Axis Principal Vrms to K1 Conversion

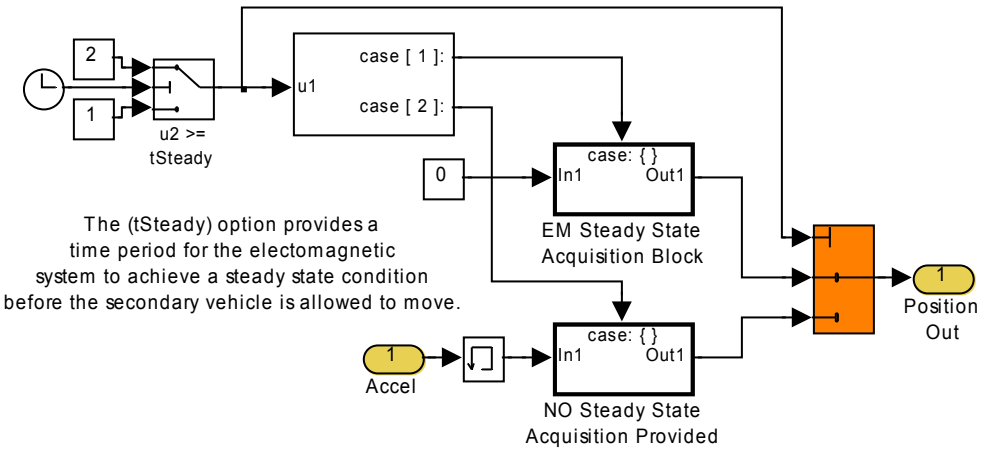

Figure C-27: Phase IV – E.M. Steady State Acquisition

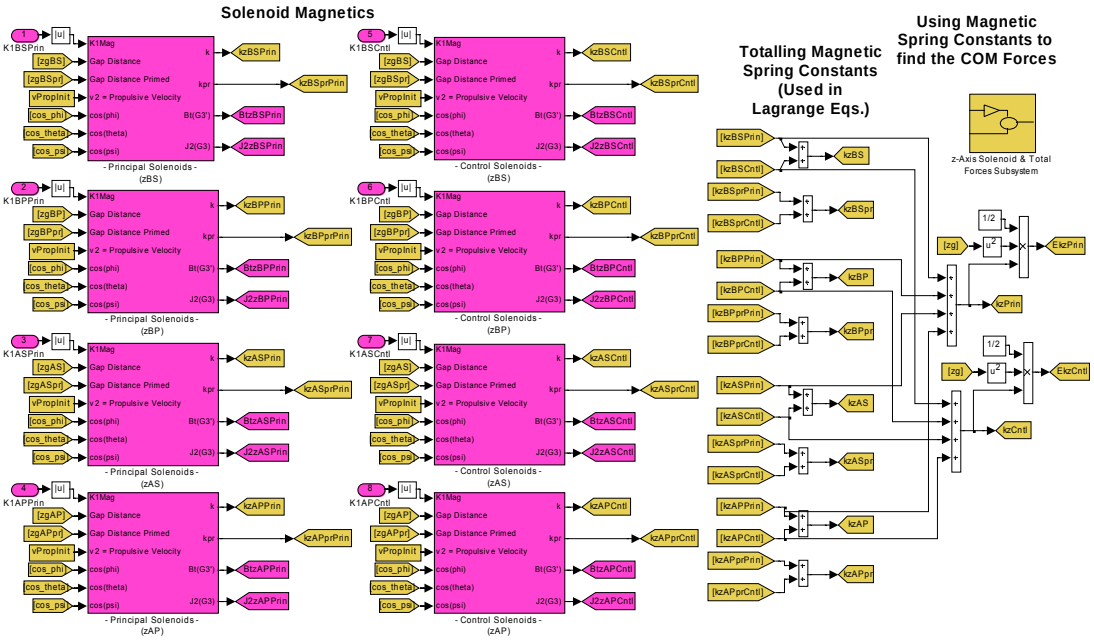

Figure C-28: Phase IV – Magnetic Spring Constant Creation

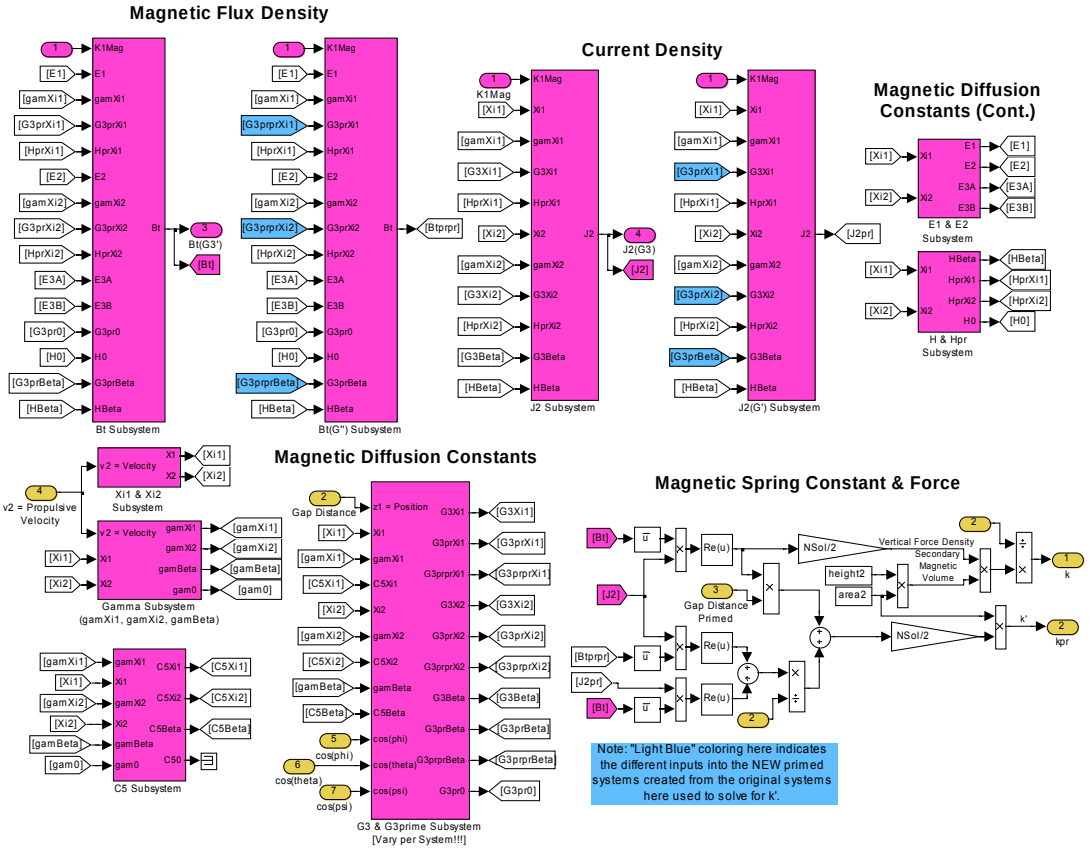

Figure C-29: Phase IV – z_{gBS} Principal B_N, B_T, & Phase J_{x2}

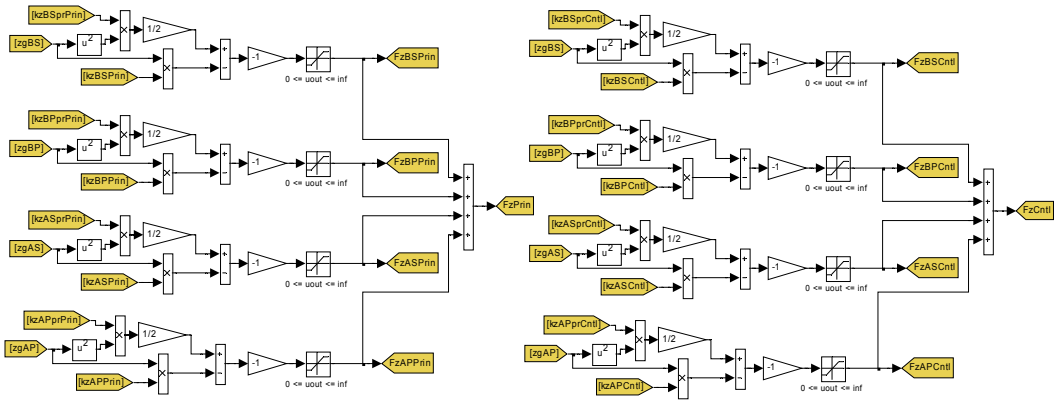

Figure C-30: Phase IV – z Axis Solenoid & C.O.M. Total Forces

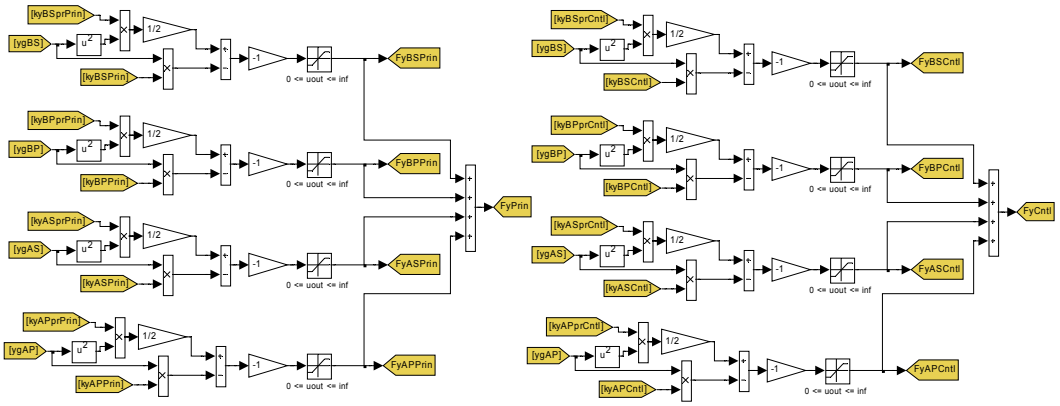

Figure C-31: Phase IV – y Axis Solenoid & C.O.M. Total Forces

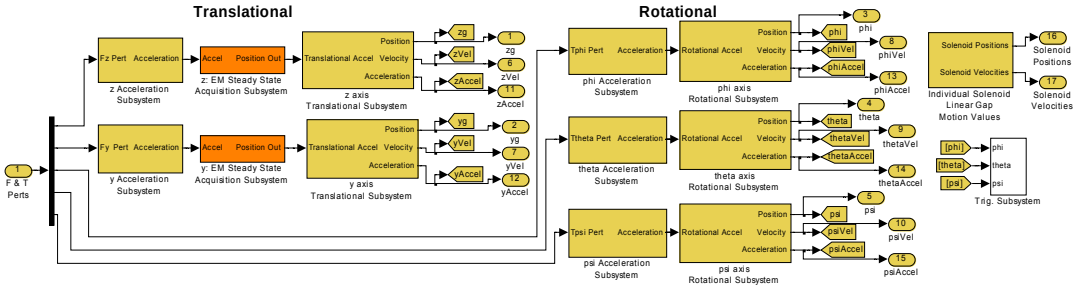

Figure C-32: Phase IV – Generalized Coordinate Solutions

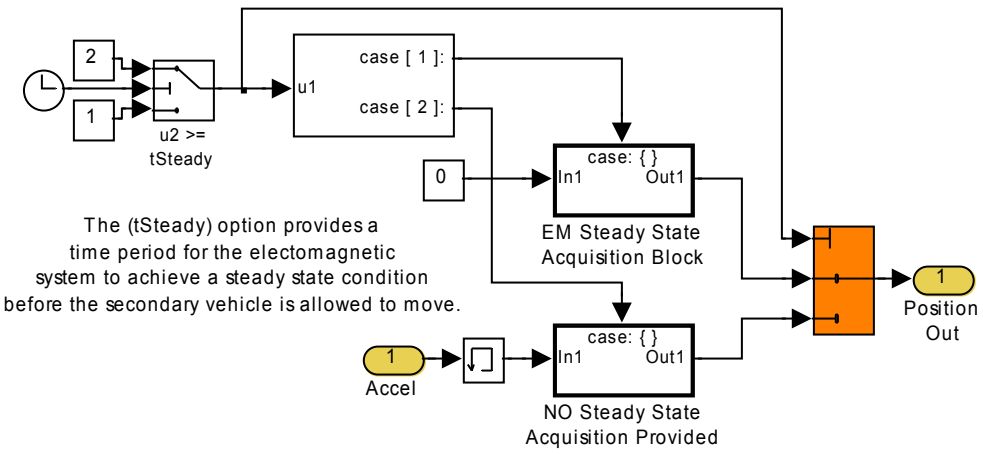

Figure C-33: Phase IV – E.M. Steady State Acquisition

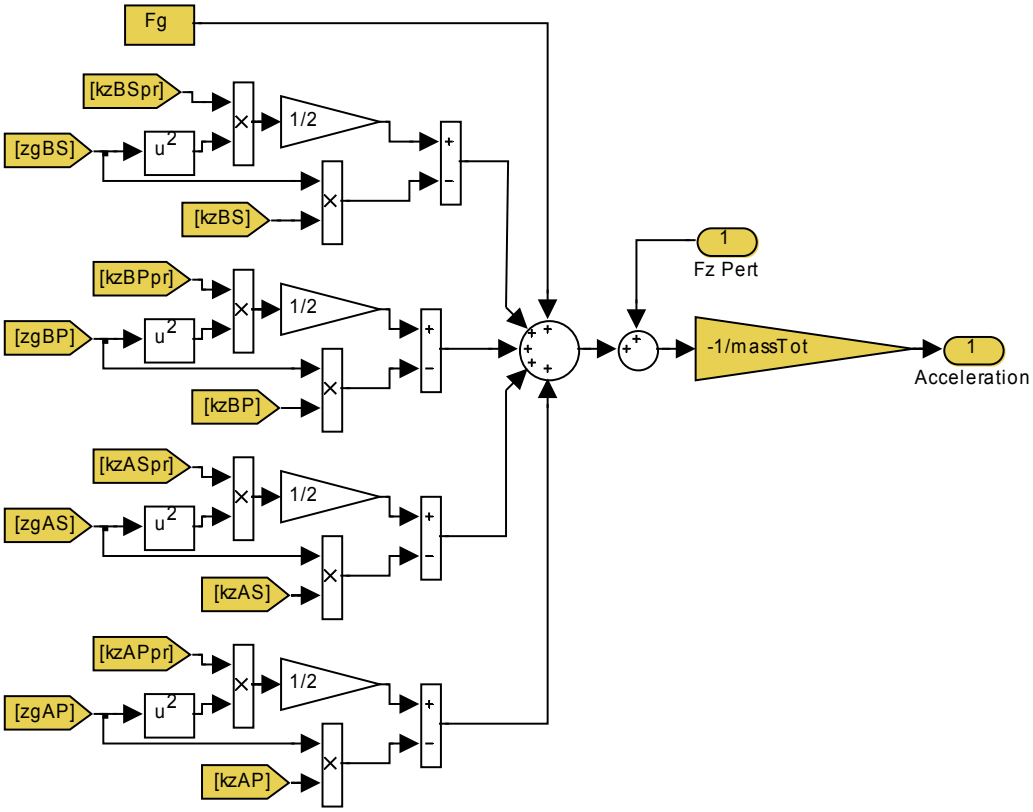

Figure C-34: Phase IV – z Axis C.O.M. Acceleration

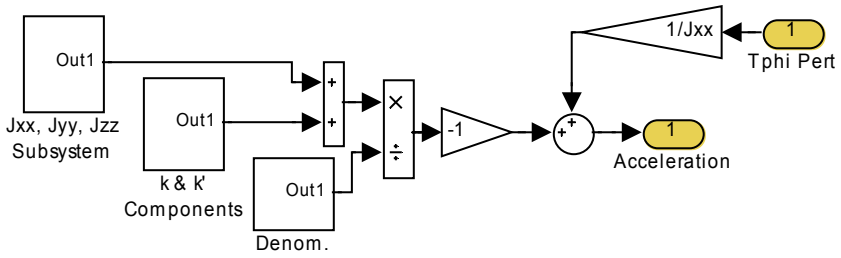

Figure C-35: Phase IV – ϕ Axis C.O.M. Acceleration

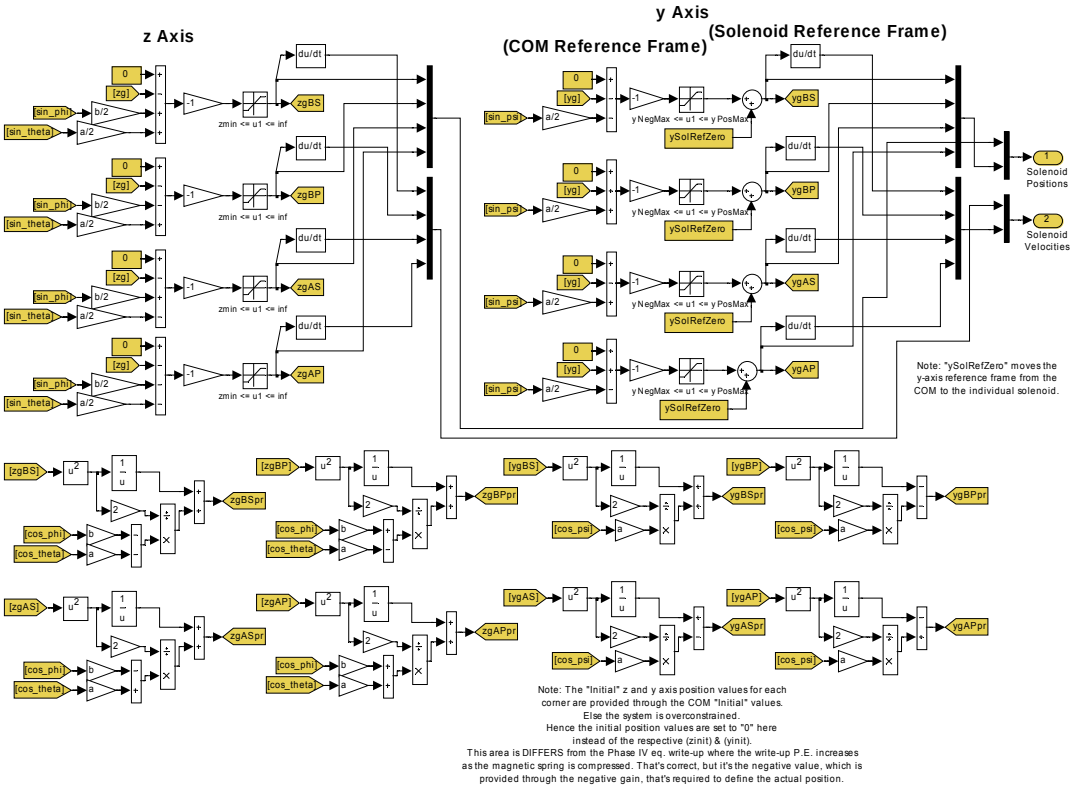

Figure C-36: Phase IV – Individual Solenoid Linear Gap Motion Values

C.1.b.iv Data Acquisition Output Subsystem

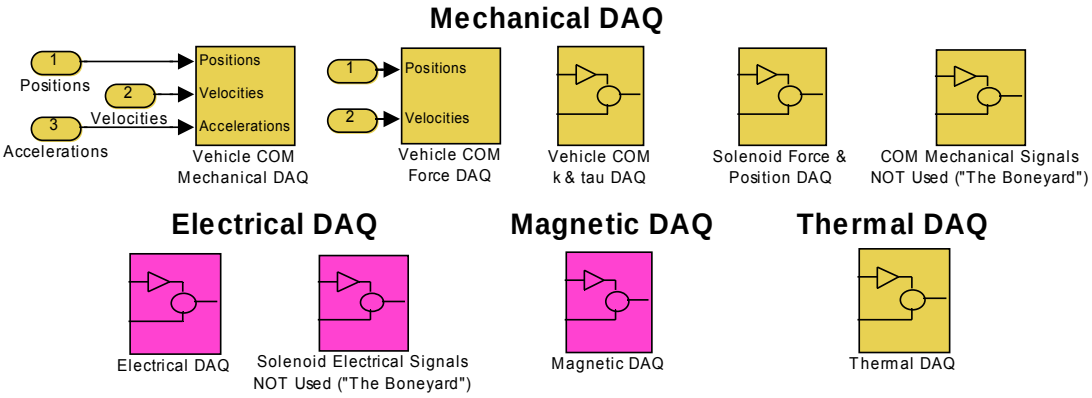

Figure C-37: Phase IV – Data Acquisition

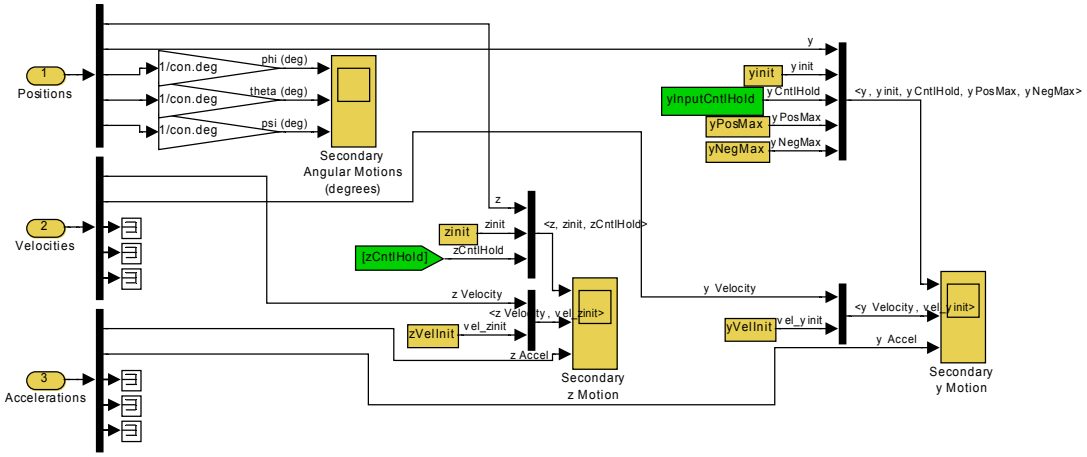

Figure C-38: Phase IV – Vehicle C.O.M. Mechanical D.A.Q.

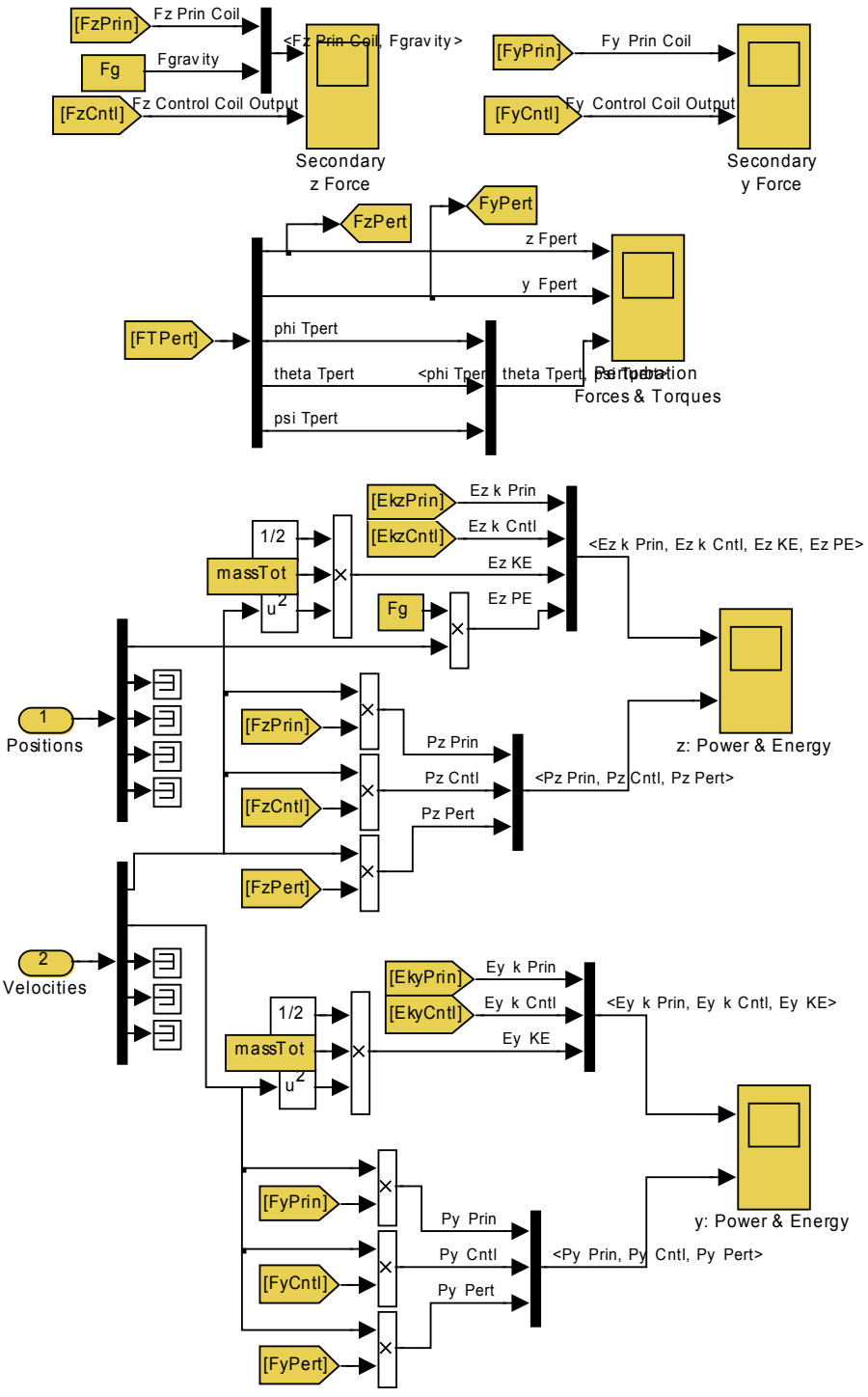
[FzPrin]
Fz Prin Coil
Fg
Fgravity
[FzCntl]
Fz Control Coil Output
<Fz Prin Coil, Fgravity>
Secondary
z Force
[FyPrin]
Fy Prin Coil
[FyCntl]
Fy Control Coil Output
Secondary
y Force
FzPert
FyPert
z Fpert
y Fpert
[FTPert]
phi Tpert
theta Tpert
psi Tpert
<phi Tpert, theta Tpert, psi Tpert>
Perturbation
Forces & Torques
[EkzPrin]
Ez k Prin
[EkzCntl]
Ez k Cntl
Ez KE
Ez PE
<Ez k Prin, Ez k Cntl, Ez KE, Ez PE>
1/2
massTot
u2
Fg
1
Positions
[FzPrin]
[FzCntl]
[FzPert]
Pz Prin
Pz Cntl
Pz Pert
<Pz Prin, Pz Cntl, Pz Pert>
z: Power & Energy
2
Velocities
[EkyPrin]
Ey k Prin
[EkyCntl]
Ey k Cntl
Ey KE
<Ey k Prin, Ey k Cntl, Ey KE>
[FyPrin]
[FyCntl]
[FyPert]
Py Prin
Py Cntl
Py Pert
<Py Prin, Py Cntl, Py Pert>
y: Power & Energy

Figure C-39: Phase IV – Vehicle C.O.M. Force D.A.Q.

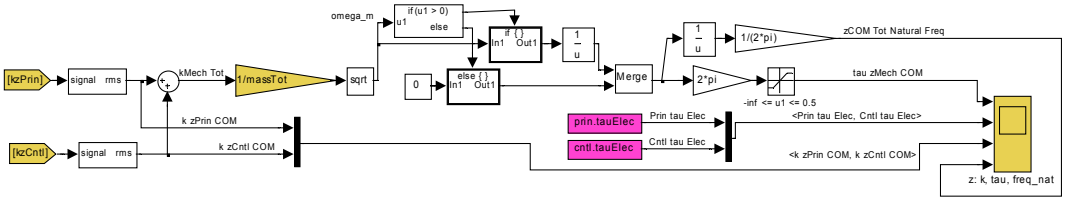

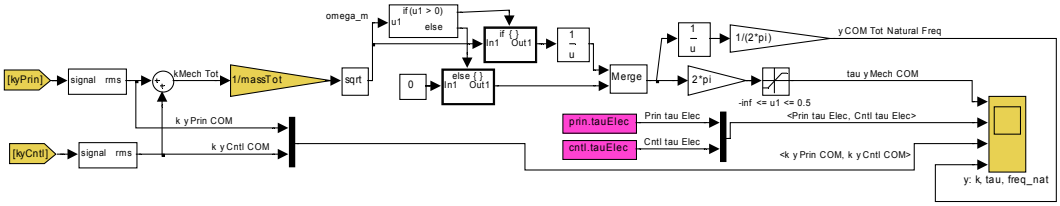

Figure C-40: Phase IV – Vehicle C.O.M. k & τ D.A.Q.

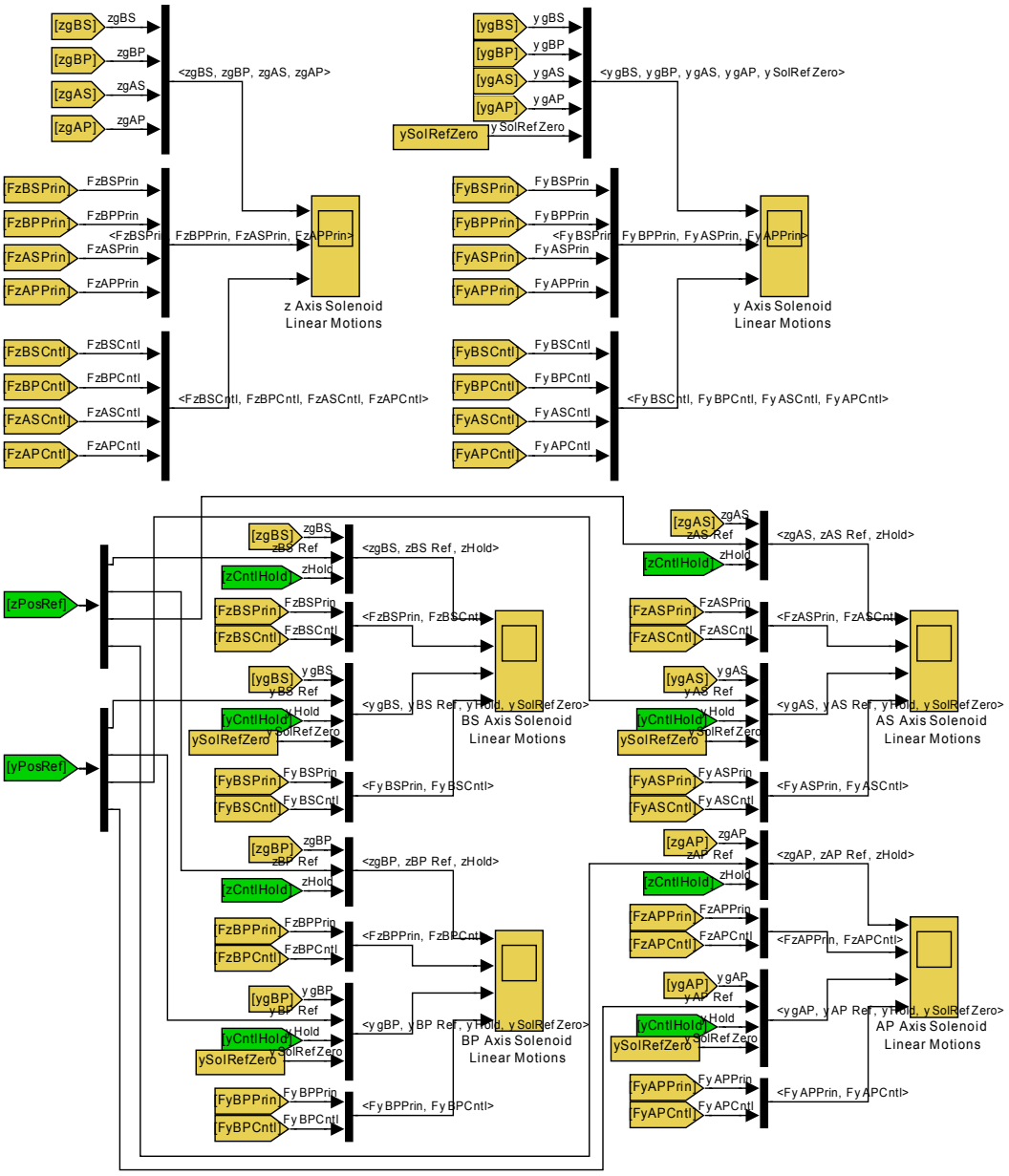

Figure C-41: Phase IV – Solenoid Force & Position D.A.Q.

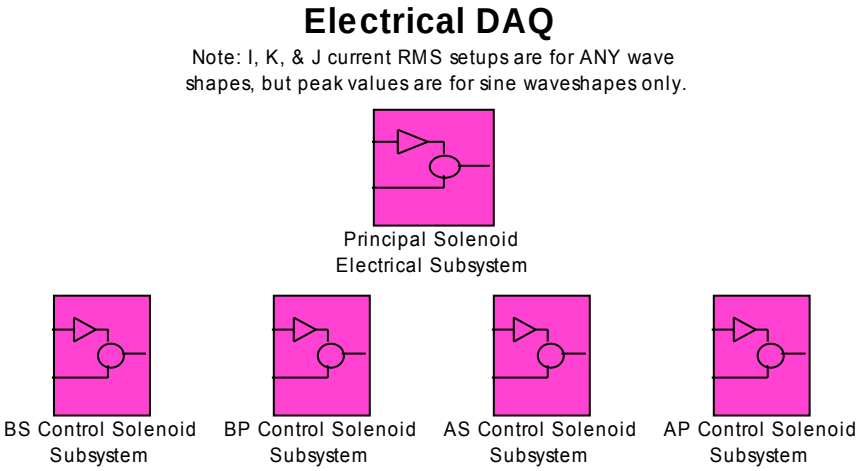

Figure C-42: Phase IV – Electrical D.A.Q.

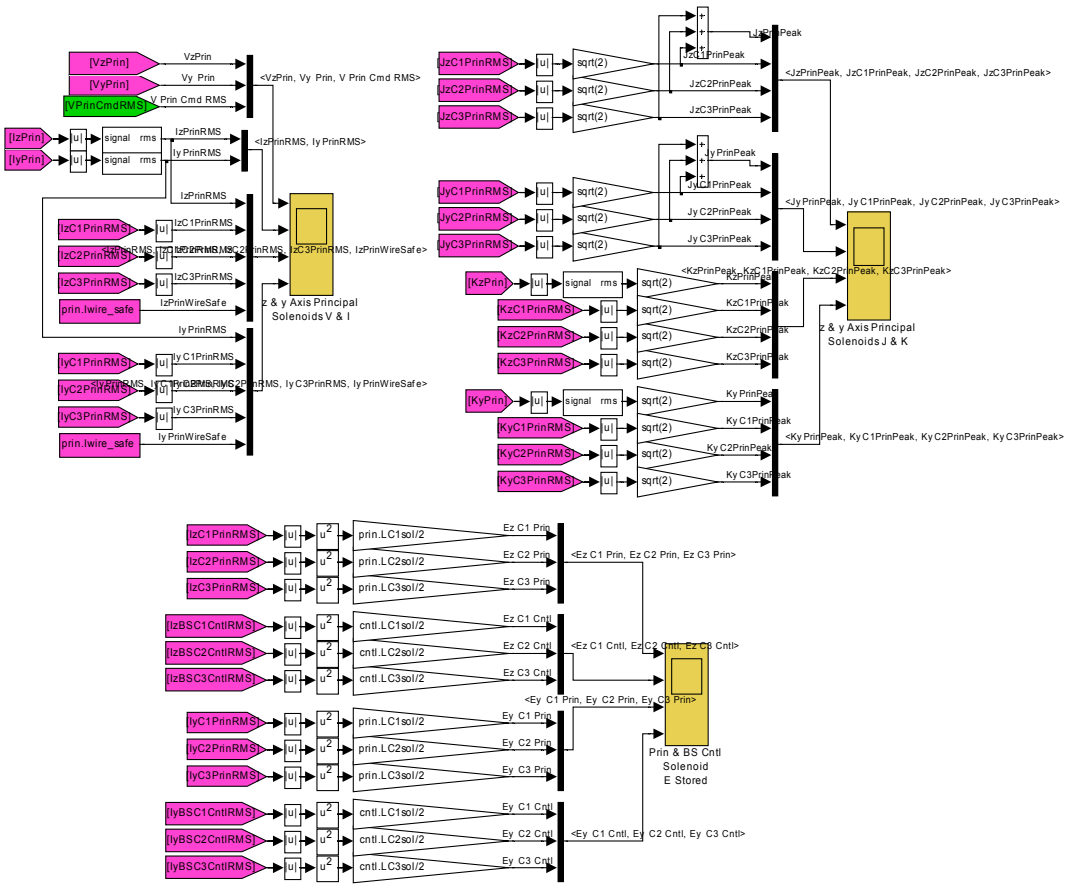

Figure C-43: Phase IV – Principal Solenoid Electrical D.A.Q.

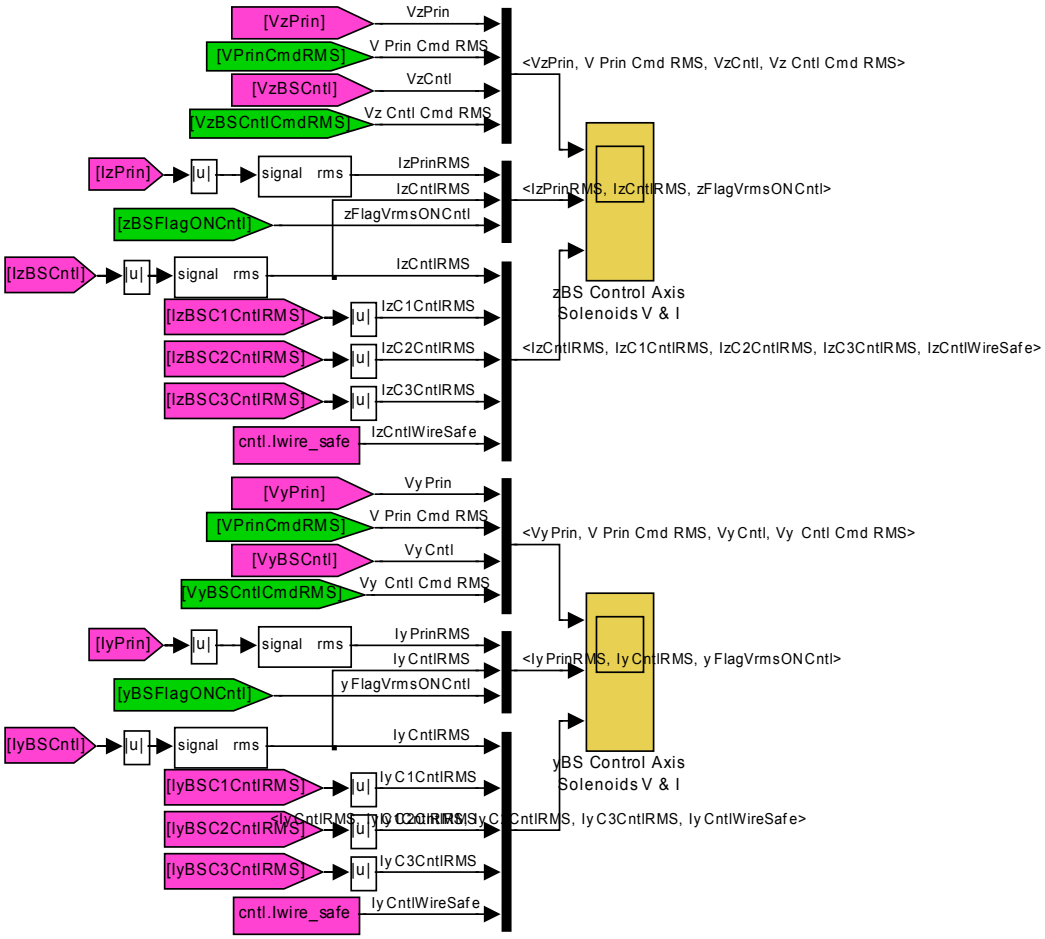

Figure C-44: Phase IV – BS Control Solenoid Electrical D.A.Q.

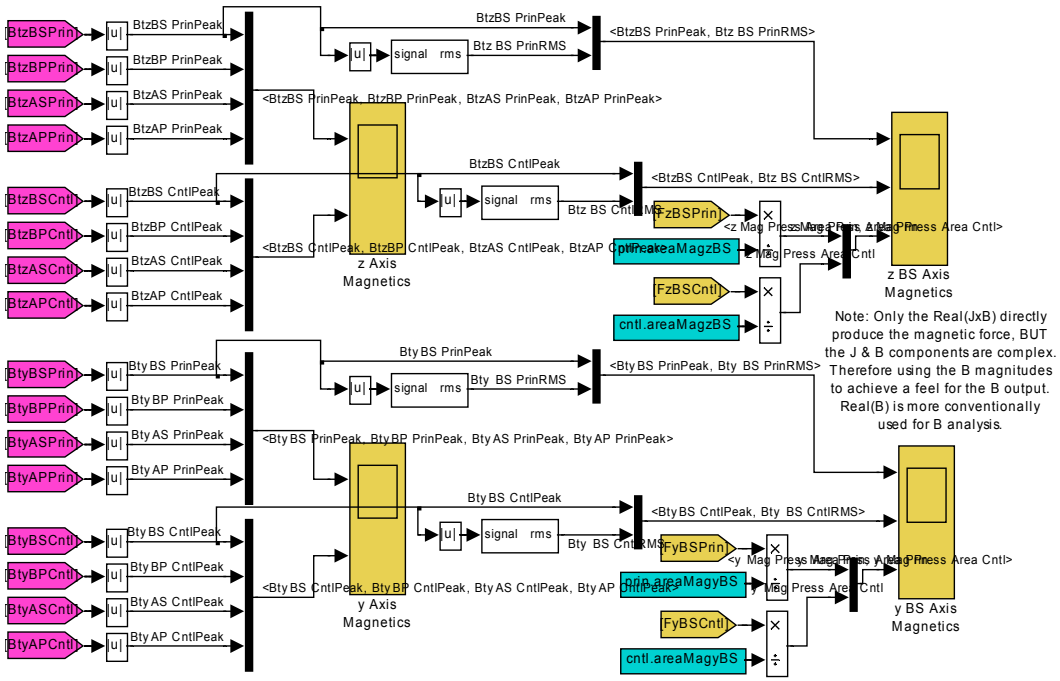

Figure C-45: Phase IV – Magnetic D.A.Q.

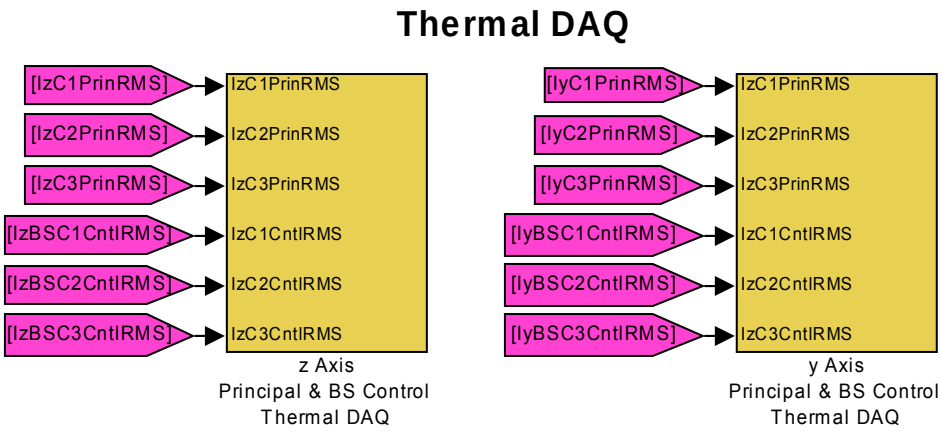

Figure C-46: Phase IV – Thermal D.A.Q.

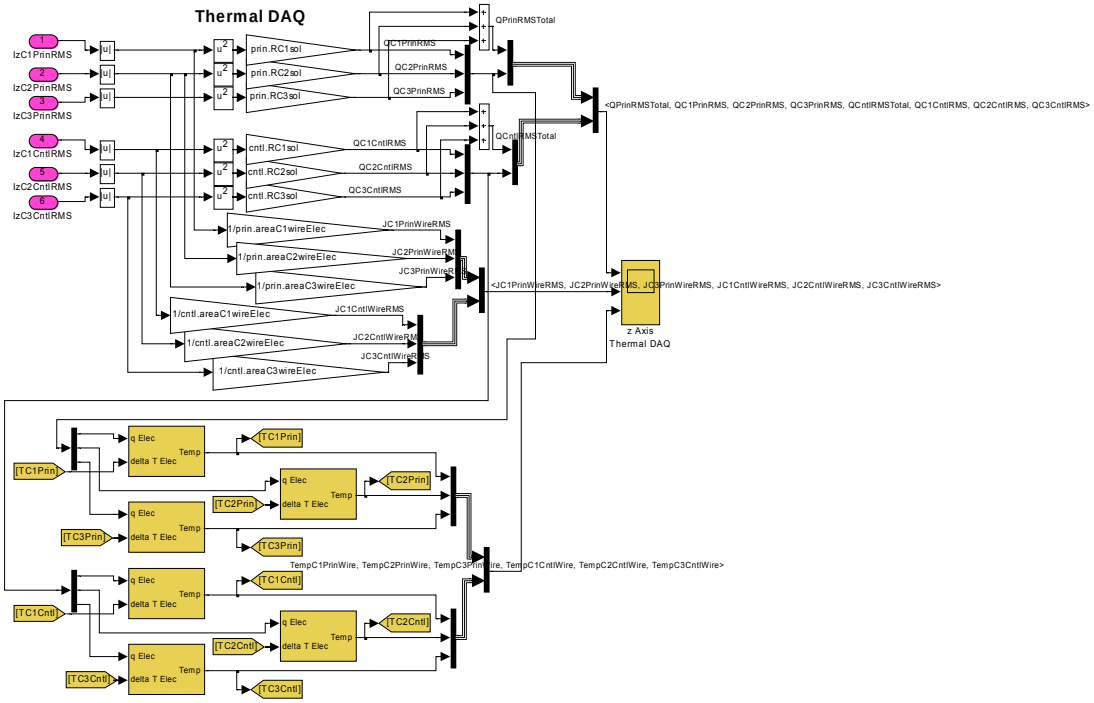

Figure C-47: Phase IV – z Axis Principal & BS Control Thermal D.A.Q.

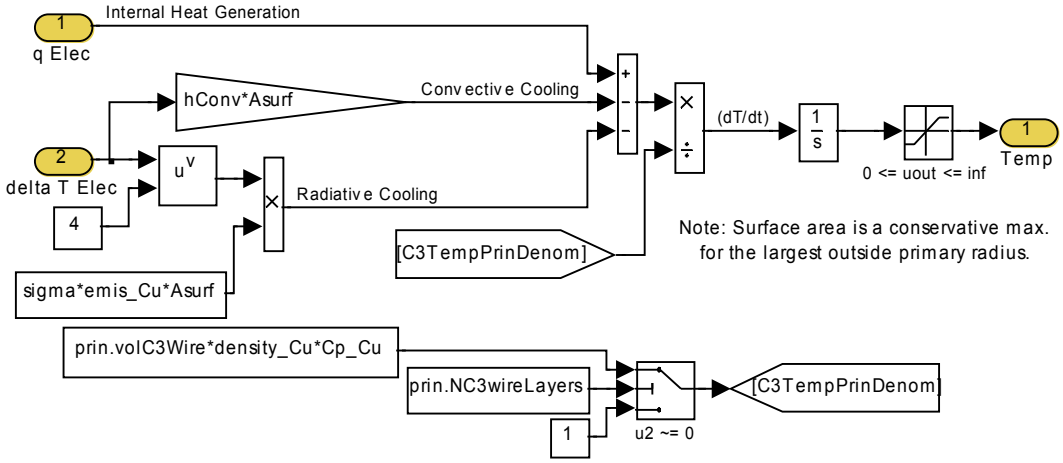

Figure C-48: Phase IV – z Axis Prin. & BS Cntl. Thermal D.A.Q. Temp. Rise

C.2 MATLAB FILES

C.2.a All Phases - Solenoid Design Matlab Function File

```
function
[radC1out,radC2out,radC3out,NturnsTot,lenWireLayersTot,pfCAvg,NC1wireHeight,NC2wireHeight,NC3wireH
eight,NC1wireLayers,NC2wireLayers,NC3wireLayers,...

areaC1wireElec,areaC2wireElec,areaC3wireElec,NC1turns,NC2turns,NC3turns,lenC1WireLayers,lenC2WireL
ayers,...

lenC3WireLayers,areaC1X,areaC2X,areaC3X,pfC1,pfC2,pfC3,volC1Wire,volC2Wire,volC3Wire,Iwire_safe,ar
eaMag,...

beta,RC1sol,RC2sol,RC3sol,tauElec,ZC1sol,ZC2sol,ZC3sol,Z3CoilParallel,LC1sol,LC2sol,LC3sol,Zcircui
tTot]...
    =
PhD_SolenoidDesigner(mur,cond1,rad1_in,rad1_out,Npedestals,HeightSinglePed,PercentPedHeightWound,p
fTurn,NC1wireLayers,...
    freq,Rexternal);

%%% SOLENOID DESIGN FILE

%%% PhD Dissertation - ALL Phases
%%% By: Glenn A. Knierim
%%% Program Started: Spring 2004
%-------------------------------------------------------------------------------------------

global prin cntl con Case


%~~ Solenoid primary mechanical geometry ~~%
```

```
switch Case.Phase
    case 1
        Case.AWG = menu('Choose the solenoid coil wire gage','26 AWG','28 AWG','30 AWG','31
AWG','32 AWG');
        switch Case.AWG
            case 1
                disp('Solenoid Coil Wire: 26 AWG wire')
                diam_WireElec = 0.0159*con.in;          % Solenoid electrical wire diameter, bare
copper (m)
                diam_WireMech = 0.0178*con.in;          % Solenoid mechanical wire diameter, Heavy
build (m)
                Iwire_safe = 1.2;                       % Solenoid wire safe constant current (A)
            case 2
                disp('Solenoid Coil Wire: 28 AWG wire')
                diam_WireElec = 0.0126*con.in;          % Solenoid electrical wire diameter, bare
copper (m)
                diam_WireMech = 0.0144*con.in;          % Solenoid mechanical wire diameter, Heavy
build (m)
                Iwire_safe = 0.761;                     % Solenoid wire safe constant current (A)
            case 3
                disp('Solenoid Coil Wire: 30 AWG wire')
                diam_WireElec = 0.0100*con.in;          % Solenoid electrical wire diameter, bare
copper (m)
                diam_WireMech = 0.0116*con.in;          % Solenoid mechanical wire diameter, Heavy
build (m)
                Iwire_safe = 0.477;                     % Solenoid wire safe constant current (A)
            case 4
                disp('Solenoid Coil Wire: 31 AWG wire')
                diam_WireElec = 0.0089*con.in;          % Solenoid electrical wire diameter, bare
copper (m)
                diam_WireMech = 0.0105*con.in;          % Solenoid mechanical wire diameter, Heavy
build (m)
                Iwire_safe = 0.377;                     % Solenoid wire safe constant current (A)
            case 5
                disp('Solenoid Coil Wire: 32 AWG wire')
```

```
                diam_WireElec = 0.0080*con.in;          % Solenoid electrical wire diameter, bare
copper (m)
                diam_WireMech = 0.0095*con.in;          % Solenoid mechanical wire diameter, Heavy
build (m)
                Iwire_safe = 0.304;                     % Solenoid wire safe constant current (A)
        end
    case 2
        Case.AWG = menu('Choose the solenoid coil wire gage','18 AWG','20 AWG','22 AWG','24
AWG','26 AWG',...
            '28 AWG','30 AWG','31 AWG','32 AWG');
        switch Case.AWG
            case 1
                disp('Solenoid Coil Wire: 18 AWG wire')
                diam_WireElec = 0.0403*con.in;          % Solenoid electrical wire diameter, bare
copper (m)
                diam_WireMech = 0.0431*con.in;          % Solenoid mechanical wire diameter, Heavy
build (m)
                Iwire_safe = 7.75;                      % Solenoid wire safe constant current (A)
            case 2
                disp('Solenoid Coil Wire: 20 AWG wire')
                diam_WireElec = 0.032*con.in;           % Solenoid electrical wire diameter, bare
copper (m)
                diam_WireMech = 0.0346*con.in;          % Solenoid mechanical wire diameter, Heavy
build (m)
                Iwire_safe = 4.89;                      % Solenoid wire safe constant current (A)
            case 3
                disp('Solenoid Coil Wire: 22 AWG wire')
                diam_WireElec = 0.0253*con.in;          % Solenoid electrical wire diameter, bare
copper (m)
                diam_WireMech = 0.0276*con.in;          % Solenoid mechanical wire diameter, Heavy
build (m)
                Iwire_safe = 3.04;                      % Solenoid wire safe constant current (A)
            case 4
                disp('Solenoid Coil Wire: 24 AWG wire')
                diam_WireElec = 0.0201*con.in;          % Solenoid electrical wire diameter, bare
copper (m)
```

```
            diam_WireMech = 0.0223*con.in;          % Solenoid mechanical wire diameter, Heavy
build (m)
            Iwire_safe = 1.93;                      % Solenoid wire safe constant current (A)
        case 5
            disp('Solenoid Coil Wire: 26 AWG wire')
            diam_WireElec = 0.0159*con.in;          % Solenoid electrical wire diameter, bare
copper (m)
            diam_WireMech = 0.0178*con.in;          % Solenoid mechanical wire diameter, Heavy
build (m)
            Iwire_safe = 1.2;                       % Solenoid wire safe constant current (A)
        case 6
            disp('Solenoid Coil Wire: 28 AWG wire')
            diam_WireElec = 0.0126*con.in;          % Solenoid electrical wire diameter, bare
copper (m)
            diam_WireMech = 0.0144*con.in;          % Solenoid mechanical wire diameter, Heavy
build (m)
            Iwire_safe = 0.761;                     % Solenoid wire safe constant current (A)
        case 7
            disp('Solenoid Coil Wire: 30 AWG wire')
            diam_WireElec = 0.0100*con.in;          % Solenoid electrical wire diameter, bare
copper (m)
            diam_WireMech = 0.0116*con.in;          % Solenoid mechanical wire diameter, Heavy
build (m)
            Iwire_safe = 0.477;                     % Solenoid wire safe constant current (A)
        case 8
            disp('Solenoid Coil Wire: 31 AWG wire')
            diam_WireElec = 0.0089*con.in;          % Solenoid electrical wire diameter, bare
copper (m)
            diam_WireMech = 0.0105*con.in;          % Solenoid mechanical wire diameter, Heavy
build (m)
            Iwire_safe = 0.377;                     % Solenoid wire safe constant current (A)
        case 9
            disp('Solenoid Coil Wire: 32 AWG wire')
            diam_WireElec = 0.0080*con.in;          % Solenoid electrical wire diameter, bare
copper (m)
```

```
                diam_WireMech = 0.0095*con.in;          % Solenoid mechanical wire diameter, Heavy
build (m)
                Iwire_safe = 0.304;                     % Solenoid wire safe constant current (A)
        end
end
diamC1_WireElec = diam_WireElec;
diamC2_WireElec = diam_WireElec;
diamC3_WireElec = diam_WireElec;
diamC1_WireMech = diam_WireMech;
diamC2_WireMech = diam_WireMech;
diamC3_WireMech = diam_WireMech;

HeightPedestal = Npedestals*HeightSinglePed;    % Overall solenoid core height (m)
heightC1PedUnused = (1 - PercentPedHeightWound/100)*HeightPedestal;
% (Height Allowed) = (Center Pedestal)-(Pedestal Groover)-(Approx. Ped. Groove Tol.)-(Polymer
Cover)-(Approx. Winding End Tol.)
heightC1wire = ((PercentPedHeightWound/100)*HeightPedestal - 0.03*con.in - 0.02*con.in) -
0.11*con.in - (6*diamC1_WireMech);
heightC2wire = heightC1wire;
heightC3wire = heightC1wire;
NC1wireHeight = ceil(heightC1wire/(pfTurn*diamC1_WireMech)); % Approx. number of solenoid wires
per layer

Case.coil = menu('Choose the # of coils per solenoid','1 Coil','2 Coils','3 Coils');
switch Case.coil
    case 1
        disp('1 Coil per Solenoid')
        NC2wireHeight = 0;
        NC3wireHeight = 0;
        NC2wireLayers = 0;
        NC3wireLayers = 0;
    case 2
        disp('2 Coils per Solenoid')
        NC2wireHeight = NC1wireHeight;
        NC3wireHeight = 0;
        NC2wireLayers = round(0.8*NC1wireLayers);   % Mult. factor: 30AWG:0.8; 28AWG:0.78
```

```
        NC3wireLayers = 0;
    case 3
        disp('3 Coils per Solenoid')
        NC2wireHeight = NC1wireHeight;
        NC3wireHeight = NC1wireHeight;
        NC2wireLayers = round(0.8*NC1wireLayers);   % Mult. factor: 30AWG:0.8; 28AWG:0.78
        NC3wireLayers = round(0.5*NC1wireLayers);
end
areaC1wireMech = pi*(diamC1_WireMech/2)^2;  % Mechanical area, includes insulation, of single wire
X-section (m^2)
areaC2wireMech = areaC1wireMech;
areaC3wireMech = areaC1wireMech;
areaC1wireElec = pi*(diamC1_WireElec/2)^2;  % Electrical area, Cu only, of single wire X-section
(m^2)
areaC2wireElec = areaC1wireElec;
areaC3wireElec = areaC1wireElec;
NC1turns = round(NC1wireLayers*NC1wireHeight);  % Solenoid wire number of turns
NC2turns = round(NC2wireLayers*NC2wireHeight);
NC3turns = round(NC3wireLayers*NC3wireHeight);
NturnsTot = NC1turns + NC2turns + NC3turns;
lenC1WireLayers = pfTurn*NC1wireLayers*diamC1_WireMech; % Approx. length of the wire stack
lenC2WireLayers = pfTurn*NC2wireLayers*diamC2_WireMech;
lenC3WireLayers = pfTurn*NC3wireLayers*diamC3_WireMech;
lenWireLayersTot = lenC1WireLayers + lenC2WireLayers + lenC3WireLayers;
radCoilInsul = 0.015*con.in;        % Radius of insulation around coils (m)
radC1out = rad1_out + lenC1WireLayers + 2*radCoilInsul; % Coil #1 outside radius (m)
radC2out = radC1out + lenC2WireLayers + radCoilInsul;   % Coil #2 outside radius (m)
radC3out = radC2out + lenC3WireLayers + radCoilInsul;   % Coil #3 outside radius (m)
areaC1X = lenC1WireLayers*heightC1wire;     % Radial direction, solenoid current density cross
sectional area (m^2)
areaC2X = lenC2WireLayers*heightC2wire;
areaC3X = lenC3WireLayers*heightC3wire;
pfC1 = NC1turns*areaC1wireElec/areaC1X;     % Solenoid wire packing factor for radial cross
section geometry
switch Case.coil
    case 1
```

```
        pfCAvg = pfC1;
        pfC2 = 0;
        pfC3 = 0;
    case 2
        pfC2 = NC2turns*areaC2wireElec/areaC2X;
        pfC3 = 0;
        pfCAvg = (pfC1 + pfC2)/2;
    case 3
        pfC2 = NC2turns*areaC2wireElec/areaC2X;
        pfC3 = NC3turns*areaC3wireElec/areaC3X;
        pfCAvg = (pfC1 + pfC2 + pfC3)/3;
end
lenC1SolWire = 0;                % Initializing the summer statement
for nlay = 0:(NC1wireLayers - 1)
    lenSolWireSummer = NC1wireHeight*2*pi*(rad1_out + (diamC1_WireMech/2) + nlay*diamC1_WireMech);
    lenC1SolWire = lenC1SolWire + lenSolWireSummer; % Total solenoid wire length (m)
end
lenC2SolWire = 0;                % Initializing the summer statement
lenC2SolWire = 0;
for nlay = 0:(NC2wireLayers - 1)
    lenSolWireSummer = NC2wireHeight*2*pi*(radC1out + (diamC2_WireMech/2) + nlay*diamC2_WireMech);
    lenC2SolWire = lenC2SolWire + lenSolWireSummer; % Total solenoid wire length (m)
end
lenC3SolWire = 0;                % Initializing the summer statement
lenC3SolWire = 0;
for nlay = 0:(NC3wireLayers - 1)
    lenSolWireSummer = NC3wireHeight*2*pi*(radC2out + (diamC3_WireMech/2) + nlay*diamC3_WireMech);
    lenC3SolWire = lenC3SolWire + lenSolWireSummer; % Total solenoid wire length (m)
end
lenTotSolWire = lenC1SolWire + lenC2SolWire + lenC3SolWire;     % Total length of sol. wire to
make all coils (m)
volC1Wire = areaC1wireElec*lenC1SolWire;           % Thermal volume of coil #1 wire
volC2Wire = areaC2wireElec*lenC2SolWire;           % Thermal volume of coil #2 wire
volC3Wire = areaC3wireElec*lenC3SolWire;           % Thermal volume of coil #3 wire
rC1windAvg =  (radC1out + rad1_out)/2;             % Coil #1 middle length radius
rC2windAvg =  (radC2out + radC1out)/2;             % Coil #2 middle length radius
```

```
rC3windAvg =  (radC3out + radC2out)/2;              % Coil #3 middle length radius

%~~ Solenoid primary electrical & magnetic parameters ~~%
switch Case.coil
    case 1
        % Setting an approximation for the max. magnetic radius for the mag. pressure (m)
        % Using the coil outside radius plus a 1/2 outside coil radius as the magnetic pressure
outside radius.
        radMagMax = radC1out + lenC1WireLayers/2;
        radLambda = rC1windAvg;
    case 2
        radMagMax = radC2out + lenC2WireLayers/2;
        radLambda = rC2windAvg;
    case 3
        radMagMax = radC3out + lenC3WireLayers/2;
        radLambda = rC3windAvg;
end
% Using the core 1/2 radius as the magnetic pressure inside radius (m)
radMagMin = (rad1_out - rad1_in)/2; % Setting an approximation for the min. magnetic radius for
the mag. pressure (m)
areaMag = pi*(radMagMax^2 - radMagMin^2);   % Magnetic pressure area approximation based on the
primary core & directly stacked coils (m^2)
lambdaEff = 2*(2*radLambda);    % Effective wavelength (m) [Initial approximation presented]
beta = 2*pi/lambdaEff;          % Wave number (A/m)
tauP = lambdaEff/2;             % Pole pitch (m)

%~~ Solenoid circuit electrical parameters ~~%
RC1sol = lenC1SolWire/(cond1*areaC1wireElec);       % Coil #1 resistance (ohm)
RC2sol = lenC2SolWire/(cond1*areaC2wireElec);
RC3sol = lenC3SolWire/(cond1*areaC3wireElec);
LC1sol = 0.8E-6*mur*(rC1windAvg/con.in*NC1turns)^2/(6*rC1windAvg/con.in + 9*heightC1wire/con.in +
10*lenC1WireLayers/con.in);   % Coil #1 inductance (H)
tauC1Elec = LC1sol/RC1sol;                  % Coil #1 solenoid electrical time constant (sec)
switch Case.coil
    case 1
        LC2sol = 0;
```

```
        LC3sol = 0;
        tauC2Elec = 0;
        tauC3Elec = 0;
    case 2
        LC2sol = 0.8E-6*mur*(rC2windAvg/con.in*NC2turns)^2/(6*rC2windAvg/con.in +
9*heightC2wire/con.in + 10*lenC2WireLayers/con.in);
        LC3sol = 0;
        tauC2Elec = LC2sol/RC2sol;
        tauC3Elec = 0;
    case 3
        LC2sol = 0.8E-6*mur*(rC2windAvg/con.in*NC2turns)^2/(6*rC2windAvg/con.in +
9*heightC2wire/con.in + 10*lenC2WireLayers/con.in);
        LC3sol = 0.8E-6*mur*(rC3windAvg/con.in*NC3turns)^2/(6*rC3windAvg/con.in +
9*heightC3wire/con.in + 10*lenC3WireLayers/con.in);
        tauC2Elec = LC2sol/RC2sol;
        tauC3Elec = LC3sol/RC3sol;
end
tauElec = max([tauC1Elec;tauC2Elec;tauC3Elec]);
ZC1sol = RC1sol + j*(2*pi*freq)*LC1sol;         % Primary solenoid coil #1 impedance (ohm)
ZC2sol = RC2sol + j*(2*pi*freq)*LC2sol;
ZC3sol = RC3sol + j*(2*pi*freq)*LC3sol;
switch Case.coil
    case 1
        Z3CoilParallel = 1/(1/ZC1sol);
        ZsolParallel = ZC1sol + Rexternal;  % Equivalent parallel Z (ohm)
        LcapResParallel = LC1sol;           % Equivalent parallel L used for the resonant
capacitor (H)
    case 2
        Z3CoilParallel = 1/((1/ZC1sol) + (1/ZC2sol));
        ZsolParallel = (ZC1sol*ZC2sol)/(ZC1sol + ZC2sol);
        LcapResParallel = (LC1sol*LC2sol)/(LC1sol + LC2sol);
    case 3
        Z3CoilParallel = 1/((1/ZC1sol) + (1/ZC2sol) + (1/ZC3sol));
        ZsolParallel = Z3CoilParallel;
        LcapResParallel = 1/((1/LC1sol) + (1/LC2sol) + (1/LC3sol));
end
```

```
Case.Cres = menu('Is there a Resonant Capacitor in series with the solenoid?','YES','NO');
switch Case.Cres
    case 1
        disp('Resonant Capacitor: Present')
        Cres = 1/((2*pi*freq)^2*LcapResParallel);
        ZcircuitTot = 1/(j*(2*pi*freq)*Cres) + ZsolParallel;
    case 2
        disp('Resonant Capacitor: NOT Present')
        Cres = 0;
        ZcircuitTot = ZsolParallel;
end
```

C.2.b Phase I Matlab Files

C.2.b.i Matlab Input Function File

```
%%% INPUT FILE

%%% PhD Dissertation - Phase I
%%% By: Glenn A. Knierim
%%% Program Started: Spring 2004
%-------------------------------------------------------------------------------------%

%%%%%%%%%%%%%%%%%%%%%%%%%
% Overall Program Notes %
%%%%%%%%%%%%%%%%%%%%%%%%%

% 1.    This program models one to three coil solenoids respectively levitating and controlling
%       the levitation of a secondary plate.
% 2.    All calculation units are S.I. excluding distances since the physical solenoid system
under
%       development is based on ANSI dimensioned based primary core, primary wire, and secondary.
% 3.    "%%%" starting a commented description after a variable means a regularly changed
variable.
```

```
%%% LINEAR CONTROLLER - Best Run to Date:
%% Solenoid Designs
%   Both Coils: 30 AWG w/ a Resonant Capacitor
%   Principal Solenoid: 2 coils
%   Control Solenoid: 1 coils
%   Coil #1: Principal coil = 21, Control coil = 24.
%% Simulation Params.
%   zinit = 0.85*con.in;
%   zInputCntlHold = 0.6*con.in;
%   zCntlLowIPD = 0.02*con.in;
%   Simulation Type: Euler Fixed Step
%   tStp = 5E-4;
%   tStpMin = tStp;


%-------------------------------------------------------------------------------------------%
%%%%%%%%%%%%%%%%%%
% PRE PROCESSING %
%%%%%%%%%%%%%%%%%%

% Clear memory, home the cursor, & increase memory size
clear prin cntl con Case
pack;clc;
set(0,'RecursionLimit',10000)

disp('Preprocessing Start')
tstart=now;                     % Start: Timer to show real time Preprocessing Time

%%%%%%%%%%%%%%%%%%%%%%%%%%%%%
% Define global parameters %
%%%%%%%%%%%%%%%%%%%%%%%%%%%%%

% Global simulation structured variable arrays for the principal & control solenoid systems:
(prin) & (cntl)
```

```
% Global simulation structured constant setup array: (con)
% Global simulation structured Case setup array: (Case)
global prin cntl con Case


%%%%%%%%%%%%%%%%%%%%%%%%%%%%%%%%%%%%%%%%%%%%%%%%%%%%
% User Defined Input for Test Case to Run %
%%%%%%%%%%%%%%%%%%%%%%%%%%%%%%%%%%%%%%%%%%%%%%%%%%%%

%%% RUN THE INPUT MENU (NOT Used)
%PhD_PhaseI_input_menu;

%%% Unable to: READ INTO WORKSPACE THE FUZZY LOGIC INFORMATION [NO method here used]


% Phase to Run
% Case.Phase = menu('Choose the Phase under analysis','Phase I','Phase IV');
Case.Phase = 1;     % Hardwiring a Phase I Analysis
disp('_____________________________________')
switch Case.Phase
    case 1
        disp('            Phase I')
        disp(' ')
    case 2
        disp('            Phase IV')
        disp(' ')
end


%%%%%%%%%%%%%%%%%%%%
% Unit Conversions %
%%%%%%%%%%%%%%%%%%%%

con.lbm = 0.4535924;                % pound mass to kg
```

```
con.lbf = 4.448222;                 % pound force to N
con.ft = 12*0.0254;                 % ft to m
con.in = 0.0254;                    % in to m
con.Ag = 9.81;                      % Acceleration due to gravity (m/sec^2)
con.cm = 100;                       % Meter to Centimeter
con.deg = pi/180;                   % Degrees to Radians


%%%%%%%%%%%%%%%%%%%%%%%%
% Defining Constants  %
%%%%%%%%%%%%%%%%%%%%%%%%

% Simulation constants
tcnt = 0;                       % Counter for displaying info. during simulation
tStp = 5E-4/2;                  % (5E-4) for testing; (5E-4/2) for final runs
tStpMin = tStp;
%maxStp = 1/120/100;            % Maximum time step (sec)
reltol = 1*1E-2;                % Relative sim. tolerance
abstol = 1*1E-2;                % Absolute sim. tolerance
%decimate = 1;                  % Plot increment (time step)
endTime = 4;                    %%% tpulse2 + thold + 0.05;       % Simulation end time (sec)

% Universal material constants
mu0 = pi*4E-7;                  % Permeability of a vacuum (H/m)
cond_Cu = 5.977E7;              % Copper conductivity (Siemens/m)
density_Cu = 8.934E3;           % Copper density (kg/m^3)
Cp_Cu = 386.023;                % Copper specific heat (m^2/(s^2*K))
Ctemp_Cu = 0.0043;              % Copper coefficient of temperature (1/K)
cond_Al = 3.766E7;              % Aluminum conductivity (Siemens/m)
density_Al = 2.692E3;           % Aluminum density (kg/m^3)
Cp_Al = 962.964;                % Aluminum specific heat (m^2/(s^2*K))
Ctemp_Al = 0.004;               % Aluminum coefficient of temperature (1/K)
CThCondFe = 1;                  % [NOT Used] Thermal conductivity of ferrite (W/(m*C))
sigma = 5.67E-8;                % Stefan-Boltzmann constant (W/(m^2*K^4))
```

```
% Simulation specific material constants
mur = 4.673;%1/2*150;           %%% Relative permeability of primary iron with factor for geometry
mu1 = mur*mu0;                  % Permeability of the primary (H/m)
mu3 = mu0;                      % Permeability of the air gap b/w the primary & secondary (H/m)
mu4 = mu0;                      % Permeability of the air behind the secondary (H/m)
Bsat = 0.8;                     %%% B fully saturated value, approx. as a step function (T)
cond1 = cond_Cu;                % Primary conductivity (Siemens/m)
emis_Cu = 0.5;                  % Approx. emissivity of copper stably oxidized under operating
conditions
hConv = 15;                     % Approx. free or natural gas convective coef. (W/(m^2*K))

% System geometric parameters
z0 = 1E-3*con.in;                   % Min. boundary condition distance b/w regions 1 & 3 b/w
primary & secondary (m)



%%%%%%%%%%%%%%%%%%%%%%%%%%%%%%%%%%%%%%%%%%%%%%%%%%%%%%%%%%%%%%%%%%%%%%%%%%%%%%%
% INPUTS: Defining "Principal" Solenoid Primary Variables %
%%%%%%%%%%%%%%%%%%%%%%%%%%%%%%%%%%%%%%%%%%%%%%%%%%%%%%%%%%%%%%%%%%%%%%%%%%%%%%%

% Solenoid material & geometric parameters
rad1_in = 0*con.in;                 %%% Solenoid inside core radius (m)
rad1_out = 0.8*con.in;              %%% Solenoid outside core radius (m)

% Solenoid mechanical geometry
prin.NSol = 1;                      %%% # of solenoids
Npedestals = 1;                     %%% # of solenoid center core pedestals (m)
HeightSinglePed = 1.615*con.in;     %%% Solenoid center core pedestal height (m)
PercentPedHeightWound = 100;        %%% Percent of pedestal available wound w/ wire (%)
pfTurn = 1.1;                       %%% Estimated packing factor per winding diam. to diam. turn
NC1wireLayers = 21;                 %%% (21) # of "Principal" coil #1 wire layers (Set for 30 AWG,
but Iwire too high w/ Cap.)
% Solenoid primary source electrical & magnetic parameters
prin.freq = 60;                     %%% Electrical frequency (Hz)
freq = prin.freq;
```

```
prin.omega_e = 2*pi*prin.freq;      % Electrical angular frequency (rad/sec)
prin.Vrms = 120;                    %%% Primary principal solenoid source rms voltage (V)
prin.Rext = 0;                      %%% External resistance [IF present] (ohm)
Rexternal = prin.Rext;

% RUN THE "SOLENOID DESIGNER" FUNCTION FILE %
[radC1out,radC2out,radC3out,NturnsTot,lenWireLayersTot,pfCAvg,NC1wireHeight,NC2wireHeight,NC3wireH
eight,NC1wireLayers,NC2wireLayers,NC3wireLayers,...

areaC1wireElec,areaC2wireElec,areaC3wireElec,NC1turns,NC2turns,NC3turns,lenC1WireLayers,lenC2WireL
ayers,...

lenC3WireLayers,areaC1X,areaC2X,areaC3X,pfC1,pfC2,pfC3,volC1Wire,volC2Wire,volC3Wire,Iwire_safe,ar
eaMag,...

beta,RC1sol,RC2sol,RC3sol,tauElec,ZC1sol,ZC2sol,ZC3sol,Z3CoilParallel,LC1sol,LC2sol,LC3sol,Zcircui
tTot]...
    =
PhD_SolenoidDesigner(mur,cond1,rad1_in,rad1_out,Npedestals,HeightSinglePed,PercentPedHeightWound,p
fTurn,NC1wireLayers,...
    freq,Rexternal);
% Principal Coil & Input Matlab file ONLY
% (radC1out,radC2out,radC3out)
% Case outputs
prin.Case.AWG = Case.AWG;
prin.Case.coil = Case.coil;
prin.Case.Cres = Case.Cres;
%~~ Solenoid primary overall mechanical geometry ~~%
prin.NC1wireHeight = NC1wireHeight;
prin.NC2wireHeight = NC2wireHeight;
prin.NC3wireHeight = NC3wireHeight;
prin.NC1wireLayers = NC1wireLayers;
prin.NC2wireLayers = NC2wireLayers;
prin.NC3wireLayers = NC3wireLayers;
%~~ Solenoid primary wire geometry ~~%
prin.areaC1wireElec = areaC1wireElec;
```

```
prin.areaC2wireElec = areaC2wireElec;
prin.areaC3wireElec = areaC3wireElec;
prin.NC1turns = NC1turns;
prin.NC2turns = NC2turns;
prin.NC3turns = NC3turns;
prin.lenC1WireLayers = lenC1WireLayers;
prin.lenC2WireLayers = lenC2WireLayers;
prin.lenC3WireLayers = lenC3WireLayers;
prin.areaC1X = areaC1X;
prin.areaC2X = areaC2X;
prin.areaC3X = areaC3X;
prin.pfC1 = pfC1;
prin.pfC2 = pfC2;
prin.pfC3 = pfC3;
prin.volC1Wire = volC1Wire;
prin.volC2Wire = volC2Wire;
prin.volC3Wire = volC3Wire;
%~~ Solenoid primary electrical & magnetic parameters ~~%
prin.Iwire_safe = Iwire_safe;
prin.areaMag = areaMag;
prin.beta = beta;
%~~ Solenoid circuit electrical parameters ~~%
prin.RC1sol = RC1sol;
prin.RC2sol = RC2sol;
prin.RC3sol = RC3sol;
prin.LC1sol = LC1sol;
prin.LC2sol = LC2sol;
prin.LC3sol = LC3sol;
prin.tauElec = tauElec;
prin.ZC1sol = ZC1sol;
prin.ZC2sol = ZC2sol;
prin.ZC3sol = ZC3sol;
prin.Z3CoilParallel = Z3CoilParallel;
prin.ZcircuitTot = ZcircuitTot;
```

```
%%%%%%%%%%%%%%%%%%%%%%%%%%%%%%%%%%%%%%%%%%%%%%%%%%%%%%%%%%%%%%%%%%%%%%%%
% INPUTS: Defining "Control" Solenoid Primary Variables %
%%%%%%%%%%%%%%%%%%%%%%%%%%%%%%%%%%%%%%%%%%%%%%%%%%%%%%%%%%%%%%%%%%%%%%%%

% Solenoid material & geometric parameters
rad1_in = 0*con.in;                 %%% Solenoid inside core radius (m)
rad1_out = 0.8*con.in;              %%% Solenoid outside core radius (m)

% Solenoid mechanical geometry
cntl.NSol = 1;                      %%% # of solenoids
Npedestals = 1;                     %%% # of solenoid center core pedestals (m)
HeightSinglePed = 1.615*con.in;     %%% Solenoid center core pedestal height (m)
PercentPedHeightWound = 100;        %%% Percent of pedestal available wound w/ wire (%)
pfTurn = 1.1;                       %%% Estimated packing factor per winding diam. to diam. turn
NC1wireLayers = 24;                 %%% (24) # of "Control" coil #1 wire layers
% Solenoid primary source electrical & magnetic parameters
cntl.freq = 60;                     %%% Electrical frequency (Hz)
freq = cntl.freq;
cntl.omega_e = 2*pi*cntl.freq;      % Electrical angular frequency (rad/sec)
% prin.IrmsMax = 2;                 %%% Maximum Irms allowed [Using a reasonable max. value from
availability & heating] (Arms)
cntl.Vrms = 120;                    %%% Primary control solenoid source rms voltage (V)
prin.Rext = 0;                      %%% External resistance [IF present] (ohm)
Rexternal = prin.Rext;

Case.CntlCoil = menu('Is the Control Solenoid Circuit exactly the same as the Principal Solenoid
Circuit','NO','YES');
switch Case.CntlCoil
    case 1
        % RUN THE "SOLENOID DESIGNER" FUNCTION FILE %

[radC1out,radC2out,radC3out,NturnsTot,lenWireLayersTot,pfCAvg,NC1wireHeight,NC2wireHeight,NC3wireH
eight,NC1wireLayers,NC2wireLayers,NC3wireLayers,...
```

```
areaC1wireElec,areaC2wireElec,areaC3wireElec,NC1turns,NC2turns,NC3turns,lenC1WireLayers,lenC2WireL
ayers,...

lenC3WireLayers,areaC1X,areaC2X,areaC3X,pfC1,pfC2,pfC3,volC1Wire,volC2Wire,volC3Wire,Iwire_safe,ar
eaMag,...

beta,RC1sol,RC2sol,RC3sol,tauElec,ZC1sol,ZC2sol,ZC3sol,Z3CoilParallel,LC1sol,LC2sol,LC3sol,Zcircui
tTot]...
            =
PhD_SolenoidDesigner(mur,cond1,rad1_in,rad1_out,Npedestals,HeightSinglePed,PercentPedHeightWound,p
fTurn,NC1wireLayers,...
            freq,Rexternal);
end
% Control Coil ONLY
cntl.NturnsTot = NturnsTot;
cntl.lenWireLayersTot = lenWireLayersTot;
cntl.pfCAvg = pfCAvg;
% Case outputs
cntl.Case.AWG = Case.AWG;
cntl.Case.coil = Case.coil;
cntl.Case.Cres = Case.Cres;
%~~ Solenoid primary overall mechanical geometry ~~%
cntl.NC1wireHeight = NC1wireHeight;
cntl.NC2wireHeight = NC2wireHeight;
cntl.NC3wireHeight = NC3wireHeight;
cntl.NC1wireLayers = NC1wireLayers;
cntl.NC2wireLayers = NC2wireLayers;
cntl.NC3wireLayers = NC3wireLayers;
%~~ Solenoid primary wire geometry ~~%
cntl.areaC1wireElec = areaC1wireElec;
cntl.areaC2wireElec = areaC2wireElec;
cntl.areaC3wireElec = areaC3wireElec;
cntl.NC1turns = NC1turns;
cntl.NC2turns = NC2turns;
cntl.NC3turns = NC3turns;
```

```
cntl.lenC1WireLayers = lenC1WireLayers;
cntl.lenC2WireLayers = lenC2WireLayers;
cntl.lenC3WireLayers = lenC3WireLayers;
cntl.areaC1X = areaC1X;
cntl.areaC2X = areaC2X;
cntl.areaC3X = areaC3X;
cntl.pfC1 = pfC1;
cntl.pfC2 = pfC2;
cntl.pfC3 = pfC3;
cntl.volC1Wire = volC1Wire;
cntl.volC2Wire = volC2Wire;
cntl.volC3Wire = volC3Wire;
%~~ Solenoid primary electrical & magnetic parameters ~~%
cntl.Iwire_safe = Iwire_safe;
cntl.areaMag = areaMag;
cntl.beta = beta;
%~~ Solenoid circuit electrical parameters ~~%
cntl.RC1sol = RC1sol;
cntl.RC2sol = RC2sol;
cntl.RC3sol = RC3sol;
cntl.LC1sol = LC1sol;
cntl.LC2sol = LC2sol;
cntl.LC3sol = LC3sol;
cntl.tauElec = tauElec;
cntl.ZC1sol = ZC1sol;
cntl.ZC2sol = ZC2sol;
cntl.ZC3sol = ZC3sol;
cntl.Z3CoilParallel = Z3CoilParallel;
cntl.ZcircuitTot = ZcircuitTot;


%%%%%%%%%%%%%%%%%%%%%%%%%%%%%%%%%%%%%%%%%%%%%%%%%%%%%%%%%%%%%%%%%%%%%%%
% INPUTS: Defining Solenoid Secondary & Control Variables %
%%%%%%%%%%%%%%%%%%%%%%%%%%%%%%%%%%%%%%%%%%%%%%%%%%%%%%%%%%%%%%%%%%%%%%%
```

```
% CONTROL SYSTEM INPUT VALUES %
zInputCntlHold = 0.6*con.in;%1.55*con.in;      %%% Controller hold z coordinate distance (m)
zCntlLowIPD = 0.02*con.in;
GainKlug = 72;                  %%% Start value: 14.5; Best yet (Phase I): 72
%%% 70 working well for coils w/ 28AWG wire & Cap., BUT oscillations building & current too high &
B too low
tauMechLim = 0.5;               % Mechanical tau plotting limit (sec)


% MECHANICAL INPUT PARAMETERS %

%~ Initial Condition Positions ~%
Case.InitCond = menu('Are the COM air gap initial conditions zeroed out or offset?',...
    'Zeroed Out','Offset (Non-Zero Values)');
% NOTE: The (tSteady) option provides a time period for the electomagnetic system to achieve a
steady state
% condition before the secondary vehicle is allowed to move.
tSteady = 0.05;                     %%% (Minimum: 0.025) Time for the electromagnetic system to
achieve steady state
switch Case.InitCond
    case 1  % Zeroed out COM air gap initial conditions
        zinit = zInputCntlHold;     %%% Initial steady state position of mass where z = zg (m)
        vzinit = 0;                 %%% Initial steady state velocity of mass in the z axis
direction (m/sec)
        vPropInit = 0;              %%% Initial steady state velocity of mass in any NON-z axis
direction (m/sec)
    case 2  % Offset (non-zero) COM air gap initial conditions
        zinit = 0.85*con.in;        %%% Initial steady state position of mass where z = zg (m)
        vzinit = 0;                 %%% Initial steady state velocity of mass in the z axis
direction (m/sec)
        vPropInit = 0;              %%% Initial steady state velocity of mass in any NON-z axis
direction (m/sec)
end

% SECONDARY INPUT VALUES %
```

```
% Secondary - Material & geometric parameters
rad2_in = rad1_in;              %%% Secondary inside radius (m)

% z AXIS PERTURBATION FORCE
Case.Pert = menu('Perturbation Force Inputs:',...
    'OFF (Zeroed out)','STEP (Use w/ NO Control to achieve Nat. Freqs.)',...
    'SINUSOID (DOF Natural Freq. Excitations)','STOCHASTIC');
switch Case.Pert
    case {1,4}  % "OFF" Zeroed out Perturbation conditions. Use for Displacement Offsets
        if Case.Pert == 1
            CasePert = sprintf('%s','OFF (Zeroed out)');
        else
            CasePert = sprintf('%s','Stochastic');
        end
        tPert = 0;                      % Perturbation "on" time
        FzPertMag = 0;                  % z axis perturbation force magnitude
        omega_z = 0;
    case 2  % STEP Perturbation conditions active
        CasePert = sprintf('%s','Step');
        tPert = 0.1;                    % Perturbation "on" time
        FzPertMag = 0.15*con.lbf;       %%% z axis perturbation force magnitude
        omega_z = 0;
    case 3  % SINUSOID Perturbation conditions active (Natural Freq. come from STEP response
above)
        CasePert = sprintf('%s','Sinusoid');
        tPert = 0.1;                    % Perturbation "on" time
        FzPertMag = -0.025*con.lbf;     %%% z axis perturbation force magnitude
        freq_zNat = 1/(1.706 - 1.495);  % z axis natural frequency for system analyzed (Hz)
        omega_z = 2*pi*(freq_zNat);
end


%%%%%%%%%%%%%%%%%%%%%%%%%%%%%%%%%%%%%%%%%%%%%%%%
% Defining Solenoid - Secondary Variables %
%%%%%%%%%%%%%%%%%%%%%%%%%%%%%%%%%%%%%%%%%%%%%%%%
```

```
% Secondary - Material & geometric parameters
density2 = density_Cu;          % Secondary material density (kg/m^3)
mu2 = mu0;                      % Permeability of the secondary (H/m)
cond2 = cond_Cu;                % Secondary conductivity (Siemens/m)
delta = sqrt(2/(prin.omega_e*mu0*cond2));    % Secondary skin depth [Use for secondary thickness]
(m)
height2max = 0.4*con.in;        % Max. secondary height (m)
height2 = delta;                % Secondary height [Set between the skin depth to a max. possible
secondary height value] (m)
if delta > height2max
    height2 = height2max;       %%% Vary the secondary height (m)
end
rad1_out = max([radC1out;radC2out;radC3out]); % Primary outside radius (m)
Asurf = HeightSinglePed*(2*pi*rad1_out) + 2*(pi*rad1_out^2);    % Primary outside surface area
(m^2)
rad2_out = rad1_out;            %%% Secondary outside radius (m)
rad2 = rad2_out;                %%% Secondary integration radius [Set as the outside radius] (m)
area2 = pi*(rad2_out^2 - rad2_in^2);    % Secondary area (m^2)
vol2 = area2*height2;           % Secondary volume (m^3)
mass2 = density2*vol2;          % Secondary mass (kg)
% mBear = 1*con.lbf/con.Ag;     % Individual bearing mass (kg)
% NBear = 2;                    % Number of bearings
% mAccel = 0.002;               % Accelerometer mass (kg)
% mSecExtra = 2*con.lbf/con.Ag; %%% Approx. mass of remaining levitated secondary material &
equip. [Gross Approx. right now] (kg)
% massTot = NSol*mass2 + NBear*mBear + mAccel + mSecExtra;   % Secondary moving mass
massTot = mass2;                % Total moving system mass (kg)
Fg = con.Ag*massTot;            % Single solenoid secondary weight (N)


%%% NOT USED!!! %%%
% % Reynolds Magnetic # specific parameters
% Kc1TotalPeak = 1.041E6/50;    %%% Coil #1 peak sheet current (A/m)
% Kc2TotalPeak = 1.035E6/50;    %%% Coil #2 peak sheet current (A/m)
```

```
% Kc3TotalPeak = 0;              %%% Coil #3 peak sheet current (A/m)
% KcTotalPeak = Kc1TotalPeak + Kc2TotalPeak + Kc3TotalPeak;   % Total coil peak sheet currents
(A/m)
% ReynoldsMagNum_NoMot = (mu2*cond2/beta^2); % Reynolds magnetic number w/o motion component
% tauElec = 0.011;              % Solenoid electrical time constant (sec)
% radMagMin = 0.338*con.in;     %%% Inside magnetic radius
% radMagMax = 1.368*con.in;     %%% Outside magnetic radius
% areaMag = pi*(radMagMax^2 - radMagMin^2);
% volMag = areaMag*height2;     % Magnetic volume (secondary height based)
%set_param('PhD_PhaseI_Master_MagReynoldsNum-TEST','simulationcommand','start')  %%% Simulink file
return call


%%%%%%%%%%%%%%%%%%%%%%%%%%%%%%%%
% Overall Control Parameters %
%%%%%%%%%%%%%%%%%%%%%%%%%%%%%%%%

% Characteristic equation constants from the Butterworth
% Pattern solved closed loop control system poles.
%%% ORIGINAL Values
alpha1 = -7.869;
alpha2 = 30.445;
alpha3 = -57.916;

% Vrms Principal & Control times & voltages
tfall = 0.01;                   % Time for control signal down slope (sec)
thold = 0.25 + tfall;           % Time for control signal down slope & hold (sec)
trise = 0.01 + thold;           % Time for control signal down slope, hold, & up slope (sec)
tpulse1 = 0.25;                 % First control pulse spike time (sec)
tpulse2 = 1.25;                 % 0.035 + (tpulse1+trise);    % Second control pulse spike time
(sec)
Vhold =  0;                     % Vrms for control signal pulse down hold (Vrms)
prin.Case.Wave = menu('Principal Coil Waveform Type','Constant Vrms','Steady Vrms w/ Single Vrms
Down Pulse','Steady Vrms w/ Double Vrms Down Pulses','NO Principal Coil');
switch prin.Case.Wave
```

```
    case 1
        CasePrinWaveform = sprintf('%s','Constant Vrms');
        tVrmsCmd = [0 0.002 0.025       endTime];
        VrmsCmd =  [0 0     prin.Vrms   prin.Vrms];
    case 2
        CasePrinWaveform = sprintf('%s','Steady Vrms w/ Single Vrms Down Pulse');
        % Principal voltage time (sec)
        tVrmsCmd = [0 0.002 0.025      tpulse1     (tpulse1+tfall) (tpulse1+thold)
(tpulse1+trise) endTime];
        % Principal voltage maintained (Vrms)
        VrmsCmd =  [0 0     prin.Vrms  prin.Vrms   Vhold           Vhold            prin.Vrms
prin.Vrms];
    case 3
        endTime = 2.5;
        CasePrinWaveform = sprintf('%s','Steady Vrms w/ Double Vrms Down Pulses');
        % Principal voltage time (sec)
        tVrmsCmd = [0 0.002 0.025       tpulse1     (tpulse1+tfall) (tpulse1+thold)
(tpulse1+trise) tpulse2...
            (tpulse2+tfall) (tpulse2+thold)  (tpulse2+trise) endTime];
        % Principal voltage maintained (Vrms)
        VrmsCmd =  [0 0     prin.Vrms   prin.Vrms    Vhold           Vhold            prin.Vrms
prin.Vrms...
            Vhold           Vhold             prin.Vrms      prin.Vrms];
    case 4
        CasePrinWaveform = sprintf('%s','NO Principal Coil');
        tVrmsCmd = [0 endTime]; % Principal solenoid control rms voltage (Vrms)
        VrmsCmd =  [0 0];       % Principal solenoid control rms voltage (Vrms)
end

Case.Cntl = menu('Controller Activation Type','No Controller','I-PD Control','Fuzzy
Control','Neuro-Fuzzy Adaptive Control');
switch Case.Cntl
    case 1
        CaseCntl = sprintf('%s','No Controller');
    case 2
        CaseCntl = sprintf('%s','I-PD');
```

```
    case 3
        CaseCntl = sprintf('%s','Fuzzy');
    case 4
        CaseCntl = sprintf('%s','Neuro-Fuzzy');
end
if Case.Cntl == 1
    tCntlStart = realmax;
else
    Case.CntlTime = menu('Controller Activation Time','Delayed Control Start','Immediate Control
Start');
    switch Case.CntlTime
        case 1  % Delayed Control Start (with separate Principal Solenoid)
            tCntlStart = 4*tpulse1;     % Control hold signal start time (sec)
        case 2  % Immediate Control Start (without separate Principal Solenoid)
            tCntlStart = 0;             % Control hold signal start time (sec)
    end
end
tCntlStartStr = num2str(tCntlStart);


%%% Training data set used for the Neuro-Fuzzy Controller
NumOscilTrain = 12;                         % Number of damping cycles
kAmp = 500/3-50;                            % Estimate of "k Prin" centroid minus offset from a
regular run
freqNatTrain = 1/(2*pi)*sqrt(kAmp/massTot); % Training oscillation damping freq. (Hz)
omegaNatTrain = 2*pi*freqNatTrain;
TauNatTrain = 1/freqNatTrain;               % Training oscillation damping period, used to help
set (freqNatTrain) eq. (sec)
tTrain = TauNatTrain*NumOscilTrain;         % Time to dampen out the oscillations (sec)
zTrainSlope = -(zinit)/tTrain;
zVelTrain = (4 + 2)*(zinit - zInputCntlHold)/TauNatTrain;   % Rough approx. for max. velocity
(m/sec)
zVelTrainSlope = -(zVelTrain)/tTrain;
% Load up "simout.signals.values"
```

```
%-------------------------------------------------------------------------------------------%
%%%%%%%%%%%%%%%%%%%%%%
%%                    %%
%% Simulation Start %%
%%                    %%
%%%%%%%%%%%%%%%%%%%%%%

tend=now;                    % Stop: Timer to show real time computational time
disp(['(Preprocessing Time = ' datestr(tend-tstart,13) ')']);

set_param('PhD_PhaseI_Master','simulationcommand','start')   % Simulink file return call
```

C.2.b.ii Matlab Output Function File

```
%%% OUTPUT PLOTS FILE

%%% PhD Dissertation - Phase I
%%% By: Glenn A. Knierim
%%% Program Started: Spring 2004
%-------------------------------------------------------------------------------------------

%%%%%%%%%%%%%%%%%%%%%%%%%%%%%%%%%%%%%%%%%%%%%%%%%%%%%%%%%%%%%%%%%%%%%%%%%%%%%%%%%%%%%%%%%%%
% POST PROCESSING %
%%%%%%%%%%%%%%%%%%%%



%%%%%%%%%%%%%%%%%%%%%%%%%%%%%%%%
% Define global parameters %
%%%%%%%%%%%%%%%%%%%%%%%%%%%%%%%%

% Global simulation structured variable arrays for the principal & control solenoid systems:
(prin) & (cntl)
% Global simulation structured constant setup array: (con)
```

```
% Global simulation structured Case setup array: (Case)
global prin cntl con Case


%%%%%%%%%%%%%%%%%%%%%%%%
% POST PROCESSING DATA %
%%%%%%%%%%%%%%%%%%%%%%%%

disp('-=> Start of Postprocessing Data <=-')
tstart=now; % Start: Timer to show real postprocessing time


%%% Plot Preparation %%%
% Note: Plotting data from Simulink output Structured Arrays w/ Time

%~ Plot Time ~%
% Note: Sim. discritization constant for all plots, so just choosing a time source
time = zMotion.time;

%~ Mechanical Plots ~%
% Mechanical position plots
z = zMotion.signals(:,1).values(:,1)./con.in;
zmax = max(z);
zinit = zMotion.signals(:,1).values(:,2)./con.in;
zCntlHold = zMotion.signals(:,1).values(:,3)./con.in;
zCntlLowPD = zMotion.signals(:,1).values(:,4)./con.in;
zRef = zMotion.signals(:,1).values(:,5)./con.in;
% Mechanical velocity plots
zVel = zMotion.signals(:,2).values(:,1);
zVelInit = zMotion.signals(:,2).values(:,2);
% Mechanical force plots
FzPrin = zForce.signals(:,1).values(:,1);
Fgravity = zForce.signals(:,1).values(:,2);
FzCntl = zForce.signals(:,2).values(:,1);
```

```
%~ Electrical Plots ~%
% System volages
VPrinCmdRMS = V_I.signals(:,1).values(:,2);
VPrinCmdMaxRMS = max(VPrinCmdRMS);
VCntlCmdRMS = V_I.signals(:,1).values(:,4);
% System currents
IprinRMS = V_I.signals(:,2).values(:,1);
ICntlRMS = V_I.signals(:,2).values(:,2);
FlagVrmsONCntl = V_I.signals(:,2).values(:,3);
% Principal solenoid currents
IPrinRMS = V_I.signals(:,3).values(:,1);
IC1PrinRMS = V_I.signals(:,3).values(:,2);
IC2PrinRMS = V_I.signals(:,3).values(:,3);
IC3PrinRMS = V_I.signals(:,3).values(:,4);
IPrinWireSafe = V_I.signals(:,3).values(:,5);
% Control solenoid currents
ICntlRMS = V_I.signals(:,4).values(:,1);
IC1CntlRMS = V_I.signals(:,4).values(:,2);
IC2CntlRMS = V_I.signals(:,4).values(:,3);
IC3CntlRMS = V_I.signals(:,4).values(:,4);
ICntlWireSafe = V_I.signals(:,4).values(:,5);

%~ Secondary Power & Energy Plots ~%
% Seconary energy plots
EkzPrin = PowerEnergy.signals(:,1).values(:,1);
EkzPrinMax = max(EkzPrin);
EkzCntl = PowerEnergy.signals(:,1).values(:,2);
EzKE = PowerEnergy.signals(:,1).values(:,3);
EzPE = PowerEnergy.signals(:,1).values(:,4);
EzPEMax = max(EzPE);
% Seconary power plots
PzPrin = PowerEnergy.signals(:,2).values(:,1);
PzCntl = PowerEnergy.signals(:,2).values(:,2);
PzPert = PowerEnergy.signals(:,2).values(:,3);
```

```
%~ System Response Plots ~%
% Tau plots
tauMech = k_tau.signals(:,1).values(:,1);
tauEPrin = k_tau.signals(:,2).values(:,1);
tauECntl = k_tau.signals(:,2).values(:,2);
tauECntlMax = max(tauECntl);
% Magnetic spring constant & mechanical natural frequency plots
kPrin = k_tau.signals(:,3).values(:,1);
kCntl = k_tau.signals(:,3).values(:,2);
kMechNatFreq = k_tau.signals(:,4).values(:,1);

%~ Thermal Plots ~%
% System thermal energy
QPrinRMSTot = Thermal.signals(:,1).values(:,1);
QPrinRMSTotMax = max(QPrinRMSTot);
QC1PrinRMS = Thermal.signals(:,1).values(:,2);
QC2PrinRMS = Thermal.signals(:,1).values(:,3);
QC3PrinRMS = Thermal.signals(:,1).values(:,4);
QCntlRMSTot = Thermal.signals(:,1).values(:,5);
QC1CntlRMS = Thermal.signals(:,1).values(:,6);
QC2CntlRMS = Thermal.signals(:,1).values(:,7);
QC3CntlRMS = Thermal.signals(:,1).values(:,8);
% System temperatures
TempC1PrinWire = Thermal.signals(:,3).values(:,1);
TempC2PrinWire = Thermal.signals(:,3).values(:,2);
TempC3PrinWire = Thermal.signals(:,3).values(:,3);
TempC1CntlWire = Thermal.signals(:,3).values(:,4);
TempC2CntlWire = Thermal.signals(:,3).values(:,5);
TempC3CntlWire = Thermal.signals(:,3).values(:,6);


%%%%%%%%%%%%%%%%%%%%%%%%%
% POST PROCESSING PLOTS %
%%%%%%%%%%%%%%%%%%%%%%%%%
```

```
% Output Setup
figure(1); delete(1);
figure(2); delete(2);
figure(3); delete(3);
figure(4); delete(4);
figure(5); delete(5);
figure(6); delete(6);
figure(7); delete(7);
figure(8); delete(8);
figure(9); delete(9);
figure(10); delete(10);


%%%%%%%%%%%%%%%%%%%%%%%%%%%%%%%%%%%%
%~ Fuzzy & Neuro-Fuzzy Logic Plots ~%

switch Case.Cntl
    case 3  % Fuzzy logic controller plot commands
        a = readfis('PhD_PhaseI_FuzzyCntl.fis');
        getfis(a);

        figure(1)
        plotfis(a);
        title(['\bf',CaseCntl,' Logic Control - ',CaseCntl,' Inference System Structure'],
'FontSize',15);
        set(gca, 'FontSize',11, 'FontWeight','bold')

        figure(2)
        gensurf(a,[1 2],1,[100 100])
        grid on
        colorbar
        title(['\bf',CaseCntl,' Logic Control - ',CaseCntl,' Inference System Structure'],
'FontSize',15);
        set(gca, 'FontSize',11, 'FontWeight','bold')
```

```
        xlabel({'\bfSecondary z Axis';['Reference Ratio'];['[Variable Name: zRefRatio]']},
'FontSize',12,...
            'HorizontalAlignment','center');
        ylabel({'\bfSecondary z Axis';['Velocity (m/sec)'];['[Variable Name: z2=Velocity]']},
'FontSize',12,...
            'HorizontalAlignment','center');
        zlabel({'\bfControl Voltage (Vrms)';['[Variable Name: VCntlRMS]']}, 'FontSize',12,...
            'HorizontalAlignment','center');
        zlim([0 prin.Vrms]);

        figure(3)
        plotmf(a,'input',1);
        grid on
        title(['\bf',CaseCntl,' Logic Control - Input Membership Function'], 'FontSize',15);
        set(gca, 'FontSize',11, 'FontWeight','bold')

        figure(4)
        plotmf(a,'input',2);
        grid on
        title(['\bf',CaseCntl,' Logic Control - Input Membership Function'], 'FontSize',15);
        set(gca, 'FontSize',11, 'FontWeight','bold')

        figure(5)
        plotmf(a,'output',1);
        grid on
        title(['\bf',CaseCntl,' Logic Control - Output Membership Function'], 'FontSize',15);
        set(gca, 'FontSize',11, 'FontWeight','bold')


    case 4  % Neuro-Fuzzy logic controller plot commands
        a = readfis('PhD_PhaseI_NeuroFuzzyCntl.fis');
        getfis(a);

        figure(1)
        plotfis(a);
```

```
        title(['\bf',CaseCntl,' Logic Control - ',CaseCntl,' Inference System Structure'],
'FontSize',15);
        set(gca, 'FontSize',11, 'FontWeight','bold')

        figure(2)
        gensurf(a,[1 2],1,[100 100])
        grid on
        colorbar
        title(['\bf',CaseCntl,' Logic Control - ',CaseCntl,' Inference System Structure'],
'FontSize',20);
        set(gca, 'FontSize',14, 'FontWeight','bold')
        xlabel({'\bfSecondary z Axis';['Reference Ratio'];['[Variable Name: zRefRatio]']},
'FontSize',16,...
            'HorizontalAlignment','center');
        ylabel({'\bfSecondary z Axis';['Velocity (m/sec)'];['[Variable Name: z2=Velocity]']},
'FontSize',16,...
            'HorizontalAlignment','center');
        zlabel({'\bfControl Voltage (Vrms)';['[Variable Name: VCntlRMS]']}, 'FontSize',16,...
            'HorizontalAlignment','center');
        zlim([0 prin.Vrms]);

        figure(3)
        plotmf(a,'input',1);
        grid on
        title(['\bf',CaseCntl,' Logic Control - Input Membership Function'], 'FontSize',15);
        set(gca, 'FontSize',11, 'FontWeight','bold')

        figure(4)
        plotmf(a,'input',2);
        grid on
        title(['\bf',CaseCntl,' Logic Control - Input Membership Function'], 'FontSize',15);
        set(gca, 'FontSize',11, 'FontWeight','bold')

        figure(5)
        plotmf(a,'output',1);
```

```
        grid on
        title(['\bf',CaseCntl,' Logic Control - Output Membership Function'], 'FontSize',15);
        set(gca, 'FontSize',11, 'FontWeight','bold')
end


%%%%%%%%%%%%%%%%%%%%%%%%
%~ Mechanical Plots ~%

% Mechanical position plot
figure(6)
subplot(3,1,1)
clear Legend_Labels;
P=plot(time, [z, zinit, zCntlHold, zCntlLowPD, zRef],'linewidth',2.8);
set(gca, 'FontSize',11, 'FontWeight','bold')
set(P(1), 'Color', 'k');
set(P(2), 'Color', 'm');
set(P(3), 'Color', 'g');
set(P(4), 'Color', 'r');
set(P(5), 'Color', 'b');
set(P(3),'LineStyle','--');
set(P(4),'LineStyle','-.');
Legend_Labels{1}='\bfz';
Legend_Labels{2}='\bfInitial z';
Legend_Labels{3}='\bfz Control Hold';
Legend_Labels{4}='\bfz Control Low I-PD Band';
Legend_Labels{5}='\bfz Reference = (zCntlHold - z)';
[legend_handle,object_handles] = legend(P,Legend_Labels,0);
set(findobj(object_handles, 'Type', 'text'), 'FontSize',10);
ylabel(['\bfz Axis Position (in)'], 'FontSize',14);
if Case.Cntl ~= 1
    T = text(tCntlStart,1.01*zmax,['\bfControl Start time: ', tCntlStartStr,' sec']);
    set(findobj(T, 'Type', 'text'), 'FontSize',12);
end
title({'\bfMechanical';['Principal Solenoid: ',CasePrinWaveform,';  Control Type: ',...
```

```
    CaseCntl,';  Perturbation Type: ',CasePert]}, 'FontSize',15);
grid on

% Mechanical velocity plot
subplot(3,1,2)
clear Legend_Labels;
P=plot(time, [zVel, zVelInit],'linewidth',2.8);
set(gca, 'FontSize',11, 'FontWeight','bold')
set(P(1), 'Color', 'k');
set(P(2), 'Color', 'm');
set(P(2),'LineStyle','--');
Legend_Labels{1}='\bfz Velocity';
Legend_Labels{2}='\bfInitial z Velocity';
[legend_handle,object_handles] = legend(P,Legend_Labels,0);
set(findobj(object_handles, 'Type', 'text'), 'FontSize',10);
ylabel(['\bfz Axis Velocity (m/sec)'], 'FontSize',14);
grid on

% Mechanical force plot
subplot(3,1,3)
clear Legend_Labels;
P=plot(time, [FzPrin, FzCntl, Fgravity],'linewidth',2.8);
set(gca, 'FontSize',11, 'FontWeight','bold')
set(P(1), 'Color', 'g');
set(P(2), 'Color', 'b');
set(P(3), 'Color', 'r', 'LineStyle','--','linewidth',3);
Legend_Labels{1}='\bfPrincipal';
Legend_Labels{2}='\bfControl';
Legend_Labels{3}='\bfGravity';
[legend_handle,object_handles] = legend(P,Legend_Labels,0);
set(findobj(object_handles, 'Type', 'text'), 'FontSize',10);
ylabel(['\bfz Axis Force (N)'], 'FontSize',14);
xlabel(['\bfTime (sec)'], 'FontSize',14);
grid on
```

```
%%%%%%%%%%%%%%%%%%%%%%%%%%%%%%%%%%%%
%~ Secondary Power & Energy Plots ~%

% Secondary energy
figure(7)
subplot(2,1,1)
clear Legend_Labels;
P=plot(time, [EkzPrin, EzKE, EzPE, EkzCntl],'linewidth',2.8);
set(gca, 'FontSize',11, 'FontWeight','bold')
set(P(1), 'Color', 'g');
set(P(2), 'Color', 'r', 'linewidth',3);
set(P(3), 'Color', 'm', 'linewidth',3);
set(P(4), 'Color', 'b', 'linewidth',3);
Legend_Labels{1}='\bfPrincipal Magnetic Spring';
Legend_Labels{2}='\bfKinetic Energy';
Legend_Labels{3}='\bfPotential Energy';
Legend_Labels{4}='\bfControl Magnetic Spring';
[legend_handle,object_handles] = legend(P,Legend_Labels,0);
set(findobj(object_handles, 'Type', 'text'), 'FontSize',10);
ylabel(['\bfInstantaneous Energy (J))'], 'FontSize',14);
if Case.Cntl ~= 1
    T = text(tCntlStart,1.01*EzPEMax,['\bfControl Start time: ', tCntlStartStr,' sec']);
    set(findobj(T, 'Type', 'text'), 'FontSize',12);
end
title({'\bfSecondary Power & Energy';['Principal Solenoid: ',CasePrinWaveform,';  Control Type:
',...
    CaseCntl,';  Perturbation Type: ',CasePert]}, 'FontSize',15);
grid on

% Secondary power
subplot(2,1,2)
clear Legend_Labels;
P=plot(time, [PzPrin, PzPert, PzCntl],'linewidth',2.8);
set(gca, 'FontSize',11, 'FontWeight','bold')
```

```
set(P(1), 'Color', 'g');
set(P(2), 'Color', 'm', 'linewidth',3);
set(P(3), 'Color', 'b', 'linewidth',3);
Legend_Labels{1}='\bfPrincipal';
Legend_Labels{2}='\bfPerturbation';
Legend_Labels{3}='\bfControl';
[legend_handle,object_handles] = legend(P,Legend_Labels,0);
set(findobj(object_handles, 'Type', 'text'), 'FontSize',10);
ylabel(['\bfPower Input (W)'], 'FontSize',14);
xlabel(['\bfTime (sec)'], 'FontSize',14);
grid on


%%%%%%%%%%%%%%%%%%%%%%%%%%%%
%~ System Response Plots ~%

% Mechanical & Electrical tau
figure(8)
subplot(3,1,1)
clear Legend_Labels;
hold on;
% H = line or graphics handle. AX = Axis handles (LEFT and RIGHT)
LEFT=1; RIGHT=2;
Conv = 1000;
[AX,H(1,LEFT),H(1,RIGHT)] = plotyy(time, (tauEPrin*Conv),...
    time, (tauMech));
P = plot(time, (tauECntl*Conv));
set(gca, 'FontSize',11, 'FontWeight','bold')
% Set the Axis Parent valus to the respective Left & Right axis.
set(H(1,LEFT),'Parent', AX(LEFT));
set(H(1,RIGHT),'Parent',AX(RIGHT));
hold off;
% Setting the y axis values for plotting
TauLim = 0.01;
set(AX(LEFT),'YLim',[0 TauLim*Conv]);
```

```
set(AX(:,RIGHT),'YLim',[0 tauMechLim]);
% Note: get() only works on one handle at a time, so pick some arbitrary one
set(get(AX(LEFT),'Ylabel'),'String','\bfElectrical Tau (msec)', 'FontSize',14, 'Color', 'k');
set(get(AX(RIGHT),'Ylabel'),'String','\bfTotal Mechanical Tau (sec)', 'FontSize',14, 'Color',
'k');
% Setting the x & y axis ticks for plotting
set(AX(LEFT),'YTick',0:(Conv*TauLim/4):(Conv*TauLim));
set(AX(:,RIGHT),'YTick',0:tauMechLim/4:tauMechLim);
% Set up Line types and colors
set(H(1,LEFT), 'Color', 'b', 'linewidth',3);
set(H(1,RIGHT), 'Color', 'k', 'linewidth',3);
set(P(1), 'Color', 'm', 'linewidth',3);
set(AX(:),'XColor','k','YColor','k', 'FontSize',12, 'FontWeight','bold')
% Legend
Legend_Labels{1}='\bfMechanical';
Legend_Labels{2}='\bfPrincipal Elec.';
Legend_Labels{3}='\bfControl Elec.';
[legend_handle,object_handles] = legend([H(1,LEFT),P],Legend_Labels{2:3});
set(findobj(object_handles, 'Type', 'text'), 'FontSize',10, 'FontWeight','bold',
'BackgroundColor', 'none');
[legend_handle,object_handles] = legend(H(1,RIGHT),Legend_Labels{1});
set(findobj(object_handles, 'Type', 'text'), 'FontSize',10, 'FontWeight','bold',
'BackgroundColor', 'none');
% Set the grid for the Left axis & turn the grid on.
grid(AX(1,1));
grid on;
if Case.Cntl ~= 1
    T = text(tCntlStart,1.05*tauECntlMax*Conv,['\bfControl Start time: ', tCntlStartStr,' sec']);
    set(findobj(T, 'Type', 'text'), 'FontSize',12);
end
title({'\bfSystem Response';['Principal Solenoid: ',CasePrinWaveform,';  Control Type: ',...
    CaseCntl,';  Perturbation Type: ',CasePert]}, 'FontSize',15);

% Magnetic spring constants
subplot(3,1,2)
clear Legend_Labels;
```

```
P=plot(time, [kPrin, kCntl],'linewidth',2.8);
set(gca, 'FontSize',11, 'FontWeight','bold')
set(P(1), 'Color', 'k');
set(P(2), 'Color', 'b');
Legend_Labels{1}='\bfPrincipal';
Legend_Labels{2}='\bfControl';
[legend_handle,object_handles] = legend(P,Legend_Labels,0);
set(findobj(object_handles, 'Type', 'text'), 'FontSize',10);
ylabel(['\bfMag. Spring Constants (N/m)'], 'FontSize',14);
grid on

% Mechanical resonant/natural frequency
subplot(3,1,3)
clear Legend_Labels;
P=plot(time, kMechNatFreq,'linewidth',2.8);
set(gca, 'FontSize',11, 'FontWeight','bold')
set(P(1), 'Color', 'k');
ylabel(['\bfMech. Natural Frequency (Hz)'], 'FontSize',14);
xlabel(['\bfTime (sec)'], 'FontSize',14);
grid on


%%%%%%%%%%%%%%%%%%%%%%
%~ Electrical Plots ~%

% System volages plot
figure(9)
subplot(4,1,1)
clear Legend_Labels;
P=plot(time, [VPrinCmdRMS, VCntlCmdRMS],'linewidth',2.8);
set(gca, 'FontSize',11, 'FontWeight','bold')
set(P(1), 'Color', 'k');
set(P(2), 'Color', 'b');
Legend_Labels{1}='\bfPrincipal';
Legend_Labels{2}='\bfControl';
```

```
[legend_handle,object_handles] = legend(P,Legend_Labels,0);
set(findobj(object_handles, 'Type', 'text'), 'FontSize',10);
ylabel(['\bfVoltage (Vrms)'], 'FontSize',14);
if Case.Cntl ~= 1
    T = text(tCntlStart,1.1*VPrinCmdMaxRMS,['\bfControl Start time: ', tCntlStartStr,' sec']);
    set(findobj(T, 'Type', 'text'), 'FontSize',12);
end
title({'\bfElectrical';['Principal Solenoid: ',CasePrinWaveform,';  Control Type: ',...
    CaseCntl,';  Perturbation Type: ',CasePert]}, 'FontSize',15);
grid on

% System currents plot
subplot(4,1,2)
clear Legend_Labels;
P=plot(time, [IprinRMS, ICntlRMS, FlagVrmsONCntl],'linewidth',2.8);
set(gca, 'FontSize',11, 'FontWeight','bold')
set(P(1), 'Color', 'k');
set(P(2), 'Color', 'b');
set(P(3), 'Color', 'm', 'LineStyle','--');
Legend_Labels{1}='\bfPrincipal';
Legend_Labels{2}='\bfControl';
Legend_Labels{3}='\bfControl Vrms "on" Flag';
[legend_handle,object_handles] = legend(P,Legend_Labels,0);
set(findobj(object_handles, 'Type', 'text'), 'FontSize',10);
ylabel(['\bfSolenoid Current (Irms)'], 'FontSize',14);
grid on

% Principal solenoid currents plot
subplot(4,1,3)
clear Legend_Labels;
P=plot(time, [IPrinRMS, IC1PrinRMS, IC2PrinRMS, IC3PrinRMS, IPrinWireSafe],'linewidth',2.8);
set(gca, 'FontSize',11, 'FontWeight','bold')
set(P(1), 'Color', 'k');
set(P(2), 'Color', 'b');
set(P(3), 'Color', 'm');
set(P(4), 'Color', 'g');
```

```
set(P(5), 'Color', 'r', 'LineStyle','--');
Legend_Labels{1}='\bfSolenoid';
Legend_Labels{2}='\bfCoil #1';
Legend_Labels{3}='\bfCoil #2';
Legend_Labels{4}='\bfCoil #3';
Legend_Labels{5}='\bfSafe Wire Level';
[legend_handle,object_handles] = legend(P,Legend_Labels,0);
set(findobj(object_handles, 'Type', 'text'), 'FontSize',10);
ylabel(['\bfPrincipal Current (Irms)'], 'FontSize',14);
grid on

% Control solenoid currents plot
subplot(4,1,4)
clear Legend_Labels;
P=plot(time, [ICntlRMS, IC1CntlRMS, IC2CntlRMS, IC3CntlRMS, ICntlWireSafe],'linewidth',2.8);
set(gca, 'FontSize',11, 'FontWeight','bold')
set(P(1), 'Color', 'k');
set(P(2), 'Color', 'b');
set(P(3), 'Color', 'm');
set(P(4), 'Color', 'g');
set(P(5), 'Color', 'r', 'LineStyle','--');
Legend_Labels{1}='\bfSolenoid';
Legend_Labels{2}='\bfCoil #1';
Legend_Labels{3}='\bfCoil #2';
Legend_Labels{4}='\bfCoil #3';
Legend_Labels{5}='\bfWire Safe';
[legend_handle,object_handles] = legend(P,Legend_Labels,0);
set(findobj(object_handles, 'Type', 'text'), 'FontSize',10);
ylabel(['\bfControl Current (Irms)'], 'FontSize',14);
xlabel(['\bfTime (sec)'], 'FontSize',14);
grid on


%%%%%%%%%%%%%%%%%%
%~ Thermal Plots ~%
```

```
% System thermal energy
figure(10)
subplot(2,1,1)
clear Legend_Labels;
P=plot(time, [QPrinRMSTot, QC1PrinRMS, QC2PrinRMS, QC3PrinRMS,...
    QCntlRMSTot, QC1CntlRMS, QC2CntlRMS, QC3CntlRMS],'linewidth',2.8);
set(gca, 'FontSize',11, 'FontWeight','bold')
set(P(1), 'Color', 'k');
set(P(2), 'Color', 'b');
set(P(3), 'Color', 'm');
set(P(4), 'Color', 'g');
set(P(5), 'Color', 'k', 'LineStyle','--');
set(P(6), 'Color', 'b', 'LineStyle','--');
set(P(7), 'Color', 'm', 'LineStyle','--');
set(P(8), 'Color', 'g', 'LineStyle','--');
Legend_Labels{1}='\bfPrincipal Solenoid';
Legend_Labels{2}='\bfPrincipal Coil #1';
Legend_Labels{3}='\bfPrincipal Coil #2';
Legend_Labels{4}='\bfPrincipal Coil #3';
Legend_Labels{5}='\bfControl Solenoid';
Legend_Labels{6}='\bfControl Coil #1';
Legend_Labels{7}='\bfControl Coil #2';
Legend_Labels{8}='\bfControl Coil #3';
[legend_handle,object_handles] = legend(P,Legend_Labels,0);
set(findobj(object_handles, 'Type', 'text'), 'FontSize',10);
ylabel(['\bfThermal Power (W)'], 'FontSize',14);
if Case.Cntl ~= 1
    T = text(tCntlStart,1.1*QPrinRMSTotMax,['\bfControl Start time: ', tCntlStartStr,' sec']);
    set(findobj(T, 'Type', 'text'), 'FontSize',12);
end
title({'\bfPrimary Solenoid Thermal';['Principal Solenoid: ',CasePrinWaveform,';  Control Type:
',...
    CaseCntl,';  Perturbation Type: ',CasePert]}, 'FontSize',15);
grid on
```

```
% System Temperatures
subplot(2,1,2)
clear Legend_Labels;
P=plot(time, [TempC1PrinWire, TempC2PrinWire, TempC3PrinWire,...
    TempC1CntlWire, TempC2CntlWire, TempC3CntlWire],'linewidth',2.8);
set(gca, 'FontSize',11, 'FontWeight','bold')
set(P(1), 'Color', 'k');
set(P(2), 'Color', 'b');
set(P(3), 'Color', 'm');
set(P(4), 'Color', 'k', 'LineStyle','--');
set(P(5), 'Color', 'b', 'LineStyle','--');
set(P(6), 'Color', 'm', 'LineStyle','--');
Legend_Labels{1}='\bfPrincipal Coil #1';
Legend_Labels{2}='\bfPrincipal Coil #2';
Legend_Labels{3}='\bfPrincipal Coil #3';
Legend_Labels{4}='\bfControl Coil #1';
Legend_Labels{5}='\bfControl Coil #2';
Legend_Labels{6}='\bfControl Coil #3';
[legend_handle,object_handles] = legend(P,Legend_Labels,0);
set(findobj(object_handles, 'Type', 'text'), 'FontSize',10);
ylabel(['\bfTemperature Change (°C)'], 'FontSize',14);
xlabel(['\bfTime (sec)'], 'FontSize',14);
grid on



tend=now; % Stop: Timer to show postprocessing real time
disp(['-=> Postprocessing took ' datestr(tend-tstart,13) ') <=-']);
```

C.2.c Phase IV Matlab Files

C.2.c.i Matlab Input Function File

```
%%% INPUT FILE
```

```
%%% PhD Dissertation - Phase IV
%%% By: Glenn A. Knierim
%%% Program Started: Spring 2004
%-------------------------------------------------------------------------------%

%%%%%%%%%%%%%%%%%%%%%%%%%
% Overall Program Notes %
%%%%%%%%%%%%%%%%%%%%%%%%%

% 1.    This program models one to three coil solenoids respectively levitating and controlling
%       the levitation of a 6 DOF vehicle.
% 2.    All calculation units are S.I. excluding distances since the physical solenoid system
under
%       development is based on ANSI dimensioned based primary core, primary wire, and secondary.
% 3.    "%%%" starting a commented description after a variable means a regularly changed
variable.
% 4.    For Phase IV currently using 18 AWG wire with 2 coils for the primary and 1 coil for the
%       secondary solenoids with a series resonant capacitor. For this
%       system [(Fz/Fy) =~ 6.5] unless using (yFGain) which then gives [(Fz/Fy) =~ 3].
%       Coil #1: Principal coil = 21, Control coil = 24.

%-------------------------------------------------------------------------------%
%%%%%%%%%%%%%%%%%
% PRE PROCESSING %
%%%%%%%%%%%%%%%%%

% Clear memory, home the cursor, & increase memory size
clear prin cntl con Case
pack;clc;
set(0,'RecursionLimit',10000)

disp('Preprocessing Start')
tstart=now;                     % Start: Timer to show real time Preprocessing Time
```

```
%%%%%%%%%%%%%%%%%%%%%%%%%%%%
% Define global parameters %
%%%%%%%%%%%%%%%%%%%%%%%%%%%%

% Global simulation variables (sim) & constants (con) throughout program
% (sim) & (con) are structured arrays
global prin cntl con Case


%%%%%%%%%%%%%%%%%%%%%%%%%%%%%%%%%%%%%%%%%%%%%%%%
% User Defined Input for Test Case to Run %
%%%%%%%%%%%%%%%%%%%%%%%%%%%%%%%%%%%%%%%%%%%%%%%%

%%% RUN THE INPUT MENU (NOT Used)
%PhD_PhaseIV_input_menu;
%%% READ INTO WORKSPACE THE FUZZY LOGIC INFORMATION [NO method here used]
%%% Load info. into workspace manually in the FIS editor & do not clear above.
% PhD_PhaseIV_FuzzyCntl.fis
% a = readfis('PhD_PhaseI_FuzzyCntl.fis');
%getfis(a);
%evalfis(a);
%writefis(a)

%%% Phase to Run
% Case.Phase = menu('Choose the Phase under analysis','Phase I','Phase IV');
Case.Phase = 2;     % Hardwiring a Phase IV Analysis
disp('_____________________________________')
switch Case.Phase
    case 1
        disp('            Phase I')
        disp(' ')
    case 2
        disp('            Phase IV')
        disp(' ')
end
```

```
%%% Active axes
Case.Axes = menu('Are both the z & y axis solenoids activated or just the z axis solenoids?',...
    'BOTH z & y axis (y axis constrained)','ONLY z axis (free to move in x-y axis plane)');
disp('_____________________________________')
switch Case.Axes
    case 1
        disp('   Active Solenoid Axis: BOTH z & y axis')
        disp(' ')
    case 2
        disp('   Active Solenoid Axis: ONLY z axis')
        disp(' ')
end


%%%%%%%%%%%%%%%%%%%%
% Unit Conversions %
%%%%%%%%%%%%%%%%%%%%

con.lbm = 0.4535924;                % pound mass to kg
con.lbf = 4.448222;                 % pound force to N
con.ft = 12*0.0254;                 % ft to m
con.in = 0.0254;                    % in to m
con.Ag = 9.81;                      % Acceleration due to gravity (m/sec^2)
con.cm = 100;                       % Meter to Centimeter
con.deg = pi/180;                   % Degrees to Radians


%%%%%%%%%%%%%%%%%%%%%%%%
% Defining Constants  %
%%%%%%%%%%%%%%%%%%%%%%%%

% Simulation constants
tcnt = 0;                       % Counter for displaying info. during simulation
tStp = 5*5E-5;%5*5E-5;          % Using: Cntl Off: 0.5*5E-5; Cntl ON: 2*5E-5
tStpMin = tStp;
```

```
%maxStp = 1/120/100;            % Maximum time step (sec)
reltol = 1*1E-2;                % Relative sim. tolerance
abstol = 1*1E-2;                % Absolute sim. tolerance
%decimate = 1;                  % Plot increment (time step)
endTime = 4;                    %%% (4) tpulse2 + thold + 0.05;       % Simulation end time (sec)

% Universal material constants
mu0 = pi*4E-7;                  % Permeability of a vacuum (H/m)
cond_Cu = 5.977E7;              % Copper conductivity (Siemens/m)
density_Cu = 8.934E3;           % Copper density (kg/m^3)
Cp_Cu = 386.023;                % Copper specific heat (m^2/(s^2*K))
Ctemp_Cu = 0.0043;              % Copper coefficient of temperature (1/K)
cond_Al = 3.766E7;              % Aluminum conductivity (Siemens/m)
density_Al = 2.692E3;           % Aluminum density (kg/m^3)
Cp_Al = 962.964;                % Aluminum specific heat (m^2/(s^2*K))
Ctemp_Al = 0.004;               % Aluminum coefficient of temperature (1/K)
CThCondFe = 1;                  % [NOT Used] Thermal conductivity of ferrite (W/(m*C))
sigma = 5.67E-8;                % Stefan-Boltzmann constant (W/(m^2*K^4))

% Simulation specific material constants
mur = 4.673;%1/2*150;           %%% Relative permeability of primary iron with factor for geometry
mu1 = mur*mu0;                  % Permeability of the primary (H/m)
mu3 = mu0;                      % Permeability of the air gap b/w the primary & secondary (H/m)
mu4 = mu0;                      % Permeability of the air behind the secondary (H/m)
Bsat = 0.8;                     %%% (0.8) B fully saturated value, approx. as a step function (T)
cond1 = cond_Cu;                % Primary conductivity (Siemens/m)
emis_Cu = 0.5;                  % Approx. emissivity of copper stably oxidized under operating
conditions
hConv = 15;                     % Approx. free or natural gas convective coef. (W/(m^2*K))

% System geometric parameters
zmin = 1E-3*con.in;             % Min. z boundary condition distance b/w primary & secondary (m)


%%%%%%%%%%%%%%%%%%%%%%%%%%%%%%%%%%%%%%%%%%%%%%%%%%%%%%%%%%%%%%%%%%%%%%%%%%%%
```

```
% INPUTS: Defining "Principal" Solenoid Primary Variables %
%%%%%%%%%%%%%%%%%%%%%%%%%%%%%%%%%%%%%%%%%%%%%%%%%%%%%%%%%%%%%%%%%%%%%%%

% Solenoid material & geometric parameters
rad1_in = 0*con.in;             %%% (0) Solenoid inside core radius (m)
rad1_out = 2.5*con.in;          %%% (2.5") Solenoid outside core radius (m)

% Solenoid mechanical geometry
prin.zNSol = 1;                 %%% (1) # of z axis principal solenoids
prin.yNSol = 1;                 %%% (1) # of y axis principal solenoids
Npedestals = 1;                 %%% (1) # of solenoid center core pedestals (m)
HeightSinglePed = 7*con.in;     %%% (7") Solenoid center core pedestal height (m)
PercentPedHeightWound = 100;    %%% (100) Percent of pedestal available wound w/ wire (%)
pfTurn = 1.1;                   %%% (1.1) Estimated packing factor per winding diam. to diam. turn
NC1wireLayers = 21;             %%% (21) # of "Principal" coil #1 wire layers (Set for 30 AWG, but
Iwire too high w/ Cap.)
% Solenoid primary source electrical & magnetic parameters
prin.freq = 60;%150;            %%% (60) Electrical frequency (Hz)
freq = prin.freq;
prin.omega_e = 2*pi*prin.freq;  % Electrical angular frequency (rad/sec)
prin.Vrms = 280;                %%% (280) Primary principal solenoid source rms voltage (V)
prin.Rext = 0;                  %%% (0) External resistance [IF present] (ohm)
Rexternal = prin.Rext;

% RUN THE "SOLENOID DESIGNER" FUNCTION FILE %
[radC1out,radC2out,radC3out,NturnsTot,lenWireLayersTot,pfCAvg,NC1wireHeight,NC2wireHeight,NC3wireH
eight,NC1wireLayers,NC2wireLayers,NC3wireLayers,...

areaC1wireElec,areaC2wireElec,areaC3wireElec,NC1turns,NC2turns,NC3turns,lenC1WireLayers,lenC2WireL
ayers,...

lenC3WireLayers,areaC1X,areaC2X,areaC3X,pfC1,pfC2,pfC3,volC1Wire,volC2Wire,volC3Wire,Iwire_safe,ar
eaMag,...
```

```
beta,RC1sol,RC2sol,RC3sol,tauElec,ZC1sol,ZC2sol,ZC3sol,Z3CoilParallel,LC1sol,LC2sol,LC3sol,Zcircui
tTot]...
    =
PhD_SolenoidDesigner(mur,cond1,rad1_in,rad1_out,Npedestals,HeightSinglePed,PercentPedHeightWound,p
fTurn,NC1wireLayers,...
    freq,Rexternal);
% Principal Coil & Input Matlab file ONLY
% (radC1out,radC2out,radC3out)
% Case outputs
prin.Case.AWG = Case.AWG;
prin.Case.coil = Case.coil;
prin.Case.Cres = Case.Cres;
%~~ Solenoid primary overall mechanical geometry ~~%
prin.NC1wireHeight = NC1wireHeight;
prin.NC2wireHeight = NC2wireHeight;
prin.NC3wireHeight = NC3wireHeight;
prin.NC1wireLayers = NC1wireLayers;
prin.NC2wireLayers = NC2wireLayers;
prin.NC3wireLayers = NC3wireLayers;
%~~ Solenoid primary wire geometry ~~%
prin.areaC1wireElec = areaC1wireElec;
prin.areaC2wireElec = areaC2wireElec;
prin.areaC3wireElec = areaC3wireElec;
prin.NC1turns = NC1turns;
prin.NC2turns = NC2turns;
prin.NC3turns = NC3turns;
prin.lenC1WireLayers = lenC1WireLayers;
prin.lenC2WireLayers = lenC2WireLayers;
prin.lenC3WireLayers = lenC3WireLayers;
prin.areaC1X = areaC1X;
prin.areaC2X = areaC2X;
prin.areaC3X = areaC3X;
prin.pfC1 = pfC1;
prin.pfC2 = pfC2;
prin.pfC3 = pfC3;
```

```
prin.volC1Wire = volC1Wire;
prin.volC2Wire = volC2Wire;
prin.volC3Wire = volC3Wire;
%~~ Solenoid primary electrical & magnetic parameters ~~%
prin.Iwire_safe = Iwire_safe;
prin.beta = beta;
% Magnetic areas
prin.areaMagzBS = areaMag;
prin.areaMagzBP = areaMag;
prin.areaMagzAS = areaMag;
prin.areaMagzAP = areaMag;
prin.areaMagyBS = areaMag;
prin.areaMagyBP = areaMag;
prin.areaMagyAS = areaMag;
prin.areaMagyAP = areaMag;
%~~ Solenoid circuit electrical parameters ~~%
prin.RC1sol = RC1sol;
prin.RC2sol = RC2sol;
prin.RC3sol = RC3sol;
prin.LC1sol = LC1sol;
prin.LC2sol = LC2sol;
prin.LC3sol = LC3sol;
prin.tauElec = tauElec;
prin.ZC1sol = ZC1sol;
prin.ZC2sol = ZC2sol;
prin.ZC3sol = ZC3sol;
prin.Z3CoilParallel = Z3CoilParallel;
prin.ZcircuitTot = ZcircuitTot;


%%%%%%%%%%%%%%%%%%%%%%%%%%%%%%%%%%%%%%%%%%%%%%%%%%%%%%%%%%%%%%%%%%%%%%%
% INPUTS: Defining "Control" Solenoid Primary Variables %
%%%%%%%%%%%%%%%%%%%%%%%%%%%%%%%%%%%%%%%%%%%%%%%%%%%%%%%%%%%%%%%%%%%%%%%

% Solenoid material & geometric parameters
```

```
rad1_in = 0*con.in;             %%% Solenoid inside core radius (m)
% rad1_out = 0.8*con.in;        %%% Solenoid outside core radius (m)

% Solenoid mechanical geometry
cntl.zNSol = 1;                 %%% (1) # of z axis principal solenoids
cntl.yNSol = 1;                 %%% (1) # of y axis principal solenoids
Npedestals = 1;                 %%% (1) # of solenoid center core pedestals (m)
HeightSinglePed = 7*con.in;     %%% (7") Solenoid center core pedestal height (m)
PercentPedHeightWound = 100;    %%% (100) Percent of pedestal available wound w/ wire (%)
pfTurn = 1.1;                   %%% (1.1) Estimated packing factor per winding diam. to diam. turn
NC1wireLayers = 24;             %%% (24) # of "Control" coil #1 wire layers
% Solenoid primary source electrical & magnetic parameters
cntl.freq = prin.freq;%60;      %%% Electrical frequency (Hz)
freq = cntl.freq;
cntl.omega_e = 2*pi*cntl.freq;  % Electrical angular frequency (rad/sec)
cntl.Vrms = prin.Vrms;          %%% Primary control solenoid source rms voltage (V)
prin.Rext = 0;                  %%% (0) External resistance [IF present] (ohm)
Rexternal = prin.Rext;

Case.CntlCoil = menu('Is the Control Solenoid Circuit exactly the same as the Principal Solenoid
Circuit','NO','YES');
switch Case.CntlCoil
    case 1
        % RUN THE "SOLENOID DESIGNER" FUNCTION FILE %

[radC1out,radC2out,radC3out,NturnsTot,lenWireLayersTot,pfCAvg,NC1wireHeight,NC2wireHeight,NC3wireH
eight,NC1wireLayers,NC2wireLayers,NC3wireLayers,...

areaC1wireElec,areaC2wireElec,areaC3wireElec,NC1turns,NC2turns,NC3turns,lenC1WireLayers,lenC2WireL
ayers,...

lenC3WireLayers,areaC1X,areaC2X,areaC3X,pfC1,pfC2,pfC3,volC1Wire,volC2Wire,volC3Wire,Iwire_safe,ar
eaMag,...

beta,RC1sol,RC2sol,RC3sol,tauElec,ZC1sol,ZC2sol,ZC3sol,Z3CoilParallel,LC1sol,LC2sol,LC3sol,Zcircui
tTot]...
```

```
            =
PhD_SolenoidDesigner(mur,cond1,rad1_in,rad1_out,Npedestals,HeightSinglePed,PercentPedHeightWound,p
fTurn,NC1wireLayers,...
            freq,Rexternal);
end
% Control Coil ONLY
cntl.NturnsTot = NturnsTot;
cntl.lenWireLayersTot = lenWireLayersTot;
cntl.pfCAvg = pfCAvg;
% Case outputs
cntl.Case.AWG = Case.AWG;
cntl.Case.coil = Case.coil;
cntl.Case.Cres = Case.Cres;
%~~ Solenoid primary overall mechanical geometry ~~%
cntl.NC1wireHeight = NC1wireHeight;
cntl.NC2wireHeight = NC2wireHeight;
cntl.NC3wireHeight = NC3wireHeight;
cntl.NC1wireLayers = NC1wireLayers;
cntl.NC2wireLayers = NC2wireLayers;
cntl.NC3wireLayers = NC3wireLayers;
%~~ Solenoid primary wire geometry ~~%
cntl.areaC1wireElec = areaC1wireElec;
cntl.areaC2wireElec = areaC2wireElec;
cntl.areaC3wireElec = areaC3wireElec;
cntl.NC1turns = NC1turns;
cntl.NC2turns = NC2turns;
cntl.NC3turns = NC3turns;
cntl.lenC1WireLayers = lenC1WireLayers;
cntl.lenC2WireLayers = lenC2WireLayers;
cntl.lenC3WireLayers = lenC3WireLayers;
cntl.areaC1X = areaC1X;
cntl.areaC2X = areaC2X;
cntl.areaC3X = areaC3X;
cntl.pfC1 = pfC1;
cntl.pfC2 = pfC2;
cntl.pfC3 = pfC3;
```

```
cntl.volC1Wire = volC1Wire;
cntl.volC2Wire = volC2Wire;
cntl.volC3Wire = volC3Wire;
%~~ Solenoid primary electrical & magnetic parameters ~~%
cntl.Iwire_safe = Iwire_safe;
cntl.beta = beta;
% Magnetic areas
cntl.areaMagzBS = areaMag;
cntl.areaMagzBP = areaMag;
cntl.areaMagzAS = areaMag;
cntl.areaMagzAP = areaMag;
cntl.areaMagyBS = areaMag;
cntl.areaMagyBP = areaMag;
cntl.areaMagyAS = areaMag;
cntl.areaMagyAP = areaMag;
%~~ Solenoid circuit electrical parameters ~~%
cntl.RC1sol = RC1sol;
cntl.RC2sol = RC2sol;
cntl.RC3sol = RC3sol;
cntl.LC1sol = LC1sol;
cntl.LC2sol = LC2sol;
cntl.LC3sol = LC3sol;
cntl.tauElec = tauElec;
cntl.ZC1sol = ZC1sol;
cntl.ZC2sol = ZC2sol;
cntl.ZC3sol = ZC3sol;
cntl.Z3CoilParallel = Z3CoilParallel;
cntl.ZcircuitTot = ZcircuitTot;

%%%%%%%%%%%%%%%%%%%%%%%%%%%%%%%%%%%%%%%%%%%%%%%%
% Defining Solenoid - Secondary Variables %
%%%%%%%%%%%%%%%%%%%%%%%%%%%%%%%%%%%%%%%%%%%%%%%%

% Secondary - Material & geometric parameters
density2 = density_Cu;          % Secondary material density (kg/m^3)
mu2 = mu0;                      % Permeability of the secondary (H/m)
```

```
cond2 = cond_Cu;                % Secondary conductivity (Siemens/m)
delta = sqrt(2/(prin.omega_e*mu0*cond2));    % Secondary skin depth [Use for secondary thickness]
(m)
height2max = 2*con.in;          % Max. secondary height (m)
c = delta;                      % Secondary height [Set between the skin depth to a max. possible
secondary height value] (m)
if delta > height2max
    c = height2max;             %%% Vary the secondary height (m)
end
height2 = c;                    % Just setting as per model variable name
a = 3.5*36*con.in;              % Secondary length (m)
b = 1/4*a;                      % Secondary width (m)
rad1_out = max([radC1out;radC2out;radC3out]); % Primary outside radius (m)
Asurf = HeightSinglePed*(2*pi*rad1_out) + 2*(pi*rad1_out^2);    % Primary outside surface area
(m^2)
rad2_out = rad1_out;            %%% Secondary outside radius (m)
rad2 = rad2_out;
vol2 = a*b*c;                   % Secondary volume (m^3)
mass2 = density2*vol2;          % Secondary mass of reaction plate (kg)
massVehicleADD = 75;            %%% (75) Additional secondary mass to provide "vehicle support"
mass (kg)
massTot = mass2 + massVehicleADD;   % Total moving system mass (kg)
Fg = con.Ag*massTot;            % Single solenoid secondary weight (N)
Jxx = massTot/12*(b^2 + c^2);   % x axis rotational mass moment of inertia (kg x m^2)
Jyy = massTot/12*(a^2 + c^2);   % x axis rotational mass moment of inertia (kg x m^2)
Jzz = massTot/12*(a^2 + b^2);   % x axis rotational mass moment of inertia (kg x m^2)


%%%%%%%%%%%%%%%%%%%%%%%%%%%%%%%%%%%%%%%%%%%%%%%%%%%%%%%%%%%%%%%%%%%%%%%%%%%%%%%
% INPUTS: Defining Solenoid Secondary & Control Variables %
%%%%%%%%%%%%%%%%%%%%%%%%%%%%%%%%%%%%%%%%%%%%%%%%%%%%%%%%%%%%%%%%%%%%%%%%%%%%%%%

%%% CONTROL SYSTEM INPUT VALUES %%%
zInputCntlHold = 1*con.in;      %%% (1") Controller hold z coordinate distance (m)
yInputCntlHold = 0*con.in;      %%% (0) Controller hold y coordinate distance (m)
```

```
yFGain = 1;                     %%% Set (1) gain. Current (Fz/Fy) force difference is (1160/720) =
1.6
GainKlug = 72;                  %%% (72) Start value: 14.5; Best yet (Phase I): 72
%%% 70 working well for coils w/ 28AWG wire & Cap., BUT oscillations
%%% building & current too high & B too low
tauMechLim = 0.5;               % Mechanical tau plotting limit (sec)

%%% ELECTRICAL INPUT PARAMETERS %%%
%~ Principal - Initial Current ~%
% NOTE:  Assume principal coils never starting from 0, but control coils always do
% and hence they're current has a natural (L/R) electrical time lag.
IPrinInitRe = real(prin.Vrms/prin.ZcircuitTot); %%% Principal primary initial current (A)
IPrinInitIm = imag(prin.Vrms/prin.ZcircuitTot); %%% Principal primary initial current (A)

%%% MECHANICAL INPUT PARAMETERS %%%
% Note: Since the purpose of this sim. is control and not an exact sim. of the system,
%   using a "quick and dirty" method to limit the angles as set here instead of the
%   proper method of setting boundary condition changes with contacts.

%~ Secondary - Material & geometric parameters ~%
rad2_in = rad1_in;              %%% Secondary solenoid reaction area inside radius (m)

%~ Initial Condition Positions ~%
Case.InitCond = menu('Are the COM air gap initial conditions zeroed out or offset?',...
    'Zeroed Out','Offset (Non-Zero Values)');
disp('_____________________________')
% Rotational (NOTE: Rotational Init. Cond. are quite low due to the long a, b, & c side
% dimensions. The program "BLOWS UP" with an error.
% NOTE: Do NOT change the Initial Angle POSITION Conditions. Keep them at
% one. Else an error occurs with the magnetic spring constant with respect to a particular
% air gap distance. This error is due to the initial air gap position inputted into the G3'
% terms, but not accounted for in the solution for each air gap. This is acceptable for
% now, but should be solved later. Input angle changes through angular velocity or external
% forcing function terms.
angleMax = 45*con.deg;          %%% Unrealitically MAX. angle for saturation block use (radians)
```

```
ymax = 2*con.in;                %%% (2) Max. y boundary condition distance b/w primary & secondary
(m)
% NOTE: The (tSteady) option provides a time period for the electomagnetic system to achieve a
steady state
% condition before the secondary vehicle is allowed to move.
tSteady = 0.03;                 %%% (Minimum: 0.025) Time for the electromagnetic system to
achieve steady state
switch Case.InitCond
    case 1  % Zeroed out COM air gap initial conditions
        phiInit = 0*con.deg;            %%% (0) [KEEP AT (0) FOR NOW!] Initial phi angle (radians)
        thetaInit = 0*con.deg;          %%% (0) [KEEP AT (0) FOR NOW!] Initial theta angle
(radians)
        psiInit = 0*con.deg;            %%% (0) [KEEP AT (0) FOR NOW!] Initial psi angle (radians)
        % z Axis Linear
        zinit = zInputCntlHold;         %%% (zInputCntlHold) Initial steady state position of mass
where z = zg (m)
        % y Axis Linear
        yinit = yInputCntlHold;         %%% (yInputCntlHold) Initial steady state position of mass
where z = zg (m)
        % Initial condition velocities
        zVelInit = 0;                   %%% Initial steady state velocity of mass in the z axis
direction (m/sec)
        yVelInit = 0;                   %%% Initial steady state velocity of mass in the z axis
direction (m/sec)
        phiVelInit = 0*con.deg;         %%% (8) Initial phi angular velocity (radians/sec)
        thetaVelInit = 0*con.deg;       %%% (-8) Initial theta angular velocity (radians/sec)
        psiVelInit = 0*con.deg;         %%% (8) Initial psi angular velocity (radians/sec)
        vPropInit = 80;                 %%% (80) Initial steady state velocity of mass in any NON-
z axis direction (m/sec)
    case 2  % Offset (non-zero) COM air gap initial conditions
        phiInit = 0*con.deg;            %%% (0) [KEEP AT (0) FOR NOW!] Initial phi angle (radians)
        thetaInit = 0*con.deg;          %%% (0) [KEEP AT (0) FOR NOW!] Initial theta angle
(radians)
        psiInit = 0*con.deg;            %%% (0) [KEEP AT (0) FOR NOW!] Initial psi angle (radians)
        % z Axis Linear
```

```
        zinit = 1.6*con.in;             %%% (1.7") Initial steady state position of mass where z =
zg (m)
        % y Axis Linear
        yinit = 0.5*con.in;             %%% (0.5") Initial steady state position of mass where z =
zg (m)
        % Initial condition velocities
        zVelInit = 0;                   %%% Initial steady state velocity of mass in the z axis
direction (m/sec)
        yVelInit = 0;                   %%% Initial steady state velocity of mass in the z axis
direction (m/sec)
        phiVelInit = 8*con.deg;         %%% (8) Initial phi angular velocity (radians/sec)
        thetaVelInit = -8*con.deg;      %%% (-8) Initial theta angular velocity (radians/sec)
        psiVelInit = 5*con.deg;         %%% (5) Initial psi angular velocity (radians/sec)
        vPropInit = 80;                 %%% (80) Initial steady state velocity of mass in any NON-
z axis direction (m/sec)
end
%%% z & y axis solenoid reference frame initial condition values - ONLY used for mag. spring
constant inputs
% NOTE: Currently setting values to the desired "Hold" Offset z & y axis positions.
% z axis
zgBSInit = zInputCntlHold;% zinit - b*sin(phiInit)/2 - a*sin(thetaInit)/2;
zgBPInit = zInputCntlHold;% zinit + b*sin(phiInit)/2 - a*sin(thetaInit)/2;
zgASInit = zInputCntlHold;% zinit - b*sin(phiInit)/2 + a*sin(thetaInit)/2;
zgAPInit = zInputCntlHold;% zinit + b*sin(phiInit)/2 + a*sin(thetaInit)/2;
% y axis
ySolRefZero = ymax/2;           % 1/2 Airgap distance used for both setting the optimum y & sol. y
reference positions
yPosMax = ySolRefZero;          % Max. positive y axis position
yNegMax = -ySolRefZero;         % Max. negative y axis position
ygBSInit = ySolRefZero;% yinit + a*sin(psiInit)/2;
ygBPInit = ySolRefZero;% yinit - a*sin(psiInit)/2;
ygASInit = ySolRefZero;% yinit - a*sin(psiInit)/2;
ygAPInit = ySolRefZero;% yinit + a*sin(psiInit)/2;
switch Case.Axes
    case 1  % BOTH z and y axis solenoids are active
        psiAngleMax = angleMax;
```

```
    case 2  % z axis solenoids only active
        psiInit = 0*con.deg;    %%% Initial psi angle (radians)
        psiVelInit = 0*con.deg; %%% Initial psi angular velocity (radians/sec)
        psiAngleMax = realmax;
end

%~ Perturbation Force & Torque Inputs ~%
Case.Pert = menu('Perturbation Force & Torque Inputs:',...
    'OFF (Zeroed out)','STEP (Use w/ NO Control to achieve Nat. Freqs.)',...
    'SINUSOID (DOF Natural Freq. Excitations)','STOCHASTIC');
disp('_____________________________________')

switch Case.Pert
    case {1,4}  % "OFF" Zeroed out Perturbation conditions. Use for Displacement Offsets

        if Case.Pert == 1
            CasePert = sprintf('%s','OFF (Zeroed out)');
        else
            CasePert = sprintf('%s','Stochastic');
        end
        tPert = 0;                      % Perturbation "on" time
        FzPertMag = 0;                  % z axis perturbation force magnitude
        omega_z = 0;
        FyPertMag = 0;                  % y axis perturbation force magnitude
        omega_y = 0;
        TphiPertMag = 0;                % phi axis perturbation torque magnitude
        omega_phi = 0;
        TthetaPertMag = 0;              % theta axis perturbation torque magnitude
        omega_theta = 0;
        TpsiPertMag = 0;                % psi axis perturbation torque magnitude
        omega_psi = 0;
    case 2  % STEP Perturbation conditions active
        CasePert = sprintf('%s','Step');
        tPert = 0.1;                    % Perturbation "on" time
        % z axis
```

```
        FzPertMag = 150*con.lbf;        %%% z axis perturbation force magnitude
        omega_z = 0;
        % y axis
        FyPertMag = 100*con.lbf;        %%% y axis perturbation force magnitude
        omega_y = 0;
        % Rotational axes
        TphiPertMag = 100;
        omega_phi = 0;
        TthetaPertMag = 100;
        omega_theta = 0;
        TpsiPertMag = 100;
        omega_psi = 0;
    case 3  % SINUSOID Perturbation conditions active (Natural Freq. come from STEP response
above)
        CasePert = sprintf('%s','Sinusoid');
        tPert = 0.1;                    % Perturbation "on" time
        % z axis
        FzPertMag = 25*con.lbf;        %%% z axis perturbation force magnitude
        xlambda = 5;                    % x axis guideway cyclic perturbation distance (m)
        (vPropInit/xlambda);            % x axis guideway frequency value (not used) (Hz)
        freq_zNat = 1/(0.930 - 0.515);  % z axis natural frequency for system analyzed (Hz)
        omega_z = 2*pi*(freq_zNat);
        % y axis
        FyPertMag = 25*con.lbf;        %%% y axis perturbation force magnitude
        freq_yNat = 1/(1.412 - 0.571);  % y axis natural frequency for system analyzed (Hz)
        omega_y = 2*pi*(freq_yNat);
        % phi axis
        TphiPertMag = 5;
        freq_phiNat = 1/(0.493 - 0.230);    % phi axis natural frequency for system analyzed (Hz)
        omega_phi = 2*pi*(freq_phiNat);
        % theta axis
        TthetaPertMag = 5;
        freq_thetaNat = 1/(0.492 - 0.230);  % theta axis natural frequency for system analyzed
(Hz)
        omega_theta = 2*pi*(freq_thetaNat);
        % psi axis
```

```
        TpsiPertMag = 10;
        freq_psiNat = 1/(0.535 - 0.246);    % psi axis natural frequency for system analyzed (Hz)
        omega_psi = 2*pi*(freq_psiNat);
end


%%%%%%%%%%%%%%%%%%%%%%%%%%%%%%%%
% Overall Control Parameters %
%%%%%%%%%%%%%%%%%%%%%%%%%%%%%%%%

% Vrms Principal & Control times & voltages
tfall = 0.01;                   % Time for control signal down slope (sec)
thold = 0.25 + tfall;           % Time for control signal down slope & hold (sec)
trise = 0.01 + thold;           % Time for control signal down slope, hold, & up slope (sec)
tpulse1 = 0.5;                  % First control pulse spike time (sec)
tpulse2 = 1.5;                  % 0.035 + (tpulse1+trise);    % Second control pulse spike time
(sec)
Vhold =  0;                     % Vrms for control signal pulse down hold (Vrms)
prin.Case.Wave = menu('Principal Coil Waveform Type','Constant Vrms','Steady Vrms w/ Single Vrms
Down Pulse','Steady Vrms w/ Double Vrms Down Pulse','NO Principal Coil');
switch prin.Case.Wave
    case 1
        CasePrinWaveform = sprintf('%s','Constant Vrms');
        tVrmsCmd = [0 0.001     endTime];
        VrmsCmd =  [0 prin.Vrms prin.Vrms];
        %          tVrmsCmd = [0 endTime];
        %          VrmsCmd =  [prin.Vrms   prin.Vrms];
    case 2
        CasePrinWaveform = sprintf('%s','Steady Vrms w/ Single Vrms Down Pulse');
        % Principal voltage time (sec)
        tVrmsCmd = [0 0.001      tpulse1     (tpulse1+tfall) (tpulse1+thold)  (tpulse1+trise)
endTime];
        % Principal voltage maintained (Vrms)
        VrmsCmd =  [0 prin.Vrms  prin.Vrms   Vhold           Vhold            prin.Vrms
prin.Vrms];
```

```
    case 3
        CasePrinWaveform = sprintf('%s','Steady Vrms w/ Double Vrms Down Pulses');
        % Principal voltage time (sec)
        tVrmsCmd = [0 0.001       tpulse1     (tpulse1+tfall) (tpulse1+thold)  (tpulse1+trise)
tpulse2...
            (tpulse2+tfall) (tpulse2+thold)  (tpulse2+trise) endTime];
        % Principal voltage maintained (Vrms)
        VrmsCmd =  [0 prin.Vrms   prin.Vrms    Vhold           Vhold            prin.Vrms
prin.Vrms...
            Vhold           Vhold             prin.Vrms      prin.Vrms];
    case 4
        CasePrinWaveform = sprintf('%s','NO Principal Coil');
        tVrmsCmd = [0 endTime];     % Principal solenoid control rms voltage (Vrms)
        VrmsCmd =  [0 0];           % Principal solenoid control rms voltage (Vrms)
end

Case.Cntl = menu('Controller Activation Type','No Controller','Fuzzy Control','Neuro-Fuzzy
Adaptive Control');
switch Case.Cntl
    case 1
        CaseCntl = sprintf('%s','No Controller');
    case 2
        CaseCntl = sprintf('%s','Fuzzy');
    case 3
        CaseCntl = sprintf('%s','Neuro-Fuzzy');
end
if Case.Cntl == 1
    tCntlStart = realmax;
else
    Case.CntlTime = menu('Controller Activation Time','Delayed Control Start','Immediate Control
Start');
    switch Case.CntlTime
        case 1  % Delayed Control Start (with separate Principal Solenoid)
            if Case.Pert == 4
                tCntlStart = 2*tpulse1;         % Control hold signal start time (sec)
            else
```

```
                tCntlStart = 3*tpulse1;         % Control hold signal start time (sec)
            end
        case 2  % Immediate Control Start (without separate Principal Solenoid)
            tCntlStart = 0;                 % Control hold signal start time (sec)
    end
end
tCntlStartStr = num2str(tCntlStart);


%%% Training data set used for the Neuro-Fuzzy Controller
NumOscilTrain = 12;                         % Number of damping cycles
kAmp = 500/3-50;                            % Estimate of "k Prin" centroid minus offset from a
regular run
freqNatTrain = 1/(2*pi)*sqrt(kAmp/massTot); % Training oscillation damping freq. (Hz)
omegaNatTrain = 2*pi*freqNatTrain;
TauNatTrain = 1/freqNatTrain;               % Training oscillation damping period, used to help
set (freqNatTrain) eq. (sec)
tTrain = TauNatTrain*NumOscilTrain;         % Time to dampen out the oscillations (sec)
zTrainSlope = -(zinit)/tTrain;
zVelTrain = (4 + 2)*(zinit - zInputCntlHold)/TauNatTrain;   % Rough approx. for max. velocity
(m/sec)
zVelTrainSlope = -(zVelTrain)/tTrain;
% Load up "simout.signals.values"


%-------------------------------------------------------------------------------------%
%%%%%%%%%%%%%%%%%%%%%%
%%                    %%
%% Simulation Start %%
%%                    %%
%%%%%%%%%%%%%%%%%%%%%%

tend=now;                                   % Stop: Timer to show real time computational time
disp(['(Preprocessing Time = ' datestr(tend-tstart,13) ')']);
```

```
set_param('PhD_PhaseIV_Master','simulationcommand','start')   % Simulink file return call
```

C.2.c.ii Matlab Output Function File

```
%%% OUTPUT PLOTS FILE

%%% PhD Dissertation - Phase IV
%%% By: Glenn A. Knierim
%%% Program Started: Spring 2004
%-------------------------------------------------------------------------------------

%%%%%%%%%%%%%%%%%%%%-----------------------------------------------------------------
% POST PROCESSING %
%%%%%%%%%%%%%%%%%%%%



%%%%%%%%%%%%%%%%%%%%%%%%%%%%%%
% Define global parameters %
%%%%%%%%%%%%%%%%%%%%%%%%%%%%%%

% Global simulation structured variable arrays for the principal & control solenoid systems:
(prin) & (cntl)
% Global simulation structured constant setup array: (con)
% Global simulation structured Case setup array: (Case)
global prin cntl con Case



%%%%%%%%%%%%%%%%%%%%%%%%
% POST PROCESSING DATA %
%%%%%%%%%%%%%%%%%%%%%%%%

disp('-=> Start of Postprocessing Data <=-')
tstart=now; % Start: Timer to show real postprocessing time
```

```
%%% Plot Preparation %%%
% Note: Plotting data from Simulink output Structured Arrays w/ Time

%~ Plot Time ~%
% Note: Sim. discritization constant for all plots, so just choosing a time source
time = zMotion.time;


%~ COM Mechanical Position Plots ~%
% z Axis Mechanical Plots
z = zMotion.signals(:,1).values(:,1)./con.in;
zmax = max(z);
zinit = zMotion.signals(:,1).values(:,2)./con.in;
zCntlHold = zMotion.signals(:,1).values(:,3)./con.in;
% Mechanical velocity plots
zVel = zMotion.signals(:,2).values(:,1);
zVelInit = zMotion.signals(:,2).values(:,2);
% Mechanical force plots
FzPrin = zForce.signals(:,1).values(:,1);
Fgravity = zForce.signals(:,1).values(:,2);
FzCntl = zForce.signals(:,2).values(:,1);
FzPert = FTPert.signals(:,1).values(:,1);

% y Axis Mechanical Plots
y = yMotion.signals(:,1).values(:,1)./con.in;
ymax = max(y);
yinit = yMotion.signals(:,1).values(:,2)./con.in;
yCntlHold = yMotion.signals(:,1).values(:,3)./con.in;
yPosMax = yMotion.signals(:,1).values(:,4)./con.in;
yPosMin = yMotion.signals(:,1).values(:,5)./con.in;
% Mechanical velocity plots
yVel = yMotion.signals(:,2).values(:,1);
yVelInit = yMotion.signals(:,2).values(:,2);
% Mechanical force plots
```

```
FyPrin = yForce.signals(:,1).values(:,1);
FyCntl = yForce.signals(:,2).values(:,1);
FyPert = FTPert.signals(:,2).values(:,1);

% Angular Mechanical Plots
phi = AngleMotion.signals(:,1).values(:,1);
phimax = max(phi);
theta = AngleMotion.signals(:,2).values(:,1);
psi = AngleMotion.signals(:,3).values(:,1);
% Angular Perturbation Force Plots
TphiPert = FTPert.signals(:,3).values(:,1);
TthetaPert = FTPert.signals(:,3).values(:,2);
TpsiPert = FTPert.signals(:,3).values(:,3);


%~ Solenoid Mechanical Position Plots ~%
% zgBS Mechanical Plots
zgBS = BSMotion.signals(:,1).values(:,1)./con.in;
zgBSmax = max(zgBS);
zgBSRef = BSMotion.signals(:,1).values(:,2)./con.in;
zgBSCntlHold = BSMotion.signals(:,1).values(:,3)./con.in;
% Mechanical force plots
FzBSPrin = BSMotion.signals(:,2).values(:,1);
FzBSCntl = BSMotion.signals(:,2).values(:,2);
% ygBS Mechanical Plots
ygBS = BSMotion.signals(:,3).values(:,1)./con.in;
ygBSRef = BSMotion.signals(:,3).values(:,2)./con.in;
ygBSCntlHold = BSMotion.signals(:,3).values(:,3)./con.in;
% Mechanical force plots
FyBSPrin = BSMotion.signals(:,4).values(:,1);
FyBSCntl = BSMotion.signals(:,4).values(:,2);

% zgBP Mechanical Plots
zgBP = BPMotion.signals(:,1).values(:,1)./con.in;
zgBPmax = max(zgBP);
```

```
zgBPRef = BPMotion.signals(:,1).values(:,2)./con.in;
zgBPCntlHold = BPMotion.signals(:,1).values(:,3)./con.in;
% Mechanical force plots
FzBPPrin = BPMotion.signals(:,2).values(:,1);
FzBPCntl = BPMotion.signals(:,2).values(:,2);
% ygBS Mechanical Plots
ygBP = BPMotion.signals(:,3).values(:,1)./con.in;
ygBPRef = BPMotion.signals(:,3).values(:,2)./con.in;
ygBPCntlHold = BPMotion.signals(:,3).values(:,3)./con.in;
% Mechanical force plots
FyBPPrin = BPMotion.signals(:,4).values(:,1);
FyBPCntl = BPMotion.signals(:,4).values(:,2);

% zgAS Mechanical Plots
zgAS = ASMotion.signals(:,1).values(:,1)./con.in;
zgASmax = max(zgAS);
zgASRef = ASMotion.signals(:,1).values(:,2)./con.in;
zgASCntlHold = ASMotion.signals(:,1).values(:,3)./con.in;
% Mechanical force plots
FzASPrin = ASMotion.signals(:,2).values(:,1);
FzASCntl = ASMotion.signals(:,2).values(:,2);
% ygBS Mechanical Plots
ygAS = ASMotion.signals(:,3).values(:,1)./con.in;
ygASRef = ASMotion.signals(:,3).values(:,2)./con.in;
ygASCntlHold = ASMotion.signals(:,3).values(:,3)./con.in;
% Mechanical force plots
FyASPrin = ASMotion.signals(:,4).values(:,1);
FyASCntl = ASMotion.signals(:,4).values(:,2);

% zgAP Mechanical Plots
zgAP = APMotion.signals(:,1).values(:,1)./con.in;
zgAPmax = max(zgAP);
zgAPRef = APMotion.signals(:,1).values(:,2)./con.in;
zgAPCntlHold = APMotion.signals(:,1).values(:,3)./con.in;
% Mechanical force plots
FzAPPrin = APMotion.signals(:,2).values(:,1);
```

```
FzAPCntl = APMotion.signals(:,2).values(:,2);
% ygBP Mechanical Plots
ygAP = APMotion.signals(:,3).values(:,1)./con.in;
ygAPRef = APMotion.signals(:,3).values(:,2)./con.in;
ygAPCntlHold = APMotion.signals(:,3).values(:,3)./con.in;
% Mechanical force plots
FyAPPrin = APMotion.signals(:,4).values(:,1);
FyAPCntl = APMotion.signals(:,4).values(:,2);


%~ Secondary Power & Energy Plots ~%
% z Axis Seconary energy plots
EkzPrin = zPowerEnergy.signals(:,1).values(:,1);
EkzCntl = zPowerEnergy.signals(:,1).values(:,2);
EzKE = zPowerEnergy.signals(:,1).values(:,3);
EzPE = zPowerEnergy.signals(:,1).values(:,4);
EzPEMax = max(EzPE);
% z Axis Seconary power plots
PzPrin = zPowerEnergy.signals(:,2).values(:,1);
PzCntl = zPowerEnergy.signals(:,2).values(:,2);
PzPert = zPowerEnergy.signals(:,2).values(:,3);
% y Axis Seconary energy plots
EkyPrin = yPowerEnergy.signals(:,1).values(:,1);
EkyCntl = yPowerEnergy.signals(:,1).values(:,2);
EyKE = yPowerEnergy.signals(:,1).values(:,3);
% y Axis Seconary power plots
PyPrin = yPowerEnergy.signals(:,2).values(:,1);
PyCntl = yPowerEnergy.signals(:,2).values(:,2);
PyPert = yPowerEnergy.signals(:,2).values(:,3);


%~ System Response Plots ~%
% z Axis Tau plots
tauzMech = zkCOM.signals(:,1).values(:,1);
tauzEPrin = zkCOM.signals(:,2).values(:,1);
```

```
tauzEPrinMax = max(tauzEPrin);
tauzECntl = zkCOM.signals(:,2).values(:,2);
% z Axis Magnetic spring constant & mechanical natural frequency plots
kzPrin = zkCOM.signals(:,3).values(:,1);
kzCntl = zkCOM.signals(:,3).values(:,2);
kzMechNatFreq = zkCOM.signals(:,4).values(:,1);
% y Axis Tau plots
tauyMech = ykCOM.signals(:,1).values(:,1);
tauyEPrin = ykCOM.signals(:,2).values(:,1);
tauyEPrinMax = max(tauyEPrin);
tauyECntl = ykCOM.signals(:,2).values(:,2);
% y Axis Magnetic spring constant & mechanical natural frequency plots
kyPrin = ykCOM.signals(:,3).values(:,1);
kyCntl = ykCOM.signals(:,3).values(:,2);
kyMechNatFreq = ykCOM.signals(:,4).values(:,1);


%~ Electrical Plots - BS Solenoid ONLY ~%
% z & y Axis Voltages
VBSPrinCmdRMS = zBSVICntl.signals(:,1).values(:,2);
VBSPrinCmdMaxRMS = max(VBSPrinCmdRMS);
VBSzCntlCmdRMS = zBSVICntl.signals(:,1).values(:,4);
VBSyCntlCmdRMS = yBSVICntl.signals(:,1).values(:,4);
% z Axis Currents
IBSzPrinRMS = zBSVICntl.signals(:,2).values(:,1);
IBSzCntlRMS = zBSVICntl.signals(:,2).values(:,2);
FlagBSzVrmsONCntl = zBSVICntl.signals(:,2).values(:,3);
IBSzC1CntlRMS = zBSVICntl.signals(:,3).values(:,2);
ICntlWireSafe = zBSVICntl.signals(:,3).values(:,5);
% y Axis Currents
IBSyPrinRMS = yBSVICntl.signals(:,2).values(:,1);
IBSyCntlRMS = yBSVICntl.signals(:,2).values(:,2);
FlagBSyVrmsONCntl = yBSVICntl.signals(:,2).values(:,3);
IBSyC1CntlRMS = yBSVICntl.signals(:,3).values(:,2);
ICntlWireSafe = yBSVICntl.signals(:,3).values(:,5);
```

```
%~ Magnetic Plots - BS Solenoid ONLY ~%
% z Axis
BtBSzPrinPeak = zBSMag.signals(:,1).values(:,2);
BtBSzPrinMaxPeak = max(BtBSzPrinPeak);
BtBSzCntlPeak = zBSMag.signals(:,2).values(:,2);
for i = 1:length(BtBSzPrinPeak)
    BsatLimit(i) = Bsat;
end
% y Axis
BtBSyPrinPeak = yBSMag.signals(:,1).values(:,2);
BtBSyCntlPeak = yBSMag.signals(:,2).values(:,2);


%~ Thermal Plots ~%
% z Axis System thermal energy
QzPrinRMSTot = zTherm.signals(:,1).values(:,1);
QzPrinRMSTotMax = max(QzPrinRMSTot);
QzCntlRMSTot = zTherm.signals(:,1).values(:,5);
% z Axis System temperatures - Coil #1 ONLY
TempC1zPrinWire = zTherm.signals(:,3).values(:,1);
TempC1zCntlWire = zTherm.signals(:,3).values(:,4);
% y Axis System thermal energy
QyPrinRMSTot = yTherm.signals(:,1).values(:,1);
QyPrinRMSTotMax = max(QyPrinRMSTot);
QyCntlRMSTot = yTherm.signals(:,1).values(:,5);
% y Axis System temperatures - Coil #1 ONLY
TempC1yPrinWire = yTherm.signals(:,3).values(:,1);
TempC1yCntlWire = yTherm.signals(:,3).values(:,4);


%%%%%%%%%%%%%%%%%%%%%%%%%
% POST PROCESSING PLOTS %
%%%%%%%%%%%%%%%%%%%%%%%%%
```

```
% Output Setup
figure(1); delete(1);
figure(2); delete(2);
figure(3); delete(3);
figure(4); delete(4);
figure(5); delete(5);
figure(6); delete(6);
figure(7); delete(7);
figure(8); delete(8);
figure(9); delete(9);
figure(10); delete(10);


%%%%%%%%%%%%%%%%%%%%%%%%%%%%%%%%%%%%
%~ Fuzzy & Neuro-Fuzzy Logic Plots ~%

switch Case.Cntl
    case 2  % Fuzzy logic controller plot commands
        a = readfis('PhD_PhaseIV_FuzzyCntl.fis');
        getfis(a);

        figure(1)
        plotfis(a);
        title(['\bf',CaseCntl,' Logic Control - ',CaseCntl,' Inference System Structure'],
'FontSize',15);
        set(gca, 'FontSize',11, 'FontWeight','bold')

        figure(2)
        gensurf(a,[1 2],1,[100 100])
        grid on
        colorbar
        title(['\bf',CaseCntl,' Logic Control - ',CaseCntl,' Inference System Structure'],
'FontSize',15);
        set(gca, 'FontSize',11, 'FontWeight','bold')
```

```
        xlabel({'\bfSecondary z Axis';['Reference Ratio'];['[Variable Name: zRefRatio]']},
'FontSize',12,...
            'HorizontalAlignment','center');
        ylabel({'\bfSecondary z Axis';['Velocity (m/sec)'];['[Variable Name: z2=Velocity]']},
'FontSize',12,...
            'HorizontalAlignment','center');
        zlabel({'\bfControl Voltage (Vrms)';['[Variable Name: VCntlRMS]']}, 'FontSize',12,...
            'HorizontalAlignment','center');
        zlim([0 prin.Vrms]);

        figure(3)
        plotmf(a,'input',1);
        grid on
        title(['\bf',CaseCntl,' Logic Control - Input Membership Function'], 'FontSize',15);
        set(gca, 'FontSize',11, 'FontWeight','bold')

        figure(4)
        plotmf(a,'input',2);
        grid on
        title(['\bf',CaseCntl,' Logic Control - Input Membership Function'], 'FontSize',15);
        set(gca, 'FontSize',11, 'FontWeight','bold')

        figure(5)
        plotmf(a,'output',1);
        grid on
        title(['\bf',CaseCntl,' Logic Control - Output Membership Function'], 'FontSize',15);
        set(gca, 'FontSize',11, 'FontWeight','bold')

    case 3  % Neuro-Fuzzy logic controller plot commands
        a = readfis('PhD_PhaseIV_NeuroFuzzyCntl.fis');
        getfis(a);

        figure(1)
        plotfis(a);
```

```
        title(['\bf',CaseCntl,' Logic Control - ',CaseCntl,' Inference System Structure'],
'FontSize',15);
        set(gca, 'FontSize',11, 'FontWeight','bold')

        figure(2)
        gensurf(a,[1 2],1,[100 100])
        grid on
        colorbar
        title(['\bf',CaseCntl,' Logic Control - ',CaseCntl,' Inference System Structure'],
'FontSize',15);
        set(gca, 'FontSize',11, 'FontWeight','bold')
        xlabel({'\bfSecondary z Axis';['Reference Ratio'];['[Variable Name: zRefRatio]']},
'FontSize',12,...
            'HorizontalAlignment','center');
        ylabel({'\bfSecondary z Axis';['Velocity (m/sec)'];['[Variable Name: z2=Velocity]']},
'FontSize',12,...
            'HorizontalAlignment','center');
        zlabel({'\bfControl Voltage (Vrms)';['[Variable Name: VCntlRMS]']}, 'FontSize',12,...
            'HorizontalAlignment','center');
        zlim([0 prin.Vrms]);

        figure(3)
        plotmf(a,'input',1);
        grid on
        title(['\bf',CaseCntl,' Logic Control - Input Membership Function'], 'FontSize',15);
        set(gca, 'FontSize',11, 'FontWeight','bold')

        figure(4)
        plotmf(a,'input',2);
        grid on
        title(['\bf',CaseCntl,' Logic Control - Input Membership Function'], 'FontSize',15);
        set(gca, 'FontSize',11, 'FontWeight','bold')

        figure(5)
        plotmf(a,'output',1);
```

```
        grid on
        title(['\bf',CaseCntl,' Logic Control - Output Membership Function'], 'FontSize',15);
        set(gca, 'FontSize',11, 'FontWeight','bold')
end


%%%%%%%%%%%%%%%%%%%%%%%%
%~ Mechanical Plots ~%

%~ z Axis Mechanical Plots ~%
% Mechanical position plot
figure(6)
subplot(3,1,1)
clear Legend_Labels;
P=plot(time, [z, zinit, zCntlHold],'linewidth',2.8);
set(gca, 'FontSize',11, 'FontWeight','bold')
set(P(1), 'Color', 'k');
set(P(2), 'Color', 'm', 'LineStyle','-.');
set(P(3), 'Color', 'r', 'LineStyle','--');
Legend_Labels{1}='\bfz';
Legend_Labels{2}='\bfInitial z';
Legend_Labels{3}='\bfz Control Hold';
[legend_handle,object_handles] = legend(P,Legend_Labels,0);
set(findobj(object_handles, 'Type', 'text'), 'FontSize',10);
ylabel(['\bfz Axis Position (in)'], 'FontSize',14);
if Case.Cntl ~= 1
    T = text(tCntlStart,0.95*zmax,['\bfControl Start time: ', tCntlStartStr,' sec']);
    set(findobj(T, 'Type', 'text'), 'FontSize',12);
end
title({'\bfCenter of Mass z Axis Mechanical';['Principal Solenoid: ',CasePrinWaveform,';  Control
Type: ',...
    CaseCntl,';  Perturbation Type: ',CasePert]}, 'FontSize',15);
grid on

% Mechanical velocity plot
```

```
subplot(3,1,2)
clear Legend_Labels;
P=plot(time, [zVel, zVelInit],'linewidth',2.8);
set(gca, 'FontSize',11, 'FontWeight','bold')
set(P(1), 'Color', 'k');
set(P(2), 'Color', 'm', 'LineStyle','--');
Legend_Labels{1}='\bfz Velocity';
Legend_Labels{2}='\bfInitial z Velocity';
[legend_handle,object_handles] = legend(P,Legend_Labels,0);
set(findobj(object_handles, 'Type', 'text'), 'FontSize',10);
ylabel(['\bfz Axis Velocity (m/sec)'], 'FontSize',14);
grid on

% Mechanical force plot
subplot(3,1,3)
clear Legend_Labels;
P=plot(time, [FzPrin, FzPert, FzCntl, Fgravity],'linewidth',2.8);
set(gca, 'FontSize',11, 'FontWeight','bold')
set(P(1), 'Color', 'g');
set(P(2), 'Color', 'm', 'linewidth',3.4);
set(P(3), 'Color', 'b','linewidth',3);
set(P(4), 'Color', 'r', 'LineStyle','--', 'linewidth',3);
Legend_Labels{1}='\bfTotal Principal';
Legend_Labels{2}='\bfPerturbation';
Legend_Labels{3}='\bfTotal Control';
Legend_Labels{4}='\bfGravity';
[legend_handle,object_handles] = legend(P,Legend_Labels,0);
set(findobj(object_handles, 'Type', 'text'), 'FontSize',10);
ylabel(['\bfz Axis Force (N)'], 'FontSize',14);
xlabel(['\bfTime (sec)'], 'FontSize',14);
grid on

%~ y Axis Mechanical Plots ~%
% Mechanical position plot
figure(7)
subplot(3,1,1)
```

```
clear Legend_Labels;
P=plot(time, [y, yinit, yCntlHold, yPosMax, yPosMin],'linewidth',2.8);
set(gca, 'FontSize',11, 'FontWeight','bold')
set(P(1), 'Color', 'k');
set(P(2), 'Color', 'm', 'LineStyle','--');
set(P(3), 'Color', 'r', 'LineStyle','-.');
set([P(4) P(5)], 'Color', 'b', 'LineStyle',':', 'linewidth',3.5);
Legend_Labels{1}='\bfy';
Legend_Labels{2}='\bfInitial y';
Legend_Labels{3}='\bfy Control Hold';
Legend_Labels{4}='\bfy Maximum';
Legend_Labels{5}='\bfy Minimum';
[legend_handle,object_handles] = legend(P,Legend_Labels,0);
set(findobj(object_handles, 'Type', 'text'), 'FontSize',10);
ylabel(['\bfy Axis Position (in)'], 'FontSize',14);
if Case.Cntl ~= 1
    T = text(tCntlStart,1.25*ymax,['\bfControl Start time: ', tCntlStartStr,' sec']);
    set(findobj(T, 'Type', 'text'), 'FontSize',12);
end
title({'\bfCenter of Mass y Axis Mechanical';['Principal Solenoid: ',CasePrinWaveform,';  Control
Type: ',...
    CaseCntl,';  Perturbation Type: ',CasePert]}, 'FontSize',15);
grid on

% Mechanical velocity plot
subplot(3,1,2)
clear Legend_Labels;
P=plot(time, [yVel, yVelInit],'linewidth',2.8);
set(gca, 'FontSize',11, 'FontWeight','bold')
set(P(1), 'Color', 'k');
set(P(2), 'Color', 'm', 'LineStyle','--');
Legend_Labels{1}='\bfy Velocity';
Legend_Labels{2}='\bfInitial y Velocity';
[legend_handle,object_handles] = legend(P,Legend_Labels,0);
set(findobj(object_handles, 'Type', 'text'), 'FontSize',10);
ylabel(['\bfy Axis Velocity (m/sec)'], 'FontSize',14);
```

```
grid on

% Mechanical force plot
subplot(3,1,3)
clear Legend_Labels;
P=plot(time, [FyPrin, FyPert, FyCntl],'linewidth',2.8);
set(gca, 'FontSize',11, 'FontWeight','bold')
set(P(1), 'Color', 'g');
set(P(2), 'Color', 'm', 'linewidth',3.4);
set(P(3), 'Color', 'b', 'linewidth',3);
Legend_Labels{1}='\bfTotal Principal';
Legend_Labels{2}='\bfPertubation';
Legend_Labels{3}='\bfTotal Control';
[legend_handle,object_handles] = legend(P,Legend_Labels,0);
set(findobj(object_handles, 'Type', 'text'), 'FontSize',10);
ylabel(['\bfy Axis Force (N)'], 'FontSize',14);
xlabel(['\bfTime (sec)'], 'FontSize',14);
grid on


%~ Angular Mechanical Plots ~%
% Angular position plot
figure(8)
subplot(2,1,1)
clear Legend_Labels;
P=plot(time, [phi, theta, psi],'linewidth',2.8);
set(gca, 'FontSize',11, 'FontWeight','bold')
set(P(1), 'Color', 'k');
set(P(2), 'Color', 'b');
set(P(3), 'Color', 'm');
Legend_Labels{1}='\bfPhi (Pitch)';
Legend_Labels{2}='\bfTheta (Roll)';
Legend_Labels{3}='\bfPsi (Yaw)';
[legend_handle,object_handles] = legend(P,Legend_Labels,0);
set(findobj(object_handles, 'Type', 'text'), 'FontSize',10);
```

```
ylabel(['\bfAngular Position (deg)'], 'FontSize',14);
if Case.Cntl ~= 1
    T = text(tCntlStart,0.95*phimax,['\bfControl Start time: ', tCntlStartStr,' sec']);
    set(findobj(T, 'Type', 'text'), 'FontSize',12);
end
title({'\bfCenter of Mass Angular Mechanical';['Principal Solenoid: ',CasePrinWaveform,';  Control
Type: ',...
    CaseCntl,';  Perturbation Type: ',CasePert]}, 'FontSize',15);
grid on

% Angular perturbation torque plot
subplot(2,1,2)
clear Legend_Labels;
P=plot(time, [TphiPert, TthetaPert, TpsiPert],'linewidth',2.8);
set(gca, 'FontSize',11, 'FontWeight','bold')
set(P(1), 'Color', 'k');
set(P(2), 'Color', 'b');
set(P(3), 'Color', 'm');
Legend_Labels{1}='\bfPhi (Pitch)';
Legend_Labels{2}='\bfTheta (Roll)';
Legend_Labels{3}='\bfPsi (Yaw)';
[legend_handle,object_handles] = legend(P,Legend_Labels,0);
set(findobj(object_handles, 'Type', 'text'), 'FontSize',10);
ylabel(['\bfAngular Perturbation Torque (N\bulletm)'], 'FontSize',14);
xlabel(['\bfTime (sec)'], 'FontSize',14);
grid on


%~ BS Air Gap Mechanical Plots ~%
% z Axis Mechanical position plot
figure(9)
subplot(4,1,1)
clear Legend_Labels;
P=plot(time, [zgBS, zgBSRef, zgBSCntlHold],'linewidth',2.8);
set(gca, 'FontSize',11, 'FontWeight','bold')
```

```
set(P(1), 'Color', 'k');
set(P(2), 'Color', 'm');
set(P(3), 'Color', 'r', 'LineStyle','--');
Legend_Labels{1}='\bfPosition';
Legend_Labels{2}='\bfReference';
Legend_Labels{3}='\bfControl Hold';
[legend_handle,object_handles] = legend(P,Legend_Labels,0);
set(findobj(object_handles, 'Type', 'text'), 'FontSize',10);
ylabel(['\bfz Axis Position (in)'], 'FontSize',14);
if Case.Cntl ~= 1
    T = text(tCntlStart,1.05*zgBSmax,['\bfControl Start time: ', tCntlStartStr,' sec']);
    set(findobj(T, 'Type', 'text'), 'FontSize',12);
end
title({'\bfSolenoid BS Mechanical';['Principal Solenoid: ',CasePrinWaveform,';  Control Type:
',...
    CaseCntl,';  Perturbation Type: ',CasePert]}, 'FontSize',15);
grid on

% z Axis mechanical force plot
subplot(4,1,2)
clear Legend_Labels;
P=plot(time, [FzBSPrin, FzBSCntl],'linewidth',2.8);
set(gca, 'FontSize',11, 'FontWeight','bold')
set(P(1), 'Color', 'b');
set(P(2), 'Color', 'g');
Legend_Labels{1}='\bfPrincipal';
Legend_Labels{2}='\bfControl';
[legend_handle,object_handles] = legend(P,Legend_Labels,0);
set(findobj(object_handles, 'Type', 'text'), 'FontSize',10);
ylabel(['\bfz Axis Force (N)'], 'FontSize',14);
grid on

% y Axis Mechanical position plot
subplot(4,1,3)
clear Legend_Labels;
P=plot(time, [ygBS, ygBSRef, ygBSCntlHold],'linewidth',2.8);
```

```
set(gca, 'FontSize',11, 'FontWeight','bold')
set(P(1), 'Color', 'k');
set(P(2), 'Color', 'm');
set(P(3), 'Color', 'r', 'LineStyle','--');
Legend_Labels{1}='\bfPosition';
Legend_Labels{2}='\bfReference';
Legend_Labels{3}='\bfControl Hold';
[legend_handle,object_handles] = legend(P,Legend_Labels,0);
set(findobj(object_handles, 'Type', 'text'), 'FontSize',10);
ylabel(['\bfy Axis Position (in)'], 'FontSize',14);
set(findobj(T, 'Type', 'text'), 'FontSize',12);
grid on

% y Axis mechanical force plot
subplot(4,1,4)
clear Legend_Labels;
P=plot(time, [FyBSPrin, FyBSCntl],'linewidth',2.8);
set(gca, 'FontSize',11, 'FontWeight','bold')
set(P(1), 'Color', 'b');
set(P(2), 'Color', 'g');
Legend_Labels{1}='\bfPrincipal';
Legend_Labels{2}='\bfControl';
[legend_handle,object_handles] = legend(P,Legend_Labels,0);
set(findobj(object_handles, 'Type', 'text'), 'FontSize',10);
ylabel(['\bfy Axis Force (N)'], 'FontSize',14);
xlabel(['\bfTime (sec)'], 'FontSize',14);
grid on


%~ BP Air Gap Mechanical Plots ~%
% z Axis Mechanical position plot
figure(10)
subplot(4,1,1)
clear Legend_Labels;
P=plot(time, [zgBP, zgBPRef, zgBPCntlHold],'linewidth',2.8);
```

```
set(gca, 'FontSize',11, 'FontWeight','bold')
set(P(1), 'Color', 'k');
set(P(2), 'Color', 'm');
set(P(3), 'Color', 'r', 'LineStyle','--');
Legend_Labels{1}='\bfPosition';
Legend_Labels{2}='\bfReference';
Legend_Labels{3}='\bfControl Hold';
[legend_handle,object_handles] = legend(P,Legend_Labels,0);
set(findobj(object_handles, 'Type', 'text'), 'FontSize',10);
ylabel(['\bfz Axis Position (in)'], 'FontSize',14);
if Case.Cntl ~= 1
    T = text(tCntlStart,1.05*zgBPmax,['\bfControl Start time: ', tCntlStartStr,' sec']);
    set(findobj(T, 'Type', 'text'), 'FontSize',12);
end
title({'\bfSolenoid BP Mechanical';['Principal Solenoid: ',CasePrinWaveform,';  Control Type:
',...
    CaseCntl,';  Perturbation Type: ',CasePert]}, 'FontSize',15);
grid on

% z Axis mechanical force plot
subplot(4,1,2)
clear Legend_Labels;
P=plot(time, [FzBPPrin, FzBPCntl],'linewidth',2.8);
set(gca, 'FontSize',11, 'FontWeight','bold')
set(P(1), 'Color', 'b');
set(P(2), 'Color', 'g');
Legend_Labels{1}='\bfPrincipal';
Legend_Labels{2}='\bfControl';
[legend_handle,object_handles] = legend(P,Legend_Labels,0);
set(findobj(object_handles, 'Type', 'text'), 'FontSize',10);
ylabel(['\bfz Axis Force (N)'], 'FontSize',14);
grid on

% y Axis Mechanical position plot
subplot(4,1,3)
clear Legend_Labels;
```

```
P=plot(time, [ygBP, ygBPRef, ygBPCntlHold],'linewidth',2.8);
set(gca, 'FontSize',11, 'FontWeight','bold')
set(P(1), 'Color', 'k');
set(P(2), 'Color', 'm');
set(P(3), 'Color', 'r', 'LineStyle','--');
Legend_Labels{1}='\bfPosition';
Legend_Labels{2}='\bfReference';
Legend_Labels{3}='\bfControl Hold';
[legend_handle,object_handles] = legend(P,Legend_Labels,0);
set(findobj(object_handles, 'Type', 'text'), 'FontSize',10);
ylabel(['\bfy Axis Position (in)'], 'FontSize',14);
set(findobj(T, 'Type', 'text'), 'FontSize',12);
grid on

% y Axis mechanical force plot
subplot(4,1,4)
clear Legend_Labels;
P=plot(time, [FyBPPrin, FyBPCntl],'linewidth',2.8);
set(gca, 'FontSize',11, 'FontWeight','bold')
set(P(1), 'Color', 'b');
set(P(2), 'Color', 'g');
Legend_Labels{1}='\bfPrincipal';
Legend_Labels{2}='\bfControl';
[legend_handle,object_handles] = legend(P,Legend_Labels,0);
set(findobj(object_handles, 'Type', 'text'), 'FontSize',10);
ylabel(['\bfy Axis Force (N)'], 'FontSize',14);
xlabel(['\bfTime (sec)'], 'FontSize',14);
grid on


%~ AS Air Gap Mechanical Plots ~%
% z Axis Mechanical position plot
figure(11)
subplot(4,1,1)
clear Legend_Labels;
```

```
P=plot(time, [zgAS, zgASRef, zgASCntlHold],'linewidth',2.8);
set(gca, 'FontSize',11, 'FontWeight','bold')
set(P(1), 'Color', 'k');
set(P(2), 'Color', 'm');
set(P(3), 'Color', 'r', 'LineStyle','--');
Legend_Labels{1}='\bfPosition';
Legend_Labels{2}='\bfReference';
Legend_Labels{3}='\bfControl Hold';
[legend_handle,object_handles] = legend(P,Legend_Labels,0);
set(findobj(object_handles, 'Type', 'text'), 'FontSize',10);
ylabel(['\bfz Axis Position (in)'], 'FontSize',14);
if Case.Cntl ~= 1
    T = text(tCntlStart,1.05*zgASmax,['\bfControl Start time: ', tCntlStartStr,' sec']);
    set(findobj(T, 'Type', 'text'), 'FontSize',12);
end
title({'\bfSolenoid AS Mechanical';['Principal Solenoid: ',CasePrinWaveform,';  Control Type:
',...
    CaseCntl,';  Perturbation Type: ',CasePert]}, 'FontSize',15);
grid on

% z Axis mechanical force plot
subplot(4,1,2)
clear Legend_Labels;
P=plot(time, [FzASPrin, FzASCntl],'linewidth',2.8);
set(gca, 'FontSize',11, 'FontWeight','bold')
set(P(1), 'Color', 'b');
set(P(2), 'Color', 'g');
Legend_Labels{1}='\bfPrincipal';
Legend_Labels{2}='\bfControl';
[legend_handle,object_handles] = legend(P,Legend_Labels,0);
set(findobj(object_handles, 'Type', 'text'), 'FontSize',10);
ylabel(['\bfz Axis Force (N)'], 'FontSize',14);
grid on

% y Axis Mechanical position plot
subplot(4,1,3)
```

```
clear Legend_Labels;
P=plot(time, [ygAS, ygASRef, ygASCntlHold],'linewidth',2.8);
set(gca, 'FontSize',11, 'FontWeight','bold')
set(P(1), 'Color', 'k');
set(P(2), 'Color', 'm');
set(P(3), 'Color', 'r', 'LineStyle','--');
Legend_Labels{1}='\bfPosition';
Legend_Labels{2}='\bfReference';
Legend_Labels{3}='\bfControl Hold';
[legend_handle,object_handles] = legend(P,Legend_Labels,0);
set(findobj(object_handles, 'Type', 'text'), 'FontSize',10);
ylabel(['\bfy Axis Position (in)'], 'FontSize',14);
set(findobj(T, 'Type', 'text'), 'FontSize',12);
grid on

% y Axis mechanical force plot
subplot(4,1,4)
clear Legend_Labels;
P=plot(time, [FyASPrin, FyASCntl],'linewidth',2.8);
set(gca, 'FontSize',11, 'FontWeight','bold')
set(P(1), 'Color', 'b');
set(P(2), 'Color', 'g');
Legend_Labels{1}='\bfPrincipal';
Legend_Labels{2}='\bfControl';
[legend_handle,object_handles] = legend(P,Legend_Labels,0);
set(findobj(object_handles, 'Type', 'text'), 'FontSize',10);
ylabel(['\bfy Axis Force (N)'], 'FontSize',14);
xlabel(['\bfTime (sec)'], 'FontSize',14);
grid on


%~ AP Air Gap Mechanical Plots ~%
% z Axis Mechanical position plot
figure(12)
subplot(4,1,1)
```

```
clear Legend_Labels;
P=plot(time, [zgAP, zgAPRef, zgAPCntlHold],'linewidth',2.8);
set(gca, 'FontSize',11, 'FontWeight','bold')
set(P(1), 'Color', 'k');
set(P(2), 'Color', 'm');
set(P(3), 'Color', 'r', 'LineStyle','--');
Legend_Labels{1}='\bfPosition';
Legend_Labels{2}='\bfReference';
Legend_Labels{3}='\bfControl Hold';
[legend_handle,object_handles] = legend(P,Legend_Labels,0);
set(findobj(object_handles, 'Type', 'text'), 'FontSize',10);
ylabel(['\bfz Axis Position (in)'], 'FontSize',14);
if Case.Cntl ~= 1
    T = text(tCntlStart,1.05*zgAPmax,['\bfControl Start time: ', tCntlStartStr,' sec']);
    set(findobj(T, 'Type', 'text'), 'FontSize',12);
end
title({'\bfSolenoid AP Mechanical';['Principal Solenoid: ',CasePrinWaveform,';  Control Type:
',...
    CaseCntl,';  Perturbation Type: ',CasePert]}, 'FontSize',15);
grid on

% z Axis mechanical force plot
subplot(4,1,2)
clear Legend_Labels;
P=plot(time, [FzAPPrin, FzAPCntl],'linewidth',2.8);
set(gca, 'FontSize',11, 'FontWeight','bold')
set(P(1), 'Color', 'b');
set(P(2), 'Color', 'g');
Legend_Labels{1}='\bfPrincipal';
Legend_Labels{2}='\bfControl';
[legend_handle,object_handles] = legend(P,Legend_Labels,0);
set(findobj(object_handles, 'Type', 'text'), 'FontSize',10);
ylabel(['\bfz Axis Force (N)'], 'FontSize',14);
grid on

% y Axis Mechanical position plot
```

```
subplot(4,1,3)
clear Legend_Labels;
P=plot(time, [ygAP, ygAPRef, ygAPCntlHold],'linewidth',2.8);
set(gca, 'FontSize',11, 'FontWeight','bold')
set(P(1), 'Color', 'k');
set(P(2), 'Color', 'm');
set(P(3), 'Color', 'r', 'LineStyle','--');
Legend_Labels{1}='\bfPosition';
Legend_Labels{2}='\bfReference';
Legend_Labels{3}='\bfControl Hold';
[legend_handle,object_handles] = legend(P,Legend_Labels,0);
set(findobj(object_handles, 'Type', 'text'), 'FontSize',10);
ylabel(['\bfy Axis Position (in)'], 'FontSize',14);
set(findobj(T, 'Type', 'text'), 'FontSize',12);
grid on

% y Axis mechanical force plot
subplot(4,1,4)
clear Legend_Labels;
P=plot(time, [FyAPPrin, FyAPCntl],'linewidth',2.8);
set(gca, 'FontSize',11, 'FontWeight','bold')
set(P(1), 'Color', 'b');
set(P(2), 'Color', 'g');
Legend_Labels{1}='\bfPrincipal';
Legend_Labels{2}='\bfControl';
[legend_handle,object_handles] = legend(P,Legend_Labels,0);
set(findobj(object_handles, 'Type', 'text'), 'FontSize',10);
ylabel(['\bfy Axis Force (N)'], 'FontSize',14);
xlabel(['\bfTime (sec)'], 'FontSize',14);
grid on


%~ BS, BP, AS, AP Air Gap Mechanical Plots ~%

%%% z Axis Plots
```

```
% BS: z Axis Mechanical position plot
figure(13)
subplot(4,2,1)
clear Legend_Labels;
P=plot(time, [zgBS, zgBSRef, zgBSCntlHold],'linewidth',2.8);
set(gca, 'FontSize',11, 'FontWeight','bold')
set(P(1), 'Color', 'k');
set(P(2), 'Color', 'm');
set(P(3), 'Color', 'r', 'LineStyle','--');
Legend_Labels{1}='\bfPosition';
Legend_Labels{2}='\bfReference';
Legend_Labels{3}='\bfControl Hold';
[legend_handle,object_handles] = legend(P,Legend_Labels,0);
set(findobj(object_handles, 'Type', 'text'), 'FontSize',10);
ylabel(['\bfBS Position (in)'], 'FontSize',14);
title({'\bfSolenoid z Axis Mechanical';['Principal Solenoid: ',CasePrinWaveform,';  Control Type:
',...
    CaseCntl]}, 'FontSize',15);
grid on

% BP: z Axis Mechanical position plot
subplot(4,2,3)
clear Legend_Labels;
P=plot(time, [zgBP, zgBPRef, zgBPCntlHold],'linewidth',2.8);
set(gca, 'FontSize',11, 'FontWeight','bold')
set(P(1), 'Color', 'k');
set(P(2), 'Color', 'm');
set(P(3), 'Color', 'r', 'LineStyle','--');
ylabel(['\bfBP Position (in)'], 'FontSize',14);
grid on

% AS: z Axis Mechanical position plot
subplot(4,2,5)
clear Legend_Labels;
P=plot(time, [zgAS, zgASRef, zgASCntlHold],'linewidth',2.8);
set(gca, 'FontSize',11, 'FontWeight','bold')
```

```
set(P(1), 'Color', 'k');
set(P(2), 'Color', 'm');
set(P(3), 'Color', 'r', 'LineStyle','--');
ylabel(['\bfAS Position (in)'], 'FontSize',14);
grid on

% AP: z Axis Mechanical position plot
subplot(4,2,7)
clear Legend_Labels;
P=plot(time, [zgAP, zgAPRef, zgAPCntlHold],'linewidth',2.8);
set(gca, 'FontSize',11, 'FontWeight','bold')
set(P(1), 'Color', 'k');
set(P(2), 'Color', 'm');
set(P(3), 'Color', 'r', 'LineStyle','--');
ylabel(['\bfAP Position (in)'], 'FontSize',14);
xlabel(['\bfTime (sec)'], 'FontSize',14);
grid on

%%% y Axis Plots
% BS: y Axis Mechanical position plot
subplot(4,2,2)
clear Legend_Labels;
P=plot(time, [ygBS, ygBSRef, ygBSCntlHold],'linewidth',2.8);
set(gca, 'FontSize',11, 'FontWeight','bold')
set(P(1), 'Color', 'k');
set(P(2), 'Color', 'm');
set(P(3), 'Color', 'r', 'LineStyle','--');
ylabel(['\bfBS Position (in)'], 'FontSize',14);
set(findobj(T, 'Type', 'text'), 'FontSize',12);
if Case.Cntl ~= 1
    T = text(tCntlStart,1.02*zgBSmax,['\bfControl Start time: ', tCntlStartStr,' sec']);
    set(findobj(T, 'Type', 'text'), 'FontSize',12);
end
title({'\bfSolenoid y Axis Mechanical';['Perturbation Type: ',CasePert]}, 'FontSize',15);
grid on
```

```
% BP: y Axis Mechanical position plot
subplot(4,2,4)
clear Legend_Labels;
P=plot(time, [ygBP, ygBPRef, ygBPCntlHold],'linewidth',2.8);
set(gca, 'FontSize',11, 'FontWeight','bold')
set(P(1), 'Color', 'k');
set(P(2), 'Color', 'm');
set(P(3), 'Color', 'r', 'LineStyle','--');
ylabel(['\bfBP Position (in)'], 'FontSize',14);
set(findobj(T, 'Type', 'text'), 'FontSize',12);
grid on

% AS: y Axis Mechanical position plot
subplot(4,2,6)
clear Legend_Labels;
P=plot(time, [ygAS, ygASRef, ygASCntlHold],'linewidth',2.8);
set(gca, 'FontSize',11, 'FontWeight','bold')
set(P(1), 'Color', 'k');
set(P(2), 'Color', 'm');
set(P(3), 'Color', 'r', 'LineStyle','--');
ylabel(['\bfAS Position (in)'], 'FontSize',14);
set(findobj(T, 'Type', 'text'), 'FontSize',12);
grid on

% AP: y Axis Mechanical position plot
subplot(4,2,8)
clear Legend_Labels;
P=plot(time, [ygAP, ygAPRef, ygAPCntlHold],'linewidth',2.8);
set(gca, 'FontSize',11, 'FontWeight','bold')
set(P(1), 'Color', 'k');
set(P(2), 'Color', 'm');
set(P(3), 'Color', 'r', 'LineStyle','--');
ylabel(['\bfAP Position (in)'], 'FontSize',14);
set(findobj(T, 'Type', 'text'), 'FontSize',12);
```

```
xlabel(['\bfTime (sec)'], 'FontSize',14);
grid on


%%%%%%%%%%%%%%%%%%%%%%%%%%%%%%%%%%%%
%~ Secondary Power & Energy Plots ~%

% z Axis seconary energy plots
figure(14)
subplot(4,1,1)
clear Legend_Labels;
P=plot(time, [EkzPrin, EzKE, EzPE, EkzCntl],'linewidth',2.8);
set(gca, 'FontSize',11, 'FontWeight','bold')
set(P(1), 'Color', 'b');
set(P(2), 'Color', 'm');
set(P(3), 'Color', 'r');
set(P(4), 'Color', 'g');
Legend_Labels{1}='\bfPrincipal';
Legend_Labels{2}='\bfKinetic Energy';
Legend_Labels{3}='\bfPotential Energy';
Legend_Labels{4}='\bfControl';
[legend_handle,object_handles] = legend(P,Legend_Labels,0);
set(findobj(object_handles, 'Type', 'text'), 'FontSize',10);
ylabel(['\bfz Axis Instantaneous Energy (J)'], 'FontSize',14);
if Case.Cntl ~= 1
    T = text(tCntlStart,1.05*EzPEMax,['\bfControl Start time: ', tCntlStartStr,' sec']);
    set(findobj(T, 'Type', 'text'), 'FontSize',12);
end
title({'\bfCenter of Mass Secondary Power & Energy';['Principal Solenoid: ',CasePrinWaveform,';
Control Type: ',...
    CaseCntl,';  Perturbation Type: ',CasePert]}, 'FontSize',15);
grid on

% z Axis seconary power plots
subplot(4,1,2)
```

```
clear Legend_Labels;
P=plot(time, [PzPrin, PzPert, PzCntl],'linewidth',2.8);
set(gca, 'FontSize',11, 'FontWeight','bold')
set(P(1), 'Color', 'b');
set(P(2), 'Color', 'm');
set(P(3), 'Color', 'g');
Legend_Labels{1}='\bfPrincipal';
Legend_Labels{2}='\bfPerturbation';
Legend_Labels{3}='\bfControl';
[legend_handle,object_handles] = legend(P,Legend_Labels,0);
set(findobj(object_handles, 'Type', 'text'), 'FontSize',10);
ylabel(['\bfz Axis Power (W)'], 'FontSize',14);
set(findobj(T, 'Type', 'text'), 'FontSize',12);
grid on

% y Axis seconary energy plots
subplot(4,1,3)
clear Legend_Labels;
P=plot(time, [EkyPrin, EyKE, EkyCntl],'linewidth',2.8);
set(gca, 'FontSize',11, 'FontWeight','bold')
set(P(1), 'Color', 'b');
set(P(2), 'Color', 'm');
set(P(3), 'Color', 'g');
Legend_Labels{1}='\bfPrincipal';
Legend_Labels{2}='\bfKinetic Energy';
Legend_Labels{3}='\bfControl';
[legend_handle,object_handles] = legend(P,Legend_Labels,0);
set(findobj(object_handles, 'Type', 'text'), 'FontSize',10);
ylabel(['\bfy Axis Instantaneous Energy (J)'], 'FontSize',14);
set(findobj(T, 'Type', 'text'), 'FontSize',12);
grid on

% y Axis seconary power plots
subplot(4,1,4)
clear Legend_Labels;
P=plot(time, [PyPrin, PyPert, PyCntl],'linewidth',2.8);
```

```
set(gca, 'FontSize',11, 'FontWeight','bold')
set(P(1), 'Color', 'b');
set(P(2), 'Color', 'm');
set(P(3), 'Color', 'g');
Legend_Labels{1}='\bfPrincipal';
Legend_Labels{2}='\bfPerturbation';
Legend_Labels{3}='\bfControl';
[legend_handle,object_handles] = legend(P,Legend_Labels,0);
set(findobj(object_handles, 'Type', 'text'), 'FontSize',10);
ylabel(['\bfy Axis Power (W)'], 'FontSize',14);
xlabel(['\bfTime (sec)'], 'FontSize',14);
grid on


%%%%%%%%%%%%%%%%%%%%%%%%%%%
%~ System Response Plots ~%

% Mechanical & Electrical tau
figure(15)
subplot(3,1,1)
clear Legend_Labels;
% H = line or graphics handle. AX = Axis handles (LEFT and RIGHT)
LEFT=1; RIGHT=2;
Conv = 1;
hold on;
[AX,H(1,LEFT),H(1,RIGHT)] = plotyy(time, (tauzEPrin*Conv),...
    time, (tauzMech));
[AX2,H(2,LEFT),H(2,RIGHT)] = plotyy(time, (tauyECntl*Conv),...
    time, (tauyMech));
% Set the Axis Parent valus to the respective Left & Right axis.
set(H(:,LEFT),'Parent', AX(LEFT));
set(H(:,RIGHT),'Parent',AX(RIGHT));
hold off;
% Setting the y axis values for plotting
TauLim = 0.15;
```

```
set(AX(LEFT),'YLim',[0 TauLim*Conv]);
set(AX(1,RIGHT),'YLim',[0 tauMechLim]);
set(AX2(1,RIGHT),'YLim',[0 tauMechLim]);
% Note: get() only works on one handle at a time, so pick some arbitrary one
set(get(AX(LEFT),'Ylabel'),'String','\bfElectrical Tau (sec)', 'FontSize',14, 'Color', 'k');
set(get(AX(RIGHT),'Ylabel'),'String','\bfTotal Mechanical Tau (sec)', 'FontSize',14, 'Color',
'k');
% Setting the x & y axis ticks for plotting
set(AX(LEFT),'YTick',0:(Conv*TauLim/4):(Conv*TauLim));
set(AX(RIGHT),'YTick',0:tauMechLim/4:tauMechLim);
set(AX2(RIGHT),'YTick',0:tauMechLim/4:tauMechLim);
% Set up Line types and colors
set(H(1,LEFT), 'Color', 'm', 'linewidth',3);
set(H(2,LEFT), 'Color', 'b', 'linewidth',3);
set(H(1,RIGHT), 'Color', 'k', 'linewidth',3);
set(H(2,RIGHT), 'Color', 'g', 'linewidth',3);
set(AX(:),'XColor','k','YColor','k', 'FontSize',12, 'FontWeight','bold')
set(AX2(:),'XColor','k','YColor','k', 'FontSize',12, 'FontWeight','bold')
% Legend
Legend_Labels{1}='\bfPrincipal Elec.';
Legend_Labels{2}='\bfControl Elec.';
Legend_Labels{3}='\bfz Axis Mech.';
Legend_Labels{4}='\bfy Axis Mech.';
[legend_handle,object_handles] = legend([H(1,LEFT),H(2,LEFT)],Legend_Labels{1:2});
set(findobj(object_handles, 'Type', 'text'), 'FontSize',10, 'FontWeight','bold');
[legend_handle,object_handles] = legend([H(1,RIGHT),H(2,RIGHT)],Legend_Labels{3:4});
set(findobj(object_handles, 'Type', 'text'), 'FontSize',10, 'FontWeight','bold',
'BackgroundColor', 'none');
% Set the grid for the Left axis & turn the grid on.
grid(AX(1,1));
grid on;
if Case.Cntl ~= 1
    T = text(tCntlStart,1.05*tauzEPrinMax*Conv,['\bfControl Start time: ', tCntlStartStr,' sec']);
    set(findobj(T, 'Type', 'text'), 'FontSize',12);
end
title({'\bfSystem Response';['Principal Solenoid: ',CasePrinWaveform,';  Control Type: ',...
```

```
    CaseCntl,';  Perturbation Type: ',CasePert]}, 'FontSize',15);

% Magnetic spring constants
subplot(3,1,2)
clear Legend_Labels;
P=plot(time, [kzPrin, kzCntl, kyPrin, kyCntl],'linewidth',2.8);
set(gca, 'FontSize',11, 'FontWeight','bold')
set(P(1), 'Color', 'k');
set(P(2), 'Color', 'g');
set(P(3), 'Color', 'b', 'LineStyle','--');
set(P(4), 'Color', 'm', 'LineStyle','--');
Legend_Labels{1}='\bfz Axis Principal';
Legend_Labels{2}='\bfz Axis Control';
Legend_Labels{3}='\bfy Axis Principal Coil';
Legend_Labels{4}='\bfy Axis Control Coil';
[legend_handle,object_handles] = legend(P,Legend_Labels,0);
set(findobj(object_handles, 'Type', 'text'), 'FontSize',10);
ylabel(['\bfMag. Spring Constants (N/m)'], 'FontSize',14);
grid on

% Mechanical resonant/natural frequency
subplot(3,1,3)
clear Legend_Labels;
P=plot(time, [kzMechNatFreq, kyMechNatFreq],'linewidth',2.8);
set(gca, 'FontSize',11, 'FontWeight','bold')
set(P(1), 'Color', 'k');
set(P(2), 'Color', 'b');
Legend_Labels{1}='\bfz Axis';
Legend_Labels{2}='\bfy Axis';
[legend_handle,object_handles] = legend(P,Legend_Labels,0);
set(findobj(object_handles, 'Type', 'text'), 'FontSize',10);
ylabel(['\bfMech. Natural Frequency (Hz)'], 'FontSize',14);
xlabel(['\bfTime (sec)'], 'FontSize',14);
grid on
```

```
%%%%%%%%%%%%%%%%%%%%%%%%%%%%%%%%%%%%%%%%%%%%%%%%
%~ Electrical Plots - BS Solenoid ONLY ~%

% System volages plot
figure(16)
subplot(3,1,1)
clear Legend_Labels;
P=plot(time, [VBSPrinCmdRMS, VBSzCntlCmdRMS, VBSyCntlCmdRMS],'linewidth',2.8);
set(gca, 'FontSize',11, 'FontWeight','bold')
set(P(1), 'Color', 'k');
set(P(2), 'Color', 'b');
set(P(3), 'Color', 'm');
Legend_Labels{1}='\bfPrincipal';
Legend_Labels{2}='\bfz Axis Control';
Legend_Labels{3}='\bfy Axis Control';
[legend_handle,object_handles] = legend(P,Legend_Labels,0);
set(findobj(object_handles, 'Type', 'text'), 'FontSize',10);
ylabel(['\bfVoltage (Vrms)'], 'FontSize',14);
if Case.Cntl ~= 1
    T = text(tCntlStart,1.05*VBSPrinCmdMaxRMS,['\bfControl Start time: ', tCntlStartStr,' sec']);
    set(findobj(T, 'Type', 'text'), 'FontSize',12);
end
title({'\bfSolenoid BS Electrical';['Principal Solenoid: ',CasePrinWaveform,';  Control Type:
',...
    CaseCntl,';  Perturbation Type: ',CasePert]}, 'FontSize',15);
grid on

% z Axis currents
subplot(3,1,2)
clear Legend_Labels;
P=plot(time, [IBSzPrinRMS, IBSzCntlRMS, IBSzC1CntlRMS, FlagBSzVrmsONCntl,
ICntlWireSafe],'linewidth',2.8);
set(gca, 'FontSize',11, 'FontWeight','bold')
set(P(1), 'Color', 'k');
```

```
set(P(2), 'Color', 'b', 'linewidth',3.8);
set(P(3), 'Color', 'g');
set(P(4), 'Color', 'm', 'LineStyle','--');
set(P(5), 'Color', 'r', 'LineStyle','--');
Legend_Labels{1}='\bfPrincipal Solenoid';
Legend_Labels{2}='\bfControl Solenoid';
Legend_Labels{3}='\bfControl Coil #1';
Legend_Labels{4}='\bfControl Vrms "on" Flag';
Legend_Labels{5}='\bfSafe Wire Level';
[legend_handle,object_handles] = legend(P,Legend_Labels,0);
set(findobj(object_handles, 'Type', 'text'), 'FontSize',10);
ylabel(['\bfz Axis Current (Irms)'], 'FontSize',14);
grid on

% y Axis currents
subplot(3,1,3)
clear Legend_Labels;
P=plot(time, [IBSyPrinRMS, IBSyCntlRMS, IBSyC1CntlRMS, FlagBSyVrmsONCntl,
ICntlWireSafe],'linewidth',2.8);
set(gca, 'FontSize',11, 'FontWeight','bold')
set(P(1), 'Color', 'k');
set(P(2), 'Color', 'b', 'linewidth',3.8);
set(P(3), 'Color', 'g');
set(P(4), 'Color', 'm', 'LineStyle','--');
set(P(5), 'Color', 'r', 'LineStyle','--');
Legend_Labels{1}='\bfPrincipal Solenoid';
Legend_Labels{2}='\bfControl Solenoid';
Legend_Labels{3}='\bfControl Coil #1';
Legend_Labels{4}='\bfControl Vrms "on" Flag';
Legend_Labels{5}='\bfSafe Wire Level';
[legend_handle,object_handles] = legend(P,Legend_Labels,0);
set(findobj(object_handles, 'Type', 'text'), 'FontSize',10);
ylabel(['\bfy Axis Current (Irms)'], 'FontSize',14);
xlabel(['\bfTime (sec)'], 'FontSize',14);
grid on
```

```
%%%%%%%%%%%%%%%%%%%%%%%%%%%%%%%%%%%%%%%%
%~ Magnetic Plots - BS Solenoid ONLY ~%

% z Axis
figure(17)
subplot(2,1,1)
clear Legend_Labels;
P=plot(time, [BtBSzPrinPeak, BtBSzCntlPeak, BsatLimit'],'linewidth',2.8);
set(gca, 'FontSize',11, 'FontWeight','bold')
set(P(1), 'Color', 'k');
set(P(2), 'Color', 'b');
set(P(3), 'Color', 'r', 'LineStyle','--');
Legend_Labels{1}='\bfPrincipal';
Legend_Labels{2}='\bfControl';
Legend_Labels{3}='\bfBt & Bn Saturation Limit';
[legend_handle,object_handles] = legend(P,Legend_Labels,0);
set(findobj(object_handles, 'Type', 'text'), 'FontSize',10);
ylabel(['\bfz Axis (T)'], 'FontSize',14);
if Case.Cntl ~= 1
    T = text(tCntlStart,1.05*BtBSzPrinMaxPeak,['\bfControl Start time: ', tCntlStartStr,' sec']);
    set(findobj(T, 'Type', 'text'), 'FontSize',12);
end
title({'\bfBS Solenoid Tangential Magnetic Flux Density';['Principal Solenoid:
',CasePrinWaveform,';  Control Type: ',...
    CaseCntl,';  Perturbation Type: ',CasePert]}, 'FontSize',15);
grid on

% z Axis
subplot(2,1,2)
clear Legend_Labels;
P=plot(time, [BtBSyPrinPeak, BtBSyCntlPeak, BsatLimit'],'linewidth',2.8);
set(gca, 'FontSize',11, 'FontWeight','bold')
set(P(1), 'Color', 'k');
set(P(2), 'Color', 'b');
```

```
set(P(3), 'Color', 'r', 'LineStyle','--');
Legend_Labels{1}='\bfPrincipal';
Legend_Labels{2}='\bfControl';
Legend_Labels{3}='\bfBt & Bn Saturation Limit';
[legend_handle,object_handles] = legend(P,Legend_Labels,0);
set(findobj(object_handles, 'Type', 'text'), 'FontSize',10);
ylabel(['\bfy Axis (T)'], 'FontSize',14);
xlabel(['\bfTime (sec)'], 'FontSize',14);
grid on


%%%%%%%%%%%%%%%%%%%
%~ Thermal Plots ~%

% System thermal energy
figure(18)
subplot(2,1,1)
clear Legend_Labels;
P=plot(time, [QzPrinRMSTot, QzCntlRMSTot, QyPrinRMSTot, QyCntlRMSTot],'linewidth',2.8);
set(gca, 'FontSize',11, 'FontWeight','bold')
set(P(1), 'Color', 'k');
set(P(2), 'Color', 'g');
set(P(3), 'Color', 'b', 'LineStyle','--');
set(P(4), 'Color', 'm', 'LineStyle','--');
Legend_Labels{1}='\bfz Axis Principal';
Legend_Labels{2}='\bfz Axis Control';
Legend_Labels{3}='\bfy Axis Principal Coil';
Legend_Labels{4}='\bfy Axis Control Coil';
[legend_handle,object_handles] = legend(P,Legend_Labels,0);
set(findobj(object_handles, 'Type', 'text'), 'FontSize',10);
ylabel(['\bfThermal Power (W)'], 'FontSize',14);
if Case.Cntl ~= 1
    T = text(tCntlStart,1.05*QzPrinRMSTotMax,['\bfControl Start time: ', tCntlStartStr,' sec']);
    set(findobj(T, 'Type', 'text'), 'FontSize',12);
end
```

```
title({'\bfPrimary Solenoid Thermal';['Principal Solenoid: ',CasePrinWaveform,';  Control Type:
',...
    CaseCntl,';  Perturbation Type: ',CasePert]}, 'FontSize',15);
grid on

% System Temperatures
subplot(2,1,2)
clear Legend_Labels;
P=plot(time, [TempC1zPrinWire, TempC1zCntlWire, TempC1yPrinWire,
TempC1yCntlWire],'linewidth',2.8);
set(gca, 'FontSize',11, 'FontWeight','bold')
set(P(1), 'Color', 'k');
set(P(2), 'Color', 'g');
set(P(3), 'Color', 'b', 'LineStyle','--');
set(P(4), 'Color', 'm', 'LineStyle','--');
Legend_Labels{1}='\bfz Axis Principal';
Legend_Labels{2}='\bfz Axis Control';
Legend_Labels{3}='\bfy Axis Principal Coil';
Legend_Labels{4}='\bfy Axis Control Coil';
[legend_handle,object_handles] = legend(P,Legend_Labels,0);
set(findobj(object_handles, 'Type', 'text'), 'FontSize',10);
ylabel(['\bfTemperature Change (°C)'], 'FontSize',14);
xlabel(['\bfTime (sec)'], 'FontSize',14);
grid on



tend=now; % Stop: Timer to show postprocessing real time
disp(['-=> Postprocessing took ' datestr(tend-tstart,13) ') <=-']);
```

APPENDIX D LABVIEW CONTROL & D.A.Q. PROGRAMS & PICS.

Appendix D and E supplement the Phase I test description provided in Chapter 4.2.

D.1 PHASE I, TEST #1: SOLENOID PARAM. DETERMINATION

The following programs are used to provide controlled voltage magnitude and frequency signals to a stack of bipolar amplifiers. The programs are organized into user operational front panel interface shown in Figure D-1 and supporting block diagram shown in Figure D-2. A picture of the Phase I bipolar amplifier solenoid test setup with the front panel interface controller is presented in Figure D-3. This test is described in Chapter 4.2.c.ii and the results of this test are discussed in Chapter 5.2.e.ii.

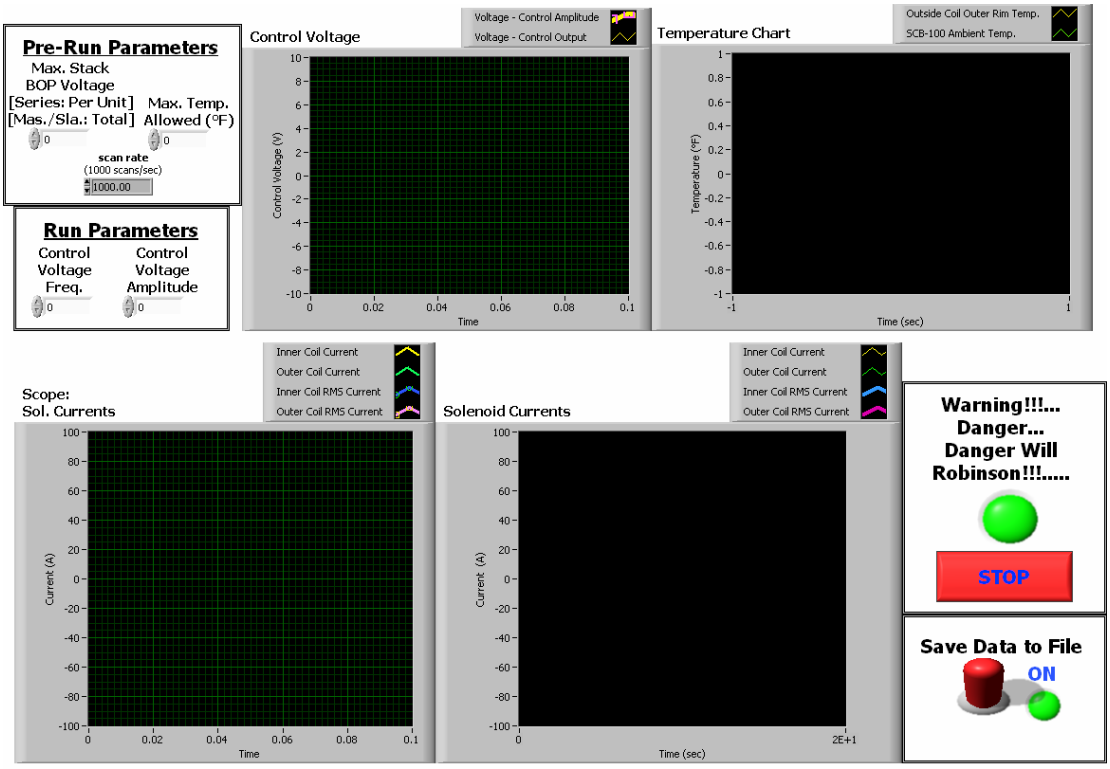

Figure D-1: Solenoid Bipolar Amplifier Test Front Panel

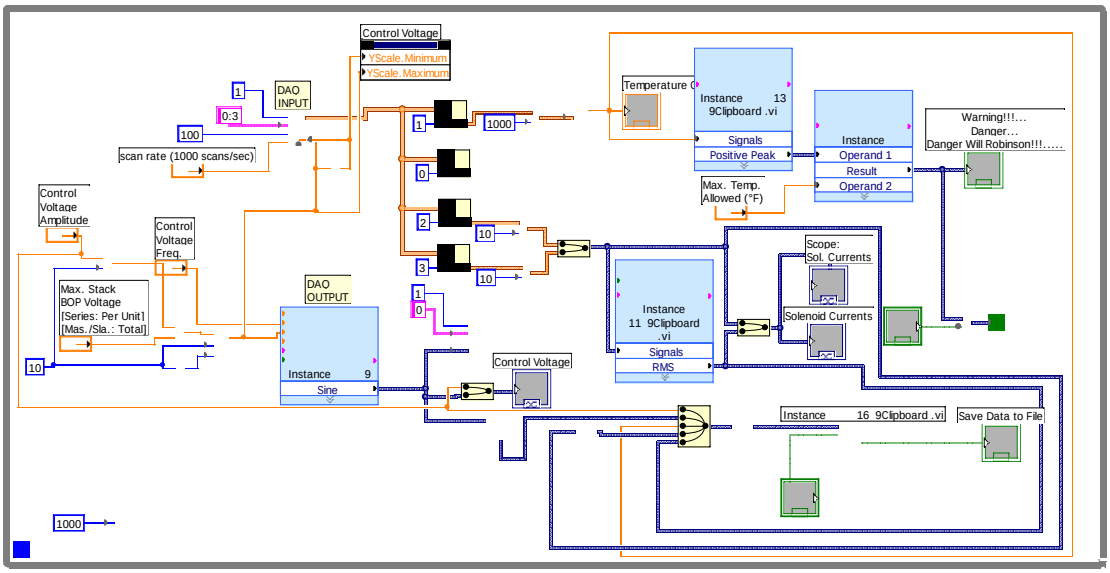

Figure D-2: Solenoid Bipolar Amplifier Test Block Diagram

Figure D-3: Phase I Initial Solenoid Bipolar Amplifier Test Setup

D.2 PHASE I, TESTS #2&3: SYSTEM RESPONSE TESTS

A picture of the rejected Phase I plastic sleeve test apparatus is presented in Figure D-4. The initial concepts and final test apparatus solution is provided in Chapter 4.2.c.i.

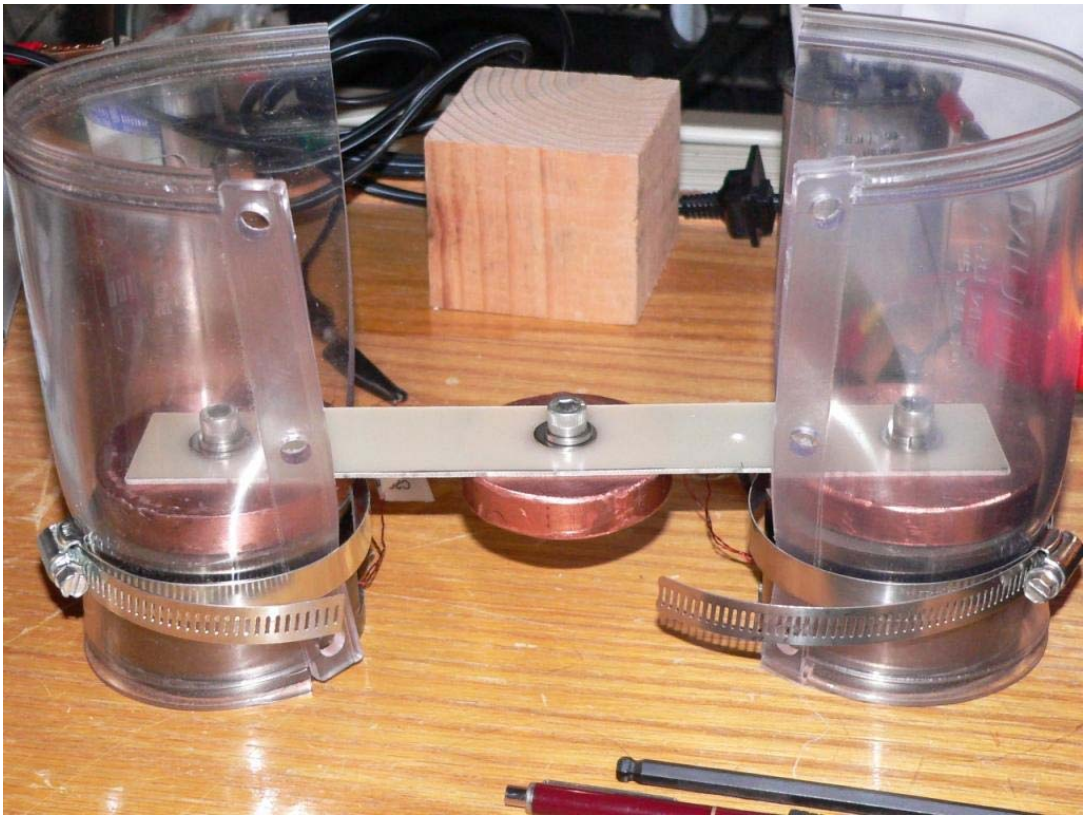

Figure D-4: Phase I Test Apparatus – Plastic Sleeve Concept

APPENDIX E SOLENOID HARDWARE

E.1 PHASE I SOLENOID HARDWARE – GENERAL

Appendix D and E supplement the Phase I test description provided in Chapter 4.2.

The following solenoid fabrication hardware developed the solenoids used for all Phase I tests. To date six solenoids, three of which are dual coil solenoids, were wound and tested. Three of these solenoids are used for Phase I testing. Two are the principal solenoids and one is the control solenoid.

E.2 PHASE I SOLENOID CORES

The Phase I principal and control coils are wound onto a solenoid bobbin which is presented in Figure E-1. This solenoid bobbin comprises the central part of the solenoid assembly body originally presented in Figure 4.2-3 and is now presented in Figure E-2. A picture of the solenoid core components is presented in Figure E-3.

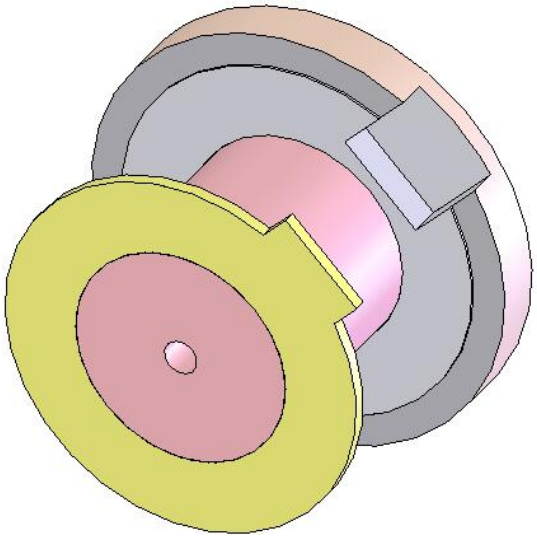

Figure E-1: Solenoid Bobbin Assembly

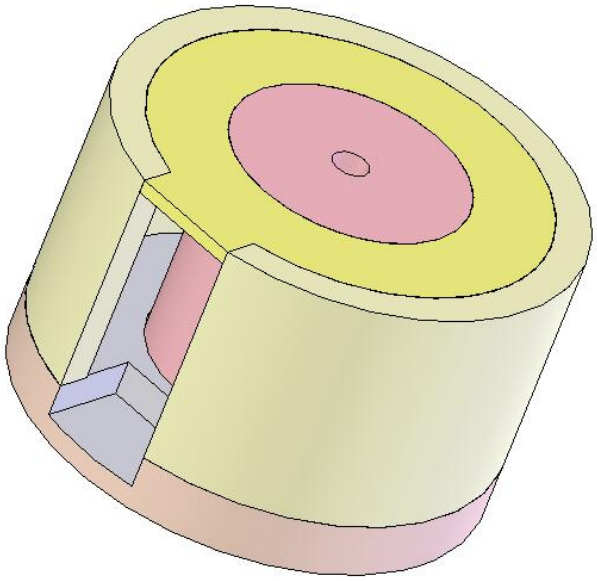

Figure E-2: Solenoid Core Assembly

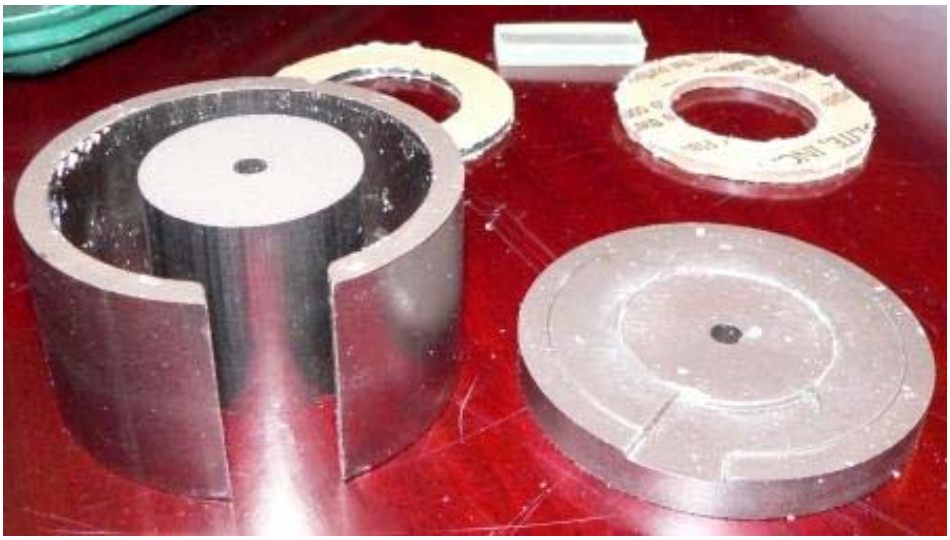

Figure E-3: Solenoid Core Assembly Components

E.3 PHASE I WINDING MACHINE

An example of solenoid winding data taking during the winding of solenoid #2 is presented in Figure E-4. The initial solenoid winding machine developed is presented in Figure E-5. Supplemental pictures of the final numerically controlled, dual axis solenoid winding machine and integrated tensiometer originally presented in Figure 4.2-2 are presented in Figures E-6 and E-7.

SOLENOID #2: WINDING DATA

Wound: Saturday - 2/18/06; Double Coil 1.45" High, 0.1" Top Insul, 28 AWG Heavy Insulation Wire

Master: Lg. Servo (Vmax 6.9V; Imax 3.75A) @ 250 RPM w/ 5 RPS Accel. & Decel., Slave: Closed Loop Stepper

Coil #	Layer #	Layer (Linear Dir.) Counter #	Δ Layer Counter #	Computer Winding Values (Radial Dir.)				Measured Values		Delta Depth	Approx. Depth Remaining for Coil (in)	Layer Radius	Winding Notes
				Counter #	Total # of Turns	# of Turns per Layer	Linear Distance (in.)	Layer Width (in)	Depth to Set Location (in)	(in)		(in)	
1	0	0		0	0.0				0.528			0.800	Coil #1 Final Wire Layer # is 15.5. Winding depth from acrylic top disk. 2 Layers of Tape on Core.
1	1	2970	2970	396000	99.0	99.0	1.426	1.466	0.479	0.049	0.517	0.849	
1	2	575		792000	198.0	99.0	1.426	1.471	0.500	-0.021	0.502	0.828	
1	3	2070	1495	1188000	297.0	99.0	1.426	1.471	0.489	0.012	0.487	0.840	
1	4	750		1584000	396.0	99.0	1.426	1.469	0.469	0.020	0.472	0.859	
1	5	2120	1370	1980000	495.0	99.0	1.426	1.459	0.465	0.004	0.457	0.863	
1	6	650		2376000	594.0	99.0	1.426	1.471	0.455	0.010	0.442	0.873	
1	7	2320	1670	2772000	693.0	99.0	1.426	1.471	0.437	0.019	0.428	0.892	
1	8	650		3168000	792.0	99.0	1.426	1.470	0.418	0.019	0.413	0.911	
1	9	2320	1670	3564000	891.0	99.0	1.426	1.470	0.421	-0.004	0.398	0.907	
1	10	650		3960000	990.0	99.0	1.426	1.470	0.368	0.053	0.383	0.960	
1	11	2320	1670	4356000	1089.0	99.0	1.426	1.473	0.363	0.005	0.368	0.965	
1	12	650		4752000	1188.0	99.0	1.426	1.475	0.355	0.008	0.353	0.973	
1	13	2320	1670	5148000	1287.0	99.0	1.426	1.475	0.350	0.005	0.338	0.978	
1	14	650		5544000	1386.0	99.0	1.426	1.470	0.350	0.000	0.323	0.978	
1	15	2320	1670	5940000	1485.0	99.0	1.426	1.476	0.322	0.028	0.308	1.006	
1	**15.5**	840	190	6138000	**1534.5**	49.5	0.713	1.475	0.308	0.014	0.301	1.020	
Tape (1 Layer)		0		0	0.0				0.304			1.020	
COIL #1 AVERAGES:						**99.0**	**1.426**	**1.518**		**0.014**			
2	16	1485		198000	49.5	49.5	0.713	1.475	0.308	-0.004	0.293	**1.016**	Coil #2 Final Wire Layer # is 12.5. Winding depth from acrylic top disk. Counters set to 0 b/w coils. 3 layers of tape outside Coil #2. No potting of final core.
2	17	2970	1485	594000	148.5	99.0	1.426	1.477	0.282	0.026	0.278	1.042	
2	18	0		990000	247.5	99.0	1.426	1.475	0.271	0.011	0.263	1.053	
2	19	2970	2970	1386000	346.5	99.0	1.426	1.478	0.255	0.016	0.249	1.069	
2	20	0		1782000	445.5	99.0	1.426	1.479	0.243	0.012	0.234	1.081	
2	21	2970	2970	2178000	544.5	99.0	1.426	1.482	0.228	0.015	0.219	1.096	
2	22	0		2574000	643.5	99.0	1.426	1.481	0.209	0.019	0.204	1.115	
2	23	2970	2970	2970000	742.5	99.0	1.426	1.483	0.204	0.005	0.189	1.120	
2	24	0		3366000	841.5	99.0	1.426	1.484	0.181	0.023	0.174	1.143	
2	25	2970	2970	3762000	940.5	99.0	1.426	1.484	0.172	0.009	0.159	1.152	
2	26	0		4158000	1039.5	99.0	1.426	1.486	0.144	0.028	0.144	1.180	
2	27	2970	2970	4554000	1138.5	99.0	1.426	1.485	0.114	0.030	0.129	1.210	
2	**28**	0	-2970	4950000	**1237.5**	99.0	1.426	1.487	0.109	0.006	0.114	1.216	
Tape (3 Layers)					0.0				0.098			1.216	
COIL #2 AVERAGES:						**99.0**	**1.426**	**1.540**		**0.016**			
TOTAL AVERAGES FOR BOTH COILS:						**99.0**	**1.426**	**1.529**		**0.015**			

Figure E-4: Solenoid Coil #2 Winding Data Chart

Figure E-5: Solenoid Coil Winding Machine - Initial

Figure E-6: Solenoid Coil Winding Machine - Overall

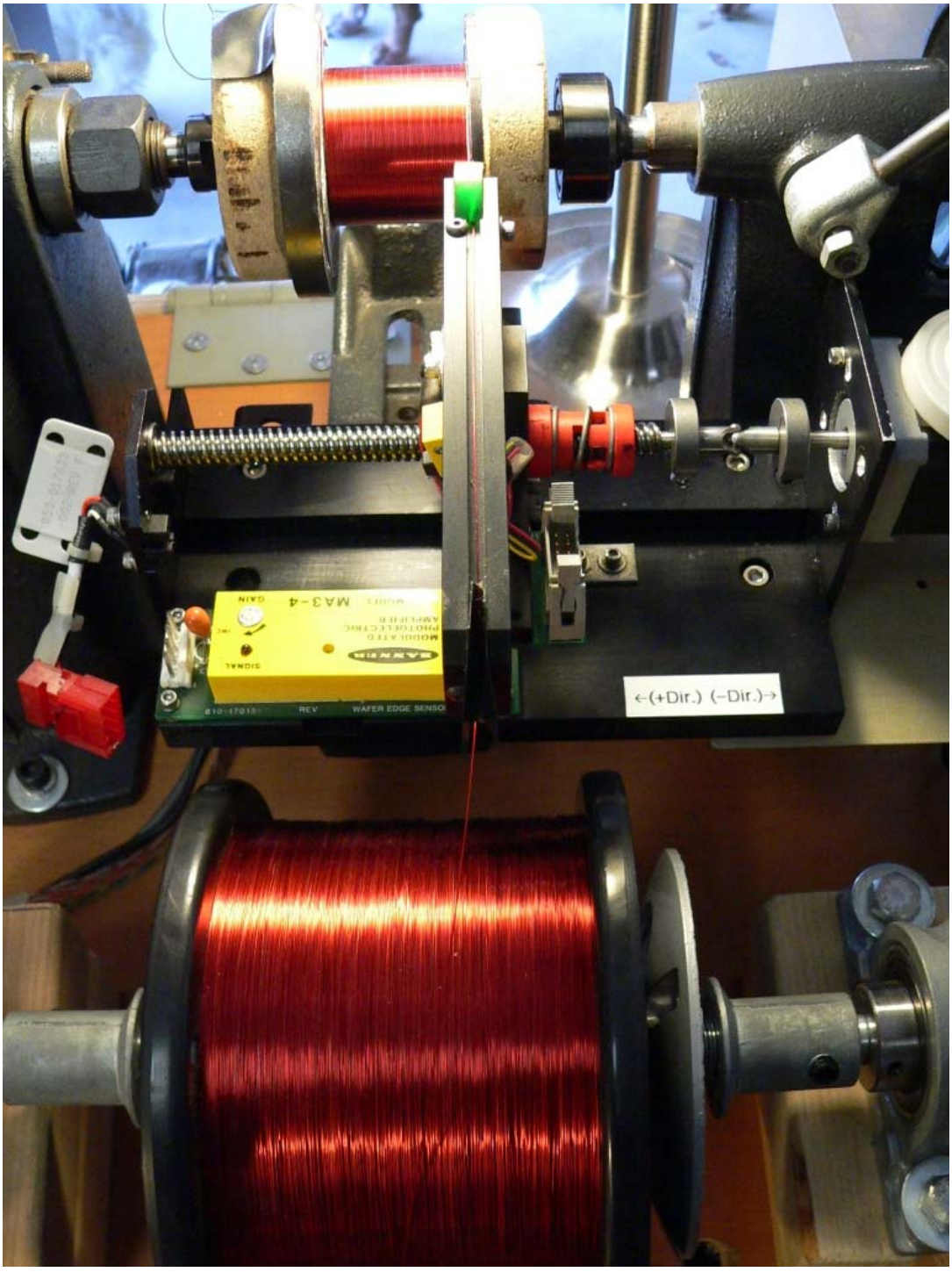

Figure E-7: Solenoid Coil Winding Machine – Winding Close Up

BIBLIOGRAPHY

1. Dukkipati, Rao, V., “Vehicle Dynamics,” C.R.C. Press LLC, 2000, pp. 364-376, 383.

2. Fausett, Laurene, “Fundamentals of Neural Networks: Architectures, Algorithms, and Applications,” Prentice-Hall Inc., 1994, pp. 1-35, 289-320, 325-330.

3. Greenwood, Donald T., “Principles of Dynamics,” Prentice Hall, Inc., 2nd Edition, 1988, pp. 354-358, 405-413.

4. Gupta, Madan M., Jin, Liang, and Homma, Noriyasu, “Static and Dynamic Neural Networks: From Fundamentals to Advanced Theory,” John Wiley & Sons, Inc., 2003, pp. 106-154, 519-520, 634-680.

5. Hayte, William H., “Engineering Electromagnetics,” McGraw-Hill, Inc., 5th Edition, 1989, pp. 336-363.

6. Hopgood, Adrian A., “Intelligent Systems for Engineers and Scientists,” C.R.C. Press LLC, 2nd Edition, 2001, pp. 195-221, 223-231, 426-431, 439-443

7. Incropera, Frank P. and De Witt, David P., "Fundamentals of Heat and Mass Transfer," John Wiley & Sons, Inc., 3rd Edition, 1990, pp. 9, 226-229.

8. Iwamoto, M., Yamada, T., and Ohno, E., “Magnetic Damping Force in Electrodynamically Suspended Trains,” *I.E.E.E. Transactions on Magnetics*, Vol. MAG-10, May 1974, pp. 458-461.

9. Jain, Lakhmi C. and Martin, N. M., “Fusion of Neural Networks, Fuzzy Sets, and Genetic Algorithms: Industrial Applications,” C.R.C. Press LLC, 1999, pp. 15-29, 71-100, 108-135.

10. Jayawant, B. V., “Electromagnetic Levitation and Suspension Techniques,” Edward Arnold Publishers Ltd., 1981, pp. 89-92.

11. Knierim, Glenn A., “Minimizing High-Speed Linear Induction Motor Longitudinal End Effects,” University of Texas at Austin Master Thesis, May 2002.

12. Kuo, Benjamin C., “Automatic Control Systems,” John Wiley & Sons, Inc., 7th Edition, 1995, pp. 802-804.

13. Lyshevski, Sergey Edward, “Control System Theory with Engineering Applications,” Birkhauser Boston, 2001, pp.179-185, 251-262.

14. Melcher, James R., "Continuum Electromechanics," Massachusetts Institute of Technology Press, 1981, pp. 6.15, 6.20-6.23.

15. Melin, Particia and Castillo, Oscar, “Modeling, Simulation, and Control of Non-Linear Dynamical Systems: An Intelligent Approach Using Soft Computing and Fractal Theory,” Taylor & Francis, 2002, pp. 9-64, 113-126, 175-214.

16. Moon, Francis C., “Magneto-Solid Mechanics,” John Wiley & Sons, Inc., 1984, pp. 137-138, 343-345.

17. Moon, Francis C., “Superconducting Levitation; Applications to Bearings and Magnetic Transportation,” John Wiley & Sons, Inc., 1994, pp. 27, 171-176.

18. Nguyen, Hung T., Prasad, Nadipuram R., Walker, Carol L., and Walker, Elbert A., “A First Course in Fuzzy and Neural Control,” C.R.C. Press LLC, 2003, pp. 85-82, 108-113, 120-123, 133-157, 165-185, 201-225, 229-246.

19. Ogata, Katsuhiko, “Modern Control Engineering,” Prentice-Hall Inc., 2nd Edition, 1990, pp. 265-269, 282, 610-613, 699-708, 772-776, 795, 827-836, 846-856.

20. Sinha, Pradip K., “Electromagnetic Suspension; Dynamics & Control,” Peter Peregrinus Ltd., 1987, pp. 16-17, 189-198.

21. Thompson, Marc T., Thornton, Richard D., “Flux-Canceling Electrodynamic Maglev Suspension: Part II Test Results and Scaling Laws,”

I.E.E.E. Transactions on Magnetics, Vol. 35, No. 3, May 1999, pp. 1964-1975.

22. Trzynadlowski, Andrezej M., “Control of Induction Motors,” Academic Press, 2001, pp. 164-173.

23. Woodson, Herbert H., Melcher, James R., "Electromechanical Dynamics, Part II: Fields, Forces, and Motion," Robert E. Krieger Publishing Co., 2nd Edition, 1985, pp. 336-337, 357, 364-369.

24. Yamamura, Sakae, “Theory of Linear Induction Motors,” University of Tokyo Press, 1972, pp. 67-79.

25. Zak, Stanislaw H., “Systems and Control,” Oxford University Press, 2003, pp. 149-170, 188-201, 393-437, 447-465, 469-529.

VITA

Glenn Auld Knierim was born in Summit, New Jersey on November 15, 1970. He is the son of Captain Thomas George and Barbara Auld Knierim. After completing his work at Jonathan Dayton Regional High School in Springfield, New Jersey in 1989, he entered Lehigh University in Bethlehem, Pennsylvania. He received a Bachelor of Science in Mechanical Engineering degree from Lehigh University in 1993. During and after his bachelor's degree he worked as a mechanical engineer at Louis Berger & Associates International in New Jersey and Washington D.C. He then worked as an automation and robotics mechanical engineer at Ismecam Inc. in Carlsbad, California. Prior to graduate school he worked as a research electromechanical engineer at General Atomics in San Diego, California. At General Atomics he enrolled in physics and electrical engineering classes and seminars at the University of California in San Diego. During the time between undergraduate and graduate coursework he traveled throughout North America, South America, Europe, and Turkey. August 1999 he entered the Electrical Engineering, Energy Systems area graduate school at University of Texas in Austin. For the majority of graduate school matriculation he performed graduate research assistant duties at the University's Center for Electromechanics. While attending University he also lectured and proctored multiple undergraduate mechanical engineering senior design teams under a teaching assistantship. Spring 2002 he completed his Master of Science in Electrical Engineering degree. Fall 2002 he returned to General Atomics in San Diego, California as a full time research electromechanical and electromagnetic engineer while completing his Doctor of Philosophy in Electrical Engineering degree.

Permanent Address: Glenn A. Knierim
40407 Chauncey Way
Temecula, CA 92591

Glenn A. Knierim typed this dissertation.